Multi-omics characterisation of phosphodiesterase enzymes in colorectal cancer & bioinformatic discovery of Dengue virus disruptor peptides

Thomas Andrew Wright (MSci)

Thesis submitted in fulfilment of the requirements for the degree of Doctor of Philosophy in Molecular, Cell, and Systems Biology

School of Cardiovascular & Metabolic Health,
College of Medical, Veterinary & Life Sciences,
University of Glasgow

Primary Supervisor: Professor George Baillie
Secondary Supervisor: Professor Andrew Jamieson

October 2024

Table of Contents

Foreword

As follows, this thesis is a culmination of the work conducted during the four years of my PhD. Notably, this research was split into two distinct projects: one focussed on characterising phosphodiesterase enzymes as drug targets in colorectal cancer by a multi-omics approach, and the other involving peptide drug discovery for the development of antiviral disruptors of Dengue virus.

This division was necessitated by the occurrence of two extraordinary events that occurred early in my research. First, I began my PhD during the COVID-19 pandemic. During this uncertain time, access to the laboratory, materials, and training was considerably limited. Three months later in December 2020, the Pfizer-BioNTech vaccine rolled out in the UK and restrictions were slowly lifted.

After three months, this difficulty was compounded. On the 19th of March 2021, we suffered a massive fire in our laboratory. Importantly, no one was injured, but our equipment and samples were completely destroyed, and the workspace was gutted. This caused significant challenges for continuing our work. Five months later, we were able to return to bench work in a temporary laboratory space, but setbacks and challenges persisted for the next year. Despite this disaster, we eventually moved back into our original laboratory once it was rebuilt 21 months later in December 2022, and it ended up being a fantastic, spacious facility with brand new equipment.

By convention, a PhD thesis is comprised of a single project with the purpose of demonstrating depth of research experience in one field. However, due to the above circumstances and my growing passion for computational biology, half of my time was dedicated towards the colorectal cancer omics project and the other half towards the Dengue drug discovery project. This was also carried out based on guidance from the MVLS graduate school, which recommended undertaking dry lab activities to mitigate the setbacks from COVID-19 and the fire. Reflecting this, I have structured this thesis into two parts, which is more typical of bioinformatics PhD theses. As such, I hope to demonstrate that both research projects stand independently as coherent and substantial contributions within the broader field of molecular drug discovery. I hope to not only demonstrate that I have become a well-rounded and independent researcher

with the following skills – evaluating literature, identifying a novel research question, designing and performing experiments, problem solving, conducting in-depth analysis, contextualising results with the literature, and directing research, as well as conference presentation and publication – but that I have developed versatility by applying these skills towards two distinct applications and methodologies. In addition, this has avoided arbitrarily forcing the two bodies of work together as one strained project, which would have obscured the original contexts and detracted from the quality of each.

Taken together, my PhD has been an amazing experience that has developed me personally and professionally, despite the vibrant happenings, and I hope that I have faithfully represented this time by the following document.

Author's Declaration

I declare that the work presented in this thesis has been carried out by myself unless where otherwise acknowledged, and that this thesis is entirely my own composition and has not been submitted elsewhere for any other degree, diploma or professional qualification at the University of Glasgow or any other institution.

Thomas Andrew Wright, October 2024

Acknowledgements

I would like to begin by expressing my deep gratitude to Professor George Baillie for his mentorship, support, and encouragement. His belief in me and the numerous opportunities he has provided have allowed me to pursue my dream career. In addition, he was the best travel companion, and I'm thankful for our adventures, shenanigans, and drams in Thailand.

Importantly, I would like to thank Dr Declan Doogan, whose generous funding of this project made everything possible.

I would also like to thank the many mentors that were instrumental in the success of this project. Thank you to my second supervisor, Professor Andrew Jamieson who was generous in offering advice and guidance in the early stages of my project. Big thanks to Dr Connor Blair, who somehow managed to convert a slightly dim chemistry student into an independent researcher in life science, and for providing support and motivation throughout. Without him, I would not have survived the visit to Lewiston 7-Eleven. A heartfelt thank you to Professor Aussara Panya for giving me the once in a lifetime opportunity to work in her lab in Thailand, looking after me, and for being unendingly kind and supportive. Her fierce dedication and leadership will always be an inspiration for me. Furthermore, I would like to extend my sincere thanks to Professor Pa-thai Yenchitsomanus for his support and for hosting me at his lab at Siriraj Hospital in Bangkok. I won't forget the durian fruit he kindly gave me, which I had to secretly eat by the river at night as to not alarm the general public by the smell. Huge thanks also to Dr Nunghathai Sawasdee for her support and patience during that time. The green tea she gifted me was the best I've ever had, and I'm worried nothing will compare again. Thank you to P' Usa and everyone else at the Siriraj lab who gave me such a warm welcome.

A huge thank you to John Cole for training me in bioinformatics, supporting my work, and for being a role model through his killer R chops and humorous approach. Additionally, I'd like to give a big thank you to Dr Jiayue Ling, as well as all the Baillies, Freemans, other residents of lab 535, and the Fullers for coaching me in all things biochemistry. I owe my gratitude to Dr Martin Rennie and Professor Helen Walden for training me in chromatography techniques and offering access to equipment, which was pivotal for this project. I wish to express a huge thank you to Dr Kathryn Pennel and Professor Joanne Edwards for

so kindly offering me tissue samples, which was a huge factor in the success of this thesis. I am also grateful towards Dr Angie Sin, Sol Olivera, and Zoë Lees for teaching me the mysterious ways of RNA and RT-qPCR. I am similarly grateful to Dr Khedidja Mosbahi for giving me advice and helping me progress on recombinant protein expression and purification techniques. Thanks also to the many people at the University of Glasgow who helped me, including Professor Will Fuller, Dr Dilys Freeman, Dr Sam Holt, June Southall, Dr Mads Gabrielsen, and Dr David McGuinness. Also, thank you also in advance to my viva examiners for taking the time to examine this thesis.

Many thanks also to my friends in 535. The hard times were much easier with such a fantastic group. Thanks to Alina Zorn and Madihah Hussain, the bedrock of 535, for fuelling our research with cake. Thank you also to those from the Aragon Research Society for the endless laughs and antics, including Dr Jack Beazer, Dr Chloe Gulliver, Michael Donnelly, Sol Olivera, Zoë Lees, Dr Max Ralston, Fiona Jordan, and Elaine Brown. Dr Jack Beazer, there are many things to be said about Jack, but I'll stick to this: stats and drams - thank you! Elaine, Queen of Peptides, thanks for all your help and for struggling through tough times with me. Thank you also to Dr Elka Kyurkchieva, my 2020 PhD classmate and US travel buddy. Special thanks to Dr Richard (Jobs) McFarlane, for trying to save my mac when I accidentally murdered it with a cup of tea. Dear mac, I'm so sorry, you nearly lasted the distance. A special thank you my friends in the Panya Lab at Chiang Mai University including Suthida Panwong, Sasithorn Saengmuang, Cartoon Ratchaneewan, Lookwha Saruda, and Dr Chutipa Chiawpanit. Thank you for your kind and warm welcome and for sharing so many amazing adventures and lifelong memories. SuSu!

Thank you also to Adam Stelmaszyc. You and Sikorski's have always had my back and I can't wait for you to read this 'essay'. Thank you also to my parents and Joe, Elen, Ffion, and Lleucu. Without you, none of this would have been possible. Thank you for always supporting and believing in me. Lastly, to my partner Emma, your constant support and tolerance has got me through this toughest of times. I'm so grateful for the extensive proofreading and feedback as well. I appreciate you.

This text is not exhaustive, and thank you to everyone else who supported me during this time.

Publications

Cooke, S.F., Wright, T.A., Sin, Y.Y., Ling, J., Kyurkchieva, E., Phanthaphol, N., Mcskimming, T., Herbert, K., Rebus, S., Biankin, A.V., Chang, D.K., Baillie, G.S. and Blair, C.M. 2024. Disruption of the pro-oncogenic c-RAF–PDE8A complex represents a differentiated approach to treating KRAS–c-RAF dependent PDAC. Scientific Reports. 14(1), p.8998.

Main, A., Mary, S., Sin, Y.Y., Wright, T.A., Ling, J., Blair, C.M., Smith, G.L., Fuller, W. and Baillie, G.S. 2024. SUMOylation of cardiac myosin binding protein-C reduces its phosphorylation and results in impaired relaxation following treatment with isoprenaline. The International Journal of Biochemistry & Cell Biology. 176, p.106668.

Sin, Y.Y., Cameron, R.T., Schepers, M., MacLeod, R., Wright, T.A., Paes, D., van den Hove, D., Willems, E., Vanmierlo, T., Prickaerts, J., Blair, C.M. and Baillie, G.S. 2024. Beta-amyloid interacts with and activates the long-form phosphodiesterase PDE4D5 in neuronal cells to reduce cAMP availability. FEBS Letters. 598(13), pp.1591–1604.

Thongyim, S., Wright, T.A., Sattayawat, P., Kaewkod, T., Baillie, G.S., Tragoolpua, Y., Jangsutthivorawat, S. and Panya, A. 2024. Clinacanthus nutans extract lowers periodontal inflammation under high-glucose conditions via inhibiting NF-κB signaling pathway. Frontiers in Pharmacology. 15.

Wright, T.A., Gemmell, A.O., Tejeda, G.S., Blair, C.M. and Baillie, G.S. 2023. Cancer: Phosphodiesterase type 4C (PDE4C), the forgotten subfamily as a therapeutic target. The International Journal of Biochemistry & Cell Biology. 162, p.106453.

Conference Participation

Computational Biology Conference (September 2024)
Poster presentation
Multi-omics characterisation of phosphodiesterase enzymes in colorectal cancer
Glasgow, United Kingdom

Gordon Research Conference, Cyclic Nucleotide Phosphodiesterases (June 2024)
Speaker and poster presentation
Multi-omics characterisation of phosphodiesterase enzymes in colorectal cancer
Lewiston Maine, USA

Scottish Biomedical Postdoctoral Research Conference (October 2023)
Flash talk and poster presentation
Multi-omics characterisation of phosphodiesterase enzymes in colorectal cancer
Glasgow, United Kingdom

Lunaphore Spatial Biology Seminar (October 2023)
Attendee
Glasgow, United Kingdom

Computational Biology Conference (July 2023)
Poster presentation
Multi-omics characterisation of phosphodiesterase enzymes in colorectal cancer
Glasgow, United Kingdom

Special Seminar, Establishment of Research Collaboration between the University of Glasgow and Chiang Mai University (March 2023)
Guest speaker
Peptide therapeutic development for Dengue Virus
Chiang Mai, Thailand

Computational Biology Conference (September 2022)
Attendee
Glasgow, United Kingdom

CEM Peptide Conference (February 2022)
Flash talk and poster presentation
Peptide therapeutic development for Dengue Virus
Liverpool, United Kingdom

Grants

Biochemical Society General Travel Grant (June 2024)
Gordon Research Conference, Cyclic Nucleotide Phosphodiesterases (June 2024)
£1152

University of Glasgow Conference Support Funding (May 2024)
Gordon Research Conference, Cyclic Nucleotide Phosphodiesterases (June 2024)
£700

Company of Biologists DMM Conference Travel Grant (April 2024)
Gordon Research Conference, Cyclic Nucleotide Phosphodiesterases (June 2024)
£600

Part 1 Summary

Multi-omics characterisation of phosphodiesterase enzymes in colorectal cancer

Colorectal cancer (CRC) originates from the malignant transformation of the colon or rectal epithelial lining and poses a significant global health concern. CRC ranks as the third most common cancer worldwide, with nearly two million new cases and approximately 900,000 deaths recorded in 2020. While rates are stabilising in developed countries among older individuals, incidence is rising in developing countries and among individuals younger than 50. Advances in chemotherapy and targeted therapies have greatly improved patient outcomes, but challenges persist, including inadequate patient responses, difficulties in predicting treatment outcomes, and the development of drug resistance. As a result, there is an urgent need for novel targets for prognosis and therapy.

Many established treatments based on phosphodiesterase (PDE) inhibition have proven effective for various conditions, but PDE inhibitors and other modulators of cAMP and cGMP have not progressed to clinical trials for CRC. cGMP signalling has been recognised as a tumour suppressor, with its attenuation identified as an early and critical event in CRC development. Additionally, inhibitors of PDE5 have demonstrated significant chemopreventative effects in CRC, leading to ongoing efforts for clinical translation. However, the other PDE genes have not been thoroughly studied in CRC, and it remains unclear whether cAMP signalling is beneficial or harmful. By profiling PDE expression and function in CRC, novel therapeutic and prognostic targets could be revealed. For this reason, this thesis had the aim of (1) characterising PDEs in CRC by a multi-omics approach using The Cancer Genome Atlas (TCGA), The Human Protein Atlas (THPA), and Clinical Proteomic Tumour Analysis Consortium (CPTAC), and (2) of using scRNA-seq analysis to verify differential PDE expression in CRC within the epithelial cell population and across microsatellite instable CRC.

This thesis first described the characterisation of PDE gene expression using RNA-seq data from CRC and normal tissue samples from TCGA colon and rectal cancer cohorts. As a result, the majority of PDEs were found downregulated in CRC, with PDE3A, PDE4D, PDE5A, PDE8A, and PDE9A exhibiting the strongest

downregulation. Conversely, weak upregulation of PDE7A and PDE10A was also shown. PDE expression was assessed based on several clinical descriptors. Differential PDE expression profiles were found almost identical between colon and rectal cancers. Additionally, by comparing between cancer stages and anatomical locations of tumours within the colon, PDEs were found homogenously downregulated in CRC and independent of these factors. By gene set enrichment analysis, this broad PDE downregulation coincided with cAMP and cGMP signalling pathway depletion in CRC. Lastly, methylation array data from TCGA cohorts was used for differential promotor methylation analysis of PDEs. Methylation probes only mapped to promotors for PDE4A, PDE4C, PDE6D, and PDE7A, but no association between promotor methylation and expression level was found. Next, associations between PDE expression and overall patient survival in CRC were explored using THPA, and PDE3B, PDE4B, PDE4D, and PDE8B were associated with prolonged survival and could participate in protective mechanisms. Following this, differential expression of PDEs were validated using IHC data from THPA and CPTAC proteomic data, and this verified downregulation of PDE3A, PDE4D, PDE8A, and upregulation of PDE7A in CRC. Validation was also performed using patient tumour and normal matched tissues, and RT-qPCR confirmed downregulation of PDE3A in CRC, and western blot confirmed downregulation of PDE9A in CRC.

scRNA-seq analysis of a publicly available CRC dataset revealed that the broad downregulation of PDEs and depletion of cAMP and cGMP pathways in the bulk RNA-seq data originated specifically from the epithelial cell population, not surrounding cell types. Furthermore, by differential expression analysis between microsatellite stable (MSS) and instable (MSI-H) CRC subtypes, most PDEs were found uniformly downregulated in both subtypes compared to normal cells. However, PDE5A indicated weak upregulation in MSI-H cells, but PDE11A was strongly upregulated in MSI-H cells, but not MSS.

This thesis supported the following model to account for these results. cGMP is a known tumour suppressor in CRC, and attenuation of cGMP signalling is an early and ubiquitous event in tumorigenesis. Since both cAMP and cGMP pathways were found depleted in CRC in this project, cAMP may also have a protective function and could be similarly attenuated as part of tumorigenesis. This is

supported by reports documenting anti-proliferative effects of AC agonism in CRC. Therefore, this would link to the broad downregulation of PDE expression found in CRC in this project. Since many PDEs are transcriptionally upregulated in response to cyclic nucleotide signalling as a feedback regulation mechanism, downregulation of cyclic nucleotides would also inhibit this stimulation of PDE expression. Taken together, this thesis supports the use of PDE inhibitors for chemoprevention in normal tissue with functional cyclic nucleotide signalling, and highlights adenylate or guanylate cyclase agonists as a promising drug targets for both chemoprevention and the treatment of established tumours. In addition, further research in characterising the regulatory links between pathogenic signalling and the few PDEs found upregulated in CRC or MSI-H CRC, such as PDE11A, may reveal novel disease mechanisms and targets for prognosis or therapy.

Part 1 Graphical Abstract

Multi-omics characterisation of phosphodiesterase enzymes in colorectal cancer

Aim: to characterise PDE expression in colorectal cancer (CRC).

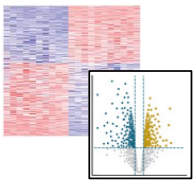

Methods: RNA-seq and scRNA-seq analysis of patient tissue and cells from TCGA and GEO.

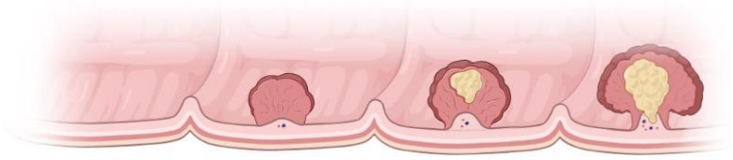

Early Tumorigenesis

?

cAMP & cGMP

PDE

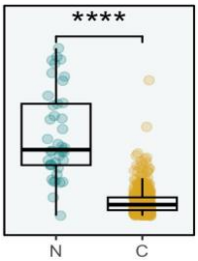

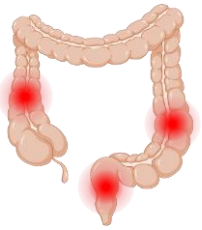

Results: cAMP and cGMP pathways and PDEs found downregulated in CRC compared to normal tissues and cells. Downregulation was independent of tumour location and cancer stage

PDEs

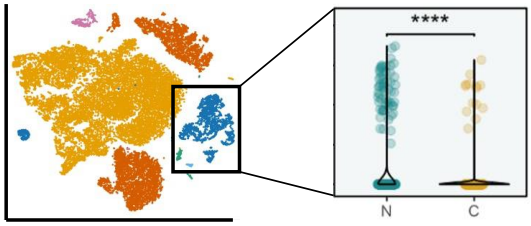

Downregulation of cAMP, cGMP, and PDEs found in the epithelial cell population by scRNA-seq.

PDE11A

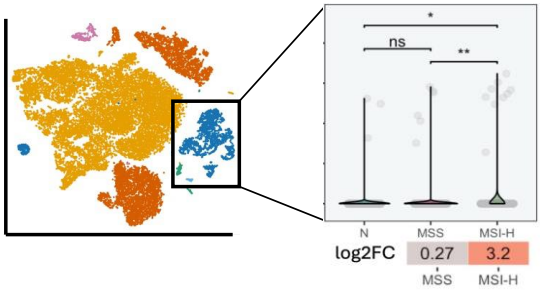

scRNA-seq identified PDE11A as upregulated in MSI-H but not MSS CRC.

Conclusion: cAMP pathway downregulation may be an important and ubiquitous event in early CRC tumorigenesis like cGMP downregulation. Low PDE expression in CRC could be due to feedback downregulation from reduced cAMP and cGMP activity. Investigation into divergent PDEs, like PDE11A upregulation in MSI-H CRC, may lead to novel prognostic methods and mechanistic insights in CRC.

Part 2 Summary

Bioinformatic discovery of Dengue Virus disruptor peptides

Dengue Virus (DENV) is the fastest spreading vector-borne viral disease in the world, accounting for approximately 100-400 million cases and 36,000 deaths every year (World Health Organization, 2009; Bhatt et al., 2013; Santana et al., 2022). Takeda's Qdenga vaccine has recently emerged from Phase III clinical trials and is hoped to provide a means for controlling this endemic (Patel et al., 2023). However, developing more than one strategy is essential. While vaccines can prevent infection, antiviral therapeutics provide a complimentary approach by enabling treatment of individuals with existing infection and could significantly reduce mortality (M.F. Lee, Wu, et al., 2023). Currently, no antiviral therapeutic for Dengue virus has been developed, and there is an urgent need for treatments (Palanichamy Kala et al., 2023).

Dengue virus exploits the human protein chaperone HSP90 as an entry receptor using the Dengue E protein for internalisation into host cells, and disruption of the E-HSP90 interaction inhibits infection (Reyes-del Valle et al., 2005; Srisutthisamphan et al., 2018). The overarching aim of this project was to discover novel peptide disruptors of E-HSP90 with the potential of providing a much-needed antiviral therapeutic for the control of Dengue virus. A development pipeline was used which focussed on peptide array screening, a high-throughput platform for the rapid discovery and rational optimisation of peptide inhibitors (Katz et al., 2011; Amartely et al., 2014). This approach has proven highly successful in the Baillie lab in similar projects (Yalla et al., 2018; Blair et al., 2019; Tibbo et al., 2022).

Towards this aim, HSP90 protein was first produced following recombinant expression in bacterial culture for use in peptide array screening. HSP90 was expressed in BL21(DE3) competent cells and purified using immobilised metal affinity chromatography, ion exchange chromatography, and size exclusion chromatography. To increase protein yield, IPTG induction conditions were optimised. A lower concentration of IPTG and an extended duration at lower temperatures after induction resulted in greater HSP90 expression. Following

chromatography steps, a stock of highly pure HSP90 protein was obtained and peptide screening could begin.

Having successfully produced the target protein, HSP90-binding epitopes were identified on the Dengue E protein by screening a discovery peptide array. This consisted of overlaying HSP90 protein on a peptide array comprised of fragments spanning the sequence of the E protein. Resultingly, a weak binding epitope E peptide 1 was discovered on E domain II, and a stronger binding epitope E peptide 2 was located in E domain III, the domain known to mediate viral entry (Hung et al., 2004; Sukupolvi-Petty et al., 2007; Frei et al., 2015; Sarker et al., 2023; González-Lodeiro et al., 2024). Both peptides were located on the E protein surface, with conservation across the four Dengue serotypes, and overlapped with epitopes for neutralising antibodies, supporting their potential role as HSP90 binding sites.

Next, physiochemical properties of the peptides were assessed by computational prediction tools. E peptide 1 adopted a partial alpha-helical conformation and E peptide 2 had a beta-hairpin fold, and both peptides had an even charge distribution and good solubility in water. Therefore, the peptides represented excellent starting points for disruptor peptide development (Di, 2015). However, both peptides contained cysteine residues, which are susceptible to oxidation and increase risk for aggregation and insolubility (Zapadka et al., 2017). This would have to be addressed in later development.

The peptides then underwent structural optimisation by peptide array screening, involving alanine scan, truncation, and point substitution analysis. During this process, E peptide 2 was prioritised over E peptide 1, due to its origin from E domain III and its stronger binding of HSP90 shown by peptide array. After optimisation, a promising candidate, Epep2, was developed and comprised residues 2-17 of the original E peptide 2 sequence. The negative control peptide Epep2AA was designed, and cytotoxicity profiles were determined using cell assays. No toxicity was found for both peptides in Vero cells up to 100 μM. However, preliminary data suggested that Epep2 affected viability of the A549 lung cancer cell line at 100 μM. This impaired viability suggested a possible disruption of endogenous HSP90 function by Epep2 at high concentrations, since cancer cells are known to exploit HSP90 for homeostasis (Li and Luo, 2023). This

highlighted the importance of characterising off-target effects in later development.

Once Epep2 and Epep2AA were found to be nontoxic for Vero cells, antiviral efficacy against Dengue virus was evaluated using cell-based ELISA. No inhibition of infection was observed. This was attributed to several possible factors. First, it was possible that Dengue virus entry into host cells is independent of the HSP90-E interaction, but this would disagree with existing reports (Reyes-del Valle et al., 2005; Srisutthisamphan et al., 2018). Second, while the Epep2 sequence bound HSP90 in peptide array screening, the free peptide in solution may not interact with HSP90. Third, Epep2 might bind HSP90 but lack affinity to displace the HSP90-E interaction. Lastly, previous reports have shown that the pathways of Dengue virus cell entry is highly dependent on cell type, and internalisation into Vero cells may be independent of HSP90 (Piccini et al., 2015). To address these factors, future work should involve testing HSP90 antibodies and Epep2 in antiviral assays using a panel of cell types to validate HSP90-E as a target and determine whether Dengue virus internalisation is mediated by HSP90 only in some cell types. Additionally, structural modification for affinity and stability may overcome potential problems in target engagement and HSP90-E disruption, while also maximising success in future clinical trials. Overall, it is hoped that these efforts can lead to the development of a greatly needed antiviral therapeutic for the control of this devastating disease.

Part 2 Graphical Abstract

Bioinformatic discovery of Dengue Virus disruptor peptides

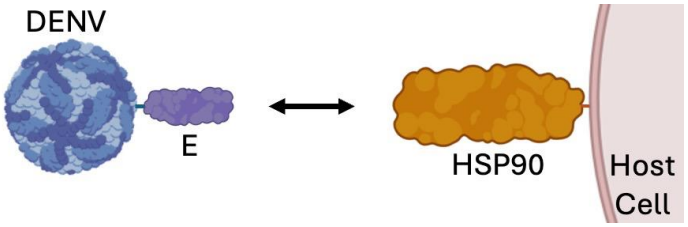

Dengue virus enters cells by interaction of the Dengue E protein with host cell surface HSP90 protein.
Aim: Develop peptide disruptors of interaction as novel antiviral therapeutics.

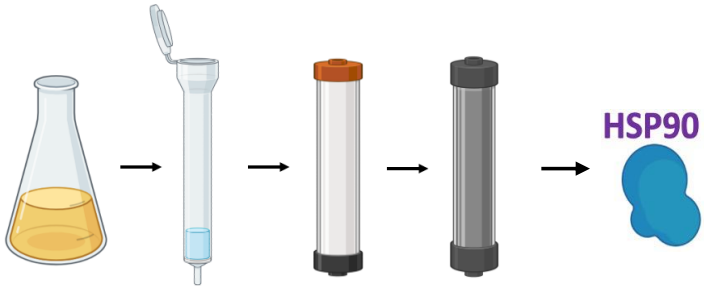

Results: HSP90 for screening was produced by recombinant expression in bacterial culture followed by chromatography purification.

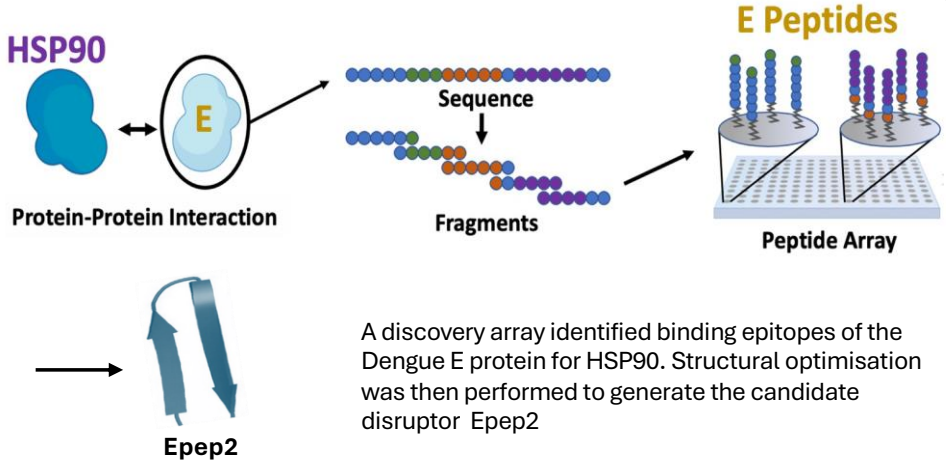

A discovery array identified binding epitopes of the Dengue E protein for HSP90. Structural optimisation was then performed to generate the candidate disruptor Epep2

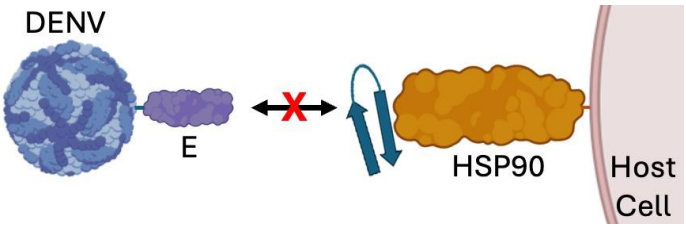

The Epep2 disruptor peptide did not affect cytotoxicity of Vero cells but failed to inhibit Dengue virus infection.

Conclusions: Epep2 may not have exhibited antiviral efficacy due to several factors, including: (1) Dengue virus entry may be independent of HSP90, (2) Epep2 may have lacked affinity to displace the HSP90-E interaction. Future work should involve verification of the role of HSP90 in virus internalisation and structural modification of Epep2 to maximise affinity.

List of Figures

List of Tables

List of Abbreviations

4G2: antibody targeting Dengue virus envelope protein

AC: adenylate cyclase

cAMP: 3', 5'-cyclic adenosine monophosphate

cGMP: 3', 5'-cyclic guanosine monophosphate

CIMP: CpG island methylator phenotype

CIN: chromosomal instability

COAD: The Cancer Genome Atlas colon adenocarcinoma dataset

COADREAD: The Cancer Genome Atlas colon and rectal adenocarcinoma dataset

CPP: cell-penetrating peptide

CRC: colorectal cancer

DENV: Dengue virus

dMMR: deficient mismatch repair

E: Dengue virus envelope protein

Epep2: peptide candidate generated from the Dengue virus envelope protein

Epep2AA: negative control peptide of Epep2

FAP: familial adenomatous polyposis

FRET: Förster resonance energy transfer

GCHP: goblet cell hyperplastic polyps

GSEA: gene set enrichment analysis

HNPCC: hereditary nonpolyposis colorectal cancer

HP: hyperplastic polyp

HSP: heat shock protein

IFN: interferon

MAP: MUTYH-associated polyposis

MMR: mismatch repair

mAB: monoclonal antibody

MSI: microsatellite instability

MSI-H: microsatellite instability-high

MSS: microsatellite stable

MVHP: microvesicular hyperplastic polyps

NES: normalised enrichment score

NGS: next-generation sequencing

Ni-NTA: nickel-nitrilotriacetic acid (used in protein purification)

NIAID: National Institute of Allergy and Infectious Diseases

PDE: phosphodiesterase

READ: The Cancer Genome Atlas rectal adenocarcinoma dataset

RNA-seq: RNA sequencing

RT-qPCR: real-time quantitative polymerase chain reaction

sAC: soluble adenylyl cyclase

scRNA-seq: single-cell RNA sequencing

SNP: single-nucleotide polymorphism

SM: small molecule

SSL: sessile serrated lesion

TCGA: The Cancer Genome Atlas

THPA: The Human Protein Atlas

TNM: tumour, node, metastasis classification system

TSA: traditional serrated adenoma

US AMRDC: United States Army Medical Research and Development Command

WB: western blot

WRAIR: Walter Reed Army Institute of Research

Part 1

Multi-omics characterisation of phosphodiesterase enzymes in colorectal cancer

Chapter 1

Introduction

1.1 Colorectal cancer is one of the most prevalent and deadly cancers

Colorectal cancer (CRC), or bowel cancer, originates from the malignant transformation of the colon or rectal epithelial lining and represents a significant health concern (Mármol et al., 2017). CRC is the third most common cancer worldwide, representing nearly two million new cases each year, and is the second most deadly cancer, accounting for 900,000 deaths in 2020 (Figure 1-1) (Mármol et al., 2017; Sung et al., 2021). Globally, the overall number of fatalities from CRC is anticipated to rise by 71.5% by the year 2035 (Araghi et al., 2019). In the UK, 1 in 17 men and 1 in 20 women will be diagnosed with CRC in their lifetime (Bowel Cancer UK, 2024). Additionally, CRC costs the UK economy 17.6 billion pounds every year (Hofmarcher and Lindgren, 2020). CRC is typically a disease of older age, but in Scotland, while overall rates have decreased since the introduction of the Scottish Bowel Screening Programme in 2007, incidence is rising in people younger than fifty years old (Clark et al., 2020).

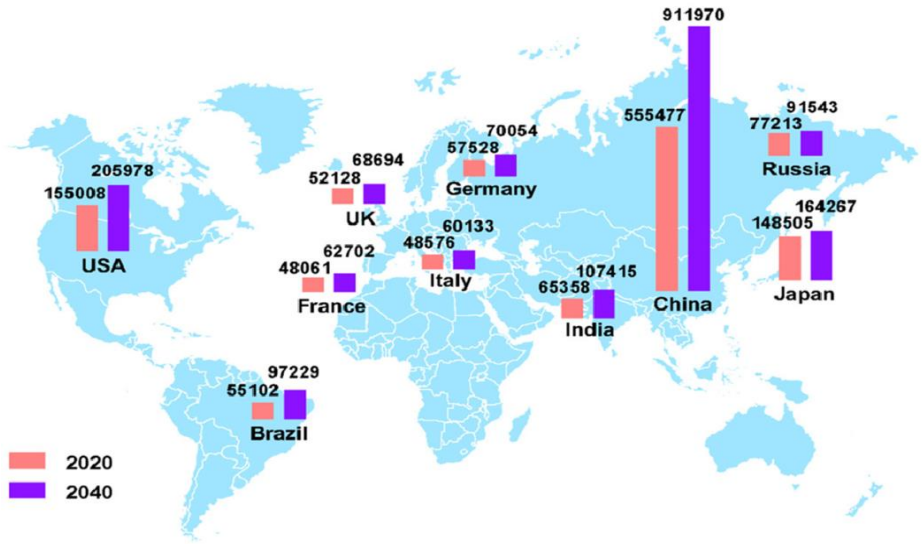

Figure 1-1: The Top 10 countries with the highest incidence of colorectal cancer in 2020. Projections for 2024 indicated in purple. (Xi and Xu, 2021).
Number of cases in 2020 and 2040 represented by red and purple bars respectively.

1.2 Anatomy of the bowel

The colon is a long tubular organ that connects the small intestine to the rectum. It is responsible for absorbing water, salts and other nutrients from food digested by the stomach and small intestine (Phillips et al., 1993). The small intestine joins the colon at a large pouch-shaped structure called the cecum (Figure 1-2) (Standring, 2019). The colon continues upwards as the ascending colon, meets a 90° bend called the hepatic flexure, then traverses the abdominal cavity from right to left as the transverse colon. After a 90° bend downwards called the splenic flexure, the descending colon meets the sigmoid colon then the rectum and anus.

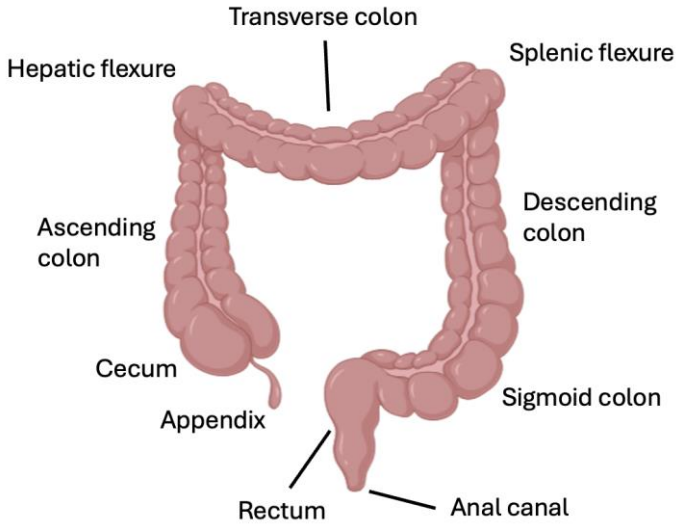

Figure 1-2: Anatomy of the large intestine.
Figure prepared using Biorender.com.

The inner lining of the bowel is comprised by the mucosa, formed by epithelial cells, absorptive enterocyte cells, and secretory goblet cells, along with a layer of connective tissue, blood vessels, and lymphatic vessels called the lamina propria (Figure 1-3) (Johansson et al., 2011). Together, these tissues absorb water and nutrients and produce mucus for the passage of stool. Under the mucosa lies a thin layer of muscle called the muscularis mucosae, which provides gentle agitation to promote contact between the mucosa and luminal contents (Siri et al., 2020). Underneath the muscularis mucosae lies another layer of connective tissue called the submucosa, which contains larger blood and lymphatic vessels, as well as nerves of the enteric nervous system (Thomson et al., 1986). Surrounding this is a thicker layer of muscle called the muscularis

propria, which is responsible for gut motility (Siri et al., 2020). Lastly, a smooth membrane mesothelial layer called the serosa connects the colon and rectum to the connective tissues of the mesentery in the abdominal cavity (Coffey and O'Leary, 2016).

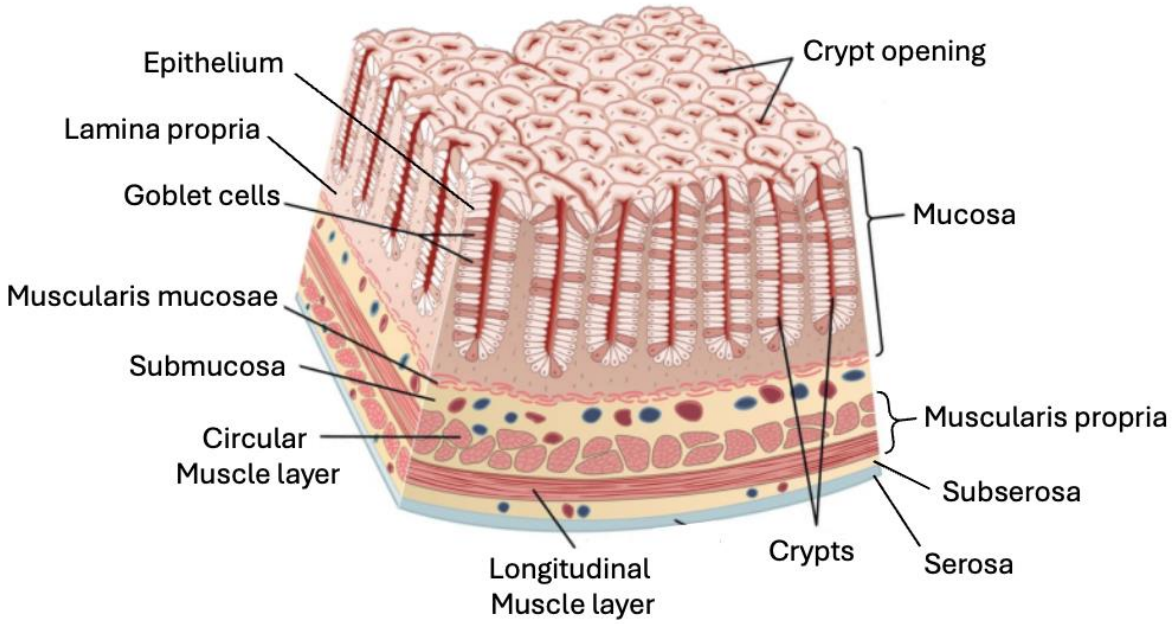

Figure 1-3: Tissue layers of the large intestine.
The tissue layers of the large intestine include the mucosa, formed by the epithelium and the underlying lamina propria. Beneath the mucosa is the muscularis mucosae, followed by the submucosa. Surrounding this is the muscularis propria, comprised of circular and longitudinal muscle layers. The outermost layer is formed by the subserosa and serosa. Figure adapted from Encyclopaedia Britannica (2025).

The mucosal surface is lined with cells arranged in an arrangement of tubular pits called colonic crypts. This arrangement increases the surface area of the colon and rectum to aid absorption of fluids and nutrients (Helander and Fändriks, 2014). At the base of the crypt, stem cells divide and differentiate into progenitor cells, also called transit amplifying cells, which migrate upwards and mature into the epithelial cells that comprise the upper surface of the crypts (Figure 1-4) (Humphries and Wright, 2008). This transition from pro-proliferation to pro-differentiation from base to lumen is mediated by a decrease in Wnt/ß-catenin signalling and an increase in bone morphogenic protein (BMP) signalling (He et al., 2004). Once differentiated, the epithelial cells are comprised mostly of enterocytes, which absorb water and nutrients. Additionally, enteroendocrine cells secrete hormones that regulate many processes including mucus secretion, motility, and appetite, and goblet cells secrete mucus to protect the mucosa

and aid stool movement (Gribble and Reimann, 2016). The colorectal lumen is a harsh environment and epithelial cells are exposed to mechanical abrasion, digestive enzymes, bile acids, and toxins from food and drink (Jani, 2023). Therefore, the terminally differentiated epithelial cells have a short lifespan of 3-5 days before undergoing apoptosis and being shed (Barker, 2014). Constant cell turnover and renewal is maintained by the balance between stem cell proliferation and differentiation with the loss of mature epithelial cells (He et al., 2004).

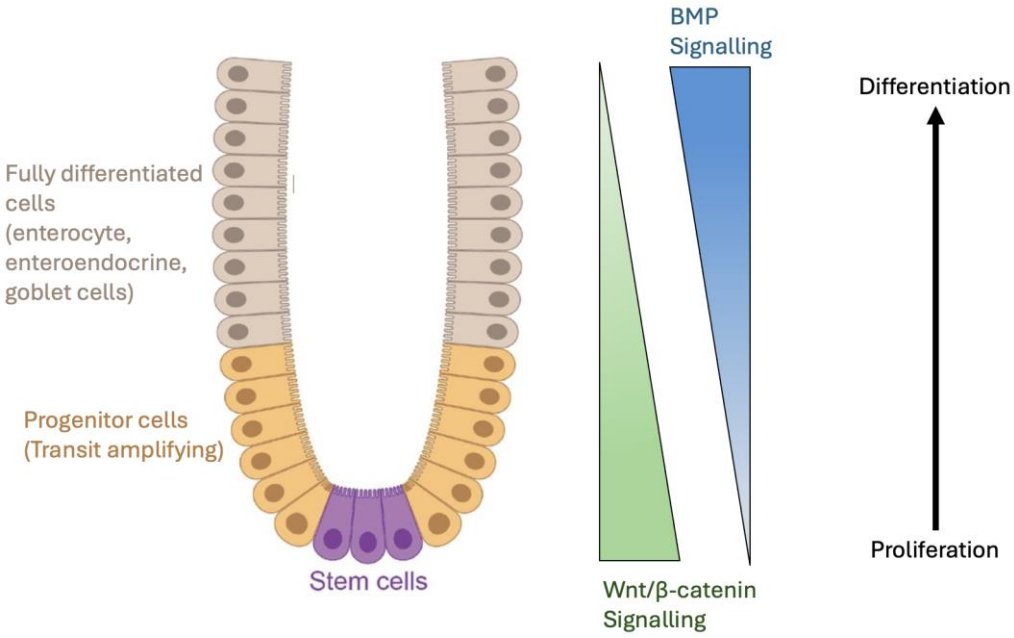

Figure 1-4: Structure of the colonic crypt and Wnt/BMP gradients that regulate the opposing gradients of pro-proliferation and pro-differentiation signalling from base to lumen.
Created using biorender.com.

1.3 Loss of genomic and epigenomic instability underlies colorectal cancer pathogenesis

Cancer is a disease of aberrant mitosis and proliferation (Williams and Stoeber, 2012). Cancerous cells develop from healthy cells by the accumulation of genetic alterations that promote unregulated growth and provide survival advantages (Islam et al., 2023). By clonal selection of more aggressive and competitive mutants, cancer cells eventually develop malignancy and metastasis which compromise bodily processes and threaten patient survival (Islam et al., 2023).

Colorectal cancer is a highly heterogeneous disease, and numerous interrelated aspects underlie tumorigenesis, including environmental and genetic risk factors,

somatic mutation, epigenetic changes, and dysregulation of pathways (Grady and Carethers, 2008). This complex interplay results in a variety of phenotypes, each with important implications for patient progression, survival, treatment options, and therapeutic response.

At the very start of CRC tumorigenesis, the mechanistic events and timings are not completely understood, but genomic and epigenomic instability are thought to initiate and hasten the accumulation of carcinogenic alterations (Al-Joufi et al., 2022). Loss of stability is comprised of three main pathways: chromosomal instability (CIN) (Pino and Chung, 2010), deficient DNA mismatch repair (MMR) with subsequent microsatellite instability (MSI) (Baretti and Le, 2018), and CpG island methylator phenotype (CIMP) (Mojarad et al., 2013).

1.3.1 Chromosomal Instability

CIN occurs in 80-85% CRC cases and is characterised by structural abnormalities of chromosomes, such as base substitutions, deletions, insertions, aneuploidy (changes in chromosome number), chromosomal rearrangements, and gene amplification (Pino and Chung, 2010). Critically, this can result in increased copy number or activity of oncogenes and loss or inhibition of tumour suppressors that result in aberrant growth and malignancy. CIN is complex and not fully understood but likely originates from defects in DNA damage repair, cell cycle regulation, and telomere function, as well as from oxidative damage and inflammation (Pino and Chung, 2010).

1.3.2 Deficiency in DNA mismatch repair and resultant microsatellite instability

Another form of genomic instability linked to CRC initiation is deficiency of the MMR system (dMMR) (Baretti and Le, 2018). In healthy cells, this mechanism corrects mistakes in base pair matching and accidental insertions or deletions made during DNA replication, recombination, or repair, and stops these modifications from being incorporated into the genome (Kunkel and Erie, 2005). The MMR system acts through a dynamic enzyme complex composed of MLH1, MLH3, MSH2, MSH3, MSH6, PMS1, and PMS2 components, and this machinery works in coordination with exonuclease, DNA polymerase and ligase proteins (Baretti and Le, 2018). dMMR linked to CRC is often caused by either

spontaneous or inherited inactivating point mutations of the MMR genes (Ijsselsteijn et al., 2020). Germline mutations in MMR genes can cause a hereditary predisposition for CRC called Lynch syndrome (Sinicrope, 2018). When MMR function is deficient, genomic stability is compromised and mutations accumulate across the genome. If mutations accumulate in oncogenes or tumour suppressors, carcinogenesis may result.

In addition to increasing overall genomic instability, dMMR underlies a major pathway of CRC pathogenesis called microsatellite instability (MSI) (Boland and Goel, 2010). Microsatellites are short motifs of 1-6 base pairs that are repeated in tandem and are common to non-coding regions across the genome but are also found infrequently in coding regions. Due to the repetitive sequence of microsatellite regions, deficient MMR complexes can slip forwards and backwards during repair, inserting or deleting base pairs (Boland and Goel, 2010). As a result, the length of microsatellite regions becomes unstable, resulting in frameshift mutations or altered protein structure that can inhibit tumour suppressors (Duval and Hamelin, 2002).

1.3.3 CpG island methylator phenotype

The third pathway of CRC-linked genomic and epigenomic instability is the CpG island methylator phenotype (CIMP) (Mojarad et al., 2013). CpG islands are regions rich in cytosine bases followed by guanine bases in the 5'-3' direction. They are an important feature of the epigenome, as they are often present in promotor regions, in which CpG island methylation can downregulate gene expression (Deaton and Bird, 2011). In a subset of CRC cases, promotors across the genome are hypermethylated at CpG islands, causing downregulation of many genes, including tumour suppressor genes (Mojarad et al., 2013). In this way, CIMP tumours often exhibit MSI, since the MMR gene MLH1 is a target for aberrant CpG island hypermethylation (Mojarad et al., 2013).

1.4 Pathways of colorectal cancer pathogenesis

1.4.1 The adenoma-carcinoma sequence

CRC is a highly heterogeneous disease with numerous subtypes, presenting a challenge for patient prognosis and treatment (Al-Joufi et al., 2022). This

heterogeneity is reflected in the multiple pathogenic pathways that emerge depending on the type of underlying genomic instability. The classic adenoma-carcinoma sequence accounts for around 70% of CRC cases and is signified by chromosomal instability and early mutation in the Wnt signalling pathway (Leslie et al., 2002). As outlined in Section 1.2, a decreasing gradient of Wnt signalling from base to lumen of the colonic crypt maintains proliferation of stem cells at the base, upwards migration of progenitor cells, and maturation of epithelium at the upper aspect (He et al., 2004). Wnt signalling in these stem cells is induced by Wnt ligands originating from fibroblasts in the lamina propria at the crypt base (Schatoff et al., 2017). These ligands prevent a destruction complex from degrading the transcriptional co-activator ß-catenin, leading to accumulation of ß-catenin in the nucleus and resultant transcription of TCF/LEF target genes including c-MYC to generate a pro-proliferation signal (Schatoff et al., 2017).

The classic adenoma-carcinoma sequence is often initiated by inactivating mutations of the critical destruction complex protein APC caused by underlying CIN (Figure 1-5) (Zhang and Shay, 2017). Resultingly, accumulation of ß-catenin leads to increased Wnt signalling and proliferation (Pino and Chung, 2010). In addition to antagonising Wnt, the APC tumour suppressor mediates proper chromosomal separation during mitosis by interaction with mitotic spindles and kinetochores (Zhang and Shay, 2017). In this way, improper chromosomal separation caused by APC mutation may exacerbate CIN further, leading to accelerated mutation rates (Zhang and Shay, 2017). Once CIN and APC mutation are established, abnormal growths called adenomas form which are characterised by increased growth and a predisposition for genomic alteration (Leslie et al., 2002). Via the accumulation of alterations in oncogenes and tumour suppressors, adenomas advance to mid and late stages, characterised by increased size, growth rate, and dysplasia. Such changes occur in genes including KRAS, PTEN, PIK3CA, SMAD4, DCC, and TP53 (Mármol et al., 2017).

Constitutively activating KRAS mutations occurs early in the adenoma-carcinoma sequence following APC mutation, and are found in 40-45% of all CRC cases (Chakraborty et al., 2024). This leads to excessive RAS-RAF-MEK-MAPK signalling and unconstrained proliferation. Additionally, mutations promoting signalling in the PI3K/AKT pathway are common to >50% of CRC cases, and most often involve

PIK3CA activation and PTEN loss (Danielsen et al., 2015). Signifying later development, tumour suppressors located on the 18q chromosome arm are lost, including SMAD4 and DCC (Popat and Houlston, 2005). SMAD4 mediates growth inhibition and apoptotic signalling in the TGF-β pathway, and loss of this tumour suppressor is found in 5-24% of CRC (Salovaara et al., 2002). DCC is linked to apoptosis and cell cycle arrest, and singe allele DCC mutations are found in 70% of CRC cases (Reale et al., 1994). Once late-stage adenomas are formed, the transition to the invasive malignant phenotype is often marked by loss of TP53, and occurs in around 60% of CRC (Hassin et al., 2022). TP53 is a critical gene that responds to DNA damage through p21-mediated cell cycle arrest or BAX-mediated apoptosis (Iacopetta, 2003). Therefore, accelerated growth of cancer cells unchecked by TP53 is another contributor to genomic instability and aggressiveness.

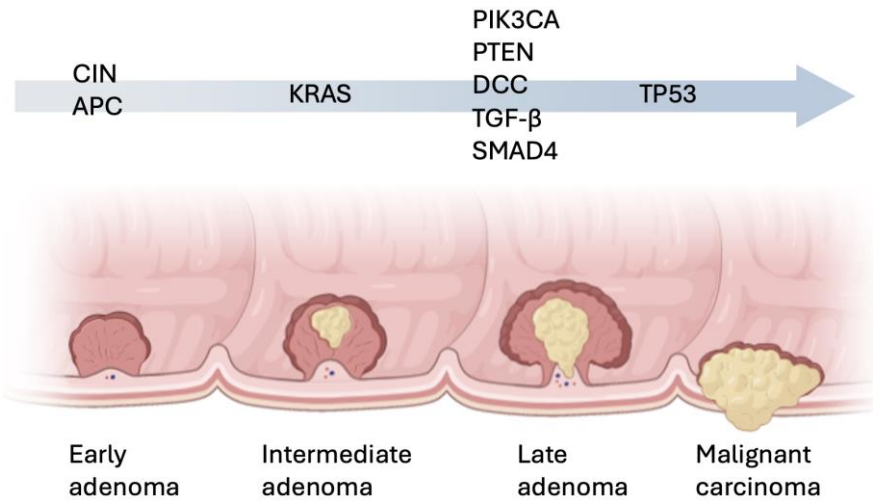

Figure 1-5. The adenoma-carcinoma pathway of colorectal cancer pathogenesis.
Figure prepared using Biorender.com.

1.4.2 Serrated pathways of colorectal cancer pathogenesis

In early research, the classic adenoma-carcinoma sequence was the first pathway of CRC pathogenesis discovered (Armaghany et al., 2012). More recently, a serrated pathway of pathogenesis has been identified, and accounts for around up to 30% of CRC cases (Figure 1-6) (Rosty et al., 2013). These pathways result in broad and flat tumours with a characteristic saw-tooth pattern formed by the crypt epithelial cells (Aiderus et al., 2024).

Serrated lesions are classified into three types. First, hyperplastic polyps (HPs) are the most common, accounting for 60-75% of serrated lesions (Aiderus et al., 2024). HPs are usually benign, have a size of <5 mm, and occur in the distal colon and rectum. They can be classified into two types based on the mucin content in the epithelial cells: microvesicular hyperplastic polyps (MVHP) and goblet cell hyperplastic polyps (GCHP). Second, sessile serrated lesions (SSL), formerly known as sessile serrated adenomas or polyps, are less common and account for 20-35% of serrated lesions (Aiderus et al., 2024). SSLs preferentially occur in the proximal colon, are larger than HPs, and are associated with higher risk of carcinogenesis and worse outcomes (Murakami et al., 2022; Aiderus et al., 2024). Third, traditional serrated adenomas (TSAs) are the rarest type, accounting for <1% of serrated lesions (Aiderus et al., 2024). TSAs can present as flat or pedunculated adenomas in the distal colon and rectum, and are distinguished from HPs by their larger size greater than 5 mm (Torlakovic et al., 2008).

The pathogenesis of serrated lesions and serrated CRC is distinct from the classic adenoma-carcinoma progression characterised by CIN and APC mutation, instead originating from BRAF or KRAS mutations with MSI and CIMP (Aiderus et al., 2024). There are two main pathways of serrated CRC pathogenesis. First, the sessile serrated pathway accounts for the majority of serrated CRC and is initiated by early BRAF mutations and predisposes for lesion formation in the proximal colon and emergence of MVHP (Kim and Kim, 2018). P16 and p53 tumour suppressors restrict the enhanced RAF/MAPK signalling, but loss of these genes in BRAF-mutated lesions or MVHP leads to uncontrolled growth and the formation of SSL (Kim and Kim, 2018). Following mutation of tumour suppressor genes like MLH1, primarily through promotor hypermethylation, malignant sessile serrated tumours arise, which are characterised by BRAF mutation, CIMP-H, and either MSI or MSS (Kim and Kim, 2018; Kang et al., 2021). For these MSI tumours, pathogenesis is liked to oncogenes and tumour suppressors containing coding-region microsatellites, including BAX, IGFR2, TGFBR2, PTEN, ACVR2 and MMR genes MSH3 and MSH6, which indicate altered microsatellite length and inactivation by frame shift mutation (Duval and Hamelin, 2002).

Second, the traditional serrated pathway gives rise to serrated tumours with CIMP-L and MSS in the distal colon and rectum and are less common than sessile serrated tumours (Kang et al., 2021). Initiation of this pathway is linked to early KRAS mutation, but early BRAF mutation can also occur, and this results in lesion formation and emergence of GCHPs (Kang et al., 2021). Following other gene alterations and methylation of tumour suppressors, including the DNA repair gene MGMT, traditional serrated lesions and MGHP progress to TSAs, which subsequently develop into malignant serrated tumours with CIMP-L and MSS (Mäkinen, 2007; Kim and Kim, 2018; Kang et al., 2021).

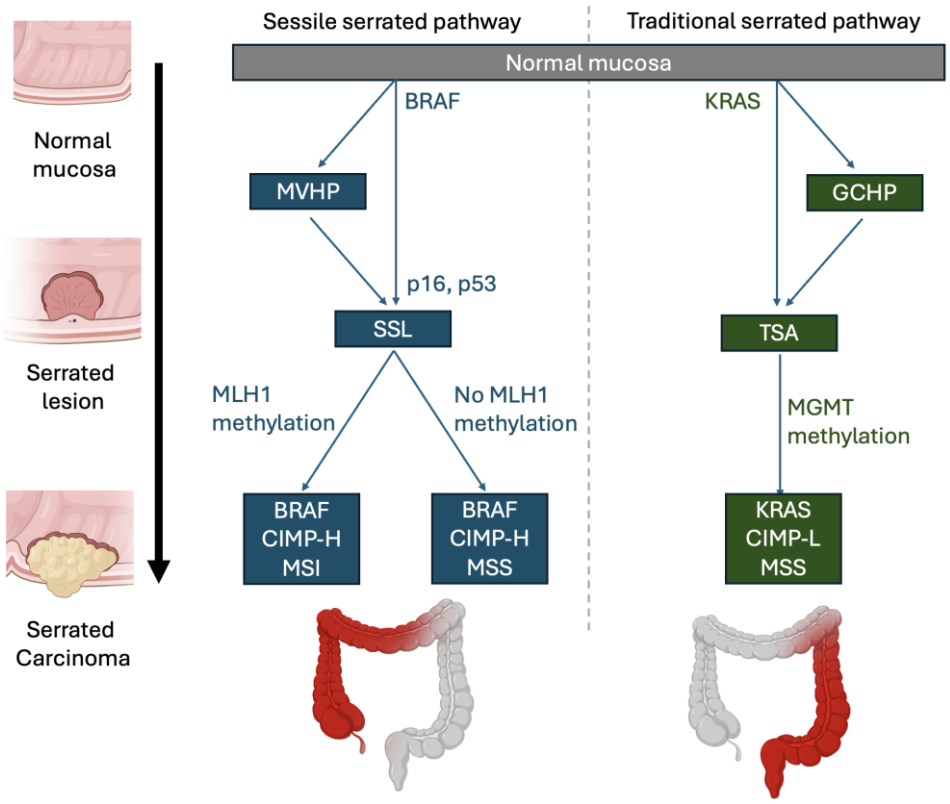

Figure 1-6. Sessile serrated pathway and traditional serrated pathway of colorectal cancer pathogenesis.
MVHP; microvesicular hyperplastic polyp, SSL; sessile serrated lesion, CIMP; CpG island methylator phenotype, MSI; microsatellite instable, MSS; microsatellite stable, GCHP; goblet cell hyperplastic polyp, TSA; traditional serrated adenoma. Polyp images prepared using Biorender.com.

1.4.3 Pathogenesis of inherited CRC

While around 95% of CRC are sporadic, 5% are hereditary, in which single highly penetrant gene mutations are passed down that predispose for CRC (Kastrinos and Syngal, 2011).

1.4.3.1 Lynch Syndrome

Around 1-5% of CRC is caused by Lynch syndrome, a condition characterised by autosomal dominant germline mutation in MMR genes MLH1, MSH2, MSH6 and PMS2, that predispose for MSI-H CRC (Table 1) (Sinicrope, 2018). As for sporadic MSI-H sessile serrated CRC, Lynch syndrome CRC pathogenesis is linked to alteration of coded microsatellite regions in oncogenes and tumour suppressors, and results in lesions in the proximal colon (Chung and Rustgi, 2003). However, Lynch Syndrome CRC lesions have adenomatous morphology, are CIMP-negative, and typically occur at a younger age than serrated sessile CRC, which is instead associated with older age-related aberrant CIMP hypermethylation (Leggett and Worthley, 2009). Individuals with Lynch syndrome have an increased risk of developing CRC, estimated at 25-75%, and are also at risk of developing other cancers depending on which MMR genes are mutated (Barrow et al., 2013).

1.4.3.2 Familial Adenomatous Polyposis (FAP)

Familial Adenomatous Polyposis (FAP) is the second most common form of hereditary CRC, and accounts for 1% of all CRC (Kastrinos and Syngal, 2011). FAP stems from an autosomal dominant germline mutation of the APC gene, proceeds according to the classic adenoma-carcinoma sequence, and is distinguished from sporadic CRC by the formation of hundreds to thousands of adenomas after the age of ten and a near 100% risk of carcinogenesis by the age of forty (Galiatsatos and Foulkes, 2006; Kastrinos and Syngal, 2011).

1.4.3.3 MUTYH-Associated Polyposis

MUTYH-Associated Polyposis (MAP) is a rare form of inherited CRC and originates from autosomal recessive mutation of the DNA base excision repair gene MUTYH (Kastrinos and Syngal, 2011). MAP progresses slower than FAP, presenting with fewer polyps and delayed carcinogenesis (Kastrinos and Syngal, 2011). Notably, MAP polyps arise primarily in the proximal colon and indicate either adenomatous or serrated morphology, with the serrated lesions being enriched for KRAS mutation (Nielsen et al., 2011). As a much rarer condition, the pathogenesis of MAPs is an area of active research.

Table 1: Summary of major colorectal cancer pathogenic pathways and subtypes.
CIN, chromosomal; CIMP, CpG island methylator phenotype; MSI/S, microsatellite instability/stability; MMR, DNA mismatch repair.

Pathogenic Pathway	Frequency	Sporadic or hereditary	Instability subtypes	Key genes and pathogenesis	Key genes	Colorectal region
Classic adenoma carcinoma sequence (Leslie et al., 2002)	70%	Sporadic	CIN	Classic sequence	APC, KRAS, PIK3CA, PTEN, DCC, TGF-ß, SMAD4, TP53	Distal, rectum
Serrated sessile pathway (Aiderus et al., 2024)	15-30%	Sporadic	CIMP+, mostly MSI	Deficient DNA mismatch repair results in MSI. MSI inhibits microsatellite containing genes	BRAF (usually V600E), p16, MLH1, BAX, IGFR2, TGFBR2, MSH2, MSH6	Proximal
Traditional serrated pathway (Aiderus et al., 2024)	< 1%	Sporadic	CIN-, CIMP-, MSS	KRAS growth and impaired MGMT DNA repair	KRAS>BRAF, MGMT	Distal, rectum
Lynch Syndrome (Sinicrope, 2018)	1-5%	Inherited	MSI, CIMP-	MMR gene mutation results in dMMR and MSI	MLH1, MSH2, MSH6, PMS2	Proximal
Familial Adenomatous Polyposis (Galiatsatos and Foulkes, 2006)	< 1%	Inherited	CIN	APC mutation initates classic sequence	APC	Distal, rectum
MUTYH-Associated Polyposis (Nielsen et al., 2011)	< 1%	Inherited	CIN-, CIMP-, MSS	Impaired base excision repair	MUTYH	Distal, rectum

1.5 CRC risk factors, prevention, and treatment

As described above, underlying genomic instability and accumulating mutations initiate various pathogenic pathways that result in heterogeneous CRC tumours. There are numerous aspects unique to the colorectal tissues that make them susceptible to cancer initiation. Firstly, the colorectum has a large surface area of epithelial cells that are rapidly turning over due to the harsh environment of the intestinal lumen, and this increases the risk of replicative errors promoting genomic instability (Sadahiro et al., 1991; Giovannucci, 2022). Furthermore, colorectal tissues have prolonged exposure to mutagens remaining present in stool (Kojima et al., 2004). For example, DNA damage can be caused heterocyclic amines or polycyclic aromatic compounds introduced from processed foods, charred foods, and red meat (Sawicki et al., 2021). Additionally, the microbiome has a large influence on colorectal homeostasis, and colonisation by deleterious bacterial species can promote inflammation and oxidative stress and produce genotoxic compounds (Sobhani et al., 2011).

In regard to these features, cancer prevention in the colorectum concerns addressing modifiable risk factors with the main goals of reducing ingestion of mutations, reducing mutagen exposure time (fibre can increase stool transit time for example), promoting microbiome diversity and homeostasis, and reducing inflammation via exercise, diet, or medications (Chan and Giovannucci, 2010). However, simply by epithelial turnover, replicative error will always present a risk of CRC occurrence. If cancer-related mutations begin to accumulate, then secondary prevention is comprised of surgical removal of precancerous polyps or neoadjuvant therapy (Chan and Giovannucci, 2010).

Tumorigenesis, the emergence of cancer, is not a single event, such as an initial APC mutation for example, but is instead a process that begins with the formation of precancerous polyps from normal tissue, which then develop to localised tumours, locally advanced and invasive tumours, and eventually metastatic cancer (Al-Joufi et al., 2022). Once a tumour becomes more advanced and aggressive, interventions for treatment become very different compared to primary or secondary prevention. For instance, patients diagnosed for cancer will accept more adverse effects of interventions compared to

healthy patients or higher risk patients because risk-benefit balance shifts significantly once cancer is diagnosed (Boland et al., 2000).

1.6 Colorectal cancer tumour classification and staging

As cancers progress, deteriorating genomic stability and accumulating oncogenic mutations result in increased growth rate, malignancy, and risk of metastasis and death (Williams and Stoeber, 2012). For this reason, treatment options, treatment response, and patient outcomes can be predicted by classifying tumour progression and identifying subtypes (Karamchandani et al., 2020). Various classifications have been designed based on molecular, morphological, and clinical characteristics.

1.6.1 TNM staging

Tumour node metastasis (TNM) staging developed by the American Joint Committee on Cancer (AJCC) is one of the most widely adopted systems to assess cancer progression and is based on anatomical analysis of resected tissues carried out by a pathologist (Weiser, 2018). TNMs scores are based on three components (Table 2). The T component describes tumour size and invasion into the intestinal wall, the N component describes invasion to lymph nodes, and the M component describes metastasis. Based on these components, cancers are classified with an overall TNM stage score ranging from 1-4, and the later stages are associated with poorer patient outcomes.

TNM staging is widely used in clinics since testing is relatively straightforward and inexpensive, and since a wide body of research has linked TNM stage to prognosis and treatment response (Li et al., 2014). Nevertheless, TNM is considered outdated since it excludes many important cancer characteristics which could improve subtype stratification and the prediction of outcomes and treatment responses (Karamchandani et al., 2020). Such characteristics include cell morphology, molecular profile, stroma composition, and the immune microenvironment (Dunne and Arends, 2024). For this reason, many clinics combine TNM staging with biomarker-based stratification to overcome these challenges.

Table 2: Summary of tumour node metastasis (TNM) staging and components.
A: The T component describes tumour size and invasion. B: The N component describes invasion to lymph nodes. C: The M component describes metastasis. D: Components of the overall TNM stage scores. (Weiser, 2018)

A

T Stage	Tumour size and invasion
T0	No tumour
Tis	*in situ*, localised to mucosa
T1	Spread to submucosa
T2	Spread to muscularis propria
T3	Spread to subserosa
T4a	Serosa penetrated, spread to visceral peritoneum
T4b	Serosa penetrated, spread to nearby organs

B

N Stage	Lymph node spread
N0	No lymph node invasion
N1a	Cancer in 1 node
N1b	Cancer in 2-3 nodes
N1c	No cancer in nodes, but present in node-adjacent adipose tissue
N2a	Cancer in 4-6 nodes
N2b	Cancer in ≧7 nodes

C

M Stage	Metastasis
M0	No metastasis
M1a	Metastasis to one organ or distant lymph node
M1b	Metastasis more than one organ or distant lymph node
M1c	Metastasis to peritoneum alone or with distant organs and lymph nodes

D

TNM Stage	Components
1	T1-2 N0 M0
2	T3-4 N0 M0
3	Any-T N1-2 M0
4	Any-T Any-N M1

1.6.2 Dukes staging

Similar to TNM, Dukes cancer staging is a clear-cut system based on anatomical features and is still used infrequently in research (Dukes, 1932). Dukes A describes tumours that have not penetrated the muscularis propria, B1 describes

penetration into the muscularis propria, and B2 describes penetration through the muscularis propria. Dukes C1 and C2 describe invasion to 1-3 and 4 or more adjacent lymph nodes respectively. Lastly, Dukes D describes cancers with metastasis to distant sites. Since Dukes staging has less segregation of cancers than the TNM system, and TNM is more commonly used in the clinic (Karamchandani et al., 2020).

1.7 Treatment of colorectal cancer

Following biopsy of a tumour, subsequent treatment is determined by assessment of cancer progression and malignancy as indicated by anatomical features, molecular markers, and stromal or immune characteristics (Biller and Schrag, 2021). The main treatment options used in clinics are surgery, radiotherapy, ablative therapy, chemotherapy, targeted therapy, and immunotherapy (Biller and Schrag, 2021).

Resection of precancerous lesions or tumours by surgery is one of the most important first-line treatment options and can often be curative. However, surgical resection can be less viable for metastasised cancers if secondary tumours are too numerous, not localised, or inaccessible (Chakedis and Schmidt, 2018). Advancements in surgical methods such as minimally invasive procedures and robotic-assisted surgeries have enhanced the precision and outcomes of cancer operations, reducing recovery times and improving prognoses (Spinelli, 2022). Furthermore, surgery allows for the collection and analysis of biopsy samples, which is essential for prognosis and guides selection of adjuvant and subsequent therapies (Biller and Schrag, 2021).

Radiotherapy is another cornerstone cancer treatment. Often combined with other treatments, radiotherapy makes use of high-energy radiation to induce cell death in cancer cells while preserving surrounding tissues (Hillson et al., 2024). This can be advantageous for sites inaccessible to surgery. Importantly, radiotherapy is a common neoadjuvant treatment which improves patient response and reduces recurrence when combined with surgical resection (Hillson et al., 2024).

1.7.1 Chemotherapy for colorectal cancer

Chemotherapeutic drugs are compounds that kill or slow the growth of rapidly dividing cells and are a critical component of cancer treatment. These treatments can be used to stabilise tumour growth before surgery, reduce risk of recurrence after surgery, or as a primary treatment in cases intractable to surgery (McQuade et al., 2017). Chemotherapy has been especially valuable for metastasised colorectal cancers, in which overall survival can be prolonged to 20 months (Goldberg, 2005). Chemotherapy is becoming more sophisticated as new compounds are discovered and regimens emerge that are optimised for reagent combination, cancer subtype, dose, and duration (McQuade et al., 2017).

The chemotherapeutic drugs currently used in the clinic are comprised of only a few compounds. 5-fluorouracil (5-FU), or the prodrug derivative capecitabine, inhibit the synthesis of thymidine by the enzyme thymidylate synthase, resulting in a deprivation of thymidine, incorporation of uracil into DNA, and subsequent cell cycle arrest and apoptosis (Vodenkova et al., 2020). Additionally, folinic acid (leucovorin) is often used as a potentiator of 5-FU to stabilise its binding to thymidylate synthase and increase efficacy (Gristan et al., 2024). Another chemotherapeutic compound, irinotecan, is a topoisomerase I inhibitor. It works by stabilising a complex formed between topoisomerase I and DNA, preventing the re-ligation of single-strand DNA breaks that occur during DNA replication (Kumar and Sherman, 2023). This action results in DNA damage accumulation, triggering cell cycle arrest and apoptosis. Finally, oxaliplatin is a platinum-based compound that interacts with DNA to form intra- and inter-strand links, preventing replication and transcription processes and inducing strand breaks (Riddell, 2018). Resulting failure of DNA damage responses induces cell cycle arrest and apoptosis.

By using combinations of chemotherapeutics, multiple cytotoxicity pathways can be targeted to increase potency, improve patient response rates, and inhibit resistance. However, drug combinations can increase toxicity and monotherapies may be preferable in some cases (McQuade et al., 2017). Guidelines directing the selection of regimens have been developed by extensive clinical testing of chemotherapeutic combinations in different colorectal cancer subtypes, and these guidelines are continually being updated as new results emerge. The main

combinations currently in use are FOLFOX (5-FU, folinic acid, oxaliplatin), FOLFIRI (5-FU, folinic acid, irinotecan), CAPOX or XELOX (capecitabine, oxaliplatin), and FOLFOXIRI (5-FU, folinic acid, oxaliplatin, irinotecan). The development of these combination therapies has had a major impact on outcomes, especially in metastatic colorectal cancer (mCRC). For example, median overall survival in mCRC has increased from 23 to 32 months from 2012 to 2024 (Gmeiner, 2024).

Despite the success of chemotherapeutics, there are important limitations. Chemotherapy treatment is accompanied by considerable toxicity and can cause long term or permanent side effects such as neuropathy and organ damage (Nurgali et al., 2018). Additionally, the heterogeneity of colorectal cancer results in varied response rates, making it difficult to predict efficacy (Xie et al., 2020). Furthermore, cancer cells will almost always develop resistance to chemotherapy, preventing the possibility of curing the cancer, and is a major factor in poor outcomes and mortality (Xie et al., 2020). These challenges necessitate continued research for the discovery of new chemotherapeutic options and the reduction of toxicity.

1.7.2 Targeted therapies for colorectal cancer

In addition to advancements in chemotherapy, the development of targeted therapies for colorectal cancer has made a significant impact on patient outcomes (Xie et al., 2020; Gmeiner, 2024). Targeted therapies inhibit specific pathways related to cancer growth, survival, and invasion, and are therefore more specific than chemotherapies which affect all rapidly dividing cells (Xie et al., 2020). Targeted therapies have been very effective in CRC, since different pathways can be targeted based on their importance in different pathogenic subtypes (Xie et al., 2020; Gmeiner, 2024). In 2004, the anti-EGFR drug cetuximab became the first targeted therapy for CRC approved by the FDA (Jonker et al., 2007). Since then, a range of therapeutics have become available, mainly consisting of monoclonal antibodies targeted against cell membrane receptors or ligands, as well as small molecule inhibitors of tyrosine kinases (Table 3, Figure 1-7).

Table 3: Targeted therapeutics approved for colorectal cancer.
mAb; monoclonal antibody, SM; small molecule, Ab; antibody.

Name	Year	Type	Pathway	Mechanism
Cetuximab	2004	mAb	EGFR	EGFR competitive inhibitor
Bevacizumab	2004	mAb	VEGFR	VEGF inhibitor
Panitumumab	2006	mAb	EGFR	EGFR competitive inhibitor
Ziv-aflibercept	2012	Recombinant protein	VEGFR	Decoy receptor of VEGF
Regorafenib	2015	SM kinase inhibitor	VEGFR	VEGFR kinase inhibitor
Ramucirumab	2017	mAb	VEGFR	VEGFR competitive inhibitor
Pembrolizumab	2017	mAb	Checkpoint Inhibitor	PD-1 competitive inhibitor
Nivolumab	2017	mAb	Checkpoint Inhibitor	PD-1 competitive inhibitor
Ipilimumab	2018	mAb	Checkpoint Inhibitor	CTLA-4 competitive inhibitor
Larotrectinib	2018		TRK	TRK kinase inhibitor
Entrectinib	2019		TRK	TRK, ROS1, ALK kinase inhibitor
Encorafenib	2020	SM+Ab	BRAF	BRAF V600E inhibitor (combined with cetuximab)
Tucatinib	2023	SM kinase + AB	HER2	HER2 kinase inhibitor (combined with trastuzumab)
Trastuzumab	2023	mAb	HER2	HER2 competitive inhibitor (combined with tucatinib)
Fruquintinib	2023	SM kinase	VEGFR	VEGFR kinase inhibitor
Adagrasib	2024	SM	KRAS	KRAS G12C inhibitor

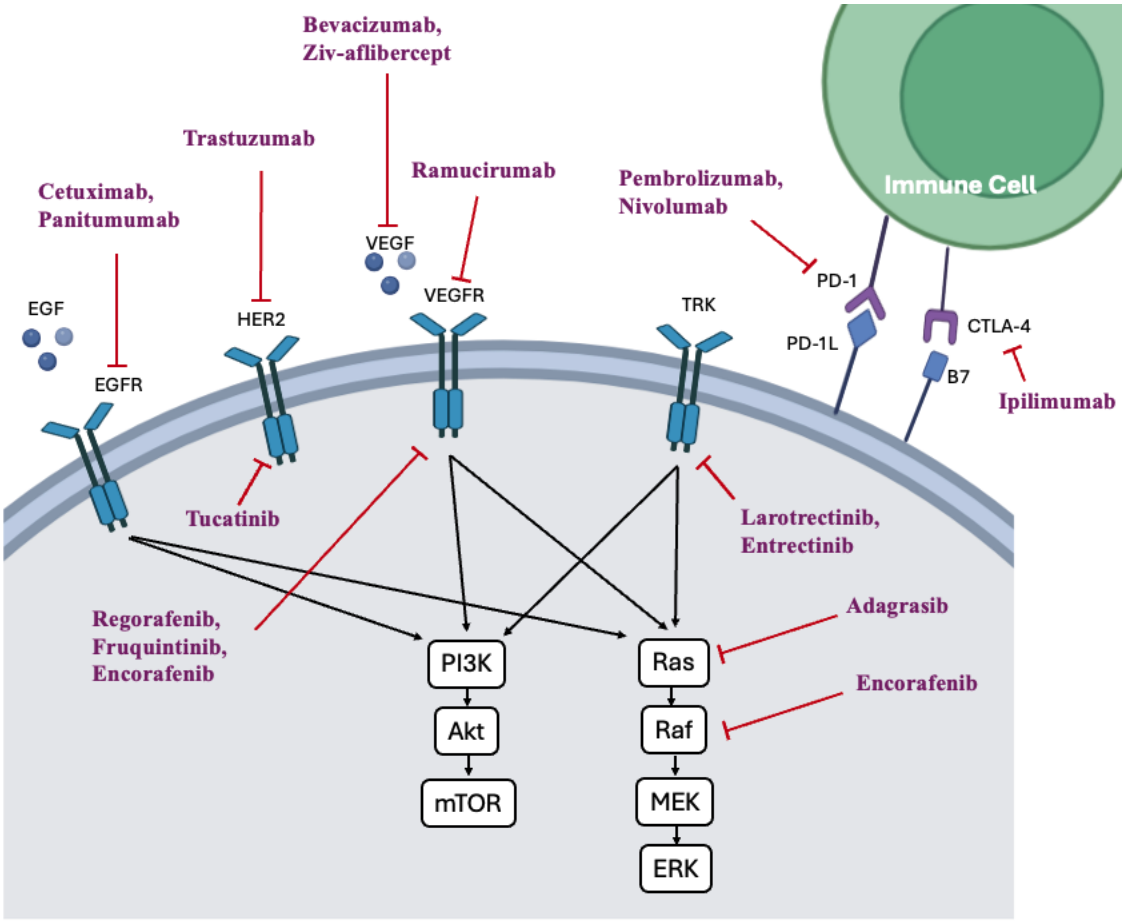

Figure 1-7. Summary of targeted therapeutics approved for colorectal cancer.
Targeted therapies for colorectal cancer are comprised of monoclonal antibodies or small molecule kinase inhibitors. Main targets include EGFR, HER2, VEGF, VEGFR, TRK, PD-1, CTLA-4, and the growth pathways PI3K/Akt/mTOR and Ras/Raf/Mek/Erk.

1.7.2.1 EGFR Inhibitors

Inhibitors of endothelial growth factor (EGF) receptor (EGFR), or HER1, are a major category of CRC targeted therapies. EGFR binds the ligands EGF and TCF-α to promote growth, proliferation, survival, and differentiation via activation of the RAS/RAF/MEK/ERK, PI3K/AKT, and JAK/STAT3 pathways (Sabbah et al., 2020). EGFR is overexpressed in 25-77% of CRCs and is associated with poor prognosis and metastasis (Spano et al., 2005). The monoclonal antibodies cetuximab and panitumumab were approved by the FDA in the mid 2000s as first-line therapies for metastatic CRC and have improved outcomes in patients when combined with 5-FU-based combination chemotherapies (García-Foncillas et al., 2019). Notably, cetuximab and panitumumab are indicated only for wild type KRAS and BRAF CRC, as mutations in these genes can constitutively activate their pathways irrespective of EGFR inhibition upstream (Sidaway, 2019).

Likewise, right side CRC tumours are also contra-indicated since they are often enriched in BRAF mutations (Holch et al., 2017).

1.7.2.2 HER2 Inhibitors

Human epidermal growth factor receptor 2 (HER2) belongs to the same family as EGFR and regulates growth and survival through the same downstream pathways (Greally et al., 2018). Although HER2 is only overexpressed in 2-5% of metastatic CRC, it is enriched in EGFR-inhibitor resistant RAS and RAF wild-type mCRC, therefore presenting a valuable drug target for this subtype (Bertotti et al., 2011; Bekaii-Saab et al., 2023). In 2023, the FDA approved a dual treatment consisting of trastuzumab, a HER2-targeted monoclonal antibody, and tucatinib, a small molecule HER2 kinase inhibitor (Casak et al., 2023).

1.7.2.3 VEGF/VEGFR Inhibitors

Similar to EGFR and HER2, the vascular endothelial growth factor (VEGF) receptor (VEGFR) activates multiple pathways including PI3K/AKT/MAPK/ERK and PLCγ/RAS/RAF/ERK/MAPK to mediate angiogenesis in response to VEGF ligand binding (Carmeliet, 2005). VEGF levels and VEGFR activity are elevated in CRC, and VEGFR-driven angiogenesis supports tumour growth and survival (Xie et al., 2020). Several targeted therapies have been approved by the FDA as first- or second-line therapies for metastatic CRC and have improved patient outcomes (Xie et al., 2020). The monoclonal antibody therapies bevacizumab, which binds VEGF, and ramucirumab, which binds VEGFR, disrupt the VEGF-VEGFR interaction to inhibit activation (Hansen et al., 2021). Ziv-aflibercept is a recombinant fusion protein based on the structure of the VEGFR receptor and acts as a decoy inhibitor to prevent VEGF-VEGFR interaction (Hansen et al., 2021). Alternatively, the small molecule kinase therapies regorafenib and fruquintinib are receptor tyrosine kinase inhibitors of VEGFR and act on its intracellular domain (Xu et al., 2022). Additionally, regorafenib is a multi-kinase inhibitor and inhibits angiogenesis by targeting receptor tyrosine kinases other than VEGFR including platelet-derived growth factor receptors and fibroblast growth factor receptors (Xu et al., 2022). Importantly, while anti-EGFR agents are most effective against left sided and RAS-wild type tumours, VEGF/VEGFR

inhibitors seem less dependent on these factors and are recommended for all other cases (Xie et al., 2020).

1.7.2.4 KRAS inhibitors

KRAS mutations occur in 40% of mCRCs and are associated with worse patient outcomes (Gmeiner, 2024). Recently in 2024, the KRAS inhibitor adagrasib was approved by the FDA in combination with the EGFR inhibitor cetuximab specifically for KRAS G12C mutant CRCs (occurring in < 4% of metastatic cases) adagrasib (Yaeger et al., 2023; Dhillon, 2023). Combination with cetuximab exhibited improved patient outcomes over adagrasib alone, an effect suggested to originate from inhibition of EGFR-compensatory feedback induced by KRAS G12C (Amodio et al., 2020).

1.7.2.5 BRAF inhibitors

BRAF mutations are found in 10% of all CRCs, of which 80% are BRAF V600E which constitutively activates BRAF and is associated with a very poor prognosis (Davies et al., 2002; Ardekani et al., 2012). While patient response rates remain low to most treatments, the FDA recently approved a regimen of a small molecule BRAF kinase inhibitor encorafenib in combination with cetuximab, which prolonged patient survival (Tabernero et al., 2021). Building upon this, research is underway include an additional inhibitor of the RAS/RAF/MEK/ERK pathway to the regimen (Gmeiner, 2024).

1.7.2.6 TRK inhibitors

Targeted therapies have recently been approved for tropomyosin receptor tyrosine kinase (TRK)-fusion positive cancers (Laetsch and Hong, 2021). TRKs are genes that mediate growth by RAS/MAPK/ERK, PLCɣ, and PI3K/AKT pathways, and in some cancers, TRKs undergo gene fusion with other genes, resulting in constitutional activation of TRK kinase activity and aberrant growth signalling (Laetsch and Hong, 2021). Even though TRK fusion is rare in CRC, accounting for only 0.7% of cases, the FDA have approved small molecule kinase inhibitors Larotrectinib and entrectinib for treatment, and second-generation inhibitors are in development (Laetsch and Hong, 2021; Gmeiner, 2024).

1.7.2.7 Immune checkpoint blockade

As part of the normal functioning of the immune system, immune checkpoint ligand and receptor recognition mediated by immune cells like CD8+ T cells, CD4+ T cells, and natural killer cells (NKs), restricts the immune response to prevent autoimmunity (Mohammadi et al., 2022). In tumours, these ligands or receptors can be overexpressed to prevent detection by the immune system (Pardoll, 2012). By developing antibody-based therapies to disrupt the ligand-receptor interaction, this immune-dampening checkpoint can be prevented, allowing the detection and killing of tumour cells by the immune system (Pardoll, 2012). Three checkpoint inhibitor drugs have been approved by the FDA for mCRC; pembrolizumab and nivolumab disrupt the interaction between the immune checkpoint receptor PD-1 and its ligand PD-1L, and ipilimumab disrupts the interaction between CTLA-4 and the ligands B7-1 and B7-2 (Makaremi et al., 2021). However, these checkpoint inhibitor therapies have only proved effective in mCRC exhibiting MSI-H and dMMR, which have been linked to increased expression of neoantigens and immune cell recruitment to the tumour (Manz et al., 2021).

1.7.2.8 Limitations of targeted therapies

Targeted therapies have transformed cancer treatment but have several important limitations. Firstly, most targeted therapies are only effective against specific CRC subtypes, and patient response is often variable even within these groups (Xie et al., 2020). Identifying which patients will benefit requires expensive genetic and molecular profiling, making patient selection a costly process (Xie et al., 2020). Secondly, resistance to targeted therapies often develops, driven by mechanisms such as compensatory feedback loops, activation of alternative signalling pathways, and genetic mutation, which allow cancer cells to bypass the targeted inhibition (Zhai et al., 2017). Lastly, targeted therapies are often expensive, particularly for the biological class drugs like monoclonal antibodies, and when combined with the expense of patient profiling and selection, especially for therapies targeting rare subtypes, the overall patient benefit may not justify the cost of these strategies (Xie et al., 2020).

To build upon the successes of targeted therapies, research efforts for the discovery of new inhibitors and novel drug targets is essential in improving patient responses, treating neglected, aggressive, or intractable CRC subtypes, and combatting resistance mechanisms.

1.8 cAMP, cGMP, and phosphodiesterase signalling

Cyclic adenosine monophosphate (cAMP) and cyclic guanosine monophosphate (cGMP) are master regulators of intracellular signalling, and together with their negative regulators cyclic nucleotide phosphodiesterases (PDEs) represent promising drug targets in cancer (Soderling and Beavo, 2000). cAMP is synthesised from ATP by adenylate cyclase (AC), and acts through the main effectors protein kinase A (PKA), EPAC, POPDC, and cAMP-gated ion channels to regulate various cellular processes including proliferation, growth, differentiation, cell cycle progression, immune function, and metabolism (Sassone-Corsi, 2012). cGMP is synthesised by guanylate cyclase from GTP and activates the main effectors of protein kinase G (PKG) and cGMP-gated cation channels to mediate cell growth, proliferation, apoptosis, immune function, and vascular and platelet homeostasis (Lucas et al., 2000).

cAMP and cGMP are central to a multitude of signalling pathways, and in order to achieve independent regulation of each, these second messengers are concentrated into compartmentalised nanodomains or microenvironments (Baillie, 2009; Zaccolo, 2011). PDEs play a crucial role in forming, shaping, and maintaining these nanodomains by selectively hydrolysing cAMP and cGMP and are positioned at the nanodomain boundaries by anchoring to membranes or by forming protein complexes (Zaccolo, 2011). This strict spatial and temporal control of cyclic nucleotide nanodomains allows the enzymatic regulation of cAMP or cGMP effectors on the scale of protein complexes (Blair et al., 2019). Nanodomain regulation by PDEs is incredibly complex, and dysfunction of PDE localisation or activity results in aberrant cAMP or cGMP signalling, which underpins many diseases (Zaccolo, 2011). For this reason, PDEs are valuable drug targets for many conditions including cancer (Peng et al., 2018).

The PDE superfamily consists of eleven distinct families (PDE1-11), each with multiple subfamilies and isoforms and classified by their homology, structural

characteristics, regulation, tissue distribution, cellular localisation, and substrate specificity (Omori and Kotera, 2007; Conti and Beavo, 2007). The domain structure of PDEs typically includes a C-terminal catalytic domain for cAMP/cGMP hydrolysis and a regulatory N-terminal domain (Keravis and Lugnier, 2010). Out of the eleven families, PDEs 4, 7, and 8 are cAMP-specific, PDEs 5, 6, and 9 are cGMP-specific, and PDEs 1, 2, 3, 10, and 11 hydrolyse both cAMP and cGMP. The diverse array of PDEs comprise over 100 isoforms, each with distinct regulation, activity, cyclic nucleotide affinity, and localisation, and these factors enhance the complexity of cAMP and cGMP nanodomain signalling. A comprehensive overview of how PDE structure, function, and spatial organisation contributes to the complexity of cAMP and cGMP signalling is provided by recent reviews (Maurice et al., 2014; Baillie et al., 2019).

1.8.1 cAMP and adenylate cyclase in colorectal cancer

The AC-cAMP-PDE and GC-cGMP-PDE pathways regulate cell proliferation, differentiation, survival, and migration, and aberrant signalling of these pathway components is important in tumorigenesis (Mehta and Patel, 2019).

1.8.1.1 cAMP as a regulator of cancer signalling

As follows, potential mechanisms of cAMP on cancer processes have been outlined. However, further detail can be found in comprehensive reviews (Cho-Chung, 1990; Fajardo et al., 2014; Ahmed et al., 2022).

cAMP affects tumorigenesis processes through a multitude of effectors acting in diverse, parallel, and often opposing pathways (Figure 1-8) (H. Zhang et al., 2020; Ahmed et al., 2022). Many outcomes from cAMP signalling originate from the effector PKA, which is a cAMP-activated serine-threonine kinase that phosphorylates targets resulting in their activation or inhibition (Sassone-Corsi, 2012). PKA has a mixed influence on apoptosis, in which inactivation of GSK3 and BAD inhibit apoptosis and activation of BIM promotes apoptosis (Jensen et al., 2007; Zambon et al., 2011; Zhao et al., 2017). PKA also affects other pathways of programmed cell death which may impact cancer cells. Pyroptosis is inhibited by PKA through the inhibition of IL1, thereby preventing GSDMD cleavage (Ye et al., 2021). Similarly, PKA inhibits ferroptosis by activating the transcription

factor CREB for the expression of GPX4, which prevents lipid peroxidation and induction of ferroptosis (Ahmed et al., 2022). Conversely, parthanatos programmed cell death is promoted by the phosphorylation of PARP1 by PKA (Brunyanszki et al., 2014). Besides effects on programmed cell death, PKA can inhibit cell proliferation and growth by inhibiting c-Raf, downregulating the Raf/MEK/ERK pathway (Kim and Juhnn, 2015). On the other hand, cAMP-PKA signalling can promote tumorigenesis through CREB-mediated expression of genes relating to metabolism, growth, and survival such as Bcl2 and cyclins (Sapio et al., 2020). CREB is recognised as an oncogene, is overexpressed in many cancers, and is associated with poor prognosis (Sapio et al., 2020).

The other main effector of cAMP is EPAC, which also affects tumorigenesis by various mechanisms (Wehbe et al., 2020). EPAC function is centred on the activation of Rap1/2 proteins by acting as a guanine exchange factor (GEF). Importantly, EPAC-Rap1/2 activation upregulates the oncogenic pathways PI3K/AKT and RAS/RAF/MEK/ERK (Wehbe et al., 2020). Additionally, EPAC suppresses apoptosis through Rap1 and inhibition of the p53-effector PUMA (Lakhter and Naidu, 2017; Wehbe et al., 2020). Conversely, EPAC promotes ferroptosis by ROS-mediated lipid peroxidation and promotes parthanatos by PARP1 activation (Musheshe et al., 2022; Zhang et al., 2023).

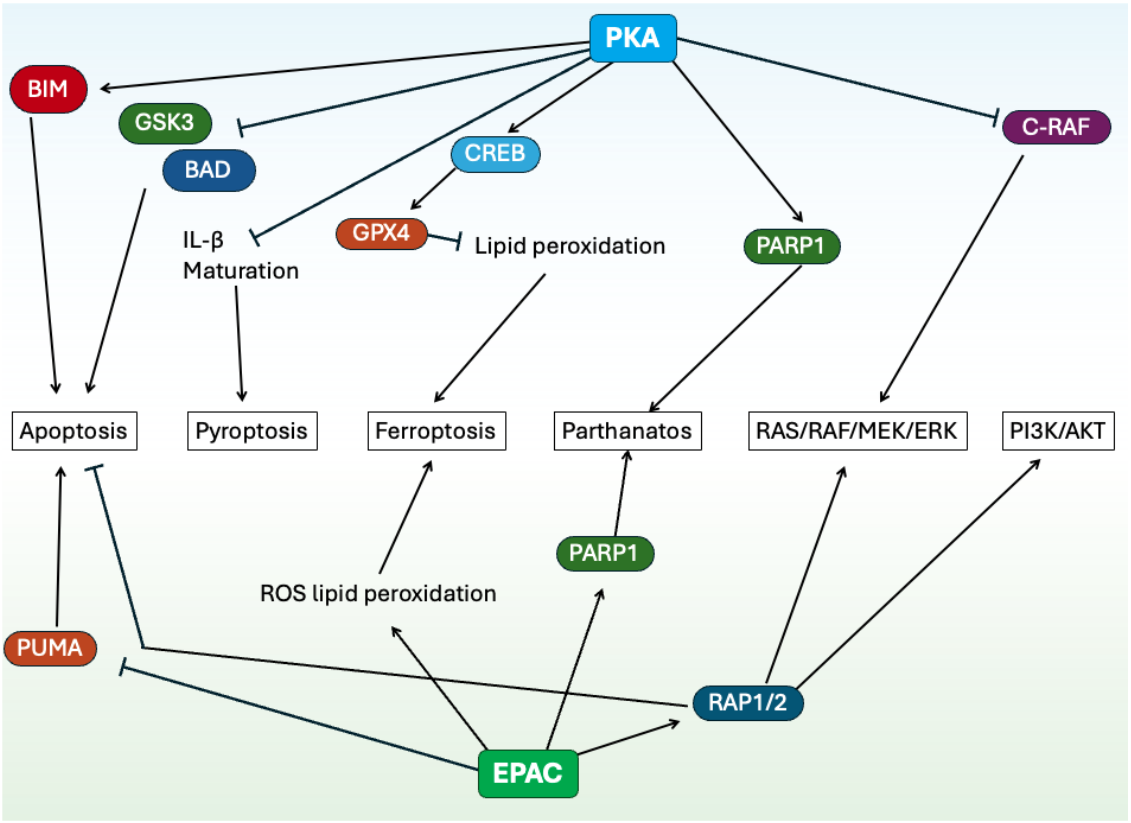

Figure 1-8. Regulation of cancer signalling by cAMP effectors PKA and EPAC.
cAMP regulates many pathways and processes important for tumorigenesis by mediating activity of main effectors PKA and EPAC. Processes affected include pathways of cell death including apoptosis, pyroptosis, ferroptosis, and parthanatos, in addition to growth pathways RAS/RAF/MEK/ERK and PI3K/AKT.

While cAMP effectors PKA and EPAC can have divergent effects on tumorigenesis, the cAMP effector POPDC is a clear tumour suppressor (Amunjela and Tucker, 2016). Firstly, POPDC inhibits RhoA, an oncogene that drives cancer cell motility, migration, invasion, and metastasis (Williams et al., 2011). Additionally, POPDC inhibits oncogenes c-Myc, ß-catenin, and MMP2/9 (Han et al., 2014; Parang et al., 2017).

As can be seen, cAMP can impact cancer pathways through multiple opposing mechanisms. This complexity is increased further considering the likelihood of AC-cAMP-PDE nanodomain regulation of these processes (Blair and Baillie, 2019). Therefore, it is not surprising that modulation of cAMP levels has been shown to either promote or inhibit cancer, depending on cancer type, pathogenic subtype, cancer stage, expression of cAMP effector proteins, and other factors.

1.8.1.2 Adenylate cyclase and cAMP as drug targets in colorectal cancer

Exploiting cAMP signalling using AC agonists, cAMP analogues, and cAMP-specific PDE inhibitors has been explored as potential therapy for CRC in multiple studies (Mehta and Patel, 2019). Conflicting effects of cAMP on CRC cell line growth have been found. Analogues theophylline and 8-Br-cAMP inhibited the growth of cell lines HT29, LIM 1215, and COLO 206F, while the analogues dibutyryl-cAMP and chlorophenylthio-cAMP promoted growth (Saba et al., 1990). In more recent work, 8-Br-cAMP inhibited growth in CT26 CRC cells and reduced tumour multiplicity and angiogenesis in a CRC mice model (Wang et al., 2018). Accounting for these divergent results, the different chemical structures of the cAMP analogues could have caused selectivity in cAMP effector activation (Niles et al., 1979). Other studies have investigated the effect of AC activation on CRC cell lines. In one study, the natural product and AC agonist forskolin was shown to increase cAMP levels, inhibit proliferation, induce apoptosis in KM12C cells (McEwan et al., 2007). In another study, forskolin and vasoactive intestinal peptide (VIP), an activator of AC via GPCR, increased cAMP, inhibited proliferation, and arrested the cell cycle at stages G0/G1 in HT29 cells (Gamet et al., 1992). However, this CRC inhibition does not generalise across the whole AC family. The AC gene ADCY9 exhibits mutation and increased expression in CRC patients, and higher expression was associated with shorter overall survival (Yi et al., 2018). The contrasting effects of ACs in CRC may originate from nanodomain regulation, and elucidation of mechanisms would facilitate the use of AC agonists or cAMP analogues as CRC therapeutics.

1.8.2 cGMP and guanylate cyclase in colorectal cancer

Like cAMP, cGMP also regulates pathways important for tumorigenesis (Fajardo et al., 2014). In the bowel, cGMP is synthesised primarily from the guanylate cyclase GUCY2C (also called GC-C), which is a membrane bound receptor expressed on the luminal aspect of the crypt (Piroozkhah et al., 2023). Under healthy conditions, the endogenous paracrine hormone guanylin is secreted by goblet cells and stimulates GUCY2C to synthesise cGMP, which exerts its action through the main effector PKG (Forte, 2004). PKGII is the only isoform expressed in colonic epithelial cells, while PKGI is predominant in intestinal smooth muscle (Francis et al., 2010; Islam et al., 2022). The GUCY2C-cGMP-PKGII pathway is

important for many aspects of intestinal homeostasis and in the prevention of CRC (Figure 1-9) (Rappaport and Waldman, 2018).

One of the most important functions of this pathway is the inhibition of proliferation to maintain the proliferation-differentiation gradient that organises intestinal crypt structure from base to lumen (Rappaport and Waldman, 2018). This organisation was described in Section 1.2. Genetic knock out of guanylin, GUCY2C, or PKGII in mice results in crypt hyperplasia and expansion of the proliferating progenitor cell compartment (Steinbrecher et al., 2002a; Li, Lin, et al., 2007; Wang et al., 2012). Furthermore, genetic knock out of GUCY2C in several CRC mice models greatly increases tumorigenesis (Li, Schulz, et al., 2007; Basu et al., 2014). The anti-proliferative mechanisms appear to involve multiple mechanisms driven by PKGII including inhibition of ß-catenin, inhibition of cell cycle by upregulation of P21 and P27, upregulation of PTEN for PI3K/AKT inhibition, and an increase in extracellular calcium sensing and influx (Rappaport and Waldman, 2018). Additionally, PKGII has been shown to reduce proliferation in gastric cancer via inhibition of EGF/EGFR induced signalling pathways, which could be important in CRC. Firstly, PKGII has been shown to bind and phosphorylate EGFR, resulting in desensitisation towards EGF binding and subsequent autophosphorylation of the EGFR receptor (Wu et al., 2012). PKGII also inhibits the MAPK/ERK pathway downstream from this by reducing Ras activation via EGFR/Grb2/Sos1 signalling, as well as by suppressing activating phosphorylation of Raf-1, MEK, and ERK (Wu et al., 2012). Furthermore, this EGFR inhibition by PKGII was shown to suppress gastric cancer cell migration by disruption of MAPK/ERK and PLCɣ1 pathways of EGFR signalling (Jiang et al., 2013).

In addition to gastric cancer, PKGII antagonism of EGFR and RAS/RAF/MAPK/ERK pathways has been demonstrated in other cancers. Firstly, PKGII was shown to inhibit activating phosphorylation of Raf-1 in chondrosarcoma, a rare type of bone cancer, by direct phosphorylation at S43 (Kamemura et al., 2017). This reflects the Raf-1 inhibition in gastric cancer as mentioned above (Wu et al., 2012). Secondly, in ovarian cancer, preliminary data suggests that PKGII can also inhibit EGFR by transcriptional suppression, resulting in reduced proliferation. (Xu et al., 2020). Further research is required to determine whether these inhibitory mechanisms also occur in CRC.

GUCY2C-cGMP-PKGII also promotes genomic stability. As outlined in Section 1.4.1, APC regulates DNA repair processes, replication, and proper mitosis beyond its function as a negative regulator of ß-catenin (Kouzmenko et al., 2008; Jaiswal and Narayan, 2011; Brocardo et al., 2011). Disruption of APC is therefore a key contributor to CIN in CRCs of the adenoma-carcinoma sequence (Giaretti et al., 2004). Genetic knockout of GUCY2C in wild type or $APC^{min/+}$ mice increased DNA double strand breakage and ROS (Li, Schulz, et al., 2007; Lin et al., 2012), while treatment of the GUCY2C ligand heat-stable enterotoxin (ST) reversed DNA double strand breaks, abnormal mitotic orientation, and aneuploidy induced by radiation exposure in a manner dependent on p53 (Li et al., 2017).

Additionally, GUCY2C-cGMP-PKGII plays a role in the integrity of the intestinal epithelial barrier, which allows the absorption of nutrients while preventing entry of harmful substances and pathogens. Tight junctions are protein complexes that regulate barrier transport between cells (Landy et al., 2016). Hyperpermeability and tight junction dysfunction is associated with intestinal pathologies like IBD, colitis, and CRC, and is driven by inflammatory stimuli (Yu, 2018). Genetic knockout of GUCY2C in mice increases inflammation and accelerates disease onset in colitis mice models (Lin et al., 2012; Harmel-Laws et al., 2013). Additionally, GUCY2C knockout promotes disassembly of tight junctions and increases permeability by IFNy upregulation, and these effects were linked to AKT signalling and downregulated tight junction gene expression (Han et al., 2011; Lin et al., 2012). Accordingly, treatment of CRC cells, primary cells from human biopsy, and DSS-induced colitis mice models inhibited AKT signalling, promoted antioxidant production, and increased barrier integrity (R. Wang et al., 2017). Taken together, GUCY2C-cGMP-PKGII appears to maintain intestinal barrier homeostasis by reducing inflammatory signalling, regulating tight junction complexes, and promoting the expression of antioxidant factors.

GUCY2C-cGMP-PKGII also regulates the gut microbiome. Dysbiosis is condition of altered and reduced diversity of gut flora and is associated with IBD and CRC (Yu, 2018). One of the main functions of PKGII in gut epithelium is to promote fluid secretion and regulate electrolyte concentration in the intestinal lumen by inhibiting sodium uptake by NHE3 and promoting chloride secretion by CFTR (Nikolovska et al., 2022). This is how the drugs Linaclotide and Plecanatide

work, which are guanylin mimetic GUCY2C agonists approved by the FDA for the treatment of constipation (Islam et al., 2018). By regulating mucus hydration and pH, PKGII is thought to favour commensal bacteria and inhibit pathogenic bacteria (Mann et al., 2013; Amarachintha et al., 2018). Consequently, genetic elimination of GUCY2C in mice has been shown to change microbiome composition and promote invasion of pathogenic bacteria into the inner mucus layer and enterocytes, while treatment of the GUCY2C agonist ST inhibited invasion (Mann et al., 2013; Amarachintha et al., 2018).

Another way cGMP signalling opposes tumorigenesis is by the inhibition of epithelial-mesenchymal crosstalk, a mechanism by which inflamed or neoplastic epithelial cells stimulate mesenchymal cells like fibroblasts via TGFß to proliferate and remodel the stroma in a manner conducive to tumour invasion (Choi et al., 2017). Such remodelling is called desmoplasia (Hewitt et al., 1993). In turn, the activated mesenchymal cells secrete growth factors like HGF which promote proliferation of epithelial cells, forming a positive feedback loop (Vermeulen et al., 2010; Koliaraki et al., 2017). cGMP has been shown to counteract this signalling and reduce tumour cell motility, invasion, and stromal remodelling. Underlying mechanisms include cGMP inhibition of fibroblast MMPs for remodelling (Lubbe et al., 2009), inhibition of motility organelles for invasion (Zuzga et al., 2012), stimulation of VASP to reduce cytoskeletal remodelling (Zuzga et al., 2012), and suppression of TGFß growth factor release by epithelial cells (Gibbons et al., 2013). In gastric cancer, one study showed cGMP activation of PKGII to inhibit RhoA, an oncogene linked to invasion, migration, transformation, proliferation, and survival processes (Wang et al., 2014). PKGII was found to directly interact with RhoA, resulting in phosphorylation of S188 and decreased migration of gastric cancer cells (Wang et al., 2014).

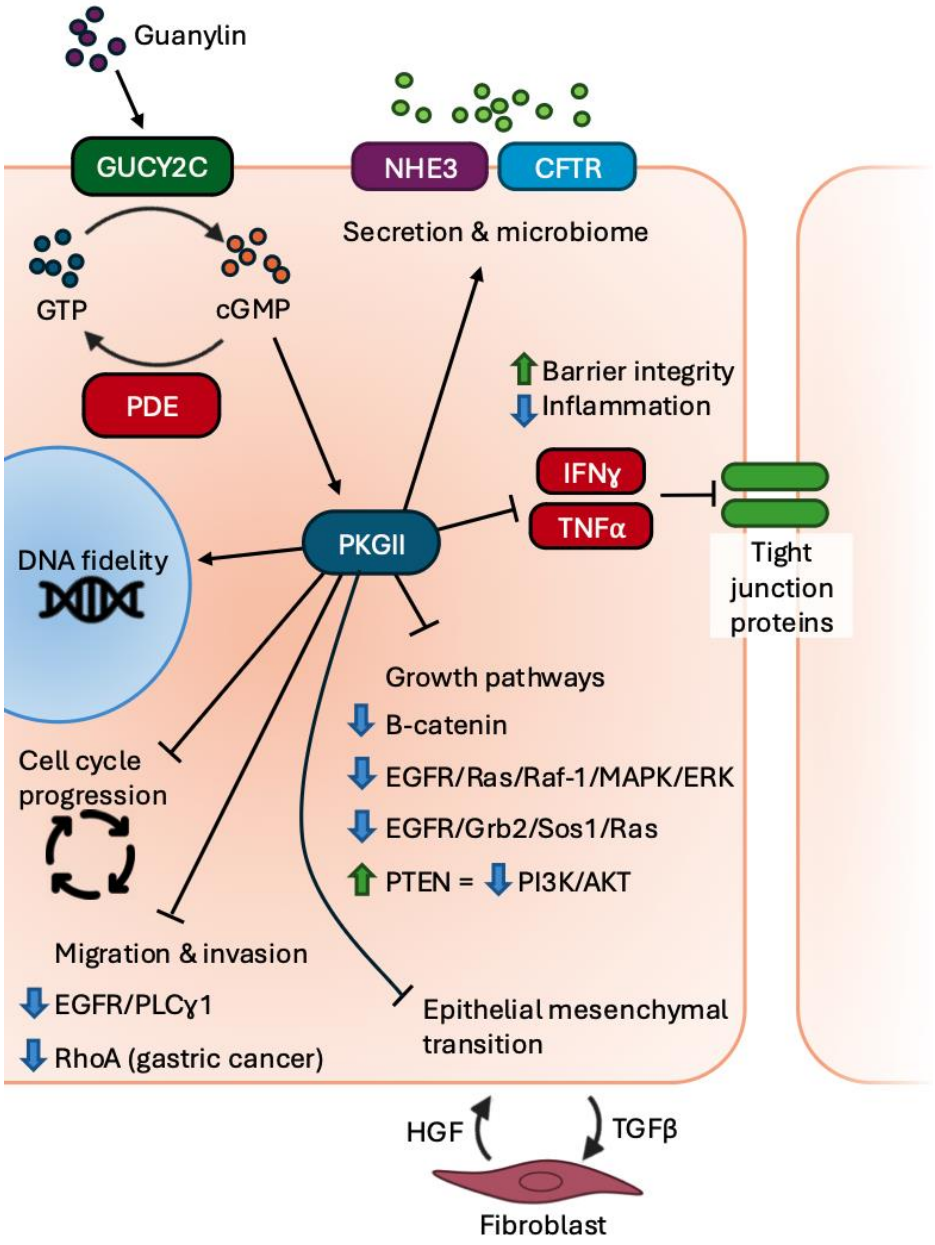

Figure 1-9. cGMP-PKG signalling homeostasis and dysfunction in colorectal cancer. cGMP-PKG regulation pathways of proliferation, genomic stability, gut barrier integrity, microbiome, and epithelial-mesenchymal crosstalk.

1.8.2.1 The paracrine hormone hypothesis and GUCY2C agonism

cGMP plays many roles in colorectal homeostasis, and since disruption of cGMP signalling is a common feature of most CRC tumours, cGMP appears to be multifaceted tumour suppressor (Rappaport and Waldman, 2020). Although the mechanism of cGMP suppression is not known, several pieces of evidence implicate loss of the GUCY2C agonist guanylin to be a driving factor. First, in a study of over 300 patients, over 85% indicated loss of uroguanylin and guanylin mRNA and protein (Wilson et al., 2014). Additionally, reduced levels of guanylin have been discovered in obese individuals and in inflamed intestinal tissue of

mice models of colitis, and this may explain why these conditions predispose for CRC (Harmel-Laws et al., 2013; Lin et al., 2016; Di Guglielmo et al., 2018). Furthermore, genetic suppression of guanylin was found to induce crypt hyperplasia in mice (Steinbrecher et al., 2002b), and guanylin administration or transgenic expression inhibited tumour formation (Shailubhai et al., 2000; Lin et al., 2016). While the mechanism underlying loss of guanylin expression observed in CRC is unknown, one study has suggested transcriptional silencing by increased Wnt/ß-catenin/TCF signalling associated with CRC (Rappaport et al., 2022). This raises the question of whether guanylin suppression in early CRC pathogenesis precedes aberrant Wnt/ß-catenin signalling, common across most CRC tumours, or whether initial Wnt/ß-catenin signalling downregulates guanylin.

In the former case, guanylin loss resulting in disruption of cGMP signalling represents the *paracrine hormone hypothesis* of CRC pathogenesis which supports the development of GUCY2C agonists and ligand mimetics for CRC treatment and chemoprevention (Pitari et al., 2007). For example, the FDA-approved anti-constipation drug Linaclotide, which is a guanylin mimetic, has undergone a phase I clinical trial, in which seven-day treatment of healthy individuals led to cGMP accumulation and reduced proliferation in epithelial cells (NCT01950403) (Weinberg et al., 2017). However, pharmacokinetic distribution to the colorectal epithelium was insufficient (Weinberg et al., 2017). Nevertheless, a phase II study of Linaclotide for the treatment of patients with stage I-III CRC is currently ongoing (NCT03796884). For these compounds, promotion of intestinal fluid secretion and subsequent diarrhoea would be a challenge in the clinic, but this side effect may be acceptable for individuals at risk for CRC tumorigenesis (Rappaport and Waldman, 2020).

1.8.2.2 cGMP elevation in colorectal cancer by guanylate cyclase agonism or inhibition of PDE5 and PDE10

In addition to GUCY2C ligands, PDE inhibition represents a promising strategy for cGMP-mediated chemoprevention of CRC. Large-scale observational case-control studies have confirmed a significant reduction of primary and secondary CRC risk in individuals treated with the PDE5 inhibitor sildenafil (Viagra) compared to untreated individuals (Huang et al., 2019; Sutton et al., 2020; Cullinane et al.,

2023). Additionally, PDE5 inhibitors have exhibited a significant reduction of CRC tumorigenesis in animal models via cGMP increase (Islam et al., 2017; Sharman et al., 2018). These reports demonstrate that PDE5 inhibitors represent a viable means for increasing cGMP and inhibiting tumorigenesis through cGMP-PKG signalling.

As opposed to prevention, PDE inhibition may not be a viable strategy for treatment of established tumours, since cGMP levels are suppressed in CRC pathogenesis (Rappaport and Waldman, 2018). As mentioned in the previous section, this may be due to loss of expression of the GUCY2C agonist guanylin, thus impairing cGMP synthesis and signalling (Pitari et al., 2007). Therefore, if cGMP synthesis is the limiting factor of this pathway, then inhibiting cGMP hydrolysis by PDEs may not result in a functionally impactful increase in cGMP. Additionally, one study demonstrated that the cGMP effector PKGII is downregulated in CRC patient tissues compared to normal tissue (Islam et al., 2022). This provides further evidence that PDE inhibition would not be viable for the treatment of established tumours, for even if cGMP levels were raised, signalling would be impaired due to loss of key cGMP effectors.

Despite this, some studies using CRC cell lines have reported that PDE5 inhibition reduces proliferation, suggesting that PDE5 inhibitors may be viable targeted therapies for established tumours, not only for chemoprevention (Thompson et al., 2000; Li et al., 2013; Mei et al., 2015). The same has been reported for PDE10 inhibition (Lee et al., 2015). However, these studies used extremely high concentrations of PDE inhibitors, and the anti-proliferative effects were found to be due to off-target mechanisms independent of cGMP elevation (Hou et al., 2022a). Regardless of PDE function, stimulating cGMP signalling does not seem to affect CRC proliferation or viability after tumorigenesis. One study found that by treatment with the reagents AOM/DSS to induce CRC, mice engineered to lack the cGMP effector PKG2 exhibited a much higher tumour multiplicity compared to wild type mice, though no difference in tumour size was found (Islam et al., 2022). This suggests that increasing cGMP would only a viable strategy for chemoprevention and not as a primary treatment for established tumours. Accordingly, preclinical development is ongoing for PDE5 inhibitors as chemopreventatives with selectivity for colorectal tissues to reduce side effects associated with systemic inhibition (A. Lee et al., 2023).

1.8.3 Phosphodiesterases in colorectal cancer

1.8.3.1 PDE2

PDE2 is a dual cAMP and cGMP specific phosphodiesterase and is the focus of growing research into cardioprotective mechanisms and potential as a therapeutic target in various central nervous system pathologies (Sadek et al., 2020; Paes et al., 2021). Research into the role of PDE2 in CRC is sparse. Some studies have shown no or negligeable protein expression in CRC cell lines NCM460, HCT116, HT29, Caco-2, SW480 or healthy colonocyte cell line FHC (Tinsley et al., 2010; N. Li et al., 2015). Furthermore, PDE2 only accounted for <12% of cGMP hydrolysis activity in HT29 cells relative to PDE3 and PDE5 (Tinsley et al., 2010). Despite this evidence of low expression, PDE2 upregulation in LS174T CRC cells has been linked to an anti-apoptotic mechanism, in which PDE2 inhibits the PKA-mediated phosphorylation of TFAM, leading to TFAM accumulation, which is implicated in suppression of apoptosis (Zhao et al., 2021a). Consequently, small molecule inhibition of PDE2 or siRNA inhibition of PDE2 or PKA inhibited proliferation in LS174T cells or mouse xenograft tumours (Zhao et al., 2021a).

1.8.3.2 PDE3

PDE3 is a dual cAMP and cGMP specific enzyme with a higher specificity for cAMP and is comprised of three isoforms: PDE3A1-3 and PDE3B1 (Murata et al., 2009). PDE3A isoforms are mainly expressed the heart, platelets, vascular smooth muscle cells, and oocytes, while PDE3B is localised to adipocytes, spermatocytes, and hepatocytes, and the PDE3 family is mainly the focus of research into cardiovascular therapeutic targets (Movsesian, 2016). PDE3 is also expressed in the colorectal tissue. Expression of the PDE3A family was found to be dominant in healthy and neoplastic colorectal biopsies compared to PDE4, PDE5, and PDE10 (Mahmood et al., 2016). Additionally, PDE3A protein was decreased in neoplastic tissue compared to healthy (Mahmood et al., 2016). Furthermore, PDE3 inhibition has been shown to decrease proliferation and motility in a number of cell lines (Murata et al., 1999; Tsukahara et al., 2013; Kangawa et al., 2017), but not the oncogenic KRAS cell line KM12C (McEwan et al., 2007). Importantly, PDE3 inhibition reduced epithelial proliferation, lesion

multiplicity, and aberrant crypt formation in mice and rat models of ulcerative colitis and CRC (Kangawa et al., 2017; Elshazly et al., 2020).

1.8.3.3 PDE4

PDE4s specifically hydrolyse cAMP and are the largest PDE family comprised of genes A-D, each with multiple isoforms (Hsien Lai et al., 2020). PDE4s play important roles in many diseases and may be the most extensively studied PDE family (Nongthombam and Haobam, 2024). PDE4s are important drug targets in COPD, psoriasis, CNS disorders, and others (Crocetti et al., 2022). Differential PDE4B and PDE4D expression are related to CRC. Several studies suggest that PDE4B expression is high in healthy tissue and early colorectal neoplasia, but lost in CRC (Mahmood et al., 2016; Pleiman et al., 2018; Bevanda et al., 2024). Paradoxically, a small study of 16 patients showed that higher PDE4B expression was associated with increased risk of tumour recurrence (Tsunoda et al., 2012). Research on PDE4D is sparse, but two studies have shown that PDE4D is downregulated in CRC and that lower PDE4D is linked to worse overall survival in patients (Chen et al., 2018; Bevanda et al., 2024). There is little information about PDE4A and PDE4C in CRC, and PDE4C is generally the most understudied subfamily of PDE4 (Wright et al., 2023).

Contrasting to the observed downregulation of PDE4B and PDE4D in CRC, almost all studies indicate that PDE4 inhibition counters tumorigenesis. One phase II clinical trial showed that the PDE4-specific inhibitor apremilast improved clinical and endoscopic parameters in ulcerative colitis patients (NCT02289417) (Danese et al., 2020). Supporting this, the use of roflumilast or piclamilast in rat models of ulcerative colitis or CRC in three studies indicated a reduction in lesion multiplicity, aberrant crypt formation and epithelial proliferation (El-Ashmawy et al., 2018; Saeedan et al., 2020; Abdel-Wahab et al., 2021). These results were also reflected in cell line mice xenograft models, in which tumour growth was reduced by inhibition of PDE4B (Nishi et al., 2017) or PDE4D (Cao et al., 2016). However, observations from one animal study opposed these findings, in which knock-out of PDE4B in $APC^{min/+}$ mice models of CRC showed an increase in lesion multiplicity (Pleiman et al., 2018).

Cell line studies also support the anti-cancer effect of PDE4 inhibition in CRC. One study showed that a combination of the AC-activator forskolin in combination with PDE4 inhibitor Rolipram inhibited growth in the oncogenic KRAS cell line KM12C as well as seven others in a panel of eleven CRC cell lines (McEwan et al., 2007). Rolipram was also shown to raise cAMP and inhibit motility in DLD-1 cells (Murata et al., 2000).

Furthermore, some cell line studies indicate anti-cancer effects related to inhibition of PDE4B specifically. Rolipram and Apremilast were shown to induce apoptosis, luminal formation, and structural regulation in 3D cell models of colonic crypts via inhibition of PDE4B (Tsunoda et al., 2012; Nishi et al., 2017). Similarly, forskolin in combination with roflumilast or rolipram reduced growth of HCT-116 and KM12C cells and was linked to inhibition of PDE4B (Kim, Kwak, et al., 2019).

Anti-cancer effects in cell lines have also been linked to PDE4D by the use of Roflumilast or Rolipram (Miklos et al., 2016; Kim, Nam, et al., 2019), miRNA (Cao et al., 2016), or the PDE4D specific inhibitor GEBR-7b (Nummela et al., 2024). Contrary to this, one study found that miRNA-mediated PDE4D inhibition reduced proliferation, migration, and invasion in two CRC cell lines (Chen et al., 2018).

Overall, PDE4 inhibition represents a promising therapeutic strategy for CRC, and further research in larger scale human CRC cohorts or in the use of PDE-isoform specific inhibitors is warranted.

1.8.3.4 PDE5/10 inhibition

PDE5 specifically hydrolyses cGMP and is well-known for its role in smooth muscle relaxation, making it an important target in the treatment of erectile dysfunction and pulmonary hypertension (Liu et al., 2023). In contrast, PDE10 degrades both cyclic AMP and cGMP, playing a crucial role in regulating dopaminergic signalling in the brain (Zagórska, 2020).

As mentioned above (Section 1.8.2.2), increasing cGMP by PDE5 and PDE10 inhibition has been shown to not affect CRC cell line proliferation (Hou et al.,

2022a), and that PDE5 and PDE10 inhibition may not be a viable strategy for established tumours (Islam et al., 2022). Despite this, increased expression of these proteins has been found in CRC cell lines and in patient tumour tissues compared to normal cells and tissues by western blot, RT-qPCR, and IHC (Tinsley et al., 2010; N. Li et al., 2015; Lee et al., 2015; Mahmood et al., 2016). While cGMP is known to be attenuated in CRC by its synthesis (Pitari et al., 2007; Rappaport and Waldman, 2018), the increased expression of these PDE families may also contribute to cGMP downregulation.

1.8.3.5 PDE6

Phosphodiesterase 6 (PDE6) is well-studied in photoreceptor cells where it plays a crucial role in the visual phototransduction pathway (Cote, 2021). Some studies have identified PDE6 mRNA expression in non-photoreceptive cells and tissues, yet protein expression and functional importance is poorly characterised (Cote, 2021). Research into the role of PDE6 in CRC is even more limited, but a recent siRNA screening study identified the PDE6 regulatory subunit PDE6ɣ' and its gene PDE6H to negatively regulate nucleotide metabolism and cell cycle progression in HCT116 CRC cells (Yalaz et al., 2024). Subsequently, PDE6H genetic knockout or siRNA inhibition suppressed proliferation of HCT116 cells and tumour growth of HCT116 mouse xenografts, and this effect was linked to increased cGMP levels and inhibition of mTOR (Yalaz et al., 2024). Interestingly, alterations in PKG were not detected, and the authors speculated that the growth arrest mechanism may be mediated by local PKG modulation or PKG-independent pathways (Yalaz et al., 2024).

1.8.3.6 PDE8

PDE8 is a cAMP-specific phosphodiesterase family with the highest affinity for cAMP out of all PDEs (Fisher et al., 1998). The PDE8 family originates from two genes PDE8A and PDE8B, accounting for over nine splice variants (Wang et al., 2001; Gamanuma et al., 2003). PDE8 is found in various tissues throughout the body, with particularly high expression in the adrenal glands, thyroid, testis, brain, and immune cells, and is being researched for immune-related diseases, inflammatory diseases, endocrine disorders, and CNS diseases (Tsai and Beavo, 2012; Epstein et al., 2021; Qiu et al., 2024).

PDE8A has a prominent role in oncogenic RAS mutated cancers, in which it interacts with c-Raf to prevent inhibition via phosphorylation by PKA (Brown et al., 2013). Disruption of the interaction has been shown to inhibit MAPK-driven growth in HeLa and pancreatic ductal adenocarcinoma cell lines (Brown et al., 2013; Cooke et al., 2024) as well as melanoma cell lines and mouse xenograft tumours (Blair et al., 2019). Similar growth inhibition was observed in HCT116 CRC cells by PDE8A-cRAF disruption by the scaffold protein 14-3-3ζ (Mukherjee et al., 2024).

Additionally, CRC-specific expression of a novel fusion transcript of PDE8A with AKAP13 was identified from cell lines and patient tissues (Nome et al., 2013), but follow up studies are required to determine functional importance and potential as a biomarker. Gene fusions have been an effective target in cancers including CRC, one example being TRK gene fusion as an indicator of MSI-H and TRK inhibitor response (H. Wang et al., 2022).

1.8.3.7 PDE9

PDE9A selectively hydrolyses cGMP with exceptionally high affinity and is expressed in various tissues, where it plays roles in neurological function, platelet aggregation, regulation of vascular smooth muscle tone, cell proliferation, apoptosis, and myocardial contractility (Soderling et al., 1998; Zheng and Zhou, 2023). Research on PDE9A in CRC is limited, but one study employed extensive database mining to characterise a distinct downregulation of PDE9A mRNA in CRC cells and tissue relative to healthy samples (Susmi et al., 2021). Furthermore, this expression pattern was linked to increased PDE9A promotor methylation, and lower PDE9A was associated with worse overall survival, progression free survival, and disease-specific survival in patients. These findings were derived by computational methods alone, and *in vitro* / *in vivo* validation is required. The observation that PDE9A appears protective in CRC is paradoxical given the tumour-suppressive role of cGMP, and valuable insight may be gained by overexpression studies of PDE9A in CRC cell lines or primary cells.

1.8.3.8 PDE11

PDE11 is a phosphodiesterase with dual specificity for cAMP and cGMP, and is highly expressed in many tissues including the prostate, liver, and adrenal gland (Kong et al., 2022). In cancer, inactivating germline mutations of PDE11A have been linked to a higher risk of adrenal hyperplasia and tumours (Pinto et al., 2020), while deleterious overexpression of PDE11A has been linked to glioblastoma (H. Lee et al., 2022). There is limited research into PDE11A and CRC, but high protein expression has been found in human colon epithelial cells, submucosal macrophages, colonic smooth muscle cells, as well as colon carcinoma tissue (D'Andrea et al., 2005).

From the above text, it is apparent that there are many links between PDEs and CRC though some associations are more tenuous than others and require further investigation.

1.9 Omics approaches for exploring PDEs in colorectal cancer

As described above, the function of cGMP signalling, PDE5, and PDE10 are well characterised in CRC, but the role of cAMP signalling and the other PDE genes remains unexplored. RNA sequencing (RNA-seq) is a powerful technique for comprehensive analysis of gene expression, and due to its sensitivity and broad scope, it is well suited for detecting subtle and complex alterations across the whole PDE family or cyclic nucleotide pathways in CRC (Hrdlickova et al., 2017). In addition, a wealth of datasets from RNA-seq and other platforms, generated by many omics studies, have been stored in freely accessible repositories such as The Cancer Genome Atlas (TCGA) and The Human Protein Atlas (THPA) (Uhlen et al., 2010; Weinstein et al., 2013). By leveraging these resources using high-level biostatistical analysis, this project aimed to gain unprecedented insight into PDE and cyclic nucleotide function in CRC, with the goal of informing prognostic and therapeutic development.

1.10 Aims

CRC is a prevalent and heterogeneous disease and is the second most deadly cancer worldwide. Advances in the understanding of pathogenesis and in the

development of novel chemotherapies and targeted therapies have revolutionised treatment and patient outcomes. However, several key challenges persist which hinder late-stage treatment, reduction in mortality, and the development of curative therapies: namely the difficulty in diagnosing early-stage CRC, and poor late-stage CRC patient outcomes stemming from inadequate response rates, disease heterogeneity, and resistance to treatment.

cAMP and cGMP are key second messengers of intracellular signalling and control many processes relating to cancer. While cGMP has defined anti-cancer functions in CRC, the role of cAMP is less clear. Nevertheless, cAMP and cGMP modulation by adenylate cyclase and guanylate cyclase agonists or phosphodiesterase inhibitors represents a promising strategy for chemoprevention of CRC. This is highlighted most by the advances in PDE5 inhibition, as well as the growing body of research into PDE4 inhibition. Beyond these PDE families, research is sparse and the roles of PDEs as biomarkers or drug targets in CRC remain underexplored. In light of this, this project had the following aims:

Chapter 1

1. To use RNA-Sequencing and database mining strategies for the identification of differentially expressed PDEs linked to CRC and CRC subtypes.

2. Investigate gene set enrichment of cAMP and cGMP signalling pathways using RNA-seq data.

3. Validate PDE expression patterns in CRC by RT-qPCR and western blotting of patient tissue samples.

Chapter 2

1. Validate differentially expressed PDEs in CRC within the epithelial cell population using scRNA-seq

2. Explore differential PDE expression between MSS and MSI-H CRC cells.

Chapter 2 Methods

2.1 PDE expression analysis between colorectal cancer and normal tissues

2.1.1 TCGA RNA-seq differential expression analysis

TCGA is a large-scale research programme launched by the National Cancer Institute (NCI) and the National Human Genome Research Institute which collects and integrates genomic, transcriptomic, epigenomic, and proteomic data with the aim of advancing cancer research (Weinstein et al., 2013). The vast datasets provided by the TCGA repository are an invaluable resource for researchers across the world. TCGA offers data from cancer and matched normal tissue from over 450 colon cancer patients (COAD cohort) and 160 rectal cancer patients (READ cohort).

Clinical and RNA-seq gene expression data of cancer and matched normal tissues from 445 colon cancer patients and 157 rectal cancer patients were downloaded from TCGA using TCGAbiolinks package (2.30.4) in R. The RNA-seq data was generated previously by TCGA using the following pipeline: FastQC and Picard Tools were used for quality assessment, and STAR was used to align reads to the GRCh38 reference genome and generate counts (National Cancer Institute, 2024). This dataset was downloaded at the raw count level. Differential expression analysis was conducted using DESeq2 (1.42.1). Differential expression was determined between cancer and normal samples, patient sex, cancer stage, and tumour location. DESeq2 quantified differential expression and tested for statistical significance by the following steps. First, the raw counts of each sample were normalised by sequencing depth to ensure that differences in gene expression were not due to one sample being sequenced with a larger input of mRNA. Next, the dispersion of each gene was estimated and used to fit a negative binomial distribution to the normalised count data. Finally, a general linear model and a Wald test were used to determine significance. Significant genes were defined as $p < 0.05$ and $|\log2FoldChange| > 1$.

2.1.2 TCGA differential methylation of PDE promotors

Using TCGAbiolinks package (2.30.4) in R, patient clinical data and Illumina Human Methylation 450 array beta values from 393 CRC patients were downloaded. This data was prepared previously by TCGA by conducting quality control and beta value conversion on raw methylation array data using the Surface Epitope Subtraction Analysis of Methylation framework (SeSAMe) (Zhou et al., 2018). Once downloaded, several quality control steps were conducted on the methylation probes. Firstly, only probes containing expression values across all samples were retained so the analysis was not influenced by missing values. Secondly, probes overlapping with single nucleotide polymorphisms (SNPs) were removed so that potential genetic confounding effects or genotype dependent binding were excluded. SNP annotation was provided by the IlluminaHumanMethylation450kanno.ilmn12.hg19 R package (0.6.1). Lastly, probes known to map to multiple sites were removed based on annotations listed online by Dr Hamid Ghaedi at Queens University Belfast, Northern Ireland (Ghaedi, 2024). Next, probes were mapped to the promotor sites on PDE genes. First, PDE gene start sites were obtained using the Ensembl genome browser (Fernández and Birney, 2010). Next, promotor regions were estimated to be within 2 kb upstream of the start sites, and probes mapping to these regions were identified using the intersect function from the command line suite BedTools (2.31.1) (Quinlan and Hall, 2010). Methylation beta values of the promotor probes were transformed into M values to reduce heteroscedasticity for statistical modelling (Du et al., 2010) by following formula:

$$m = log_2(\frac{\beta}{1-\beta})$$

The R package Limma (3.58.1) was used for differential statistics (Ritchie et al., 2015). Limma tests for significance by linear modelling in addition to empirical Bayes moderation to improve the estimation of gene-wise variance Ritchie et al., 2015). Limma is a conventional tool for analysing continuous data like methylation M values (Maksimovic et al., 2016). To visualise the differential methylation, beta values were used to generate density plots between cancer and normal tissues. For patient-matched cancer and normal samples, paired line plots were prepared to show changes in PDE promotor methylation at the

individual level. To investigate whether promotor methylation was linked to gene expression, Spearman correlation with Benjamini-Hochberg correction was performed between the methylation M values and RNA-seq counts normalised by DESeq2.

2.1.3 Pathway analysis

Pathway analysis using Gene Set Enrichment Analysis (GSEA) (4.3.2) and Pathview (1.42.0) was conducted for the cAMP signalling pathway (hsa04024) and the cGMP-PKG signalling pathway (hsa04022). The pathway gene sets were downloaded and extracted using the KEGGREST package (1.42.0) and were exported to GSEA in .gmt file format. Differentially expressed genes identified by DESeq2 were pre-ranked by a signed score metric (log2FoldChange * (-log10(p_value))), allowing genes to be ranked by log2FoldChange and significance. Gene set enrichment was performed using GSEA, and differentially expressed genes across the cAMP and cGMP-PKG pathways were visualised using Pathview.

2.1.4 THPA protein expression by immunohistochemistry and survival analysis

THPA is a research initiative conducted by Swedish institutions with the goal of mapping all human proteins across cells, tissues, and organs using a variety of omics technologies (Uhlen et al., 2010). Similar to TCGA, THPA provides a vast resource that has greatly facilitated research in human biology and disease. In particular, THPA offers RNA-seq and IHC data obtained from cancer patient tissues at the Department of Pathology, Uppsala University Hospital, Uppsala, Sweden. Additionally, THPA also provides Kaplan Meier survival analysis of gene expression data for 597 CRC TCGA patients.

To assess PDE expression at the protein level between CRC and normal tissues, immunohistochemistry (IHC) data was obtained from THPA. IHC images on the database were prepared from tissue microarrays with 1 mm cores of surgical specimens of cancer and adjacent normal tissue fixed with formalin and embedded in paraffin (FFPE). Tissue slides were stained with 3,3'-diaminobenzidine-conjugated antibodies (DAB) and counterstained using haematoxylin. Antibody specificity was verified by THPA by antigen microarray,

similar to the peptide array platform used in this project (see methods described in Chapter 7), or by western blot of lysates from human tissue or cell lines, providing a high level of confidence (O'Hurley et al., 2014). To assess PDE expression in this project, representative images from each group were selected, and figures of the full slide and a magnified section were prepared.

Similarly, Kaplan-Meier survival data were obtained from THPA. Survival analysis was conducted by THPA on gene expression and outcome data from COADREAD patients from TCGA. Stratification of samples into low and high expression groups was decided by an expression value set for the maximisation of p value as determined using a log rank test. In this way, stratification was performed to produce the biggest difference in survival between the groups.

2.1.5 PDE protein expression from the Clinical Proteomic Tumour Analysis Consortium

The Clinical Proteomic Tumour Analysis Consortium (CPTAC) was launched by the NCI to enhance understanding of cancer at the molecular level (Edwards et al., 2015). This national initiative focuses on large-scale proteomic and genomic analysis, to uncover the complex biological mechanisms driving cancer. The CPTAC offers a protein expression dataset of 97 CRC tumour and 100 normal tissue samples of mass-spectrometry-based proteomic data.

To further characterise PDE protein expression, colon cancer proteomic data was obtained from CPTAC using the University of Alabama at Birmingham Cancer (UALCAN) data analysis portal (Chandrashekar et al., 2017; Chandrashekar et al., 2022).

2.1.6 Tissue collection

Colorectal tumour and normal adjacent matched tissue samples were derived from surplus resection tissue from 10 patients undergoing surgery with curative intent within the NHS Greater Glasgow and Clyde health board through the Glasgow Biorepository. Samples were labelled with a unique identifier, immediately snap frozen, and stored at –80 °C.

2.1.7 RNA extraction

Total RNA was extracted from the snap-frozen tissue samples using the Qiagen RNeasy Mini Kit (Qiagen, Hilden, Germany) according to the manufacturer's instructions. Briefly, approximately 30 mg of tissue was homogenised in 600 µL RLT lysis buffer containing 1% v/v ß-mercaptoethanol to protect the RNA from degradation by RNases. The tissue was homogenised using a Tissue Homogeniser (TH) (Omni International) at full power for approximately 6-8 pulses of 2 s or until complete tissue disruption was achieved. The lysates were then centrifuged at 13,000 rpm for 5 minutes, and one volume of 70% ethanol was added to the supernatant. 700 µL of this mixture was added to a RNeasy column and centrifuged for 30 s at 10,000 rpm. On column DNase digestion was performed according to the Qiagen RNeasy Mini Kit protocol. 350 µL of buffer RW1 was added to the column, followed by centrifugation for 30 s at 10,000 rpm. DNase I incubation mix was prepared by diluting 10 µL of DNase I stock solution with 70 µL buffer RDD, and all 80 µL was added to the column and incubated at room temperature for 20 minutes. 350 µL of buffer RW1 was added to the column, followed by centrifugation for 30 s at 10,000 rpm. After DNase treatment, the column was washed with 500 µL of Buffer RPE and centrifuged for 30 s at 10,000 rpm. This washing step was repeated with an additional 500 µL of Buffer RPE and centrifugation at 10,000 rpm was extended to 2 minutes. The column was then centrifuged at 13,000 rpm for 5 minutes then left to air dry for 20 minutes at room temperature. For elution, 20 µL of nuclease-free water was added to the column and centrifuged for 5 minutes at 13,000 rpm. Elution was performed again with a second volume of 20 µL nuclease-free water to maximise yield. The RNA concentration was determined using a Nanodrop Spectrophotometer (Thermo Scientific). The purity of the RNA was assessed by measuring both the A260/A280 and A260/A230 absorbance ratios. An A260/A280 ratio close to 2.0 was used to confirm protein-free RNA, while an A260/A230 ratio between 2.0 and 2.2 was used to ensure minimal contamination from organic compounds introduced during RNA extraction. Only RNA samples meeting these criteria were selected for further analysis.

2.1.8 Reverse Transcription

A second round of DNase digestion was performed to ensure removal of chromosomal DNA before RT-qPCR using the DNA-free DNA removal kit (Qiagen) according to the manufacturer's instructions. Briefly, rDNase I enzyme and DNAase buffer were added to the RNA according to the RNA concentration and incubated for 30 minutes at 37 ºC. 0.1 volume of DNase inactivation reagent was added and incubated for 2 minutes with regular agitation. The sample was centrifuged at 13,000 rpm for 5 minutes and the supernatant was used for reverse transcription. Reverse transcription was performed using the Applied Biosystems High-Capacity cDNA Reverse Transcription Kit (Thermo Fisher Scientific) according to the manufacturer's protocol. 10 µL of 2X reverse transcription master mix was prepared by combining 2 µL of 10X RT Buffer, 0.8 µL of 25X dNTP Mix (100 mM), 2 µL of 10X RT Random Primers, 1 µL of MultiScribe Reverse Transcriptase, and 4.2 µL of nuclease-free H_2O. This was added to 10 µL of DNase treated RNA. The thermocycler protocol consisted of an initial incubation at 25°C for 10 minutes, followed by reverse transcription at 37°C for 2 h, and heat inactivation at 85°C for 5 minutes.

2.1.9 Quantitative Real-Time PCR (RT-qPCR)

RT-qPCR was performed using the Power SYBR Green PCR Master Mix (Invitrogen) according to the manufacturer's instructions. Applied Biosystems MicroAmp Fast Optical 96 well qPCR plates (Thermo Fisher Scientific) were used. 5 µL of SYBR green master mix from the kit was added to each well of the plate. A cDNA solution was prepared by adding 1.4 µL nuclease free water, 3 µL cDNA, and 0.6 µL of 5µM dual primer stock (for a working concentration of 300 nM) for well and added to the plate containing the SYBR green master mix for a total volume of 10 µL. RT-qPCR was then performed on an Applied Biosystems 7500 Fast RT-qPCR machine (Thermo Fisher Scientific). The temperature cycling protocol consisted of an initial denaturation step at 95 ºC for 10 minutes followed by 40 cycles between 60 ºC for 30 s and 90 ºC for 30 s. Finally, a melt curve was included to check for a single specific amplicon by increasing the temperature from 60 to 90 ºC at a rate of 1.5 ºC/minute. PDE gene expression was determined relative to both GAPDH and 18S rRNA using the comparative Ct method (Schmittgen and Livak, 2008). The primers used are listed below (Eurofins Genomics).

Table 4: PDE primers
PDE primers used to detect gene expression in patient tissue samples are listed. Bracketed numbers indicate alternative primer combinations that were used if the previous primer pair were unsuccessful.

Gene Primer	Sequence (5' to 3')
PDE3A forward	GGTTTGAGAGGGTGCTTGTG
PDE3A forward	TGGAGGAGGGCATTTGGAAT
PDE4D reverse	TTCTTCAAGCAGCCTCCCTT
PDE4D reverse	TCCACATCAAAACAAACTGCCT
PDE5A forward	CCCGAAGCCTGAGGAATTGA
PDE5A forward	CTCCTCGACCATCACTGCC
PDE6A reverse	TGAATGGGAAGGATGTGGTG
PDE6A reverse	CGATGTCCGTAAGTTCTTCAAAG
PDE6A (2) forward	GCCATGTCGCACACTCTAAG
PDE6A (2) forward	TTCATCTCTCTTGGTGAAGTGG
PDE9A forward	TAGTAAGGAGTCATGGGCGTC
PDE9A forward	AGCACGCTCTGGATTAATTCT
PDE9A (2) reverse	ATGACCAACTGCCCCTGTAA
PDE9A (2) reverse	GGAGTCAACTTCTTGTGGTTATC
PDE9A (3) forward	GTCCCACCAGCACTCCGTA
PDE9A (3) forward	AGCACGCTCTGGATTAATTCTTC

2.1.10 Protein extraction and western blot

To extract protein from the patient tissue samples, 30-50 mg of tissue was homogenised in 700 µL Pierce lysis buffer (Tris-HCl (25 mM), pH 7.4, NaCl (150 mM), EDTA (1 mM), NP-40 (1% v/v), glycerol (5% v/v) at 4 ºC with protease inhibitor (Complete Protease Inhibitor Cocktail, Roche). The tissue was homogenised using a Tissue Homogeniser (TH) (Omni International) at full power for approximately 6-8 pulses of 2 s or until complete tissue disruption was achieved. The lysates were then centrifuged at 13,000 rpm for 5 minutes. Bradford assay and western blot were performed as described later (Section 7.7.1, Section 7.7.4). The antibodies used are listed in Table 5.

Table 5: Primary and secondary antibodies used for western blotting.
WB; western blot.

Antibody	Dilution	Company	Catalogue Number
α-PDE3 (rabbit polyclonal)	WB: 1:1000	Custom antibody, Baillie Lab, University of Glasgow	NA
α-PDE4D (goat polyclonal)	WB: 1:1000	Custom antibody, Baillie Lab, University of Glasgow	NA
α-PDE4D9 (Rabbit polyclonal)	WB: 1:1000	ImmunoKontact	IKS-LY-090923-4
α-PDE6A (mouse monoclonal)	WB: 1:2000	Proteintech	67832-1-Ig
α-PDE9A (rabbit polyclonal)	WB: 1:1000	Proteintech	12648-1-AP
α-GAPDH (mouse monoclonal)	WB: 1:80,000	Proteintech	60004-1-Ig
α-rabbit IgG (donkey, 800 nm)	WB: 1:5000	Licor	926-32213
α-mouse IgG (donkey, 800 nm)	WB: 1:5000	Licor	926-32212
α-sheep IgG (donkey, 594 nm)	WB: 1:5000	Invitrogen	A-11016

2.2 Single cell RNA-seq PDE expression in colorectal cancer

2.2.1 Data Acquisition

A scRNA-seq dataset (GSE200997) published on the Gene Expression Omnibus database (Edgar et al., 2002) was identified, consisting of sequenced cells from 16 CRC patients who underwent curative colon tumour resection at Rush University Medical Center (Chicago, IL, USA). Of these patients, nine were Caucasian, six African American, and one Asian. The protocol of single cell capture and sequencing from these authors is summarised as follows. From each patient, single cells were captured from tumour tissue alongside normal matched tissue from seven of the patients using the 10X Genomics Single Cell 5' Platform. Following library preparation, sequencing was conducted using the Illumina NextSeq 550, and reads were aligned and counted using Cell Ranger (3.1.0) with the hg38 reference assembly. For this project, the raw count matrix and cell annotation files were manually downloaded from GEO and was comprised of 49,860 total cells.

2.2.2 Quality Control

The single cell data was processed using a standard workflow in Seurat (5.1.0) and R (4.3.2) (Chen et al., 2019). A Seurat object was created from the downloaded raw count matrix and cell annotation files. 'Cells' expressing less than 200 or more than 2500 genes were filtered out to remove empty droplets or multiplets. Additionally, cells expressing a proportion of >5% mitochondrial genes were filtered out, as that was an indication of stress or poor viability. Lastly, low signal genes expressed in fewer than three cells were removed. This filtered the dataset from 49,860 to 26,212 cells.

After quality control, counts were normalised by cell sequencing depth. Highly variable genes were identified, the gene expression was scaled, and principal component analysis (PCA) was used to reduce the dimensionality of the data. An elbow plot was generated, and the first 20 principal components were found to capture most of the variation in gene expression.

In single-cell RNA-Seq, multiple cells can be captured at once, resulting in anomalous results. DoubletFinder (2.0.4) was used to remove doublets. First, the optimal pK value, a parameter for doublet detection rate, was found by performing a parameter sweep over principal components. Next, the homotypic doublet rate was estimated from the cluster number annotations and was used to adjust an initial assumed doublet formation rate of 7.5%. Doublets were then identified and removed using the first 20 principal components, the optimised pK value, and the adjusted doublet rate estimate.

2.2.3 Clustering of major cell types

With the filtered cells, the first 20 principal components were used with the Seurat *FindNeighbours* function to generate a shared nearest neighbours (SNN) graph of the cells. The SNN graph was partitioned into clusters using the Seurat *FindClusters* function based on the Louvain algorithm. Granularity of clustering was set by a resolution of 0.1. To estimate the cell types of each cluster, t-SNE dimensionality reduction was used to visualise marker gene expression for epithelial cells (*KRT8, KRT18,* and *EPCAM*), fibroblasts (*THY1*), endothelial cells (*PECAM1*), T cells (*CD3D*), B cells (*CD79A*), and myeloid cells (*LYZ*).

2.2.4 Differential expression analysis

Differential expression between epithelial cells originating from cancer and normal samples was determined at the single cell level using the Seurat FindMarkers function, which is based on the Wilcoxon Rank Sum test (Satija et al., 2015). Differential expressed genes were defined by p.adj < 0.05 and |log2FC| > 1. For visualisation, dimensionality reduction by t-SNE was performed on the epithelial cell subset, and plots were generated using the FeaturePlot_scCustom function from the scCustomize package. Differential expression of epithelial cells stratified by microsatellite instability status was also carried out using the FindMarkers function. Genes were not filtered by log2FC so that small changes in PDE expression could also be shown.

To perform differential expression on the pseudobulk scale, epithelial cells were combined by patient and tissue type using the Seurat AggregateExpression function. Differential expression was determined using DESeq2 (1.42.1) between

Cancer and Normal groups. PDE genes and the markers *CA2*, *CST1*, and *LYZ* were extracted, and Benjamini-Hochberg adjusted p values were calculated for this subset.

2.2.5 Pathway analysis

Pathway analysis using GSEA (desktop application, 4.3.2) and Pathview (1.42.0) was conducted for the cAMP signalling pathway (hsa04024) and the cGMP-PKG Signalling pathway (hsa04022). The pathway gene sets were downloaded and extracted using the KEGGREST package (1.42.0) and were exported to GSEA in .gmt file format. Single cell level differentially expressed genes from the FindMarkers function were preranked by a signed score metric (log2FoldChange * (-log10(p_value))), accounting for both log2FoldChange and p_value. Gene set enrichment was performed using GSEA, and differential gene expression across the cAMP and cGMP-PKG pathways were visualised using Pathview.

Chapter 3 PDE expression analysis between colorectal cancer and normal tissues

3.1 Introduction

In colorectal cancer, patient outcomes have been greatly improved by advancements in chemotherapy and targeted therapeutics, but treatment is ineffective for some, and prediction of patient response remains a significant challenge (Xie et al., 2020; Gmeiner, 2024). Furthermore, the link between patient response and the complex heterogenous subtypes of CRC is largely unclear (Xie et al., 2020). Dysregulation of cAMP, cGMP, and PDEs are features of many diseases, and PDE inhibitors and other cAMP/cGMP modulators have been greatly successful as licensed drugs (Baillie et al., 2019). In CRC, no such compounds have reached the clinic (Mehta and Patel, 2019). However, cGMP has been identified as a tumour suppressor of CRC, and PDE5 inhibitors are undergoing preclinical development (A. Lee et al., 2023; Ramesh et al., 2023). Nonetheless, the role of cAMP in CRC is not well characterised, and the expression and function of the other PDE genes are largely unexplored. By delineating PDE expression in CRC, expression patterns could be found that inform pathologic understanding, subtype prognosis, and therapeutic development. This chapter describes the leveraging of publicly accessible repositories The Cancer Genome Atlas (TCGA), The Human Protein Atlas (THPA), and the Clinical Proteomic Tumour Analysis Consortium (CPTAC) to investigate PDE expression and function in CRC.

As follows, datasets from these repositories were leveraged to achieve the following aims:

1. To analyse TCGA colon cancer and rectal cancer cohorts separately to identify differentially expressed PDEs between cancer and normal samples, cancer grades, males and females, and tumour location.

2. To compare the PDE expression profile between colon and rectal cancers.

3. To analyse TCGA methylation array data to identify differentially methylated PDE gene promotors in cancer and relate methylation to gene expression level.

4. To explore whether the cAMP and cGMP pathways are enriched or depleted in CRC and normal tissue using gene set enrichment analysis (GSEA).

5. For the main differentially expressed PDE genes identified from TCGA RNA-seq data, to determine whether the differential mRNA expression translates to protein expression by analysing THPA IHC and CPTAC proteomic datasets.

6. To survey THPA survival analysis data to see if any PDEs are linked to CRC patient outcomes.

Additionally, since these aims all involved computational analysis of omics resources and databases, validation was performed on patient tumour and normal-matched tissues provided by Dr Kathryn Pennel and Professor Joanne Edwards as part of a collaboration within the University of Glasgow. Using these samples, this project had the additional aim:

7. To validate differential expression of PDEs found by the above computational methods by RT-qPCR and western blot on patient-matched tumour and normal tissues.

3.2 Results

3.2.1 TCGA RNA-Seq differential expression analysis

3.2.1.1 Differentially expressed PDE genes in colon cancer

Transcriptomic data from TCGA were analysed, beginning with the colon cancer dataset (TCGA COAD) consisting of 445 patients, 445 cancer samples, and 42 matched normal samples. After data acquisition and pre-processing, 14,200 genes were significantly differentially expressed, with 10,187 upregulated genes and 4,013 downregulated genes (Figure 3-1). There was a stark difference in expression profile between normal and colon cancer samples, reflected by clear clustering into sample groups (Figure 3-1:A). Of the differentially expressed genes, the majority of PDEs genes were downregulated, with only PDE7A and PDE10A upregulated (Figure 3-1:B)

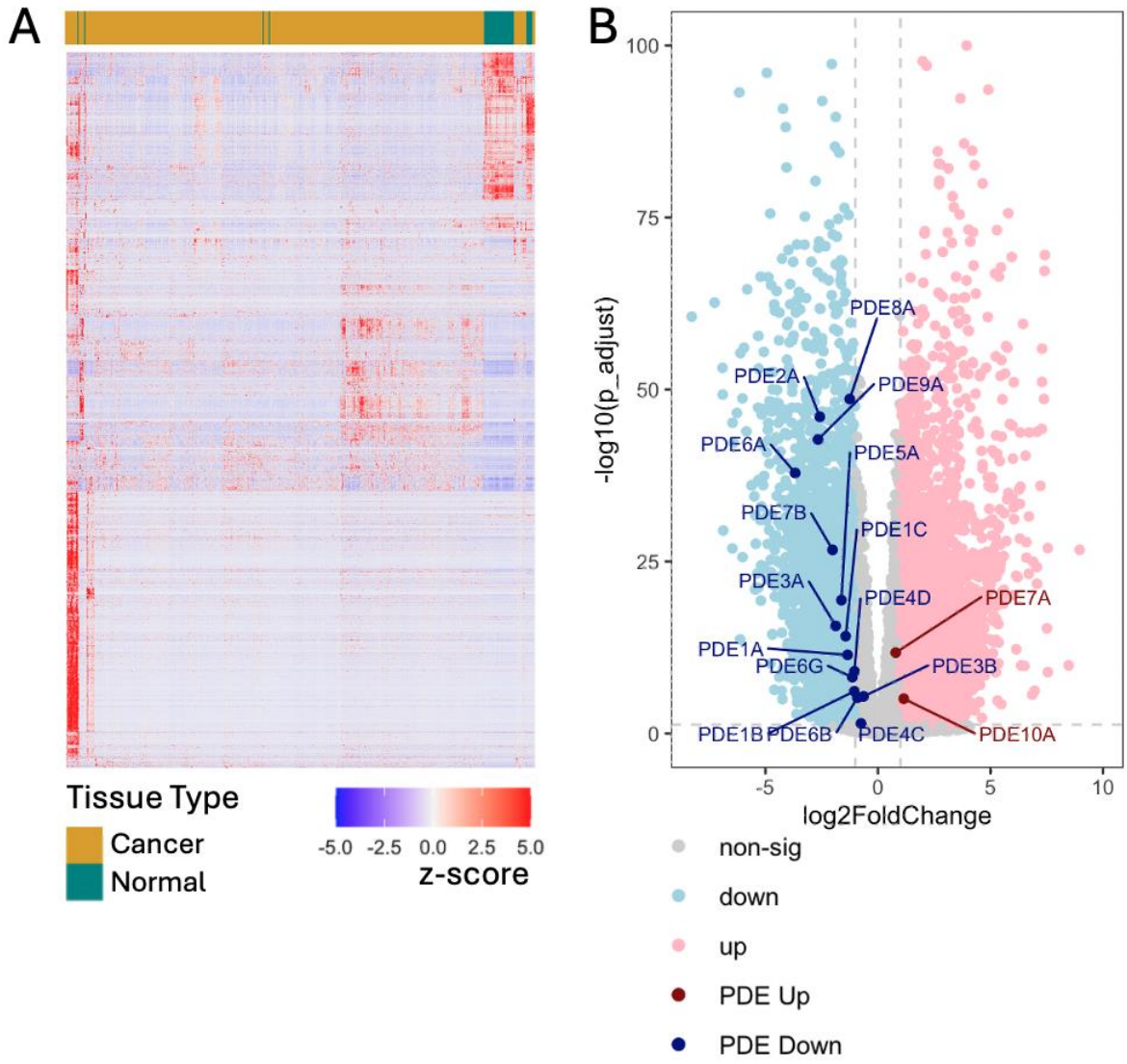

Figure 3-1: Differential expression between cancer and normal tissues in The Cancer Genome Atlas colon cancer dataset (COAD).
A total of 14,200 differentially expressed genes were identified by DESeq2, of which 10,187 were significantly upregulated and 4,013 were significantly downregulated. A: A clustered heatmap of differentially expressed genes. Expression from low (blue) to high (red) shown as z-score scaled DESeq2 normalised counts. B: Volcano plot of differentially expressed genes with significant phosphodiesterase (PDE) genes highlighted. Cancer n=445, normal n=42.

When expression of each PDE gene was viewed individually, significant downregulation was found for PDE1A, PDE1B, PDE1C, PDE2A, PDE3A, PDE3B, PDE4C, PDE4D, PDE5A, PDE6A, PDE6B, PDE6G, PDE7B, PDE8A, and PDE9A, while significant upregulation was observed for PDE7A and PDE10A in colon cancer samples compared to normal tissue (Figure 3-2).

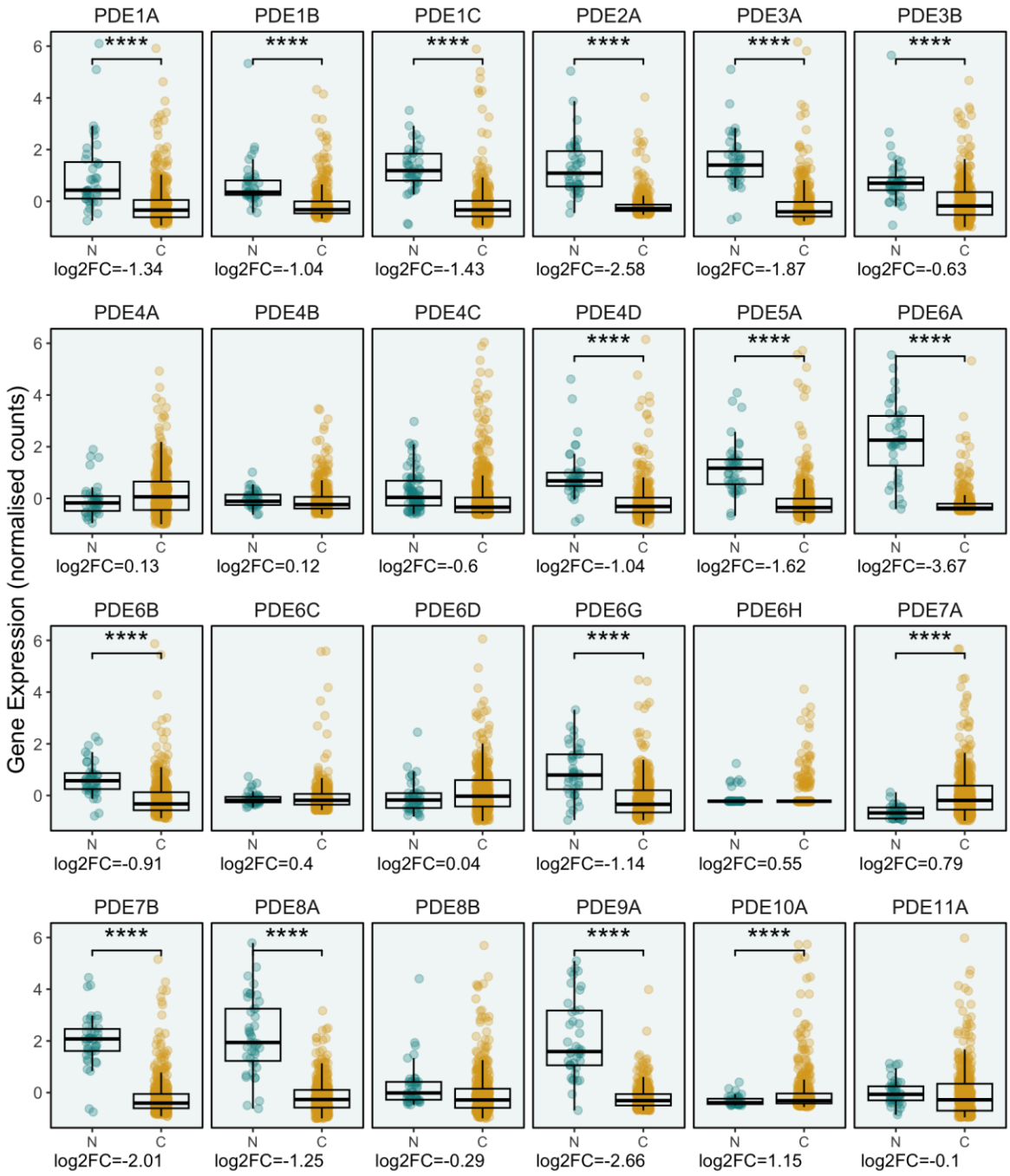

Figure 3-2. Scaled phosphodiesterase (PDE) gene expression in cancer and normal tissue from the colon cancer cohort (COAD) of The Cancer Genome Atlas (TCGA).
Differential analysis and count normalisation performed using DESeq2. Boxplots generated from normalised counts scaled by z-score. N; normal, C; cancer. Significance indicated by Benjamini-Hochberg corrected p values: *p< 0.05, **p<0.01, ***p<0.001, ****p<0.0001. Cancer n=445, normal n=42.

By examination of unscaled expression data, the relative expression level in the tissues could be seen (Figure 3-3), revealing PDE3A, PDE4D, PDE5A, PDE8A and PDE9A to be highly expressed in the colon tissue and strongly downregulated in the cancer samples. Of the upregulated genes, PDE7A had a moderate to low level of expression while PDE10A appeared lowly expressed.

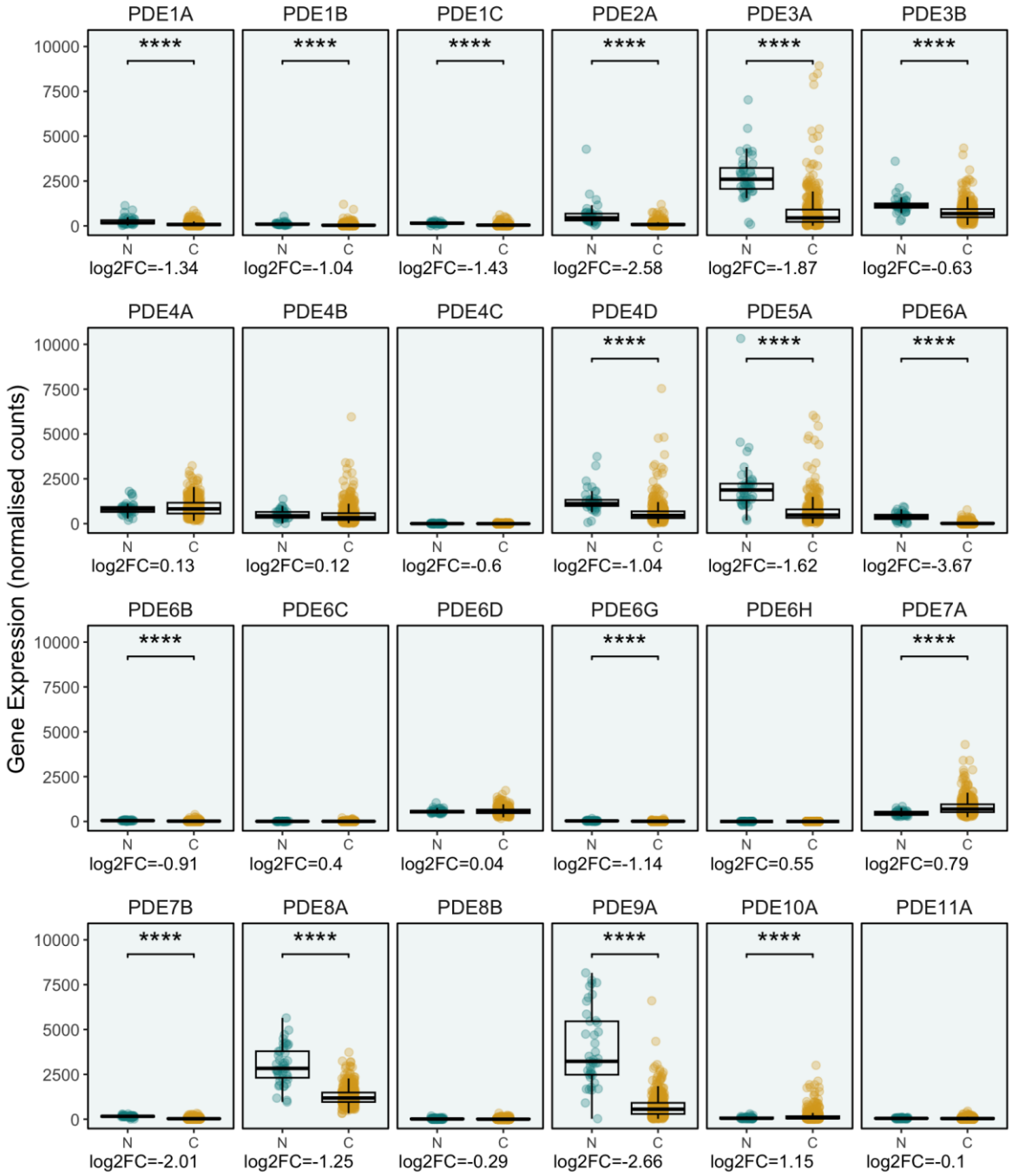

Figure 3-3. Unscaled phosphodiesterase (PDE) gene expression in cancer and normal tissue from the colon cancer cohort (COAD) of The Cancer Genome Atlas (TCGA).
Differential analysis and count normalisation performed using DESeq2. Boxplots generated from normalised counts. N; normal, C; cancer. Significance indicated by Benjamini-Hochberg corrected p values: *p<0.05, **p<0.01, ***p<0.001, ****p<0.0001. Cancer n=445, normal n=42.

3.2.1.2 Differentially expressed PDE genes across colon cancer grades and tumour location

TCGA colon dataset included cancer stage information of patients that was used to relate PDE expression to stage and cancer progression. By examination of PDE expression across cancer stages, the majority of PDEs were downregulated in the cancer samples compared to normal with a low homogenous expression across stages (Figure 3-4). However, some PDE genes suggested a different expression pattern but were not significant. PDE3A exhibited a progressive decrease with greatly reduced expression at stage IV. PDE7B was homogenously downregulated in the cancer samples but was especially reduced at stage IV similar to PDE3A. Interestingly, PDE6A was downregulated across cancer samples but seems to have slightly recovered at stage III, though this was also not significant. Of the upregulated genes, both PDE7A and PDE10A were upregulated in the cancer samples, but expression did not depend on cancer stage. Lastly, PDE2A and PDE6B indicated significant differential expression between stages, but the magnitude of change was negligeable.

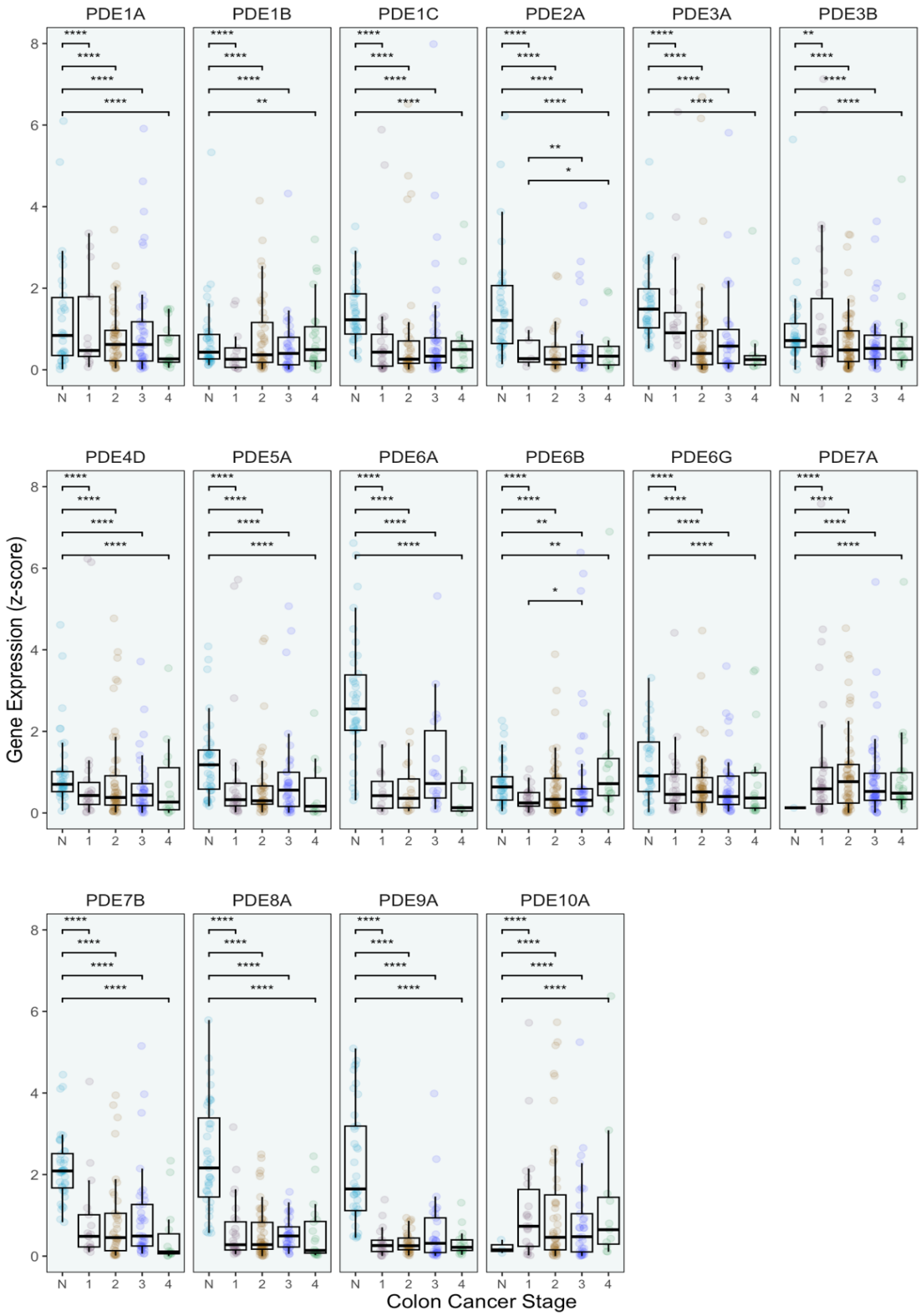

Figure 3-4. Phosphodiesterase (PDE) gene expression across cancer grades in the colon cancer cohort (COAD) of The Cancer Genome Atlas (TCGA).
Differential analysis and count normalisation performed using DESeq2. Boxplots generated from normalised counts scaled by z-score. N; normal; cancer stage I-IV. Significance indicated by Benjamini-Hochberg corrected p-values: *p<0.05, **p<0.01, ***p<0.001, ****p<0.0001. Normal n=67, stage I n=81, stage II n=187, stage III n=133, stage IV n=67.

After analysing PDE expression by cancer stage, the impact of tumour location on PDE expression was investigated. As discussed in Section 1.4.2, tumour location within the bowel is strongly associated with CRC pathogenic pathway, somatic mutation profile, tumour phenotype and patient outcome. Therefore, it was hypothesised that PDE expression would be similarly impacted by tumour location. To investigate this, PDE expression across all 24 genes was plotted against colon location from the cecum to the rectosigmoid junction (Figure 3-5). Expression across the whole PDE family was altogether homogenous across the bowel tract. However, higher expression of most PDE genes was observed in the normal tissue relative to colon cancer, which was found previously (Figure 3-2, Figure 3-3). Additionally, samples were organised by cancer stage in the plot (Figure 3-5), and no clear link between cancer stage and PDE expression was found, which was also demonstrated in the cancer stage analysis (Figure 3-4).

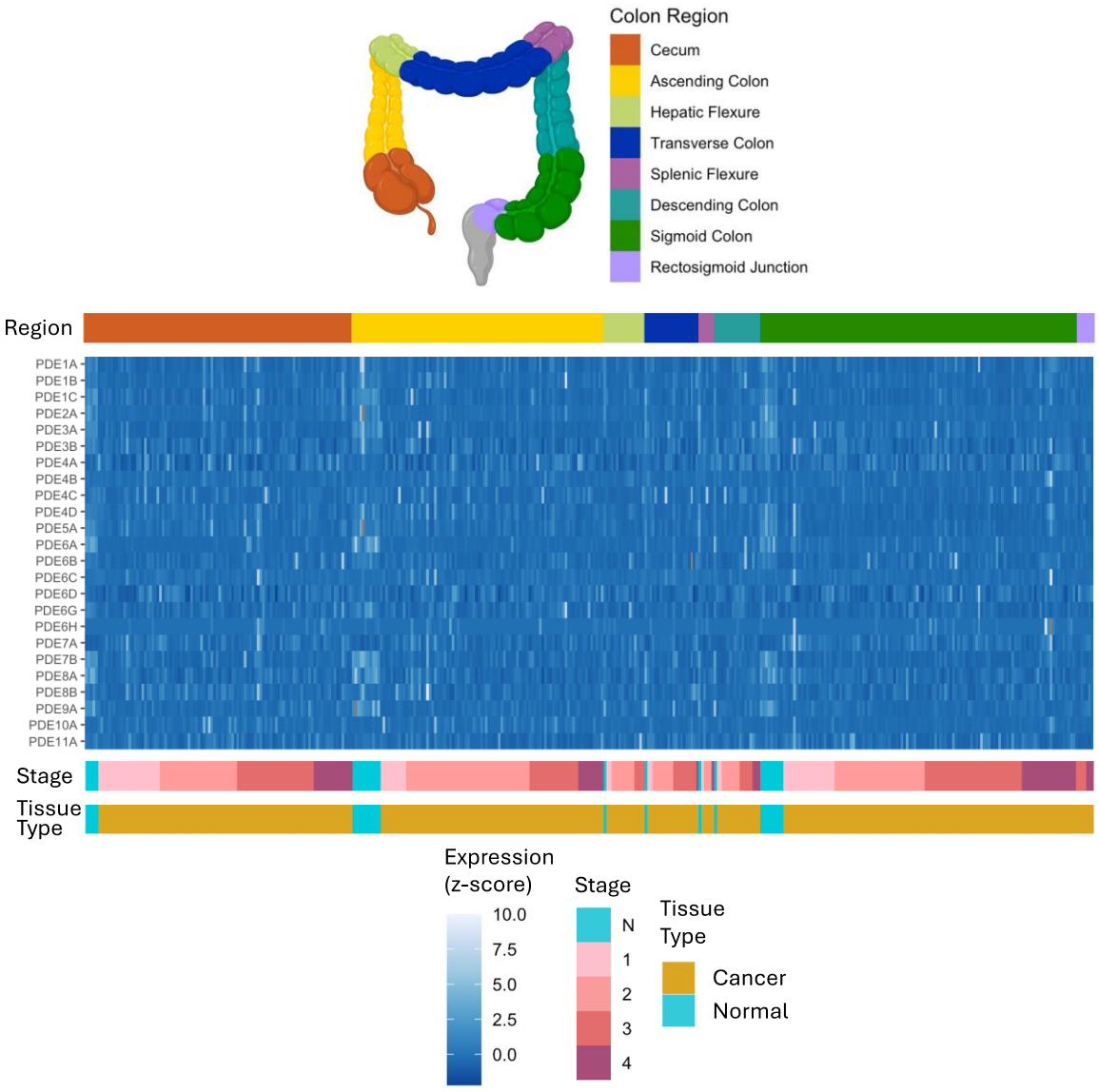

Figure 3-5. Phosphodiesterase (PDE) gene expression of normal and cancer samples across the colon.
Gene expression of all 24 PDE genes indicated as DESeq2 normalised counts scaled by z-score. Tissue samples are sorted from left to right by biopsy location through the colon from cecum to rectosigmoid junction. Within tumour location, samples are ordered by cancer stage. N; normal, 1; stage I, 2; stage II, 3; stage III, 4; stage IV. Normal n=67, stage I n=81, stage II n=187, stage III n=133, stage IV n=67.

Showing these trends more clearly, principal component analysis (PCA) of relative PDE family expression profile was carried out (Figure 3-6). Samples clearly clustered into cancer and normal groups when stratified by sample type (Figure 3-6:A). As shown in the previous heatmap (Figure 3-5), classification of the samples by cancer stage revealed no clear difference in PDE family expression, and cancer samples clustered tightly (Figure 3-6:B). Similarly, stratification by tumour location signified a homogenous PDE expression profile of the cancer samples which clustered together (Figure 3-6:C).

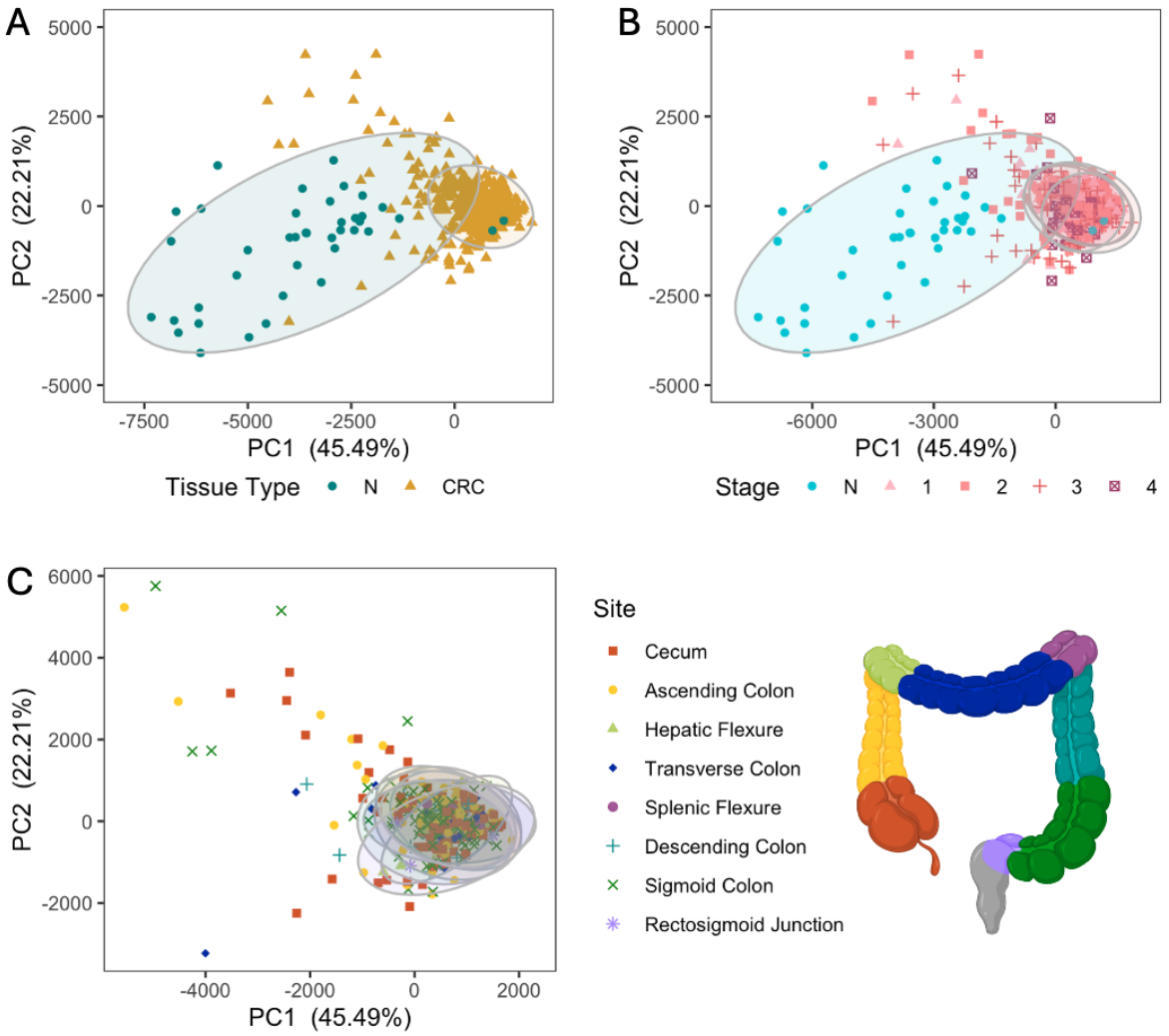

Figure 3-6. Principal component analysis (PCA) of phosphodiesterase (PDE) gene expression.
PCA of PDE gene expression profile by DESeq2 normalised counts. A: samples segregated by sample type. N; normal, CRC; colorectal cancer. B: samples classified by cancer stage. N; normal, 1; stage I, 2; stage II, 3; stage III, 4; stage IV. C: cancer samples classified by tumour location. A diagram of colon regions indicates tumour location. Normal n=67, stage I n=81, stage II n=187, stage III n=133, stage IV n=67.

3.2.1.3 Differentially expressed PDE genes in rectal cancer

Having characterised PDE expression in TCGA colon cancer cohort, it was important to analyse the rectal cancer cohort and determine whether colon and rectal cancers exhibit divergent PDE expression profiles. To this end, TCGA rectal cohort datasets (READ) were analysed, consisting of 157 patients, 157 cancer samples and 10 matched normal tissues. After data acquisition and pre-processing, 10,723 genes were significantly differentially expressed, with 6,178 upregulated genes and 4,545 downregulated genes (Figure 3-7).

Similar to the colon dataset, the rectal samples were clustered into normal and cancer tissue types with each group showing a starkly different global expression profile (Figure 3-7:A). Within the differentially expressed genes, many PDEs were downregulated, with only one upregulated gene: PDE7A (Figure 3-7:B). Unlike the colon cohort which indicated PDE10A as upregulated in the cancer samples, PDE10A showed no significant change in expression in the rectal cohort.

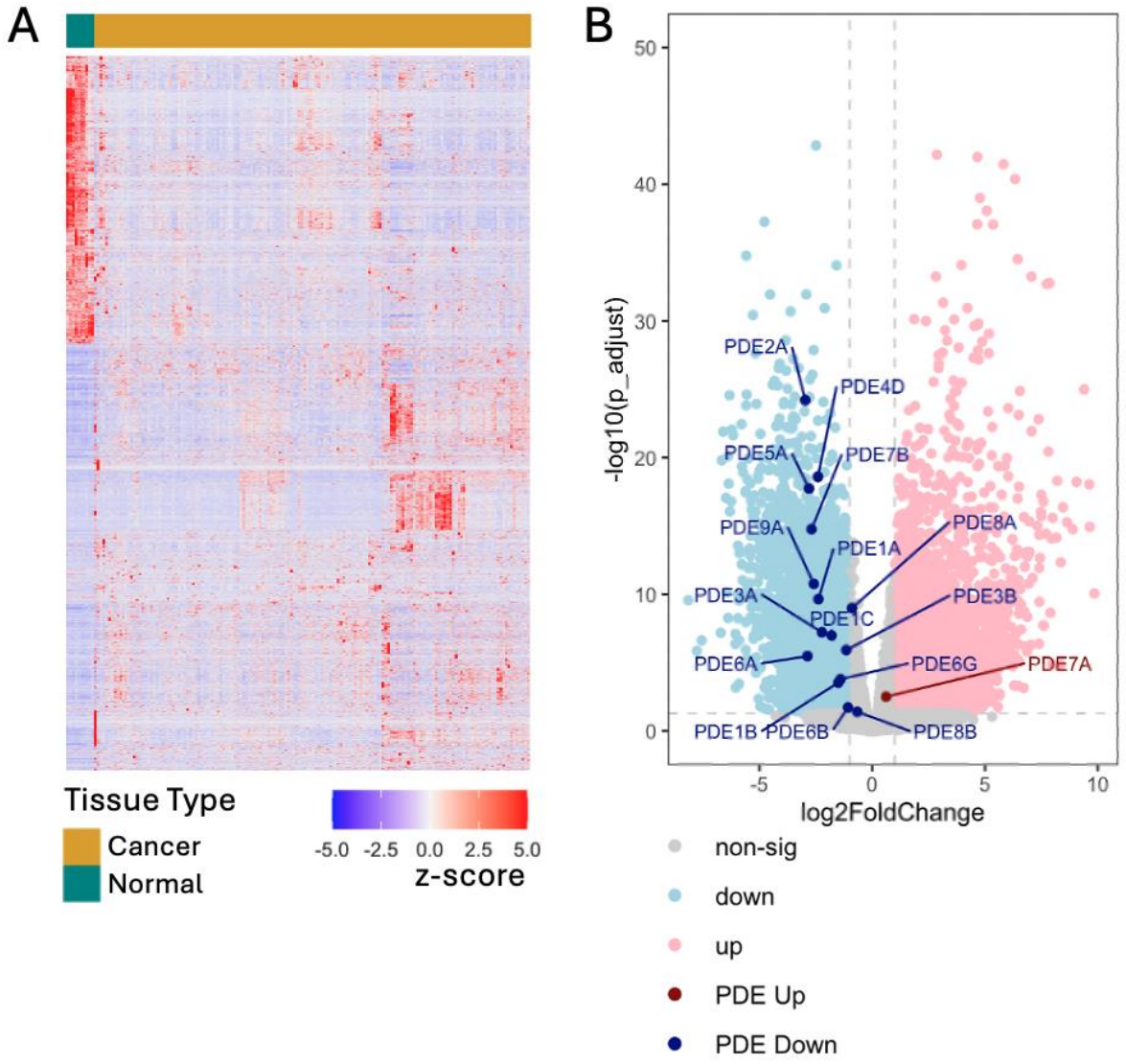

Figure 3-7: Differential expression between cancer and normal tissues in The Cancer Genome Atlas (TCGA) rectal cancer dataset (READ).
A total of 10,723 differentially expressed genes were identified by DESeq2, of which 6,178 were significantly upregulated and 4,545 were significantly downregulated. A: A clustered heatmap of differentially expressed genes. Expression from low (blue) to high (red) shown as z-score scaled DESeq2 normalised counts. B: Volcano plot of differentially expressed genes with significant phosphodiesterase (PDE) genes highlighted. Cancer n=157, normal n=10.

Gene expression between rectal cancer and normal samples across the PDE family is shown in Figure 3-8. Significant downregulation was found for PDE1A, PDE1B, PDE1C, PDE2A, PDE3A, PDE3B, PDE4D, PDE5A, PDE6A, PDE6B, PDE6G, PDE7B, PDE8A, PDE8B, and PDE9A, while significant upregulation was observed for PDE7A.

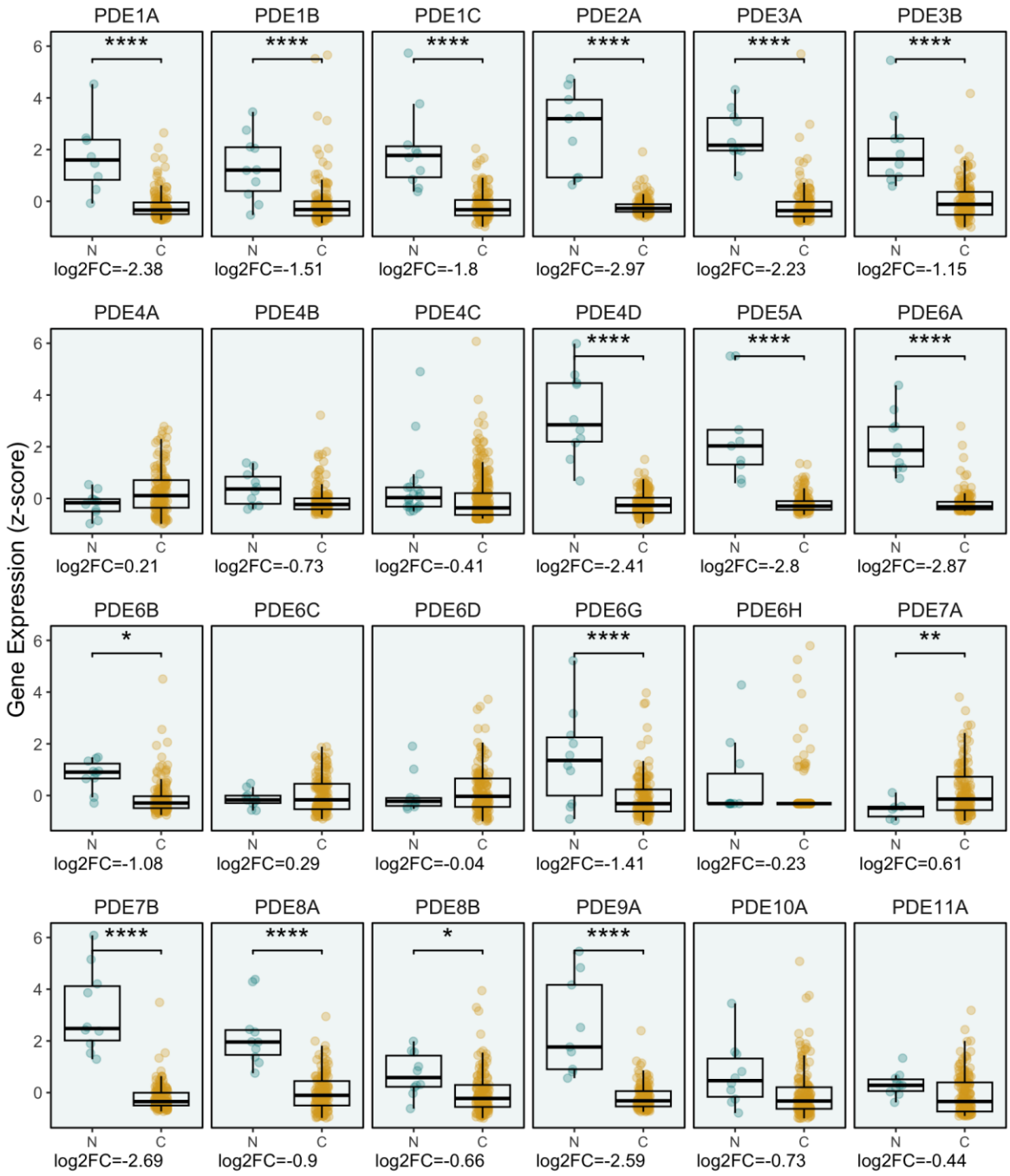

Figure 3-8. Scaled phosphodiesterase (PDE) gene expression in cancer and normal tissue from the rectal cancer cohort (READ) of The Cancer Genome Atlas (TCGA).
Differential analysis and count normalisation performed using DESeq2. Boxplots generated from normalised counts scaled by z-score. N; normal, C; cancer. Significance indicated by Benjamini-Hochberg corrected p-values: *p<0.05, **p<0.01, ***p<0.001, ****p<0.0001. Cancer n = 157, normal n = 10.

By examination of unscaled expression data, relative expression of the PDEs in the tissues could be seen (Figure 3-9), revealing PDE3A, PDE4D, PDE5A, PDE8A and PDE9A to be highly expressed in rectal tissue and strongly downregulated in cancer samples. Of the upregulated genes, the expression of PDE7A was relatively low while still indicating upregulation in the rectal cancer samples.

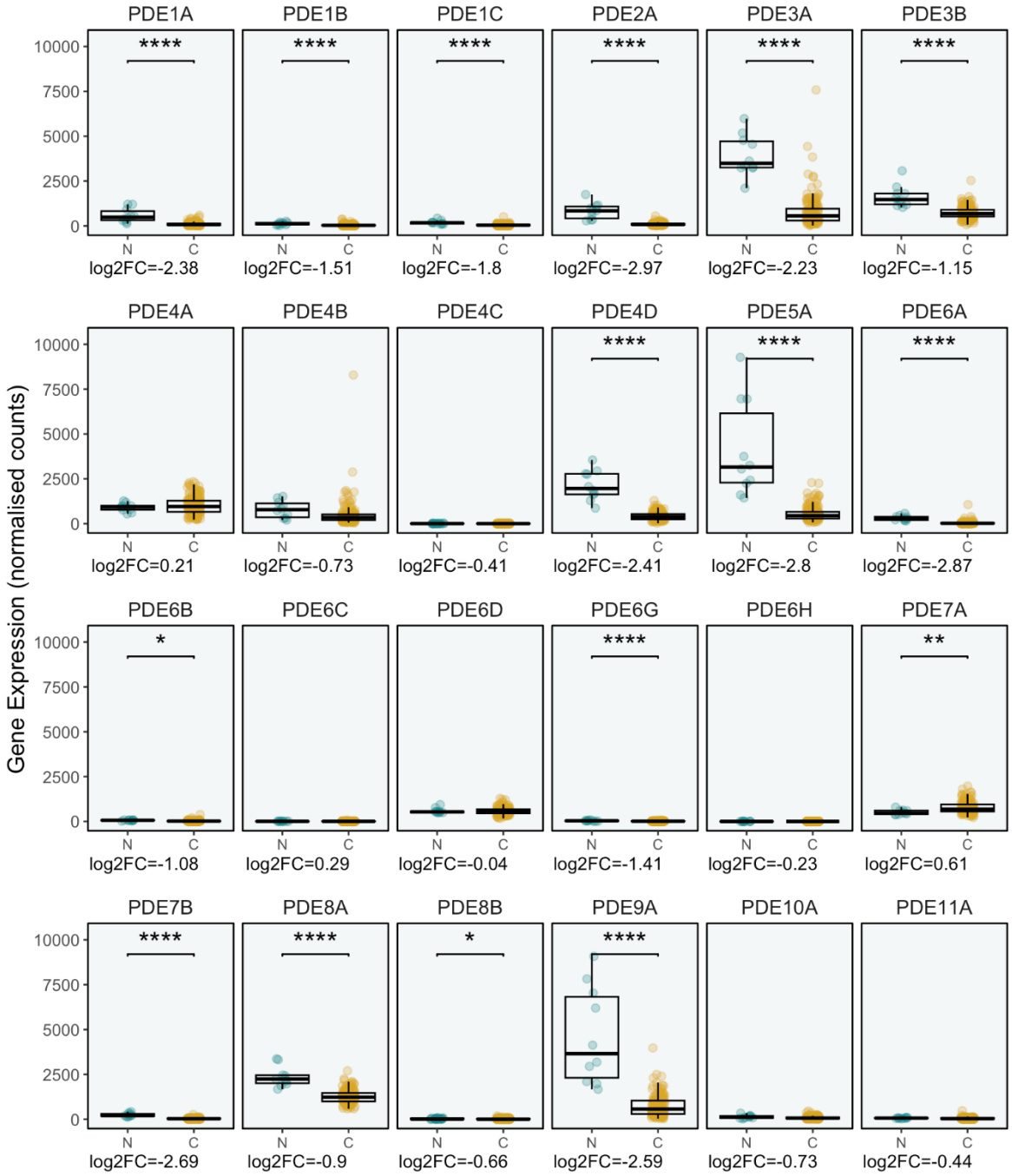

Figure 3-9. Unscaled phosphodiesterase (PDE) gene expression in cancer and normal tissue from the rectal cancer cohort (READ) of The Cancer Genome Atlas (TCGA).
Differential analysis and count normalisation performed using DESeq2. Boxplots generated from normalised counts. N; normal, C; cancer. Significance indicated by Benjamini-Hochberg corrected p values: *p < 0.05, **p < 0.01, ***p < 0.001, ****p < 0.0001. Cancer n=157, normal n=10.

3.2.1.4 Differentially expressed PDE genes across rectal cancer grades

As for TCGA colon cohort, the rectal cohort included cancer stage information. By plotting PDE expression by cancer stage, most PDE genes were downregulated in the cancer samples relative to normal tissue indicating no dependency on the individual cancer stage (Figure 3-10). Contrastingly, some PDE genes indicated different expression patterns. For instance, PDE4B indicated little difference in expression between stages but was only downregulated in stage III compared to normal tissue. Notably, PDE8B expression indicated stage-specific expression, being downregulated in stage I cancer compared to normal tissue with expression returning to levels similar to the normal tissue in stages III and IV. Furthermore, diverging from the colon cohort, PDE10A expression was not upregulated in the rectal cancer samples relative to normal, showing little deviation in expression. In fact, PDE10A was slightly downregulated in stage I cancer relative to normal.

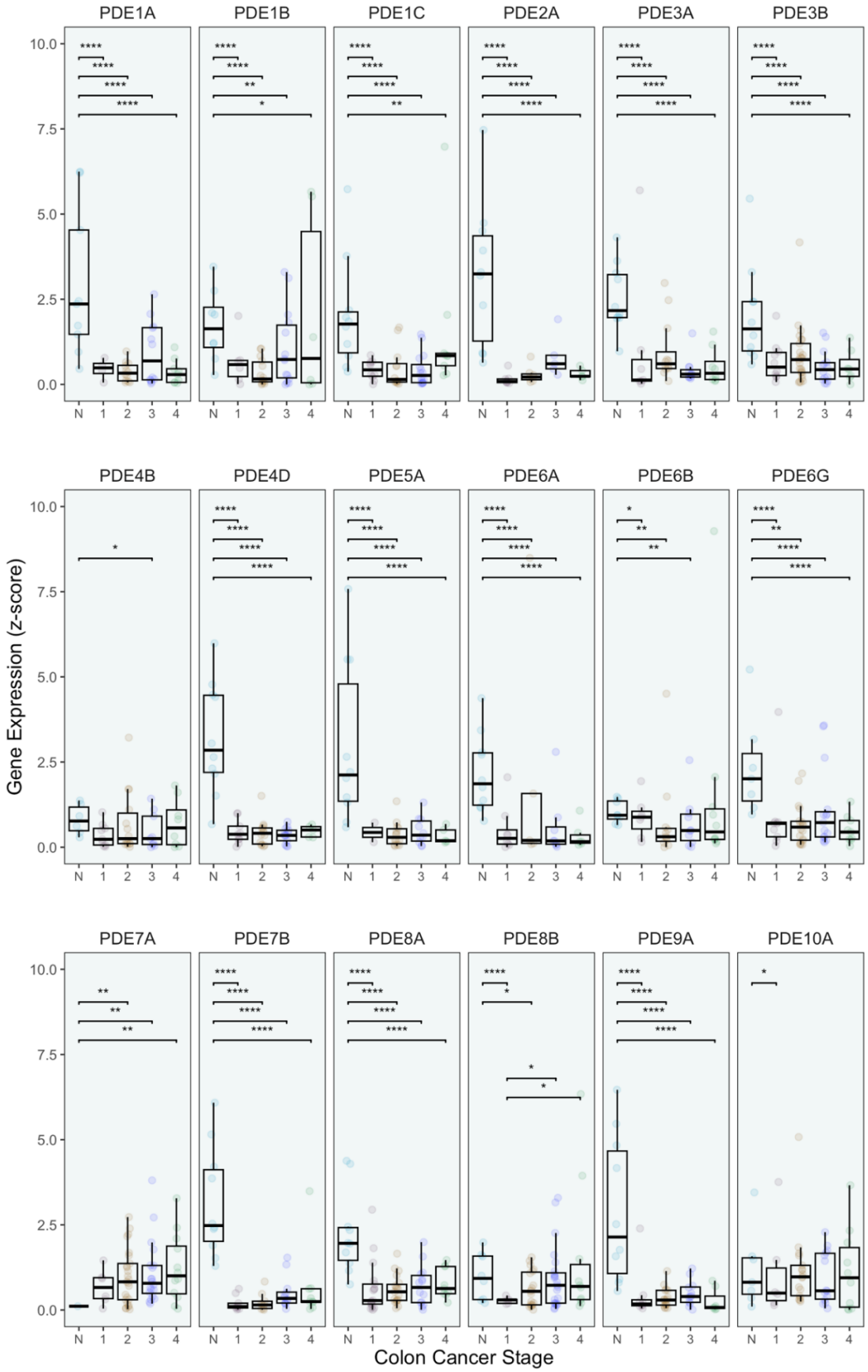

Figure 3-10. Phosphodiesterase (PDE) gene expression across cancer grades in the rectal cancer cohort (READ) of The Cancer Genome Atlas (TCGA).
Differential analysis and count normalisation performed using DESeq2. Boxplots generated from normalised counts scaled by z-score. N; normal; cancer stage I-IV. Significance indicated by Benjamini-Hochberg corrected p values: *p<0.05, **p<0.01, ***p<0.001, ****p<0.0001. Normal n=10, stage I n=30, stage II n=51, stage III n=51, stage IV n=24.

3.2.2 Differential methylation of PDE promotors in colorectal cancer

Gene methylation array data from TCGA cohorts was used to investigate correlation between PDE promotor methylation and gene expression. To this end, methylation beta values for colon and rectal TCGA cohorts were acquired and combined (COADREAD), consisting of 350 colon cancer patients with 312 cancer and 38 normal-matched samples, and 105 rectal cancer patients with 98 cancer and 7 normal-matched samples. The analysis began with filtering methylation probes to only retain those of high quality. The probes were then overlayed onto PDE promotor regions, and probes only mapped to PDE4A, PDE4C, PDE6D, and PDE7A promotors. By differential expression analysis, the promotor regions for PDE4A, PDE4C, and PDE7A were significantly hypomethylated in the cancer samples relative to normal tissue, while the PDE6D promotor was significantly hypermethylated (Figure 3-11).

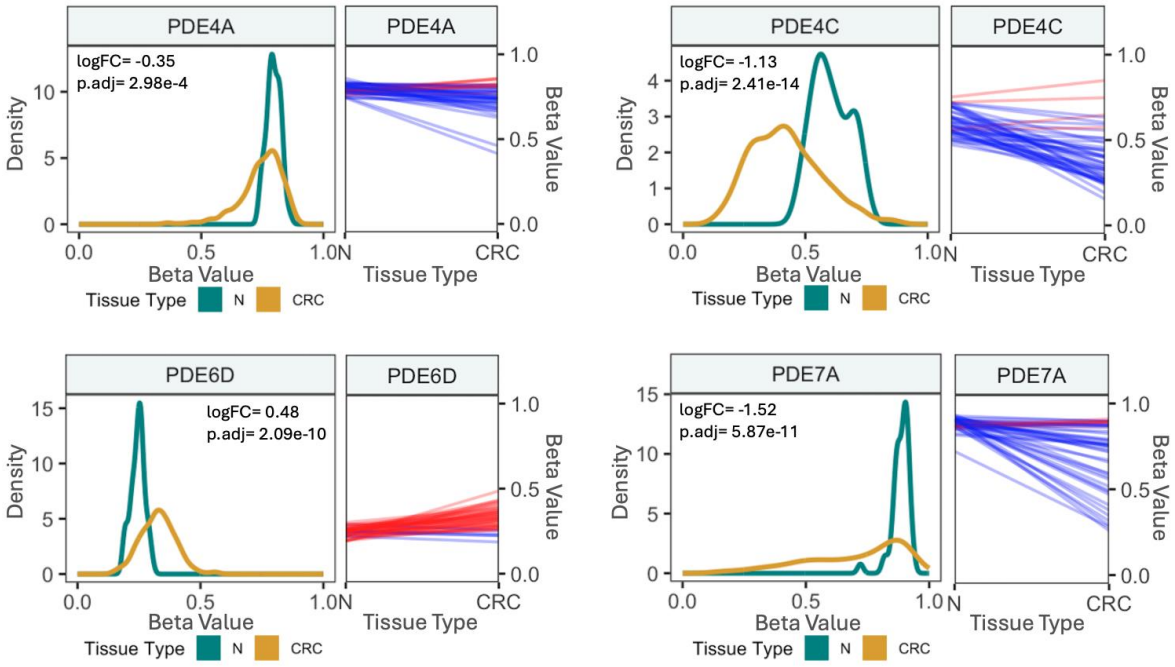

Figure 3-11: Differential phosphodiesterase (PDE) promotor methylation in colorectal cancer (CRC).
PDE promotor methylation in CRC compared to normal tissue from The Cancer Genome Atlas (TCGA) gene methylation array data (COADREAD). Density plots of methylation beta value presented with differential methylation statistics. logFC; log2FoldChange, p.adj; Benjamini-Hochberg corrected p-values, N; normal, CRC; colorectal cancer. Cancer n=410, normal n=45. For patient matched cancer-normal tissues, a paired line plot indicates change in promotor methylation within individuals. Cancer n=45, normal n=45.

Next, Spearman correlation was performed between PDE promotor methylation and gene expression to assess the strength and direction of any association (Figure 3-12). No association was found for PDE4A, PDE4C, PDE6D, or PDE7A.

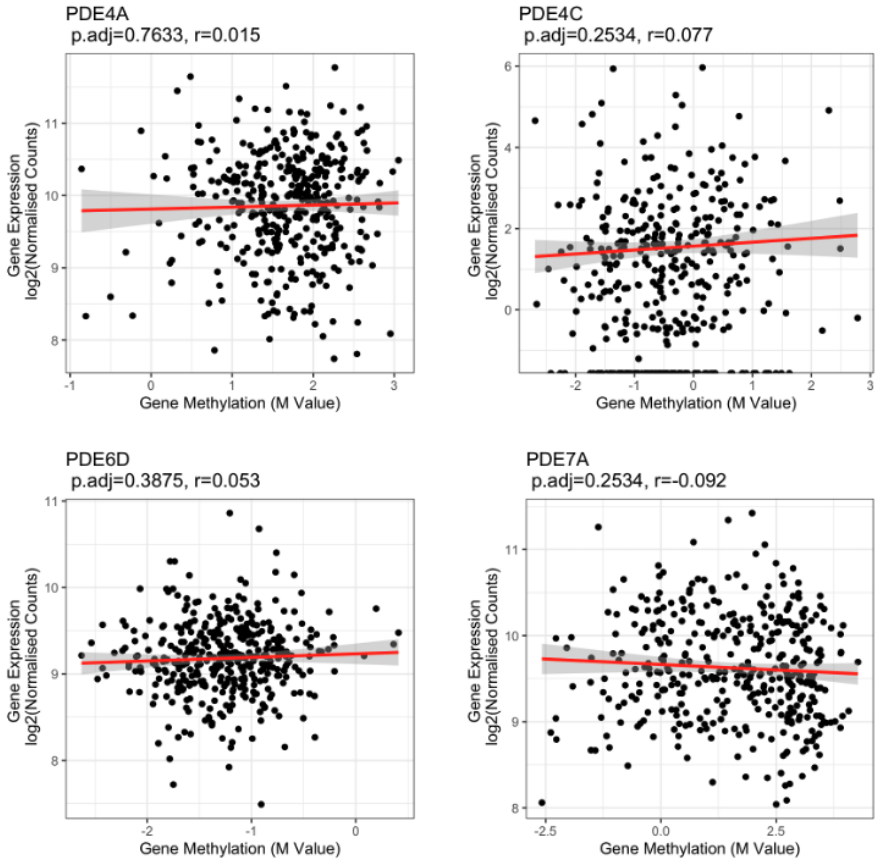

Figure 3-12: Spearman correlation between phosphodiesterase (PDE) promotor methylation and gene expression in The Cancer Genome Atlas colorectal cancer cohort (COADREAD). Methylation and gene expression tested as m value and log2-transformed DESeq2 normalised counts respectively. p.adj represents Benjamini-Hochberg adjusted p-value. A trend line was fitted to the data in red with a 95% confidence interval shown in grey. N=410.

3.2.3 cAMP and cGMP gene set enrichment analysis in colorectal cancer

Next, gene set enrichment analysis (GSEA) was performed to determine whether the cAMP and cGMP signalling pathways were differentially enriched beyond the PDE family in cancer tissues compared to normal tissues.

Given that PDE expression patterns in the colon and rectal cancer cohorts were highly similar (section 2.1.1), the datasets were combined to increase group numbers and statistical power (COADREAD). This is commonly done in the literature, but may mask disease-specific patterns (Gao et al., 2019). The dataset consisted of 445 colon cancer patients with 445 cancer samples and 42

normal samples, and 157 rectal cancer patients with 156 cancer samples and 10 normal samples. After differential expression, GSEA analysis was conducted on the differentially expressed genes for the cAMP signalling pathway and the cGMP-PKG signalling pathway (Figure 3-13). Both pathways were significantly depleted in the CRC samples compared to the normal samples, with a normalised enrichment score of -1.45 for the cAMP pathway and -1.78 for the cGMP-PKG pathway.

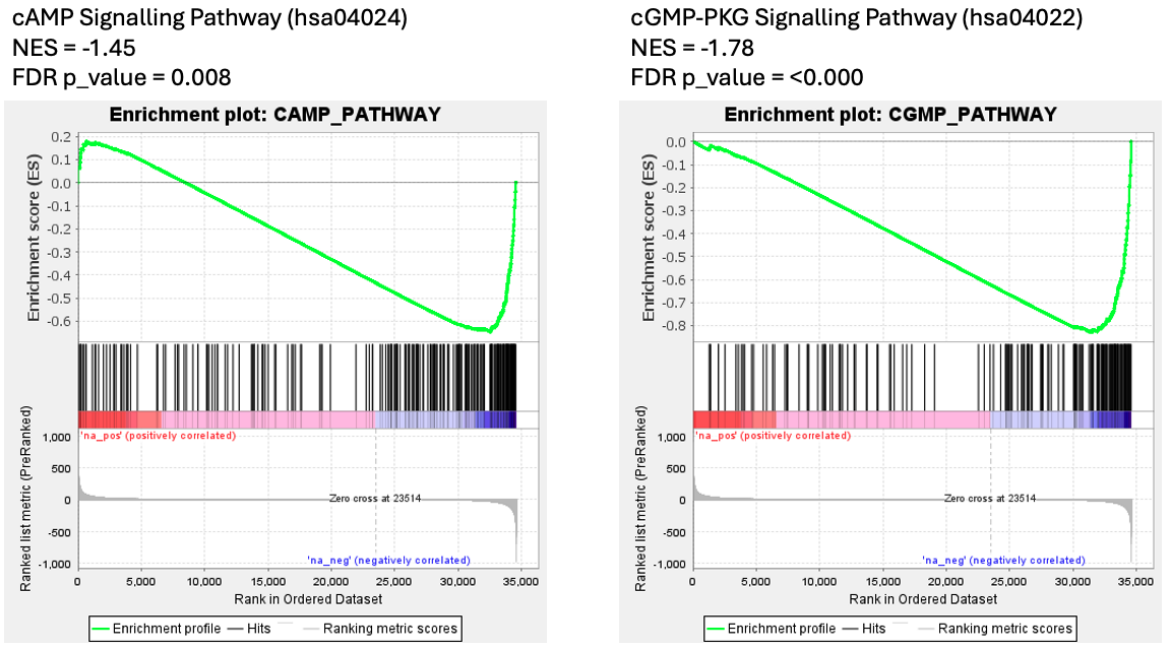

Figure 3-13: Gene set enrichment analysis for cAMP and cGMP-PKG signalling pathways in colorectal cancer (CRC).
Differentially expressed genes from CRC and normal samples in The Cancer Genome Atlas (TCGA) COADREAD cohort were ranked by a signed score metric (log2FoldChange * (-log10(p_value))) and analysed by gene set enrichment analysis (GSEA). NES; normalised enrichment score, FDR p-value; Benjamini-Hochberg adjusted p-values. The enrichment plot shows the enrichment score (ES) in green across the ranked gene list for the gene set. The x-axis represents the ranked genes ordered by the signed score metric, with the most upregulated genes on the left and the most downregulated on the right. The peak/trough of the curve represents the point of maximum enrichment, indicating where the gene set is most overrepresented. The shaded region shows the position of gene-set genes.

Next, to get an overview of the individual genes and their arrangements in the pathways, the R package Pathview was used to visualise differential expression. By inspection of the cAMP signalling pathway, broad downregulation across most genes could be seen (Figure 3-14). Upstream in the pathway, both membrane-bound and soluble adenylate cyclase were downregulated. Additionally, the cAMP effectors *PKA* and *POPDC* were downregulated, while *EPAC* was upregulated. Following cAMP, *PKA* formed a central hub in the pathway with

many of the target genes downregulated. Downstream from *PKA*, *CREB* was downregulated, and the cancer-related submodules comprising of *RAF1-MEK-ERK* and *PI3K-AKT* were uniformly downregulated. Additionally, the oncogene *SOX9* was strongly upregulated while *RhoA* was downregulated.

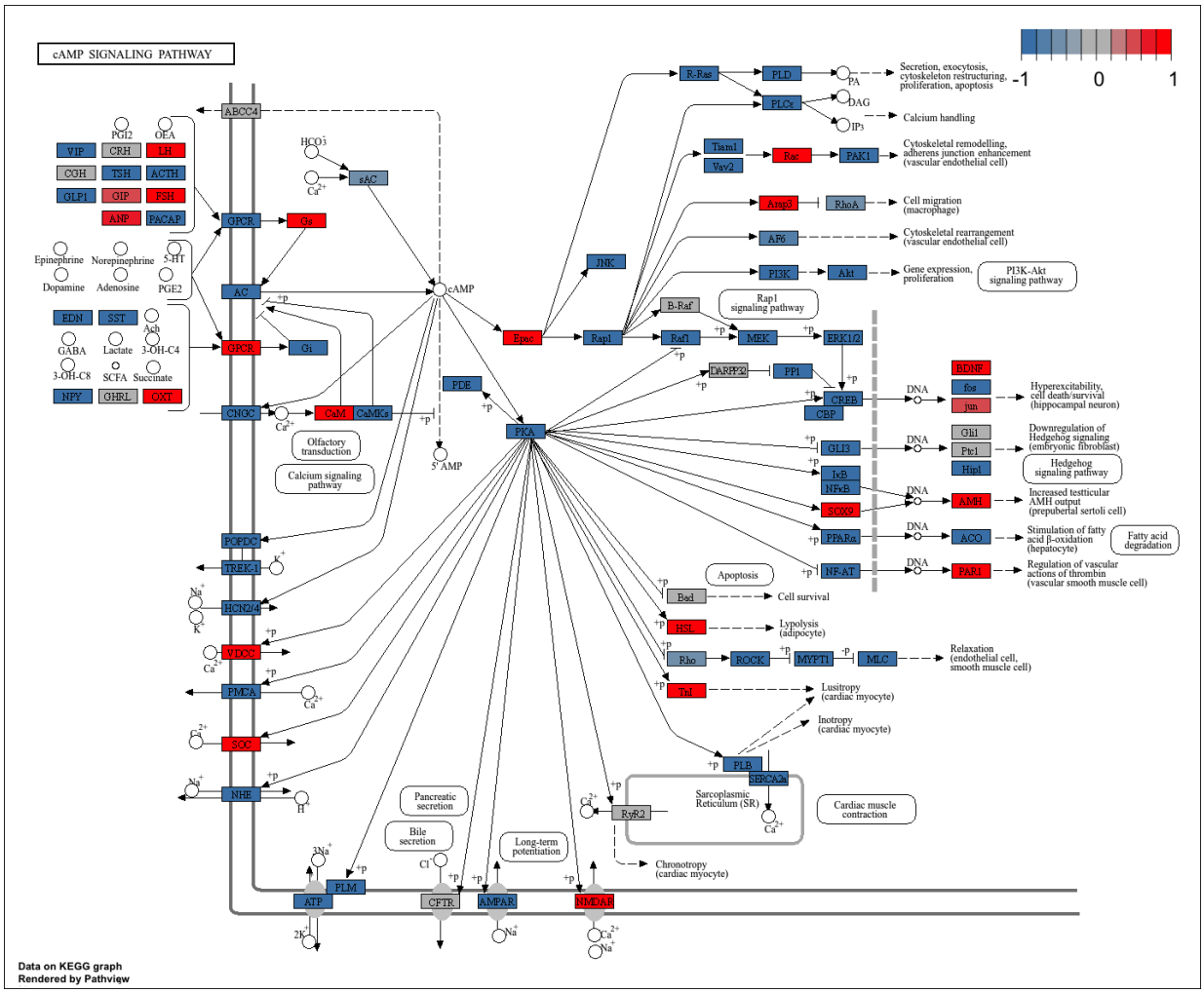

Figure 3-14: Pathview plot of differentially expressed genes in the cAMP signalling pathway. Differentially expressed genes in CRC compared to normal tissues in The Cancer Genome Atlas (TCGA) COADREAD cohort coloured by a signed score metric (log2FoldChange * (-log10(p_value))) from low (blue) to high (red). Pathway accession hsa04024.

Pathview analysis of differential gene expression in the cGMP-PKG pathway revealed broad downregulation in cancer tissues compared to normal tissues (Figure 3-15). Upstream in the pathway, downregulation of guanylate cyclases was observed (*NPRA/GUCY2A*, *NPRB/GUCY2B*). *PKG* was also downregulated and formed a hub with many of its target genes that were also downregulated. Of these, the *PKG* target *CREB* was also downregulated. As seen in the cAMP pathway above, the cancer-related submodules *RAF1-MEK-ERK* and *PI3K-AKT* were downregulated.

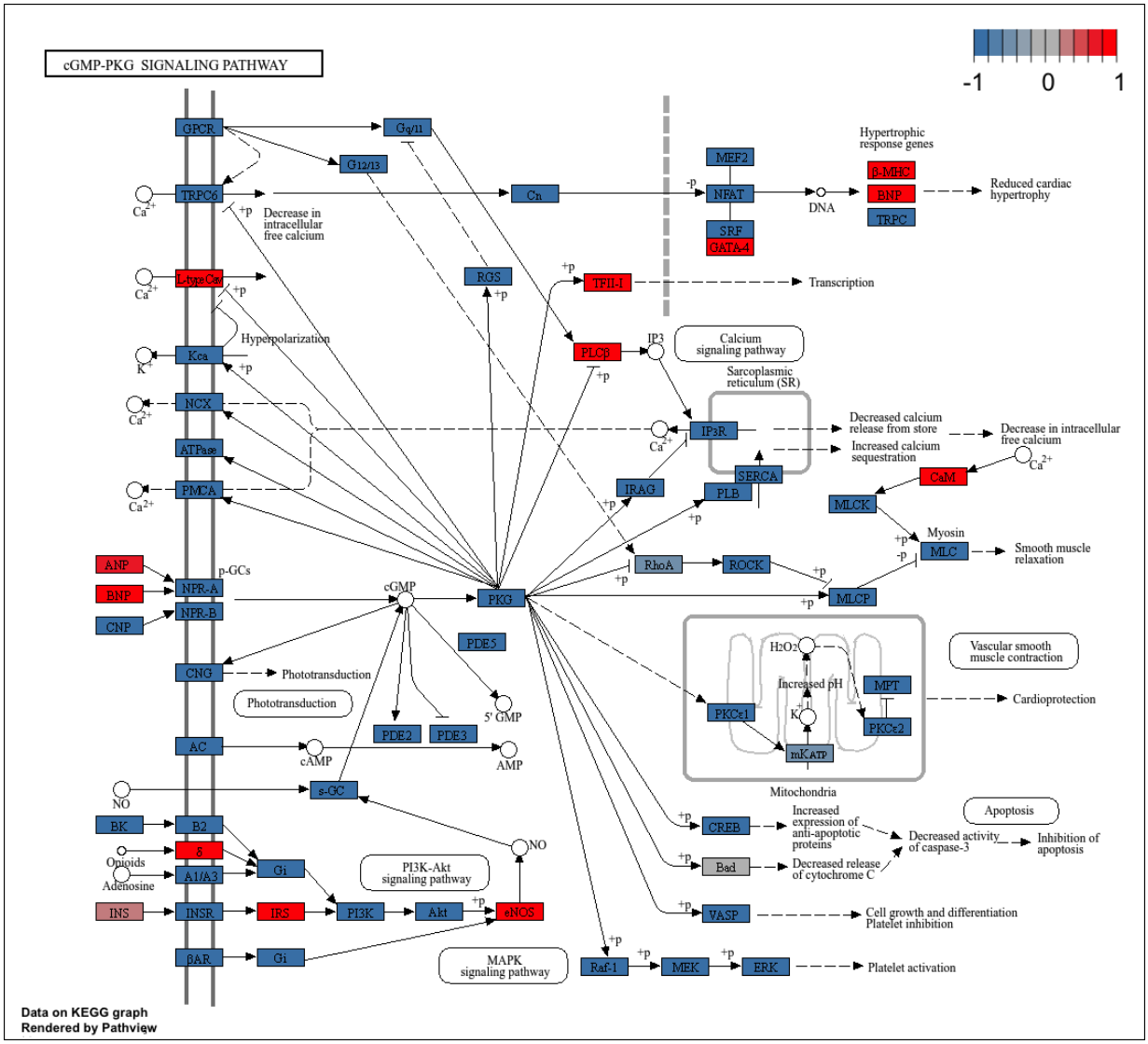

Figure 3-15: Pathview plot of differentially expressed genes in the cGMP-PKG signalling pathway.
Differentially expressed genes in CRC compared to normal tissues in The Cancer Genome Atlas (TCGA) COADREAD cohort coloured by a signed score metric (log2FoldChange * (-log10(p_value))) from low (blue) to high (red). Pathway accession hsa04022.

3.2.4 PDE protein expression in colorectal cancer by immunocytochemistry and proteomic analysis

To assess whether differential PDE mRNA expression transferred to protein expression, the most highly expressed and downregulated PDE genes found by RNA-seq (section 3.2.1.1) were selected, and IHC data from THPA was obtained (Figure 3-16). PDE3A exhibited a strong downregulation in protein expression in the colonic crypt cells, while an increase in expression was found in the surrounding stromal cells. For PDE4D and PDE5A, there was wide variation in protein expression, but a consistent slight upregulation was observed for PDE5A.

PDE7A indicated consistent expression across patients, and a slight increase in protein expression in the cancer samples may have been present. PDE8A was also generally consistent across patients, and a strong decrease in expression could clearly be seen in the cancer samples. Lastly, PDE9A was undetected in both tissue types.

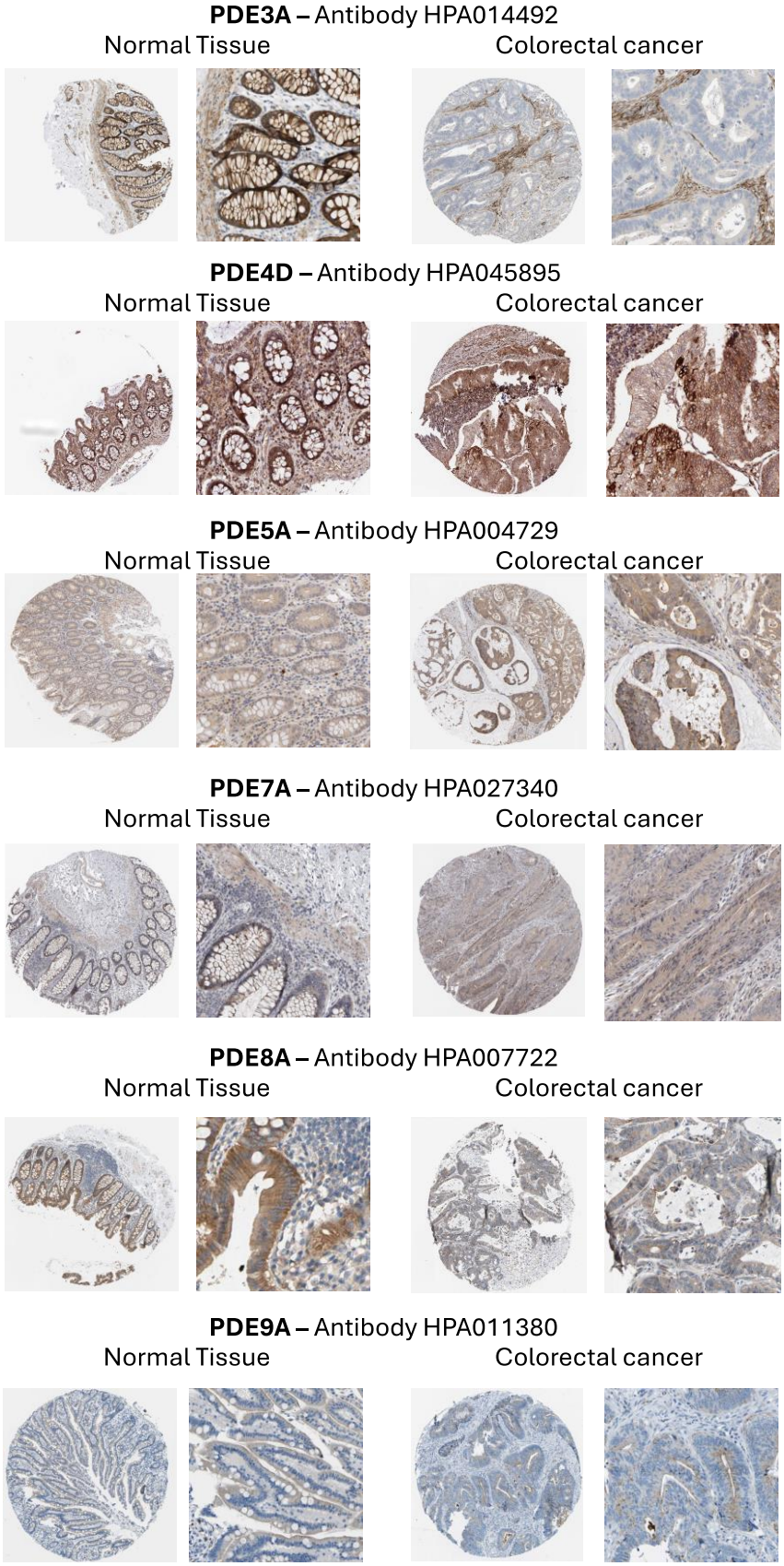

Figure 3-16: Tissue protein expression by immunohistochemistry (IHC) from The Human Protein Atlas (THPA).
Representative images obtained from THPA of normal and colorectal cancer (CRC) tissues (Thul and Lindskog, 2018). Protein expression indicated by brown staining and negative expression indicated by blue staining. Colonic crypts can be seen in the normal tissues as regular circular or elongated structures which are distorted in the cancer tissues.

To provide validation for the PDE protein expression by IHC, mass spectrometry-based proteomic data from CPTAC were analysed (Figure 3-17). Only three PDE genes were present in the dataset, consisting of PDE4A, PDE4D and PDE5A, each showing strong significant downregulation in protein expression.

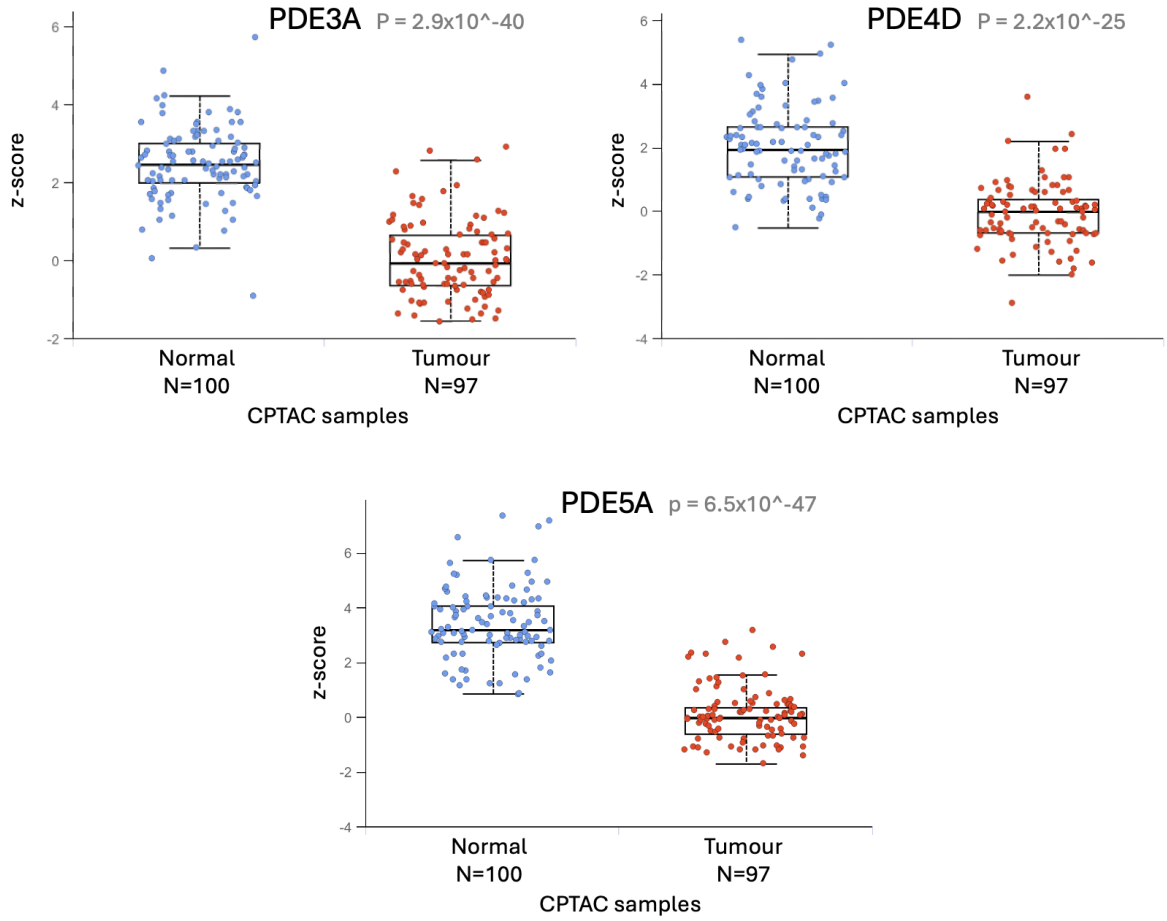

Figure 3-17: Protein expression of phosphodiesterases (PDEs) from Clinical Proteomic Tumour Analysis Consortium (CPTAC) data.
Data was obtained through the University of Alabama at Birmingham cancer data analysis portal (UALCAN) (Chandrashekar et al., 2017; Chandrashekar et al., 2022). Figures represent CPTAC mass spectrometry-based proteomic counts, log2 normalised and z-scaled by UALCAN. Normal n=100, tumour n=97.

3.2.5 The impact of PDE gene expression on colorectal cancer patient survival

To investigate the impact of PDE mRNA expression on patient overall survival, Kaplan Meier data provided by THPA was surveyed and key metrics were summarised (Figure 3-18). Many PDE genes had a significant impact on overall patient survival, but only PDE3B, PDE4B, PDE4D, and PDE8A exhibited a biologically relevant expression level near 1 FPKM, with each gene showing better outcomes for the higher expression groups. From the Kaplan-Meier

curves, clear separation in survival could be seen low and high expression groups (Figure 3-19).

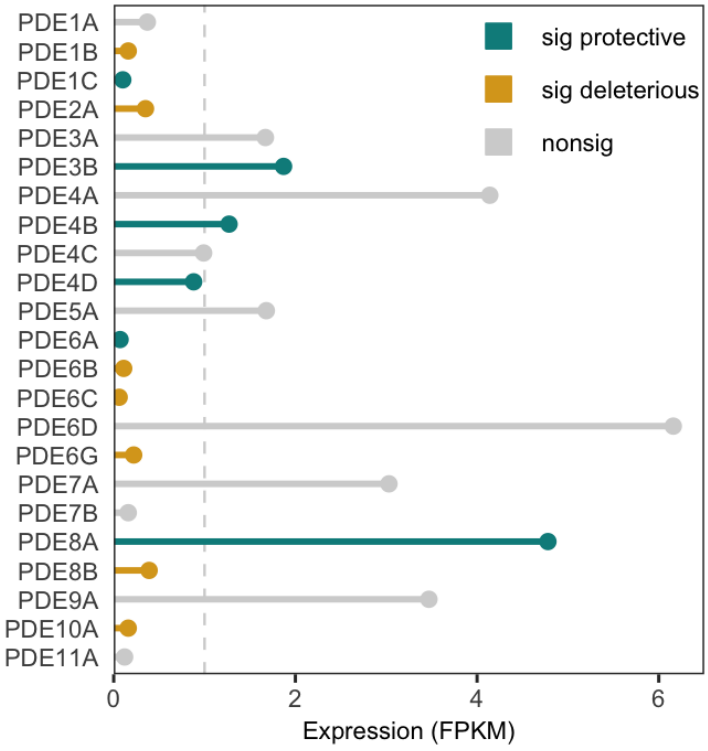

Figure 3-18: Overall survival analysis of phosphodiesterase (PDE) genes from The Human Protein Atlas (THPA).
Patient gene expression and outcome data from the Cancer Genome Atlas (TCGA) was subjected to Kaplan-Meier analysis by THPA (Weinstein et al., 2013; Thul and Lindskog, 2018). Samples were stratified into high and low-expression groups by an expression value threshold optimised by log rank test p-value. Lollipop plot indicates mean expression value in Fragments Per Kilobase of transcript per Million mapped reads (FPKM). Significant protective or deleterious impact of gene expression as determined by log rank testing is indicated by colour. A mean expression value of 1 FPKM is indicated by a grey vertical line.

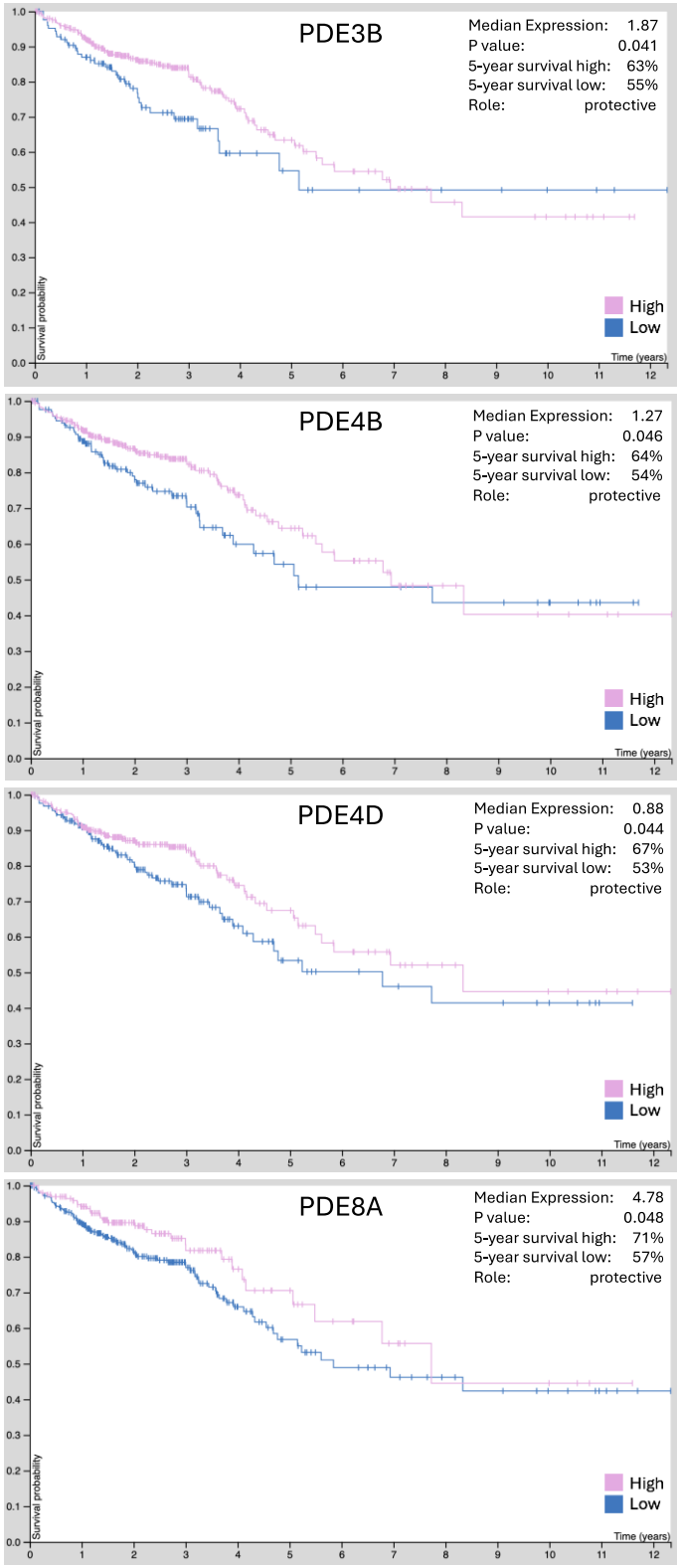

Figure 3-19: Kaplan-Meier overall survival curves of significant phosphodiesterase (PDE) genes from The Human Protein Atlas (THPA).
Patient gene expression and outcome data from the Cancer Genome Atlas (TCGA) were subjected to Kaplan-Meier analysis by THPA (Weinstein et al., 2013; Thul and Lindskog, 2018). Samples were stratified into high and low-expression groups by an expression value threshold optimised by log rank test p-value. Data obtained from THPA. Significance of impact on patient overall survival indicated by log rank testing.

3.2.6 Experimental validation of differential PDE expression in colorectal cancer

CRC and normal-matched tissues from ten patients were provided by Dr Kathryn Pennel and Professor Joanne Edwards at the University of Glasgow. RT-qPCR was performed for PDE3A, PDE4D, PDE5A, PDE6A and PDE9A. Of these, the transcript amplification of PDE3A, PDE4D, and PDE5A was detected (Figure 3-20). For each gene, most patient samples indicated downregulation but there was a high level of variability and potential outliers were present. Only PDE3A indicated a significant change and was downregulated in the tumour samples relative to the normal tissues.

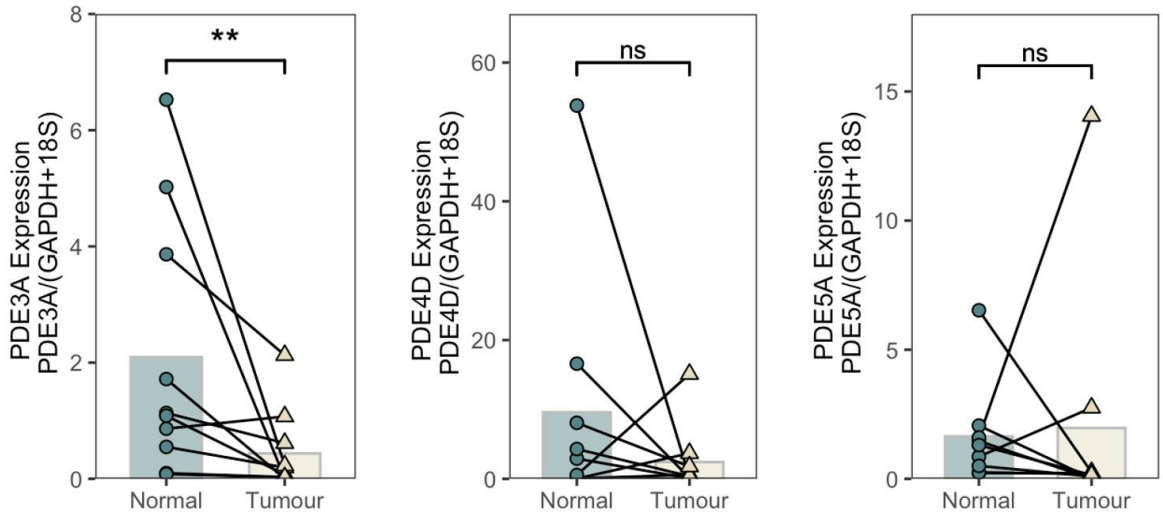

Figure 3-20: Phosphodiesterase (PDE) expression by RT-qPCR of colorectal cancer (CRC) tissue samples and matched normal tissues.
Statistical significance determined by a paired one-tailed t-test. Normality of the expression data was assessed by Shapiro-Wilk test of normality and inspection of QQ plots. A log10 transformation was performed on PDE3A expression before statistical testing. *p<0.05, **p<0.01, ***p<0.001, ****p<0.0001. Normal n=10, tumour n=10. Gene expression normalised to GAPDH and 18S rRNA.

Similarly, western blot analysis was performed on the patient tissues to validate protein expression of PDEs in colorectal cancer using antibodies targeted against PDE3A, PDE4B, PDE4C, PDE4D, PDE6A, and PDE9A. Of these, only PDE9A protein was detected and exhibited significant downregulation of protein expression in the tumour tissue relative to normal tissue. Of the ten patients, nine exhibited downregulation of protein expression with one indicating upregulation in the tumour tissues.

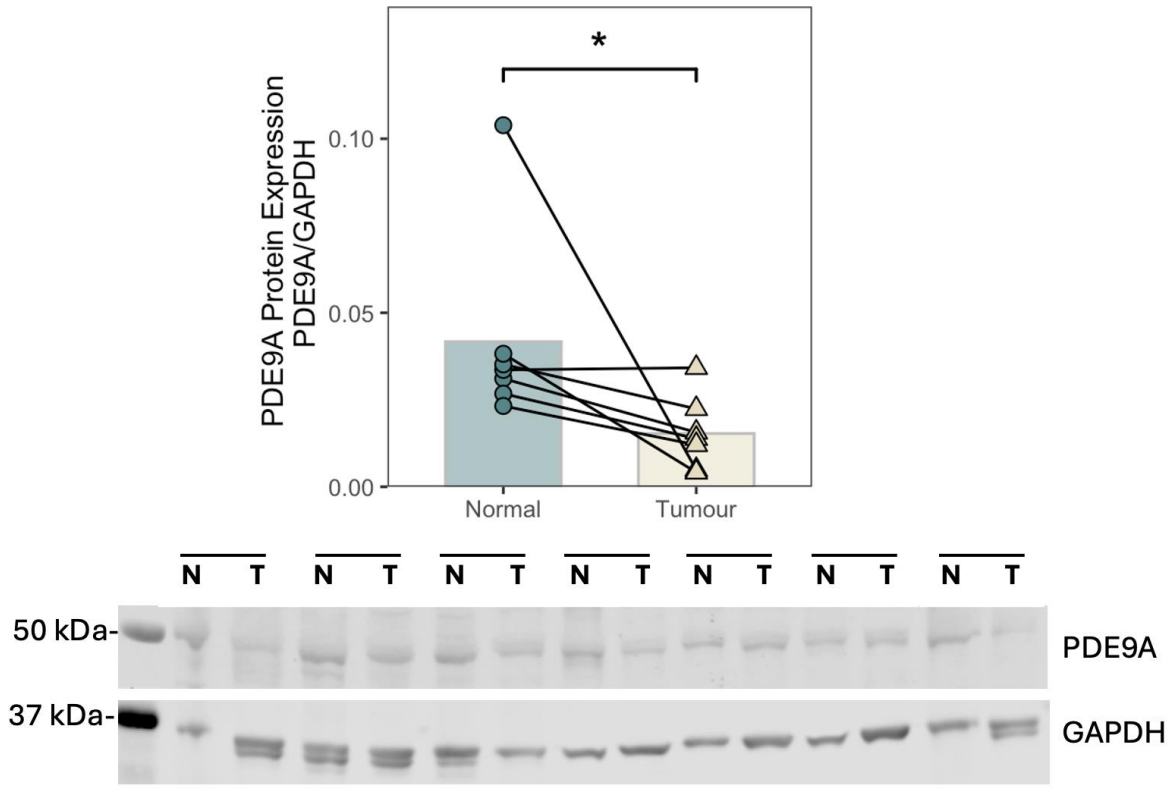

Figure 3-21: PDE9A protein expression by western blot analysis of colorectal cancer (CRC) and matched normal tissues.
Detection of PDE9A was normalised to GAPDH. Statistical significance between groups was determined by a paired one-tailed t-test. Normality of the expression data was assessed by Shapiro-Wilk test of normality and inspection of QQ plots. *p<0.05, **p<0.01, ***p<0.001, ****p<0.0001. Normal n=7, tumour n=7.

3.3 Discussion

This chapter set out to characterise PDE expression and function between CRC and normal tissue using TCGA RNA-seq and methylation array data, THPA IHC, CPTAC proteomics, and TCGA-THPA survival analysis. Lastly, PDE expression was investigated using RT-qPCR and western blot in the laboratory to confirm the computational results.

3.3.1 PDE expression profiles of colon and rectal cancer were highly similar

Colon and rectal cancers are often considered subtypes of the same disease, since they originate from neighbouring anatomical sites, share the same risk factors, and show similar pathogenesis and landscapes of mutation and signalling (Hong et al., 2012). Resultingly, these cancers have often been treated as one disease in research, therapeutic development, prognosis, and treatment. In terms of treatment, while surgery and radiotherapy are necessarily different between the cancers due to anatomical differences, targeted therapy and treatment of metastatic disease are the same (Tamas et al., 2015). However, colon and rectal cancers exhibit defined expression patterns for certain genes and have distinct patterns of metastatic spread despite their similar expression profiles (Tamas et al., 2015). For this reason, distinguishing between colon and rectal cancer in research and in the clinic may ultimately lead to improved outcomes for patients (Sanz-Pamplona et al., 2011).

Considering these differences between the two cancer types, PDE expression was expected to be distinct. Identifying these unique patterns could reveal possible associations to cancer type-specific pathways of pathogenesis or indicate targets for prognosis or therapy. To this end, differential gene expression analysis of TCGA RNA-seq data between cancer and normal tissues was performed, and PDE expression changes were compared between colon and rectal cancer. As a result, PDE expression patterns in cancer tissues were found largely the same between the colon and rectal cohorts. In colon cancer, downregulation in PDE1A-C, PDE2A, PDE3A-B, PDE4C-D, PDE5A, PDE6A-B, PDE6G, PDE7B, PDE8A, PDE9A and upregulation for PDE7A and PDE10A was found. From the unscaled expression data, it was clear that PDE3A, PDE4D, PDE5A, PDE8A and PDE9A had

the highest baseline level of expression in the normal colon tissues. These PDE changes were largely reflected in the rectal cohort, with the exception of PDE4C and PDE10A which were not differentially expressed. Additionally, PDE8B was found significantly downregulated in rectal cancer tissues but not in the colon cohort. These differences found in the rectal cohort could be biologically representative, but may instead be attributed to sample bias due to the smaller group sizes (157 cancer and 10 normal) compared to the colon cancer cohort (455 cancer and 42). These findings could be validated by RNA-seq analysis of larger rectal cohorts available on the GEO database (Edgar et al., 2002).

With these minor differences aside, these data support the view that PDE expression profiles are almost identical between colon and rectal cancers. For this reason, the mechanistic importance of PDEs in pathogenesis and their potential as prognostic and therapeutic targets are likely to be the same across the diseases. Similarly, CRC pathogenic genes KRAS, NRAS, PIK3CA, PTEN, and SMAD4 are equally mutated between colon and rectal cancers, while BRAF, CTNNB1 (encoding ß-catenin), APC, HER2, and TP53 show preferential mutation in one or the other (Hong et al., 2012). With the shift in research towards personalised medicine and tumour genotyping, these data suggest that potential targeted therapies involving cyclic nucleotides or PDEs could be applied equally to colon or rectal tumours.

3.3.2 PDE expression and colorectal cancer progression

Dynamic regulation of gene expression across cancer stages is important for understanding the pathogenic mechanisms driving tumour progression. For example, early gene expression may relate to tumorigenesis, while late-stage upregulation may reflect adaptive responses to nutrient exhaustion, hypoxia, invasion and metastasis (Wang and Luo, 2021). Dynamic expression patterns may allow for the prognosis of cancer progression and patient outcomes or inform the timing of treatments.

To this end, samples in the colon and rectal cohorts were stratified by cancer stage to investigate PDE expression in CRC progression. As a result, most PDEs were downregulated in CRC with no dependency on cancer stage. Only in rectal cancer, PDE8B found to have dynamic expression with early-stage

downregulation and late-stage upregulation. However, the magnitude of these changes was small and PDE8B exhibited low expression overall. Taken together, these data indicate that PDE expression does not depend on cancer stage after tumorigenesis.

3.3.3 PDE expression and colorectal tumour location

TCGA RNA-seq analysis revealed PDE expression to be almost identical between colon and rectal cancer. Within the colon however, proximal and distal tumours exhibit divergent pathogenic pathways, somatic mutation profiles, tumour phenotypes and patient outcomes (Al-Joufi et al., 2022). Furthermore, it has been suggested that differences in gene expression and phenotype between proximal and distal colon tumours are greater than those between distal colon and rectal tumours (Tamas et al., 2015). This divergence may result from the proximal colon originating from the embryonic midgut and the distal colorectum developing from the hindgut (Hong et al., 2012). In light of this, it was expected that PDE expression would vary by tumour location within the colon, even though no such difference was found between colon and rectal tumours by RNA-seq analysis.

To investigate this, cancer samples were stratified by tumour location as well as by cancer stage for each location. Expression across the whole PDE family was altogether homogenous across the bowel tract and site-specific cancer stages. A difference was only observed between normal and CRC samples as determined in the previous analysis.

Pathogenic genes pathways in CRC are either highly dependent on tumour location and progression, such as TP53, BRAF, and MLH1 mutation, or are early and ubiquitous across subtypes, such as Wnt/ß-catenin pathway activation. (Müller et al., 2016; Al-Joufi et al., 2022). Taken together, these data suggest that PDE downregulation could be a similar early event in CRC tumorigenesis and ubiquitous across tumours regardless of anatomical site, cancer stage, and specific tumour location.

3.3.4 No link between PDE promotor methylation and gene expression in colorectal cancer

CpG islands are regions of the genome rich in cytosine and guanine dinucleotides and are often found in the promoter regions of genes. Hypermethylation of CpG islands in promoter regions is a well-known method of epigenetic silencing, as the addition of methyl groups can inhibit transcription (Deaton and Bird, 2011). The epigenome in cancer exhibits general hypomethylation across the genome but also promotor hypermethylation of specific genes, many of which are tumour suppressors or important for pathogenesis (Baylin and Jones, 2011). For example, negative regulators of the Wnt pathway are common targets for transcriptional silencing in CRC (Suzuki et al., 2004).

This pattern of epigenetic modification suggests that the same mechanism could be responsible for the broad downregulation of PDE genes in CRC as observed in this project. Elucidating the source of PDE downregulation may inform pathogenic importance and provide new biomarkers. For instance, SEPT9 and MLH1 methylation are used as biomarkers both commercially and in the clinic for CRC diagnosis and determination of microsatellite stability status (Pérez-Carbonell et al., 2010; Lin, 2019).

Using TCGA CRC datasets, probes from gene methylation array data were mapped to PDE promotor regions, and differential methylation was determined between cancer and normal tissues. Because of the limited size of gene methylation arrays, the genome cannot be comprehensively covered (Peters et al., 2015). Accordingly, probes only mapped to promotors of PDE4A, PDE4C, and PDE7A, which were found less methylated in cancer tissues, and also PDE6D, which was more methylated. By Spearman correlation, no association between promotor methylation and RNA-seq gene expression was found for any of the PDE genes. This supports the view that the CRC-linked differential expression of PDE4A, PDE4C, PDE6D and PDE7A is not regulated by promotor methylation.

However, these results may not be biologically representative since this analysis approximated promotor regions as a 2 kb window upstream from PDE transcription start sites. If the promotors did not span this whole region, and methylation probes mapped to sites outside the promotors, the results would not

reflect epigenetic regulation. By detailed characterisation of PDE promotors combined with increased genome coverage by probes using larger methylation arrays, such as the Infinium MethylationEPIC BeadChip, more confidence could be placed in the results (Walker et al., 2015; Wu et al., 2022). Furthermore, the results could be cross-validated by other epigenetic methods like ATAC-seq, which would indicate PDE genes accessible to chromatin that may be undergoing translation (Grandi et al., 2022).

Taken together, this data suggested that the broad downregulation of PDEs in CRC was not influenced by PDE promotor regulation, but further epigenetic characterisation across the whole PDE family is required. The signalling pathways of cAMP and cGMP are far-reaching and very complex, and PDE transcription may instead be regulated by a multitude of stimuli, either acting alone or in coordination. These may include regulation by a network of transcription factors, enhancers, or silencers, or by other means such as chromatin remodelling or RNA-level regulation (Lee and Young, 2013).

3.3.5 Gene set enrichment analysis of cAMP and cGMP signalling pathways

To determine whether the cAMP and cGMP signalling pathways exhibit differential expression beyond PDE genes, gene set enrichment analysis was performed on differentially expressed genes between cancer and normal tissues in TCGA COADREAD cohort.

cGMP is a known tumour suppressor in CRC, and early attenuation of cGMP is a key step in CRC tumorigenesis (Pitari et al., 2007; Rappaport and Waldman, 2018). This was reflected by cGMP pathway analysis, in which downregulation of guanylate cyclases and PKG in CRC was suggestive of impaired cGMP synthesis and signalling.

The role of cAMP in CRC is less clear than for cGMP, but adenylate cyclase agonism by forskolin has consistently exhibited anti-proliferative effects by increasing cAMP in cell lines (Gamet et al., 1992; Höpfner et al., 2001; McEwan et al., 2007; Cristóbal et al., 2014) and mouse xenograft models (Yoshizawa et al., 1995). By pathway analysis of cAMP signalling, broad downregulation of

many genes was observed, and downregulation of adenylate cyclases, *PKA*, and *POPDC* suggested that the synthesis and action of cAMP was disrupted in the cancer tissues. Given this disruption and the anti-proliferative effects of cAMP in CRC, downregulation of cAMP may be an early and important event necessary for CRC tumorigenesis analogous to cGMP downregulation.

While the Pathview analysis served to provide a broad overview of the cAMP and cGMP pathways, unexpected downregulation of oncogenes such as *CREB*, *MEK-ERK* and *PI3K-AKT* was found in the CRC tissues. This finding may reflect that CRC subtypes and stages have divergent dependencies on different pathways (Al-Joufi et al., 2022), and that averaging subtypes into one CRC group for the RNA-seq analysis may have led to these unexpected results. Alternatively, this could have been caused by genes being averaged by family during the Pathview analysis, and this representation does not indicate individual gene expression. For instance, inspection of gene expression in the same TCGA dataset using the UALCAN data analysis portal (Chandrashekar et al., 2017; Chandrashekar et al., 2022) revealed CREB1 and CREB5 to be upregulated in CRC, while CREB3 was downregulated (data not shown). For this reason, separate pathway analysis or analysing patient tissues by RT-qPCR or western blot would better suit the investigation of cancer signalling pathways.

3.3.6 Validation of differential PDE expression by immunohistochemistry and proteomic analysis

At this point, broad downregulation of PDEs was observed by RNA-seq analysis in CRC compared to normal tissue, and this was found independent of colon or rectum location, cancer stage, and specific tumour site. To verify whether these changes in gene expression translated to the protein level, IHC and mass-spectrometry proteomic data was acquired from public databases and analysed.

Firstly, IHC images were obtained from THPA for the PDEs found most highly expressed in colorectal tissues and downregulated in CRC by the RNA-seq analysis (section 3.2.1.1). In agreement with the transcript level results, protein detection of PDE3A and PDE8A were found strongly downregulated in CRC compared to normal tissue. Also in agreement, a slight upregulation in expression was observed for PDE7A. However, contrasting with the

transcriptomic data, which found a strong downregulation of PDE5A transcripts, the IHC data showed that some cancer samples exhibited a slight increase in PDE5A, although this may be attributed to the high level of individual variation observed. This discrepancy between PDE5A transcript and protein may accurately represent the expression in patient tissues but may also be caused by non-specific binding of the antibody. Although THPA validates antibodies used for IHC by western blot or antigen array (section 2.1.4), there is a chance that the lysates used for blotting do not correspond to the tissue, therefore failing to indicate non-specificity, or that the antigen array did not capture antigens binding non-specifically present in the tissue. Without this information, specificity could be validated by in-house western blot of appropriate lysates to increase confidence of the results (O'Hurley et al., 2014).

Additionally, no clear trends were seen for PDE4D, which showed strong and highly variable staining. The strength of staining suggests that the staining protocol required optimisation and lower antibody concentrations or shorter incubations may allow better comparison of protein expression between samples. Lastly, PDE9A was not detected in either tissue type, and this may reflect lack of binding by the antibody or a need to optimise the protocol.

One limitation of this dataset from THPA was the relatively low number of normal samples, which made it difficult to identify conclusive changes in expression. For instance, there were only 2 normal patient tissues and 12 cancer patient tissues for PDE5A. There was also high variation within the groups. For this reason, validation using larger group numbers would provide more representative results. For example, with permission and further time, larger cohorts could be analysed such as the Colorectal Cancer Glasgow Royal Infirmary Tumour Micro Array Cohort and the INCISE Longitudinal Polyp Study Cohort prepared by the group of Professor Joanne Edwards at the University of Glasgow (Park and Edwards, 2021; Edwards and Ritchie, 2023). Additionally, the use of automated quantification tools like Visiopharm would avoid subjective error.

To cross validate these IHC data, PDE expression was analysed in the CPTAC dataset. Unlike IHC, which can be prone to variability due to human interpretation, mass spectrometry offers a sensitive and objective method for quantifying protein expression (Rezaul et al., 2010). However, this method does

not provide spatial and cell distribution information of protein expression. Additionally, expression data may be influenced or masked by signals from the surrounding stroma or microenvironment, which is dependent on how the samples are prepared. Nevertheless, by comparing the IHC data, proteomic analysis, and later western blot results in this project, these limitations of the individual techniques could be overcome.

Surprisingly, only PDE3A, PDE4D, and PDE5A were found by survey of PDE genes in the CPTAC proteomic data. The other PDE genes may have been filtered out during quality control steps if they had low abundance or signal to noise ratio. Additionally, since there is a high level of conservation within the PDE family, proteins might not be digested into peptides that uniquely map to sequences that are characteristic of specific PDE proteins, or they may not be produced in sufficient quantities, and thus may not be quantified (Nesvizhskii, 2014).

All three of the detected genes, PDE3A, PDE4D, and PDE5A, were significantly downregulated in CRC compared to normal tissues. For PDE3A, this agreed with the RNA-seq TCGA data and THPA IHC data, supporting the view that PDE3A is robustly downregulated in CRC. For PDE4D, this was congruous with the RNA-seq TCGA data, although the IHC data was inconclusive. For PDE5A, it was surprising that PDE5A was downregulated. This agreed with the transcript-level RNA-seq TCGA data, but the IHC data was suggestive of a slight increase in protein expression. In order to validate these findings, RT-qPCR and western blot analysis were conducted and will be discussed shortly.

3.3.7 PDE genes as prognostic markers for colorectal cancer patient outcomes

Due to the urgent need for reliable methods to determine patient subtypes and predict treatment responses in CRC, the prognostic potential of PDE gene expression for overall patient survival was evaluated. TCGA survival data was analysed using the THPA web application. Patients were stratified into high and low expression groups for Kaplan-Meier analysis, and the expression threshold was optimised by log rank test significance. Additionally, a cut-off for mean expression of 1 FPKM was chosen, ensuring that only genes with a biologically relevant expression level were detected and reducing the impact of background

noise. THPA also takes this approach using mean expression cut-offs when classifying genes as prognostic or not (Thul and Lindskog, 2018). Resultingly, PDE3B, PDE4B, PDE4D, and PDE8A were found to be significantly associated with overall survival, and the high expression groups indicated better prognosis and longer survival duration.

From the unscaled RNA-Seq TCGA data (see section 3.2.1.1), PDE3A, PDE4D, PDE5A, PDE8A and PDE9A exhibited a high level of expression in the colorectal tissues and were greatly reduced in the cancer samples. For this reason, it was plausible that they could be important for CRC pathogenesis and prognosis. Of these, only PDE4D and PDE8A were prognostic and predicted better patient outcomes, and this highlights these genes as potentially important for pathogenesis. Additionally, PDE3B was not highly expressed in the RNA-seq data but was still significantly downregulated in cancer tissues, while PDE4B was lowly expressed and not differentially expressed. These data indicate that a gene does not need to be highly or differentially expressed to be prognostic, and a small relative change in expression within cancer samples, even at low abundance, could have significant impacts on cancer-related processes. Furthermore, these data suggest that PDE3B, PDE4B, PDE4D, and PDE8A may be involved in mechanisms related to CRC aggression and severity.

3.3.8 RT-qPCR validation of PDE expression in colorectal cancer

At this point, PDE family expression in colon and rectal cancers had been characterised and cross-validated using various omics methods, cohorts, and databases. Nevertheless, it was important to verify that these changes were experimentally observable *in vitro*. A collaboration was initiated with Dr Kathryn Pennel and Professor Joanne Edwards at the University of Glasgow who provided tumour and normal-matched tissue samples of ten colorectal cancer patients. Changes in mRNA expression in cancer compared to normal tissues were assessed using RT-qPCR for some of the PDE genes that were most highly expressed and most differentially regulated by RNA-seq, comprising PDE3A, PDE4D, PDE5A, PDE6A and PDE9A.

In RT-qPCR, the use of reference genes is essential for the normalisation of target gene expression. However, this relies on the assumption that reference

gene expression is stable across experimental conditions. This may not be the case, and reference genes can exhibit variation (Lü et al., 2018). To reduce this risk, the two common CRC reference genes, GAPDH and 18S rRNA, were used together to increase accuracy and confidence of results (Hu et al., 2023).

Of the PDE genes analysed, transcript amplification was only detected for PDE3A, PDE4D, and PDE5A. The lack of PDE6A detection was not entirely unexpected given its low expression in the colorectal tissues shown by the TCGA RNA-seq data. Contrastingly, PDE9A indicated a high level of expression by RNA-seq, so it was surprising that amplification was not observed by RT-qPCR. Instead, the lack of detection may be attributed to non-specificity or inadequate affinity of primers (Rodríguez et al., 2015). The limited amount of tissue available was a significant challenge in this experiment, but with more tissue, alternative primers could be tested using more replicates to increase precision of the results.

Even though PDE3A, PDE4D, and PDE5A were detected, significant differential expression was detected only for PDE3A, which indicated downregulation in the cancer tissues. This suggests that expression of PDE4D and PDE5A was not perturbed in CRC. However, given that differential expression was found by RNA-seq and CPTAC, the lack of change found by RT-qPCR may originate from the low sample number and high variability of expression values within the groups. With more time, analysing more samples would increase statistical power and increase confidence in these results.

3.3.9 Western blot validation of PDE expression in colorectal cancer

To validate PDE protein expression in CRC, western blot analysis was carried out on patient tissues. Antibodies for PDE3A, PDE4B, PDE4D, PDE6A, and PDE9A were tested. Only PDE9A was detected and was significantly downregulated in tumour compared to normal tissue, which agreed with the transcript-level TCGA RNA-seq data. For the other antibodies, protein was not observed at the expected molecular weight, with many non-specific bands being detected outside this range. This may be attributed to several factors: the abundance of the proteins could be too low, suggesting that with more time and material, larger amounts

of protein could be loaded to increase detection. Alternatively, the protein could have been degraded in the tissue or during lysis, which could explain the presence of lower molecular weight non-specific bands. Using freshly resected tissues or performing lysis in a cold room at 4 ºC may counteract this. Additionally, the antibodies may lack specificity, and other antibodies could be tested given more time and tissue. Furthermore, other techniques such as IHC could be employed, although antibody specificity would be a key determinant. Immunoprecipitation-enriched western blot analysis would be another valid option, and may overcome the issue of low protein abundance (Trieu et al., 2009). In either case, these data support PDE9A to be robustly downregulated in CRC.

3.3.10 Literature context of PDE expression in colorectal cancer

3.3.10.1 PDE2

There is little existing research on PDE2 in CRC, but one study showed downregulation in HT29 cells compared to FHC normal colonocytes (Tinsley et al., 2010). Considering that CRC cell lines have been shown to completely lack PKG expression, an essential component of the cGMP pathway that is expressed in CRC patient tissues, CRC cell lines are not representative of the disease in critical ways (Hou et al., 2022b). Additionally, few conclusions can be made from a single comparison of healthy vs CRC cell lines. Nevertheless, this preliminary data agreed with TCGA RNA-seq data in this project, supporting downregulation of PDE2 in CRC. Also in agreement, one study demonstrated that PDE2 inhibition in HT29 lysates accounted for only a 12% reduction in overall cGMP hydrolysis (compared to 31% and 42% reduction for PDE3 and PDE5 inhibition respectively), supporting that PDE2 expression has a minor influence on cGMP in CRC (Tinsley et al., 2010). Counterintuitively, while these observations show PDE2 to be downregulated in CRC compared to normal tissues, inhibition of PDE2 reduced proliferation in CRC cell lines and murine cell line xenograft models (Zhao et al., 2021b). This mechanism was linked to an increase in cAMP levels and PKA-mediated phosphorylation of TFAM, preventing mitochondrial calcium induced growth (Zhao et al., 2021b). Additionally, THPA survival analysis in this project linked PDE2A to worse patient outcomes. This

highlights that while PDE2 appears downregulated in CRC, further inhibition in CRC or for chemoprevention in normal tissues presents a therapeutic opportunity. Furthermore, since the reduction of proliferation upon inhibition of PDE2 proceeded via an increase in cAMP and activation of PKA, it would be interesting to see if inhibition of other cAMP-specific PDEs, such as PDE4s, would exhibit the same effect. This could be easily investigated by testing PDE inhibitors on CRC cell lines and conducting western blotting to assess TFAM phosphorylation.

3.3.10.2 PDE3

PDE3A was found to be strongly downregulated in CRC compared to normal tissues by TCGA RNA-seq, THPA IHC, CPTAC proteomics, and by RT-qPCR conducted on patient tissues. RT-qPCR was performed by another group on patient tissues, in which PDE3A, while showing a high level of expression compared to other PDEs, indicated no change in CRC relative to normal tissues (Mahmood et al., 2016). The discrepancy of these results may be explained by the researchers using adenomatous tissue instead of carcinoma tissue that was used in TCGA RNA-seq and the RT-qPCR data in the present work. It could be that PDE3A expression is still at basal levels in the pre-cancerous adenomatous tissue. Nevertheless, IHC analysis by that same group indicated strong downregulation of PDE3A in CRC, which agreed with the protein level data presented in this project. In addition, one further study involving western blot analysis of CRC cell lines also supported these findings (Tinsley et al., 2010). Aside from PDE3A, PDE3B was found downregulated by TCGA RNA-seq in this project, and THPA survival analysis linked higher PDE3B expression to better patient outcomes. However, there is little data about PDE3B as distinct from PDE3A in CRC in the literature. While PDE3 appears robustly downregulated in CRC compared to normal tissues, inhibition of PDE3 has consistently inhibited growth in murine models of CRC (Kangawa et al., 2017; Elshazly et al., 2020) as well as in cell lines (Murata et al., 1999; Tinsley et al., 2010; Tsukahara et al., 2013; Kangawa et al., 2017). As for PDE2, while PDE3 appears downregulated in CRC, further inhibition in combination with AC or GC agonists could present a promising therapeutic option, or as a means of chemoprevention in precancerous tissue.

3.3.10.3 PDE4B

Existing research is discordant about the role of PDE4B in CRC. PDE4B was found upregulated by RT-qPCR and IHC of patient pre-cancerous adenoma tissues (Mahmood et al., 2016) and also in normal and early CRC tissues by IHC before downregulation in mid and late stage CRC (Pleiman et al., 2018; Bevanda et al., 2024). In one study, PDE4B was found to be protective in mouse models of CRC, and genetic knockout significantly increased tumour multiplicity and morbidity (Pleiman et al., 2018). A proposed mechanism described early upregulation of PDE4B mediated by ß-catenin signalling as a protective compensatory feedback mechanism which is lost in late-stage CRC (Pleiman et al., 2018). According to the model, increased PDE4B reduces cAMP levels, thereby inhibiting the pro-tumorigenic action of cAMP signalling, PKA, and CREB (Pleiman et al., 2018). However, this theory depicts cAMP as a pro-cancerous factor, which goes against a large body of research supporting anti-cancer effects of cAMP in cell lines (Gamet et al., 1992; Höpfner et al., 2001; McEwan et al., 2007; Cristóbal et al., 2014) and murine xenograft models (Yoshizawa et al., 1995). Also in contrast, pharmacologic or siRNA-mediated inhibition of PDE4B in cell lines and xenograft models reduced proliferation (Tsunoda et al., 2012; Nishi et al., 2017; Kim, Kwak, et al., 2019). Additionally, some reports have linked PDE4B to oncogenic mechanisms. One study demonstrated that c-Myc directly upregulates PDE4B expression to oppose cAMP pathway inhibition of c-Myc (Kim, Kwak, et al., 2019). Another study involving 16 CRC patients showed that PDE4B expression was enriched in patients who exhibited recurrence following polyp resection (Bandrés et al., 2007; Tsunoda et al., 2012).

In this project, PDE4B was not found to be differentially expressed by TCGA RNA-seq in CRC relative to normal tissue or across cancer stages. This disagreed with the dynamic expression pattern described in the literature (Mahmood et al., 2016; Pleiman et al., 2018; Bevanda et al., 2024). Given that the RNA-seq analysis was performed on a much larger cohort compared to the RT-qPCR and IHC data in these reports (Mahmood et al., 2016; Bevanda et al., 2024), the lack of differential PDE4B expression shown by RNA-seq is more likely to be representative. Additionally, THPA analysis associated higher PDE4B expression with improved patient outcomes, and this agreed with the protective effects reported in CRC mice models (Pleiman et al., 2018), but disagreed with the

finding of increased PDE4B in patients with polyp recurrence (Bandrés et al., 2007; Tsunoda et al., 2012). Despite conflicting results, these reports implicate PDE4B in CRC pathogenesis, and validation by RT-qPCR, western blot, and IHC in larger cohorts, as well as by inhibition or overexpression assays would clarify the potential of PDE4B as a prognostic or therapeutic target.

3.3.10.4 PDE4D

Previous findings on PDE4D in CRC are also conflicting. One study demonstrated the downregulation of PDE4D in CRC using RT-qPCR analysis of eight matched pairs of CRC and normal tissues, as well as by examining gene expression microarray data (Chen et al., 2018). This was also supported by IHC of patient tissue in other work (Bevanda et al., 2024). These reports agreed with the PDE4D downregulation shown by TCGA RNA-seq and CPTAC data in this project. However, PDE4D did not exhibit differential expression by RT-qPCR of 10 CRC and normal pairs of patient tissue in this project, but the small sample number and high variability may have masked differential expression.

Contrasting to these results, one study showed no change in PDE4D expression by RT-qPCR and IHC in patient tissues (Mahmood et al., 2016), while another study showed strong upregulation in CRC by RT-qPCR analysis of a larger cohort (Cao et al., 2016). PDE4D inhibition studies are equally conflicting. Anti-proliferative effects of PDE4D inhibition were found in cell lines (Kim, Nam, et al., 2019; Nummela et al., 2024), and mice xenograft models (Cao et al., 2016), while other cell line data showed PDE4D inhibition to increase proliferation, migration, and survival (Chen et al., 2018). Furthermore, PDE4D was found to be negatively regulated by two miRNAs. PDE4D inhibition by one miRNA exhibited anti-proliferative effects in CRC (Cao et al., 2016), while inhibition of the other promoted proliferation (Chen et al., 2018), but this may be attributed to divergent PDE4D-independent effects.

From TCGA survival analysis in this project, PDE4D was found to be protective. However, given the conflicting results of PDE4D inhibition on CRC in the literature, steadfast conclusions could not be made. Validation of expression by IHC in larger cohorts and testing the effect of inhibition or overexpression using proliferation assays on cell lines may reveal the prognostic and therapeutic

potential of PDE4D. Additionally, mouse- or patient-derived CRC tumour organoids would better represent the CRC molecular profile compared to cell lines and could be used to validate initial cell line data. Furthermore, delineation of PDE4D isoform expression in CRC may support the use of isoform-specific inhibitors for treatment which may produce fewer side effects (Liu et al., 2019). Lastly, exploring PDE4D expression between CRC subtypes may reveal pathogenic importance and indicate prognostic potential. This could be done by RNA-seq analysis of datasets with this clinical information, or by RT-qPCR or western blot of tissues from these subtypes.

3.3.10.5 PDE5

PDE5 is one of the more extensively studied genes in CRC. One network of researchers, primarily based at universities in Alabama, have shown PDE5 to be upregulated in CRC cell lines by western blot (Tinsley et al., 2010; Whitt et al., 2012; Li et al., 2013; Nan Li et al., 2015). However, the control group consisted of only one normal colonocyte cell line in each study, making it difficult to draw decisive conclusions. Additionally, cell lines do not fully recapitulate the molecular profile of CRC tumours, as indicated by a lack of PKG expression in CRC cell lines that is present in patient tissues (Hou et al., 2022b). For these reasons, these PDE5 western blot results should be interpreted with caution.

Reports of PDE5 differential expression analysis by other methodologies are also conflicting. RT-qPCR experiments have shown PDE5 to be upregulated in CRC patient tissues (Mahmood et al., 2016) but downregulated in murine mice models of CRC (Islam et al., 2022). Similarly, IHC of patient tissues indicated PDE5 upregulation in CRC by one study (Tinsley et al., 2010) but no differential expression in another (Mahmood et al., 2016).

The results from this project are equally incongruous. PDE5A was found downregulated in CRC by TCGA RNA-seq, possibly upregulated by THPA IHC, and downregulated by CPTAC proteomics. With these discordant results in this project and in the literature, no steadfast conclusions could be made. Nevertheless, these context dependent results may be attributed to a highly variable expression of PDE5 in CRC, or by uneven representation in each cohort of CRC subtypes, which could exhibit heterogeneous PDE5 expression. More

insight may be gained by RT-qPCR or western blot analysis of PDE5 expression using multiple large cohorts which include subtype representation. Additionally, meta-analysis of publicly available RNA-seq data from the Gene Expression Omnibus or other repositories may identify overarching patterns of expression between CRC and normal tissues or between CRC subtypes (Edgar et al., 2002). Despite the ambiguity of PDE5 expression in CRC, inhibition and resultant cGMP increase has a clear chemopreventative effect in CRC (Islam et al., 2017; Sharman et al., 2018).

3.3.10.6 PDE8

In this project, TCGA RNA-seq data and THPA IHC analysis showed PDE8A to be downregulated in CRC. Furthermore, THPA survival data linked higher PDE8A expression to improved patient outcomes. In the literature, PDE8A has been shown to promote growth of K-Ras/c-Raf dependent cancers by preventing inhibition of c-Raf via phosphorylation by PKA (Mukherjee et al., 2024; Cooke et al., 2024). This pro-cancer role seems to conflict with the downregulation of PDE8A and its prognostic role in CRC shown in this project. However, given that PDE8A opposes c-Raf inhibition by forming cAMP deficient nanodomains around c-Raf (Cooke et al., 2024), this inhibition may operate regardless of bulk-level PDE8A expression. Furthermore, the RNA-seq data in this project did not account for subtypes dependent on K-Ras/c-Raf, and any differential expression specific to these subtypes may have been masked by averaging into one cancer group. Nevertheless, given the strong downregulation in CRC and the protective role of PDE8A, it may participate in protective mechanisms opposing CRC tumorigenesis independent of c-Raf. Exploratory analysis of PDE8A expression across CRC subtypes may identify associations between PDE8A and specific pathogenic pathways. This could be done by IHC, RT-qPCR, or western blot of large cohorts with subtype representation.

3.3.10.7 PDE9

PDE9A was found downregulated in CRC by TCGA RNA-seq and western blot of patient tissues. In the literature, one study similar to this project employed a database mining approach centred mainly on TCGA and THPA to characterise PDE9A and also discovered strong downregulation in CRC (Susmi et al., 2021).

However, their analysis of THPA PDE9A IHC images, which were also used in this project, was misguided. They misleadingly claimed PDE9A to be downregulated in the CRC tissue, with no reference to the images of the normal tissue, which indicated an equal absence of PDE9A expression (Susmi et al., 2021). The authors also made misleading claims regarding the association between PDE9A expression and patient survival. They generated numerous Kaplan-Meier survival analyses of patients stratified by high and low PDE9A expression and claimed a correlation between PDE9A and patient outcomes, despite the fact that none of the plots showed statistical significance (Susmi et al., 2021).

Regardless, TCGA RNA-seq analysis in this project indicated strong downregulation in CRC compared to normal tissue. Additionally, this pattern was also demonstrated at the protein level for the first time by western blot of patient tissues. Together these data support strong downregulation of PDE9A in CRC. In follow up studies, a possible dependence of PDE9A downregulation on CRC subtype could be investigated by RNA-seq, IHC, RT-qPCR, or western blot using cohorts with subtype representation. Furthermore, a similar approach could be used to determine an association with CRC treatment response, and these results would indicate the value of PDE9A as a prognostic marker.

3.3.10.8 PDE10

A large body of literature describes PDE10 as upregulated in CRC by RT-qPCR, western blot, and IHC of cell lines, mice models of CRC, and patient tissues (N. Li et al., 2015; Nan Li et al., 2015; Lee et al., 2015; Lee et al., 2021). This agreed with TCGA RNA-seq data in this project which showed PDE10A to be upregulated. However, PDE10A upregulation was not found in the rectal cohort by RNA-seq, but this may be attributed to the lower sample number compared to the colon cohort.

As for PDE5, PDE10 inhibition in CRC cell lines was shown to reduce proliferation, suggesting that PDE inhibitors could be used for primary CRC treatment beyond chemoprevention (Lee et al., 2015). However, this effect was shown to be due to off-target effects induced by the extremely high dose of compound (Hou et al., 2022b). Additionally, cGMP signalling, while exhibiting efficacy for chemoprevention, was shown not to inhibit proliferation of CRC

tumours in a mice model (Islam et al., 2022). This suggests that inhibition of PDE10 for the increase of cGMP in established tumours would not be an effective treatment, even though PDE10 appears upregulated in CRC. Furthermore, since cGMP synthesis is downregulated in CRC, inhibiting hydrolysis by PDE inhibition may not result in an impactful increase of cGMP. It would be useful to validate this by testing PDE10 inhibitors, and also PDE5 inhibitors, on mouse- or patient-derived organoids or mouse models (Heyer et al., 1999). Changes in cGMP concentration could be detected by ELISA (Hackett et al., 2014), and effects on proliferation could be assessed by tracking organoid size or by western blot analysis of proliferation markers like Ki-67.

3.3.11 Conclusions

Generally, reports in the literature about PDE expression and function in CRC are either sparse or in disagreement. In this project, broad downregulation of PDEs in CRC was found in addition to upregulation of a few genes, and some of these findings were in agreement and some in disagreement with previous reports. This highlights the need for comprehensive profiling of PDE expression in CRC, which could be achieved by RNA-seq, RT-qPCR, IHC, and western blot analysis of multiple large cohorts. Furthermore, if data or samples from different CRC subtypes is available, subtype-specific PDE expression patterns could be characterised, which could be valuable for prognosis or reveal subtype-specific pathogenic mechanisms. Serving as a starting point, this research paves the way for future efforts that could provide more tangible targets for prognosis and treatment. By addressing these gaps in understanding, subsequent studies can enhance the development of prognostic methods and targeted therapies and improve patient outcomes.

All of the methods in this chapter were based on computational methods, except from THPA IHC datasets. For this reason, it was important to ensure that expression patterns were representative of the epithelial cells in CRC and did not originate from stromal tissues or the immune microenvironment. This investigation is described in the proceeding chapter.

Chapter 4 scRNA-seq analysis of PDE expression in colorectal cancer

4.1 Introduction

In the previous chapter, PDE expression in CRC was assessed by data mining of publicly available repositories to uncover pathogenic associations and identify potential targets for prognosis or therapeutic development. Furthermore, validation of differential PDE expression found by computational methods was performed on patient tissues using RT-qPCR and western blot. Resultingly, most PDE genes and the cAMP and cGMP signalling pathways were found to be downregulated in CRC, with the exception of PDE7A and PDE10A which were upregulated.

Having identified these expression patterns, it was important to ensure that they were biologically representative of normal and cancerous epithelial cells in CRC rather than alterations of the stroma or immune microenvironment. For this purpose, scRNA-seq analysis was used to determine differential expression within specific cell populations. In addition, the pathogenic pathways and mutational landscapes of CRC are highly divergent between subtypes, such as MSI status (Al-Joufi et al., 2022). Stratification of samples by CRC subtype could reveal subtype-specific changes which may be masked by analysing all CRC samples together as a single cancer group. Although the results described in the previous chapter indicated that PDE expression was homogenous across tumour stage and location within the colon and rectum, PDE expression may be dependent on other subtype classifications, such as MSI status. To determine if this was the case, a scRNA-seq dataset with MSI classification was chosen for analysis from the Gene Expression Omnibus.

To this end, the work presented in this chapter was carried out with the following aims:

1. To perform scRNA-seq analysis on a publicly available dataset from the Gene Expression Omnibus to analyse differential PDE expression within the epithelial cell population.

2. To carry out gene set enrichment analysis of the cAMP and cGMP signalling pathways.

3. To conduct differential expression analysis on epithelial cells stratified by MSI status to identify MSI-linked PDE genes.

4.2 Results

4.2.1 Cell clustering and annotation

The scRNA-seq dataset GSE200997 was selected for analysis and comprised 16 tumour and 7 normal tissues. The raw count matrix and cell annotations were downloaded and consisted of 49,828 cells. This dataset was processed using a standard Seurat pipeline. After quality control and doublet removal, the 26,212 remaining cells were clustered and visualised by t-distributed stochastic neighbour embedding (t-SNE) (Figure 4-1). The cells formed numerous clusters and grouped together by cell type (cancer or normal) within the clusters.

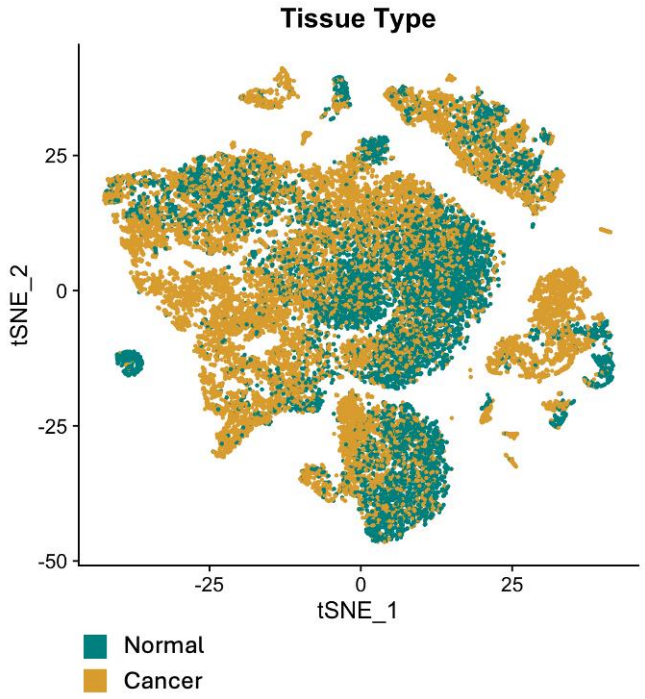

Figure 4-1. Cells from normal and colorectal cancer clustered and annotated by tissue type. 26,212 total cells clustered and visualised using t-SNE.

The expression of marker genes was then visualised across the clusters for approximation of major cell types (Figure 4-2). Accordingly, the expression of KRT8, KRT18, and EPCAM identified the epithelial cell population, THY1 marked fibroblasts, PECAM1 located endothelial cells, CD3D revealed T cells, CD79A identified B cells, and LYZ indicated myeloid cells.

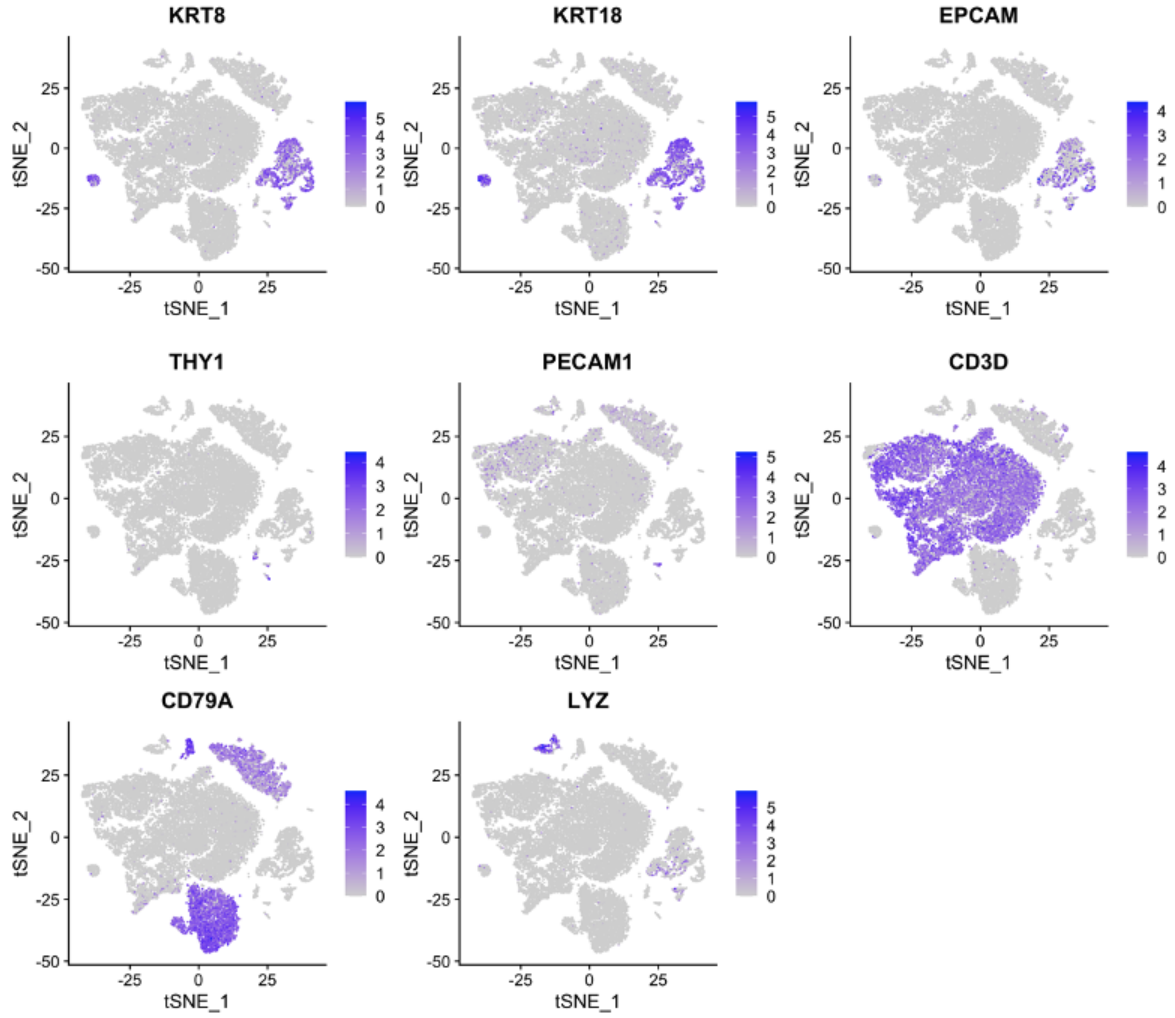

Figure 4-2. Marker gene expression of normal and colorectal cancer cells.
Canonical marker genes were visualised to identify epithelial cells (*KRT8*, *KRT18*, and *EPCAM*), fibroblasts (*THY1*), endothelial cells (*PECAM1*), T cells (*CD3D*), B cells (*CD79A*), and myeloid cells (*LYZ*). Expression level indicated by normalised counts. Cells n=26,212.

The clusters were then annotated by cell type, and strong separation of cells by cell type could be seen (Figure 4-3). Notably, epithelial cells shown in blue formed two clusters: cluster 1 comprised the majority of epithelial cells and contained a mix of both normal and cancer cells, while cluster 2 was much smaller and was formed of mostly normal cells.

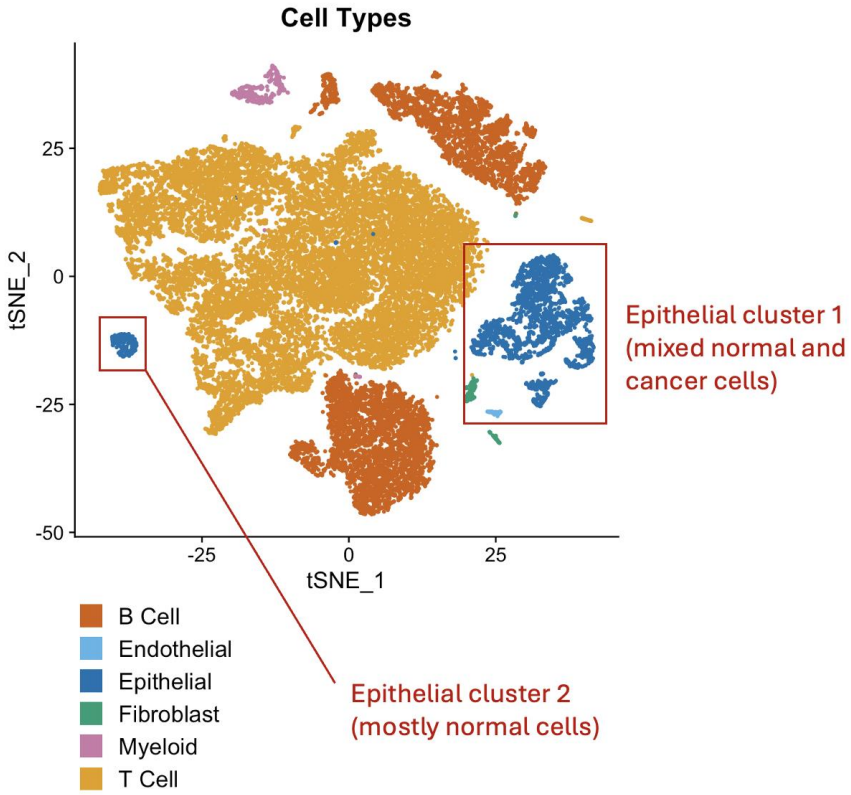

Figure 4-3: Cells from normal and colorectal cancer clustered and annotated by cell type. 26,212 total cells clustered and visualised using t-SNE. Cell type was determined by marker gene expression. Cells n=26,212. The epithelial cells formed two clusters, which are indicated by red boxes.

4.2.2 Differential expression of epithelial cells

All epithelial cells were combined into a separate dataset, and differential expression was determined between CRC and normal cells at the single-cell level. To provide initial validation, expression of marker genes associated with normal and CRC cells were checked. In the cancer epithelial cells compared to normal, the normal epithelial cell marker CA2 was found downregulated and the CRC markers CST1 and LYZ were found upregulated, reflecting expression profiles consistent with their physiological state (Figure 4-4:A). Next, differential expression across the PDE family was assessed, and PDE1C, PDE2A, PDE3A, PDE4D, PDE8A, and PDE9A were found downregulated in CRC compared to normal epithelial cells (Figure 4-4:B).

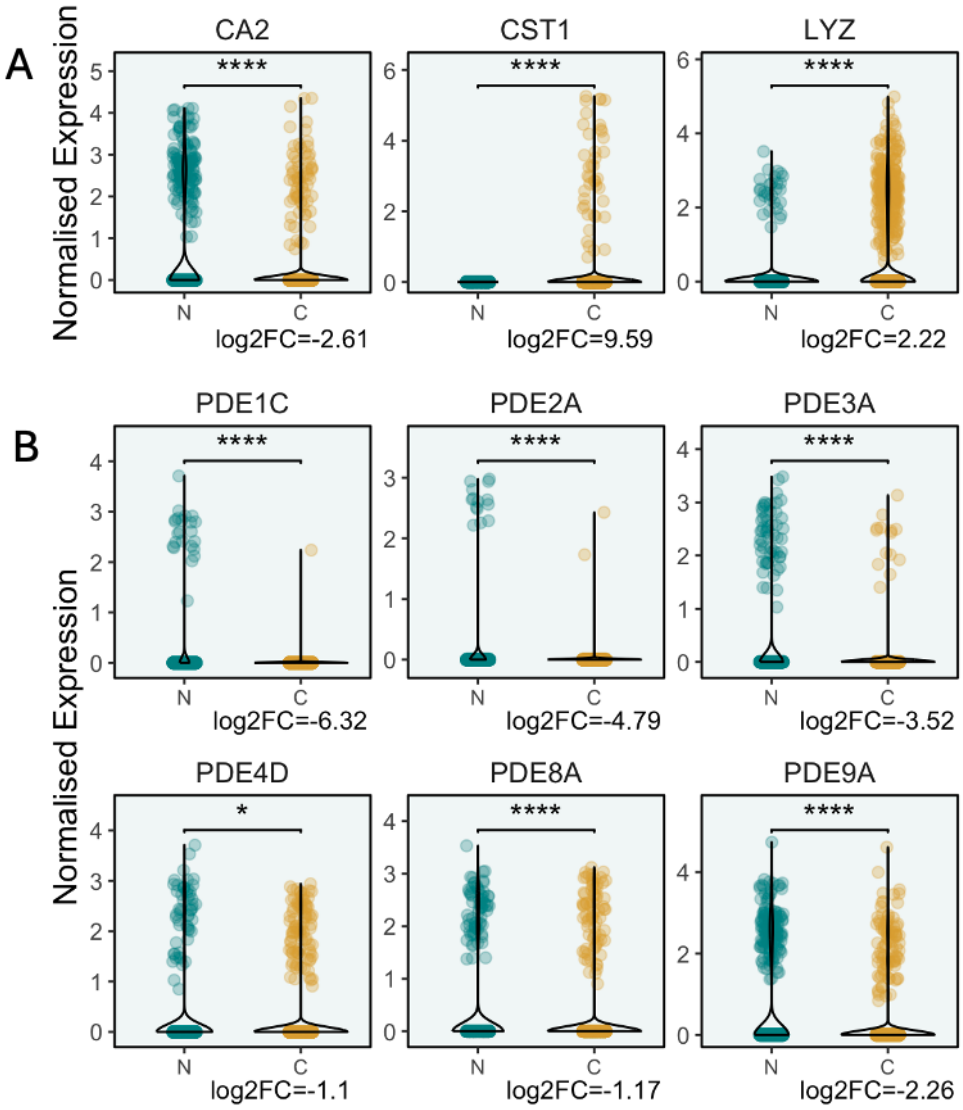

Figure 4-4. Differentially expressed genes between colorectal cancer and normal epithelial cells.
A: Differential marker gene expression of malignant colorectal epithelial cells and normal epithelial cells. B: Differential phosphodiesterase (PDE) expression. Significance signified by Benjamini-Hochberg adjusted p values. *p<0.05, **p<0.01, ***p<0.001, ****p<0.0001. Cancer n=1762, normal n=726.

To visualise the spatial distribution of gene expression across the cancer and normal epithelial cells, the epithelial cells were clustered separately from other cell types and t-SNE plots were generated (Figure 4-5). Notably, there was an inverse and spatially separated expression profile within the normal epithelium between PDE1C, PDE2A, and PDE4D (localised to cluster 1) and PDE3A and PDE9A (localised to cluster 2), while PDE8A was evenly distributed.

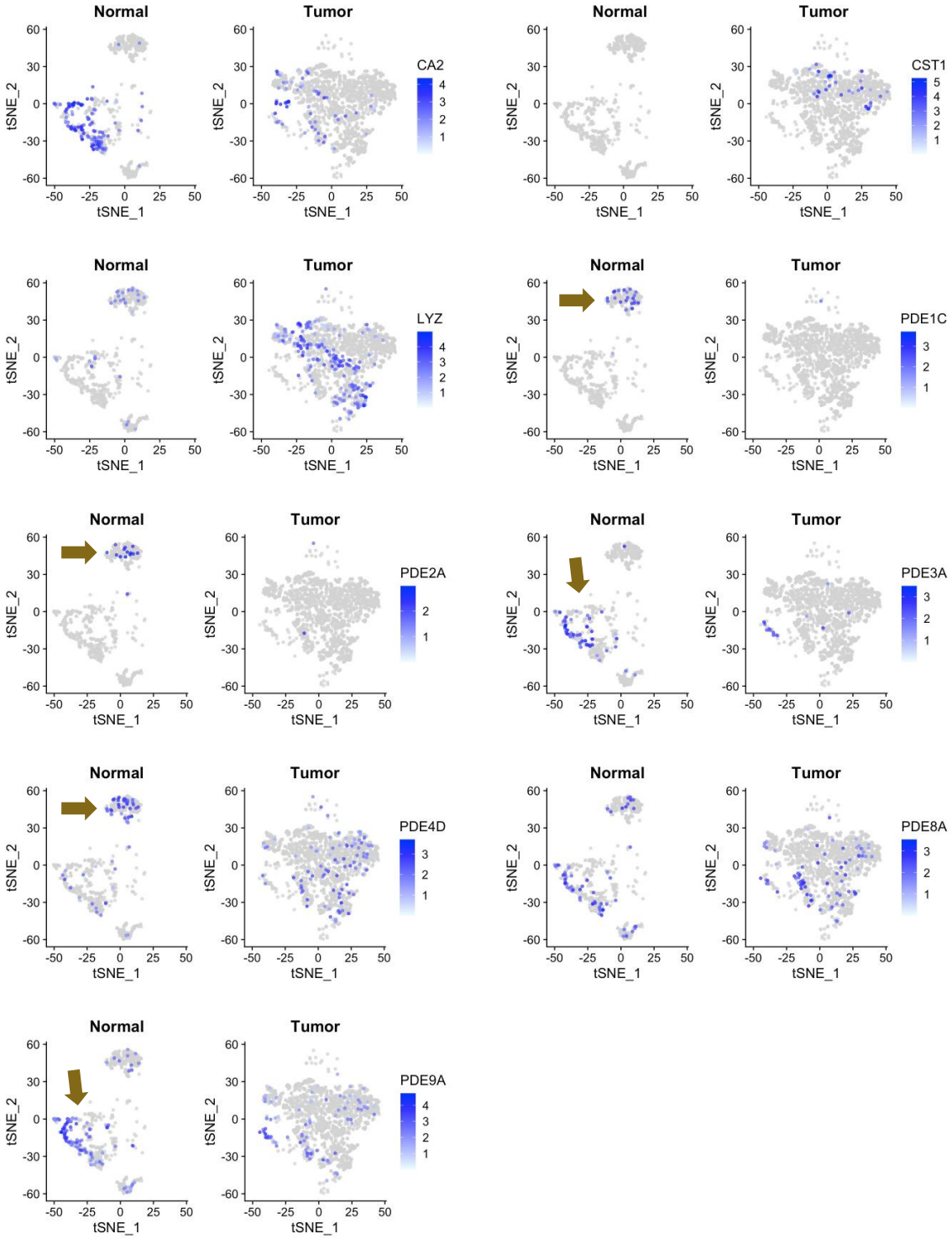

Figure 4-5. Gene expression of marker genes and phosphodiesterases in colorectal cancer and normal epithelial cells.
t-SNE plots indicating gene expression as log-normalised counts. Some phosphodiesterase (PDE) genes were found to localise to the upper epithelial cluster (cluster 2) or the lower cluster (cluster 1) in normal cells. Cancer n=1762, normal n=726.

Differential expression at the single-cell level can lead to a high level of false positives, as each cell is treated as an individual sample with no consideration of sample or patient groupings (Lee and Han, 2024a). In order to assess PDE expression more rigorously, pseudobulk differential analysis was performed, in

which cells were aggregated by patient and tissue type. Reflecting the stricter statistical method and the relatively low sample number (cancer n=16, normal n=7) compared to the cell-based analysis (cancer n=1762, normal n=726), significant differential expression was only found for CA2, PDE8A, and PDE9A, while PDE3A showed a trend towards significance (Figure 4-6:A-B).

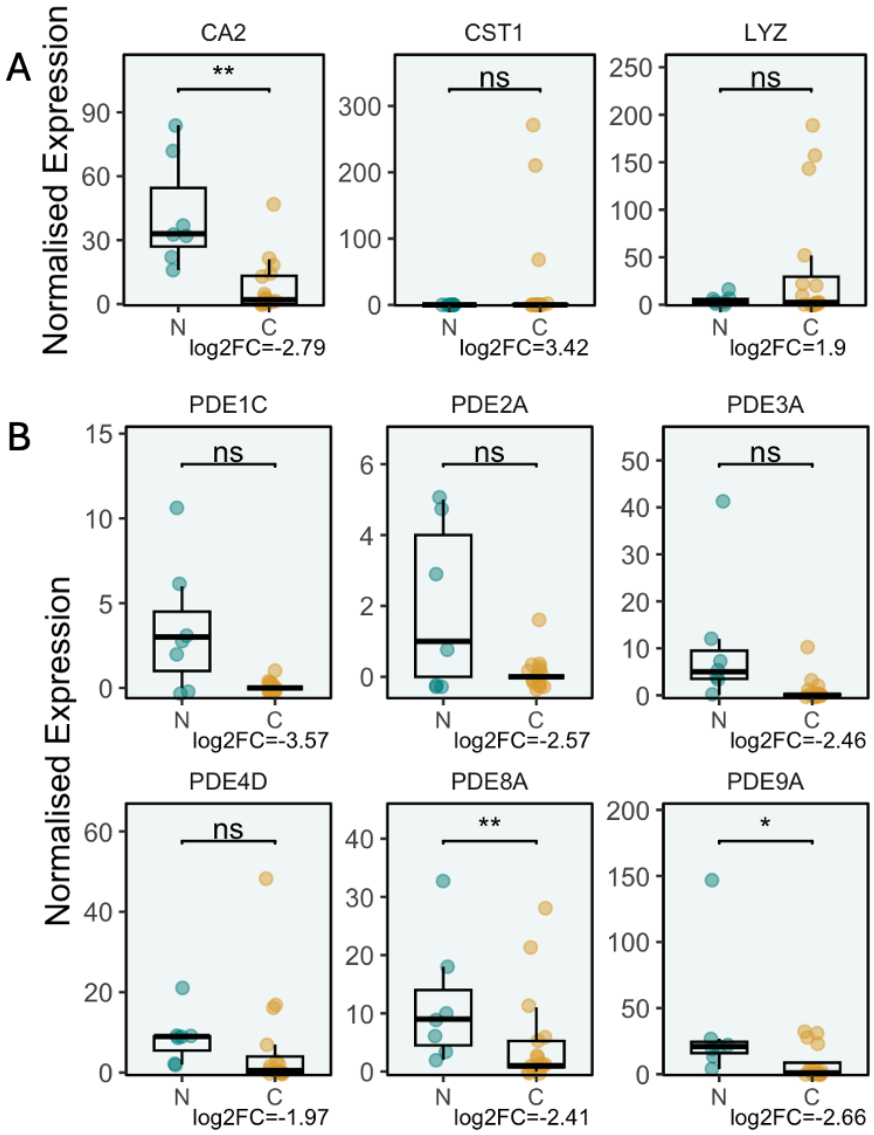

Figure 4-6. Differentially expressed genes between colorectal cancer and normal epithelial cells at the pseudobulk level.
A: Differential marker gene expression of malignant colorectal epithelial cells and normal epithelial cells. B: Differential phosphodiesterase (PDE) expression. Cells were aggregated by patient and tissue type, and differential expression was determined using DESeq2. Significance was signified by Benjamini-Hochberg adjusted p values. ns>0.05, *p<0.05, **p<0.01, ***p<0.001, ****p<0.0001. Cancer n=16, normal n=7.

4.2.3 cAMP and cGMP pathway gene set enrichment analysis

To determine whether the cAMP and cGMP signalling pathways were perturbed as a whole beyond PDE expression in the cancer epithelial cells compared to the normal epithelial cells, GSEA was carried out. The differentially expressed genes between cancer and normal epithelial cells, determined at the single-cell level, were tested against the cAMP pathway (hsa04024) and the cGMP-PKG pathway (hsa04024) using GSEA (Figure 4-7). Both pathways were found significantly depleted, as indicated by a negative normalised enrichment score (NES), in the cancer epithelial cells compared to the normal epithelial cells.

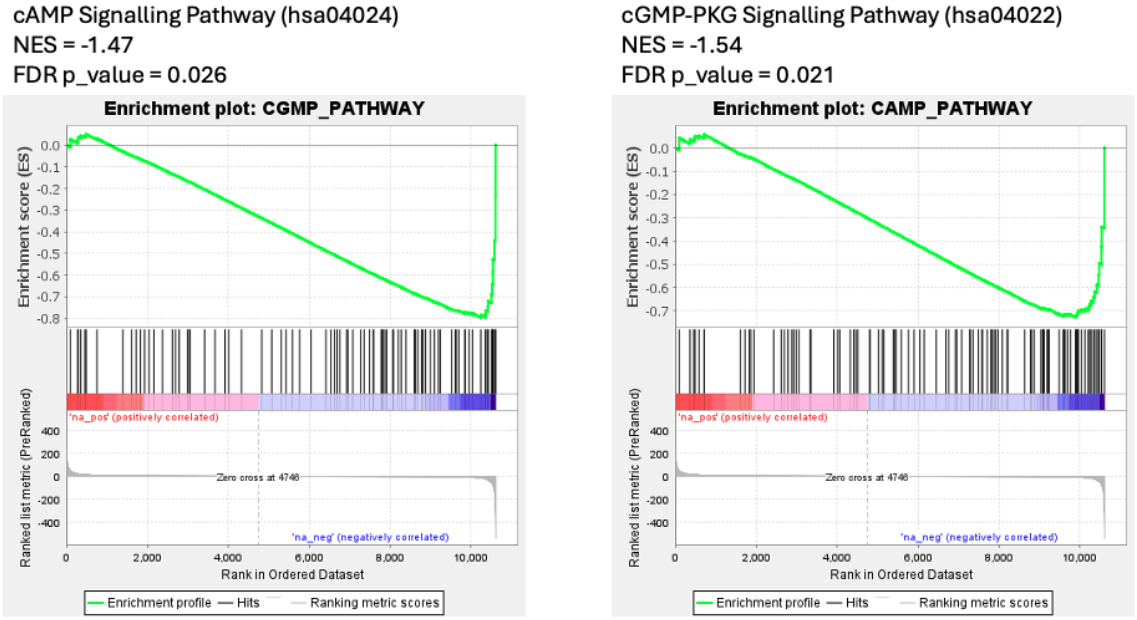

Figure 4-7. Gene set enrichment analysis (GSEA) of cAMP and cGMP signalling pathways between cancer and normal epithelial cells.
Differentially expressed genes were pre-ranked by a signed score metric (log2FoldChange * (-log10(p_value))) and tested against the hsa04024 and hsa04022 pathways using GSEA. Normalised Enrichment Score (NES) indicates gene set upregulation or downregulation normalised for gene set size. Benjamini-Hochberg corrected p values are indicated by FDR p_value. Cancer n=1762, normal n=726.

To get an overview of the individual genes and their arrangements in the pathways, the R package Pathview was used to visualise the differential expression. By inspection of the cAMP signalling pathway (hsa04024), broad downregulation of many genes could be seen (Figure 4-8). Upstream in the pathway, adenylate cyclase (AC) was downregulated. After cAMP, *PKA* was downregulated and formed a central hub of target genes, many of which were

also downregulated. In contrast, key components of this pathway were found upregulated, including the *PKA* target *CREB* and the cAMP effector *EPAC*.

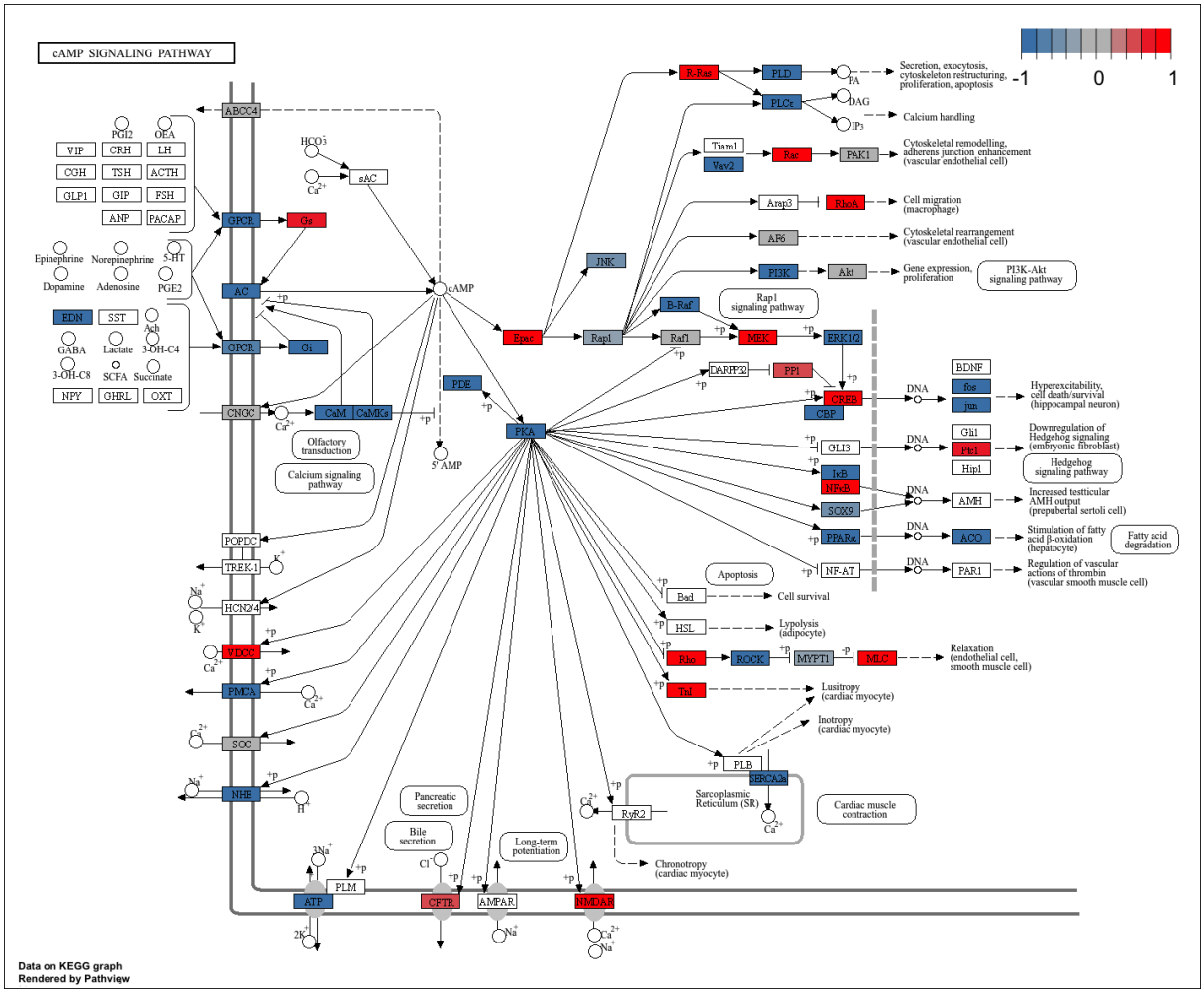

Figure 4-8. Pathview visualisation of differential gene expression in the cAMP signalling pathway (hsa04024).
Differential gene expression represented by a signed score metric (log2FoldChange * -log10(p_value)), with values ranging from low to high indicated by a blue to red gradient. Cancer n=1,762, normal n=726.

Using Pathview analysis of differential gene expression in the cGMP-PKG pathway, broad downregulation of genes was found in CRC compared to normal epithelial cells, many of which formed a hub around *PKG*, which was also downregulated. However, expression of guanylate cyclases (NPR-A/GUCY2A, NPR-B/GUCY2B) could not be determined. Interestingly, homogenous differential expression was not observed in the PI3K/AKT and RAF/MEK/ERK cancer-linked pathway modules, with genes indicating mixed modulation. Within the PI3K/AKT module for instance, *PI3K* was downregulated, *AKT* was not differentially expressed, whereas in the RAF/MEK/ERK module, *RAF1* was not differentially expressed, *MEK* was upregulated, and *ERK* was downregulated.

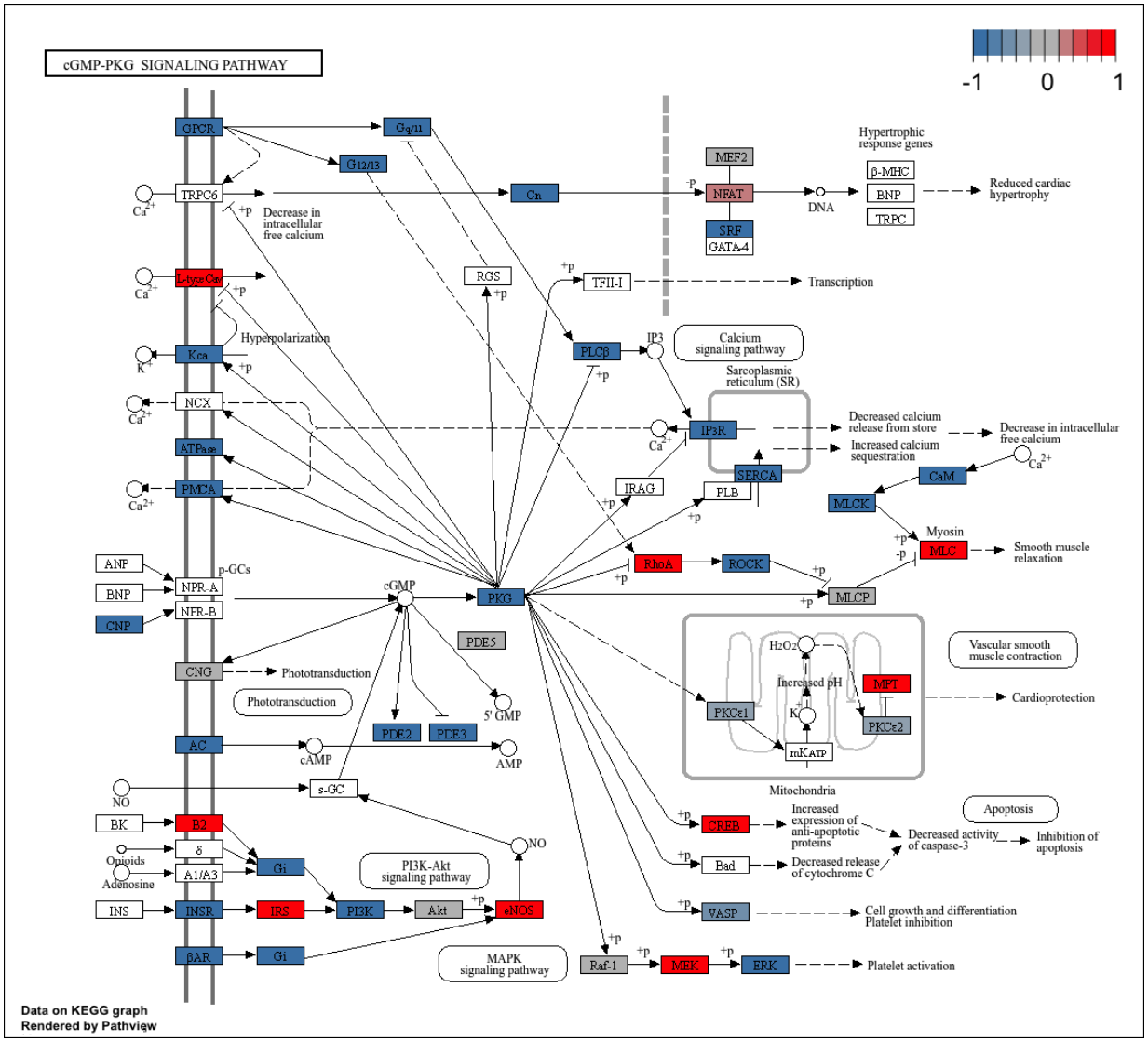

Figure 4-9. Pathview visualisation of differential gene expression in the cGMP-PKG signalling pathway (hsa04022).
Differential gene expression represented by a signed score metric (log2FoldChange * -log10(p_value)), with values ranging from low to high indicated by a blue to red gradient. Cancer n=1,762, normal n=726.

4.2.4 Differential PDE expression in microsatellite instable colorectal cancer

Differential expression analysis was carried out across normal, MSS, and MSI-H samples (Figure 4-10). By dimensionality reduction, the cells were shown to cluster by MSI status (Figure 4-10:A). To verify that the gene expression of the cells was representative of MSI status, expression of four marker genes was checked: MLH1, MSH2, MSH6, and PMS2. MLH1 was found downregulated in MSI-H cells compared to normal epithelial cells, but MSH2, MSH6, and PMS2 were not differentially expressed. For the PDE superfamily, PDE1C, PDE2A, PDE3A, PDE8A, and PDE9A were significantly downregulated in both CRC subtypes relative to

normal cells, and expression was not significantly different between MSS and MSI-H cells (Figure 4-10:B). On the other hand, PDE5A was upregulated in MSI-H compared to MSS cells, and PDE11A was strongly upregulated in MSI-H compared to MSS and normal cells.

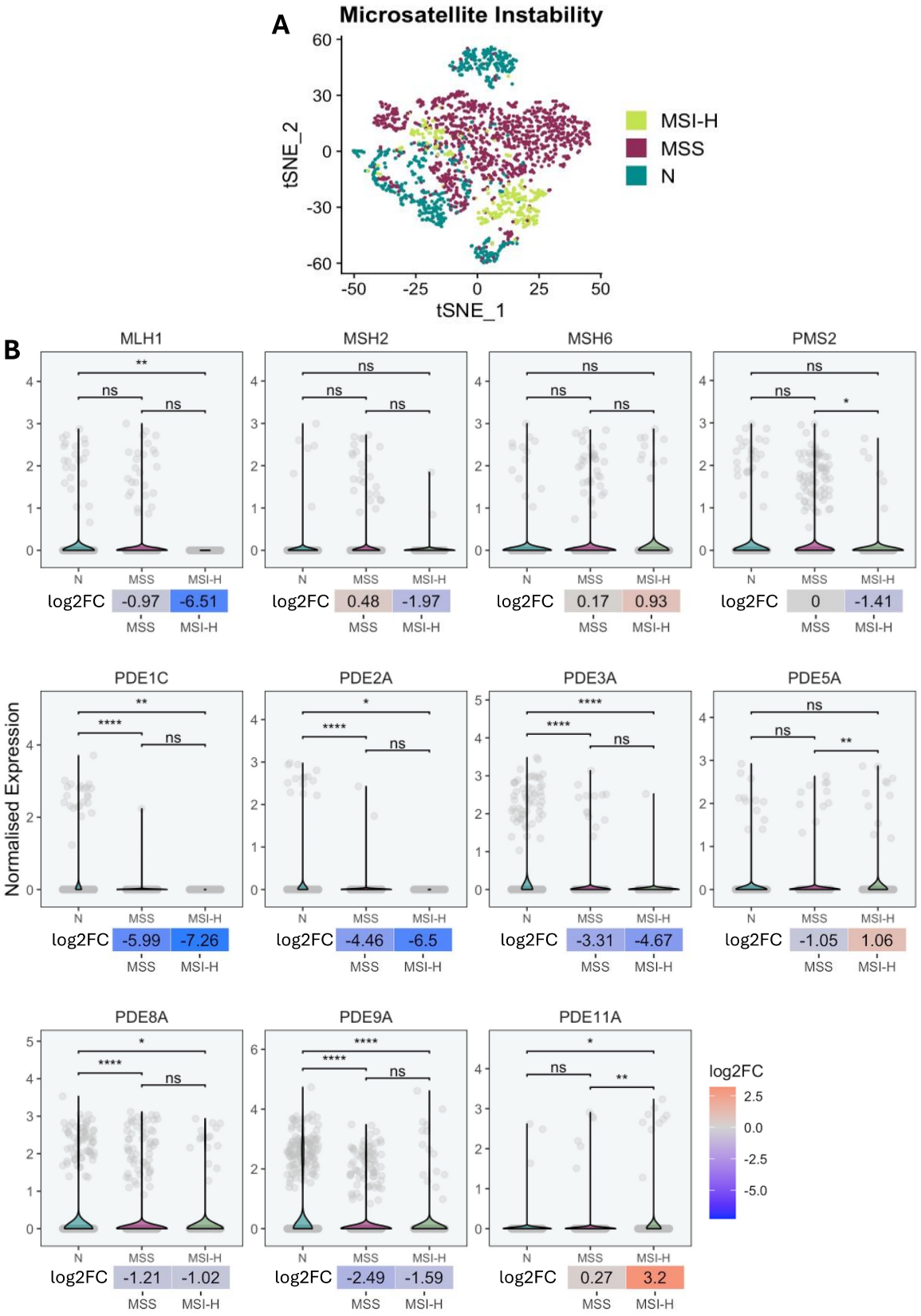

Figure 4-10. Differential expression of epithelial cells stratified by microsatellite instability status

A: t-SNE plot of cells coloured by microsatellite instability (MSI) status. B: Differential expression of MSI marker genes and phosphodiesterase (PDE) genes. MSI-H; microsatellite instable colorectal cancer (CRC), MSS; microsatellite stable CRC, N; normal cells, log2Fc; log2(fold change). Significance indicated by Benjamini-Hochberg adjusted p values. ns>0.05, *p<0.05, **p<0.01, ***p<0.001, ****p<0.0001. MSI-H n=726, MSS n=1401, N n=361.

4.3 Discussion

4.3.1 Cell clustering and annotation

In this chapter, scRNA-seq analysis was employed to examine differential expression of PDEs within the epithelial cell population as opposed to the stroma and immune microenvironment. Additionally, a scRNA-seq CRC dataset was selected, which included MSI status of patients, allowing for PDE expression to be analysed across MSI-H, MSS, and normal epithelial cell types. Since mutational landscape and pathogenic pathway are highly dependent on CRC subtypes, such as MSI status (Al-Joufi et al., 2022), it is plausible that PDE expression is similarly dependent. Identification of MSI-specific PDEs could be of value for prognosis and therapeutic development or reveal associations with MSI pathogenesis.

After standard quality control, doublet removal and clustering, the cluster cell types were determined by examining expression of canonical marker genes (R. Wang et al., 2022). Resultingly, expression of KRT8, KRT18, and EPCAM led to the identification of two epithelial cell clusters: a smaller cluster of normal cells, and a large cluster of both normal and CRC cells.

In the original work published on this dataset, these two epithelial clusters were also identified by the authors (Khaliq et al., 2022). Given that the smaller epithelial cluster was comprised almost entirely of normal cells, this group may represent a certain cell type within the normal epithelium, such as goblet cells or enteroendocrine cells (Colony, 1989). To explore differences in expression profile between the two clusters, gene ontology (GO) analysis was performed. However, the eclectic mix of pathways found enriched did not provide a clear physiological explanation for the difference between the clusters (data not shown). Given that this second cluster represented only a small proportion of normal cells, and that characterisation of normal epithelial cell subtypes was beyond the scope of this project, distinction between the two clusters was not made during differential expression analysis between the normal and cancer epithelial cells. Nevertheless, further characterisation could reveal associations between PDE expression and normal epithelial cell subtypes or CRC pathogenic pathways before tumorigenesis. This could be done by visualising expression of

more granular marker genes associated with epithelial subpopulations (Montoro et al., 2020). Also, these normal epithelial cell clusters may originate from patients with specific subtypes. For example, hypothetically, cluster 1 may originate from patients with MSI-H CRC, while cluster 2 originates from MSS CRC patients, or vice versa. By detailed examination of differential gene expression between these clusters, genes associated with subtype-specific CRC pathogenesis before tumorigenesis could be found.

4.3.2 Differential expression in colorectal cancer epithelial cells

Once the epithelial population was identified, differential PDE expression in the cancer cells was determined at the single-cell level by Wilcoxon Rank Sum test (Satija et al., 2015). As an initial validation step, expression of three marker genes was assessed. The carbonic anhydrase gene CA2 has been inversely linked to colorectal adenoma and tumour growth and is a marker for non-cancerous epithelial cells (Maurya et al., 2023). Conversely, the cysteine protease inhibitor gene CST1 and a gene coding for an enzyme that digests bacterial cell walls LYZ are both associated with proliferation and CRC progression (Jiang et al., 2018; Glyn et al., 2024). By single-cell level differential analysis, CA2 was downregulated, and CST1 and LYZ were upregulated. These findings indicated that the expression profile of the cancer and normal epithelial groups are representative of their expected biological state and supported the validity of subsequent PDE expression analysis.

By scRNA-seq differential expression analysis between CRC and normal epithelial cells, significant downregulation was found for PDE1C, PDE2A, PDE3A, PDE4D, PDE8A, and PDE9A. This agreed with the bulk-level TCGA RNA-seq data (Section 3.2.1.1), supporting downregulation of these genes to be a robust pattern in CRC. Nevertheless, differential expression of many PDE genes identified at the bulk level were not found at the single-cell level. This was true for genes PDE1A, PDE1B, PDE3B, PDE5A, PDE6A, PDE6B, PDE6G, PDE7B, and PDE8B found downregulated, and genes PDE7A and PDE10A found upregulated in TCGA colon and rectal cohorts. Since the scRNA-seq analysis indicated the same findings as the bulk analysis, albeit with fewer of the PDE genes found significantly changed, the difference could be attributed to the reduced statistical power of scRNA-seq compared to bulk RNA-seq, resulting from lower sequencing depth

and signal-to-noise ratio (Zyla et al., 2023). This would prevent weaker changes in PDE expression from being detected. Alternatively, it was possible that these differential PDEs detected only by bulk RNA-seq originated from alterations in stromal cells or the immune microenvironment in CRC. Though unlikely, this could not be ruled out, and further investigation could be done by scRNA-seq differential PDE expression analysis within these non-epithelial cell populations. Nonetheless, these results, in addition to bulk-level cross-validation in TCGA cohort, support PDE1C, PDE2A, PDE3A, PDE4D, PDE8A, and PDE9A to be strongly downregulated in CRC epithelial cells. In future work, having comprehensively characterised these genes at the mRNA level, it would be important to validate that these changes translate to the protein level.

4.3.3 Differential PDE expression at the single-cell and pseudobulk level

The single-cell level differential expression results were validated using pseudobulk analysis. Single-cell level analysis is advantageous since the large number of cells is leveraged, leading to increased sensitivity (Lee and Han, 2024a). However, each cell is treated as an independent sample with no consideration for patient-origin dependency, increasing the risk for p value inflation and false positives (Lee and Han, 2024a). Additionally, single-cell level count data often has a complex and inconsistent distribution with many zero counts. This can be difficult to model, and real expression changes can be obscured (Lee and Han, 2024a). Pseudobulk analysis overcomes this by averaging cells across patients and tissue types, which accounts for patient grouping and reduces variability and zero-inflation of count distributions (Lee and Han, 2024b). However, weaker expression patterns can be lost, and statistical power is reduced due to the smaller sample size (Lee and Han, 2024b).

By pseudobulk analysis, only CA2, PDE8A, and PDE9A were found differentially expressed while the other significant genes identified by single-cell analysis were lost, reflecting the smaller group sizes and the reduced statistical power after cell aggregation. Also of note, PDE3A approached significance and was downregulated. Overall, this highlights PDE8A and PDE9A downregulation as a strong and consistent change in CRC, increasing confidence in the findings, as

the strongest expression patterns were consistent across both methods used in this project.

4.3.4 PDE expression distribution across the normal epithelial cells

Once certain PDEs were identified as downregulated in the CRC epithelial cells compared to the normal cells, their expression was visualised across the epithelial cell cluster using t-SNE. Upon inspection, downregulation could clearly be seen, but it was surprising to see that some PDEs had an almost mutually exclusive distribution in the normal cells. While PDE8A was evenly expressed across the two normal epithelial clusters, PDE1C, PDE2C, and PDE4D were localised mainly to the smaller cluster, cluster 2, while PDE3A, and PDE9A were restricted to the larger cluster, cluster 1. This binary expression pattern clearly shows that there are subtypes within the normal epithelial cells which are characterised by distinct PDE expression profiles. Although beyond the scope of this project, it would be fascinating to see if PDE expression correlates to specific cell lineages within the epithelia (Colony, 1989), or to patients predisposed to tumours of a specific pathogenic subtype or phenotype, as discussed above (Section 4.3.1).

4.3.5 Pathway analysis

GSEA and Pathview analysis indicated that the cAMP and cGMP-PKG pathways were broadly downregulated in the cancer epithelial cells compared to the normal cells, and this agreed with the bulk-level TCGA RNA-seq dataset (Section 3.2.1.1). For cGMP, this was consistent with its established tumour suppressive role in CRC and the downregulation necessary for tumorigenesis (Rappaport and Waldman, 2018). For cAMP, these findings suggest that cAMP could play a similar protective role in CRC and could be equally downregulated during tumorigenesis.

Interesting expression patterns of other genes were shown by the Pathview representation of cAMP and cGMP pathway depletion. The cAMP effector EPAC and the PKA effector CREB were found upregulated in the CRC epithelial cells. EPAC has demonstrated both pro- and anti-cancer effects depending on cancer type and context (Wehbe et al., 2020; Zhang et al., 2024), but these data support a deleterious action of EPAC in CRC. Conversely, CREB has a clear

deleterious action in cancer and CRC (Cheng et al., 2020; Sapio et al., 2020), and this was reflected by the upregulation found by Pathview. Nonetheless, the Pathview data represented a gene family average, and inspecting differential expression of separate EPAC and CREB genes would be much more insightful. Similarly, this may explain the mixed modulation of PI3K/AKT and RAF/MEK/ERK genes shown by Pathview. Furthermore, this analysis did not account for CRC subtypes, which exhibit highly divergent pathways of pathogenesis. Therefore, averaging subtypes together as one group here likely obscured subtype-specific expression of cancer signalling pathways. For detailed characterisation of cancer signalling pathways, separate GSEA and Pathview analysis could be conducted in addition to examining individual gene expression and performing validation by RT-qPCR, western blot, and IHC on patient tissues while accounting for CRC subtypes.

4.3.6 Differential PDE expression in microsatellite instable colorectal cancer

Microsatellite stable and instable CRC tumours exhibit different mutational profiles and pathogenic pathways (Boland and Goel, 2010). Profiling PDEs across these subtypes may reveal mechanistic roles and targets for prognosis or therapy that were obscured by averaging into a single cancer group. To this end, differential gene expression analysis was performed at the single-cell level between MSI-H, MSS, and normal epithelial cells.

To validate the reliability of the data, the expression of MSI marker genes was determined. The genes MLH1, MSH2, MSH6, and PMS2 are essential components of the MMR system that maintains genomic stability (Baretti and Le, 2018). Genetic or epigenetic loss of these genes is central to pathogenesis of inherited CRC (Lynch Syndrome/HNPCC) and MSI CRC (Boland and Goel, 2010). For more information, see Section 1.3.2. By scRNA-seq, strong downregulation of MLH1 was observed in the MSI-H but not the MSS cells. On the other hand, MSH2, MSH6, and PMS2 were not found differentially expressed. This was unexpected but may be explained by the low sequencing depth and statistical power of scRNA-seq (Zyla et al., 2023). In addition, MLH1 may be a stronger biomarker for MSI CRC compared to the other genes. This is supported by two studies which described the development of gene signatures for the classification of MSI CRC,

and both included MLH1 but not MSH2, MSH6, or PMS2 (Zhang et al., 2018; Pačínková and Popovici, 2019). Taken together, the strong downregulation of MLH1 in the MSI group validated that the gene expression of these groups in this dataset was representative of their biological states. However, the lack of differential expression detected for the other MMR system genes suggests that larger datasets may be required to detect weaker patterns of expression.

Across the PDE family, PDE1C, PDE2C, PDE3A, PDE8A, and PDE9A were found significantly downregulated in both CRC subtypes relative to normal epithelial cells, and this agreed with the single-cell differential expression conducted between cancer and normal epithelial cells. Importantly, expression of these genes was not dependent on MSI status.

Intriguingly, PDE5A was found significantly increased in MSI compared to MSS cells, but this was not significantly different to normal cells. This suggests that PDE5A may be slightly increased in MSI CRC. However, existing data about PDE5A expression in CRC is conflicting, and cannot provide support for this finding. For instance, bulk RNA-seq and CPTAC proteomic analysis in the previous chapter showed PDE5A to be downregulated in CRC compared to normal tissues. Additionally, reports in the literature involving western blot analysis of CRC cell lines as well as IHC and RT-qPCR analysis of patient tissues indicate divergent results (Tinsley et al., 2010; Whitt et al., 2012; Li et al., 2013; N. Li et al., 2015; Mahmood et al., 2016; Islam et al., 2022). This was discussed in detail in Section 1.8.3.4. For this reason, differential expression of PDE5A across MSI CRC subtypes requires validation in other scRNA-seq cohorts with larger sample numbers. Alternatively, IHC analysis of normal patient tissues and both MSS and MSI-H CRC would validate this finding at the protein level. Nevertheless, these results may reflect a biologically representative upregulation of PDE5A in MSI-H CRC. While one study indicated that cGMP signalling did not reduce proliferation in established tumours, only showing efficacy for reducing polyp initiation in mice models (Islam et al., 2022) (See Section 1.8.2), it would be interesting to validate this finding by testing PDE5 inhibitors on models of MSI-H CRC after tumorigenesis. This could involve the comparison of CRC cell lines exhibiting dMMR like HCT116 and DLD-1 or MMR like WiDr and SW403 (Genther Williams et al., 2015). Alternatively, tumour organoids of MSI and MSS mice models could be used, such as those bearing mutations for MLH1 and APC respectively, but this

would be considerably more expensive (Heyer et al., 1999). Additionally, testing could be performed using patient-derived organoids, which would provide more clinically relevant results but would also be more costly. Though unlikely, if efficacy is discovered, this could represent a strategy for personalised targeted therapy for MSI-H CRC. Additionally, since cGMP synthesis is downregulated in CRC, the increase in cGMP induced by PDE inhibitors may not be sufficient for possible tumour suppression (Hou et al., 2022b). In other words, if there is no substrate present for PDE hydrolysis, then inhibiting PDEs could have no effect.

Aside from PDE5A, PDE11A was found strongly upregulated in MSI compared to MSS and normal cells. This was intriguing, since differential expression was not detected by bulk or scRNA-seq analysis between normal samples and all CRC samples grouped together. In the literature, there are no reports about the role of PDE11 in CRC, but deleterious associations have been found in other cancers including brain, prostate and adrenocortical cancer (Faucz et al., 2011; Kong et al., 2022). As for PDE5, it would be interesting to determine whether PDE11 inhibitors, such as BC11-38 (Ceyhan et al., 2012), could provide a means for personalised targeted therapy of MSI-H CRC.

4.3.7 Summary

Taken together, the results described in this chapter suggest that the broad downregulation of the PDE family in CRC, along with disruption in cAMP and cGMP signalling pathways, is representative of epithelial cells specifically and not of the stroma or immune microenvironment. Additionally, this downregulation was shown to be largely independent of MSI status subtype and the respective pathways of pathogenesis. In theory, potential prognostic or therapeutic methods exploiting these changes in PDE expression or the cAMP and cGMP pathways should be equally effective across MSI subtypes. Crucially, PDE5A and PDE11A displayed a possible upregulation in MSI-H CRC and further research involving functional studies could pave the way for MSI prognostic methods or novel personalised therapies.

Chapter 5 Final Discussion

In CRC, advancements in chemotherapy and targeted therapies have been transformative for patient outcomes, yet major challenges persist, including inadequate patient response, difficulty in predicting patient responses, the development of drug resistance, and the lack in understanding of the link between pathogenic subtypes and patient response (Xie et al., 2020; Gmeiner, 2024). For this reason, there is an urgent need for novel targeted therapies, improved means for predicting patient response and prognosis, as well as increased understanding of the mechanisms underpinning pathogenic subtypes (Xie et al., 2020; Gmeiner, 2024).

PDE inhibitors have been greatly successful as established drugs for the treatment of several diseases, including pulmonary hypertension, chronic obstructive pulmonary disease, and heart failure (Schudt et al., 2011). While PDE inhibitors and modulators of cyclic nucleotides cAMP and cGMP have demonstrated utility in preclinical studies in CRC, none have yet completed clinical trials for CRC (Peng et al., 2018). In CRC, the cGMP signalling axis has been well established to have tumour suppressive effects, and cGMP attenuation has been demonstrated as an early and essential event in CRC tumorigenesis (Pitari et al., 2007; Rappaport and Waldman, 2018). Furthermore, inhibitors of PDE5 have been found to reduce CRC risk in population studies (Huang et al., 2019; Sutton et al., 2020; Cullinane et al., 2023), and have exhibited consistent reduction of CRC tumorigenesis in animal models via cGMP increase (Islam et al., 2017; Sharman et al., 2018). For these reasons, PDE5 and PDE10 inhibitors are undergoing preclinical development as CRC chemopreventatives (A. Lee et al., 2023; Ramesh et al., 2023). Considering current research on cGMP hydrolysis by PDE5, the other PDE genes remain understudied in CRC, and it is unclear whether cAMP signalling is protective or deleterious. By characterising the expression of the whole PDE superfamily in CRC, the goal of this thesis was to elucidate the role of PDEs and cyclic nucleotides in CRC and its pathogenic subtypes and to highlight promising targets for the development of therapies or prognostic methods.

5.1 Major findings

By RNA-seq analysis of TCGA datasets, the majority of the PDE superfamily were downregulated in CRC compared to normal tissue, with the highest expression in normal tissue and strongest downregulation observed for PDE3A, PDE4D, PDE5A, PDE8A, and PDE9A. In contrast to this trend, only PDE7A and PDE10A exhibited weak upregulation in CRC tissues. Next, PDE expression was assessed based on several clinical descriptors. By comparison of TCGA cohorts, the colon and rectum exhibited an almost identical profile of differential PDE expression between CRC and normal tissue. This was not entirely unexpected, as colon and rectal cancers occupy neighbouring anatomical sites and share risk factors and similar landscapes of cancer mutation and pathogenesis (Hong et al., 2012). Similarly, comparison of cancer stages after tumorigenesis and of tumour locations within the colon revealed PDE expression to be independent of these factors, and homogenous PDE downregulation was observed across all tumours. This was more surprising, since proximal and distal colon tumours have been proposed to be more distinct in mutational landscape and tumour phenotype than for distal colon and rectal tumours (Hong et al., 2012).

One major finding of the omics analysis in this project was that both the cAMP and cGMP signalling pathways were depleted in CRC compared to normal tissue. This attenuation of cGMP and its protective signalling has been well characterised in CRC, but downregulation of the cAMP signalling pathway was a novel discovery. Given the protective effects of adenylate cyclase agonists in CRC (Gamet et al., 1992; Yoshizawa et al., 1995; Höpfner et al., 2001; McEwan et al., 2007; Cristóbal et al., 2014), this downregulation may reflect an analogous anti-cancer effect of cAMP signalling in CRC. Importantly, scRNA-seq analysis linked downregulation of PDEs and pathways of cAMP and cGMP specifically to the epithelial cell population and not to other cell types present in the surrounding tissue. Of these, PDE3A, PDE8A, and PDE9A were reaffirmed as strongly downregulated in CRC, but downregulation was also shown at the single-cell level for PDE1C, PDE2A, and PDE4D. Furthermore, scRNA-seq analysis also revealed a weak upregulation of PDE5A and a strong upregulation of PDE11A in MSI compared to MSS CRC cells, but PDE1C, PDE2A, PDE3A, PDE8A, and PDE9A exhibited strong and homogenous downregulation regardless of microsatellite instability subtype.

5.2 Conceptual model of major findings

With the key findings of broad downregulation of PDE signalling in CRC tumours regardless of anatomical site, cancer stage, and MSS/MSI pathogenic subtype, in addition to the downregulation observed for cAMP and cGMP pathways in CRC, this project supports the following model (Figure 5-1). Attenuation of cGMP signalling and tumour suppressive functions has been identified as an early and important event in CRC pathogenesis (Pitari et al., 2007; Rappaport and Waldman, 2018). Downregulation of cAMP in CRC found by this project suggests that cAMP has a similar protective role and could be equally attenuated during CRC tumorigenesis. This is supported by preclinical studies demonstrating the anti-proliferative effects of adenylate cyclase agonism and consequent cAMP increase in CRC models (Gamet et al., 1992; Yoshizawa et al., 1995; Höpfner et al., 2001; McEwan et al., 2007; Cristóbal et al., 2014). These two observations could also explain the broad downregulation of PDEs seen here in CRC.

Many PDEs are transcriptionally upregulated in response to cyclic nucleotide signalling in different tissue types, and this could form a means for long term homeostatic negative regulation (Swinnen et al., 1989). For instance, cAMP signalling can trigger transcription of many genes via activating phosphorylation of the transcription factor CREB by PKA. Such pCREB-mediated transcription has been found for PDE3A and PDE3B (Liu et al., 2006; Sucharov et al., 2019). Both genes were found to contain cAMP response elements (CREs) in their promotor regions, which bind pCREB to induce transcription. Accordingly, increase in cAMP levels or treatment of cAMP agonists stimulated PDE3A and PDE3B transcription in various cell types (Swinnen et al., 1989; Swinnen et al., 1991; Liu et al., 2006; Sucharov et al., 2019).

The same mechanism was discovered for PDE4D5, PDE4D6, and PDE4D7, which all contain promotor CREs, and treatment of cAMP agonist induced expression of PDE4D5 (Le Jeune et al., 2002; Wang et al., 2003). Similarly, other work showed transcription of PDE4B, PDE4D1, and PDE4D2 to be inducible by cAMP agonism, but the exact mechanism may involve cAMP-responsive transcription factors Sp1 and AP2 instead of CREB (Swinnen et al., 1991; Vicini and Conti, 1997; Ma et al., 1999). Additionally, promotor Sp1 binding elements have been found for PDE4A10 and PDE4A11. In the promotor region for PDE5A, binding elements have

been found for CREB, Sp1, and AP2, and both sites have been linked to transcriptional upregulation in response to cAMP and cGMP agonism (Kotera et al., 1999; Lin et al., 2001). CRE elements have also been found in the promotor of PDE7A, and ectopic overexpression of CREB or cAMP agonism both were shown to induce transcription of the gene (Lee et al., 2002; Torras-Llort and Azorín, 2003). Similarly, cAMP agonism by 8-Br-cAMP induced expression of PDE7B, although the mechanism remains unelucidated (Sasaki et al., 2004).

From these studies, it is clear that cyclic nucleotide signalling can influence transcription of PDE genes, and this possible homeostatic feedback mechanism would explain broad PDE downregulation in response to disrupted cyclic nucleotide signalling shown in this project. However, these mechanisms described above have only been found for a subset of PDE genes in non-colorectal cell types. Further study is clearly required to determine whether these observations apply to colorectal tissues and are broadly applicable across PDE genes, thus explaining the model proposed here.

Taken together, attenuation of both cAMP and cGMP signalling could be an important event facilitating CRC carcinogenesis, resulting in downstream PDE downregulation as a secondary effect. Critically, PDEs were found to be homogenously downregulated in this project irrespective of tumour location, cancer stage, or MSI subtype, suggesting that this signalling attenuation is an early and ubiquitous event in CRC carcinogenesis. This type of ubiquitous pathogenic pattern has already been demonstrated by the Wnt pathway, which exhibits strong upregulation early in tumorigenesis and is shared across almost all CRC tumours regardless of genotype and phenotype, although the specific activating mutations vary (Müller et al., 2016).

If this model is accurate, then increasing cAMP concentration could be effective for CRC chemoprevention like for cGMP, and could be achieved by either AC agonists, cAMP-specific PDE inhibitors, or a combination of both. In terms of primary targeted treatments after CRC tumorigenesis, this model suggests that PDE inhibitors may not be effective. If PDEs are already downregulated in CRC, as shown by the present work, then further inhibition may not significantly impact cyclic nucleotide levels. Furthermore, cGMP synthesis is well characterised as downregulated in CRC (Pitari et al., 2007). Therefore, if

synthesis is the limiting factor, inhibiting PDEs may not significantly affect cGMP levels. As a work around, PDE inhibitors could be combined with GC agonists. In any case, one study demonstrated that cGMP signalling, while reducing tumour multiplicity, did not impact tumour proliferation, as shown by comparison of CRC mice models with and without genetic knockout of PKG (Islam et al., 2022). This suggests that even if cGMP concentration could be elevated by PDE inhibition in CRC tumours, tumour suppression may not result. Since the cAMP signalling pathway was shown to be downregulated in CRC in this project like for cGMP, cAMP synthesis could be similarly downregulated, albeit by a different mechanism. This would therefore discourage development of PDE inhibitors the treatment of CRC tumours.

In this project, insight into the expression of cAMP and cGMP signalling pathways and PDEs in CRC has been gained, but many questions remain about the role of cAMP and cGMP in CRC and their potential as drug targets. Given the clear efficacy of cGMP elevation for chemoprevention, further research in this area could reveal further impactful discoveries.

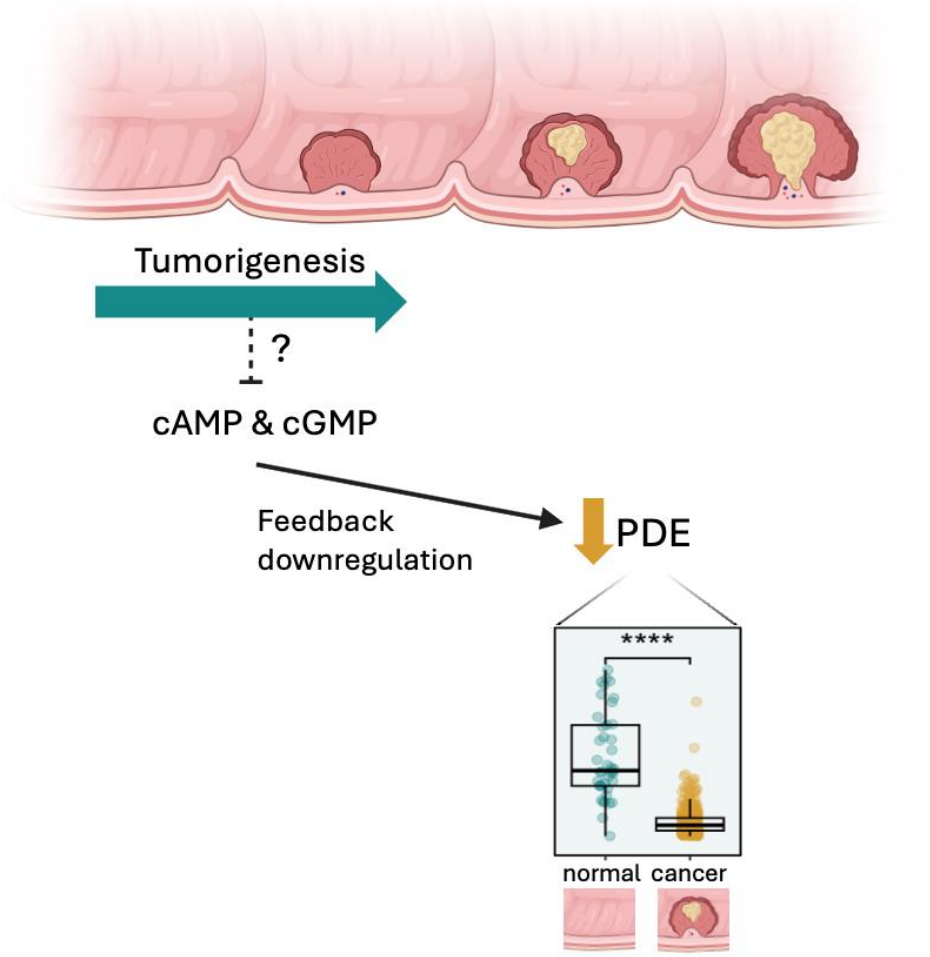

Figure 5-1: Model of cAMP, cGMP, and PDE downregulation in colorectal cancer pathogenesis.
cAMP may be a tumour suppressor in colorectal cancer. Therefore, downregulation of cAMP and cAMP-mediated signalling may be an important and early event for colorectal cancer tumorigenesis analogous to cGMP downregulation. This may cause downregulation of phosphodiesterase (PDE) enzymes as a secondary effect due to feedback transcriptional regulation, in which low cyclic nucleotide levels fail to stimulate PDE transcription. Tumour image generated using Biorender.com.

5.3 Limitations and future work

5.3.1 Validation of differential PDE expression in colorectal cancer

This project comprehensively characterised differential PDE expression in CRC at the mRNA level using RNA-seq. However, comprehensive validation of these changes at the protein level was not possible due to limitations of the datasets available and practical challenges during *in vitro* experiments. For this reason, confidence in these findings would be greatly increased by broad validation in larger cohorts using proteomics, IHC and western blot of patient tissues. By establishing new collaborations, these cohorts could include the Colorectal Cancer Glasgow Royal Infirmary Tumour Micro Array Cohort and the INCISE

Longitudinal Polyp Study Cohort prepared by the group of Professor Joanne Edwards at the University of Glasgow (Park and Edwards, 2021; Edwards and Ritchie, 2023).

Importantly, representation of CRC subtypes would allow for subtype-specific alterations to be detected. This would validate the proposed model of subtype-agnostic downregulation of cAMP, cGMP, and PDEs in CRC pathogenesis described above, and would also affirm upregulation of divergent genes, such as PDE11A in MSI-H CRC. Additionally, carrying out proteomic analysis on patient tissues would enable comprehensive characterisation of PDE protein and pathways of cAMP and cGMP analogous to the mRNA profiling used in this project.

5.3.2 Validation of cAMP and cGMP downregulation in colorectal cancer

Signalling pathways of cAMP and cGMP were found to be downregulated by RNA-seq and scRNA-seq in this project, which was proposed to be critical for CRC pathogenesis. This has been characterised for cGMP previously (Pitari et al., 2007; Rappaport and Waldman, 2018), but this is a novel finding for cAMP. Since the levels of these cyclic nucleotides were inferred indirectly from mRNA expression of their pathway genes, changes in their concentration should be directly validated in further work. For instance, cyclic nucleotide levels could be measured by ELISA between normal and CRC patient tissue samples (Hackett et al., 2014).

Moreover, disruption of cyclic nucleotide dynamics could be investigated using Förster resonance energy transfer (FRET) (Förster, 1948). Domains of a protein that change proximity to each other upon a conformational shift can be genetically fused to donor and acceptor fluorophores. Such a change in fluorophore proximity can be detected by a shift in FRET wavelength. In this way, fluorescent probes for protein binding events can be generated. For instance, reporters for indicating the presence of cyclic nucleotides can be made by inserting fluorophores near a cyclic nucleotide binding domain (DiPilato and Zhang, 2009). Alternatively, FRET reporters for cyclic nucleotide effector activity can be generated by positioning probes near binding domains for effectors on substrate proteins (Allen and Zhang, 2006). Using such probes, the

distribution across the cell of the activation of cyclic nucleotide effectors, such as PKA and PKG, could be visualised using confocal microscopy (Sample et al., 2012). These dynamics could be compared between CRC and normal patient tissues or in organoids of mice models or patients, and if the model of cAMP downregulation in CRC proposed by this project is correct, a reduced presence of cAMP and lower activation of PKA could be directly observed.

FRET probes could also be used to investigate alterations in the regulation of cyclic nucleotide nanodomains, which have been associated with cancer. In melanoma for instance, soluble AC (sAC) has been shown by IHC to migrate to the nucleus as part of a shift from differentiation to proliferation during tumorigenesis of melanocytes (Desman et al., 2014). Furthermore, this pattern was diagnostic of melanoma subtypes and was hypothesised to be prognostic of patient progression (Desman et al., 2014). Analogous changes of nanodomain regulatory components could be investigated in CRC by IHC in patient tissues and FRET of CRC cell lines or primary cells from patients.

5.3.3 Validation of cAMP in chemoprevention and tumour treatment

Since the cAMP signalling pathway was found to be downregulated in CRC in this project like cGMP, cAMP may have a similar tumour suppressive role, and further investigation might reveal its potential as a drug target for chemoprevention. Additionally, it would be valuable to characterise the effect of cAMP on CRC tumours after carcinogenesis. This could be assessed by testing AC agonists like forskolin or cAMP analogues in various CRC models. These could include normal and CRC cell lines, or mouse- or patient-derived organoids, which would be more representative (Lechuga et al., 2023). Alternatively, an approach could be adopted similar to the study involving the comparison of CRC mice models with and without genetic knockout of PKG (Islam et al., 2022). In this case, the impact of genetic knockout of PKA or other cAMP effectors on tumour multiplicity and size could be assessed, therefore revealing the role of cAMP on tumorigenesis and proliferation respectively. Lastly, if cAMP is identified as a tumour suppressor like cGMP, then the signalling components and effectors responsible for the mechanism should be investigated. This could involve testing cAMP-elevating agents alongside inhibitors of cAMP signalling components to

observe their impact on CRC proliferation and apoptosis. For example, inhibitors of EPAC, PKA, and their downstream effectors could be evaluated (Cho-Chung, 1990; Fajardo et al., 2014; Ahmed et al., 2022).

5.3.4 Investigation of subtype-specific PDEs

PDE11A was found to be strongly upregulated in MSI-H compared to normal cells by scRNA-seq, while no differential expression was found between normal and CRC cells. This suggests that PDEs can have specific mechanisms that result in upregulation instead of the hypothetical superfamily-wide PDE downregulation proposed in this work. For example, studies have suggested PDE4B to be a target for transcriptional upregulation by c-Myc and β-catenin (Pleiman et al., 2018; Kim, Kwak, et al., 2019). It would be interesting to see if PDE11A upregulation is similarly linked to MSI-specific pathogenic pathways such as MMR dysfunction or constitutive BRAF signalling (Boland and Goel, 2010).

To investigate this in further work, PDE11A differential expression should first be validated by IHC of MSI patient tissues or by RT-qPCR or western blot analysis of models for CRC MSI subtypes. This could include cell lines representative for MMR or dMMR CRC like WiDr and SW403 respectively (Genther Williams et al., 2015), or could involve mice models that recapitulate MSI subtypes, such as those bearing APC or BRAF mutations (Heyer et al., 1999). Meanwhile, the mechanisms underlying PDE11A upregulation could be investigated by GSEA of genes co-expressed with PDE11A in the scRNA-seq dataset used in this project. If promising candidate pathways are identified, their involvement could be investigated by testing the effect of inhibitors on the expression level of PDE11A in CRC MSI-H/dMMR cell lines. Lastly, the functional role of PDE11A could be assessed by observing the effect of PDE11A inhibition on proliferation and apoptosis in CRC dMMR cell lines. Following this, mouse- or patient-derived organoid models representing MSI-H and MSS would provide more representative results but would be more costly (Lechuga et al., 2023). These efforts may result in increased understanding of MSI-H CRC pathogenesis and reveal the value of PDE11A as a therapeutic target.

5.3.5 PDE expression as a biomarker for patient treatment response

One of the major challenges in current CRC treatment is the unpredictable response and outcomes among patients (Xie et al., 2020). Some individuals receive treatments they do not require or will not respond to and are then subject to the adverse effects (Foersch et al., 2023). Therefore, an increased understanding of the factors that influence treatment responses, as well as the development of reliable prediction methods, is essential for improving patient outcomes in CRC.

The discovery of PDE11A upregulation in MSI-H CRC suggests that analogous responder-specific PDEs may exist that could allow for the prediction of patient response and outcomes to chemotherapeutics or targeted therapies. This could be explored by conducting RNA-seq, RT-qPCR, IHC, and western blot in patient tissues representing responder and non-responder groups. This work could potentially be done in the context of rectal cancer in collaboration with Dr Campbell Roxburgh at the University of Glasgow, whose research group uses these techniques on patient tissues to predict response to radiotherapy in rectal cancer (Hillson et al., 2024).

5.4 Conclusion

In conclusion, this thesis has identified broad downregulation of PDEs and cyclic nucleotide signalling pathways in colorectal cancer, suggesting that attenuation of both cAMP and cGMP signalling is an early and ubiquitous event in tumorigenesis. These findings support the use of PDE inhibitors for chemoprevention rather than treating established tumours and point toward the promise of AC or GC agonists as therapeutic strategies. Additionally, identification of PDE genes upregulated in CRC subtypes could reveal specific disease mechanisms or prognostic targets. Future validation of these results and further exploration of the mechanisms underlying PDE dysregulation, particularly in MSI-H CRC, will be essential for advancing novel targeted therapies and improving patient outcomes.

Part 2

Bioinformatic discovery of Dengue virus disruptor peptides

Chapter 6 Introduction

6.1 Dengue virus epidemiology and clinical features

Dengue virus (DENV) is the fastest spreading vector-borne viral disease in the world and is a severe detriment to global health (World Health Organization, 2009). Dengue virus is a positive-sense single-stranded RNA flavivirus transmitted by Aedes mosquitos throughout tropical and subtropical regions (Figure 6-1) (Nanaware et al., 2021). Nearly half of the global population lives under risk of infection (Bos et al., 2018). Currently, no antiviral treatments are available, and candidate vaccines are undergoing late-stage clinical trials (Palanichamy Kala et al., 2023). Every year, there are approximately 100-400 million cases and 36,000 deaths from Dengue virus infection worldwide (Bhatt et al., 2013; Santana et al., 2022). One in four cases manifest in acute febrile illness, and one in twenty require hospitalisation, in which case fatality rates range from 2.5 - 5 % (Castro et al., 2017; Bere et al., 2021). For these reasons the World Health Organization has classified Dengue virus as one of the top ten threats to global health (World Health Organization, 2019).

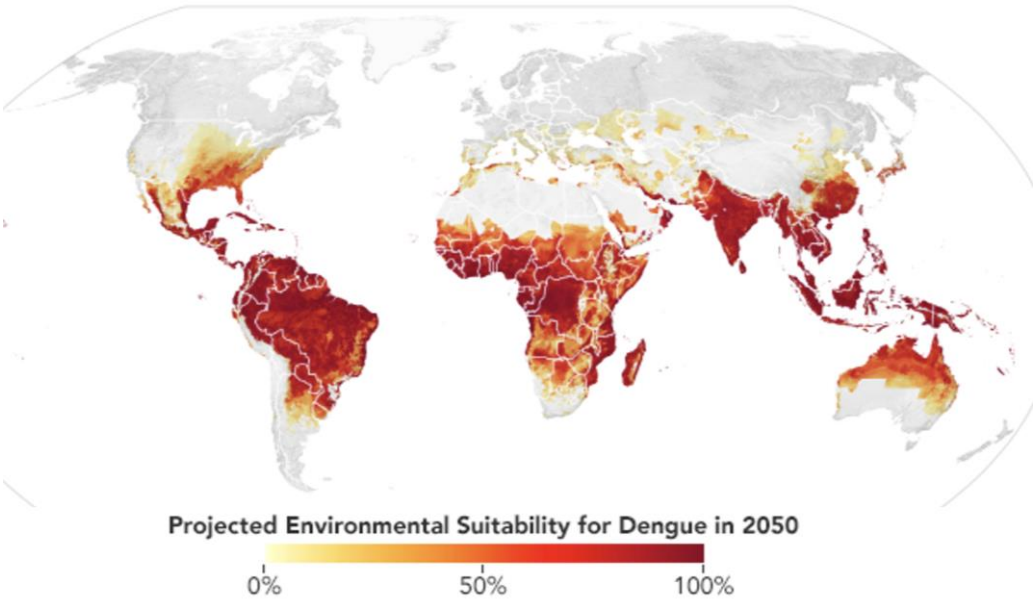

Figure 6-1: Predicted environmental suitability for Dengue virus in 2050.
Based on models of projected temperature, rainfall, and mosquito population growth. NASA Earth Observatory map by Lauren Dauphin generated from data from Janey Messina, University of Oxford (Patel and Dauphine, 2020).

Mild cases of Dengue virus infection present as a typical fever, with symptoms of high body temperature, headache, abdominal pain, musculature pain, joint pain, orbital pain, flushing, rash, and swollen glands (Oishi et al., 2007). However, around one in twenty individuals develop severe infection, characterised by low platelet count and haemorrhaging (Tsheten et al., 2021). Severe infection is life threatening, and afflicted individuals need urgent supportive care and symptomatic treatment (Tsheten et al., 2021). There are four genetic variants of Dengue virus called serotypes, each with distinct epitopes (Soo et al., 2016). The serotypes cocirculate and are individually capable of inciting full disease (Srikiatkhachorn et al., 2017). Once an individual recovers, serotype-specific neutralising antibodies provide lifelong immunity from reinfection with that serotype (Srikiatkhachorn et al., 2017). However, antibodies cross-reactive with other serotypes are rarely neutralising and can even increase risk of severe symptoms upon re-infection with a different serotype (Srikiatkhachorn et al., 2017). For these reasons, repeat infection of Dengue virus is common (St. John and Rathore, 2019).

Dengue virus is endemic in over 128 countries in South Asia, Southeast Asia, the West Pacific, Africa, the Americas, and the East Mediterranean (Brady et al., 2012). Countries most affected include Brazil, Vietnam, India, Colombia, and the Philippines (Akter et al., 2024). Dengue virus is mainly spread by the Aedes aegypti mosquito, which thrives in tropical urban environments with open water (Schmidt et al., 2011). This is a prominent issue in areas with rapid urban expansion without access to piped water, where the Aedes aegypti mosquito can lay eggs and reproduce in open water sources such as water tanks, drains and artificial debris that collect rainwater (Schmidt et al., 2011). With this growing urbanisation in combination with global warming, the regions hospitable to this mosquito are rapidly expanding (Murugesan and Manoharan, 2020). A recent outbreak in Brazil in January and February 2024 is a prime example of this (Lenharo, 2024). With a warming climate and expanding urban zones, Dengue infection is intensifying in cities and advancing south into more temperate regions of Brazil (Lenharo, 2024). In these two months alone, there were over a million cases of infection (Lenharo, 2024). This is larger than the peak in 2023, which usually occurs from March to May (Lenharo, 2024). In addition to Aedes aegypti, Dengue virus is also spread by Aedes albopictus, also known as the Asian

tiger mosquito (Lambrechts et al., 2010). Aedes albopictus is adapted to more temperate climates and is spreading Dengue virus into Europe and China (Akter et al., 2024). With all these factors taken together, Dengue virus is expanding rapidly in terms of incidence and geography.

6.2 Dengue virus structure and life cycle

Dengue virus is a flavivirus belonging to the *Flaviviridae* family (Roy and Bhattacharjee, 2021). Other members include West Nile Virus, Japanese Encephalitis Virus, Zika Virus, and Yellow Fever. The 11 kB genome of Dengue virus is comprised of positive-sense (+) single-stranded RNA containing a single open reading frame that is translated in host cells into a single polyprotein, which is cleaved into the ten Dengue proteins (Figure 6-2) (Murugesan and Manoharan, 2020). There are three structural proteins: envelope (E), membrane (M/PrM), and capsid (C), and seven non-structural proteins NS1, NS2A, NS2B, NS3, NS4A, NS4B, and NS5 (Roy and Bhattacharjee, 2021). The nonstructural proteins function after virus entry into the host cell and perform vRNA replication, virus particle assembly, and modulate the host immune system, whereas the structural proteins comprise the mature virus particle (Roy and Bhattacharjee, 2021). This particle, called a virion, is a smooth enveloped sphere with a diameter of 50 nm (Figure 6-2) (Roy and Bhattacharjee, 2021). Forming the outer surface, 90 homodimers of the E protein are organised in an icosahedral herringbone pattern (Roy and Bhattacharjee, 2021). In addition, the E proteins are glycosylated at two sites, which is important for function (Yap et al., 2017). Below the E protein is a layer of M protein and a lipid bilayer originally derived from the host endoplasmic reticulum (Chew et al., 2017). Both the E and M proteins possess transmembrane domains, which anchor the proteins to the bilayer and maintain structural integrity of the virus particle (Chew et al., 2017). Below the lipid bilayer, capsid protein encapsulates a single copy of the RNA genome (Kuhn et al., 2002).

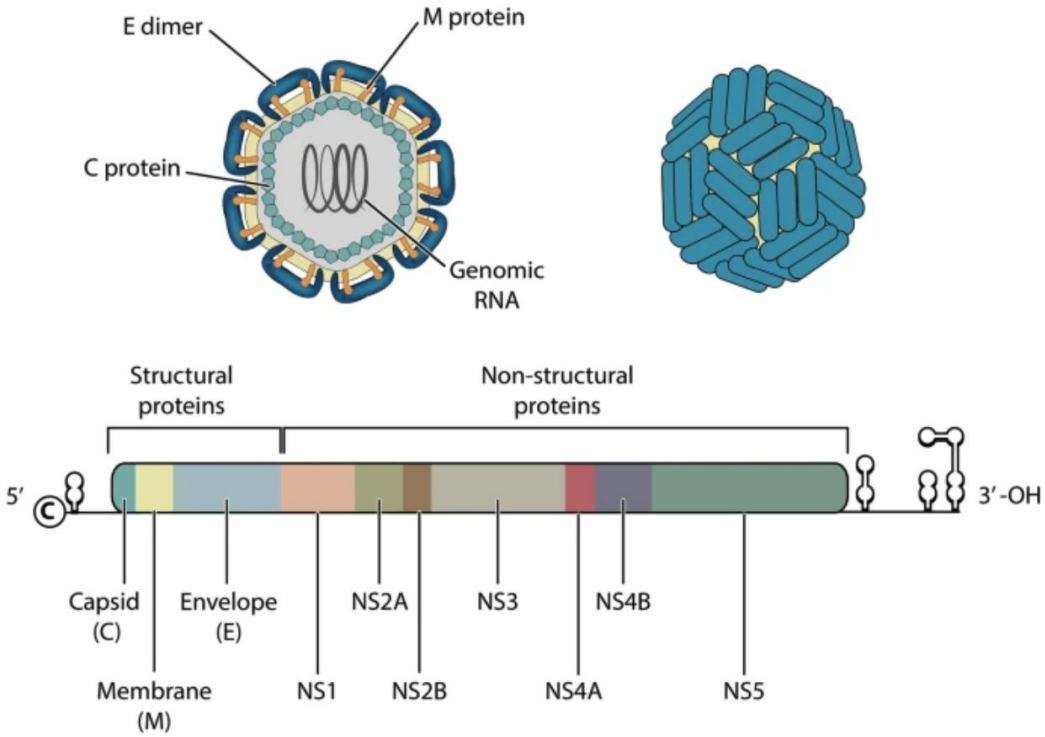

Figure 6-2: Structure of the Dengue virus particle.
The Dengue virion is composed of a layer of E protein dimer (blue) and M protein (yellow) anchored to a lipid bilayer. Within the membrane is the nucleocapsid comprised of C protein and one molecule of the RNA genome. The genome codes for the Dengue polyprotein which is translated shortly after virus internalisation. Image sourced from (Souza et al., 2022). Reuse is permitted under a CC BY 4.0 License (https://creativecommons.org/licenses/by/4.0/).

Infection with Dengue virus begins when an infected female Aedes mosquito takes a bloodmeal and injects saliva containing virus into the dermis (Figure 6-3) (Chew et al., 2017). The process of virus internalisation then proceeds by three stages. First, Dengue virus attaches to host cells by protein-protein interaction between the E protein and host receptors on the membrane (Yap et al., 2017). Second, further receptor interactions trigger endocytosis, in which the virus is engulfed in a membrane-bound vesicle and taken into the cell (Piccini et al., 2015). This process is not fully understood, but putative receptors include DC-SIGN, heparan sulfate, CD14, HSP90/HSP70, claudin-1, GRP78, mannose, laminin, integrins, and TIM and TAM proteins (Nanaware et al., 2021). Third, the virus must then escape the endosome to release the nucleocapsid into the cytoplasm (Yap et al., 2017). This is achieved by the Dengue E protein mediating fusion of the viral and endosome membranes (Kuhn et al., 2002). The low pH environment of the endosome triggers drastic conformational changes in the E protein, and E homodimers dissociate and reform as trimers (Kuhn et al., 2002). Resultingly, a structure on the E protein called the fusion loop becomes exposed

and merges the membranes to form pores through which the nucleocapsid is released (Schmidt et al., 2010).

The vRNA migrates to the rough endoplasmic reticulum (RER) and is translated by host machinery to produce the Dengue polyprotein (Figure 6-3) (Yap et al., 2017). After cleavage and post-transcriptional modification, the ten Dengue proteins are produced (Yap et al., 2017). The non-structural proteins interact with host factors to form the 'replication complex' which carries out replication of vRNA (Lescar et al., 2018). This complex is composed of the Dengue NS2A, NS2B, NS4A, NS4B, and NS5 proteins interacting with host proteins embedded in the membranes of the RER, Golgi Apparatus, or associated vesicles (Lescar et al., 2018). Virion formation begins when the structural proteins accumulate and become enclosed in the RER membrane, which buds into the lumen (Nanaware et al., 2021). The immature virion is produced when one molecule of the vRNA genome is coated in capsid protein and incorporated into the bud (Kuhn et al., 2002). The immature virion is characterised by the presence of the Pr domain linked to the M protein (Vázquez et al., 2002), which caps the M protein and prevents the E fusion loop from prematurely fusing the virus and host membranes during secretion from the infected cell (Nicholls et al., 2020). The immature virion travels through the trans-Golgi network secretory pathway, in which furin protease in the low pH environment cleaves the Pr domain to produce the mature particle characterised by a smooth outer coat (Nicholls et al., 2020). Virions then exit the cell via exocytosis and continue the life cycle by infecting a new host cell (Nicholls et al., 2020).

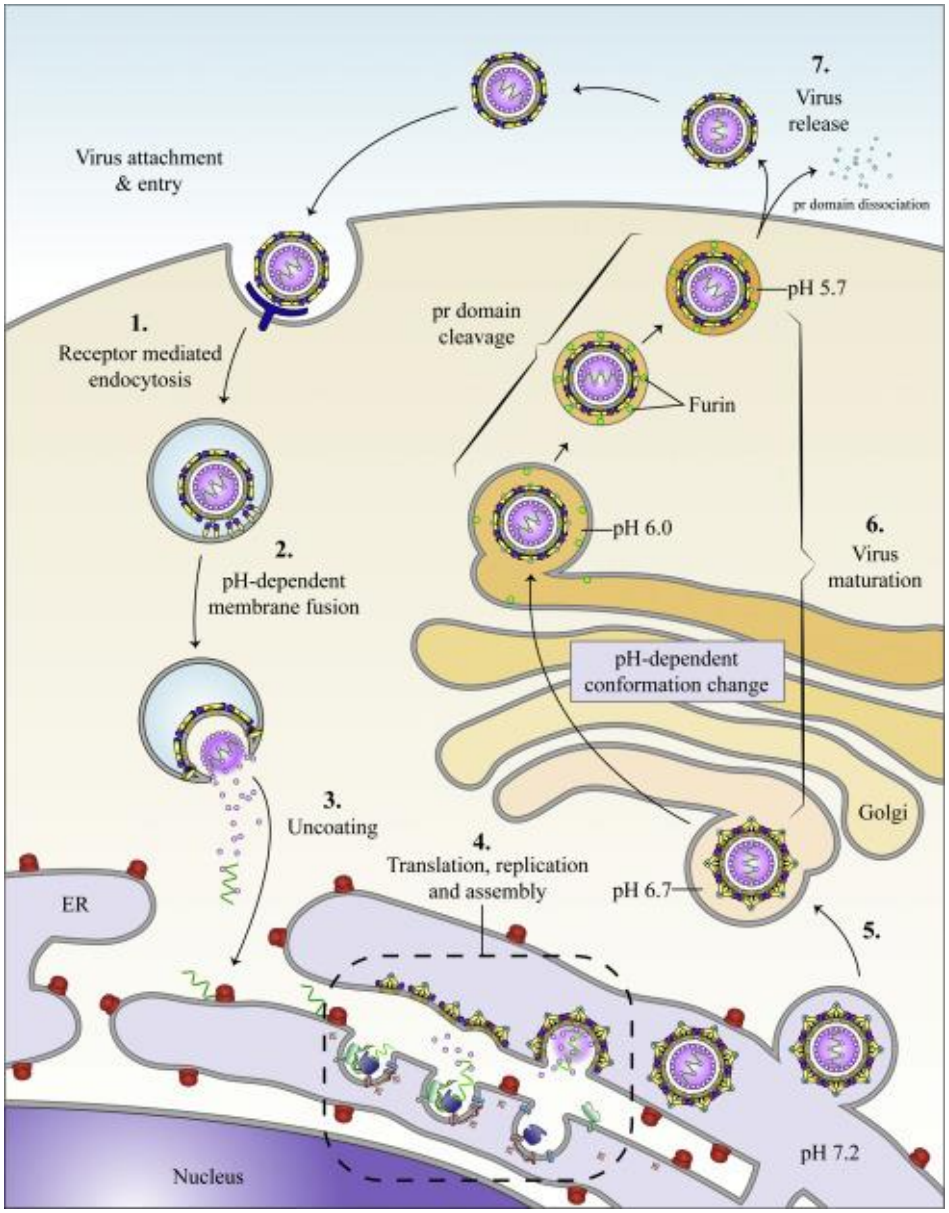

Figure 6-3: The Dengue virus life cycle.
Dengue virions interact with host factors for cell attachment and internalisation. Inside endosomes, the acidic environment triggers conformational change of the E protein to expose the fusion loop structure. The E fusion loop initiates fusion of endosome and virion membranes, releasing the Dengue nucleocapsid into the host cytoplasm. The capsid is shed, and the Dengue genome travels to the rough endoplasmic reticulum. The genome is translated into the Dengue polyprotein which is then processed into the ten mature Dengue proteins. A membrane bound replication complex forms consisting of Dengue and host proteins. This machinery replicates vRNA. New vRNA and Dengue proteins assemble with membrane and bud off into immature virions. These particles travel through the secretory pathway to exit the cell. In the acidic environment of the secretory vesicles, furin cleaves the Pr domain off of the PrM protein to form the mature virions. The Pr peptide remains associated with the virions to prevent premature membrane fusion. The virus is secreted, and the Pr peptides dissociate. Image sourced from Nicholls et al., 2020.

6.3 Dengue virus pathogenesis and host immune response

6.3.1 From mosquito bite to viremia

Following injection of Dengue virus into the dermis during a blood meal from a female Aedes mosquito, Langerhans cells and keratinocytes are among the first cells to become infected (Garcia et al., 2017). These immune cells migrate and spread infection to the lymph nodes (Garcia et al., 2017). Subsequently, infected monocytes and macrophages circulate the virus throughout the lymphatic system which eventually leads to viremia (Garcia et al., 2017). The main sites of replication are the liver, kidney, spleen, and lungs (Jain et al., 2023). Viremia lasts 10-12 days and febrile symptoms emerge within 24-48 hours (Mansour and Abu-Naser, 2019).

6.3.2 The innate immune response

The interferon (IFN) pathway is the main antiviral defence mechanism of the innate immune system (Figure 6-4) (Uno and Ross, 2018). Once a cell becomes infected, the IFN response is triggered when pattern recognition receptors (PRRs) interact with pathogen-associated molecular patterns (PAMPs) (Loo and Gale, 2011). For Dengue virus, the main PRRs are the RIG-1-like receptors (RLRs) (Loo and Gale, 2011) and toll-like receptors (TLR) 3 and 7 (Wang et al., 2006; Nasirudeen et al., 2011), and both systems detect viral replication inside the cell. RLRs are responsible for vRNA detection in the cytoplasm (Loo and Gale, 2011). Upon vRNA binding with RIG-1 or MDA5, signalling begins with recruitment of the mitochondrial membrane associated MAVS (Nasirudeen et al., 2011). This leads to activation of IKKε and TBK1 kinases, which in turn activate IRF3 and IRF7, ultimately triggering production of IFNs (Ngono and Shresta, 2018). Complimentary to the RLR pathway, vRNA binding to TLRs also triggers IFN production. TLR3 is an important receptor which recognises vRNA in endosomes, inducing activation of TRIF then TRAF3 (Baum and García-Sastre, 2010). TRAF3 goes on to activate IKKε and TBK1 kinases which mediate IFN production (Akira and Takeda, 2004). TLR7 has a different action from TLR3, in that it detects vRNA in the endosomes of dendritic cells and induces an antiviral proinflammatory response through NFκB (Wang et al., 2006). Following vRNA

binding, TLR7 recruits the adaptor protein MyD88 to activate TRAF6, which subsequently activates IKKα/ß/ɣ kinases (Wang et al., 2006). This triggers the nuclear translocation of NFκB to induce inflammatory signalling, and at the same time, TRAF6 also initiates INF production via the activation of IRF7 (Ngono and Shresta, 2018).

In addition to the RLR and TLR pathways, the cGAS/STING pathway also induces TNF signalling in response to viral infection (Figure 6-4) (Sun et al., 2017). Upon infection with Dengue virus, mitochondria become damaged and release mtDNA, and this is detected by cyclic GMP-AMP synthase (cGAS) (Sun et al., 2017). Production of the cGAMP second messenger then promotes IFN signalling in an activation sequence involving STING, TBK1, and finally IRF3/7 (Wu et al., 2013).

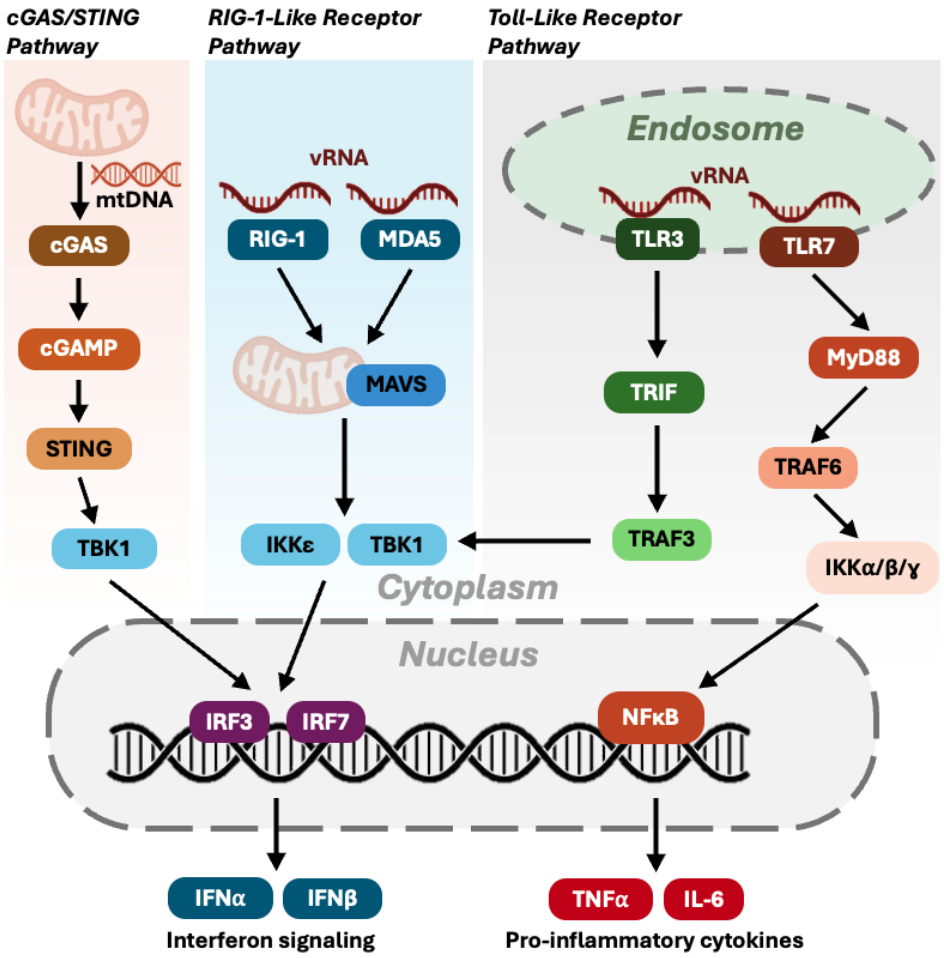

Figure 6-4: Innate immune response pathways.
The RIG-1-like receptor and Toll-like receptor pathways initiate IFN production in response to vRNA detection in endosomes. Additionally, Toll-like receptors activate proinflammatory signalling via NFκB. The cGAS/STING pathway also activates IFN production in response to mtDNA recognition, indicative of virus-induced mitochondrial damage. Figure prepared in Microsoft PowerPoint.

Once IFNs are produced and secreted, they bind to cell surface IFNAR receptors, which activate JAK1 and Tyk2 kinases (Figure 6-5) (Morrison and García-Sastre, 2014). These enzymes phosphorylate STAT proteins, so that phosphorylated STAT1 and STAT2 along with IRF9 form the ISGF3 transcription factor complex, which triggers expression of interferon-stimulated genes (ISGs) (Morrison and García-Sastre, 2014). These genes can disrupt the life cycle and replication of viruses by affecting many cellular processes. For example, ISGs can modulate the immune response, the cell cycle, and metabolism, as well as induce apoptosis (Stark et al., 1998). ISGs also bind to and directly interfere with viral protein function to inhibit infection (Stark et al., 1998).

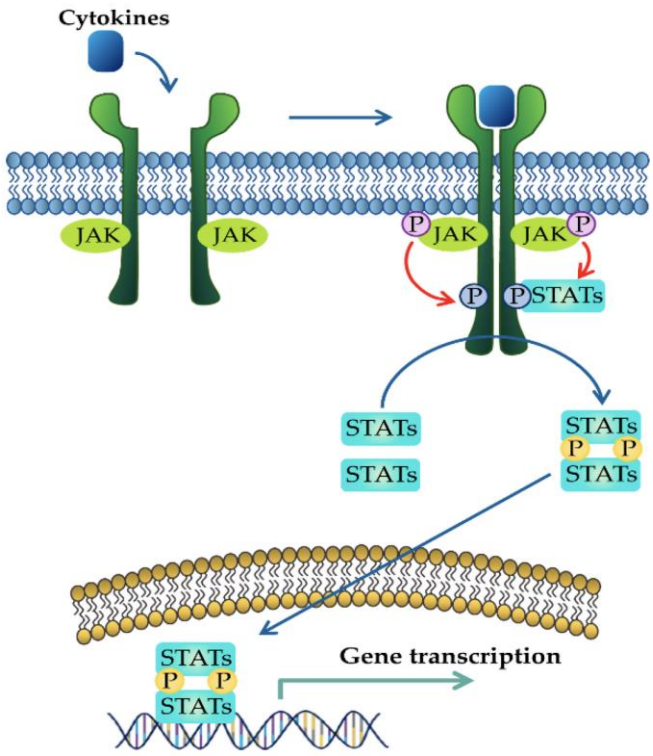

Figure 6-5: Interferon (IFN) and cytokine induced expression of antiviral interferon-stimulated genes (ISGs).
Binding of IFN and other cytokines induces the phosphorylation of STAT1 and STAT2 by JAK1 and Tyk2. Phosphorylated STAT1 and STAT2 form transcription factor complexes to promote expression of ISGs. Figure sourced from Moon et al., 2021.

6.3.3 The adaptive immune response

If the innate response fails to resolve the infection locally, the infected Langerhans cells and other immune cells will reach lymphatic tissues, where they activate B cells and $CD4^+$/$CD8^+$ T cells (M.F. Lee et al., 2022). This

interaction initiates both a humoral (antibody-mediated) and cell-mediated response which comprise adaptive immunity.

In the humoral response, the Langerhans cells and other immune cells present viral antigens on major histocompatibility complex (MHC) type-II proteins at the cell surface to $CD4^+$ T cells, which become activated and undergo clonal expansion with specificity towards that antigen (Figure 6-6) (Luckheeram et al., 2012). The $CD4^+$ T cells then distribute throughout the body. Some subtypes, especially T follicular helper cells migrate to B cell follicles in the lymphatic system where they interact with B cells (Ma et al., 2012). B cells which have also encountered the same antigen become activated by the T follicular helper cells via cytokine release and ligand-receptor interactions (Ma et al., 2012). Subsequently, the B cells proliferate, differentiate, and begin antibody production (Hoffman et al., 2016). Antibodies of different isotypes are produced, which have different effector functions, such as neutralisation of viral epitopes or opsonisation by phagocytic cells (Spiegelberg, 2009). To provide long term immunity, some B cells differentiate into memory B cells, which can rapidly re-initiate the adaptive immune response upon subsequent infection (Hoffman et al., 2016).

Contrastingly, the cell-mediated adaptive response primarily involves $CD8^+$ T cells. When the Langerhans, dendritic cells, and other cell types become infected or internalise Dengue antigens, they present the antigen peptides on class I MHC proteins (Schmid et al., 2014). They then migrate to the lymph node where they activate $CD8^+$ T cells, which undergo clonal expansion, proliferation, and differentiation into cytotoxic T lymphocytes (CTL) (Figure 6-6) (Rivino, 2018). Additionally, $CD4^+$ T cells can promote the ability of antigen presenting cells (APCs) like the Langerhans cells to activate $CD8^+$ T cells (Luckheeram et al., 2012). Alternatively, the $CD4^+$ cells can activate the $CD8^+$ T cells directly by cytokine release or receptor-ligand interaction (Luckheeram et al., 2012). As a result, levels of CTLs rise and they spread throughout the body. Cells infected with Dengue virus will present Dengue antigens on class I MHCs (Rivino, 2018). The CTLs recognise the antigens and induce apoptosis by release of perforin and granzymes (Rivino, 2018).

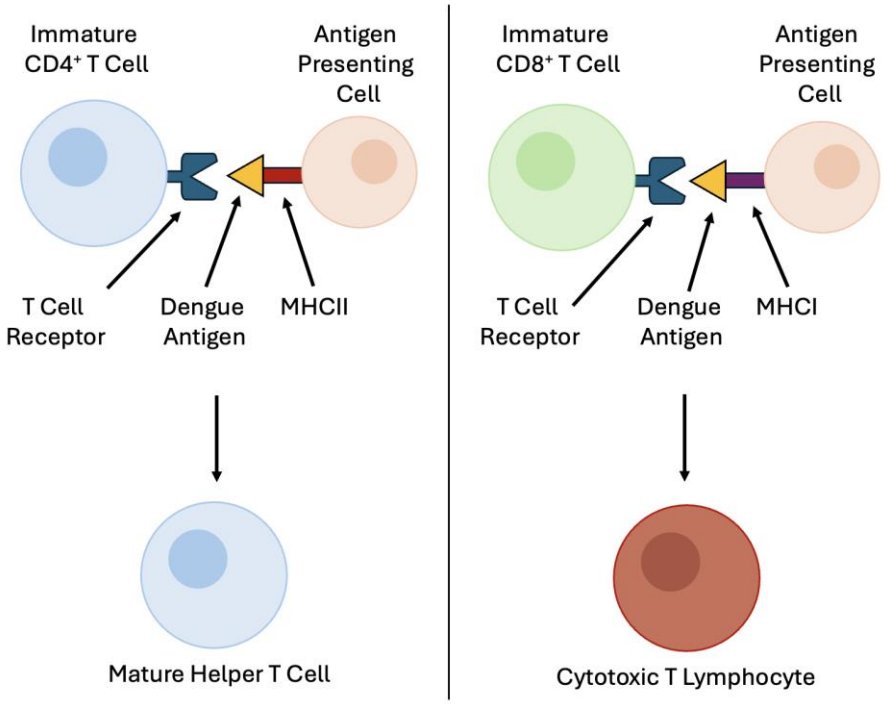

Figure 6-6: T cell activation in the adaptive immune response.
$CD4^+$ T cells are activated when APCs present Dengue antigens on MHC class II proteins. $CD8^+$ T cells are activated when APCs present Dengue antigens on MHC class I proteins.

Taken together, the adaptive immune system combats viral infection by the combination of virus neutralisation and clearance by the binding of antibodies produced by the humoral response as well as the targeted cell death of infected cells by CTLs as part of the cell-mediated response.

6.3.4 Severe Dengue infection

Severe infection of Dengue virus is much less prevalent than mild infection, representing only one in twenty cases (Pintado Silva and Fernandez-Sesma, 2023). However, severe infection presents with very contrasting clinical features and has a much higher fatality rate (Md-Sani et al., 2018). Counterintuitively, onset of severe disease occurs when viremia and acute fever subside, and severe symptoms can last two to seven days (World Health Organization, 2024). Severe infection is classified into two types. Dengue Haemorrhagic Fever (DHF) is associated with plasma leakage, thrombocytopenia (low platelet count), and coagulopathy (deficient blood clotting) which predisposes an individual to oedema, heavy bleeding, and haemorrhaging, particularly in the chest and abdominal cavity (Kalayanarooj, 2011). Dengue Shock Syndrome (DSS) is the most serious form of infection and is characterised by hypovolemic shock that

arises from escalation of DHF (Kalayanarooj, 2011). Such circulatory impairment can lead to tissue and organ damage and death (Kalayanarooj, 2011). The underlying mechanisms of severe Dengue infection are not well understood, and studying these conditions is very challenging for several reasons (Srikiatkhachorn et al., 2017). Firstly, the pathogenesis of DHF and DSS is a complex interaction between viral influences, host immune response, and vascular and circulatory dysfunction (Srikiatkhachorn et al., 2017). Secondly, animal models can only recapitulate some aspects of severe infection, and data on vaccine and drug interventions may not be representative (Srikiatkhachorn et al., 2017). Thirdly, the infrequency of DHF and DSS coupled with the seasonality of Dengue outbreaks makes it difficult to recruit individuals for human studies and clinical trials (Wallace et al., 2013). Adding to this, the tropical and subtropical countries most affected by Dengue virus often lack the funding and facilities necessary to conduct research (Wallace et al., 2013).

Despite these challenges, researchers have managed to achieve insight into mechanism, prognostic biomarkers, and potential drug targets (Srikiatkhachorn et al., 2017). Antibody-dependent enhancement (ADE) has been shown to play a big role in severe Dengue virus infection (Shukla et al., 2020). Primary infection of a specific Dengue serotype provides lifelong immunity against that serotype via the production of neutralising antibodies (Shukla et al., 2020). However, primary infection has been shown to greatly increase the risk of severe disease following infection by the other three serotypes (Katzelnick et al., 2017). This has been linked to high concentrations of non-neutralising serotype cross-reactive antibodies produced alongside the serotype-specific neutralising antibodies (Shukla et al., 2020). These cross-reactive antibodies cannot neutralise virions because they either lack sufficient affinity or may target non-neutralising epitopes (Tsai et al., 2013). Furthermore, these antibodies can promote infection by binding to immune cells expressing Fc receptors for the immunoglobulin constant region (Figure 6-7) (Halstead et al., 2010). This triggers internalisation of Dengue virions via the phagocytic pathway (Halstead et al., 2010). Furthermore, cells infected in such a manner exhibit suppressed immune responses characterised by decreased INF-α and increased IL-10 (Ubol et al., 2010). Taken together, ADE exacerbates Dengue virus infectivity and viremia and increases the risk of severe infection.

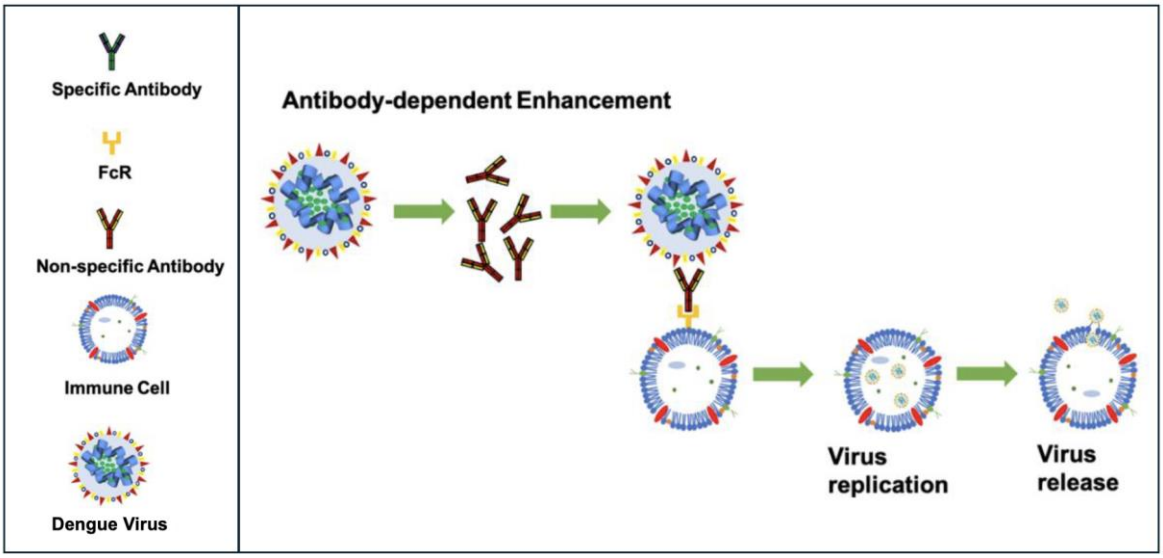

Figure 6-7: Antibody-dependent enhancement (ADE).
ADE facilitates Dengue virus entry into cells with Fc receptors. Non-neutralising or subneutralising antibodies bind to Dengue virus. Subsequent interaction with immune cells expressing Fc receptors leads to phagocytic internalisation and infection. Figure adapted from Farouq et al., 2022.

As well as ADE, numerous studies have implicated a dysregulated immune response and cytokine storm effect in the pathogenesis of severe Dengue infection (Srikiatkhachorn et al., 2017). One key piece of evidence is that severe circulatory symptoms rapidly and completely resolve at the end of infection (Screaton et al., 2015). This suggests a fully reversible functional change in the vasculature and circulatory systems induced by short-acting immune effectors (Srikiatkhachorn et al., 2017). Correspondingly, the current understanding is that uncontrolled infection, exacerbated by ADE, triggers an intensified and unbalanced immune response (Srikiatkhachorn et al., 2017). High levels of cytokines and chemokines circulate, causing aberrant vascular permeability, thrombocytopenia, and coagulopathy (McBride et al., 2020). TNF-α and VEGF-A in particular are known to strongly influence these pathways, but other immune mediators seem to be involved, such as IL-6, IL-8, IL-10, CCl2/MCP-1, and CXCL10/IP10 (Srikiatkhachorn et al., 2017). However, reported levels of these biomarkers in patients have been variable and conflicting (Srikiatkhachorn et al., 2017). Further research is required to validate these findings and to delineate inter-individual variation from structured, time-dependent patterns. In this way, novel drug targets may be found. For example, TNF-α or angiogenesis inhibitors have been suggested (Srikiatkhachorn et al., 2017).

6.4 Vaccine development for Dengue virus

6.4.1 Challenges to Dengue virus vaccine development

Currently, there is a lack of effective vaccines for Dengue virus, though promising candidates are emerging from clinical trials (Akter et al., 2024). Vaccine candidates will be described in Section 6.4.2. Dengue vaccine development is incredibly challenging for several reasons. Firstly, the four serotypes of Dengue virus are antigenically distinct, and a separate full immune response against each serotype is required for immunity (Pintado Silva and Fernandez-Sesma, 2023). If vaccine-induced antibodies are non-neutralising, cross-reactive, and capable of ADE, risk of severe infection is increased (Shukla et al., 2020). Secondly, there is a lack of animal models that are cheap, accessible, and representative of the Dengue infection (Yauch and Shresta, 2008). This is especially true for severe Dengue infection. Compared to humans, Dengue virus cannot inhibit IFN signalling in mice, making mice naturally resistant (Yauch and Shresta, 2008). However, the AG129 mice model, deficient in type-1 and type-2 IFN signalling, has been a useful tool in research (Johnson and Roehrig, 1999). AG129 can exhibit viremia, vascular permeability, thrombocytopenia, coagulopathy, haemorrhaging and cytokine storm (Yauch and Shresta, 2008). Nonetheless, the model is limited in that the influence of IFN signalling is absent. Nonhuman primates are another useful model for Dengue virus infection and can generate a robust immune response (Jain et al., 2023). However, they are incapable of developing overt disease and so are more useful for studies on tolerance and safety of candidate vaccines (Jain et al., 2023). Additionally, swine models are not useful since Dengue virus infection is asymptomatic (Zompi and Harris, 2012). Lastly, the pathology and immune response of Dengue infection and severe Dengue infection involve many physiological systems and are incredibly complex. Our limited understanding, especially of the protective and deleterious role of the immune response, makes it challenging to induce adequate immunity and avoid adverse effects during vaccine development (Akter et al., 2024).

6.4.2 The current state of Dengue virus vaccine development

Different types of vaccine strategy have been employed in Dengue virus research (Table 6). These include live-attenuated virus, inactivated virus, DNA and RNA vaccines, and recombinant protein and peptide vaccines. Of these, live-attenuated vaccines have been the focus of most research and have been most successful (Pintado Silva and Fernandez-Sesma, 2023).

Table 6: Dengue virus vaccines currently licensed or under development.
NIAID, National Institute of Allergy and Infectious Diseases; WRAIR, Walter Reed Army Institute of Research; GSK, GlaxoSmithKline; AMRDC, U.S. Army Medical Research and Development Command; NMRC, U.S. Naval and Medical Research Center.

Name	Type	Developer	Stage	Adjuvant	ref
Dengvaxia / CYD-TVD	Chimeric live-attenuated	Sanofi Pasteur	Licensed	N/A	(Thomas and Yoon, 2019)
Qdenga / TAK-003	Chimeric live-attenuated	Takeda	Licensed	N/A	(Patel et al., 2023)
TV003/TV005 / Butantan	Chimeric live-attenuated	NIAID, Butantan	Phase III	N/A	(Whitehead, 2016)
TDEN	Live-attenuated	WRAIR, GSK	Phase II	N/A	(Watanaveeradej et al., 2016)
DPIV	Inactivated	WRAIR, GSK, FIOcruz	Phase I/II	Alum	(Diaz et al., 2018)
D1ME100	DNA	US AMRDC	Phase I	N/A	(Beckett et al., 2011)
TVDV	DNA	US AMRDC, WRAIR, NMRC, Vical	Phase I	Vaxfectin	(Porter et al., 2012)
DDV	DNA	Molecular Virology Laboratory, Rajiv Gandhi Centre for Biotechnology (RGCB), India	Pre clinical	N/A	(Sankaradoss et al., 2022)
E80 mRNA	mRNA	CAS laboratory of Molecular Virology and Immunology, Institute Pasteur of Shanghai	Pre clinical	N/A	(M. Zhang et al., 2020)
V180	Recombinant Protein LNP	Merck and co.	Phase I	ISCOMATRIX	(Manoff et al., 2019)
PepGNP-Dengue	Peptide GNP	Unisanté Institute, Emergex	Pre clinical	GNP carbohydrate layer	(Miauton et al., 2024)

6.4.2.1 Live attenuated and chimeric vaccines

Dengvaxia (CYD-TDV) developed by Sanofi Pasteur was the first Dengue vaccine to be developed and was made commercially available in 2016 (Thomas and Yoon, 2019). Dengvaxia is a live-attenuated vaccine composed of four chimeric components. Each component consists of the PrM and E proteins of one Dengue serotype inserted into an attenuated yellow fever backbone (Thomas and Yoon, 2019). Dengvaxia was licensed in many countries in 2016, approved by the FDA in 2019, and was rolled out in several national public vaccination programmes (Mendoza et al., 2020). However, the immunity induced by Dengvaxia was insufficient and unbalanced between serotypes (Salje et al., 2021). Moreover, the vaccine was shown to provide limited protection in children younger than nine years, and seronegative individuals had increased risk for severe disease, an observation linked to ADE (Shukla et al., 2020; Tully and Griffiths, 2021). For this reason, Dengvaxia use has been restricted to seropositive individuals over nine years of age who live in endemic regions (Thomas and Yoon, 2019). In particular, this serostatus requirement has limited the use of the vaccine, as serostatus testing is expensive and requires laboratory facilities for conducting biomarker detection assays (Luo et al., 2019; Pearson et al., 2019). Taken together, the first Dengue vaccine Dengvaxia has not been as impactful in Dengue virus control as was initially hoped, and alternative vaccines are urgently needed.

Qdenga (TAK-003) is another live-attenuated chimeric vaccine that completed phase III clinical trials and was first licensed in 2022 in Indonesia (Mallapaty, 2022). The vaccine is composed of a live-attenuated PDK-53 DENV2 backbone with DENV1, 3, and 4 proteins inserted (Patel et al., 2023). In clinical trials, Qdenga provided strong and balanced immune protection with no adverse effects (Patel et al., 2023). The vaccine was approved by the European Medicines Agency (EMA) in 2022, and is licensed in Brazil, Indonesia, the United Kingdom, Thailand, and Argentina (Freedman, 2023). Additionally, Brazil will be the first country to undertake public vaccination programmes using Qdenga (Alves, 2024). Overall, Qdenga is a very promising emerging vaccine that seems to lack the efficacy and adverse effect of Dengvaxia.

Another live-attenuated chimeric vaccine is TV003 (Butantan vaccine). TV003 is composed of three non-chimeric components of mutagenically attenuated

DENV1, 3, and 4, and a fourth chimeric component of a mutagenically attenuated DENV4 backbone with DENV 2 proteins inserted (Whitehead, 2016). The related vaccine TV005 has the same composition but with different ratios of components (Whitehead, 2016). TV003/T005 have undergone several phase I and II clinical trials (Whitehead, 2016), and TV003 is undergoing a phase III clinical trial in Brazil (Kallás Esper G. et al., 2024). Both vaccines have demonstrated a balanced immune response and have been well tolerated (Akter et al., 2024).

In addition to Dengvaxia, Qdenga, and TV003/TV005, one further live-attenuated vaccine had some initial success in clinical trials. The Walter Reed Army Institute of Research (WRAIR) and GlaxoSmithKline (GSK) developed the vaccine TDEN, which is composed of four non-chimeric DENV components attenuated by cell culture passage (Watanaveeradej et al., 2016). After demonstrating varied success in phase I/II trials, development was ultimately terminated due to a lack of durable immunogenicity (Watanaveeradej et al., 2016).

6.4.2.2 Inactivated vaccines

Research into inactivated vaccines have also proven successful. Instead of attenuating viruses by genetic mutation or serial passage, viruses are inactivated by chemical or heat treatment (Sanders et al., 2015). In this way, the vaccine candidate DPIV was developed by WRAIR, GSK, and FIOcruz, and is comprised by formalin inactivated viruses from each serotype (Diaz et al., 2018). In addition, the immune response to the Dengue antigens is boosted by the use of Alum as an adjuvant (Diaz et al., 2018). DPIV has undergone several phase I trials and has completed a phase II trial (Pintado Silva and Fernandez-Sesma, 2023). As of yet, the vaccine has demonstrated good immunogenicity and has been well tolerated with no adverse effects (Pintado Silva and Fernandez-Sesma, 2023).

6.4.2.3 DNA and mRNA vaccines

DNA or mRNA vaccine strategies involve introducing nucleic acids into cells to induce expression of viral epitopes that trigger the immune response and generate immunogenicity (Jain et al., 2023). One DNA vaccine candidate D1ME^{100} was a monovalent DENV2 vaccine containing the sequence of the PrM and E proteins cloned into a pVR1012 vector (Beckett et al., 2011). In a phase I trial begun in 2006, D1ME^{100} failed to induce a strong immune response (Beckett et

al., 2011). Following this, a tetravalent equivalent TVDV was developed and contained the PrM and E sequences from all four serotypes and was combined with the cationic lipid-based adjuvant Vaxfectin (Beckett et al., 2011). In a phase I clinical trial begun in 2016, poor immunogenicity was observed similar to D1ME^{100} (Beckett et al., 2011). Recently a new tetravalent preclinical DNA vaccine candidate DDV was reported, and is comprised of tandem EDIII domain sequences of each serotype linked to the DENV2 NS1 sequence (Sankaradoss et al., 2022). DDV induced robust and balanced immunogenicity in murine preclinical studies and is yet to undergo clinical development (Sankaradoss et al., 2022).

Efforts in mRNA vaccine development have been limited, and only monovalent candidates have been tested in preclinical *in vivo* studies. One vaccine comprised of mRNA encoding the PrM and E proteins of Dengue serotype 1 in a lipid nano particle induced strong immunisation in mice and protected immunocompromised AG129 mice from a lethal dose of live virus (Wollner et al., 2021). In a similar study, candidates were designed by packaging mRNA encoding either the PrM and E proteins, a truncated E protein (E80), or the NS1 protein of DENV2 into lipid nanoparticles (M. Zhang et al., 2020). The E80 alone or E80 combined with the NS1 candidate both induced a robust immune response in mice (M. Zhang et al., 2020). Recently, mRNA vaccines have proven very successful in preventing infection and reducing severity in the SARS-Cov-2 pandemic which began in late 2020 (Szabó et al., 2022). With further development, the Dengue DNA and mRNA candidates may lead to vaccines with similar success.

6.4.2.4 Recombinant protein and peptide vaccines

Like mRNA vaccines, there has been limited research on recombinant protein vaccines. One study outlined the design of the V180 vaccine from a mixture of the E80 truncated E proteins of each serotype adjuvanted with ISCOMATRIX (Govindarajan et al., 2015). In a phase I clinical trial, V180 elicited a strong immune response and was well tolerated with no adverse effects (Manoff et al., 2019).

Like recombinant vaccines, peptide-based vaccines use virus epitope peptides to stimulate an immune response. There have been many studies reporting the identification of peptide vaccine candidates via computational methods with no experimental validation. Recently however, a peptide vaccine candidate that activates $CD8^+$ T cells has emerged (Miauton et al., 2024). To identify $CD8^+$ T cell activator peptides, human leukocyte antigen (HLA) typed cells were infected with Dengue virus, and virus peptides presented on class I MHC proteins were submitted to proteomic analysis (Miauton et al., 2024). Nine peptides of capsid and non-structural proteins covering each serotype were selected for packaging into gold nanoparticles to generate the candidate PepGNP-Dengue (Miauton et al., 2024). Furthermore, a 'self-adjuvanting' carbohydrate layer was incorporated to enhance immunogenicity (Miauton et al., 2024). In a phase I clinical trial, PepGNP-Dengue was well tolerated and successfully induced a Dengue-specific $CD8^+$ T cell response with little activation of the humoral response (Miauton et al., 2024). In this way, the researchers aim to provide cell-mediated immunity whilst avoiding risk of ADE-mediated adverse effects (Miauton et al., 2024).

There have also been efforts into development of viral vector and virus-like particle vaccines, but current candidates remain in preclinical stages (Akter et al., 2024).

Taken together, given the preclinical and clinical success of live-attenuated virus vaccines as well as emerging candidates developed via diverse strategies, it is likely that new tools for controlling Dengue virus will become available in the next few decades.

6.5 Antiviral development for Dengue virus

6.5.1 Challenges to Dengue antiviral research

Antiviral therapies are an alternative and complimentary strategy to vaccines for the control of Dengue virus (M.F. Lee, Wu, et al., 2023). Antiviral compounds inhibit infectivity or the lifecycle of viruses and can be of different molecular classes, such as small molecules, proteins, peptides, monoclonal antibodies, oligomers, DNA/RNA aptamers, or carbohydrates (M.F. Lee, Wu, et al., 2023). They can disrupt any part of the lifecycle to induce an antiviral effect. Some examples include entry inhibitors, structural disruptors, fusion inhibitors, polymerase inhibitors, helicase inhibitors, protein-protein interaction disruptors, and immune modulators (Obi et al., 2021; M.F. Lee, Wu, et al., 2023). Antivirals typically have a different patient use-case compared to vaccines, because they are often administered to individuals already infected with the virus, for whom the antiviral can quickly reduce symptoms, reduce severity, and shorten duration of infection (Andrei, 2021). Antivirals are also useful when no vaccine is available or for administration to immunocompromised individuals who do not respond to vaccination (See, 2022). Contrastingly, vaccines have a prophylactic use in preventing or reducing severity of infection and provide long-term protection instead of the transitory benefit of antiviral therapeutics (Andrei, 2021).

Antiviral compounds can be classified as targeting either host or viral factors, and each strategy has impactful advantages and disadvantages, which are summarised in Figure 6-8. One major consideration is drug resistance. Viruses have a high mutation rate, and this combined with the selective pressure of a vaccine or an antiviral can lead to the emergence of resistant strains (Kimberlin and Whitley, 1996). By targeting host proteins, it is much harder for the virus to circumvent the action of a treatment by mutation (Ji and Li, 2020). On the other hand, this strategy has the risk of interfering with the endogenous function of those targeted proteins, and this can lead to toxicity (Ji and Li, 2020). By targeting virus factors, this is avoided (Ji and Li, 2020). Another important consideration is specificity. Many viral proteins are unique to the virus without a human or host homologue, and targeting these proteins greatly reduces the risk of off-target binding and toxicity (Xia and Liang, 2019). In contrast, the target

epitopes of host proteins may be conserved across protein families and pathways (Xia and Liang, 2019). Lastly, one important advantage of host-targeted antivirals is that a single host protein or pathway can be exploited by multiple viruses, making broad-spectrum activity possible (He et al., 2024). Conversely, viral proteins can be divergent between serotypes or strains, and it can be challenging to identify conserved epitopes or viral mechanisms (Ji and Li, 2020).

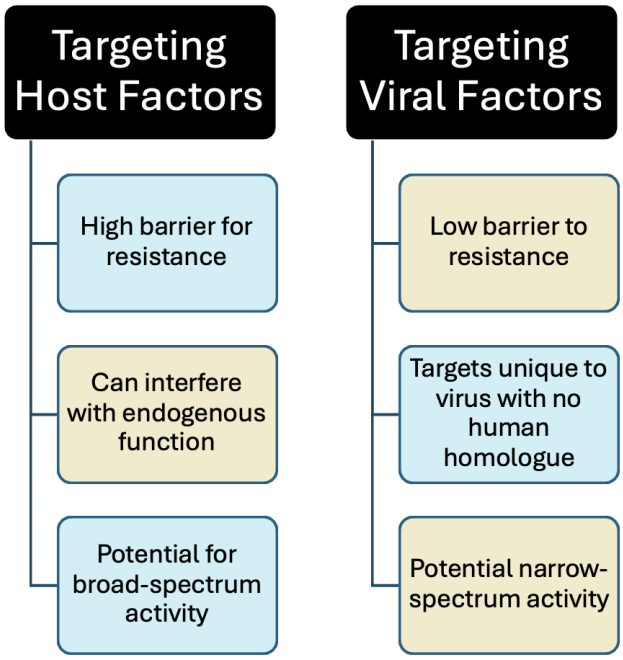

Figure 6-8: Advantages and disadvantages of targeting host or viral factors.

Even though effective vaccines for Dengue virus are starting to emerge, there has been relatively little progress in Dengue virus antivirals, and there are currently no licensed Dengue-targeted antivirals (M.F. Lee, Wu, et al., 2023). This is because antiviral development is challenging and faces similar obstacles as vaccine research. Firstly, the four virus serotypes need to be addressed, and an effective antiviral would need to inhibit each variant, which is difficult to achieve (Lim, 2019). Secondly, many compounds have undergone *in vitro* development, but few have progressed to animal models or clinical testing (M.F. Lee, Wu, et al., 2023). This is mainly due to the lack of accessible and cheap animal models, which makes it difficult to model safety and efficacy before investment in clinical trials (M.F. Lee, Wu, et al., 2023). Thirdly, given the relative rarity and unpredictability of severe Dengue infection combined with the shortfall of research facilities in many endemic areas, conducting clinical

trials can be difficult (Wallace et al., 2013). Lastly, pharmaceutical research is mainly incentivised by return on investment, and areas most affected by Dengue virus often have limited resources and healthcare funding (Mueller-Langer, 2013).

6.5.2 The current state of Dengue virus antiviral development

Despite these difficulties, there has been a marked rise in the clinical development of Dengue antivirals in the last decade, and compounds targeting both viral and host factors have achieved some clinical success (Table 7) (Palanichamy Kala et al., 2023). Research into viral factors is mostly focused on the E, NS3 and NS5 proteins because of their multiple roles and importance to the Dengue lifecycle (M.F. Lee, Wu, et al., 2023). This is exemplified by the small molecule compounds JNJ-64281802 and doxycycline which inhibit NS3 from acting as a protease in cleaving the Dengue polyprotein (Rothan et al., 2014; Kesteleyn et al., 2024). Furthermore, the small molecule AT-752 is a guanosine analogue and inhibits NS5 vRNA replication by acting as a chain terminator for new vRNA strands (Good et al., 2021). These compounds are currently being assessed in clinical trials (NCT05201794, NCT05048875).

In contrast, host-targeting antivirals mainly act on pathways responsible for vascular pathology. For example, the small molecules ketotifen, montelukast, and rupatadine counteract mast cells and other immune cells from producing vasoactive mediators that disrupt endothelial function and promote vascular leakage (St John et al., 2013; Malavige et al., 2018). Acting on a different pathway, the small molecule Zanamivir, a repurposed influenza drug, was suggested to normalise platelet levels and relieve symptoms of bleeding and plasma leakage (Glasner et al., 2017). Zanamivir is a neuraminidase inhibitor that prevents platelet clearance driven by neuraminidase enzymes, which remove sialic acid from platelet membranes (Quach et al., 2018). In addition to small molecules, Carica papaya leaf extract also increases platelet levels, though the mechanism remains unclear (Kasture et al., 2016; Gadhwal et al., 2016).

The increased momentum in antiviral research and clinical research is promising, and a licensed drug may emerge in the near future (M.F. Lee, Wu, et al., 2023).

However, Dengue antiviral research has been historically underfunded and remains neglected in comparison to other viruses like human immunodeficiency virus (HIV) (Perry et al., 2011). As such, further funding and research into Dengue virus antivirals is urgently warranted, especially given the uncertainty of emerging vaccine candidates.

Table 7: Antiviral compounds for Dengue virus in advanced clinical development.

Name	Phase	Status	Class	Mechanism	Clinical data	Trial ID or Trial Reference
JNJ-64281802	II	In progress	Small molecule	NS4B-NS3 interaction disruptor	N/A	NCT05201794 NCT04906980
AT-752	I/II	In progress	Small molecule	guanosine analogue, vRNA chain terminator, inhibits vRNA replication by NS5	N/A	NCT05366439 NCT05466240
Doxycycline	N/A	Compete / In progress	Small molecule	Tetracycline antibiotic, NS2B/NS3 protease inhibitor	Reduction in inflammatory cytokines, faster platelet recovery, reduced length of hospitalisation	CTRI/2018/01/011548 CTRI/2021/09/036661
Eltrombopag	II	Complete	Small molecule	Thrombopoietin receptor agonist normalises platelet levels	Improved platelet recovery and count, reduced bleeding	SLCTR/2019/037 Chakraborty et al., 2020
UV-4B	I	Complete	Small molecule, modified monosaccharide	Iminosugar, alpha-glucosidase inhibitor	Safe and well tolerated in phase I	NCT02061358 Callahan et al., 2022
Zanamivir	I	In progress	Small molecule	Inhibits host sialidase, inhibits NS1 directed endothelial hyperpermeability	N/A	NCT04597437
VIS513	II	In progress	Monoclonal antibody	Neutralising antibody targeting EDIII	N/A	CTRI/2021/07/035290
Ketotifen	IV	In progress	Small molecule	Mast cell stabiliser inhibits release of vasoactive compounds by mast cells and others	N/A	NCT02673840
Montelukast	II/III	Compete / In progress	Small molecule	Leukotriene receptor antagonist inhibits release of vasoactive compounds by mast cells and others	Decreased risk of severe disease	NCT04673422 Ahmad et al., 2018
Rupatadine	II	Complete	Small molecule	Platelet-activating factor and histamine-1 receptor agonist	Improved platelet counts and liver function biomarkers	SLCTR/2014/023 Malavige et al., 2018
Metformin	I/II	Compete / In progress	Small molecule	AMPK activator, counteracts virus induced increased ER colesterol	Decreased risk of severe disease	NCT04377451 Htun et al., 2018 Nguyen et al., 2021
Carica papaya leaf extract	N/A	Complete	Plant extract	Anti-inflammatory and increases platelet production.	Improved platelet counts	Gadhwal et al., 2016 Kasture et al., 2016 Srikanth et al., 2019
Vitamin E	IV	Complete	Small molecule	Unclear mechanism	Faster recovery and liver biomarkers	Vaish et al., 2012 Chathurangana et al., 2017 SLCTR/2015/012
Vitamin C	II	Compete / In progress	Small molecule	Unclear mechanism	Improved platelet recovery and reduced hospitalisation	Kothai Ramalingam et al., 2019 SLCTR/2017/028 CTRI/2019/09/021244
Zinc	N/A	Complete	Metal	Unclear mechanism	Reduced hospitalisation	Rerksuppaphol and Rerksuppaphol, 2018 TCTR20151110001
Melatonin	II	In progress	Small molecule	Unclear mechanism	N/A	NCT05034809

6.6 Peptides as Dengue virus antivirals

As described in the previous section, Dengue antiviral candidates have only recently entered clinical trials, and development has had a predominant focus on small molecules. To increase clinical success, emphasis should also be placed on the development of peptide therapeutics, since they have distinct advantages that allow them to outperform small molecules and other drug classes in many contexts (Craik et al., 2013; Fosgerau and Hoffmann, 2015; Henninot et al., 2018). Reflecting this, licensing and FDA approvals of peptide-based drugs have been steadily increasing over the last 60 years, despite the dominance of small molecules (Muttenthaler et al., 2021). Currently, there are over 80 FDA-approved peptide therapeutics, 150 peptides in clinical trials, and 400-600 peptides in preclinical testing (Fosgerau and Hoffmann, 2015; Lau and Dunn, 2018; Muttenthaler et al., 2021).

6.6.1 Advantages of peptides as therapeutics

This success of peptide therapeutics is due to their exceptional pharmacokinetic properties (Muttenthaler et al., 2021). Compared to small molecules, peptides have a larger binding surface allowing for more interactions with target sites, ensuring remarkable potency and specificity while reducing the risk of off-target binding and subsequent toxicity (Henninot et al., 2018). Such benefits are becoming increasingly important for the pharmaceutical industry, since toxicity and low efficacy are the leading cause of compound attrition in clinical development, and safety regulations are becoming more stringent (Craik et al., 2013; Roberts et al., 2014).

Additionally, the larger binding surface of peptides allows the targeting of the mostly large, flat, and featureless interfaces of protein-protein interactions, which are intractable for small molecules (Lee et al., 2019). This profoundly increases the range of targets accessible for modulation and may lead to breakthroughs for diseases lacking small molecule treatments (Lee et al., 2019).

Another advantage of peptides is that their modular structure makes them easy to rationally design and optimise for affinity, specificity, and pharmacokinetics (Wang et al., 2021). Furthermore, because their amino acid structure is

endogenous to the body and has established metabolic pathways, peptides are less likely to form toxic metabolites (Kong and Heinis, 2021). On the other hand, small molecules have incredibly diverse structures, and it can be difficult to predict metabolic pathways and ensure safety of metabolites (Lomana et al., 2022).

Peptides are also advantageous compared to proteins and antibodies as therapeutics due to their smaller size, allowing for better tissue penetration and less accumulation in the body (Craik et al., 2013; Muttenthaler et al., 2021).

6.6.2 Disadvantages of peptides as therapeutics

Despite the advantages of peptides, small molecule drugs are predominant in the pharmaceutical industry due to key drawbacks of peptides that have historically limited their use (Muttenthaler et al., 2021). Firstly, peptides are often highly charged and polar, preventing membrane permeability and limiting their use to extracellular targets alone (Henninot et al., 2018). Secondly, peptides are highly sensitive to protease degradation in the digestive tract and blood stream, as well as to hydrolysis in the acidic and basic environments of the stomach and gut (Henninot et al., 2018). Adding to this, peptides are rapidly removed from circulation by renal clearance, whereas small molecules are often retained by binding to plasma proteins (Zolla, 2008). Taken together, peptides are poorly bioavailable and must be administered by non-oral routes (Verma et al., 2021). In contrast, small molecules are often membrane permeable and bioavailable by oral administration (Gurevich and Gurevich, 2015). This key drawback of peptides limits their use significantly, since alternative administration routes such as injection are costly and have low patient adherence (Patel et al., 2014).

Another key limitation of peptides is the cost of manufacture. While peptides may be cheaper to produce than proteins and antibodies, organic synthesis and purification of small molecules is significantly cheaper (Di, 2015). This combined with the lack of bioavailability of peptides explains why small molecules have been the predominant focus in therapeutic development (Muttenthaler et al., 2021).

Peptides also have other limitations such as insolubility or aggregation risk, which can be difficult to address by structural modification without compromising affinity and specificity (Li et al., 2018). Lastly, because the immune system recognises pathogens through the protein structure of epitopes, peptides can induce immune responses, which can be a critical source of toxicity and need to be thoroughly assessed to mitigate risk (Fernandez et al., 2018).

6.6.3 Pharmacokinetic optimisation of peptides

Historically, the unfavourable pharmacokinetic properties of peptides have largely precluded their use as therapeutics (Muttenthaler et al., 2021). Nevertheless, given advances in strategies to overcome these limitations, as well as breakthroughs in peptide synthesis and manufacture, peptide drug development has seen remarkable growth and gain in momentum since the late 1980s (Muttenthaler et al., 2021).

Many methods have been developed to overcome protease susceptibility, rapid renal clearance, and short half-life (Di, 2015). Cyclisation of peptides, either head to tail, head to side chain, tail to side chain, or side chain to side chain, confines the conformation and hides cleavage sites from proteases (Figure 6-9) (Hayes et al., 2021). This is achieved by lactonisation, lactamisation, or instalment of sulfide linkages (Di, 2015). Similarly, peptides can be stapled using covalent linkages to increase rigidity and prevent protease recognition, and this is most commonly done on alpha helices (Ali et al., 2019).

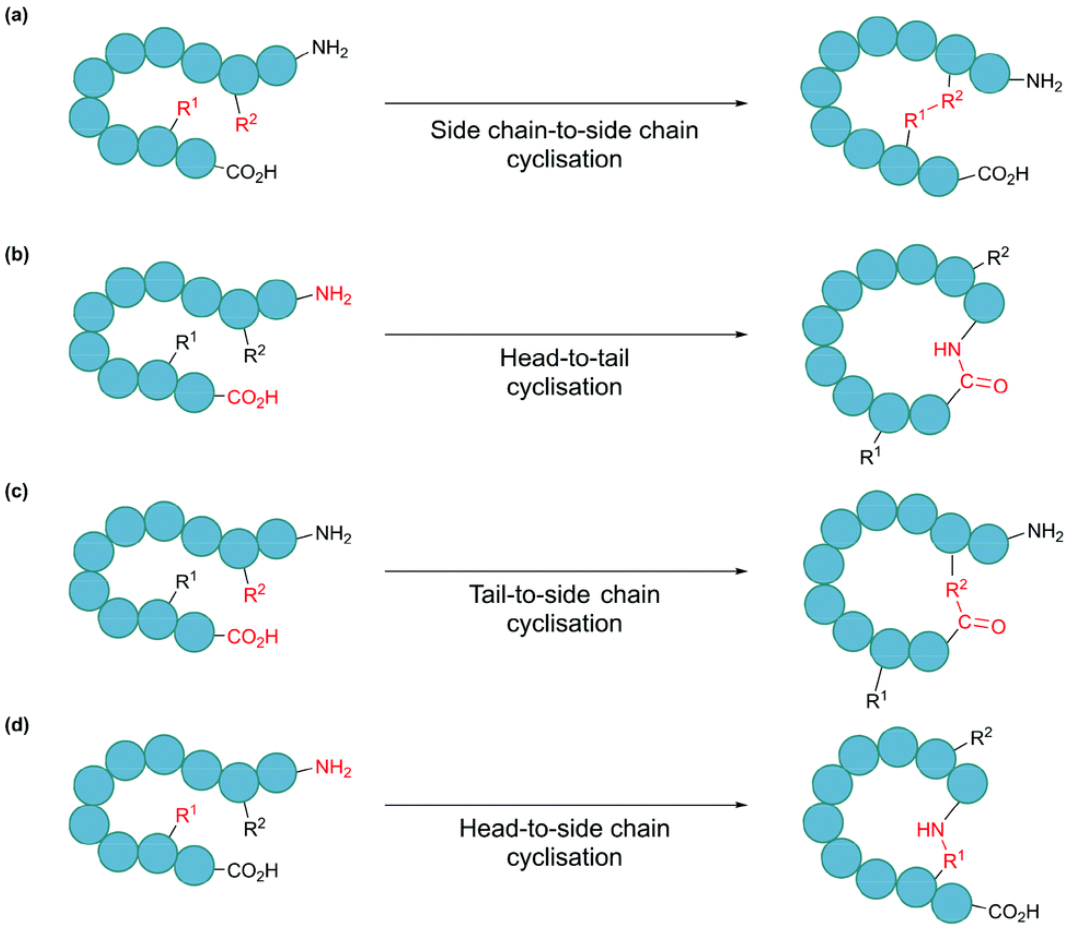

Figure 6-9: Approaches to peptide cyclisation.
Peptides can be cyclised in different ways to improve pharmacokinetic properties. Figure sourced from (Hayes et al., 2021). Reuse is permitted under a CC BY 3.0 License (https://creativecommons.org/licenses/by/3.0/).

Another common technique to improve stability and clearance of peptides is conjugation (Pollaro and Heinis, 2010; Pisal et al., 2010). Peptides can be linked to large polymers such as polyethylene glycol (PEG) or polysialic (PSA) to increase their size and hydrodynamic volume, which reduces glomerular filtration (Pollaro and Heinis, 2010). Additionally, conjugation can block termini or sterically block recognition sites for proteases (Pollaro and Heinis, 2010). Likewise, peptides can be conjugated to plasma proteins like albumin or immunoglobulin which have particularly long circulation times (Pollaro and Heinis, 2010). In this way, the half-life of peptides can be increased from hours to weeks (Di, 2015). This strategy has been applied in the design of the two FDA-approved GLP1 analogue drugs dulaglutide and albiglutide for the treatment of diabetes and has allowed for a once-weekly treatment regimen (Jimenez-Solem et al., 2010; Poole and Nowlan, 2014). Instead of direction conjugation, plasma proteins can also be exploited by addition of small molecule binders such as

small fatty acids (Pollaro and Heinis, 2010). Fatty acid conjugation can provide a further benefit by reducing risk of immunogenicity by shielding binding of T cell receptors (Kurtzhals et al., 2023).

Chemical modification of termini or cleavage sites is another powerful way to prevent recognition by proteases (Di, 2015). Many types of modification have been established, but the most common strategies include termini acetylation and amidation, N-methylation, alpha carbon modification, or use of non-proteinogenic amino acids (Di, 2015). One important example of non-proteinogenic amino acids are D-amino acids, which are stereoisomers of L-amino acids (Feng and Xu, 2016). While D-amino acids share very similar physiochemical properties with their L counterparts, proteases are much less likely to recognise them, increasing the stability and half-life of the peptide (Feng and Xu, 2016). While chemical modification is an effective and versatile way to optimise peptide pharmacokinetics, introduction of non-endogenous structures can increase the risk of metabolic toxicity, tissue accumulation, and immunogenicity (Di, 2015). Therefore, it is important to balance and mitigate these trade-offs during development (Di, 2015).

Permeability is key for the targeting of intracellular proteins, and many techniques have been developed to address peptide impermeability (Di, 2015). Many of the strategies that improve protease resistance also promote permeability. For example, conformational restriction by cyclisation or stapling can mask intramolecular hydrogen bonds and reduce hydrodynamic volume, which promotes membrane permeation (Jwad et al., 2020). To the same effect, methylation of backbone nitrogen atoms removes hydrogen bond donors and promotes hydrophobicity and permeability (Chatterjee et al., 2008). In addition to permeability, cyclisation and stapling have the additional benefits of enhancing potency and specificity (Jwad et al., 2020). These constraints limit the conformational flexibility of peptides to reduce the entropic penalty of binding (Unal et al., 2009).

Permeability can also be addressed by the use of cell-penetrating peptides (CPPs) (Guidotti et al., 2017). CPPs are short 5-30 amino acid long peptides that are either polycationic, containing many basic positively charged residues, or amphipathic, comprising an alternating sequence of charged and hydrophobic

residues (Guidotti et al., 2017). CPPs can traverse cell membranes by either direct penetration or endocytosis by mechanisms that are not fully elucidated, and can carry therapeutic peptides as cargo inside the cell (Pirhaghi et al., 2024). Despite representing a powerful approach, CPPs have only recently entered clinical development and have been limited by the need to characterise toxicity risk and tissue/cell specificity (Pirhaghi et al., 2024). Nevertheless, the first CPP containing protein therapeutic was approved by the FDA in 2022 for the treatment of glabellar lines, and many CPP candidates are undergoing advanced clinical testing (Bottens and Yamada, 2022; Dowdy et al., 2023).

Such advancements have resolved the challenges of peptide pharmacokinetics, and the full potential of peptide therapeutics can now be exploited in the treatment of disease.

6.7 Drug targets for Dengue virus

6.7.1 The Dengue Envelope protein as a drug target

Dengue antiviral research has focussed mainly on the E, NS1, and NS5 proteins because of their multiple functions critical to the virus life cycle (M.F. Lee, Wu, et al., 2023). The Dengue E protein comprises the outer surface of the mature virus particle (Figure 6-10), maintains structural integrity of the virion and mediates the functions of host cell attachment (Chen et al., 1996), receptor mediated endocytosis (Piccini et al., 2015), and endosomal membrane fusion (Modis et al., 2004). For more detail on the E protein and the Dengue life cycle, see Section 6.2. The E protein has a weight of 53 kDa, contains two critical glycosylation sites, and forms the virion surface as homodimers arranged in a herringbone pattern (Kuhn et al., 2002). The E protein is comprised of three domains: Domain I has a beta barrel structure and is located centrally between the other two domains (Modis et al., 2005); Domain II has an elongated finger like structure and contains the hydrophobic fusion loop that mediates fusion of the virus and endosomal membranes (Modis et al., 2005); Domain III has an immunoglobulin structure and forms the solvent exposed surface of the virus particle (Zhang et al., 2004). Domain III is thought to mediate receptor binding during internalisation and is the main target for serotype-specific neutralising antibodies (Bhardwaj et al., 2001). On the C-terminus after domain III, the E

protein has a stem region, which secures the E and M proteins, and a transmembrane motif, which anchors the E protein to the lipid bilayer of the virus (Zhang et al., 2003).

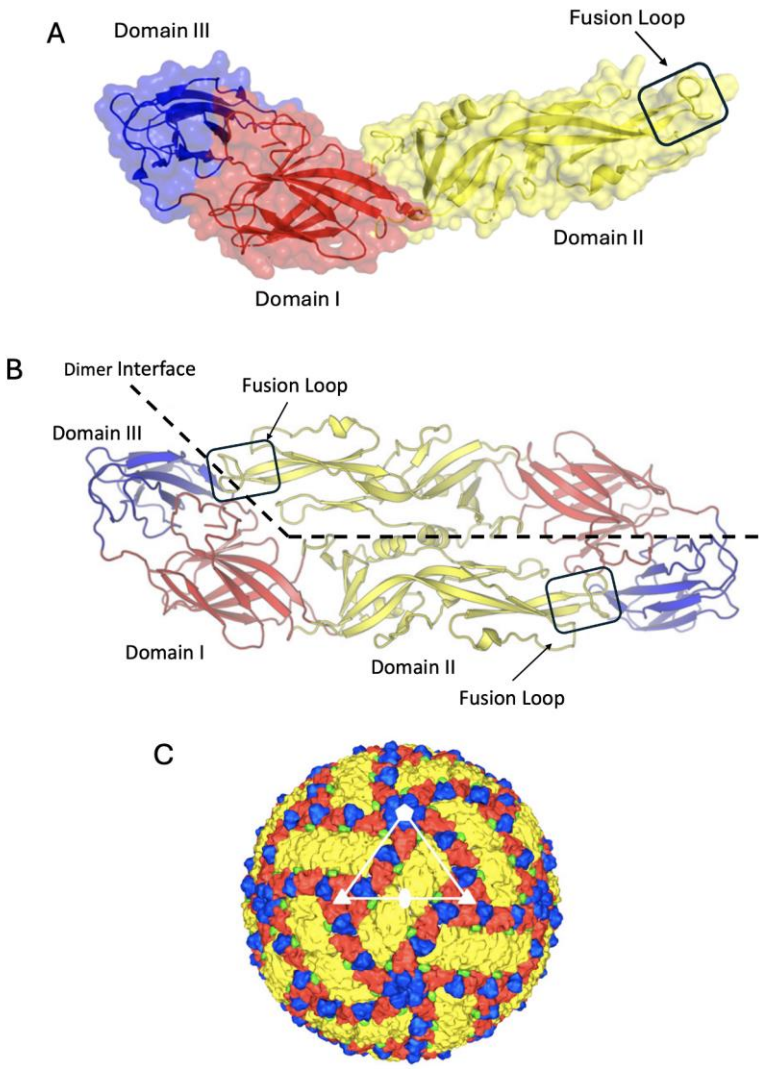

Figure 6-10: Structure of the Dengue E protein.
A: Domain organisation of the E protein. The Domain II fusion loop is indicated. B: E homodimer orientation. Dimer interface and Domain II fusion loop indicated. C: Virion particle. Icosahedral herringbone organisation of E homodimers on the virion surface. An icosahedral asymmetric unit is indicated by a white triangle. Figure adapted from (Wilken and Rimmelzwaan, 2020).

6.7.2 Peptide inhibitors of the Dengue Envelope protein

Efforts in peptide drug development targeting the Dengue E protein have resulted in several preclinical compounds with high efficacy and pan-serotype activity (Table 8) (Anasir et al., 2020; Akshantha et al., 2021). These peptides target three main functions: virion structure and integrity, host cell attachment and endocytosis mediated by receptors, and membrane fusion (Anasir et al., 2020). The compounds DN57opt and MLH40 are biomimetic peptides designed to

target host cell attachment and endocytosis (Costin et al., 2010; Panya et al., 2015). DN57opt is an optimised analogue of an E domain II (EDII) hinge region peptide, and MLH40 originates from the N-terminal ectodomain of the M protein (Costin et al., 2010; Panya et al., 2015). Both peptides were shown to bind the Dengue E protein, disrupting its conformation on the virion surface to hinder host cell attachment and endocytosis (Costin et al., 2010; Panya et al., 2015). DN57opt was more potent with an IC_{50} of 8 μM and was revealed to cause structural abnormalities in Dengue virions by cryogenic electron microscopy (Costin et al., 2010).

P7 is another biomimetic peptide originating from domain III of the E protein (Cui et al., 2018). Instead of disrupting Dengue E conformation, P7 was designed as a competitive inhibitor of a Dengue host cell receptor integrin ß3 (Cui et al., 2018). Binding of P7 disrupted the integrin ß3-E domain III interaction, resulting in impaired virus attachment and internalisation with an IC_{50} of 13 μM against serotypes 1 and 2 (Cui et al., 2018). Acting in a similar mechanism, the peptide DET4 was developed by *de novo* computational design (Alhoot et al., 2013). DET4 was designed to bind to a lateral loop structure on E domain III implicated in receptor interaction, possibly with the receptor heparan sulfate (Hung et al., 2004; Mazumder et al., 2007). DET4 inhibited Dengue serotype 2 with an IC_{50} of 35 μM and was found to disrupt the virion surface structure by transmission electron microscopy (Figure 6-11) (Alhoot et al., 2013).

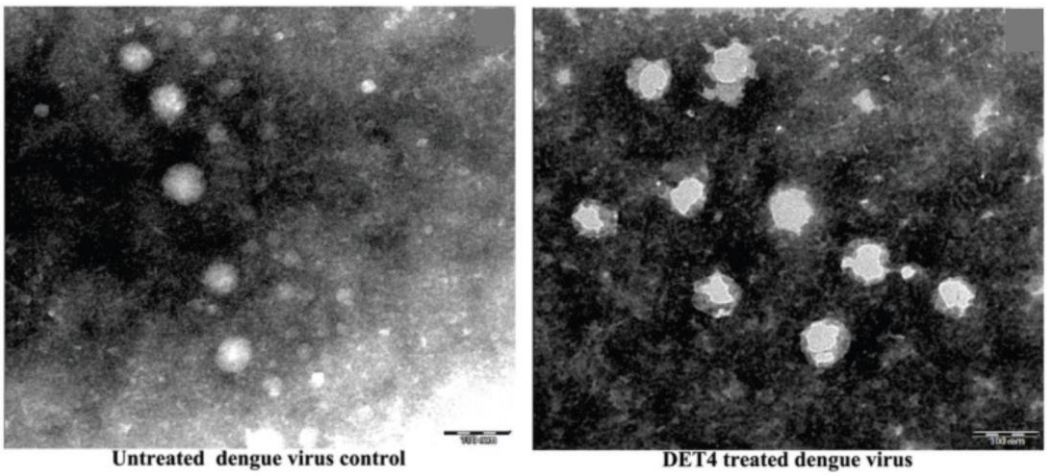

Figure 6-11: Disruption of Dengue Virion Structure by DET4 shown by transmission electron microscopy.
Untreated virions indicate a regular round structure, whereas DET4-treated virions show distorted irregular structures. Image sourced from Alhoot et al., 2013.

E inhibitors have also been discovered from natural products. LL-37 is an antimicrobial peptide found in human skin and was found to inhibit infection of Dengue serotype 2 at 10-15 μM (Alagarasu et al., 2017). Likewise, the bioactive peptide Pep-RTYM was discovered from *Acacia catechu* and inhibited Dengue serotype 2 with the low IC_{50} of 7.9 μM (Panya et al., 2020). Both peptides were shown to bind E domain III but the inhibitory mechanism remains unclear (Alagarasu et al., 2017; Panya et al., 2020).

Other peptides target E-mediated membrane fusion and subsequent nucleocapsid release. In this process, the E protein undergoes extensive conformational changes to expose the fusion loop and bring the virus and endosomal membranes into contact (Modis et al., 2004). Potent biomimetic peptide inhibitors have been designed to bind the E fusion intermediates and disrupt this process. The peptides $DV^{419-447}$ and DN59 both originate from the N-terminal stem region of the E protein and effectively inhibit infection by preventing membrane fusion (Hrobowski et al., 2005; Schmidt et al., 2010). $DV^{419-447}$ in particular exhibits pan-serotype inhibition with an impressive IC_{50} of 0.1-2 μM (Schmidt et al., 2010). Additionally, cryogenic electron microscopy revealed that DN59 had virucidal action by disruption of the virion surface, causing pore formation and release of vRNA (Lok et al., 2012).

Another fusion inhibitor peptide was designed by *do novo* docking to a conserved β-OG pocket positioned at a E domain I/II hinge region (Modis et al., 2003; Panya et al., 2014). The glutamic acid–phenylalanine dipeptide EF was found to occupy this site, and inhibited fusion by hindering E conformational mobility (Panya et al., 2014). EF inhibited DENV2 infection with an IC_{50} of 96 μM. Given the smaller structure of EF relative to other fusion inhibitors like $DV^{419-447}$, EF may form fewer bonding interactions with the envelope protein, resulting in a higher IC_{50} (Panya et al., 2015).

In a recent large-scale investigation into biomimetic peptides, several inhibitory sequences were discovered from different positions on the E protein (M.F. Lee, Anasir, et al., 2023). Peptide 5F was the most potent and inhibited Dengue serotype 2 with an IC_{50} of 33 μM (M.F. Lee, Anasir, et al., 2023). Intriguingly, these compounds were found to act on both the pre and post-fusion stages and were active across serotypes (M.F. Lee, Anasir, et al., 2023). The mechanisms

were not elucidated in this study, and further investigation using techniques such as molecular docking or X-ray crystallography may reveal novel E target sites or strategies for inhibition.

In summary, several preclinical peptide inhibitors of the Dengue E protein have been developed that exhibit high potency and pan-serotype activity. Analogous to these, two first-in-class peptides have been approved for use as therapeutics against other viruses. Bulevirtide was approved in 2020 by the European Medical Agency for the treatment of hepatitis D infection (HDV) (Kang and Syed, 2020). Bulevirtide is a biomimetic peptide of the hepatitis surface protein and binds to the host receptor sodium taurocholate co-transporter polypeptide (NTCP) to inhibit infection with an IC_{50} of 50 nM (Nkongolo et al., 2014). This strategy of competitive inhibition of host receptors is exactly analogous to the Dengue peptide P7 mentioned above.

Similar to Bulevirtide, Enfuvirtide is another first-in-class peptide drug which was approved in 2003 by the FDA for the treatment of AIDS/HIV (Dando and Perry, 2003). Enfuvirtide was designed as a biomimetic peptide of the HIV gp41 surface protein to bind and disrupt protein-protein interactions necessary for conformational rearrangement and membrane fusion (Dando and Perry, 2003). Like Bulevirtide, Enfuvirtide has a low nanomolar IC_{50} of 100 nM (Wild et al., 1994). This allosteric fusion inhibitor strategy is directly analogous to the Dengue peptides $DV2^{419-447}$ and DN59.

Given the preclinical advances and diversity of Dengue E disruptor peptides, antiviral peptide research on this target is a promising route for the development of a successful drug for Dengue virus similar to the HDV and HIV drugs Bulevirtide and Enfuvirtide. To achieve such a potent and viable drug, additional research and funding is required for the discovery of more peptide disruptors, optimisation, and testing at *in vivo* and clinical stages.

Table 8: Antiviral peptides targeting the Dengue E protein.

Peptide	Type	Design Method	Mechanism	IC_{50} and Serotype	Reference
DN57opt	Attachment or entry, structural disruptor	EDII hinge peptide	Disrupts conformation of DII hinge, disrupts virus surface (cryo-EM)	DENV2, 8 μM	Costin et al., 2010
MLH40	Attachment inhibitor	M peptide	Disrupts M-E interaction, alters E dimer conformation, inhibits attachment	DENV1-4, 24-31 μM	Panya et al., 2015
DET4	Attachment or entry, structural disruptor	*de novo*	Binds EDIII, may block heparan sulfate receptor	DENV2, 35 μM	Alhoot et al., 2013
P7	Attachment or entry	DIII peptide	Binds integrin ß3 to disrupt DIII-integrin ß3 receptor	DENV1-2, 13 μM	Cui et al., 2018, p.7
LL-37	Unknown	Natural product, human antimicrobial peptide	Binds EDIII-EDII groove	DENV2, 10-15 μM	Alagarasu et al., 2017
Pep-RTYM	Attachment or entry	Natural Product, plant peptide	Binds to EDIII, disrupts attachment or receptor mediated internalisation	DENV2, 7.9 μM	Panya et al., 2020
$DV2^{419-447}$	Fusion conformation inhibitor	Stem peptide	Disrupts fusion conformation, binds E stem	DENV1-4, 0.1-2μM	Schmidt et al., 2010
DN59	Fusion conformation inhibitor, structural disruptor	Stem peptide	Disrupts fusion conformation, binds E stem, disrupts virus surface (cryo-EM)	DENV1-4, 2-5 μM	Hrobowski et al., 2005 Lok et al., 2012
EF	Fusion conformation inhibitor	*de novo*	Disrupts fusion conformation, binds ß-OG pocket	DENV2, 96 μM	(Panya et al., 2014)
Peptide 3, 4, 5F	Multiple mechanisms	E peptides	Various activities pre-attachment and pre and post-fusion	5F: DENV2, 33 μM, Peptides active against all serotypes	(M.F. Lee, Anasir, et al., 2023)

6.8 Heat shock proteins and viral infection

Since peptides are advantageous over small molecules, particularly in the disruption of protein-protein interactions, they have the potential to become effective Dengue antivirals. In developing a peptide disruptor, heat shock proteins (HSPs) are promising targets because they form extensive interactions with viral proteins to facilitate their life cycle (Zhang and Yu, 2022).

HSPs are a superfamily of protein chaperones which maintain proteostasis and protein turnover (Lindquist and Craig, 1988). HSPs are fundamental to cell biology and are expressed in all prokaryotic and eukaryotic organisms (Lindquist and Craig, 1988). They are highly conserved across species and comprise 5-10 % of all expressed protein (Pockley, 2003). HSPs regulate the folding, degradation, and transport of many proteins involved in diverse pathways and cellular processes (Lindquist and Craig, 1988). While fulfilling many functions under basal conditions, HSPs are upregulated in response to cell stressors such as heat, cold, hypoxia, heavy metals, toxins, starvation, irradiation, and microbial infection (Tkačová and Angelovičová, 2012). HSPs enhance cell survival against these factors by counteracting protein denaturation and coordinating cellular responses (Tkačová and Angelovičová, 2012).

Among these external factors, viral infection is a significant cell stressor (Zhang and Yu, 2022). Because HSPs influence many cell processes, the relationship between HSPs and viral infection is complex. As antiviral factors, HSPs primarily activate and regulate the immune response, but direct inhibition of viral processes may also occur (Pockley, 2003; Zhang and Yu, 2022). Conversely, HSPs can be proviral when their function is usurped by viral factors to promote replication and infectivity (Zhang and Yu, 2022). Because viral genomes are small, viral proteins must be highly versatile and fulfil multiple functions in the lifecycle (Wei et al., 2024). To adopt the wide range of conformations required for these roles, viral proteins often exploit HSP chaperone function (Wei et al., 2024). In addition, viral proteins disrupt HSP signalling pathways for immune suppression and to tune the cellular environment to favour viral replication (Pockley, 2003; Zhang and Yu, 2022).

6.9 HSP90 in viral infection

By exploitation of chaperone function and signalling, the heat shock protein 90 (HSP90) family have been found to provide pro-viral functions for many different viruses including Dengue virus (Y. Wang et al., 2017; Zhang and Yu, 2022; Wei et al., 2024). HSP90 family proteins have a molecular weight of 90 kDa and have three main categories based on localisation and homology: cytoplasmic (HSP90α, HSP90ß), ER (GRP94/endoplasmin), and mitochondrial (TRAP-1) (Hoter et al., 2018). Of the cytoplasmic isoforms, HSP90α is inducible upon cell stress, and

HSP90ß is constitutively expressed (Hoter et al., 2018). These isoforms have high sequence homology of 85 % and share similar function (Johnson, 2012). Because of this, HSP90α and HSP90β are often not distinguished in the literature, simply being termed HSP90 (Hoter et al., 2018). Like other HSPs, cytoplasmic HSP90 has an essential role in proteostasis by regulation of protein folding and aggregation (Wei et al., 2024). Compared to other HSPs, HSP90 is distinguished by an extensive involvement in cell signalling pathways, providing conformational maturation of transcription factors, kinases, and steroid hormone receptors (Wei et al., 2024). In this way, HSP90 influences processes including the cell cycle, apoptosis, development, differentiation, and immune signalling (Hoter et al., 2018).

HSP90 exists primarily as a homodimer and consists of three conserved domains (Figure 6-12) (Jackson, 2013). The N-terminal domain (NTD) contains an ATP binding site, which allows HSP90 to exert an active chaperone function on client proteins as part of an association-dissociation folding cycle (Li et al., 2011). This site is also a target for competitive inhibition by the main HSP90 inhibitors geldanamycin, 17-AAG, and radicicol (Sanchez et al., 2020). The middle or M domain (MD) is the main site for the binding of client proteins (Jackson, 2013). Lastly, the C-terminal domain (CTD) contains a dimerisation motif, a calmodulin binding site, and an additional nucleotide binding site that allosterically modulates ATP hydrolysis (Jackson, 2013). To regulate chaperone activity and specificity, HSP90 coordinates with a complex network of co-chaperones via binding sites located in each domain (Sanchez et al., 2020). In the CTD specifically, a characteristic MEEVD motif acts as a binding site for co-chaperones with TPR-domains (Scheufler et al., 2000). HSP90 function is also regulated transcriptionally and by post-transcriptional modifications including phosphorylation, acetylation, nitrosylation and SUMOylation (Prodromou, 2016; Hoter et al., 2018).

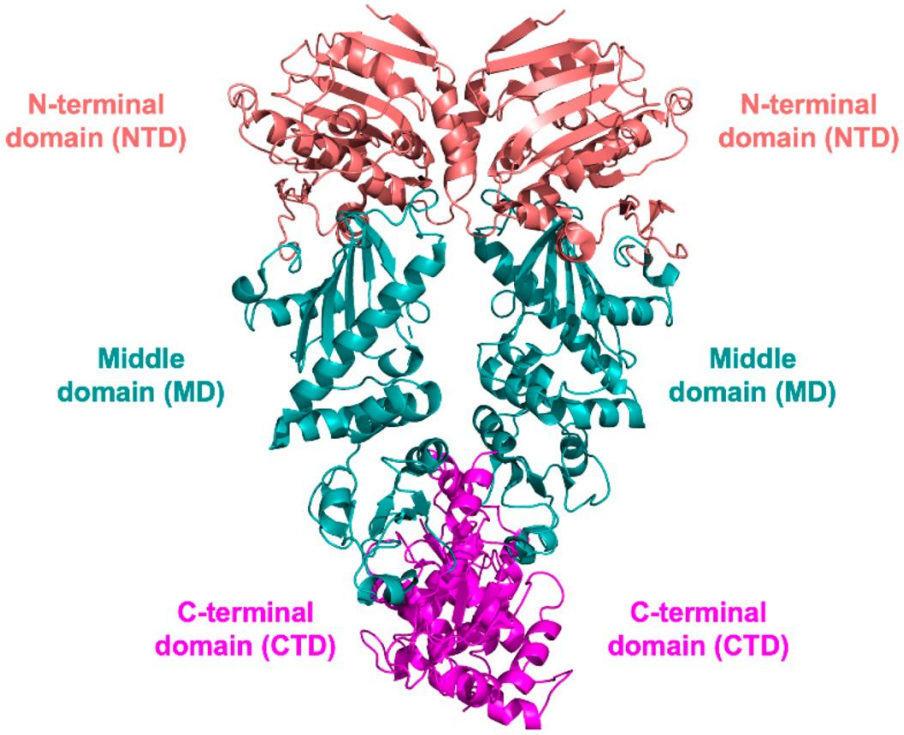

Figure 6-12: Domain structure of HSP90.
The HSP90 protein is homodimeric and is comprised of three domains. The N-terminal domain, middle domain, and C-terminal domain are shown in red, cyan, and magenta respectively. Figure sourced from Tassone et al., 2022.

HSP90 is heavily implicated in viral infection (Y. Wang et al., 2017). The conformational maturation of HSP90 is known to be exploited by several viruses (Y. Wang et al., 2017). Polymerases of Indiana vesiculovirus (VSV), chikungunya virus, and respiratory syncytial virus (RSV) bind to HSP90 to promote stability and enzyme activity (Connor et al., 2007; Geller et al., 2013; Rathore et al., 2014). Intracellular trafficking functions of HSP90 are also exploited by viruses. For example, the viral DNA polymerase of herpes simplex virus (HSV-1) and Epstein-Barr Virus (HBV) have been shown depend upon HSP90 for nuclear translocation (Burch and Weller, 2005; Kawashima et al., 2013). In the case of HSV-1, inhibition of HSP90 resulted in mis-localisation of the DNA polymerase and decreased viral yields in infected cells (Li et al., 2004; Burch and Weller, 2005). Additionally, viral factors bind to HSP90 to inhibit its role in the immune response. For example, the HBV DNA polymerase was shown to bind to HSP90 and disrupt the interaction between the HSP90/Cdc37 complex and IKK/NEMO, thereby preventing NFκB nuclear translocation and suppressing immune signalling (Liu et al., 2014).

Importantly for this thesis, HSP90 is a proviral factor in Dengue virus infection. HSP90 was found to interact with much of the Dengue proteome (Srisutthisamphan et al., 2018), facilitate host cell entry (Reyes-del Valle et al., 2005; Chavez-Salinas et al., 2008; Howe et al., 2016), and modulate host innate immune responses (Roby et al., 2020; Li et al., 2021). This raises the possibility that HSP90 inhibition may be a valuable strategy for antiviral development against Dengue virus. However, HSP90 inhibitors for viral infection have failed to reach clinical use, despite increasing attention and research efforts (Zhang and Yu, 2022). This has been attributed to small molecule toxicity, stability, and adverse effects caused by inhibition of endogenous HSP90 function (Zhang and Yu, 2022). By using peptides to disrupt pro-viral interactions of HSP90 with Dengue factors rather than HSP90 inactivation or degradation, endogenous HSP90 function may be preserved, mitigating toxicity. Peptides are in a prime position to exploit this orthogonal mechanism and may prove to be effective Dengue antivirals.

6.10 Roles of HSP90 in Dengue virus infection

6.10.1 HSP90-E interaction

Several studies have implicated HSP90 to be involved with Dengue virus internalisation mediated by the E protein (Reyes-del Valle et al., 2005; Chavez-Salinas et al., 2008; Howe et al., 2016). Reyes-del Valle et al. (2005) discovered the interaction of HSP90 with the E protein using E affinity chromatography and pull-down assays in a neuroblastoma cell line, a monocytic cell line, and peripheral blood monocytes (PBMCs). This was corroborated by Srisutthisamphan et al. (2018) who surveyed the HSP90 Dengue interactome and validated E-HSP90 binding by reciprocal co-immunoprecipitation and colocalisation experiments. Moreover, in the study by Reyes-del Valle et al. (2005), HSP90 was found to bind HSP70 and form a E receptor complex on the cell membrane of peripheral blood monocytes and macrophages. Competitive inhibition of Dengue virus infection was demonstrated using recombinant HSP90 as a decoy inhibitor, or by treatment of HSP90 or HSP70-directed antibodies in the neuroblastoma cell line (Figure 6-13) and PBMCs and macrophages (Reyes-del Valle et al., 2005). Furthermore, the HSP90/HSP70 receptor complex associated with lipid-enriched microdomains or rafts on the cell membrane of monocytic cells, and treatment

of a raft disruptor induced a strong antiviral effect (Reyes-del Valle et al., 2005).

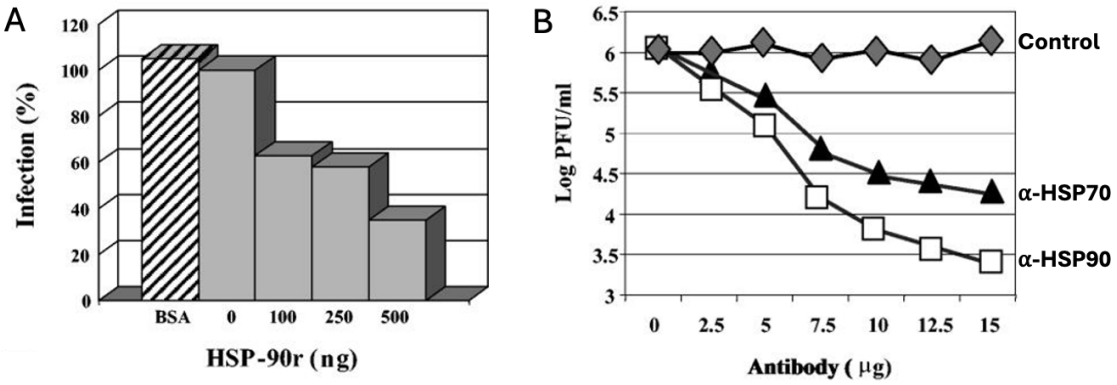

Figure 6-13: Competitive inhibition of the E-HSP90/HSP70 interaction.
Recombinant HSP90 or antibodies directed against HSP90 or HSP70 inhibited Dengue virus infection in in SH-SY5Y neuroblastoma cells. A: virus was incubated for 1 h before exposure to host cells and infection was inhibited. B: Cells were incubated with antibody for 1 h before exposure to Dengue virus. Treatment of control, anti-HSP70 or anti-HSP90 antibodies are indicated as diamonds, triangles, and squares respectively. Figure sourced from Reyes-del Valle et al., 2005.

In a follow-up study by the same group, heat shock of monocytic cells increased cell surface expression of the HSP90/HSP70 complex, and Dengue virus infectivity was increased two-fold (Chavez-Salinas et al., 2008). Intriguingly, heat shock had no effect on virus attachment to host cells, but instead facilitated virus entry as shown by flow cytometry (Chavez-Salinas et al., 2008). HSP90 was therefore implicated in receptor-mediated endocytosis of Dengue virus and not in cell attachment (Chavez-Salinas et al., 2008).

Taken together, the clear role of HSP90 as an endocytosis receptor for Dengue virus infection highlights its potential as a drug target. HSP90 inhibition may therefore prevent virus entry or interfere with E function after host cell engagement. However, existing data on the impact of chemical HSP90 inhibition on Dengue infectivity are conflicting. Srisutthisamphan et al. (2018) described that HSP90 inhibition by geldanamycin resulted in only a slight antiviral effect, and only the detection of Dengue E in the cell decreased with no effect on the other proteins. This was accompanied by increased E protein in the cell media (Srisutthisamphan et al., 2018). In another study, researchers investigating the impact of Dengue infection on a complex of HSP90 with NLRP12 showed that it mediates an antiviral IFN-induced innate immune response (Li et al., 2021). In

monocytic cells infected with Dengue virus, overexpression of NLRP12 potently reduced detection of NS5 and viral RNA (Li et al., 2021). Inhibition of HSP90 by 17-DMAG exerted a pro-viral effect and reversed this change, and this vRNA restoration was also shown in Japanese Encephalitis, Yellow Fever and Zika Viruses (Li et al., 2021). This observation seemingly conflicts with the geldanamycin data from Srisutthisamphan et al. (2018). However, this pro-viral effect of HSP90 inhibition may be specific to NLRP12 overexpression, where pro-immune signalling may be a limiting factor for Dengue infection. Results from HSP90 inhibition in other flaviviruses is also conflicting. In Japanese encephalitis virus, HSP90 inhibition resulted in NS5 degradation and reduced virus copy numbers (Lu et al., 2017). Contrastingly, HSP90 inhibition in WNV and ZIKV seemingly increased expression of virus genomic RNA and viral protein including NS5 (Roby et al., 2020).

These discordant findings reflect that HSP90 has wide-reaching endogenous functions and has both proviral and antiviral roles during infection of Dengue virus and other flaviviruses. Therefore, chemical inhibition of HSP90 may disrupt both protective and deleterious HSP90 pathways and may not be a viable strategy. Compared to broad chemical inhibition, the study by Reyes-del Valle et al. (2005) showed that specific disruption of the Dengue E–HSP90 interaction resulted in robust inhibition of viral entry and infectivity. Given the advantages of peptides in disrupting PPIs, disruption of the E-HSP90 interaction by a peptide candidate may reproduce the viral entry inhibition shown by antibodies and recombinant HSP90 (Reyes-del Valle et al. 2005). In addition, the unique potency and selectivity of peptide compounds may increase the chance of success in clinical testing. This strategy of competitive inhibition of viral entry receptors has been proven by the licensed peptide drugs Bulevirtide for HBV and Miraviroc for HIV, which exhibit near picomolar affinity and are well tolerated (MacArthur and Novak, 2008; Kang and Syed, 2020). In conclusion, development of a peptide disruptor of the HSP90-E interaction may lead to a novel Dengue virus entry inhibitor which is urgently needed for treatment and control of this disease.

6.11 Peptide array screening for peptide discovery

As postulated above, proviral interactions of HSP90 with the Dengue virus E protein represent promising drug targets. The project described in this thesis has the goal of advancing towards the development of an urgently needed Dengue antiviral therapeutic by the discovery and development of protein-protein interaction disruptor peptides. To this end, a discovery pipeline was designed centred on the screening of peptide arrays. Peptide array screening is a rapid, cost effective, and versatile technique for the high-throughput screening of hundreds of peptide sequences (Katz et al., 2011; Amartely et al., 2014). Peptide arrays are synthetic libraries of 2-25mer peptides immobilised on cellulose membranes (Katz et al., 2011). By use of a far-western screening method, peptides binding to a protein target can be identified for applications including epitope mapping of protein-protein interactions as well as rational peptide discovery and structural optimisation.

6.12 Research aims

Dengue virus is an increasingly critical threat to global health that remains unchecked. While second-generation vaccines are only just emerging into clinical use worldwide, research into antiviral inhibition is an underdeveloped field. Peptide therapeutics are demonstrating increasing clinical success, especially for targets intractable for small molecules such as protein-protein interactions. Given the limited progress in small molecule Dengue antivirals, peptide disruptors of viral protein-protein interactions are an unexplored and promising strategy.

Studies have shown that Dengue virus exploits HSP90 chaperone function and signalling to promote infectivity and replication through interaction with the Dengue E protein (see Section 6.10.1). Disruption of the E-HSP90 interaction has been shown to inhibit receptor-mediated endocytosis of Dengue virus into host cells. In light of these findings, the following aims were addressed in this thesis with the overarching goal of developing novel antiviral peptide compounds of Dengue virus.

Chapter 8

- To develop a method for preparing HSP90 protein by recombinant bacterial expression, IMAC isolation, and purification by ion exchange and size exclusion chromatography.

Chapter 9

- To identify binding epitopes on the Dengue E protein for HSP90 by peptide array screening.

- To assess the pharmacokinetic suitability of E epitopes as peptide therapeutic candidates using computational prediction tools.

- To develop epitopes into candidate peptides by structural optimisation using peptide array screening.

- To evaluate cytotoxicity and antiviral efficacy of candidates by *in vitro* assays.

Chapter 7 Materials and Methods

7.1 Antibodies

7.1.1 Primary antibodies

Table 9: List of primary antibodies.
WB, western blot; PLA, proximity ligation assay; IFA, Dengue Virus immunofluorescence assay.

Antibody	Dilution	Company	Catalogue Number
α-HSP90 (rabbit polyclonal)	WB: 1:2000 PLA: 1:200 Arrays: 1:1000	Santa Cruz	sc7947
α-6His HRP (mouse monoclonal)	WB: 1:2000	Sigma-Aldrich	A7058
α-DYKDDDDK (flag tag) M2 (rabbit polyclonal)	WB: 1:5000 PLA: 1:200	Sigma-Aldrich	F3165
α-GAPDH (mouse monoclonal)	WB: 1:80,000	Proteintech	60004-1-Ig
4G2 α-Dengue E (mouse monoclonal)	-	In-house, Chiang Mai University	-
α-NS5 (mouse monoclonal)	IFA: 1:100	Invitrogen	MA5-17295

7.1.2 Secondary antibodies

Table 10: List of secondary antibodies.
WB, western blot; IFA, Dengue Virus immunofluorescence assay.

Antibody	Dilution	Company	Catalogue Number
α-rabbit IgG (donkey, 800 nm)	WB: 1:5000	LI-COR	926-32213
α-mouse IgG (donkey, 800 nm)	WB: 1:5000	LI-COR	926-32212
α-mouse IgG (goat, 680 nm)	WB: 1:5000	Invitrogen	A-21057
α-mouse IgG (rabbit, HRP)	ELISA: 1:2000	Agilent/Dako	P026002-2
α-mouse IgG (goat, 488 nm)	IFA: 1:1000	Invitrogen	A28175

7.2 Bacterial transformation and isolation of plasmid DNA

7.2.1 HSP90 plasmids

A plasmid containing HSP90 was ordered from GenScript Biotech (New Jersey, U.S.). The protein sequence of HSP90AA1 (GenBank accession NP_001017963.2) was converted to a nucleotide sequence based on the E. coli codon table. Additionally, CC and CTCGAG were added to the 5' and 3' ends respectively to facilitate cloning. This sequence was then inserted into pET-32b(+) vector using NcoI/XhoI restriction sites. By use of the pET-32b(+) vector, transformed bacteria could be grown in the presence of Ampicillin, and the recombinant HSP90 had a C-terminal His tag for purification.

7.2.2 Bacterial Transformation

A working stock of HSP90 plasmid was obtained by transforming competent E. coli cells and isolating plasmid DNA. First, HSP90 plasmid was resuspended in nuclease-free water. DH5α competent E. coli (Invitrogen, cat. 18263012) were thawed on ice. 100 µL of bacteria were transferred to pre-chilled microcentrifuge tubes. 50 ng of plasmid DNA was added, and pUC19 DNA or nuclease-free water were used as positive and negative controls respectively. The bacteria were incubated at 4°C for 30 minutes, heat shocked for 45 seconds at 42 °C in a water bath, then returned to 4 °C for 2 minutes. 950 µL of **Super Optimal broth with Catabolite repression** (S.O.C.) media was added to each tube. The bacteria were shaken at 37 °C for 1 hour at 225 rpm. 100 µL of bacteria was spread on lysogeny broth (LB) agar plates (1% bacto-tryptone (w/v), 0.5% yeast extract (w/v), 1% NaCl (w/v), and 1.5% agar (w/v)) containing 100 µg/mL ampicillin and incubated for 16 hours at 37 °C.

7.2.3 Plasmid DNA Isolation

In order to obtain a stock of plasmid DNA from the transformed E. coli, a culture of E. coli was grown, and plasmid DNA was extracted. A single colony of HSP90 transformed-DH5α bacteria was picked and used to inoculate 10 mL of LB medium with ampicillin (1% bacto-tryptone (w/v), 0.5% yeast extract (w/v),150mM NaCl (w/v), 100 µg/mL ampicillin). This was incubated at 37 °C

overnight with shaking at 225 rpm. Plasmid was isolated using a Miniprep kit (Qiagen, cat. 27104) following the manufacturer's protocol. At the last step, plasmid was eluted from the spin columns using nuclease-free water. The resultant plasmid stock was analysed on a Nanodrop spectrophotometer (Thermo Scientific, cat. ND-2000) for concentration and purity by A260/A280 and A260/A230 ratios, as contaminants can affect subsequent transfection or bacterial transformation. An A260/A280 ratio below 1.8 indicates the presence of protein, phenol, or other contaminants, and an A260/A280 ratio above 2.0 indicates contamination with RNA. An A260/A230 ratio outside the range of 2.0 – 2.2 indicates the contamination of phenol, guanidine, or other organic residues left over from the isolation process.

7.2.4 DNA agarose gel electrophoresis

Following plasmid isolation, the purity and molecular weight of the DNA was assessed using agarose gel electrophoresis. A 1 % agarose gel was prepared by dissolving agarose (Merck, cat. A9539) in TAE buffer (40 mM Tris-acetate, 1 mM EDTA, pH 8.0) using a microwave. The gel was allowed to cool and solidify in a casting tray with comb. The gel was placed in a Bio-Rad Sub-Cell GT electrophoresis tank (Bio-Rad, cat. 1704401) filled with TAE buffer. Plasmid DNA samples (4 µL each) were mixed with 1 µL of 6X loading dye (Thermo Scientific, cat. R0611) and 1 µL of SYTO 60 nucleic acid stain (Invitrogen, cat. S11342) and loaded into the wells alongside a 1 kb DNA ladder (5 µL). The gel was run at 100 V for 1 hour. The DNA bands were visualised using a gel and blot imaging system (LI-COR Odyssey CLx).

7.3 Growth, expression, and purification of recombinant HSP90 protein

7.3.1 Recombinant production of HSP90 protein

The DH5α strain of E. coli was used to prepare plasmid DNA stocks because it has a high transformation efficiency and mutations that reduce alterations of the plasmid DNA sequence (Phue et al., 2008). On the other hand, the BL21(DE3) strain was used for the production of recombinant HSP90 protein, because it can express a T7 RNA polymerase when induced with IPTG (isopropyl-ß-D-

thiogalactopyranoside), allowing for high level expression of plasmid DNA protein under the control of the T7 promotor, such as pET-32b(+)-HSP90.

BL21(DE3) competent E. coli were transformed with HSP90 plasmid (See Section 7.2.2). A single colony was used to inoculate 10 mL of LB medium containing 100 µg/mL ampicillin and was incubated overnight at 37 °C with shaking at 225 rpm. This starter was used to inoculate a 500 mL sample of LB medium with ampicillin, and this culture was incubated at 37 °C with shaking at 225 rpm for approximately 4 hours until an OD600 reading of 0.6-0.8 was reached. The main culture was then induced with 0.1 mM IPTG, VWR chemicals, cat. 437145X) to stimulate expression of the HSP90-pET-32b(+) construct. The culture was incubated for 18 hours at 18 °C with shaking at 225 rpm. The culture was pelleted by centrifugation at 6000 rpm for 10 min at 4 °C and frozen at -80 °C to aid lysis. The pellet was thawed and resuspended in 10 mL imidazole lysis buffer (50 mM tris base, 300 mM NaCl, 10 mM imidazole, pH 7.4, protease inhibitor (Roche, cat. 11873580001)). The solution was sonicated using a model 120 sonic dismembrator (Fisherbrand, cat. 12337338) with a 0.5-15 mL probe (Fisherbrand, cat. 12991171). Sonication was performed on ice at 40 % amplitude in cycles of 30 seconds on, 10 seconds off for a total of 4 minutes. The lysate was divided into 1 mL aliquots and centrifuged at 13,000 rpm at 4 °C for 15 minutes. The supernatant was pooled and frozen at -80 °C.

7.3.2 Immobilised metal affinity chromatography

The pET-32b(+) plasmid of the HSP90 construct expresses the protein with a C-terminal polyhistidine tag, which allows for the isolation of HSP90 by immobilised metal affinity chromatography (IMAC) (Block et al., 2009). By the use of a column loaded with beads conjugated to metal ions, such as Ni^{2+} or Co^{2+}, to which the imidazole side chains of the polyhistidine tag coordinate to, recombinant protein can be isolated from bacterial lysate. Coordinating protein can then be eluted by applying an increasing concentration gradient of imidazole solution to the column. Proteins are therefore separated by affinity to the metal ions.

Nickel NTA beads (Thermo Scientific, cat. 10449164) were washed three times with imidazole buffer (50 mM tris base, 300 mM NaCl, 10 mM imidazole, pH 7.4),

and resuspended to 1 mL in imidazole buffer. This bead solution was added to the HSP90 lysate and rotated for 1 hour at 4 °C. The bead-lysate mixture was added to a 20 mL Econo-Pac chromatography column (Bio-Rad, 7321010), and the flow through was collected. The column was then washed three times with imidazole buffer cooled to 4 °C. A buffer with an increasing gradient of imidazole was then applied to the column in 3 x 1 mL increments, and the elutes were collected. The buffer consisted of a tris buffer (50 mM tris base, 300 mM NaCl, pH 7.4) with increasing concentrations of imidazole (25, 50, 75, 100, 150, 250 mM imidazole). The protein content and purity were analysed by Bradford assay, SDS-PAGE, Coomassie staining, and western blot (See Section 7.7).

7.3.3 Ion exchange chromatography

HSP90 elutes isolated by affinity chromatography were subjected to purification by anion exchange chromatography. This experiment makes use of a column loaded with stationary phase positively charged beads to separate proteins. Negatively charged proteins will bind to the column. By applying a solution gradient of increasing ionic strength (increasing NaCl concentration), sodium and chloride ions will compete with the protein for column-binding, and proteins will elute based on their net negative charge. Proteins with more negative charge will bind to the column more strongly and elute later than less negatively proteins.

After analysing protein content and purity of HSP90 affinity chromatography elutes, the cleanest and most concentrated samples were loaded onto a pre-equilibrated 1 mL-capacity Resource Q column (Cytiva, cat. 17117701) using an ÄKTA pure chromatography system (Cytiva). Low salt (100 mM NaCl) and high salt (1000 mM NaCl) solutions were prepared in tris buffer (50 mM tris, 5 % glycerol, 1 mM TCEP, pH 8). These were used to apply an increasing gradient of salt solution through the column and elute the protein. Fractions were collected in 1 mL increments, and protein elution was monitored by absorbance at 280 nm.

7.3.4 Gel filtration chromatography

Gel filtration was carried out to further purify the protein and normalise NaCl concentration. This experiment makes use of a column loaded with a porous resin. Proteins are separated by size/molecular weight. Small proteins will enter the pores in the gel and travel down the column slowly. Larger proteins cannot enter the pores and will travel through the column in a more direct and quicker route. Therefore, large proteins are eluted first, and smaller proteins are eluted later.

HSP90 eluted from anion exchange chromatography was analysed by SDS-PAGE and Coomassie staining (see Section 7.7). By comparing protein bands, the fractions most concentrated with HSP90 protein and with the fewest impurities were applied onto a pre-equilibrated Superdex 200 Increase 10/300 GL column (Cytiva, cat. 28990944) connected to an ÄKTA pure chromatography system (Cytiva). The column was pre-equilibrated with gel filtration buffer (20 mM Tris-base, 150 mM NaCl, 5% glycerol, 5 mM DTT, pH 8). The sample was loaded at a flow rate of 0.5 mL/min, and elutes were collected in 1 mL increments. Protein elution was monitored by 280 nm absorbance. The protein content and purity were assessed using SDS-PAGE and Coomassie staining (See Section 7.7).

7.4 Peptide Arrays

7.4.1 Peptide array SPOT synthesis

Peptide arrays produced by SPOT synthesis allow for the high throughput screening of synthetic peptides for applications of epitope mapping, and rational peptide discovery and optimisation (Katz et al., 2011; Amartely et al., 2014). Peptide SPOT synthesis relies on standard solid phase Fmoc chemistry but is differentiated by the use of derivatised cellulose membrane as a solid support instead of beads. Peptides are synthesised from the C-terminus, which is attached to a PEG linker of the membrane, to the N-terminus. Reagents, such as amino acids and coupling reagents are spotted onto the membrane to synthesise the peptide. This droplet forms a miniature vessel in which the reaction is confined. By the synthesis of many peptide spots arranged in a grid formation, peptide array libraries can be made, in which each spot consists of thousands of peptide copies in an area of only around 2 mm^2.

Peptide arrays were synthesised by SPOT synthesis using a Multipep RSi automated parallel peptide synthesiser (Intavis). DIC (N,N'-Diisopropylcarbodiimide, Sigma-Aldrich, cat. D125407) and Oxyma Pure (Ethyl 2-cyano-2-(hydroxyimino)acetate, Merck, cat. 8510860500) were used to 'activate' Fmoc amino acids dissolved in DMF (n,n-dimethylformamide, Rathburn, cat. RG2014) before spotting to the membrane (Figure 7-1). In the case of the first amino acid spotted, the amino acid reacts with PEG groups on the membrane to begin the peptide chain. Before spotting of the next amino acid building block, unreacted peptide chains were capped by washing with acetic anhydride (Sigma-Aldrich, cat. 539996) to prevent elongation of deletion peptides. Fmoc groups on the nascent peptide chain were deprotected using piperidine (Sigma-Aldrich, cat. 104094). The membrane was then washed with NMP (1-Methyl-2-pyrrolidinone ,Sigma-Aldrich, cat. 443778) to remove waste products. The next amino acid was then spotted to repeat the cycle, and peptides up to 25 amino acids in length were synthesised.

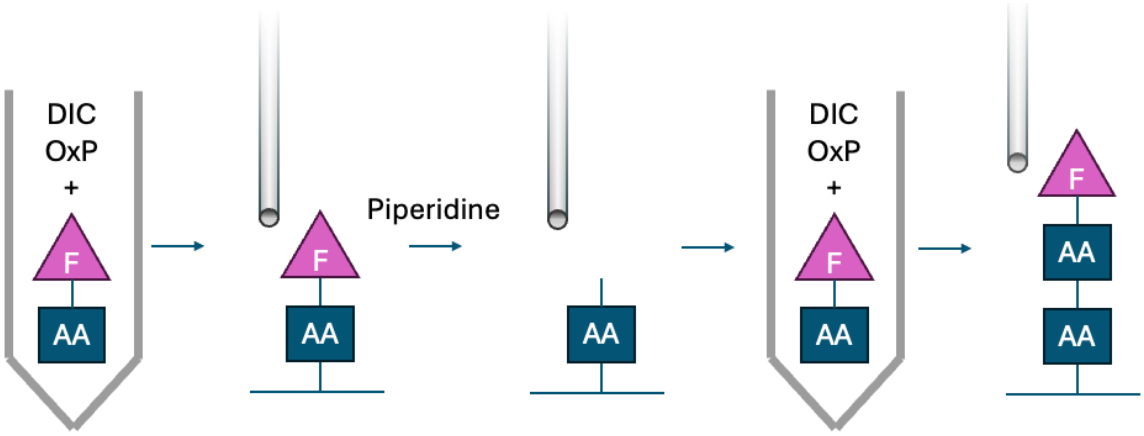

Figure 7-1: Overview of SPOT synthesis of peptide arrays.
Amino acids dissolved in DMF are 'activated' with DIC and Oxyma Pure (OxP). The synthesiser spots these reagents onto the membrane, and the first amino acid links to the membrane via the C-terminus. The synthesiser washes piperidine over the membrane to deprotect the Fmoc group from the N-terminus. The new peptide chain is ready for the next amino acid. The second amino acid then reacts with DIC and Oxyma Pure, and is spotted onto the membrane to build the peptide chain. This process is repeated until the full peptide is synthesised.

To work up, the arrays were incubated with deprotection solution (2 % triisopropylsilane (Sigma-Aldrich, cat. 233781) and 5 % distilled water in trifluoroacetic acid (Fluorochem, cat. F008708)) at room temperature for two hours with gentle agitation. The membranes were then washed three times for 2 minutes each with gentle agitation using DMF, DCM (Sigma-Aldrich, cat. 650463),

then ethanol. After drying, the peptide arrays were visualised and cut to size using a transilluminator (Fisher Scientific, cat. 16515180) then stored at 4 °C.

7.4.2 Peptide array screening by far-western blot

For peptide array applications such as mapping binding epitopes or screening rationally designed peptide libraries, a far-western blot technique is used (Figure 7-2). In the process of mapping the epitopes of a protein-protein interaction, the sequence of one of the proteins is divided up into short overlapping fragments, typically 20mers. An example using the HSP90-E interaction is illustrated in Figure 7-2. These fragments are synthesised in a grid arrangement of peptide spots, with each spot containing many copies of a peptide sequence. A target protein is overlaid, and the binding sequences comprising the epitope are identified by immunodetection. Binding peptides can be developed into candidate disruptors by further peptide array screening for structural optimisation.

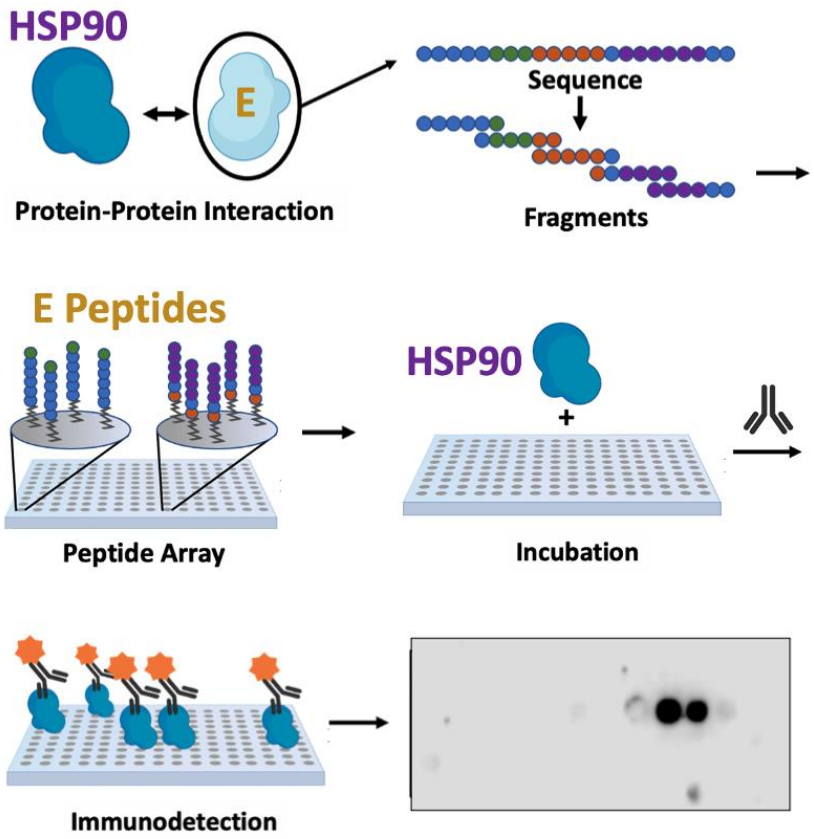

Figure 7-2: Fine-mapping of epitopes in a protein-protein interaction by peptide array screening.
The HSP90-E interaction is used as an example. The sequence of one of the protein partners, in this case E, is synthesised on a peptide array as overlapping fragments. Each spot consists of many copies of one of those fragments. A protein sample of the other binding partner, in this case HSP90, is overlaid, and E binding peptides are identified by immunodetection.

The protocol for this peptide array screening process is summarised in Figure 7-3. Firstly, peptide arrays were rinsed with ethanol and Tris-buffered saline with Tween 20 (TBST) (20 mM tris base, 150 mM NaCl, 0.1 % Tween 20, pH 7.6). The arrays were blocked for two hours at room temperature with gentle agitation with 5 % (w/v) non-fat dry milk in Tris-buffered saline (TBS) (20 mM tris base, 150 mM NaCl, pH 7.6). After a rinse with TBS, the arrays were incubated with target protein overnight at 4 °C with gentle agitation. For cell lysates, a mass of 1-3 mg of total protein was used, which was diluted in TBS with 2.5 % (w/v) non-fat dry milk. For purified protein, a concentration of 0.1-2 µM was used, and was diluted in TBS with 2.5 % (w/v) non-fat dry milk. A buffer-only solution was used to incubate the negative control peptide. After protein incubation, the arrays were washed three times for 10 minutes with TBST. The arrays were then incubated with primary antibody overnight at 4 °C with gentle agitation. Antibodies were diluted in TBST with 2.5 % (w/v) non-fat dry milk (See

Table 5 for dilutions). Following this, the arrays were washed as before, then incubated with secondary antibody for 1 hour at room temperature with gentle agitation (See Table 10 for dilutions). The arrays were washed for a final time, then incubated for 5 minutes at room temperature with gentle agitation with either (i) Pierce Enhanced chemiluminescent substrate (Thermo Scientific, cat. 32106), or (ii) WesternSure Premium Substrate (LI-COR, cat. 926-95000) to detect weak array-protein interactions. Arrays were then imaged on the C-DiGit blot scanner (LI-COR) on high sensitivity for 12 minutes. Spot densitometry and figure preparation were carried out using the PepGenie web application (http://pepgenie.pythonanywhere.com/).

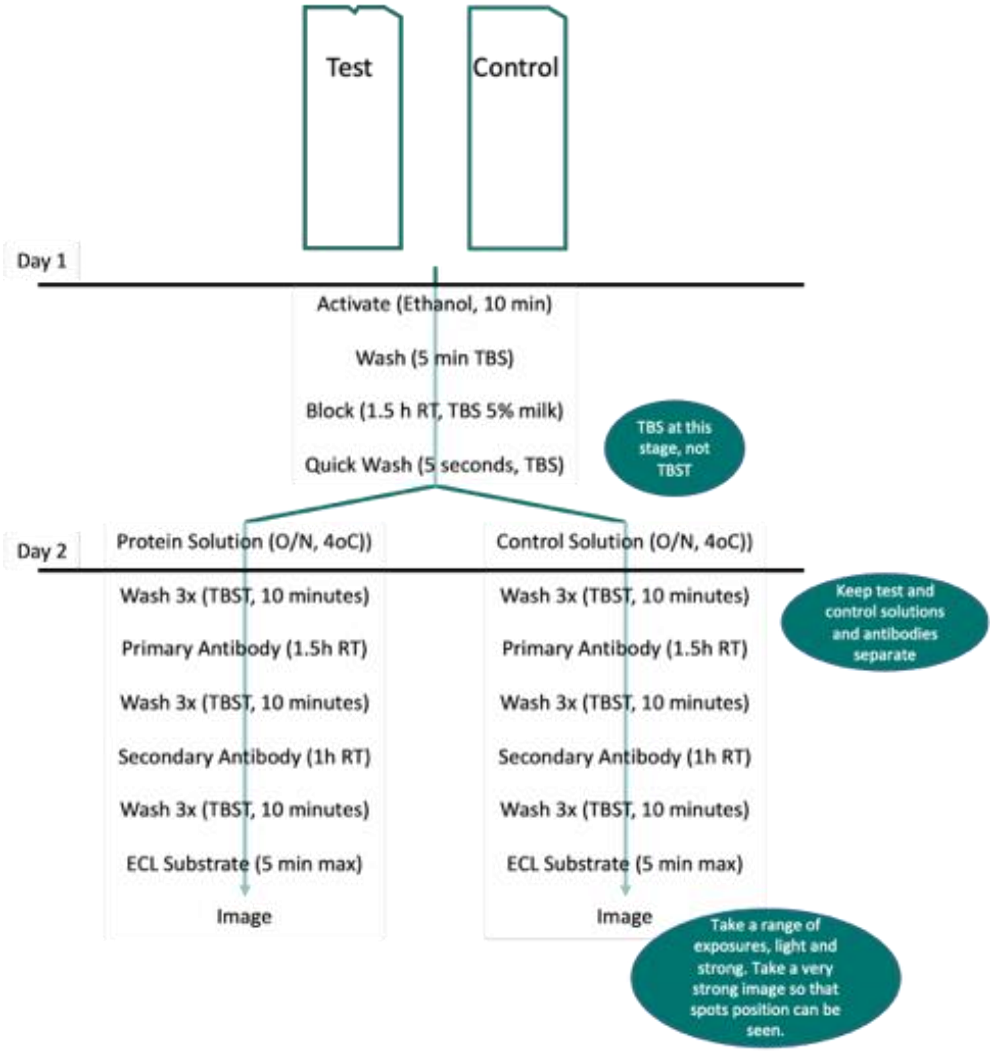

Figure 7-3: Summary of the peptide array screening process.
Peptide arrays are first blocked then incubated with either target protein for the test array, or buffer-only solution for the control array. After incubation with primary and secondary antibodies, binding peptides can be identified using enhanced chemiluminescence (ECL). TBS, Tris-buffered saline; TBST, Tris-buffered saline with Tween 20; O/N, overnight; RT, room temperature.

7.5 Computational peptide analysis tools

7.5.1 3D structural modelling of proteins using PyMOL

Protein and peptide structures were visualised using the PyMOL open-source molecular graphics system (version 3.0.0, Schrödinger Inc) (DeLano, 2002). Existing molecular structures were downloaded from the Research Collaboratory for Structural Bioinformatics (RCSB) Protein Data Bank (PDB, https://www.rcsb.org/) (Berman et al., 2000) in .pdb format. PDB accession codes are stated in figure legends.

7.5.2 Prediction of peptide conformation using PEP-FOLD3

Peptide secondary structure is a major determinant of physiochemical and pharmacokinetic properties, and therefore influences their efficacy as therapeutic agents. The prediction of peptide secondary structure was carried out using the *de novo* peptide structure prediction server PEP-FOLD3 (version 3.5, https://bioserv.rpbs.univ-paris-diderot.fr/services/PEP-FOLD3/). PEP-FOLD3 predicts predict the 3D structures of peptides ranging from 9 to 50 residues by using a coarse-grained force field and a greedy algorithm to sample conformations (Lamiable et al., 2016). Peptide models generated using PEP-FOLD3 were exported to PyMOL for visualisation.

7.5.3 Multiple sequence alignment using Clustal Omega

In order to evaluate the conservation of protein sequences between Dengue Virus serotypes, multiple sequence alignment was performed using Clustal Omega, a robust and scalable multiple sequence alignment (MSA) tool designed for large datasets (Sievers and Higgins, 2018), accessible at https://www.ebi.ac.uk/jdispatcher/msa/clustalo. Alignment output was downloaded in FASTA or Clustal format (.aln-clustal_num) and visualised using Jalview.

7.5.4 Visualisation of multiple sequence alignment using Jalview

Multiple sequence alignments generated by Clustal Omega were analysed and prepared into figures using the open source tool Jalview (desktop application version 2.11.3.3) (Waterhouse et al., 2009). Overall conservation was determined as the average of pairwise alignment scores calculated by Jalview. Per residue conservation scores were calculated by Jalview, which considered both amino acid identity and physiochemical properties. The scale ranged 0-11, with 11 being represented by '*'. The '+' symbol indicated where physiochemical properties are conserved despite an identity mismatch.

7.5.5 PepCalc for estimation of peptide physiochemical properties

The net charge, charge distribution, water solubility, and per-residue polarity of peptides were calculated using the online web application PepCalc (Innovagen AB Inc.) (http://pepcalc.com/). Per-residue hydrophobicity was calculated using the Hopp and Woods scale (Hopp and Woods, 1983). Figures prepared using the application were downloaded from the web server.

7.5.6 Prediction of aggregation potential using Aggrescan

Peptide aggregation is a major obstacle to peptide solubility. Aggregation potential was predicted using the online web application Aggrescan (http://bioinf.uab.es/aggrescan/) (Conchillo-Solé et al., 2007). To identify regions of high aggregation potential, Aggrescan calculates a sliding window average (A_4V) of the A_3V aggregation propensity of each amino acid (de Groot et al., 2005). Five consecutive amino acids with a A_4V above a threshold of -0.02 were classified as an aggregation hotspot. Figures prepared using the application were downloaded from the web server.

7.6 Mammalian cell culture

7.6.1 Media, subculturing, and cryopreservation

All cell lines used in this project are listed in

Table 11. Cells were cultured in 25 cm^2, 75 cm^2, 150 cm^2 culture flasks (Corning, cat. 430639, 430641, 430823) at 37 °C, 5 % CO_2, and 95 % humidity in a cell incubator. Cells were passaged at 70-80 % confluence, and media was refreshed every 3-4 days. Passaging was carried out by the following process. The media was removed, and the cells were washed with sterile-filtered phosphate buffered saline (PBS) warmed to 37 °C. To detach the cells, 0.05% trypsin-EDTA with phenol red (Gibco, 25300054) was added and incubated at 37 °C for 3 minutes or longer until cells detached. The trypsin was inactivated by addition of an equal volume of media warmed to 37 °C, and the solution was centrifuged at 1000 rpm for 3 minutes. The supernatant was removed, and the cell pellet was resuspended in warm media, loaded into a culture flask, and returned to the incubator. A volume of 7, 10, or 25 mL were used for the 25, 75, and 150 cm2 culture flasks respectively. Cell stocks for long-term storage were prepared by resuspending cells with 10 % DMSO (Sigma-Aldrich, cat. 5.89569) in media and storing at -80 °C for 24 hours in a cell freezing container (Thermo Scientific, cat. 5100-0001) before transfer to liquid nitrogen storage. Mycoplasma was regularly screened for using a MycoAlert kit (Lonza, cat. LT07-318).

Table 11: Summary of cell lines used.

Cell line	Origin	Supplier	Media	Passage
HEK293	Human embryonic kidney, epithelial	ATCC: CRL-1573	**DMEM:** 2mM L- Glutamine, 100 U/µg penicillin-streptomycin, 10% fetal bovine serum	1:2-1:10
Vero	African Green Monkey kidney, epithelial	ATCC: CCL-81	**MEM:** 2mM L- Glutamine, 100U/µg penicillin-streptomycin, 10% fetal bovine serum	1:2-1:6
Huh7	Human hepatocellular carcinoma	Cytion: 300156	**DMEM:** 2mM L- Glutamine, 100U/µg penicillin-streptomycin, 10% fetal bovine serum	1:2-1:6
Hmec-1	Human microvascular dermal cells, endothelial	ATCC: CRL-3243	**MCDB:** 2mM L- Glutamine, 10 ng/mL epidermal growth factor, 1 µg/mL hydrocortisone, 100U/µg penicillin- streptomycin, 10% fetal bovine serum	1:2-1:12
C6/36	*Aedes albopictus mosquito embryonic cells*	ATCC: CRL-1660	**Leibowitz-15:** 1 % fetal bovine serum, 10 % tryptose phosphate broth	1:2-1:5

7.6.2 Transfection of mammalian cells with plasmid DNA

NS5 was expressed in mammalian cells by chemical transfection for use in in vitro assays such as proximity ligation assay. A pcDNA3.2 construct containing the NS5 sequence (GenBank accession P29990.1) with a C-terminal flag tag (DYKDDDDK) was provided by Professor Aussara Panya from Chiang Mai University. Transfections were carried out using the Lipofectamine LTX and PLUS reagents (Invitrogen, cat. A12621) according to the manufacturer's protocol. In order to determine the optimal transfection conditions for each cell line, a pilot transfection was conducted to test a range of ratios of plasmid DNA mass to transfection reagents with incubation at 24 or 48 hours. Transfection success was evaluated using western blot.

7.6.3 Cell lysis for protein extraction

Media was removed from cells, and the cells were washed with PBS. Pierce lysis buffer (25 mM tris base, 150 mM NaCl, 1 mM EDTA, 1 % NP-40, 5 % glycerol, pH 7.6) containing protease inhibitor (Roche, cat. 11873580001) was cooled to 4 ˚C and added to the cells. 100-250 µL or 500-1000 µL of lysis buffer was added to each well of 6-well plates or a 10 cm dishes respectively. The cells were

incubated in the buffer for 10 minutes on ice with gentle agitation. The cells were then scraped, and the lysate was rotated at 4 °C for 30 minutes. The lysate was then centrifuged at 14,000 rpm for 15 minutes, and the protein-containing supernatant was collected and either stored at -80 °C or used immediately.

7.7 Protein analysis

7.7.1 Bradford assay

Protein concentration of samples was assessed using Bradford protein assay. The experiment is based on the non-covalent interaction of Coomassie brilliant blue R-250 with protein, causing a change in the charge distribution of the dye. This results in a colour change from brown to blue that is proportional to the protein concentration, which can be quantified by 595 nm absorbance (Bradford, 1976).

A standard protein curve was prepared in triplicate in a clear 96-well plate using bovine serum albumin (BSA, Sigma-Aldrich, cat. A4612). BSA was dissolved in distilled water to prepare 50 µL volumes at concentrations of 0, 0.1, 0.25, 0.5, 0.75, and 1 mg/mL. Protein samples were diluted to an appropriate concentration, and 50 µL volumes were loaded into wells in triplicate. 200 µL of dye reagent (Bio-Rad, cat. 5000006) was added to each well, and the plate was incubated for 15 minutes at room temperature. 595 nm absorbance was measured using a plate reader (Berthold Tristar 5 Multimode Plate Reader). Protein concentration was calculated from the linear equation of the standard curve.

7.7.2 SDS-PAGE

The protein content of isolated recombinant protein or cell/tissue lysates was assessed using sodium dodecyl sulphate polyacrylamide gel electrophoresis (SDS-PAGE). A mini gel tank (Invitrogen, cat. 15384604) was filled with 1x NuPAGE MOPS buffer (Invitrogen, cat. NP0001) and loaded with 10-, 12-, or 15-well NuPAGE Bis-Tris mini protein gels (Invitrogen, cat. NP0321). 5x Lamelli buffer (0.25 % Bromophenol blue (w/v), 5 % ß-mercaptoethanol, 50 % glycerol, 10 % SDS (w/v), 0.25 M tris base, pH 7) was added to the protein samples for a final concentration of 1x and boiled at 80 °C for 10 minutes. Once cool, the samples were loaded into the wells along with a pre-stained protein ladder (Bio-Rad, cat.

1610373). Voltage was applied in three stages of 120 V for 30 minutes, 150 V for 20 minutes, then 170 V for 20 minutes.

7.7.3 Coomassie Protein Staining

SDS-PAGE gels were stained with Coomassie solution to visualise total protein content. The gel was incubated for 30 minutes with gentle agitation in Coomassie stain (0.1 % (w/v) Coomassie brilliant blue R-250 (Bio-Rad, cat. 1610400), 50 % ethanol, 10 % acetic acid, 40 % distilled water). The gel was then rinsed with distilled water, and washed with de-staining solution (40 % ethanol, 10 % acetic acid, 50 % distilled water) in 30-minute periods until bands were resolved from background staining. The gel was then imaged using a document scanner.

7.7.4 Western blot

After SDS-PAGE, protein gels were loaded into mini blot modules (Invitrogen, B1000) with 0.45 µm nitrocellulose membrane (Thermo Scientific, cat. 88018) and placed into a mini gel tank (Invitrogen, cat. 15384604) filled with 1x NuPAGE transfer buffer (Invitrogen, NP00061) containing 25 % methanol. Wet transfer was carried out by applying 25 V for 1 hour to transfer protein from the gel to the membrane. The membranes were then blocked in TBS with 5 % non-fat dry milk for 1 hour at room temperature with gentle agitation. The membranes were rinsed with TBS, then incubated with primary antibody diluted in TBS with 2.5 % non-fat dry milk overnight at 4 °C with gentle agitation (primary antibody dilutions listed in Table 5). The membranes were washed three times for 10 minutes in TBST at room temperature with gentle agitation. Secondary antibody was incubated for 1 hour at room temperature with gentle agitation (secondary antibody dilutions listed in Table 10). The membranes were washed three times as before, then visualised using a gel and blot imager (LI-COR Odessy CLx). Bands were quantified relative to GAPDH using the Image Studio software (LI-COR, version 5.5.4).

7.8 Dengue disruptor peptides

Peptides were designed by epitope mapping and subsequent structural optimisation by peptide array screening of HSP90-Dengue protein interactions

(Table 12). For the NS5 peptide, an N-terminal R8 sequence was included to enable membrane permeability and intracellular targeting of HSP90. This was not required for the E peptides, as cell surface HSP90 was the target. Each peptide was modified with N-terminus acetylation and C-terminus amidation to increase stability against protease-mediated degradation (Di, 2015). Peptides were ordered from GenScript Biotech (New Jersey) and resuspended in either nuclease-free water or a mixture of nuclease-free water and DMSO to a stock concentration of 10 mM.

Table 12: Summary of Dengue disruptor peptides.

Peptide	Sequence	Purity	Mass	Stock Concentration	Buffer
Epep2	Ac-IRVQYEGDGSPCKIPF-Am	>= 95 %	9.2 mg	10 mM	Nuclease-free water
Epep2AA	Ac-IRVQYEGDGSP**A**K**A**PF-Am	>= 95 %	9.6 mg	10 mM	Nuclease-free water
NS5pep1	Ac-RRRRRRRR-LLCDIGESSP-Am	>= 95 %	9.6 mg	10 mM	Nuclease-free water
NS5pep1AA	Ac-RRRRRRRR-LL**A**D**A**GESSP-Am	>= 95 %	9.3 mg	10 mM	Nuclease-free water

7.9 Cell viability assays

7.9.1 PrestoBlue cell viability assay

The PrestoBlue cell viability assay makes use of the non-fluorescent blue dye resazurin, which is reduced by mitochondrial or cellular reductases to the fluorescent pink dye resorufin, which has an excitation peak at 560 nm and an emission peak at 590 nm (Byth et al., 2001). The ratio of 560 nm / 590 nm fluorescence is proportional to the number of viable cells in the sample (Byth et al., 2001). These experiments were conducted in Professor Panya's laboratory, Chiang Mai University, Thailand.

Vero, Huh7, or A549 cells were grown to a confluency of 80 % in a 96 well plate at 37 °C, 5 % CO_2, and 95 % humidity in a cell incubator. To treat with peptide, the media was removed, and 200 µL of media containing peptide was added. The peptide concentrations used were 0, 6.25, 12.5, 25, 50 and 100 µM in addition to vehicle-only treatment. The peptides were incubated for 4 hours in the incubator. 20 µL of PrestoBlue reagent (Invitrogen, A13261) was added directly to each well, and the plate was incubated for 2 hours before fluorescence

emission was read at 560 nm / 590 nm using a plate reader (MRC, cat. UT-6550). Cell viability was calculated as a percentage of vehicle.

7.9.2 MTS colourimetric cell proliferation assay

While the PrestoBlue experiments were conducted in Professor Panya's lab, Chiang Mai University, Thailand, the later stage work was continued in Professor Baillie's lab at the University of Glasgow, where MTS reagent was accessible. There are numerous types of cell viability assays available, and the selection of reagents often depends on the personal preferences of the laboratory staff. Both PrestoBlue and MTS assays are effective options for measuring cell viability (Luzak et al., 2022).

The MTS assay measures cell viability based on the reduction of the tetrazolium compound MTS (3-(4,5-dimethylthiazol-2-yl)-5-(3-carboxymethoxyphenyl)-2-(4-sulfophenyl)-2H-tetrazolium) to a soluble formazan product by NADPH-dependent dehydrogenase enzymes in viable cells (Barltrop et al., 1991). The formazan product can be measured at 490 nm absorbance, and the amount produced is proportional to the number of viable cells (Cory et al., 1991).

Hmec-1 cells were grown to a confluency of 80 % in a 96 well plate at 37 °C, 5 % CO_2, and 95 % humidity in a cell incubator. To treat with peptide, the media was removed, and 200 µL of media containing peptide was added. The peptide concentrations used were 0, 12.5, 25, 50 and 100 µM in addition to vehicle-only control and 0.05 % Triton X-100 (Sigma-Aldrich, X100) toxic control. The peptides were incubated for 24 hours in the incubator. At 21 hours, 20 µL of MTS reagent (Abcam, ab197010) was added to each well, and the plate was loosely covered in aluminium foil to protect from light. At 24 hours, the plate was shaken for 20 s by a plate reader (Tristar 5 Multimode Plate Reader) and 490 nm absorbance was read. Cell viability was calculated as a percentage of vehicle.

7.10 *In vitro* antiviral assays

7.10.1 Preparation of Dengue Virus stock

Dengue Virus media stocks were prepared previously in Chiang Mai University. Dengue Virus serotype 2 (strain: Thailand/16681/84 [NCBI: txid31634]) was

propagated in C6/36 cells grown in Leibowitz-15 (Gibco, cat. 11415064) culture medium (1 % FBS, 10 % tryptose phosphate broth) and exposed to a multiplicity of infection (MOI) of 0.1. Cells were grown under the conditions of 37 °C, 5 % CO2, and 95 % humidity in a cell incubator. 5 days following infection, the media containing virus was collected and immediately stored at -80 °C.

7.10.2 Monoclonal anti-Dengue E neutralising antibody 4G2

A mouse monoclonal anti-Dengue E antibody 4G2 was prepared previously in Chiang Mai University from hybridoma cells (ATCC, cat. VR-1852).

7.10.3 Cell-based ELISA for Dengue Virus infection

Cell-based enzyme-linked immunosorbent assay (ELISA) was employed to assess the antiviral activity of peptide treatments by quantifying the reduction in viral protein expression in infected cells.

Vero and Huh7 cells were grown to a confluency of 70 % in a 96-well plate at 37 °C, 5 % CO2, and 95 % humidity in a cell incubator. The media was removed, and media containing live Dengue Virus was added for an MOI of 0.025 for Vero cells and 0.05 for Huh7 cells. The cells were incubated with virus for 2 hours in the cell incubator. The virus-containing media was removed, and the cells were washed once with PBS warmed to 37 °C. 100 µL of media containing peptide was added to the wells. For Huh7 cells, concentrations of 3.12, 6.25, 12.5, 25, 50, and 100 µM peptide were used in addition to Dengue Virus-only and vehicle-only controls, as well as cells treated with the neutralising 4G2 antibody as a positive control. The cells exposed to virus were incubated with these solutions for 48 hours in the cell incubator. Following this treatment, cells were rinsed twice with PBST (PBS, 0.5 % Tween 20), then fixed for 15 minutes at room temperature using paraformaldehyde (PFA, Sigma-Aldrich, cat. 47608). The cells were washed twice with PBST then permeabilised with 0.2 % triton X-100 in PBS for 15 minutes at room temperature. The cells were blocked with 1 % BSA in PBS for 30 minutes at room temperature with gentle agitation. Incubation with the 4G2 primary antibody was carried out for 3 hours at 37 °C. The cells were washed and incubated in a horseradish peroxidase (HRP)-conjugated rabbit anti-mouse secondary antibody (1:2000 dilution, Agilent, cat. P026002-2) for 1 hour at room

temperature with gentle agitation. The cells were washed, and 100 µL of TMB substrate (3,3,5,5-tetramethylbenzidine, Thermo Scientific, cat. N301) was added to each well. After 20 minutes of incubation at room temperature, stop solution was added, and absorbance at 450 nm was measured using a plate reader (MRC, cat. UT-6550). E epitope detection was read as a percentage relative to the Dengue Virus-only control.

7.11 Statistical analysis

Due to differences in experimental design and resultant data, statistical analysis for each experiment are described separately in each figure. Statistical significance was defined as $P < 0.05$. The majority of graphs were prepared using R (version 4.3.2 “Eye Holes”, (R Core Team, 2023)) and RStudio (version 2023.12.1+402, (Posit team, 2024)), or were prepared using GraphPad Prism software (version 9.5, (Swift, 1997)) or Microsoft Excel software (version 16.81).

Chapter 8 Preparation of HSP90 Recombinant Protein

8.1 Introduction

Dengue virus exploits the human chaperone protein HSP90 for entry into host cells as well as for many steps in the life cycle. Disruption of the E-HSP90 interaction by development of a peptide inhibitor could provide an urgently needed antiviral therapeutic. Working towards this objective, this chapter sets out the preparation of purified recombinant HSP90 protein for use in peptide screening and future target engagement assays.

The approach adopted consisted of several stages (Figure 8-1). First, a plasmid containing the HSP90 gene was designed for expression in bacterial culture. The plasmid contained a T7 promoter, which allowed for controlled expression of the HSP90 protein when introduced into BL21(DE3) competent E. coli. In this system, the T7 promoter is recognised by T7 RNA polymerase, which is present in BL21(DE3) cells but remains inactive until induced. Upon addition of IPTG, a LacI repressor is removed from the Lac operon of the T7 RNA polymerase, allowing for the production of T7 RNA polymerase, which then drives expression of HSP90 protein from the T7 promoter.

The plasmid was designed to include a C-terminal His tag on the HSP90 protein, allowing for isolation by IMAC following expression in bacterial culture. This technique exploits the strong coordination of the His tag with metal ions, such as nickel, present on the chromatography resin (Porath, 1988). When the cell lysate is passed over the resin, His-tagged proteins bind to the immobilised metal ions, allowing isolation from the lysate. By addition of an increasing gradient of imidazole, which competes with the His tag for resin binding, the His-tagged proteins can be selectively eluted.

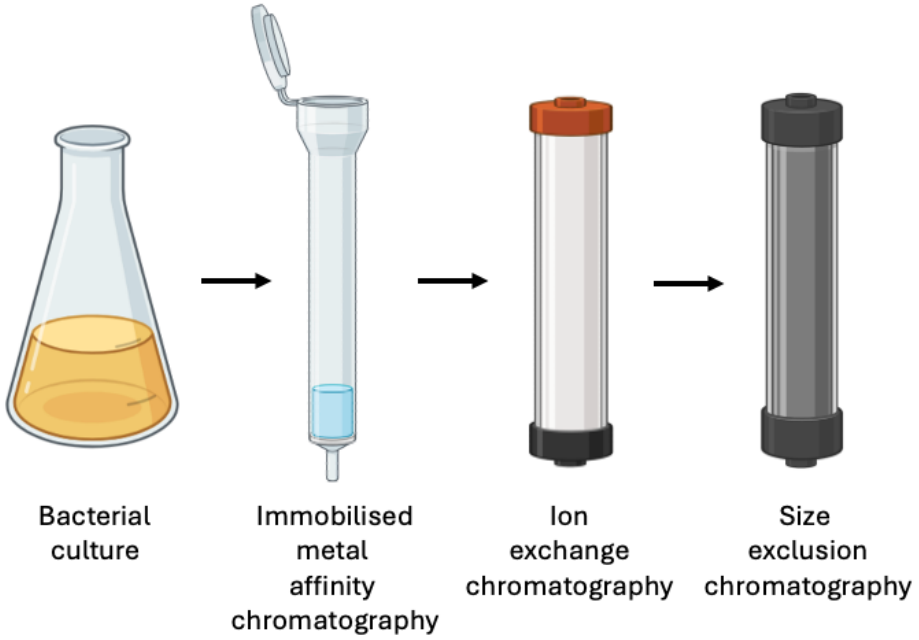

Figure 8-1. Preparation and purification of HSP90 recombinant protein.
HSP90 protein was first grown using BL21 competent E. coli. HSP90 was then isolated by the His tag using immobilised metal affinity chromatography and subsequently purified by ion exchange and size exclusion chromatography.

To increase purity, the samples were also processed by ion exchange and size exclusion chromatography. Ion exchange chromatography separates proteins based on charge (Yamamoto et al., 1988). First, a resin with a charge complementary to that of the target protein is used. Proteins with the matching charge bind to the resin, while other proteins are washed away. By applying a gradient of increasing ionic strength, the bound proteins are gradually eluted and separated based on their affinity for the column. On the other hand, size exclusion chromatography separates proteins based on their size (Mori and Barth, 1999). In this technique, a resin with pores of varying sizes is used. Smaller proteins can enter the pores and therefore travel through the column by a less direct, slower route. In contrast, larger proteins cannot enter the pores, pass around them, and move more quickly through the column. This allows proteins to be separated, with larger proteins eluting first and smaller proteins eluting later. After preparation and purification of HSP90 in this way, peptide array screening could be conducted to discover disruptors of the E-HSP90 interaction, and this is described in the next chapter. As such, the goals of the current chapter are outlined as follows:

1. To design and obtain a HSP90 plasmid for recombinant expression using bacterial cell culture.

2. To transform competent bacteria for the preparation of plasmid DNA and the expression of recombinant protein.

3. To optimise the IPTG-induction conditions of HSP90 expression.

4. To perform IMAC, ion affinity chromatography and size exclusion chromatography for the preparation of pure HSP90 stock.

8.2 Results

8.2.1 Transformation of DH5α and BL21(DE3) competent cells with HSP90

A pET-32b(+) plasmid was obtained from GenScript, into which a sequence of HSP90AA1 (accession NP_001017963.2) was inserted using the Nco1 and Xho1 restriction sites. A C-terminal 6His tag was also included. This plasmid was then transformed into DH5α competent E. coli for storage and plasmid preparation. After purification of a plasmid stock from the DH5α E. coli, the plasmid was transformed into BL21(DE3) competent E. coli for protein preparation. These E. coli strains were chosen for their specialised functions: DH5α is engineered for enhanced plasmid stability and yield, whereas BL21(DE3) is optimised for higher protein production and reduced protease expression (Phue et al., 2008).

8.2.2 Optimisation of IPTG induction conditions

Once stocks of BL21(DE3) competent cells transformed with the HSP90 plasmid were obtained, the conditions of IPTG induction were optimised. The general process of protein preparation was as follows. First, an overnight starter culture was grown from a glycerol stock of the HSP90-transformed competent cells. The next day, this was used to grow a main culture to an optical density of 0.6-0.8 (600 nm). IPTG was then added to induce HSP90 expression, and harvesting was carried out by centrifugation and sonication. To optimise induction, four protocols with different temperatures, durations, and IPTG concentrations were tested (Table 13).

Table 13: Conditions for IPTG optimisation.

Condition	Temperature (°C)	Duration (h)	IPTG (mM)
1	37	3	0.1
2	37	3	1
3	18	18	0.1
4	18	18	1

The protein content of samples from the uninduced culture, induced culture, soluble fraction, and pellet was evaluated using Coomassie staining, and the

impact of the induction conditions was assessed (Figure 8-2). First, a 100 kDa band was observed in the induced samples but not the uninduced samples, and this indicated successful HSP90 expression induced by IPTG in all conditions. Next, this band was thicker in the soluble fraction than the pellet, signifying effective cell lysis. The band sizes of HSP90 in the soluble fraction (SF) were compared, and condition 3 led to the highest expression, but conditions 1 and 4 were nearly as favourable. Therefore, condition 3, consisting of a 0.1 mM IPTG induction at 18 °C for 18 hours, was chosen for further experiments of HSP90 expression.

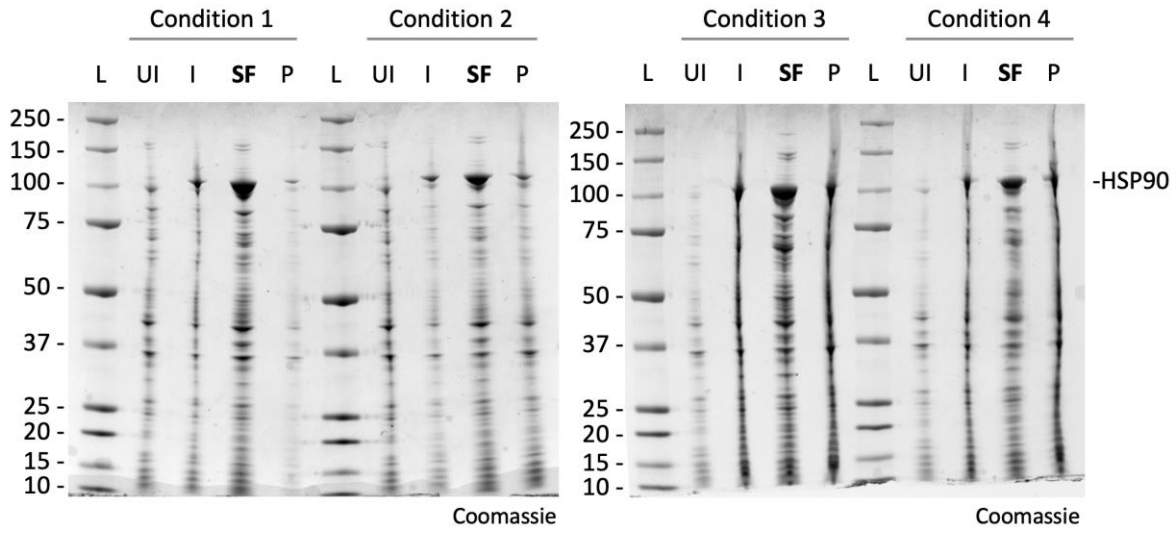

Figure 8-2: Coomassie stained protein samples from IPTG induction conditions 1-4. Protein content of samples was visualised to compare yield of HSP90 at 100 kDa. The uninduced and induced samples verified whether HSP90 expression was successfully induced by IPTG. Comparison of soluble fraction and pellet indicated successful lysis. The protein bands of known molecular weight in the ladder lane are indicated in kDa. L, ladder; UI, uninduced; I, induced; SF, soluble fraction; P, pellet.

8.2.3 Immobilised Metal Affinity Chromatography

The plasmid for HSP90 was designed to incorporate a His tag to enable protein isolation by IMAC. An initial isolation experiment was performed on the soluble fractions from the IPTG optimisation. These samples were fed into a column packed with Ni-NTA agarose beads. The column was washed three times, and imidazole solution was added to bind the beads and displace the His tagged proteins. By addition of an increasing concentration gradient of imidazole, the proteins were eluted by their strength of affinity to the nickel.

After carrying out this isolation process on the samples from IPTG induction conditions 1-4, the fractions were analysed by Coomassie staining (Figure 8-3). In the flow-through of all conditions, a 100 kDa band corresponding to HSP90 could be seen, indicating that the column bound only a portion of the HSP90. By the third wash after flow-through, little protein was eluted, showing successful removal of products in the lysate without His tags. By addition of increasing concentrations of imidazole, HSP90 was eluted, and this increased, peaked and tailed off in each condition sample. For conditions 1, 3, and 4, this peak occurred at 150 mM imidazole. This elution peak for condition 2 occurred earlier at 50 mM. In each condition, there was significant elution of lower molecular weight proteins in addition to HSP90. Overall, the protein isolated from each induction condition had a similar composition, and none appeared particularly pure.

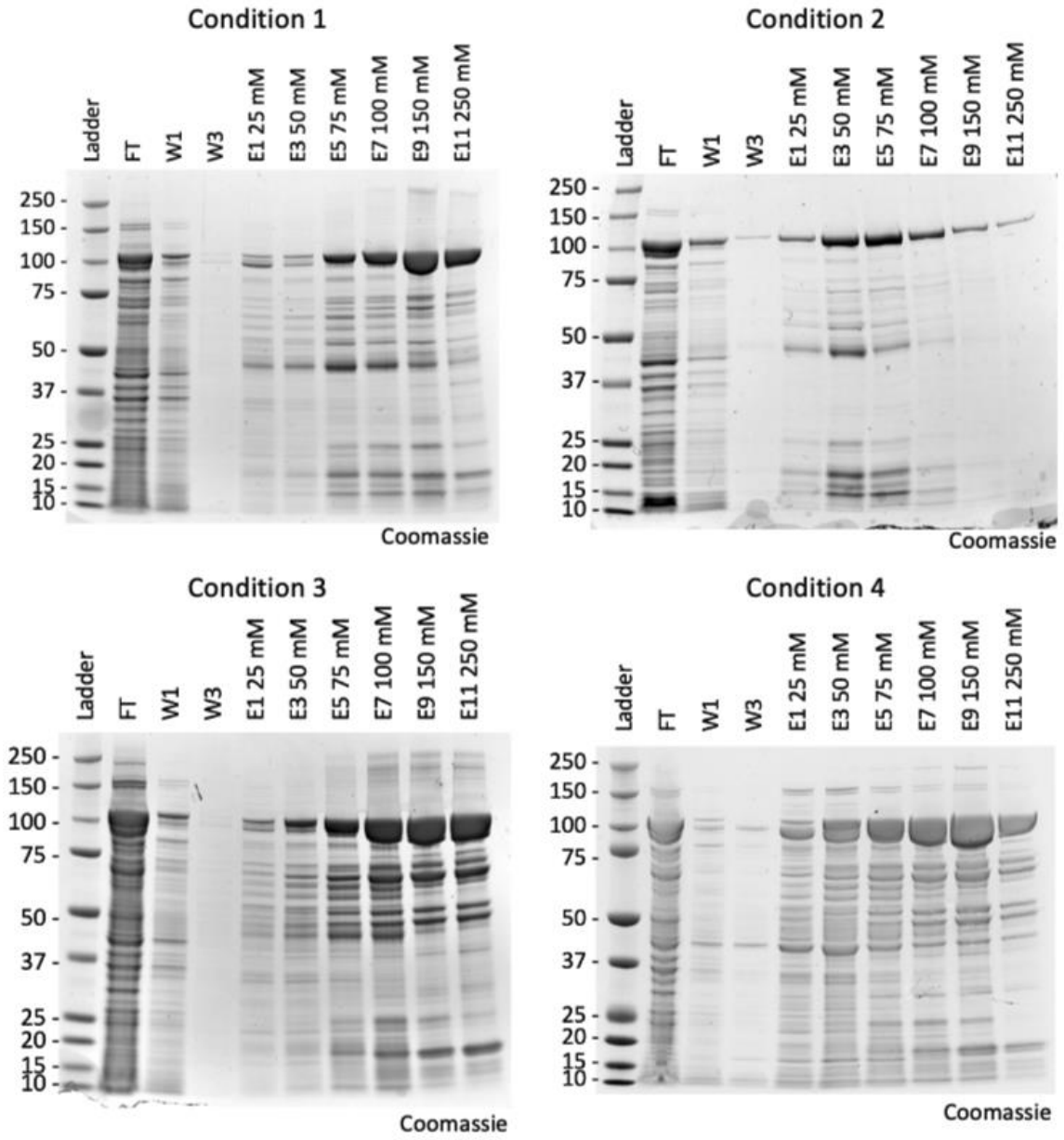

Figure 8-3: His-tagged proteins isolated by immobilised metal affinity chromatography (IMAC) from the soluble fractions from IPTG optimisation.
Fractions show protein eluted from the Ni-NTA agarose column using a concentration gradient of imidazole. Protein stained with Coomassie for visualisation. The protein bands of known molecular weight in the ladder lane are indicated in kDa. FT, flowthrough; W, wash; E, elute.

To verify the identity of the band at 100 kDa, the elutes were immunoblotted for HSP90 and His tag (Figure 8-4). A 100 kDa band was detected using both antibodies, but many lower molecular weight products were present, suggesting degradation. For this reason, follow up methods for purification were used to ensure purity.

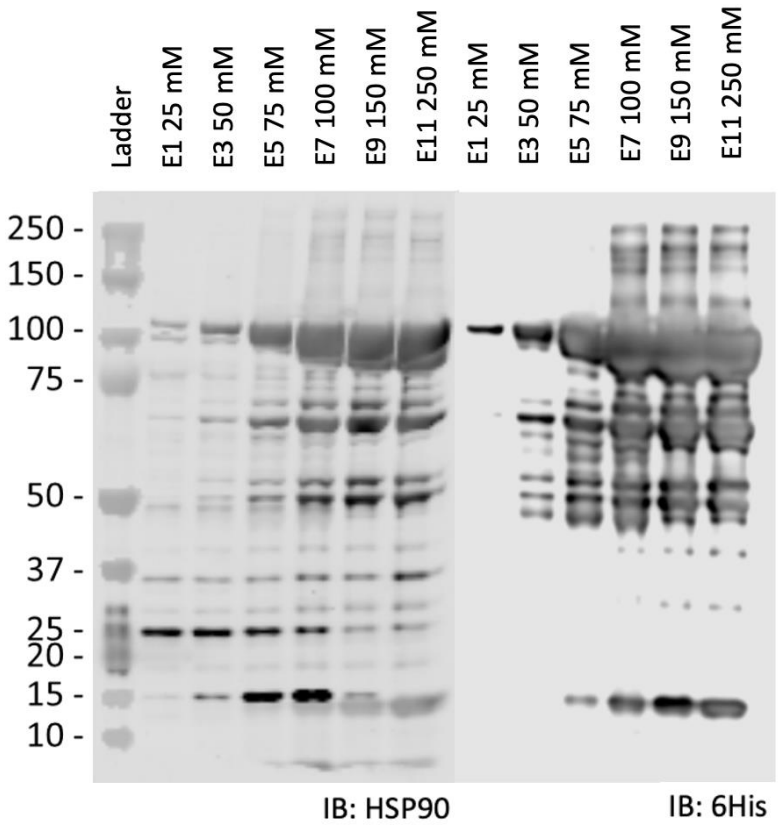

Figure 8-4: Immunoblotting of fractions from immobilised metal affinity chromatography for HSP90 and His tag.
Protein was eluted from the column by increasing concentrations of imidazole. Bands corresponding to HSP90 or HSP90 epitope-containing proteins were detected by antibody staining. The protein bands of known molecular weight in the ladder lane are indicated in kDa. E; elute, IB; immunoblot.

8.2.4 Scale up of immobilised metal affinity chromatography

Having successfully optimised IPTG induction and isolated HSP90 using Nickel IMAC, protein could now be produced for subsequent purification. To scale up and prepare the amount of protein needed, a total of four litres of culture were grown, lysed, and processed using nickel IMAC columns. Instead of the previous imidazole gradient used for protein elution, a two-step elution of 75 mM and 250 mM was used. The isolates were assessed using Coomassie staining and western blot, revealing HSP90 to be successfully eluted from the column and most concentrated in fractions 1-4 (Figure 8-5). As before, many products of lower molecular weight were co-eluted. By western blotting for both HSP90 and His tag, the presence of HSP90 at 100 kDa was confirmed. However, many of the lower molecular weight products were also detected, and further purification was required. For this purpose, fractions 1-5 were pooled together and concentrated to ~7 µg/µL (80 µM, 1.5 mL, 10.5 mg) using ultrafiltration spin columns. This protein was then stained using Coomassie and revealed to be

relatively pure (Figure 8-6).

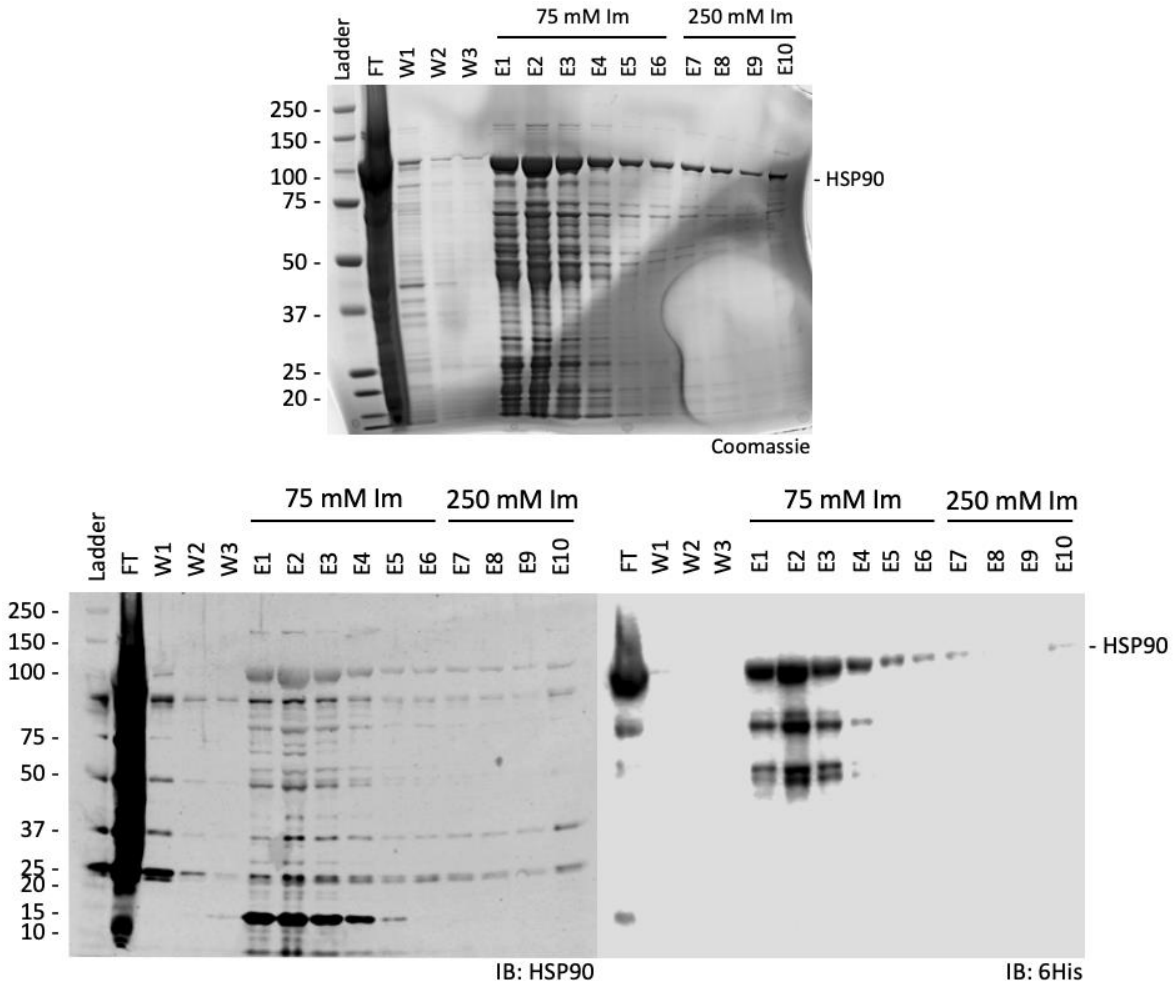

Figure 8-5: Scaled up isolation of HSP90 using immobilised metal affinity chromatography (IMAC) with nickel beads.
Protein content of elutes from IMAC were assessed for HSP90 at 100 kDa and the presence of other products. A: Elutes were stained with Coomassie stain to show protein composition. B: Fractions were immunoblotted for HSP90 and His tag. The protein bands of known molecular weight in the ladder lane are indicated in kDa. FT; flow-through, W; wash, E; elute, IB; immunoblot, Im; imidazole.

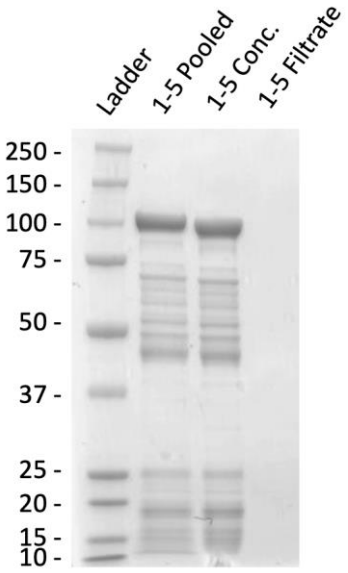

Figure 8-6: Coomassie stain of pooled and concentrated fractions 1-5 of immobilised metal affinity chromatography (IMAC)-isolated HSP90.
Protein content of pooled fractions was assessed for HSP90 at 100 kDa and the presence of impurities. Fractions were concentrated using centrifugal ultrafiltration. The protein bands of known molecular weight in the ladder lane are indicated in kDa.

8.2.5 Ion Exchange and Size Exclusion Chromatography

After isolating a large amount of HSP90 by IMAC, further purification was necessary to remove the lower molecular weight products. Ion exchange chromatography was used to separate the proteins by charge. To select the resin, the isoelectric constant for HSP90 was calculated. With an isoelectric constant of ~5, HSP90 should be negatively charged at pH 7.4. Therefore, a positively charged anion exchange resin was used. To begin, HSP90 was loaded onto the column, and a concentration gradient of 100-1000 mM NaCl was applied. The protein content of elutes was monitored by UV absorbance at 280 nm, and four main peaks were observed (Figure 8-7). These elutes were analysed by Coomassie staining, and a 100 kDa band corresponding to HSP90 was identified from elutes 8-10. Fraction 8 covered a shoulder peak conjoined to this main HSP90 peak, and it was found to contain many lower molecular weight products. Because of this, only fractions 9 and 10 were combined and used for further rounds of purification. When combined, this sample had a concentration of 2.0 µg/µL (23 µM, 1.6 mL, 3.2 mg). In addition, fractions 14 and 15 corresponding to the fourth peak were analysed by Coomassie staining but were found to contain little protein.

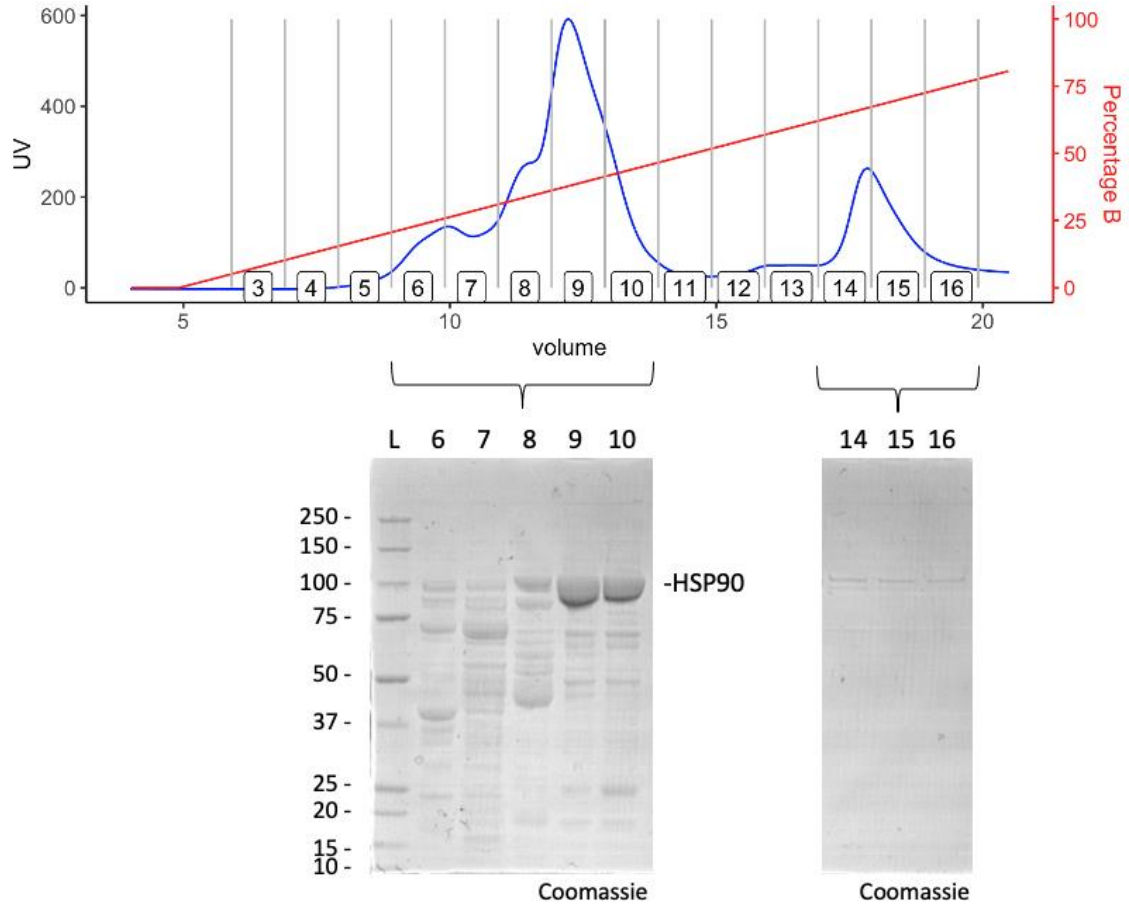

Figure 8-7: Ion exchange chromatography of HSP90 samples isolated by immobilised metal affinity chromatography (IMAC).
Protein was eluted from the column using a NaCl concentration gradient of 100-1000 mM. Percentage B indicates the percentage ratio of 1000 mM NaCl solution to 100 mM NaCl solution applied. Elution was monitored by UV absorbance at 280 nm and is shown in absorbance units (AU). The x-axis indicates the volume eluted from the column in mL. The fraction number is noted by boxed labels. Protein composition of elutes was determined by Coomassie staining. The protein bands of known molecular weight in the ladder lane are indicated in kDa. L; ladder.

Fractions 9 and 10 from ion exchange chromatography underwent a second round of purification by size exclusion chromatography. These samples were fed through a size exclusion column, and protein elution was measured by 280 nM absorbance (Figure 8-8). One large peak was observed by UV, and Coomassie staining of these fractions revealed a large 100 kDa HSP90 band and a small amount of lower molecular weight bands. Protein from fractions 7 and 8 were pooled together and had a concentration of 1.9 µg/µL (22 µM, 1.6 mL, 3.0 mg). Samples 6, 9, 10, and 11 were also pooled and had a concentration of 0.98 µg/µL (10.8 µM, 3.2 mL, 3.1 mg). These samples were analysed by Coomassie staining and were revealed to have a high purity (Figure 8-8).

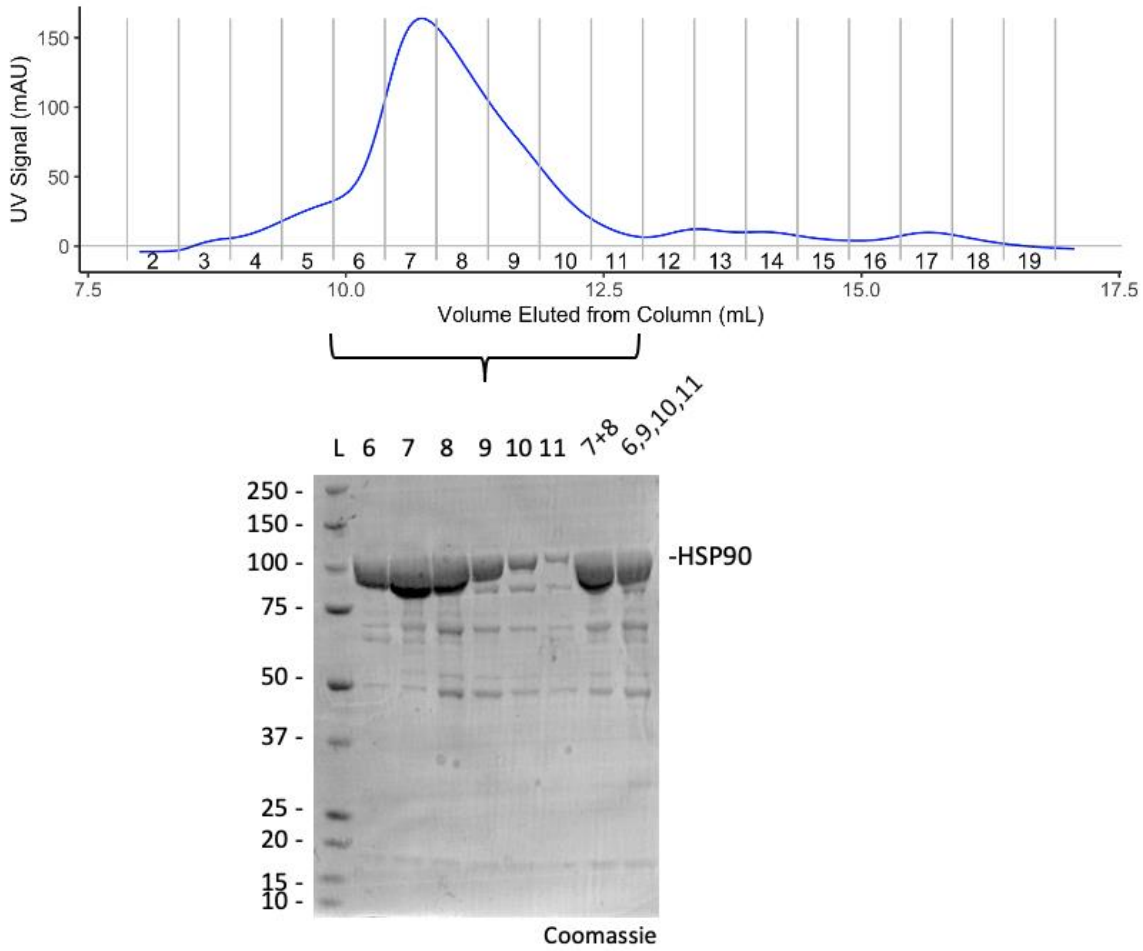

Figure 8-8: Size exclusion chromatography of HSP90 protein obtained from ion exchange chromatography.
Elution was monitored by 280 nm absorbance and is shown in absorbance units (AU), and protein composition was assessed by Coomassie staining. The x-axis indicates the volume eluted from the column in mL. The fraction number is noted by numbered labels. Fractions 7 and 8 were pooled together, and fractions 6, 9, 10, and 11 were collected in a separate pool. These two samples were prepared for Coomassie staining. The protein bands of known molecular weight in the ladder lane are indicated in kDa.

8.3 Discussion

8.3.1 Optimisation of IPTG induction conditions

A large stock of purified recombinant HSP90 protein was required for peptide array screening and target engagement assays. However, a pilot experiment was first carried out for the optimisation of IPTG induction conditions with the goal of increasing yield. IPTG concentration and post-induction temperature and duration are important factors that greatly affect protein yield: high temperature and short durations after induction can be beneficial by saving time and increasing growth rate of bacteria but can negatively affect yields by resulting in plasmid loss and mis-partitioning as the bacteria replicate, as well as incorrect protein folding, and formation of insoluble aggregates called inclusion bodies (Schein and Noteborn, 1988; Papaneophytou and Kontopidis, 2014). In addition, a sufficient concentration of IPTG is essential to relieve inhibition of the lac operon to stimulate protein expression. However, higher concentrations of IPTG increase the rate of protein synthesis but can stunt the growth and replication of bacteria, resulting in decreased overall yields (Bentley et al., 1991; Glick, 1995). For these reasons, four induction conditions were tested, each varying these factors so that the optimal balance could be identified. After growth and harvesting of the cultures, the protein composition of the culture was assessed by Coomassie staining. Resultingly, condition 3 provided the greatest yield, which comprised induction with 0.1 mM IPTG and a post-induction duration of 18 hours at 18 ºC. This suggested that the lower IPTG concentration, lower temperature, and extended duration post-induction provided a better balance between protein expression and bacterial replication. If greater yields of HSP90 are required in future work, IPTG concentration could be further optimised by testing concentrations between 0.1 and 1 mM and above 1 mM (Papaneophytou and Kontopidis, 2014). Additionally, the use of a more nutrient-dense media such as terrific broth may result in higher yields (Lozano Terol et al., 2019).

8.3.2 Impurities from immobilised metal affinity chromatography

After optimisation of IPTG induction, a pilot IMAC isolation demonstrated successful pull down of HSP90 and an improvement in protein purity. However,

many lower molecular weight impurities could be seen. Since many of these were detected by western blotting for HSP90 and His tag, these proteins were probably degradation products which still contained the epitopes necessary for antibody binding. In following rounds of HSP90 production, several changes could be made to reduce potential degradation. First, the post-induction duration of 18 hours could be reduced to prevent exposure of protein to bacterial proteases. Although the BL21(DE3) strain has been engineered to be deficient in Lon and OmpT proteases, levels of these enzymes may still be present in addition to other proteases (Gopal and Kumar, 2013). Furthermore, the harvesting protocol included several rounds of sonication for cell lysis. An optimisation experiment could be performed to see if a better balance between cell lysis and potential HSP90 degradation induced by sonication could be achieved. During IMAC, protease inhibitors were already present in the buffers, but performing the procedure in a cold room would ensure that the equipment was at a cold temperature to slow down degradation.

The lower molecular weight products could also be proteins that bound nonspecifically to the nickel resin during IMAC. This was expected, since IMAC isolation is not as specific as other pull down techniques (Charlton and Zachariou, 2008). Nevertheless, IMAC was chosen in this project since it is a very common and cost-effective method that is simple to perform. Additionally, the small size of the His tag was essential to prevent interference with the HSP90 conformation or its interaction during peptide array screening or target engagement assays (Carson et al., 2007). Even so, non-specific binding could be reduced by adopting a different tag isolation system, such as FLAG tag or strep-tag-II, which also have a small size but are much more specific (Young et al., 2012). However, these resins are costly and have less capacity than nickel IMAC resins (Young et al., 2012). In any case, additional purification steps would be necessary to remove the eluting agent of these isolation methods, and the yield of HSP90 from IMAC was sufficient to accommodate loss by further purification.

8.3.3 Simplification of imidazole elution

Once the pilot IMAC experiment demonstrated effective HSP90 pulldown, growth and harvesting of HSP90 bacterial culture was scaled up and processed by IMAC. However, the protocol for imidazole elution was simplified. Since the pilot IMAC

showed that the ratio of HSP90 protein to impurities did not change with increasing imidazole, incremental increases in imidazole were not necessary. Additionally, follow up purification steps would effectively remove the impurities anyway. To streamline the IMAC and speed up the process to avoid protein degradation, a two-step protocol was employed: a first flush of 75 mM imidazole was performed to elute the majority of HSP90, followed by a 250 mM flush to recover residual HSP90 on the column. This was effective, and the pooled fractions indicated a good yield of HSP90. Ion exchange and size exclusion chromatography were then performed on the samples, and the lower molecular weight impurities were successfully removed.

In summary, a successful method for preparing recombinant HSP90 was designed, resulting in a stock of HSP90 with sufficient yield and purity for peptide array screening and peptide binding affinity assays. Through optimisation of the IPTG induction conditions and the IMAC imidazole elution protocol, yields were increased, and the process was streamlined. The next chapter describes how this HSP90 stock was used for the discovery of peptide disruptors of the HSP90-Dengue E protein by array screening.

Chapter 9 Peptide array discovery of HSP90-E disruptor peptides

9.1 Introduction

This chapter describes the discovery and optimisation of peptide disruptors of the Dengue E-HSP90 interaction based on E epitopes, followed by evaluation of antiviral potential (Figure 9-1). To achieve this, purified recombinant HSP90 was prepared as described in the previous chapter and used for screening against a peptide array of the Dengue E protein. Once HSP90-binding epitopes of the E protein were discovered, the physiochemical properties were assessed, and promising sequences were developed into disruptor candidates by peptide array structural optimisation. The optimised candidates were then synthesised for cell assays, and cytotoxicity profiles were characterised. Lastly, antiviral efficacy of the peptides was determined by cell-based ELISA.

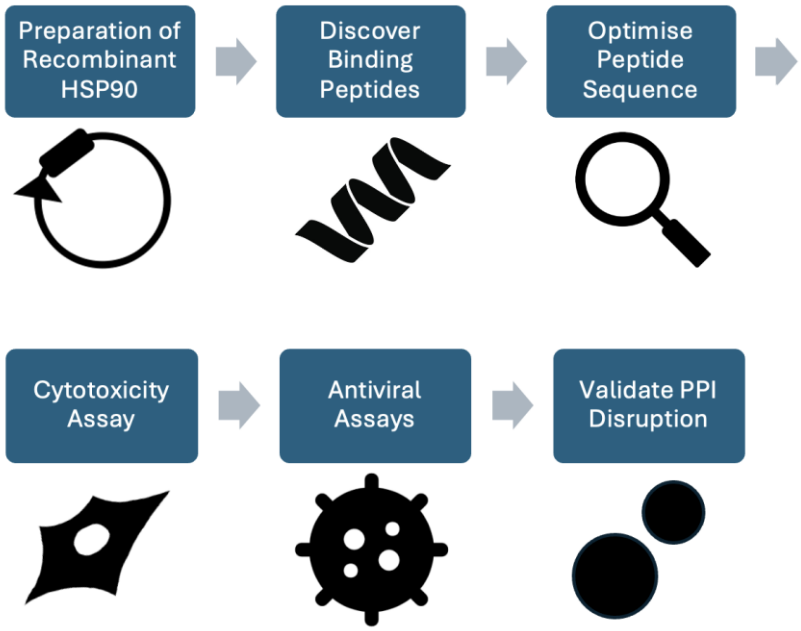

Figure 9-1: Development pipeline for the development of antiviral peptide candidates
HSP90 protein was first produced by recombinant expression in bacterial culture. Peptide array screening was used for the discovery of HSP90-binding epitopes on the E protein. Structural optimisation was then performed using peptide array screening to generate disruptor peptide candidates from the epitopes. Cytotoxicity and antiviral efficacy of the peptides were determined by cell assays. Lastly, disruption of the protein-protein interaction would be carried out on successful candidates. PPI; protein-protein interaction.

The Dengue E protein has been a valuable target in the development of antiviral peptide inhibitors (Section 6.7.1). In particular, the interaction between the E

protein and host cell chaperone HSP90 is a promising and unexplored drug target, as highlighted by antiviral assays using HSP90-directed antibodies (Reyes-del Valle et al., 2005). However, the binding sites on each protein partner remains unknown. On the E protein, several pieces of evidence implicate domain III (DIII) to be responsible for host cell attachment, receptor mediated endocytosis, and membrane fusion: (a) soluble recombinant DIII protein competitively inhibits Dengue virus infection *in vitro* in different cell types (Hung et al., 2004), (b) neutralising antibodies against Dengue virus are directed towards DIII (Sarker et al., 2023), (c) mutagenesis of DIII residues prevents neutralisation of the virus by the adaptive immune system (Sukupolvi-Petty et al., 2007; Frei et al., 2015), (d) the external structure of the virion particle is comprised mostly by DIII, which is orientated outwards and protrudes from the surface (González-Lodeiro et al., 2024), and (e) the immunoglobulin-like structure of DIII is widely associated with adhesion (Bork et al., 1994). For these reasons, interaction with HSP90 may be mediated by DIII.

Towards the goal of developing peptide inhibitors of the E-HSP90 interaction, this chapter had the following aims:

1) To identify binding epitopes on the Dengue E protein for HSP90 by peptide array screening.

2) To assess physiochemical properties of epitope sequences.

3) To develop binding epitopes into peptide disruptor candidates by peptide array structural optimisation.

4) To establish the non-toxic working concentration of disruptors by *in vitro* cytotoxicity assays.

5) To evaluate antiviral activity of disruptor peptides using cell-based ELISA.

9.2 Chapter methods

9.2.1 Structural optimisation by peptide array screening

In this chapter, HSP90-binding epitopes from the Dengue E protein were developed into candidate disruptors by structural optimisation using peptide array screening. Epitope mapping has been described previously (Section 7.4.2). After discovery of epitopes, three structural modification techniques were employed. First, alanine scanning was used to identify residues essential for binding, termed hotspots, as well as superfluous residues which could be removed or substituted (Morrison and Weiss, 2001). For this technique, each amino acid in the peptide sequence was substituted with alanine in subsequent spots, and the impact on binding was observed (Figure 9-2). By alanine substitution, the side chain of a residue was largely removed and the contribution of that side chain to binding affinity via direct interaction or allosteric support of neighbouring residues could be determined (Morrison and Weiss, 2001). If binding decreased after alanine substitution, the side chain of the original residue was important for the interaction. For residues that were already alanine in the native sequence, glycine was substituted, since it has a single hydrogen atom instead of a methyl group like alanine.

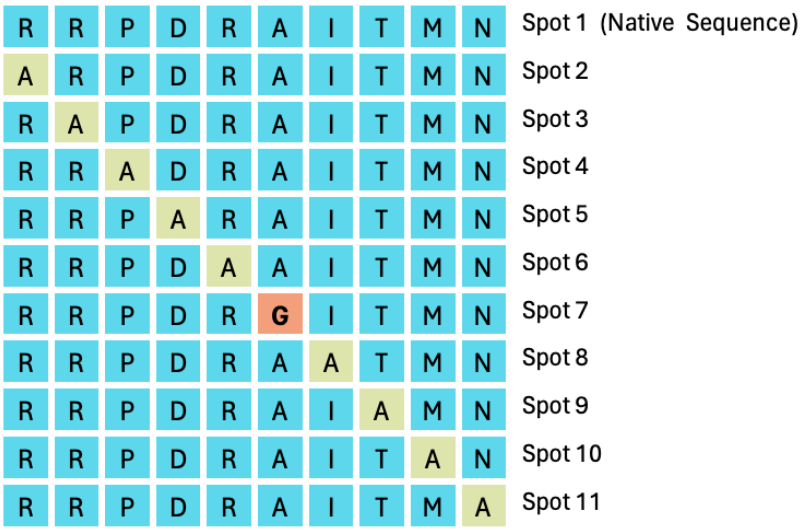

Figure 9-2: Alanine scanning to determine the importance of each residue.
In subsequent peptide array spots, each amino acid of the original peptide sequence is substituted with alanine. Substitution with alanine indicates the importance of the side chain of the original residue to binding. Alanine residues are substituted with glycine.

The second sequence optimisation technique employed in this project was truncation of termini residues. This method has been employed in peptide array screening in previous work from my group (Mahindra et al., 2021). By observing the change in binding after truncating the native peptide sequence, termini residues superfluous to binding were identified, and the shortened core binding motif was found (Figure 9-3). By use of epitope mapping, alanine scanning, and truncation, optimised disruptor peptides could be developed from protein-protein interactions.

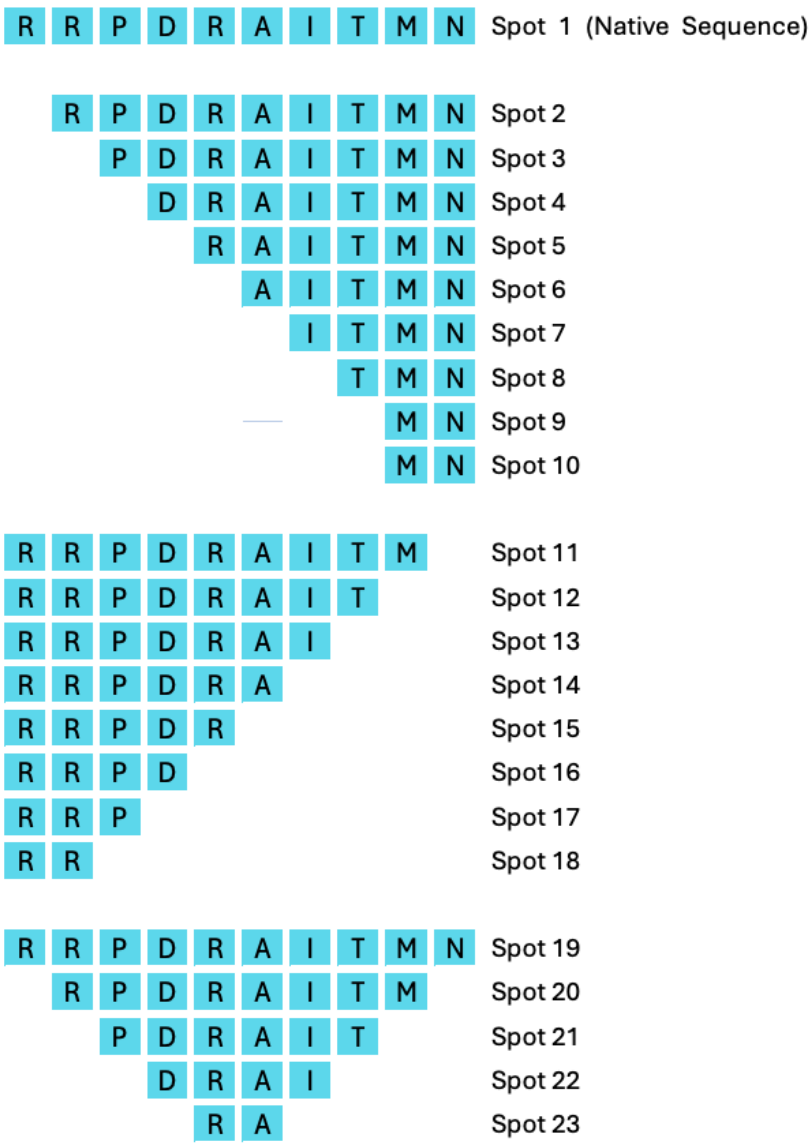

Figure 9-3: Termini truncation to identify core binding motifs.
The binding of truncated peptides is observed to identify termini residues that are unimportant for binding. Removal of terminal residues can reveal the core binding motif.

The last structural optimisation method used in this project was point substitution, also called saturation mutagenesis or scanning site saturation (Miyazaki and Arnold, 1999). This involved the substitution of each residue position with all other proteinogenic amino acids, meaning that all amino acids were tested at each residue position (Figure 9-4). By screening such a library by peptide array, the key residue positions important for target binding could be identified, along with the amino acid properties that enhanced binding at each position, such as charge, hydrophilicity, or other physiochemical properties. This technique therefore provided rich information which can be leveraged for rational optimisation (Lutz, 2010).

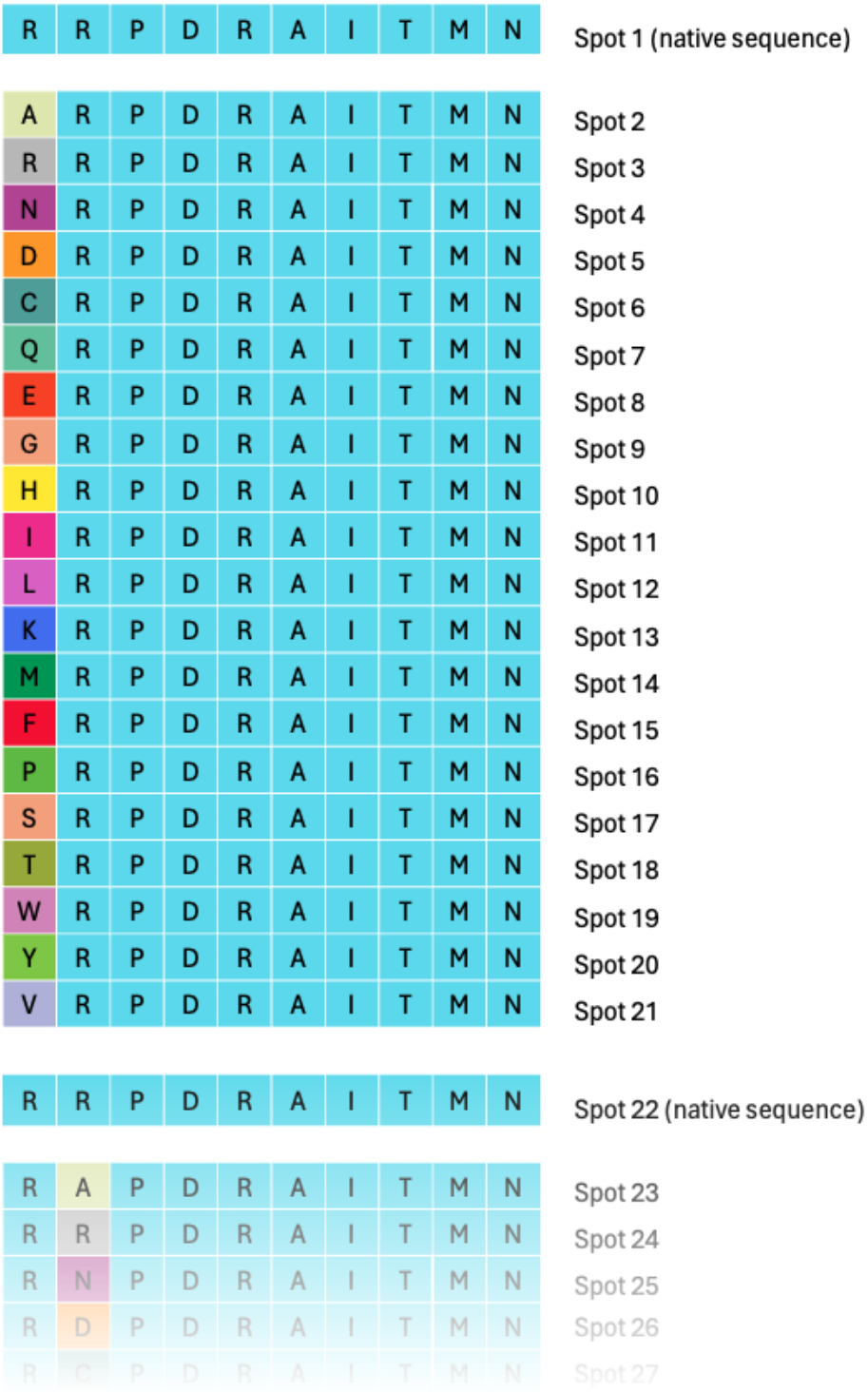

Figure 9-4: Point substitution for peptide optimisation.
All twenty proteinogenic amino acids are tested at each residue position to gain detailed information about important positions and physiochemical properties beneficial to binding. Point substitution only shown for the first residue.

9.3 Results

9.3.1 Peptide array discovery of HSP90 epitopes on the Dengue E protein

To begin, the binding sites for HSP90 on the Dengue E protein were mapped by synthesising and screening a peptide array that spanned the sequence of the E protein by 20mer peptides, each shifted by five amino acids in sequence. This array was screened using a far-western blot technique with HSP90 recombinant protein produced in the previous chapter (Figure 9-5). Two putative binding sites were identified. The weaker binding site was located earlier in the sequence in Domain II and was comprised of residues K56-P75. The stronger binding site was located later in the sequence in Domain III and spanned two peptide spots covering residues V321-R345. Within this, the stronger peptide spanned the residues V321-M340. The two epitopes K56-P75 and V321-M340 were taken forward for optimisation and were designated E peptide 1 and E peptide 2 respectively.

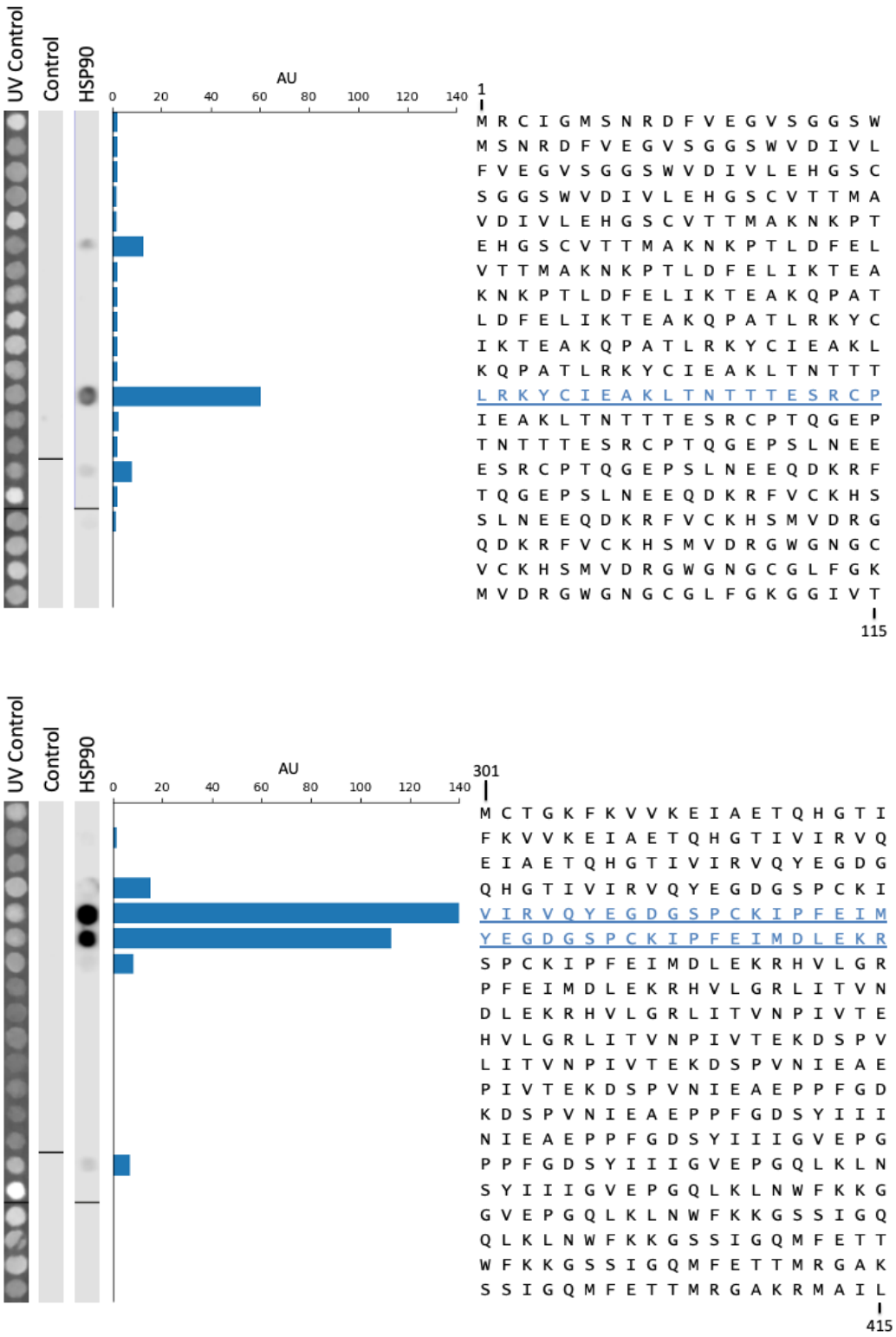

Figure 9-5: HSP90 overlaid onto a peptide array spanning the DENV E sequence.
An array overlaid with a buffer and antibody-only control was included to detect non-specific binding. Spot quantification is shown as control-corrected inverted pixel value. Black lines show where consecutive spots span different columns. Numbering relative to accession AAA42954.1.

The position of E peptide 1 and E peptide 2 in the domain structure of the Dengue E protein was analysed (Figure 9-6:A), and the epitope sequences were highlighted on a crystal structure of the E protein (Figure 9-6:B-C). The epitopes

were exposed on the protein surface and therefore accessible for interaction with HSP90 (Figure 9-6:C). Furthermore, the binding peptides were separated in space and were unlikely to comprise the same binding site. To see whether the epitopes were conserved across the four Dengue serotypes, multiple sequence alignment was carried out (Figure 9-7). E peptide 1 had a sequence homology of 73.3 % across serotypes, while conservation was lower at 53.3 % for the stronger binding sequence E peptide 2.

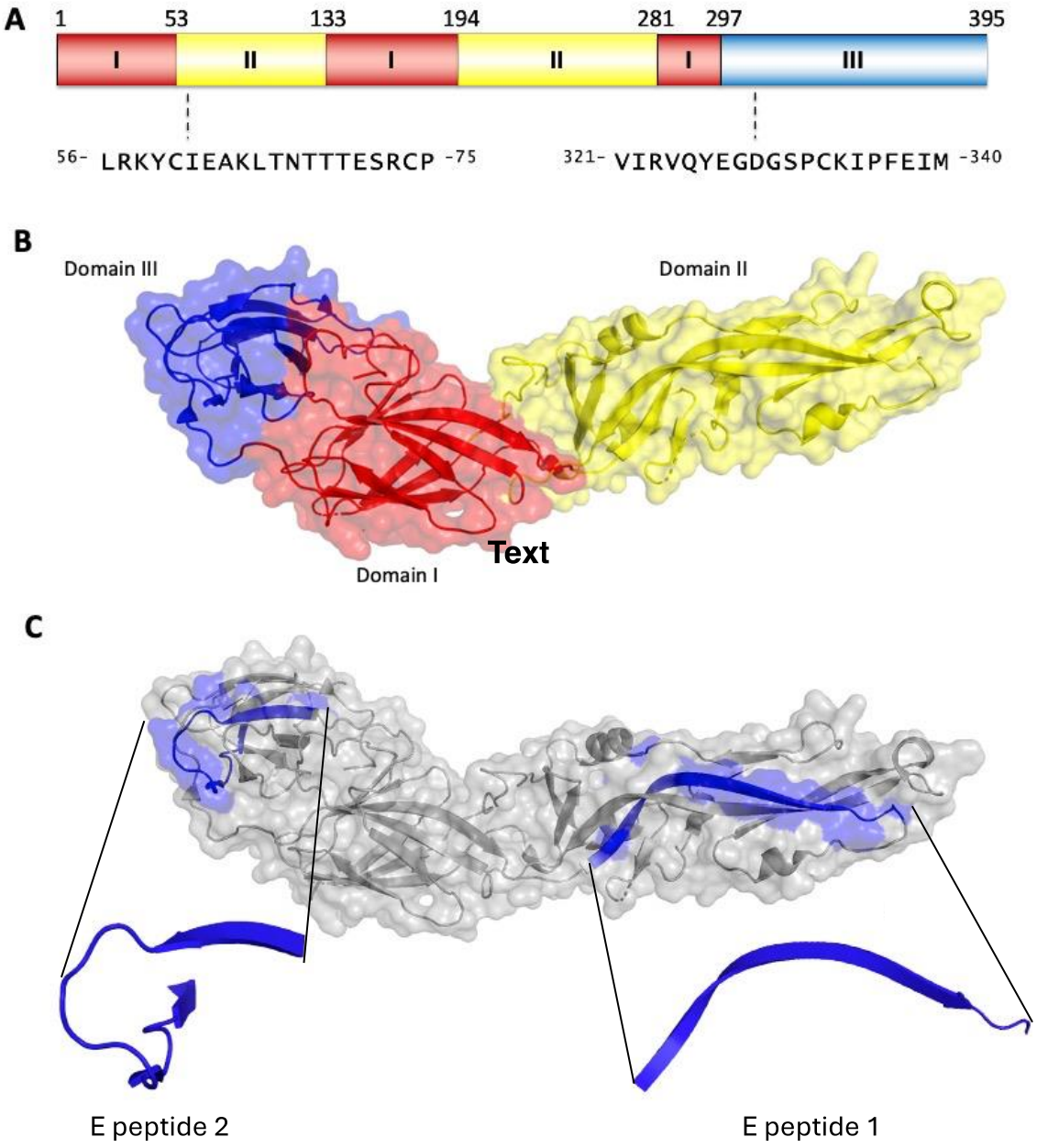

Figure 9-6: Domain structure of Dengue E and HSP90 binding peptides.
A: Domains of the DENV E protein and position of binding peptides. Domains are comprised of noncontinuous stretches of amino acids. B: Domain organisation overlaid onto an existing crystal structure. C: Location of the HSP90 binding epitopes E peptide 1 and E peptide 2 within the DENV E structure. PDB accession 1TG8.

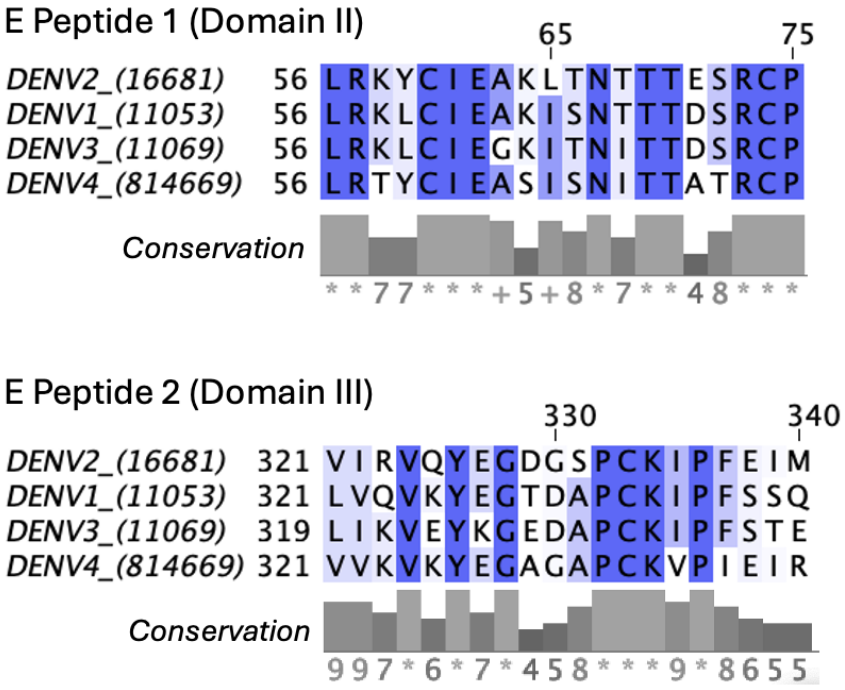

Figure 9-7: Multiple sequence alignment of E peptides.
Alignment relative to DENV2. Viral strain shown in brackets. Alignment performed using Clustal Omega. Diagram and conservation score generated using Jalview. Conservation score considers both amino acid identity and physiochemical properties. The scale ranges 0-11, with 11 being represented by '*'. The '+' symbol indicates where physiochemical properties are conserved despite an identity mismatch.

9.3.2 Physiochemical and Pharmacokinetic Assessment

Having identified the two binding sites on the Dengue E protein for HSP90, E peptide 1 and E peptide 2, physiochemical and pharmacokinetic properties were assessed. Since secondary structure greatly impacts affinity and pharmacokinetic properties, peptide conformers were predicted using PepFold3, a tool for sequence-based conformation prediction. E peptide 1 was estimated to be partially α-helical from K3 to L10, and E peptide 2 was estimated to adopt a ß-hairpin structure (Figure 9-8).

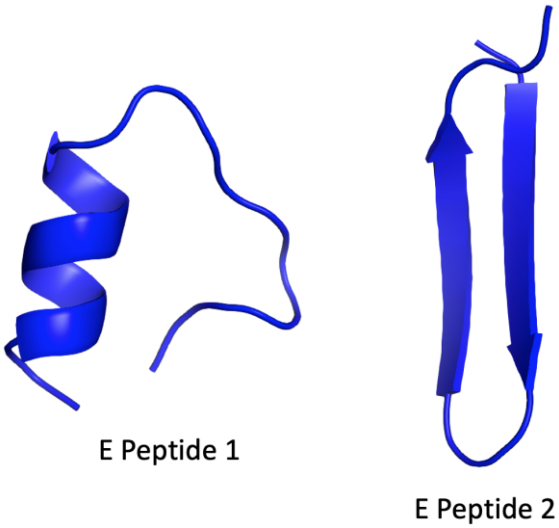

Figure 9-8: Conformation of HSP90 binding peptides as predicted by PepFold3.
Predicted conformations of the HSP90-binding epitopes E peptide 1 and E peptide 2 discovered by peptide array screening. E peptide 1 exhibited a partial α-helical structure, and E peptide 2 adopted a β-hairpin fold.

Charge, solubility, and aggregation propensity of the peptides were also investigated. The web-based tool PepCalc was used to assess charge and solubility. For aggregation, the tool AGGRESCAN was employed to calculate aggregation potential and highlight aggregation hotspots. E peptide 1 was estimated to have good water solubility, a net charge of +2 at pH 7, and several charged residues evenly distributed along the sequence (Figure 9-9:A). Using AGGRESCAN, a hotspot of aggregation potential was identified between K3 and A8, which overlapped with the α-helical section (Figure 9-9:B-C). Additionally, the presence of two cysteines was noted, which may promote aggregation under oxidative conditions.

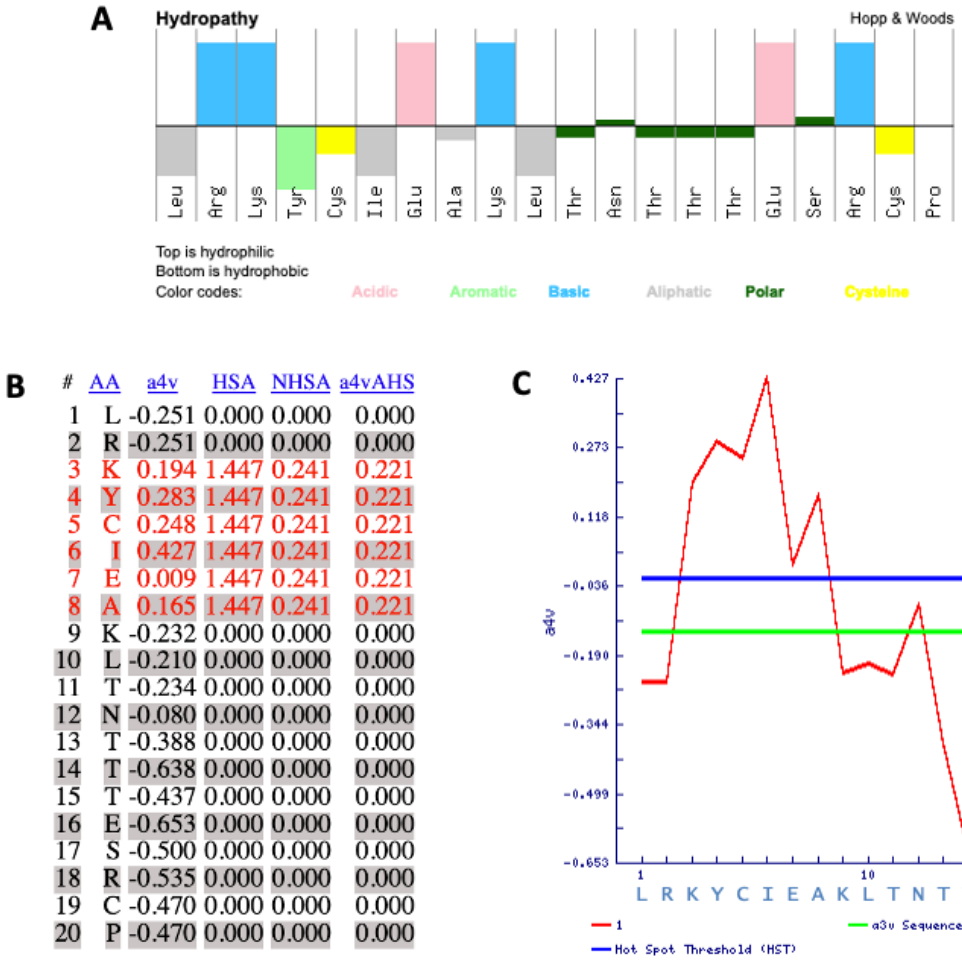

Figure 9-9: Predicted physiochemical properties of E peptide 1.
A: Charge distribution depicted using PepCalc. Residue properties are indicated by colour: pink, acidic; light-green, aromatic; blue, basic; grey, aliphatic; dark-green, polar; yellow, cysteines. Bar chart shows Hopp and Woods Hydophobicity scale (Hopp and Woods, 1983). B: Aggregation potential calculated by AGGRESCAN. a4v indicates the sliding window average of a3v amino acid aggregation propensity. HSA (Hot spot area) is the area of aggregation potential above the hotspot threshold. NHSA is the HSA normalised for the number of residues. a4vAHS is the average a4v within a hotspot. C: Plot of AGGRESCAN aggregation potential (a4v) against residue. Blue line indicates the hotspot threshold (-0.02), and the green line depicts the average aggregation potential for the sequence.

E Peptide 2 was similarly assessed and was predicted to have good water solubility, several charged amino acids evenly distributed, and a net charge of -1 at pH 7 (Figure 9-10:A). E peptide 2 was also predicted to have an area of high aggregation potential, but it was not considered a hotspot since it spanned less than five consecutive amino acids (Conchillo-Solé et al., 2007) (Figure 9-10:B-C).

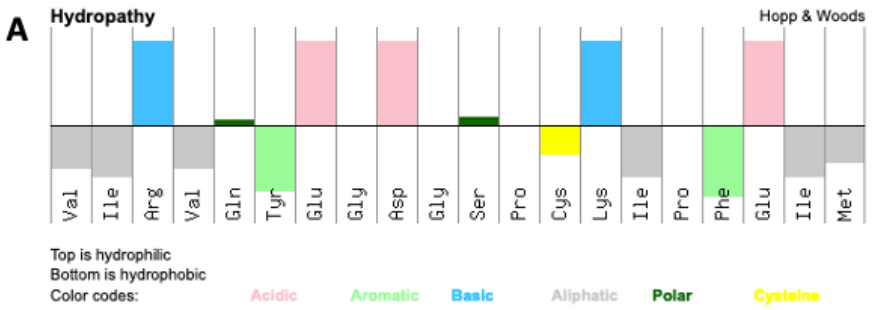

B

#	AA	a4v	HSA	NHSA	a4vAHS
1	V	0.429	2.092	0.000	0.447
2	I	0.429	2.092	0.000	0.447
3	R	0.508	2.092	0.000	0.447
4	V	0.421	2.092	0.000	0.447
5	Q	-0.226	0.000	0.000	0.000
6	Y	-0.085	0.000	0.000	0.000
7	E	-0.771	0.000	0.000	0.000
8	G	-0.632	0.000	0.000	0.000
9	D	-0.922	0.000	0.000	0.000
10	G	-0.707	0.000	0.000	0.000
11	S	-0.479	0.000	0.000	0.000
12	P	-0.298	0.000	0.000	0.000
13	C	0.173	0.982	0.000	0.307
14	K	0.165	0.982	0.000	0.307
15	I	0.583	0.982	0.000	0.307
16	P	0.180	0.000	0.000	0.000
17	F	0.730	2.154	0.000	0.518
18	E	0.548	2.154	0.000	0.518
19	I	0.398	2.154	0.000	0.518
20	M	0.398	2.154	0.000	0.518

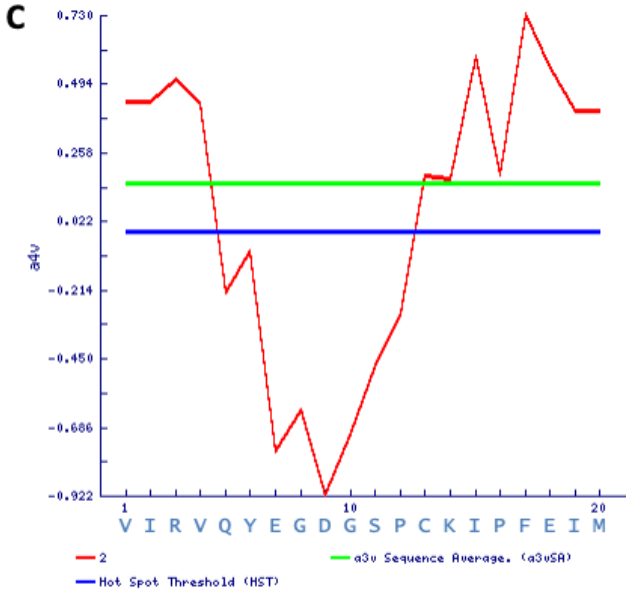

Figure 9-10: Predicted physiochemical properties of E Peptide 2.
A: Charge distribution depicted using PepCalc. Residue properties are indicated by colour: pink, acidic; light-green, aromatic; blue, basic; grey, aliphatic; dark-green, polar; yellow, cysteines. Bar chart shows Hopp and Woods Hydophobicity scale (Hopp and Woods, 1983). B: Aggregation potential calculated by AGGRESCAN. a4v indicates the sliding window average of a3v amino acid aggregation propensity. HSA (Hot spot area) is the area of aggregation potential above the hotspot threshold. NHSA is the HSA normalised for the number of residues. a4vAHS is the average a4v within a hotspot. C: Plot of AGGRESCAN aggregation potential (a4v) against residue. Blue line indicates the hotspot threshold (-0.02), and the green line depicts the average aggregation potential for the sequence.

9.3.3 Alanine scan and truncation analysis

Following computational pharmacokinetic characterisation, a small follow up array screen was conducted to validate and compare HSP90-binding of the two binding site peptides. (Figure 9-11). These were screened in triplicate. A peptide spanning residues G112-V130 was included as a negative control, since it did not bind HSP90 in the discovery array (data not shown). As found previously, both peptides bound HSP90, and E peptide 2 bound stronger than E peptide 1 (Figure 9-11). Also as before, the negative control sequence did not show any signal.

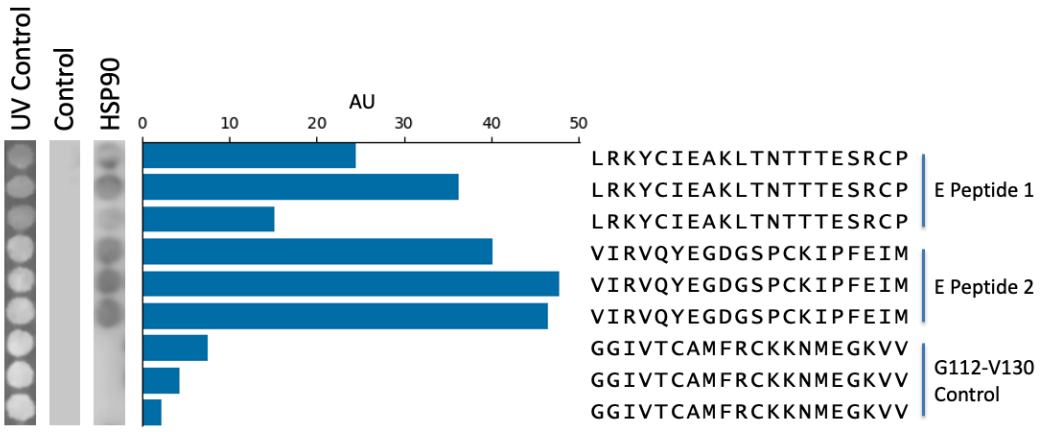

Figure 9-11: Validation of HSP90 binding DENV E peptides.
The two peptides identified as possible HSP90 binding sites on the DENV E protein were screened by peptide array in triplicate. A third sequence which did not show binding in the discovery array was included as a negative control. An array overlaid with a buffer and antibody-only control was included to detect non-specific binding. Spot quantification is shown as control-corrected inverted pixel value.

Structural analysis was then carried out by further peptide array screening to investigate the importance of each residue for binding HSP90. This information would provide insight into the protein binding sites and guide optimisation of the resultant peptide candidates. By alanine scan analysis of E peptide 1, several patterns were observed (Figure 9-12). First, residues in the C-terminal half of the peptide were generally found to be more important for binding than the N-terminal side. Second, alanine substitution of each basic residue greatly increased binding, especially K3A. Lastly, substitution of C19 abrogated binding, identifying it as a hotpot residue.

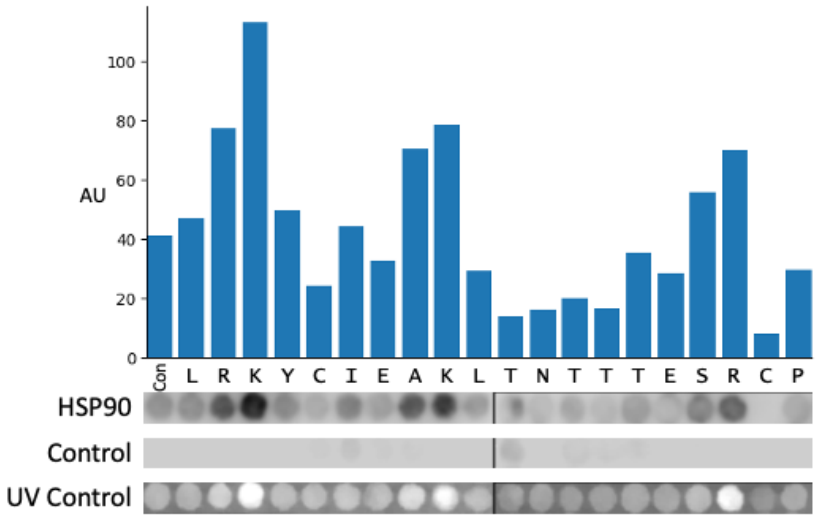

Figure 9-12: Alanine scan of E peptide 1:
Each spot represents where a residue has been substituted with alanine. An array overlaid with a buffer and antibody-only control was included to detect non-specific binding. Spot quantification is shown as control-corrected inverted pixel value. Black lines show where consecutive spots span different columns.

Subsequently, truncation analysis was performed (Figure 9-13). Upon truncation of the N-terminus, binding was improved by removing L1 and R2 and was mostly maintained until removal of Y4 (Figure 9-13:A). By C-terminal truncation, binding was immediately curtailed by the removal of P20 and almost fully undetectable after removal of C19 (Figure 9-13:B). The importance of C19 was also seen in the alanine scan (Figure 9-12). Following further C-terminal truncation, binding recovered in later truncates (Figure 9-13:B). Due to their short length however, this recovery may be due to nonspecific interaction. By dual truncation of both termini, the importance of P20 and C19 was observed again since binding was inhibited upon their removal. (Figure 9-13:C). Taken together, these findings indicated that the peptide could be shortened from the N-terminus but not the C-terminus, affinity may be optimised by substitution of basic residues, and the preservation of C19 was essential.

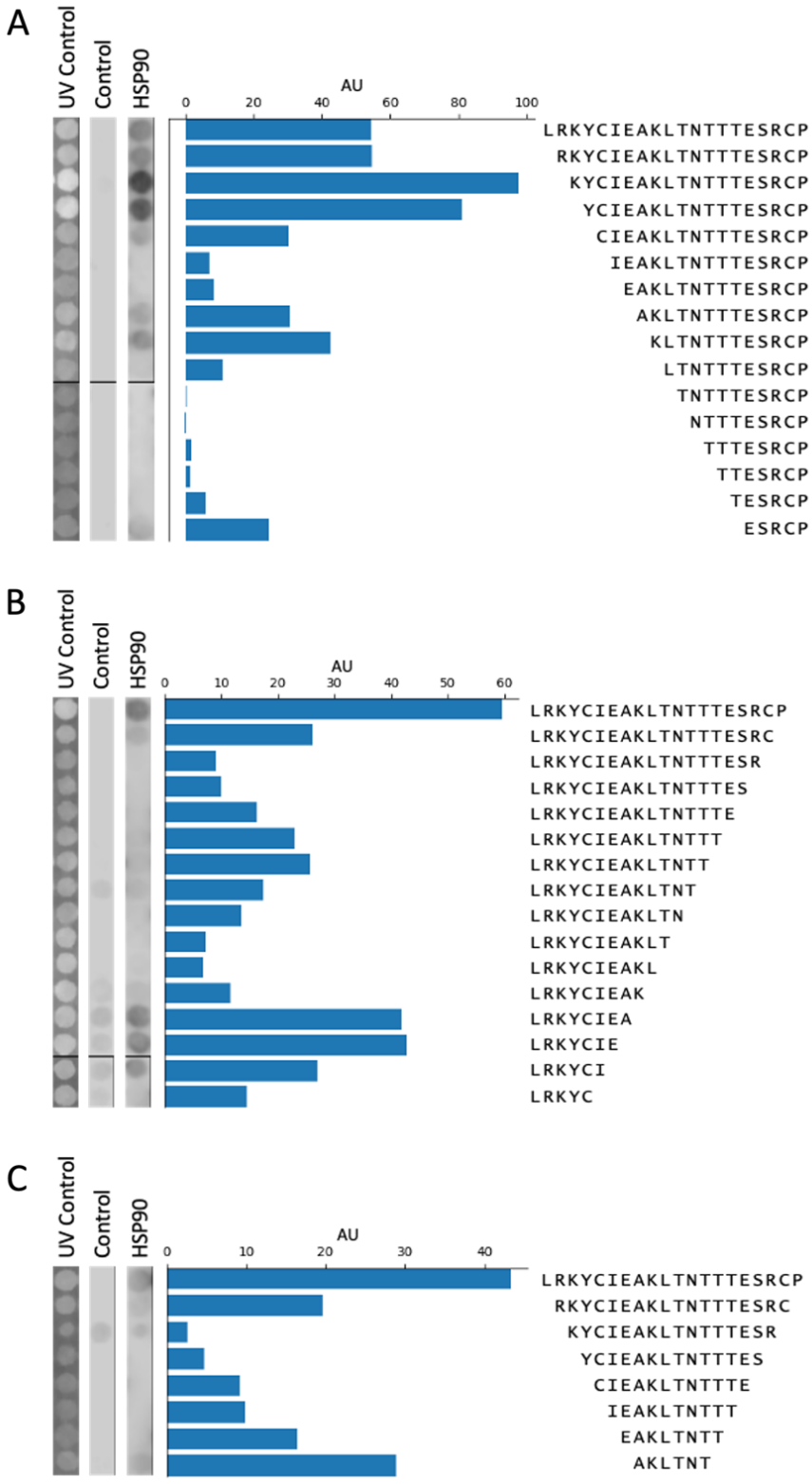

Figure 9-13: Truncation analysis of E peptide 1:
A: N-terminal truncation. Each consecutive peptide spot has a residue removed from the N-terminus. B: C-terminal truncation. Each consecutive peptide spot is shortened by one residue at the C-terminus. C: Dual truncation showing concurrent removal of one residue from each terminus in consecutive peptide spots. An array overlaid with a buffer and antibody-only control was included to detect non-specific binding. Spot quantification is shown as control-corrected inverted pixel value. Black lines show where consecutive spots span different columns.

Having investigated the structure of E peptide 1, the same procedure for E peptide 2 was carried out. By alanine scan, numerous residues were found to be important for binding, particularly the stretch of residues from C13 to P16, and that binding was improved upon P12A and E18A substitution (Figure 9-14).

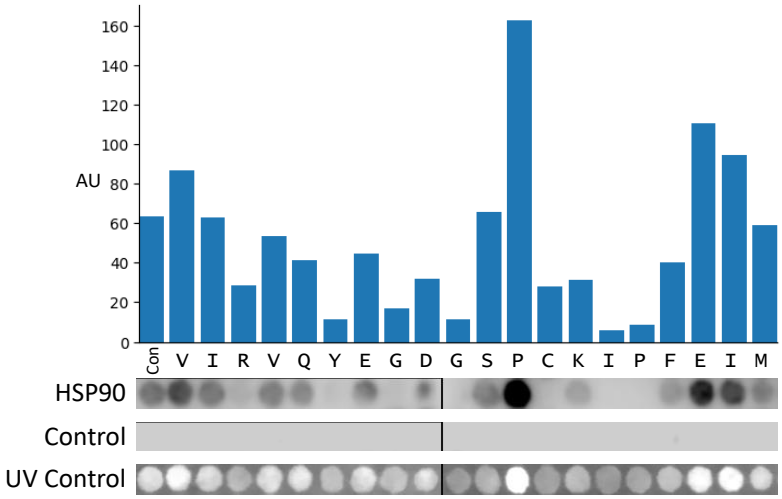

Figure 9-14: Alanine scan of E peptide 2.
Each spot represents where a residue has been substituted with alanine. An array overlaid with a buffer and antibody-only control was included to detect non-specific binding. Spot quantification is shown as control-corrected inverted pixel value. Black lines show where consecutive spots span different columns.

Next, truncation analysis was carried out on E Peptide 2. Following N-terminal truncation, binding was maintained after the removal of V1 and I2 but tailed off after exclusion of R3 (Figure 9-15:A). Following C-terminal truncation, binding was improved after removal of E18, I19 and M20, and decreased after the omission of F17 (Figure 9-15:B). This pattern from C-terminal truncation was also observed in the dual-truncation (Figure 9-15:C). These trends were concurrent with the alanine scan, in which substitution of these superfluous terminal residues did not affect binding (Figure 9-14). Taken together, these data indicated that each terminus could be trimmed, and that the P12A substitution may offer increased affinity towards HSP90.

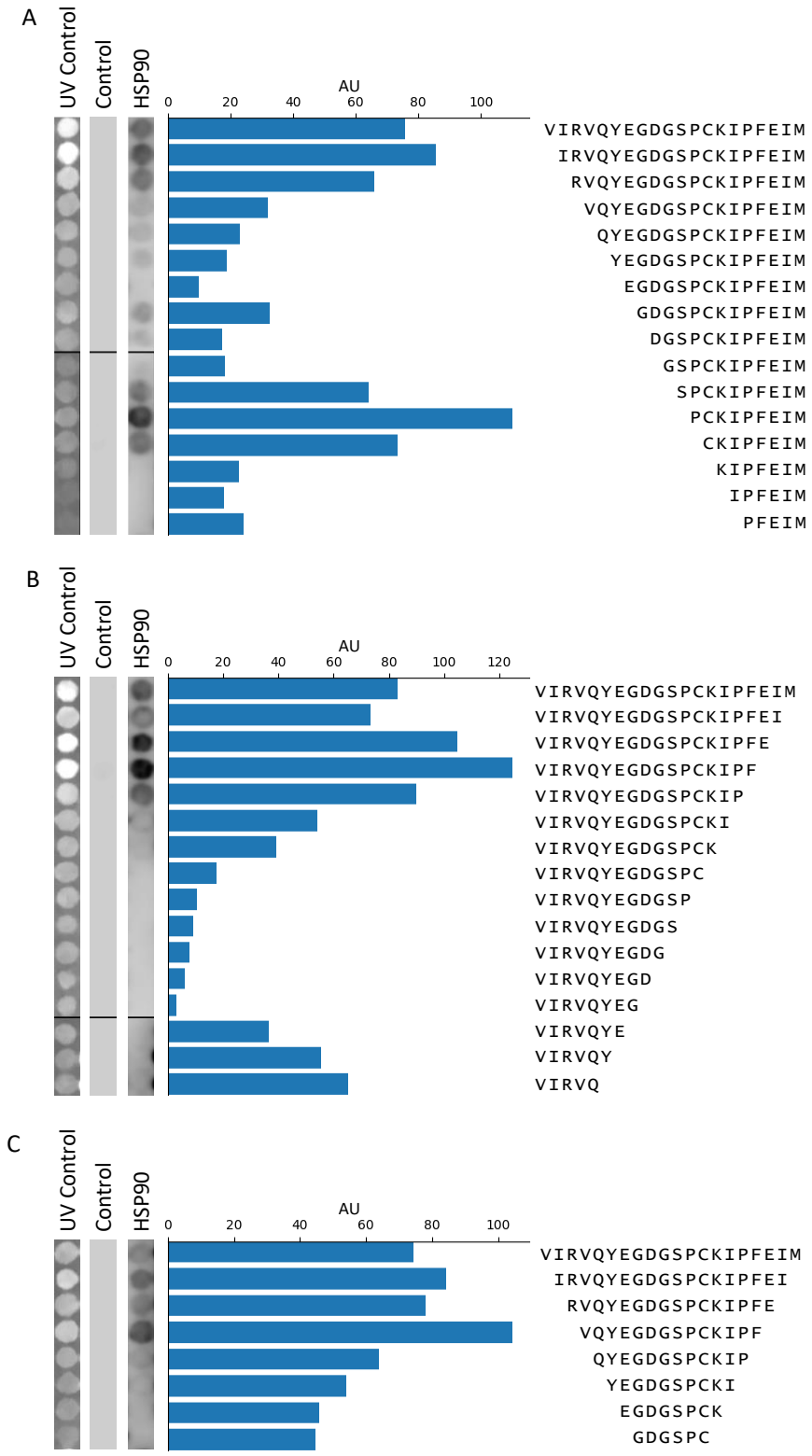

Figure 9-15: Truncation analysis of E peptide 2.
A: N-terminal truncation. Each consecutive peptide spot has a residue removed from the N-terminus. B: C-terminal truncation. Each consecutive peptide spot has one residue removed from the C-terminus. C: Dual truncation showing concurrent removal of one residue from each terminus in consecutive peptide spots. An array overlaid with a buffer and antibody-only control was included to detect non-specific binding. Spot quantification is shown as control-corrected inverted pixel value. Black lines show where consecutive spots span different columns.

9.3.4 Structural optimisation of E Peptide 2 and selection of truncates

Having identified hotspot residues and inessential residues at the termini, a second round of optimisation was conducted to select the strongest binding truncate to take forward into *in vitro* assays. With a view to avoid synthesising a large volume of arrays, only one binding site peptide was taken forward for further development at this stage. E Peptide 2 was chosen due to the stronger binding of its native sequence, and because of the potential of the P12A substitution to improve affinity. Nonetheless, E Peptide 1 remained a viable candidate and could serve as a contingency option in subsequent stages.

A selection of E Peptide 2 truncates were selected based on binding signal from the truncation analysis. These were synthesised and screened as duplicates, and HSP90 binding signal was compared (Figure 9-16). These truncates comprised 1-20, 12-20, 1-17, and 4-17. A novel truncate, 2-17, was designed based on the previous alanine scan and truncation data that suggested the redundancy of residues V1, E18, I19 and M20 (Figure 9-14; Figure 9-15). When screened together, most truncates indicated weak binding except for the rationally inferred truncate 2-17, which appeared to bind HSP90 strongly (Figure 9-16).

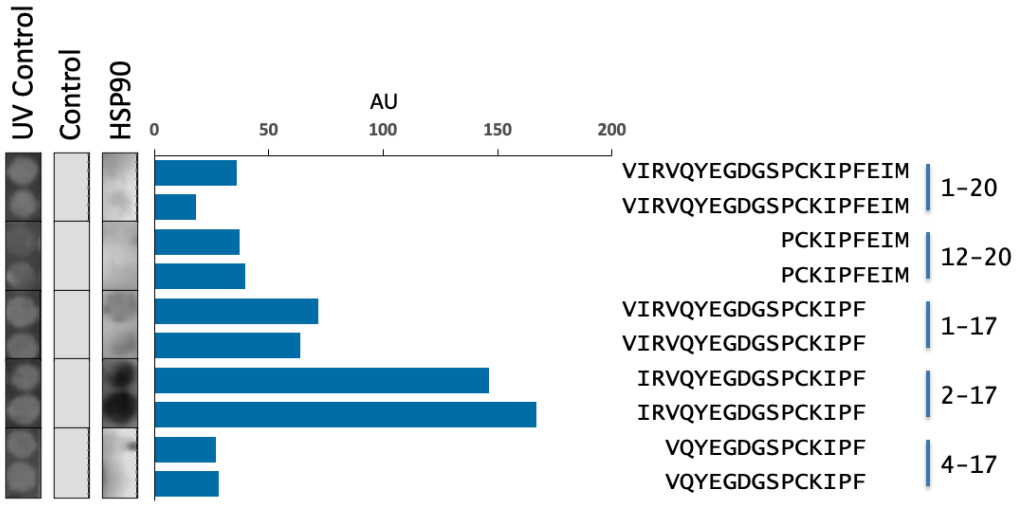

Figure 9-16: Comparison of E Peptide 2 truncates.
An array overlaid with a buffer and antibody-only control was included to detect non-specific binding. Spot quantification is shown as control-corrected inverted pixel value. Black lines indicate where non-consecutive peptide spots have been joined.

The truncate 2-17 was selected for further optimisation because of its exceptionally strong signal. Next, the role of key residues in the sequence was

investigated by performing targeted substitution (Figure 9-17). First, the potential oxidation of C13 presents a risk of aggregation and insolubility. By substitution with serine, a less nucleophilic and redox insensitive residue with similar physiochemical properties, this risk can be avoided (Moroder, 2005). However, binding was abrogated by the C13S substitution (Figure 9-17), and this affirms the necessity of cysteine 13 as shown previously (Figure 9-14). In addition, substitution of acidic residues was investigated. Upon substitution of E7 and D9 with lysine to invert the charge, binding decreased substantially, indicating necessity of the negative charge (Figure 9-17). Of note, these substitutions also resulted in binding in the negative control, indicating non-specific interaction.

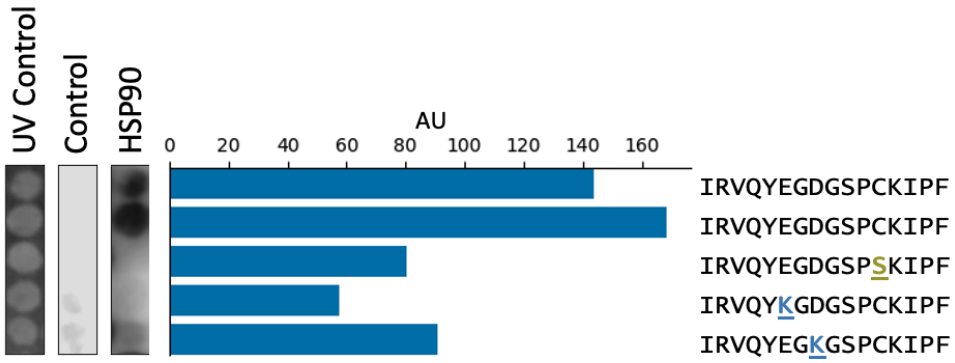

Figure 9-17: Point Substitution analysis of the E Peptide 2 2-17 truncate.
From the native truncate, cysteine at position 13 was substituted with the isostere serine to avoid redox sensitivity and aggregation risk. E7K and D9K were introduced to assess the role of charge at those positions. An array overlaid with a buffer and antibody-only control was included to detect non-specific binding. Spot quantification is shown as control-corrected inverted pixel value.

Continuing our study into the structure of the E Peptide 2 2-17 truncate, another alanine scan was carried out (Figure 9-18). Similar results to the native sequence alanine scan were observed (Figure 9-14). Notably, the decrease in binding upon alanine substitution of residues C13, K14, I15, and P16 was observed once more (Figure 9-18). In addition, an increase in binding was found following the P12A substitution, similar to the native alanine scan (Figure 9-14). This substitution therefore remained a valid option for optimisation of affinity. Notably, substitution of E7 and D9 with alanine led to non-specific binding (Figure 9-18), similar to the charge inversion experiment (Figure 9-17).

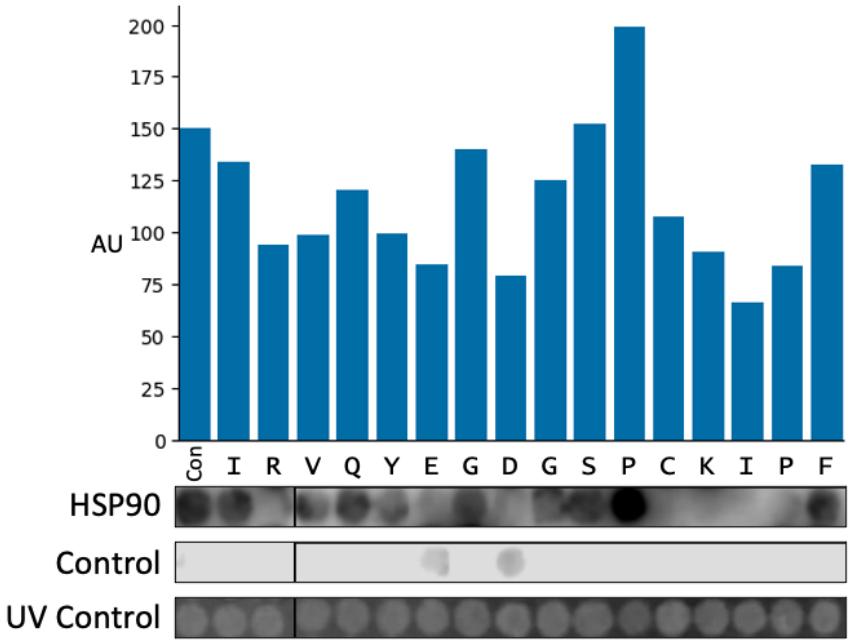

Figure 9-18: Alanine scan analysis of the E Peptide 2 2-17 truncate.
Each spot represents where a residue has been substituted with alanine. An array overlaid with a buffer and antibody-only control was included to detect non-specific binding. Spot quantification is shown as control-corrected inverted pixel value. Black lines show where consecutive spots span different columns.

9.3.5 Point substitution analysis of E peptide 2 2-17

Before conducting assays to evaluate cytotoxicity and antiviral efficacy of E Peptide 2 2-17, a full point substitution analysis was carried out to gain detailed information on the importance of each residue to binding. In this experiment, each residue position was substituted with all other 19 natural amino acids. In the array, each column shows all substituents for one position, revealing information about what type of side chain is beneficial at each part of the peptide. Because the P12A substitution of truncate 2-17 resulted in the strongest binding observed, point substitution was carried out on this peptide with the aim of identifying even stronger derivatives.

The array overlaid with HSP90 is shown in Figure 9-19:A, along with the control array in Figure 9-19:B. A heatmap of control-corrected signal values is shown in Figure 9-20. From this, several patterns were observed. First, most substitutions of residues C13, K14, I15, and P16 resulted in a loss of binding (Figure 9-20), as also seen in alanine scans of the native peptide (Figure 9-14) and 2-17 truncate (Figure 9-18). This confirms this area as a hotspot region for binding. Second, a decrease in binding from substitution of the acidic residues E7 and D9 was also

found (Figure 9-20), which agrees with previous charge inversion substitutions and alanine scan analysis (Figure 9-17; Figure 9-18). Additionally, E7D and D9E substitutions maintained the negative charge and seemed to preserve binding. (Figure 9-20). Congruent with this, substitution with lysine or arginine at the 7 and 9 positions as well as most positions on the C-terminal resulted in a loss of binding.

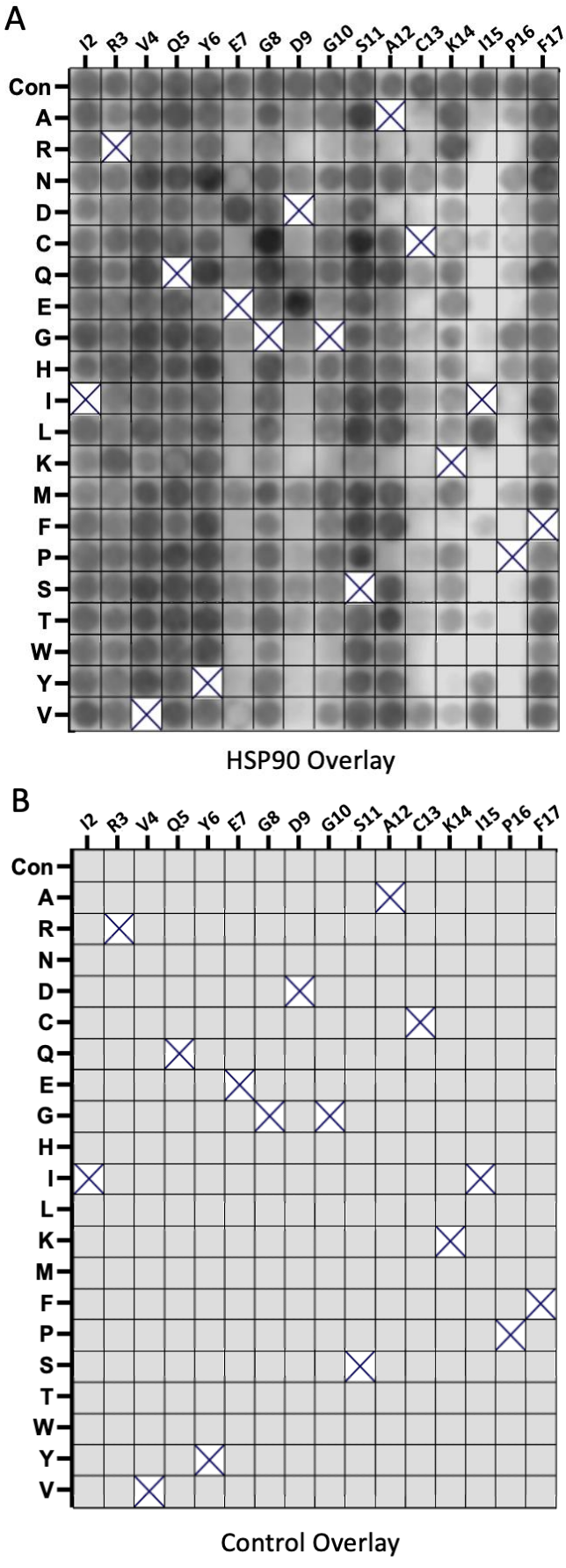

Figure 9-19: Point substitution analysis of E Peptide 2 2-17. Each residue is substituted with all other natural amino acids. A: Array overlaid with HSP90. B: Array overlaid with a buffer and antibody-only control to detect non-specific binding.

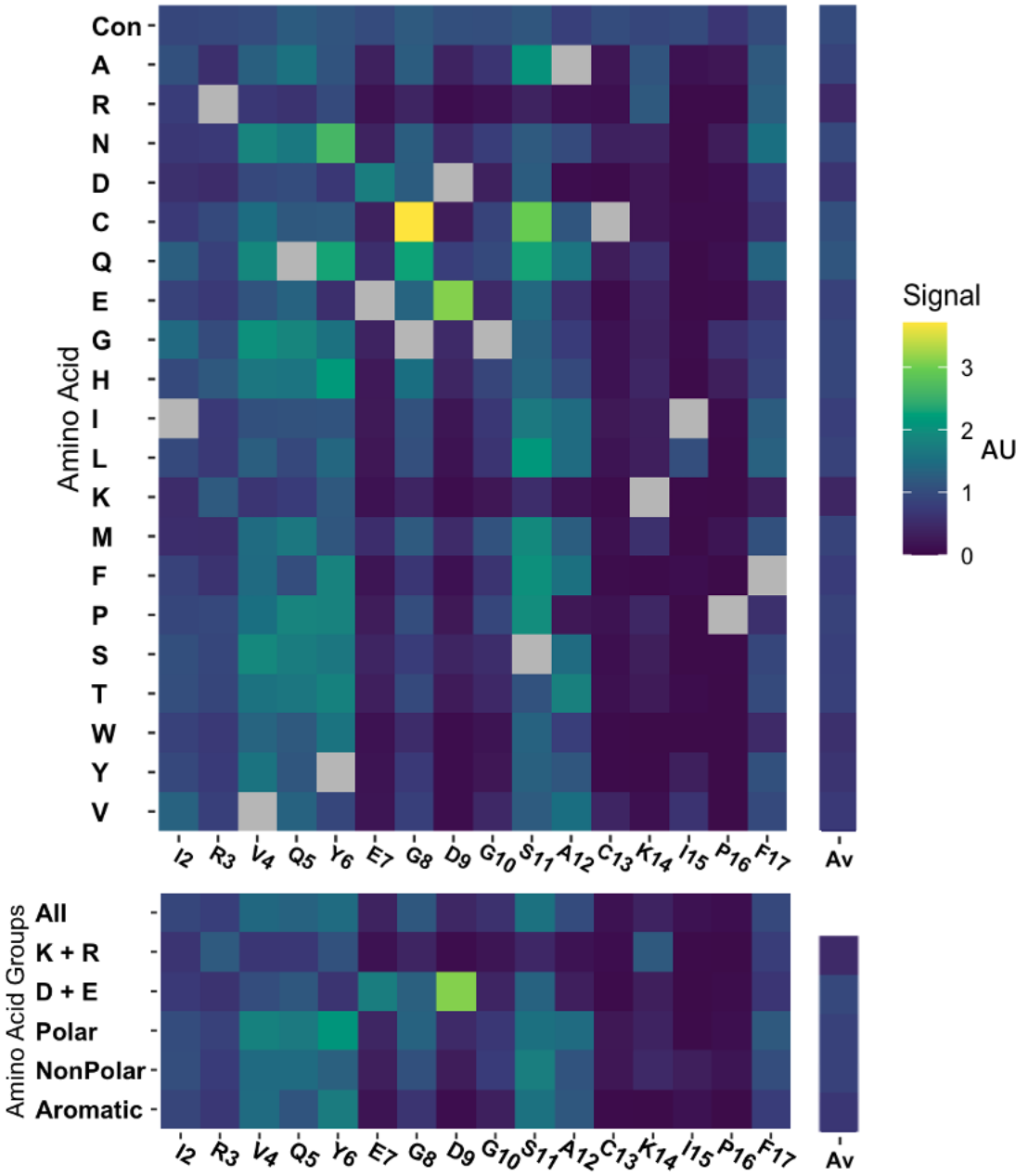

Figure 9-20: Heatmap of point substitution analysis of E Peptide 2 2-17.
The native sequence is repeated in the first row as a control. Each column shows all possible 19 substitutions at one residue position. Grey squares indicate the native residue identity. Signal is normalised to mean native value. Con, control; Av, average signal.

Substitution was beneficial to binding at some positions as well. Positions V4, Q5, Y6, and S11 exhibited increased binding by most substitutions. (Figure 9-20). To clearly show these patterns, the mean change at each position was calculated (Figure 9-21). To highlight the strongest binding substituents, the peptides were ranked by binding signal (Figure 9-22). Amongst these, the strongest binding substituents were G8C, D9E, and S11C.

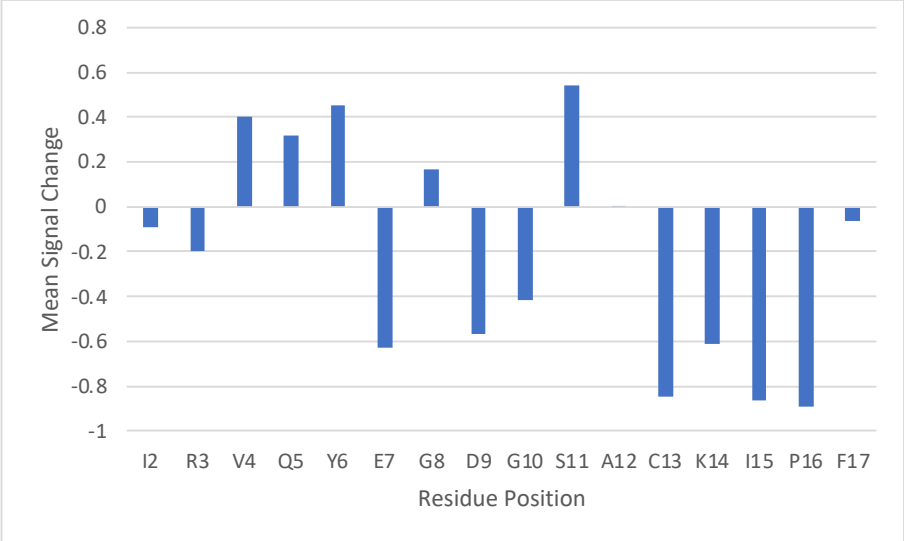

Figure 9-21: Mean signal change of each residue in point substitution analysis. Signal is normalised to the mean control value.

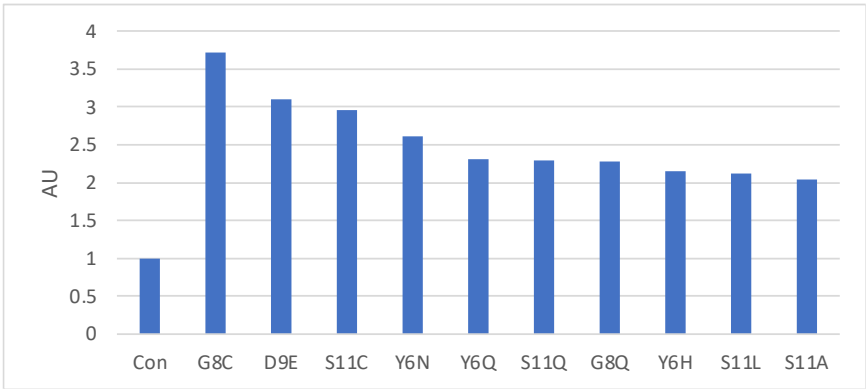

Figure 9-22: Top ten substitutions that increased binding in the point substitution analysis. Signal was normalised to the mean native value.

9.3.6 Cytotoxicity of E peptides

Now that the strong binding derivative E Peptide 2 2-17 had been developed from the HSP90 binding site on Dengue DIII, and point substitution data had been obtained, cytotoxicity and antiviral efficacy were characterised. First, a negative control peptide was required to distinguish the effects of specific interaction. For this peptide, substitutions C13A and I15A were incorporated together with the aim of abolishing specific interaction with HSP90. These hotspot substitutions demonstrated loss of activity in the alanine scan of the truncate (Figure 9-18) and the native sequence E Peptide 2 (Figure 9-14). Moving forward, E Peptide 2 2-17 and the double alanine control peptide were termed Epep2 and Epep2AA (Table 14).

Table 14: Sequences of candidate inhibitor peptides for the HSP90-E interaction.
Candidate disruptor Epep2 was developed from the HSP90 binding epitope E peptide 2 from the Dengue E protein and spanned residues 2-17 of that original sequence. Amino acid sequence indicated, and the inactivating double alanine substitutions in the negative control peptide Epep2AA are indicated in bold blue text.

Peptide Name	Sequence
E Peptide 2 2-17 (Epep2)	IRVQYEGDGSPCKIPF
E Peptide 2 2-17 AA (Epep2AA)	IRVQYEGDGSP**A**K**A**PF

Additionally, the secondary structure of the candidates was predicted using PEP-FOLD3, and both adopted a ß-hairpin-like structure. (Figure 9-23).

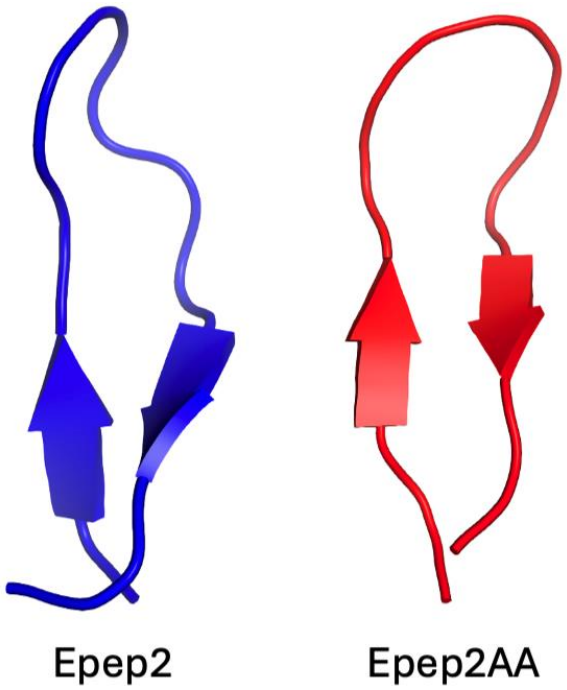

Figure 9-23: Peptide Conformers of Epep2 and Epep2AA predicted by PEP-FOLD3.
Conformation prediction of the peptide candidate Epep2 and the negative control peptide Epep2AA. Both peptides exhibited a β-hairpin like conformation.

With these candidates, cytotoxicity assays were conducted so that any decrease in virus infection observed could be differentiated from peptide-induced cell death. To this end, these two peptides were synthesised by GenScript with modifications of N-terminal acetylation and C-terminal amidation, which are commonly used to increase stability against proteases for linear peptides (Di,

2015). Cytotoxicity assays were then carried out by Professor Aussara Panya at Chiang Mai University. Vero and Huh7 cells were specifically chosen since they are highly susceptible to viral infection and, originating from the kidney and liver respectively, are representative of the main cell types infected by RNA viruses (Emeny and Morgan, 1979; Sun and Nassal, 2006). These cells were treated with the two peptide compounds Epep2 and Epep2AA at 24 and 48 hours, and cell viability was measured using the PrestoBlue assay (Figure 9-24). The results indicated no cytotoxicity in Vero or Huh7 cell lines at a concentration range from 0 to 100 µM. In A549 cells however, a reduction in viability was observed for Epep2 at 48 hours, and at 24 and 48 hours for Epep2AA. Moving forward, subsequent antiviral assays were conducted in Vero cells. Of note, the cytotoxicity data for Huh7 and A549 cell was preliminary and consisted of one biological replicate.

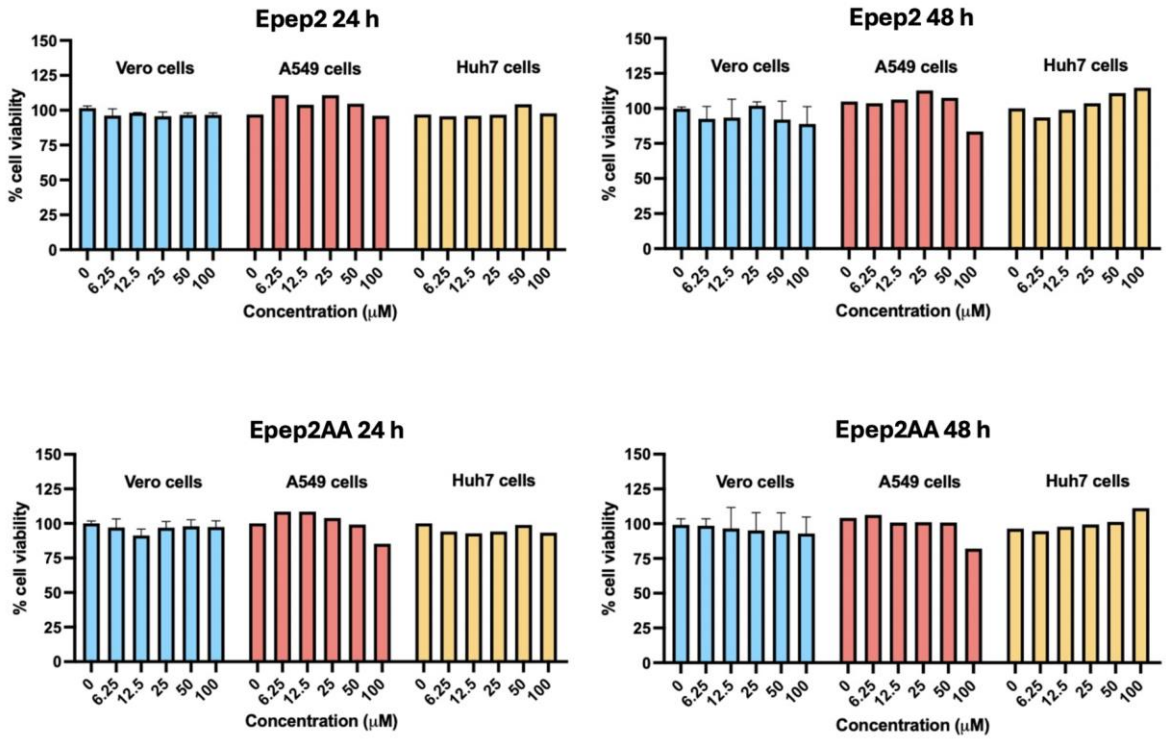

Figure 9-24: Presto Blue cell viability assay of Epep2 and Epep2AA.
Viability was determined by 590/560 nm fluorescence expressed as a percentage of the vehicle control. Experiment carried out by Professor Aussara Panya at Chiang Mai University. (Vero n=3, A549 and Huh7 n=1). Column plot and error bars represent mean and standard deviation.

9.3.7 Antiviral assessment of E peptides by live virus ELISA

With the toxicity profile of Epep2 and Epep2AA in Vero cells established, antiviral activity was determined. This assay was performed by Professor Aussara

Panya at Chiang Mai University. This was a decisive moment in the project, as any antiviral effect would validate the HSP90-E PPI as a drug target. Furthermore, the degree of potency would signify the value of the peptide as a therapeutic candidate relative to existing peptide inhibitors. For this purpose, cell-based ELISA was used to quantify infectivity. Cells were incubated with live Dengue virus serotype 2 together with Epep2 or Epep2AA for 2 hours. Unbound viruses and peptide were removed by washing, and the cells were left for 24 or 48 hours. The presence of Dengue E antigens was then measured relative to a Dengue-only treatment control by using the E protein antibody 4G2 and ELISA reagents. 4G2 was also used as a positive control treatment condition, since it is an anti-viral Dengue-neutralising antibody. As a result, no decrease in infection was observed for Epep2 or Epep2AA, while 4G2 induced an antiviral effect (Figure 9-25).

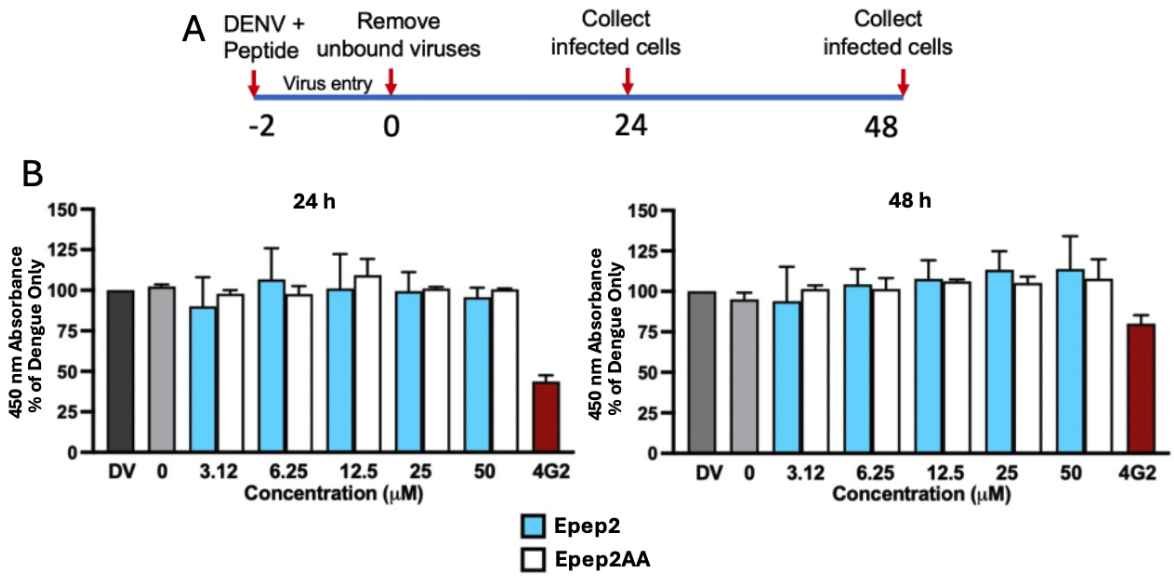

Figure 9-25: Cell-based ELISA of Vero cells exposed to Dengue virus and treated with peptides Epep2 and Epep2AA.
A: Treatment protocol for assay. Time represented in hours. B: ELISA results. Experiment carried out by Professor Aussara Panya at Chiang Mai University. DV; Dengue virus only, 4G2; 4G2 antibody targeted to E protein. (n=3). Column plot and error bars represent mean and standard deviation.

Since Epep2 did not produce an antiviral effect, the experiment was repeated, but the cells were incubated with peptide for 30 minutes before being exposed to virus. Resultingly, no antiviral activity was observed for Epep2 relative to the Dengue virus-only control with this new treatment regimen, while 4G2 exhibited an inhibition of infection (Figure 9-26).

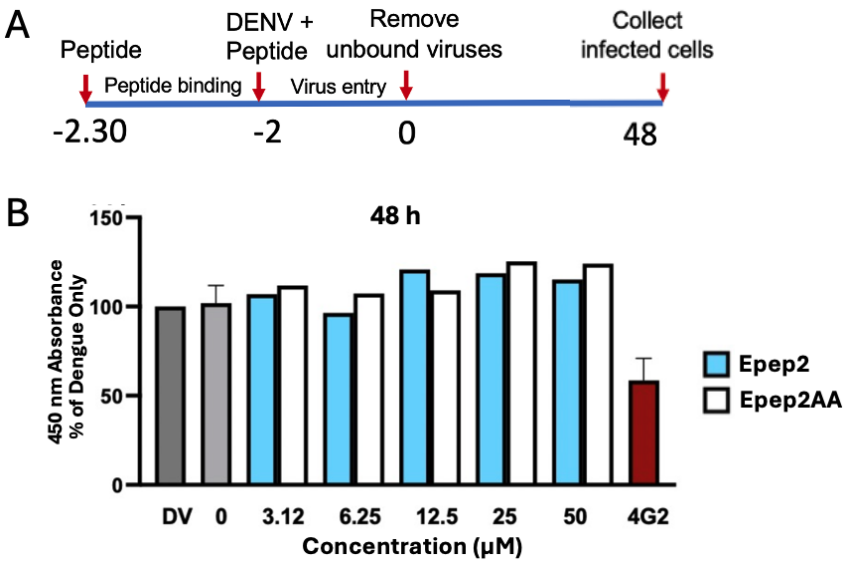

Figure 9-26: Cell-based ELISA of Vero cells exposed to Dengue virus and treated with peptides Epep2 and Epep2AA.
A: Treatment protocol for assay. Time represented in hours. B: ELISA results. Experiment carried out by Professor Aussara Panya at Chiang Mai University. DV; Dengue virus only, 4G2; 4G2 antibody targeted to E protein. (n=1). Column plot and error bars represent mean and standard deviation respectively. Three technical replicates were used for the untreated and 4G2 controls.

9.4 Discussion

9.4.1 Discovery of HSP90-binding epitopes of the Dengue E protein

Peptide array screening of Dengue E peptides against HSP90 recombinant protein revealed two main binding sites. The weaker binding site originated from Domain II at residues K56-P75, and the stronger binding site was located downstream in domain III at residues V321-M340. These were termed E Peptide 1 and E Peptide 2 respectively. By examination of the E protein crystal structure, these two binding sites for HSP90 were found to be exposed on the protein surface and could therefore comprise the binding interface with HSP90. Because of their separation in space, the sites were unlikely to form a single binding motif. Next, multiple sequence alignment was carried out to compare the homology of the peptides between the four Dengue serotypes. Conservation of a sequence during the evolution of multiple serotypes would suggest a functional role (Cooper and Brown, 2008). Overall, both sequences showed some level of conservation, and E peptide 1 exhibited higher overall homology than E peptide 2. Residue identity was not conserved beyond three consecutive amino acids in both peptides, but physiochemical properties were conserved over longer stretches. This was especially true in E peptide 1. In summary, the level of conservation found makes it plausible for HSP90-binding sites to be present at either peptide location, which could be important for Dengue virus cell entry.

In addition to serotype conservation, the presence of neutralising antibody binding sites can indicate functional importance (Burton, 2023). If infection is inhibited by an antibody binding to a specific site, then that site may be involved in processes essential to the virus life cycle, such as the interaction with host receptors for internalisation (Sicca et al., 2018). The sequence of E Peptide 1 overlapped with a serotype-conserved structural feature at residues R73-E79 called the BC loop, which is a known binding site for potent neutralising antibodies (Smith et al., 2013). E Peptide 1 shared its three C-terminal residues R73, C74 and P75 with this structure, of which R73 was shown to be a hotspot residue for antibody binding by mutagenesis studies (Smith et al., 2013). Considering these overlaps, it is possible that antibody-induced neutralisation

originates from the disruption of interaction between the E peptide 1 epitope and HSP90.

Besides neutralising antibodies, there is also a conserved glycosylation site at N67 (Hu et al., 2021). This residue is critical for recognition of DC-SIGN, a lectin-like protein and verified receptor for Dengue virus internalisation (Hu et al., 2021). DC-SIGN binds the glycosylated N67 and N153 residues of the Dengue E protein to trigger cell entry of the virus. This interaction is dependent on glycosylation, as substitution with non-glycosylated N67Q reduces virus infectivity (Hu et al., 2021). This possible overlap of binding sites for DC-SIGN and HSP90 raises the question of cooperativity. It may be that there is sequential binding, in which recognition of the first protein receptor promotes recruitment of the second. Alternatively, HSP90, DC-SIGN and the Dengue E protein may form a pro-viral complex as part of cell entry. Further research is required, and peptide array or docking studies would reveal any interactions between these proteins, and the use of simultaneous HSP90 and DC-SIGN inhibition may produce synergistic effects.

While E Peptide 1 was discovered on Domain II, E Peptide 2 was found in Domain III, the domain suggested to participate in host cell receptor binding (Hung et al., 2004; Sukupolvi-Petty et al., 2007; Frei et al., 2015; Sarker et al., 2023; González-Lodeiro et al., 2024). The E Peptide 2 epitope contains many residues important for the binding of neutralising antibodies. In a western blot study, such affinity was found for a peptide comprising residues C333-L351, which overlaps with E Peptide 2 located at V321-M340 (Roehrig et al., 1998). Looking closer at individual residues, experiments including mutagenesis assays (Huang et al., 2008; Gromowski et al., 2010), phage display (Frei et al., 2015), and yeast display methods (Sukupolvi-Petty et al., 2007) have revealed residues Q325, E327, G330, S331, and I335 to be important in the binding of neutralising antibodies. Additionally, P332 was identified as a hotspot residue critical for binding neutralising antibodies, but was suggested to play an allosteric role instead of forming direct interactions (Gromowski et al., 2010; Frei et al., 2015). The same was true for D329, but mutagenesis of this position did not result in as strong inhibition of antibody binding to E as for the P332 mutation (Gromowski et al., 2010). With so many residues within E Peptide 2 acting as important

epitopes for neutralising antibodies, it was plausible that this site could play a functional role in virus internalisation.

On E Domain III, a lateral loop structure has been shown to bind the host cell receptor heparan sulfate to trigger cell entry of the Dengue virus (Hung et al., 2004; Bressanelli et al., 2004; Mazumder et al., 2007). Compellingly, the peptide inhibitor DET4 was designed against this motif and exhibited a moderate antiviral effect with an IC50 of 35 μM (Alhoot et al., 2013; Isa et al., 2019). It was possible that E peptide 2 overlapped with the lateral loop to form a single binding site for both HSP90 and heparan sulfate. This was not the case however, and the E Peptide 2 epitope at V321-M340 was located upstream from the lateral loop at I380-L389. Nevertheless, when the two motifs were highlighted on a crystal structure of the E protein, they were found to be in close proximity (Figure 9-27). Although these were two distinct sites, this proximity may indicate cooperative binding between HSP90 and heparan sulfate. This could be investigated by peptide array, virtual docking, or pulldown assays. If co-dependence between HSP90 and heparan sulfate in binding the E protein is found, a combination therapy may provide an additive antiviral effect. Taken together, the level of conservation and presence of neutralising antibody epitopes in E Peptide 1 and E Peptide 2 support the notion of a functional role in Dengue virus infection, which may be the binding of HSP90 receptors on host cells.

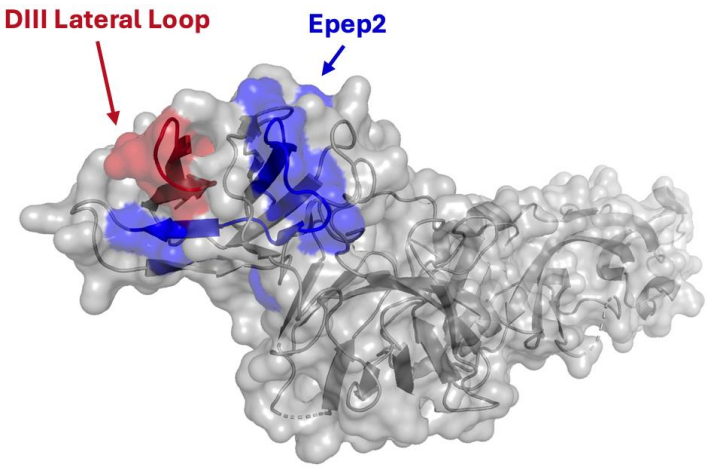

Figure 9-27: E peptide 2 epitope and the lateral loop structure shown on a crystal structure of the Dengue E protein.
PDB accession 1TG8.

The two binding sites described in this chapter were discovered by peptide array. However, one limitation of peptide array screening is that the peptides are fixed to a cellulose membrane by a C-terminal PEG linker, which may constrain peptide conformation or sterically occlude the C-terminus (Katz et al., 2011). Therefore, the peptides may not be representative of the E protein HSP90 binding sites. Validation by another method would increase confidence of these findings. For example, obtaining an X-ray crystal structure of HSP90 bound by the E protein domain III would provide detailed structural information and would inform late-stage optimisation of peptide structure activity relationship (SAR).

9.4.2 Pharmacokinetic assessment of E Peptide 1 and E Peptide 2

Peptide secondary structure greatly impacts pharmacokinetics and pharmacodynamics (Lee et al., 2019). E Peptide 1 and 2 were predicted to adopt a partial α-helix and a ß-hairpin structure respectively. Such constrained conformations can increase stability against proteases, promote membrane permeability, and increase potency by offsetting the entropic penalty of binding (Henninot et al., 2018).

Furthermore, when several physiochemical parameters were estimated, both peptides were found to be charged at pH 7 and indicated good solubility in water. However, both peptides presented an aggregation risk since cysteine residues were found in both sequences (Moroder, 2005). Cysteine residues are prone to oxidation, which can lead to the formation of disulfide bonds and the formation of peptide aggregates (Zapadka et al., 2017). Additionally, a hotspot for aggregation was found in E Peptide 1. These factors may lead to insolubility, presenting a challenge during *in vitro* assay testing and eventual therapeutic administration (Fosgerau and Hoffmann, 2015). To improve the chance of clinical success, these features should be addressed in later optimisation. Cysteine could be substituted for serine, a redox-insensitive residue with similar physiochemical properties (Moroder, 2005). Polar residues could be substituted into the aggregation hotspot to disfavour non-polar and aromatic interactions (Fosgerau and Hoffmann, 2015).

Overall, the constrained conformations of E peptide 1 and 2 in addition to the good water solubility makes these peptides excellent starting points for

therapeutic development, but aggregation risk remained a potential challenge. In later development, aggregation could be checked for using solubility assays and could be addressed by substitution of cysteine for a non-redox sensitive isostere or by increasing polarity and charge across the peptide (Moroder, 2005).

9.4.3 Sequence optimisation of HSP90-binding E peptides

Alanine scan analysis and truncation of termini were carried out to identify hotspot residues and optimise peptide length. From an alanine scan experiment, E Peptide 1 was found to have a cluster of important residues on the C-terminal side. Additionally, substitution of positively charged basic residues with alanine improved interaction, suggesting that the binding site on HSP90 may be positively charged. It would be interesting to see whether the introduction of negatively charged aspartic or glutamic acid would increase affinity for HSP90 further. Lastly, C19 was found to be a hotspot residue since alanine substitution was not tolerated. However, serine substitution may avoid redox sensitivity like alanine but may preserve HSP90 interaction, since it is more physiochemically similar to cysteine (Moroder, 2005). Truncation analysis of E Peptide 1 mostly reflected the alanine scan in which N-terminal residues could be removed, but C-terminal residues proved important for binding.

By alanine scan analysis of E Peptide 2, many residues across the sequence were found to be important for HSP90 binding, particularly C13-P16. Conversely, P12A and E18A substitutions increased binding. This is interesting, since P12A corresponds to residue P332 of the E protein. As found by mutagenesis, this residue was thought to provide a critical allosteric role in the binding of neutralising antibodies, highlighting P332 as potentially important to viral entry (Gromowski et al., 2010; Frei et al., 2015). It is surprising that removal of this residue by the P12A substitution in this project increased binding to HSP90, suggesting that P12 plays a different role in binding HSP90 and neutralising antibodies. Finally, truncation analysis of E Peptide 2 affirmed the alanine scan results showing several residues from both termini to be redundant. As a result of these experiments, the hotspot residues and redundant termini residues of both peptides were identified, and this information was used as a starting point to optimise peptide length in the following work.

9.4.4 Prioritisation of E peptide 2 and further optimisation

To reduce the cost of peptide array synthesis, only E peptide 2 was taken forward for further screening, since it indicated stronger binding affinity, originated from EDIII, and the P12A substitution could potentially increase binding affinity further.

In the previous array screening experiments, redundant residues at the termini of E peptide 2 were identified. In subsequent screening, various truncates of E peptide 2 were compared, and 2-17 was identified as the strongest binding derivative. Targeted substitution was then carried out by peptide array, in which a C13S modification was made to remove the redox sensitivity and risk of aggregation due to the cysteine residue (Moroder, 2005). Unfortunately, this abrogated binding with HSP90, affirming C13 as a hotspot residue. Moving forward, C13 had to be preserved, but substitution with the non-proteinogenic amino acid selenocysteine could potentially remove aggregation risk while preserving HSP90 binding (Moroder, 2005). Otherwise, introduction of polar residues elsewhere in the peptide would be another option to discourage aggregation (Zapadka et al., 2017).

Next, an alanine scan was carried out on the 2-17 truncate, and the results largely reflected the findings from the alanine scan of the full-length native sequence, increasing confidence in these findings. These data highlighted the importance of preserving the hotspot residues of E7, D9, and C13-P16 during structural modification in later development.

9.4.5 Point substitution of E peptide 2

Given that C13 could not be substituted with alanine or serine without hindering binding to HSP90, and that detailed information on the role of each amino acid would be useful for optimisation, a full point substitution was carried out. For this analysis, the derivative E Peptide 2 2-17 P12A was selected as the sequence to be substituted. This was a stronger binding peptide than the native sequence and provided a higher baseline to improve upon for the discovery of even stronger binding derivatives. As also shown by the previous alanine scans, point substitution validated that most substitutions of E7, D9, and C13-P16

substantially reduced binding. Intuitively, preservation of the negative charge by E7D and D9E maintained binding. Correspondingly, introduction of lysine or arginine at these positions or at most positions on the C-terminal half of the peptide greatly reduced binding. This propensity for negative charge suggested again that the HSP90 binding site for this peptide was positively charged, and a negative charge is favoured for prospective ligands.

Some substitutions resulted in stronger binding. Most substitutions of R3-Y6 and S11 were beneficial, and the highest binding substituents were G8C, D9E, and S11C. Of these, the D9E modification is most valuable for the optimisation of affinity in later development, as introduction of cysteine by G8C would not be viable due to increased redox-sensitivity and aggregation risk (Moroder, 2005). In other work, point substitution analysis was carried out to characterise the binding of broad-spectrum chemokine inhibitor peptides, in which a similar anionic region was found essential for target binding (Vales et al., 2023). Additionally, increasing negative charge further by aspartic or glutamic acid substitution was identified as a means for improving affinity (Vales et al., 2023). This emphasises the utility of point substitution analysis for characterising charge-based interactions to inform peptide drug development.

9.4.6 Design of the negative control peptide Epep2AA

Now that an optimised candidate had been developed, termed Epep2, spanning residues 2-17 of the E peptide 2 epitope, assay testing for target disruption, cytotoxicity, and antiviral characterisation could be performed. First, a negative control peptide was required to distinguish specific peptide effects from off-target actions. A control peptide, Epep2AA, was designed by incorporating two loss-of-binding substitutions, C13A and I15A, into the 2-17 truncate as identified by the alanine scan data. This type of double-alanine control was selected over a scrambled control, since alanine controls preserve more of the native sequence and are more likely to be representative. Additionally, scrambled controls contain all residues of the native sequence and therefore retain the risk for specific interaction (Farkas et al., 2022). For these reasons, double alanine controls are sometimes preferred, despite being less common, and have been successful in other studies of peptide therapeutic development (Victor et al., 1999; Chang et al., 2013; Wei et al., 2021).

9.4.7 Epep2 cytotoxicity characterisation

Following design of the Epep2 candidate and corresponding negative control, cytotoxicity assays indicated no impact of the peptides on Vero cell viability up to a concentration of 100 µM. Additionally, while preliminary data suggested a similar tolerance in Huh7 cells, some cytotoxicity was observed in A549 cells upon treatment of Epep2 and Epep2AA above 50 µM.

It was interesting that this effect was observed only in the cancer cell line A549. HSP90 function is known to be exploited in cancer cells for stabilisation of signalling factors and misfolded proteins for the promotion of survival, proliferation, migration, and invasion (Li and Luo, 2023). Furthermore, HSP90 inhibitors have been shown to suppress oncogenic pathways and have entered clinical development (Li and Luo, 2023). Therefore, the cytotoxic effect of the peptides in A549 cells suggests a similar inhibition of endogenous non-viral functions of HSP90. This was surprising, since peptides are typically not membrane permeable, and Epep2 should therefore not interfere with intracellular HSP90. Instead, Epep2 could have disrupted endogenous functions of HSP90 at the cell membrane (Taha et al., 2019; Chakraborty and Edkins, 2021), which could be plausible given the high concentration of 100 µM. Alternatively, this high concentration could have resulted in Epep2 permeation and disruption of endogenous HSP90 function inside the cell. These results emphasised that potential disruption of endogenous HSP90 function should be thoroughly characterised in later development and would be especially important for avoiding off-target toxicity for clinical translation. For example, degradation HSP90 client proteins or disrupted client protein interaction could be assessed by western blot or co-immunoprecipitation respectively (Neckers et al., 2018).

9.4.8 Epep2 antiviral efficacy

Having confirmed the absence of off-target toxicity of Epep2 in Vero cells up to 100 µM, antiviral activity was determined against Dengue virus using cell-based ELISA. However, at all experimental conditions tested, no inhibition of viral infection was observed.

These results imply that disruption of the HSP90-Dengue E interaction for the inhibition of viral entry may be an ineffective strategy, and that internalisation may proceed by pathways independent of HSP90 (Piccini et al., 2015). However, lack of efficacy may originate from challenges specific to the Epep2 peptide. For instance, it is possible that Epep2 did not bind HSP90 as a free linear peptide. The binding shown in the peptide array experiments may be representative of a conformation specific to that assay, namely of a conformation imposed by the necessity of the C-terminal PEG linker (Katz et al., 2011; Amartely et al., 2014). Therefore, Epep2 may have adopted a different inactive conformation as a free linear peptide in solution which did not bind HSP90 and disrupt Dengue virus infection.

Alternatively, it was also possible that Epep2 may have bound HSP90 in the cell-based ELISA experiment but failed to disrupt the HSP90-E interaction. Therefore, the affinity of Epep2 for HSP90 may have been too low to compete with the E protein and displace the interaction. This was found in other work, in which researchers developed an analogous cell entry inhibitor peptide against the SARS-CoV-2 virus, and the peptide did not disrupt virus internalisation (Mahindra et al., 2021). The peptide was hypothesised to lack sufficient affinity to disrupt the target interaction (Mahindra et al., 2021). This could be the case for Epep2.

9.4.9 Cell type dependency of HSP90-mediated internalisation

Lack of antiviral efficacy of Epep2 could also originate from a discrepancy between cell types. In the seminal paper characterising HSP90 as a Dengue virus receptor for cell entry, researchers identified recombinant HSP90 protein and HSP90 antibodies to inhibit infection (Reyes-del Valle et al., 2005). This was established in both neurological SH-SY5Y cells and human peripheral monocytes/macrophages, which are major targets of Dengue virus and are relevant models of infection (Reyes-del Valle et al., 2005). Conversely, HSP90 antibodies were found to provide no inhibition of Dengue virus in HepG2 liver cells, another primary target of Dengue virus infection (Cabrera-Hernandez et al., 2007). Furthermore, upregulation of HepG2 cell membrane HSP90 by heat shock did not result in increased Dengue virus infection (Cabrera-Hernandez et al., 2007). Accounting for this, it has been shown that the mechanism employed by Dengue virus for cell entry is highly dependent on cell type, and multiple

pathways can occur concurrently (Piccini et al., 2015). While one pathway can be dominant, others can be redundant or even counterproductive to infection (Piccini et al., 2015). Therefore, HSP90 may facilitate Dengue virus entry in SH-SY5Y and human peripheral monocytes/macrophages, while virus internalisation into HepG2 cells may be HSP90-independent. Likewise, viral entry may proceed by HSP90-independent pathways in Vero cells and would explain the lack of efficacy of Epep2. In this project, the testing conducted for cytotoxicity and antiviral activity should have included SH-SY5Y cells which were used in the seminal paper describing the antiviral activity of recombinant HSP90 and HSP90 antibodies against Dengue Virus (Reyes-del Valle et al., 2005). This would have allowed for direct comparison of present results with those previously reported. However, testing began with the cell lines that were immediately available in our group and representative of the main organs affected in Dengue Virus infection (for more information, see section 6.3.1). These were comprised of the kidney cell line Vero and the liver cell line Huh7. Additionally, use of the Vero cell line would allow for any antiviral effects of the peptides to be seen without interference from the innate immune response, since Vero cells are deficient in IFN signalling (Barrett et al., 2009). Because of this susceptibility to infection, Vero cells are commonly used in antiviral research (Barrett et al., 2009).

Interestingly, HSP90-mediated internalisation of Dengue virus may be linked to clathrin-mediated internalisation, a process by which the clathrin protein regulates uptake of nutrients and signalling molecules by endocytosis (Kaksonen and Roux, 2018). Many viruses, including dengue virus, exploit this mechanism for entry into host cells (Piccini et al., 2015; Carro and Cherry, 2021). Dengue virus internalisation has been shown to be clathrin-dependent in SH-SY5Y and human peripheral monocytes/macrophages but clathrin-independent in HepG2 and Vero cells (Alhoot et al., 2011; Piccini et al., 2015; Ho et al., 2017). Similarly, Dengue virus internalisation has been shown to be HSP90-dependent in SH-SY5Y and human peripheral monocytes/macrophages (Reyes-del Valle et al., 2005; Srisutthisamphan et al., 2018), but HSP90-independent in HepG2 (Cabrera-Hernandez et al., 2007), and possibly in Vero cells as suggested in this project. Together, these coincidental observations suggest a possible link between HSP90 and clathrin in Dengue virus internalisation. Importantly, if cell types show the same dependence of HSP90- and clathrin-mediated internalisation pathways of

Dengue virus, this would suggest that internalisation is independent of HSP90 in Vero cells, just as internalisation is independent of clathrin in Vero cells (Piccini et al., 2015).

In conclusion, the discovery of two HSP90-binding epitopes on the Dengue E protein highlights potential targets for disrupting viral entry. While E Peptide 2 demonstrated stronger binding affinity and was further optimised, its lack of antiviral efficacy in initial assays suggests the need for further refinement. Modifications to enhance binding affinity and stability could achieve antiviral efficacy. Alternatively, lack of efficacy may originate from a cell-type dependency of HSP90-mediated internalisation by Dengue virus, in which case Epep2 should be tested in other cell types for inhibition of infectivity.

Chapter 10 Final discussion

Exploitation of HSP90 function and signalling by many viruses has been well characterised (Y. Wang et al., 2017; Zhang and Yu, 2022; Wei et al., 2024). Similarly, Dengue virus has been shown to interact with HSP90 on the surface of host cells via the E protein to facilitate internalisation, and disruption of this interaction has demonstrated antiviral effects (Reyes-del Valle et al., 2005; Chavez-Salinas et al., 2008; Srisutthisamphan et al., 2018). Accordingly, this thesis had the goal of developing peptide disruptors of this interaction as novel antiviral therapeutics for Dengue virus by use of a peptide array screening approach with the following aims:

Chapter 6

- To develop a method for preparing HSP90 protein by recombinant bacterial expression, IMAC isolation, and purification by ion exchange and size exclusion chromatography.

Chapter 7

- To identify binding epitopes on the Dengue E protein for HSP90 by peptide array screening.

- To assess the pharmacokinetic suitability of E epitopes as peptide therapeutic candidates using computational prediction tools.

- To develop epitopes into candidate peptides by structural optimisation using peptide array screening.

- To evaluate cytotoxicity and antiviral efficacy of candidates by *in vitro* assays.

10.1 Major findings and conclusions

10.1.1 Preparation of purified recombinant HSP90 protein

This project began by the development of a method for recombinant bacterial expression and purification of HSP90 protein. Once an appropriate plasmid was designed and obtained, IPTG induction conditions of BL21(DE3) competent bacteria were optimised. A lower temperature of 18 ºC and an extended duration of 18 hours after induction resulted in greater protein yield, possibly by promoting correct protein folding, reducing the loss and mis-partitioning of plasmid DNA, and decreasing protein aggregation in inclusion bodies (Schein and Noteborn, 1988; Papaneophytou and Kontopidis, 2014). In addition, a lower concentration of 0.1 mM IPTG resulted in a greater yield of HSP90. This suggested a better balance between recombinant protein expression and metabolic burden, which can inhibit bacterial replication and decrease overall yield (Bentley et al., 1991; Glick, 1995). With these conditions, a sufficient quantity of HSP90 was produced and successfully purified by IMAC, ion exchange chromatography, and size exclusion chromatography.

10.1.2 Peptide array discovery of HSP90-E disruptor peptides

Next, peptide array screening was carried out using recombinant HSP90 protein for the discovery of peptide disruptors of the HSP90-E interaction. By screening a discovery array, two HSP90-binding epitopes were found on the E protein. A weaker binding site, E peptide 1, originated from EDII, while the stronger site, E peptide 2, was located in EDIII. E peptide 2 was especially promising since EDIII is the putative binding site of Dengue virus for host cell internalisation (Hung et al., 2004; Sukupolvi-Petty et al., 2007; Frei et al., 2015; Sarker et al., 2023; González-Lodeiro et al., 2024). Further investigation of the epitopes revealed conservation of the sequences across Dengue serotypes and their location at the protein surface, supporting their role as putative HSP90 binding sites important for virus internalisation. Using bioinformatic prediction, both peptides were shown to adopt constrained conformations: E peptide 1 displayed a partial α-helical structure, while E peptide 2 adopted a ß-hairpin conformation. In addition to this, both peptides had an even charge distribution and good solubility in water, making them excellent candidates for therapeutic

development (Henninot et al., 2018; Lee et al., 2019). However, high aggregation propensity was found for E peptide 1, and both peptides contained cysteine residues. These factors may hinder solubility and would need to be addressed in later development (Fosgerau and Hoffmann, 2015).

Several rounds of structural optimisation were performed on the epitopes by peptide array screening. During this process, E peptide 2 was prioritised over E peptide 1, since it exhibited stronger binding and originated from EDIII. Resultingly, the promising peptide candidate Epep2 was developed and spanned residues 2-17 of the E peptide 2 epitope. By alanine scan and point substitution, hotspot residues were identified at E7, D9, C13, K14, I15, and P16. The necessity of C13 was unfortunate, since it renders the peptide redox-sensitive and increases risk for aggregation (Moroder, 2005). However, this risk could be attenuated in future development by reducing aggregation propensity across the rest of the peptide or perhaps by substitution with isosteres like selenocysteine (Moroder, 2005). In addition, alanine scan and point substitution experiments identified P12A and D9E as promising options for increasing affinity for HSP90.

Having developed a promising candidate peptide, a negative control peptide was designed, and cytotoxicity and antiviral efficacy were assessed. Neither peptide indicated cytotoxic effects, except for Epep2 in A549 cells at 100 μM, as shown by preliminary data. This suggested possible disruption of endogenous HSP90 function at high concentrations and highlighted the importance of characterising off-target effects before clinical translation. Lastly, a cell-based ELISA antiviral assay determined that Epep2 had no antiviral efficacy in Vero cells up to 50 μM. This was attributed to several possible factors. First, disruption of the HSP90-E interaction may not prevent Dengue virus entry. Second, it was possible that Epep2 did not bind HSP90. Third, even if Epep2 did bind, it may not have displaced the HSP90-E interaction. This could be caused by insufficient affinity or stability of the peptide. Fourth, pathways of Dengue virus internalisation have been found dependent on cell type (Piccini et al., 2015), and HSP90-independent mechanisms may be dominant in Vero cells, accounting for lack of Epep2 efficacy.

10.1.3 Future work and Limitations

Future work should be directed towards addressing the lack of antiviral efficacy of Epep2 in inhibiting Dengue virus, which may be due to several factors: (a) Dengue virus entry into cells could be independent of HSP90, (b) Epep2 may lack affinity to bind HSP90, (c) Epep2 may lack affinity to displace the HSP90-E interaction, and (d) Dengue virus entry could be independent of HSP90 cell types like Vero (Figure 10-1).

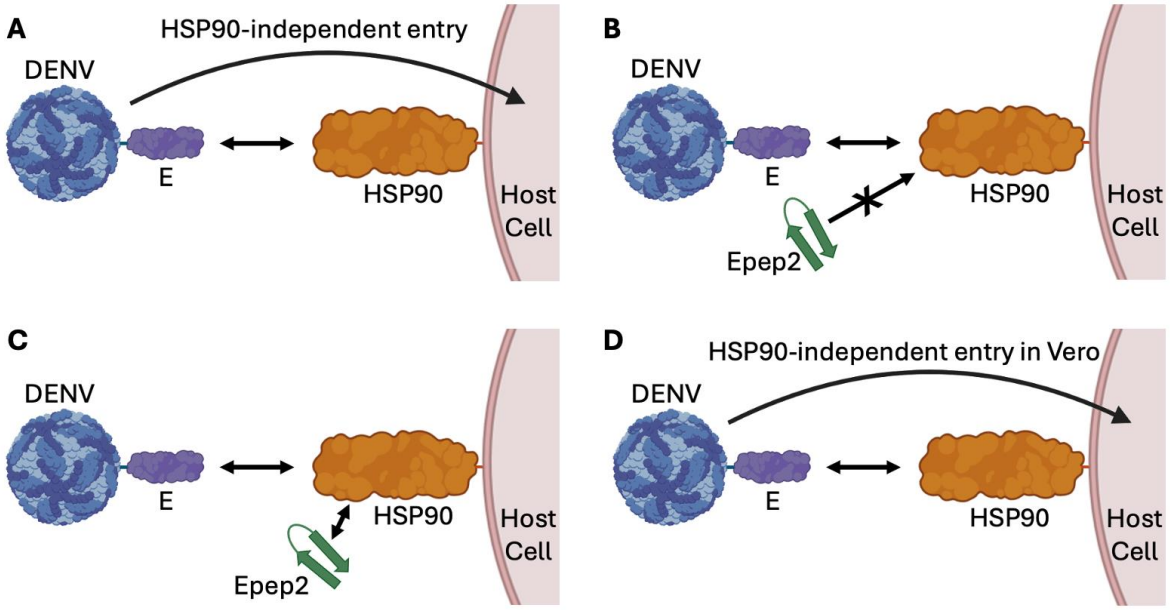

Figure 10-1. Potential causes of the lack of antiviral efficacy of Epep2.
Possible factors contributing to the lack of Epep2 antiviral efficacy include A: dengue virus entry may be independent of HSP90, B: Epep2 may have insufficient affinity to bind HSP90, C: Epep2 may not have sufficient affinity to disrupt the HSP90-virus interaction, and D: dengue virus entry may occur independently of HSP90 in cell types such as Vero.

10.1.3.1 Dengue virus cell entry is independent of HSP90

These challenges could be overcome by the following strategies. First, the dependence of Dengue virus internalisation on HSP90 should be confirmed by testing the antiviral effect of HSP90 antibodies on a panel of cell types (Figure 10-1:A). These should include the cell lines SH-SY5Y and HepG2, in addition to primary human peripheral monocytes/macrophages, which were tested in previous reports (Reyes-del Valle et al., 2005; Cabrera-Hernandez et al., 2007; Srisutthisamphan et al., 2018). This should affirm the validity of the HSP90-E interaction as a drug target.

10.1.3.2 Epep2 may not bind HSP90

Next, Epep2 may have not interacted with HSP90, therefore not inhibiting Dengue virus infection (Figure 10-1:B). This could be due to the free peptide in solution adopting a different inactive conformation compared to the binding conformation adopted during peptide array screening, which may have been influenced by the C-terminal PEG membrane linker. Binding of Epep2 to HSP90 could be verified by target engagement assays like fluorescence polarisation and surface plasmon resonance, which are offered by the Integrated Protein Analysis facility at the University of Glasgow. Ideally, this confirmation of target binding would have been achieved before cytotoxicity and antiviral testing, but initial attempts at preparing E protein stock for target engagement assays by ectopic expression in mammalian cells were unsuccessful (data not shown). With more time however, further troubleshooting may establish a viable protocol. Alternatively, recombinant E protein could be procured from suppliers, and this would avoid these challenges of in-house preparation.

10.1.3.3 Epep2 may not disrupt HSP90-E

Similarly, Epep2 may have successfully bound HSP90, but could lack the affinity required to displace the HSP90-E interaction (Figure 10-1:C). This problem was encountered in another study focussed on developing entry disruptor peptides for SARS-CoV-2, where lack of efficacy of the peptide was attributed to insufficient affinity to disrupt interaction of the virus with the entry receptor protein (Mahindra et al., 2021). This suggests that the approach of entry disruptor peptide development is not viable. Nevertheless, this strategy was successful for Dengue virus in other work, as demonstrated by the P7 disruptor, which blocked the EDIII-integrin ß3 interaction (Cui et al., 2018), or the DET4 disruptor, which targeted the EDIII-heparan sulfate interaction (Alhoot et al., 2013). This precedent demonstrates the validity of this approach and supports further optimisation of Epep2 to achieve antiviral efficacy.

The ability of Epep2 to disrupt the HSP90-E interaction could be validated using co-immunoprecipitation or proximity ligation assay (Söderberg et al., 2008; Zhu et al., 2017). As for target engagement, assays for target disruption would ideally have been performed before cytotoxicity and antiviral testing but were

hindered by problems in E protein ectopic expression in mammalian cell culture. As a first step in further work, target disruption of the peptides could be demonstrated by pull-down assays using recombinant E protein procured from suppliers, avoiding the challenges of in-house preparation. If Epep2 does not disrupt the interaction, increasing affinity by structural modification may enable efficacy. Epep2 already adopts a ß-hairpin structure, and such confined conformations can increase potency by reducing entropic binding penalty (Unal et al., 2009). Stapling of the ß-hairpin could further increase conformational restriction and binding affinity (Selvarajan et al., 2023). This could be achieved by standard Fmoc solid-phase peptide synthesis, but with the inclusion of one alkenyl glycine residue at each terminus and an extra step of olefin metathesis before cleavage from the solid support (Selvarajan et al., 2023). This type of synthesis was accomplished in other work for the development of novel antimicrobial ß-hairpin peptides, which exhibited enhanced potency and stability due to stapling (Selvarajan et al., 2023). Such a protocol could be accomplished in collaboration Professor Andrew Jamieson at the University of Glasgow, whose research group specialises in peptide synthesis and research. As an alternative strategy, peptide affinity could be increased by incorporating substitutions shown by alanine scan and point substitution to increase binding, such as P12A or D9E.

In addition, an inability to disrupt the HSP90-E interaction may stem from a lack of stability against protease-mediated degradation. This could be assessed by plasma stability assay services offered by contract research organisations like Charles River. If vulnerability to proteases is discovered, incorporation of D-amino acids or conjugation to PEG or PSA polymers could hinder enzyme recognition and hydrolysis (Pollaro and Heinis, 2010; Feng and Xu, 2016). Additionally, ß-hairpin stapling would hinder protease recognition as well as improve potency (Di, 2015).

10.1.3.4 HSP90-mediated internalisation of Dengue virus may depend on cell type

Further work should also investigate if Epep2 lacked efficacy in Vero cells due to the dominance of Dengue virus internalisation pathways independent of HSP90 in that cell line (Figure 10-1:D) (Piccini et al., 2015). This could involve testing the

use of Epep2 and HSP90 antibodies in a panel of cell lines, including SH-SY5Y cells and human peripheral monocytes/macrophages, which were shown to be protected against Dengue virus infection by HSP90 antibodies (Reyes-del Valle et al., 2005), and HepG2, which showed no change in infection with HSP90 antibody treatment (Cabrera-Hernandez et al., 2007). This would determine if Epep2 and HSP90-mediated internalisation is dependent on cell type. Furthermore, antiviral effects of clathrin inhibitors should also be investigated, which may reveal a link between clathrin- and HSP90-mediated internalisation.

10.1.3.5 Further development

If the above challenges of target viability, HSP90 binding, HSP90-E disruption, and cell line dependency are resolved, the next steps should focus on maximising both the affinity and stability of Epep2 to enhance the likelihood of success in future clinical trials. Furthermore, several other peptide disruptors have exhibited antiviral activity against other Flaviviruses, like Zika virus, Yellow Fever virus, and West Nile virus (see Section 6.7.2). After achieving efficacy in Dengue virus, testing Epep2 in other Flaviviruses would greatly increase its clinical potential (Wang and Shi, 2015). In parallel, it will be crucial to assess potential disruption of endogenous HSP90 functions so that off-target toxicity can be avoided, which is the greatest cause of compound attrition in clinical trials (Leeson and Empfield, 2010). This could involve western blotting or co-immunoprecipitation analysis of client proteins (Neckers et al., 2018). Additionally, Epep2 could be tested in combination with other inhibitors with complimentary mechanisms, which may result in synergistic effects. For example, Epep2 could be investigated with the $DV^{419-447}$ inhibitor, which was shown to disrupt E-mediated membrane fusion during viral entry and exhibited potent pan-serotype inhibition (Schmidt et al., 2010). Lastly, if Epep2 demonstrates success in *in vitro* experiments, recapitulating this efficacy using animal models like AG129 mice would be essential for attracting investment to fund clinical trials (Zellweger and Shresta, 2014).

10.1.4 Conclusion

Although Epep2 did not demonstrate antiviral efficacy against the Dengue virus, several promising strategies have been presented for achieving efficacy and raises hope for successful development of antiviral inhibitors in the future. If these approaches do not succeed, other strategies could be pursued using the discovery pipeline used in this project. For instance, peptide array technology is especially powerful for rational optimisation of peptides. Various promising entry inhibitors targeting the Dengue E protein already exist, some with exceptional affinity and pan-flavivirus activity, but have not progressed beyond the cell culture development stage (see Section 6.7.2). Collaborating with other researchers to optimise these inhibitors further using peptide array screening could lead to antivirals with unprecedented activity that could progress to clinical development.

Furthermore, the peptide array strategy used in this project has been successful in numerous projects in the Baillie Research group (Yalla et al., 2018; Blair et al., 2019; Tibbo et al., 2022). Therefore, targeting other Dengue virus interactions using this pipeline could result in more successful inhibitors than Epep2. For example, Dengue virus has been shown to exploit HSP90 through other viral proteins, such as NS1 and NS5, for various roles in its life cycle (Srisutthisamphan et al., 2018; Li et al., 2021). Additionally, the inhibition of other entry receptors, including HSP70, claudin-1, and GRP78, remains largely unexplored (Wang and Shi, 2015; Taguwa et al., 2015).

In conclusion, Dengue virus poses a devastating and increasingly severe threat to global health and lacks effective measures for control. The development of antivirals, whether disrupting HSP90-E or other targets, is crucial for enhancing our ability to combat this disease.

References

Abdel-Wahab, B.A., Alqhtani, H., Walbi, I.A., Albarqi, H.A., Aljadaan, A.M., Khateeb, M.M. and Hassanein, E.H.M. 2021. Piclamilast mitigates 1,2-dimethylhydrazine induced colon cancer in rats through modulation of Ras/PI3K/Akt/mTOR and NF-κß signaling. *Chemico-Biological Interactions*. 350, p.109686.

Ahmad, A., Waseem, T., Butt, N.F., Randhawa, F.A., Malik, U. and Shakoori, T.A. 2018. Montelukast Reduces the Risk of Dengue Shock Syndrome in Dengue Patients. *Tropical Biomedicine*. 35(4), pp.1115–1122.

Ahmed, M.B., Alghamdi, A.A.A., Islam, S.U., Lee, J.-S. and Lee, Y.-S. 2022. cAMP Signaling in Cancer: A PKA-CREB and EPAC-Centric Approach. *Cells*. 11(13).

Aiderus, A., Barker, N. and Tergaonkar, V. 2024. Serrated colorectal cancer: preclinical models and molecular pathways. *Trends in Cancer*. 10(1), pp.76–91.

Akira, S. and Takeda, K. 2004. Toll-like receptor signalling. *Nature Reviews Immunology*. 4(7), pp.499–511.

Akshantha, H.S., Pujar, G.V., Sethu, A.K., Bhagyalalitha, M. and Singh, M. 2021. Dengue structural proteins as antiviral drug targets: Current status in the drug discovery & development. *European Journal of Medicinal Chemistry*. 221, p.113527.

Akter, R., Tasneem, F., Das, S., Soma, M.A., Georgakopoulos-Soares, I., Juthi, R.T. and Sazed, S.A. 2024. Approaches of dengue control: vaccine strategies and future aspects. *Frontiers in Immunology*. 15, p.1362780.

Alagarasu, K., Patil, P.S., Shil, P., Seervi, M., Kakade, M.B., Tillu, H. and Salunke, A. 2017. *In-vitro* effect of human cathelicidin antimicrobial peptide LL-37 on dengue virus type 2. *Peptides*. 92, pp.23–30.

Alhoot, M.A., Rathinam, A.K., Wang, S.M., Manikam, R. and Sekaran, S.D. 2013. Inhibition of Dengue Virus Entry into Target Cells Using Synthetic Antiviral Peptides. *International Journal of Medical Sciences*. 10(6), pp.719–729.

Alhoot, M.A., Wang, S.M. and Sekaran, S.D. 2011. Inhibition of Dengue Virus Entry and Multiplication into Monocytes Using RNA Interference. *PLOS Neglected Tropical Diseases*. 5(11), p.e1410.

Ali, A.M., Atmaj, J., Van Oosterwijk, N., Groves, M.R. and Dömling, A. 2019. Stapled Peptides Inhibitors: A New Window for Target Drug Discovery. *Computational and Structural Biotechnology Journal*. 17, pp.263–281.

Al-Joufi, F.A., Setia, A., Salem-Bekhit, M.M., Sahu, R.K., Alqahtani, F.Y., Widyowati, R. and Aleanizy, F.S. 2022. Molecular Pathogenesis of Colorectal Cancer with an Emphasis on Recent Advances in Biomarkers, as Well as Nanotechnology-Based Diagnostic and Therapeutic Approaches. *Nanomaterials*. 12(1), p.169.

Allen, M.D. and Zhang, J. 2006. Subcellular dynamics of protein kinase A activity visualized by FRET-based reporters. *Biochemical and Biophysical Research Communications*. 348(2), pp.716–721.

Alves, L. 2024. Brazil to start widespread dengue vaccinations. *The Lancet*. 403(10422), p.133.

Amarachintha, S., Harmel-Laws, E. and Steinbrecher, K.A. 2018. Guanylate cyclase C reduces invasion of intestinal epithelial cells by bacterial pathogens. *Scientific Reports*. 8(1), p.1521.

Amartely, H., Iosub-Amir, A. and Friedler, A. 2014. Identifying Protein-protein Interaction Sites Using Peptide Arrays. *JoVE (Journal of Visualized Experiments)*. (93), p.e52097.

Amodio, V., Yaeger, R., Arcella, P., Cancelliere, C., Lamba, S., Lorenzato, A., Arena, S., Montone, M., Mussolin, B., Bian, Y., Whaley, A., Pinnelli, M., Murciano-Goroff, Y.R., Vakiani, E., Valeri, N., Liao, W.-L., Bhalkikar, A., Thyparambil, S., Zhao, H.-Y., de Stanchina, E., Marsoni, S., Siena, S., Bertotti, A., Trusolino, L., Li, B.T., Rosen, N., Di Nicolantonio, F., Bardelli, A. and Misale, S. 2020. EGFR Blockade Reverts Resistance to KRASG12C Inhibition in Colorectal Cancer. *Cancer Discovery*. 10(8), pp.1129–1139.

Amunjela, J.N. and Tucker, S.J. 2016. POPDC proteins as potential novel therapeutic targets in cancer. *Drug Discovery Today*. 21(12), pp.1920–1927.

Anasir, M.I., Ramanathan, B. and Poh, C.L. 2020. Structure-Based Design of Antivirals against Envelope Glycoprotein of Dengue Virus. *Viruses*. 12(4), p.367.

Andrei, G. 2021. Vaccines and Antivirals: Grand Challenges and Great Opportunities. *Frontiers in Virology*. 1.

Araghi, M., Soerjomataram, I., Jenkins, M., Brierley, J., Morris, E., Bray, F. and Arnold, M. 2019. Global trends in colorectal cancer mortality: projections to the year 2035. *International Journal of Cancer*. 144(12), pp.2992–3000.

Ardekani, G.S., Jafarnejad, S.M., Tan, L., Saeedi, A. and Li, G. 2012. The Prognostic Value of BRAF Mutation in Colorectal Cancer and Melanoma: A Systematic Review and Meta-Analysis. *PLOS ONE*. 7(10), p.e47054.

Armaghany, T., Wilson, J.D., Chu, Q. and Mills, G. 2012. Genetic Alterations in Colorectal Cancer. *Gastrointestinal Cancer Research : GCR*. 5(1), pp.19–27.

Baillie, G.S. 2009. Compartmentalized signalling: spatial regulation of cAMP by the action of compartmentalized phosphodiesterases. *The FEBS Journal*. 276(7), pp.1790–1799.

Baillie, G.S., Tejeda, G.S. and Kelly, M.P. 2019. Therapeutic targeting of 3’,5’-cyclic nucleotide phosphodiesterases: inhibition and beyond. *Nature Reviews. Drug Discovery*. 18(10), pp.770–796.

Bandrés, E., Malumbres, R., Cubedo, E., Honorato, B., Zarate, R., Labarga, A., Gabisu, U., Sola, J.J. and García-Foncillas, J. 2007. A gene signature of 8 genes could identify the risk of recurrence and progression in Dukes' B colon cancer patients. *Oncology Reports*. 17(5), pp.1089–1094.

Baretti, M. and Le, D.T. 2018. DNA mismatch repair in cancer. *Pharmacology & Therapeutics*. 189, pp.45–62.

Barker, N. 2014. Adult intestinal stem cells: critical drivers of epithelial homeostasis and regeneration. *Nature Reviews Molecular Cell Biology*. 15(1), pp.19–33.

Barltrop, J.A., Owen, T.C., Cory, A.H. and Cory, J.G. 1991. 5-(3-carboxymethoxyphenyl)-2-(4,5-dimethylthiazolyl)-3-(4-sulfophenyl)tetrazolium, inner salt (MTS) and related analogs of 3-(4,5-dimethylthiazolyl)-2,5-diphenyltetrazolium bromide (MTT) reducing to purple water-soluble formazans As cell-viability indicators. *Bioorganic & Medicinal Chemistry Letters*. 1(11), pp.611–614.

Barrett, P.N., Mundt, W., Kistner, O. and Howard, M.K. 2009. Vero cell platform in vaccine production: moving towards cell culture-based viral vaccines. *Expert Review of Vaccines*. 8(5), pp.607–618.

Barrow, E., Hill, J. and Evans, D.G. 2013. Cancer risk in Lynch Syndrome. *Familial Cancer*. 12(2), pp.229–240.

Basu, N., Saha, S., Khan, I., Ramachandra, S.G. and Visweswariah, S.S. 2014. Intestinal Cell Proliferation and Senescence Are Regulated by Receptor Guanylyl Cyclase C and p21 *. *Journal of Biological Chemistry*. 289(1), pp.581–593.

Baum, A. and García-Sastre, A. 2010. Induction of type I interferon by RNA viruses: cellular receptors and their substrates. *Amino Acids*. 38(5), pp.1283–1299.

Baylin, S.B. and Jones, P.A. 2011. A decade of exploring the cancer epigenome — biological and translational implications. *Nature Reviews Cancer*. 11(10), pp.726–734.

Beckett, C.G., Tjaden, J., Burgess, T., Danko, J.R., Tamminga, C., Simmons, M., Wu, S.-J., Sun, P., Kochel, T., Raviprakash, K., Hayes, C.G. and Porter, K.R. 2011. Evaluation of a prototype dengue-1 DNA vaccine in a Phase 1 clinical trial. *Vaccine*. 29(5), pp.960–968.

Bekaii-Saab, T.S., Lach, K., Hsu, L.-I., Siadak, M., Stecher, M., Ward, J., Beckerman, R. and Strickler, J.H. 2023. Impact of Anti-EGFR Therapies on HER2-Positive Metastatic Colorectal Cancer: A Systematic Literature Review and Meta-Analysis of Clinical Outcomes. *The Oncologist*. 28(10), pp.885–893.

Bentley, W.E., Davis, R.H. and Kompala, D.S. 1991. Dynamics of induced CAT expression in E. coli. *Biotechnology and Bioengineering*. 38(7), pp.749–760.

Bere, A.W., Mulati, O., Kimotho, J. and Ng'ong'a, F. 2021. Carica papaya Leaf Extract Silver Synthesized Nanoparticles Inhibit Dengue Type 2 Viral Replication In Vitro. *Pharmaceuticals*. 14(8), p.718.

Berman, H.M., Westbrook, J., Feng, Z., Gilliland, G., Bhat, T.N., Weissig, H., Shindyalov, I.N. and Bourne, P.E. 2000. The Protein Data Bank. *Nucleic Acids Research*. 28(1), pp.235–242.

Bertotti, A., Migliardi, G., Galimi, F., Sassi, F., Torti, D., Isella, C., Corà, D., Di Nicolantonio, F., Buscarino, M., Petti, C., Ribero, D., Russolillo, N., Muratore, A., Massucco, P., Pisacane, A., Molinaro, L., Valtorta, E., Sartore-Bianchi, A., Risio, M., Capussotti, L., Gambacorta, M., Siena, S., Medico, E., Sapino, A., Marsoni, S., Comoglio, P.M., Bardelli, A. and Trusolino, L. 2011. A Molecularly Annotated Platform of Patient-Derived Xenografts ("Xenopatients") Identifies HER2 as an Effective Therapeutic Target in Cetuximab-Resistant Colorectal Cancer. *Cancer Discovery*. 1(6), pp.508–523.

Bevanda, M., Kelam, N., Racetin, A., Filipović, N., Bevanda Glibo, D., Bevanda, I. and Vukojević, K. 2024. Expression Pattern of PDE4B, PDE4D, and SFRP5 Markers in Colorectal Cancer. *Medicina*. 60(8), p.1202.

Bhardwaj, S., Holbrook, M., Shope, R.E., Barrett, A.D.T. and Watowich, S.J. 2001. Biophysical Characterization and Vector-Specific Antagonist Activity of Domain III of the Tick-Borne Flavivirus Envelope Protein. *Journal of Virology*. 75(8), pp.4002–4007.

Bhatt, S., Gething, P.W., Brady, O.J., Messina, J.P., Farlow, A.W., Moyes, C.L., Drake, J.M., Brownstein, J.S., Hoen, A.G., Sankoh, O., Myers, M.F., George, D.B., Jaenisch, T., Wint, G.R.W., Simmons, C.P., Scott, T.W., Farrar, J.J. and Hay, S.I. 2013. The global distribution and burden of dengue. *Nature*. 496(7446), pp.504–507.

Biller, L.H. and Schrag, D. 2021. Diagnosis and Treatment of Metastatic Colorectal Cancer: A Review. *JAMA*. 325(7), pp.669–685.

Blair, C.M. and Baillie, G.S. 2019. Reshaping cAMP nanodomains through targeted disruption of compartmentalised phosphodiesterase signalosomes. *Biochemical Society Transactions*. 47(5), pp.1405–1414.

Blair, C.M., Walsh, N.M., Littman, B.H., Marcoux, F.W. and Baillie, G.S. 2019. Targeting B-Raf inhibitor resistant melanoma with novel cell penetrating peptide disrupters of PDE8A – C-Raf. *BMC Cancer*. 19(1), p.266.

Block, H., Maertens, B., Spriestersbach, A., Brinker, N., Kubicek, J., Fabis, R., Labahn, J. and Schäfer, F. 2009. Chapter 27 Immobilized-Metal Affinity Chromatography (IMAC): A Review *In*: R. R. Burgess and M. P. Deutscher, eds. *Methods in Enzymology* [Online]. Guide to Protein Purification, 2nd Edition. Academic Press, pp.439–473.

Boland, C.R. and Goel, A. 2010. Microsatellite Instability in Colorectal Cancer. *Gastroenterology*. 138(6), pp.2073-2087.e3.

Boland, C.R., Sinicrope, F.A., Brenner, D.E. and Carethers, J.M. 2000. Colorectal cancer prevention and treatment. *Gastroenterology*. 118(2), pp.S115–S128.

Bork, P., Holm, L. and Sander, C. 1994. The Immunoglobulin Fold: Structural Classification, Sequence Patterns and Common Core. *Journal of Molecular Biology*. 242(4), pp.309–320.

Bos, S., Gadea, G. and Despres, P. 2018. Dengue: a growing threat requiring vaccine development for disease prevention. *Pathogens and Global Health*. 112(6), pp.294–305.

Bottens, R.A. and Yamada, T. 2022. Cell-Penetrating Peptides (CPPs) as Therapeutic and Diagnostic Agents for Cancer. *Cancers*. 14(22), p.5546.

Bowel Cancer UK 2024. What is bowel cancer? Available at: https://www.bowelcanceruk.org.uk/about-bowel-cancer/bowel-cancer/. Accessed: September 2024.

Bradford, M.M. 1976. A rapid and sensitive method for the quantitation of microgram quantities of protein utilizing the principle of protein-dye binding. *Analytical Biochemistry*. 72(1), pp.248–254.

Brady, O.J., Gething, P.W., Bhatt, S., Messina, J.P., Brownstein, J.S., Hoen, A.G., Moyes, C.L., Farlow, A.W., Scott, T.W. and Hay, S.I. 2012. Refining the Global Spatial Limits of Dengue Virus Transmission by Evidence-Based Consensus. *PLOS Neglected Tropical Diseases*. 6(8), p.e1760.

Bressanelli, S., Stiasny, K., Allison, S.L., Stura, E.A., Duquerroy, S., Lescar, J., Heinz, F.X. and Rey, F.A. 2004. Structure of a flavivirus envelope glycoprotein in its low-pH-induced membrane fusion conformation. *The EMBO journal*. 23(4), pp.728–738.

Brocardo, M.G., Borowiec, J.A. and Henderson, B.R. 2011. Adenomatous polyposis coli protein regulates the cellular response to DNA replication stress. *The International Journal of Biochemistry & Cell Biology*. 43(9), pp.1354–1364.

Brown, K.M., Day, J.P., Huston, E., Zimmermann, B., Hampel, K., Christian, F., Romano, D., Terhzaz, S., Lee, L.C.Y., Willis, M.J., Morton, D.B., Beavo, J.A., Shimizu-Albergine, M., Davies, S.A., Kolch, W., Houslay, M.D. and Baillie, G.S. 2013. Phosphodiesterase-8A binds to and regulates Raf-1 kinase. *Proceedings of the National Academy of Sciences*. 110(16), pp.E1533–E1542.

Brunyanszki, A., Olah, G., Coletta, C., Szczesny, B. and Szabo, C. 2014. Regulation of mitochondrial poly(ADP-Ribose) polymerase activation by the ß-adrenoceptor/cAMP/protein kinase A axis during oxidative stress. *Molecular Pharmacology*. 86(4), pp.450–462.

Burch, A.D. and Weller, S.K. 2005. Herpes Simplex Virus Type 1 DNA Polymerase Requires the Mammalian Chaperone Hsp90 for Proper Localization to the Nucleus. *Journal of Virology*. 79(16), pp.10740–10749.

Burton, D.R. 2023. Antiviral neutralizing antibodies: from in vitro to in vivo activity. *Nature Reviews Immunology*. 23(11), pp.720–734.

Byth, H.-A., Mchunu, B.I., Dubery, I.A. and Bornman, L. 2001. Assessment of a simple, non-toxic alamar blue cell survival assay to monitor tomato cell viability. *Phytochemical Analysis*. 12(5), pp.340–346.

Cabrera-Hernandez, A., Thepparit, C., Suksanpaisan, L. and Smith, D.R. 2007. Dengue virus entry into liver (HepG2) cells is independent of hsp90 and hsp70. *Journal of Medical Virology*. 79(4), pp.386–392.

Callahan, M., Treston, A.M., Lin, G., Smith, M., Kaufman, B., Khaliq, M., DeWald, L.E., Spurgers, K., Warfield, K.L., Lowe, P., Duchars, M., Sampath, A. and Ramstedt, U. 2022. Randomized single oral dose phase 1 study of safety, tolerability, and pharmacokinetics of Iminosugar UV-4 Hydrochloride (UV-4B) in healthy subjects. *PLOS Neglected Tropical Diseases*. 16(8), p.e0010636.

Cao, B., Wang, K., Liao, J.-M., Zhou, X., Liao, P., Zeng, S.X., He, M., Chen, L., He, Y., Li, W. and Lu, H. 2016. Inactivation of oncogenic cAMP-specific phosphodiesterase 4D by miR-139-5p in response to p53 activation K. Struhl, ed. *eLife*. 5, p.e15978.

Carmeliet, P. 2005. VEGF as a key mediator of angiogenesis in cancer. *Oncology*. 69 Suppl 3, pp.4–10.

Carro, S.D. and Cherry, S. 2021. Beyond the Surface: Endocytosis of Mosquito-Borne Flaviviruses. *Viruses*. 13(1), p.13.

Carson, M., Johnson, D.H., McDonald, H., Brouillette, C. and DeLucas, L.J. 2007. His-tag impact on structure. *Acta Crystallographica Section D: Biological Crystallography*. 63(3), pp.295–301.

Casak, S.J., Horiba, M.N., Yuan, M., Cheng, J., Lemery, S.J., Shen, Y.L., Fu, W., Moore, J.N., Li, Y., Bi, Y., Auth, D., Fesenko, N., Kluetz, P.G., Pazdur, R. and Fashoyin-Aje, L.A. 2023. FDA Approval Summary: Tucatinib with Trastuzumab for Advanced Unresectable or Metastatic, Chemotherapy Refractory, HER2-Positive RAS Wild-Type Colorectal Cancer. *Clinical Cancer Research*. 29(21), pp.4326–4330.

Castro, M.C., Wilson, M.E. and Bloom, D.E. 2017. Disease and economic burdens of dengue. *The Lancet Infectious Diseases*. 17(3), pp.e70–e78.

Ceyhan, O., Birsoy, K. and Hoffman, C.S. 2012. Identification of Biologically Active PDE11-Selective Inhibitors Using a Yeast-Based High-Throughput Screen. *Chemistry & Biology*. 19(1), pp.155–163.

Chakedis, J. and Schmidt, C.R. 2018. Surgical Treatment of Metastatic Colorectal Cancer. *Surgical Oncology Clinics of North America*. 27(2), pp.377–399.

Chakraborty, A., Dey, S., Ghatak, I., Ray, P., Bhattacharya, S. and Sengupta, A. 2024. KRAS Mutation Status in Colorectal Epithelial Tumors of Colorectal Cancer. *Asian Pacific Journal of Cancer Biology*. 9(1), pp.37–40.

Chakraborty, A. and Edkins, A.L. 2021. HSP90 as a regulator of extracellular matrix dynamics. *Biochemical Society Transactions*. 49(6), pp.2611–2625.

Chakraborty, S., Alam, S., Sayem, M., Sanyal, M., Das, T., Saha, P., Sayem, M., Byapari, B.K., Tabassum, C.T., Kabir, A., Amin, M.R. and Nabi, A.H.M.N. 2020. Investigation of the efficacy and safety of eltrombopag to correct thrombocytopenia in moderate to severe dengue patients - a phase II randomized controlled clinical trial. *eClinicalMedicine*. 29.

Chan, A.T. and Giovannucci, E.L. 2010. Primary Prevention of Colorectal Cancer. *Gastroenterology*. 138(6), pp.2029-2043.e10.

Chandrashekar, D.S., Bashel, B., Balasubramanya, S.A.H., Creighton, C.J., Ponce-Rodriguez, I., Chakravarthi, B.V.S.K. and Varambally, S. 2017. UALCAN: A Portal for Facilitating Tumor Subgroup Gene Expression and Survival Analyses. *Neoplasia (New York, N.Y.)*. 19(8), pp.649–658.

Chandrashekar, D.S., Karthikeyan, S.K., Korla, P.K., Patel, H., Shovon, A.R., Athar, M., Netto, G.J., Qin, Z.S., Kumar, S., Manne, U., Creighton, C.J. and Varambally, S. 2022. UALCAN: An update to the integrated cancer data analysis platform. *Neoplasia (New York, N.Y.)*. 25, pp.18–27.

Chang, Y.S., Graves, B., Guerlavais, V., Tovar, C., Packman, K., To, K.-H., Olson, K.A., Kesavan, K., Gangurde, P., Mukherjee, A., Baker, T., Darlak, K., Elkin, C., Filipovic, Z., Qureshi, F.Z., Cai, H., Berry, P., Feyfant, E., Shi, X.E., Horstick, J., Annis, D.A., Manning, A.M., Fotouhi, N., Nash, H., Vassilev, L.T. and Sawyer, T.K. 2013. Stapled α−helical peptide drug development: A potent dual inhibitor of MDM2 and MDMX for p53-dependent cancer therapy. *Proceedings of the National Academy of Sciences*. 110(36), pp.E3445–E3454.

Charlton, A. and Zachariou, M. 2008. Immobilized Metal Ion Affinity Chromatography of Histidine-Tagged Fusion Proteins *In*: M. Zachariou, ed. *Affinity Chromatography: Methods and Protocols* [Online]. Totowa, NJ: Humana Press, pp.137–150.

Chathurangana, P.W.P., Samaranayake, D.B.D.L., Quienters, V.G. and Wickramasinghe, V.P. 2017. Effects of vitamin E supplementation on the clinical outcome of dengue fever and dengue haemorrhagic fever in children. *Asian Pacific Journal of Tropical Disease*. 7(11), pp.645–649.

Chatterjee, J., Gilon, C., Hoffman, A. and Kessler, H. 2008. N-methylation of peptides: a new perspective in medicinal chemistry. *Accounts of Chemical Research*. 41(10), pp.1331–1342.

Chavez-Salinas, S., Ceballos-Olvera, I., Reyes-del Valle, J., Medina, F. and del Angel, R.M. 2008. Heat shock effect upon dengue virus replication into U937 cells. *Virus Research*. 138(1), pp.111–118.

Chen, G., Ning, B. and Shi, T. 2019. Single-Cell RNA-Seq Technologies and Related Computational Data Analysis. *Frontiers in Genetics*. 10.

Chen, L., Gao, H., Liang, J., Qiao, J., Duan, J., Shi, H., Zhen, T., Li, H., Zhang, F., Zhu, Z. and Han, A. 2018. miR-203a-3p promotes colorectal cancer

proliferation and migration by targeting PDE4D. *American Journal of Cancer Research*. 8(12), pp.2387–2401.

Chen, Y., Maguire, T. and Marks, R.M. 1996. Demonstration of binding of dengue virus envelope protein to target cells. *Journal of Virology*. 70(12), pp.8765–8772.

Cheng, Y., Wu, J., Qin, B., Zou, B., Wang, Y. and Li, Y. 2020. CREB1-induced lncRNA LEF1-AS1 contributes to colorectal cancer progression via the miR-489/DIAPH1 axis. *Biochemical and Biophysical Research Communications*. 526(3), pp.678–684.

Chew, M.-F., Poh, K.-S. and Poh, C.-L. 2017. Peptides as Therapeutic Agents for Dengue Virus. *International Journal of Medical Sciences*. 14(13), pp.1342–1359.

Cho-Chung, Y.S. 1990. Role of Cyclic AMP Receptor Proteins in Growth, Differentiation, and Suppression of Malignancy: New Approaches to Therapy. *Cancer Research*. 50(22), pp.7093–7100.

Choi, J.E., Bae, J.S., Kang, M.J., Chung, M.J., Jang, K.Y., Park, H.S. and Moon, W.S. 2017. Expression of epithelial-mesenchymal transition and cancer stem cell markers in colorectal adenocarcinoma: Clinicopathological significance. *Oncology Reports*. 38(3), pp.1695–1705.

Chung, D.C. and Rustgi, A.K. 2003. The Hereditary Nonpolyposis Colorectal Cancer Syndrome: Genetics and Clinical Implications. *Annals of Internal Medicine*. 138(7), pp.560–570.

Clark, G.R., Anderson, A.S., Godfrey, T.G., Strachan, J.A., Fraser, C.G. and Steele, R.J. 2020. Variation in changes in the incidence of colorectal cancer by age and association with screening uptake: an observational study. *BMJ open*. 10(9), p.e037925.

Coffey, J.C. and O'Leary, D.P. 2016. The mesentery: structure, function, and role in disease. *The Lancet Gastroenterology & Hepatology*. 1(3), pp.238–247.

Colony, P.C. 1989. The Identification of Cell Types in the Normal Adult Colon *In*: *Cell and Molecular Biology of Colon Cancer*. CRC Press.

Conchillo-Solé, O., de Groot, N.S., Avilés, F.X., Vendrell, J., Daura, X. and Ventura, S. 2007. AGGRESCAN: a server for the prediction and evaluation of 'hot spots' of aggregation in polypeptides. *BMC Bioinformatics*. 8, p.65.

Connor, J.H., McKenzie, M.O., Parks, G.D. and Lyles, D.S. 2007. Antiviral activity and RNA polymerase degradation following Hsp90 inhibition in a range of negative strand viruses. *Virology*. 362(1), pp.109–119.

Conti, M. and Beavo, J. 2007. Biochemistry and Physiology of Cyclic Nucleotide Phosphodiesterases: Essential Components in Cyclic Nucleotide Signaling. *Annual Review of Biochemistry*. 76(Volume 76, 2007), pp.481–511.

Cooke, S.F., Wright, T.A., Sin, Y.Y., Ling, J., Kyurkchieva, E., Phanthaphol, N., Mcskimming, T., Herbert, K., Rebus, S., Biankin, A.V., Chang, D.K., Baillie, G.S. and Blair, C.M. 2024. Disruption of the pro-oncogenic c-RAF–PDE8A complex represents a differentiated approach to treating KRAS–c-RAF dependent PDAC. *Scientific Reports*. 14(1), p.8998.

Cooper, G.M. and Brown, C.D. 2008. Qualifying the relationship between sequence conservation and molecular function. *Genome Research*. 18(2), pp.201–205.

Cory, A.H., Owen, T.C., Barltrop, J.A. and Cory, J.G. 1991. Use of an aqueous soluble tetrazolium/formazan assay for cell growth assays in culture. *Cancer communications*. 3(7), pp.207–212.

Costin, J.M., Jenwitheesuk, E., Lok, S.-M., Hunsperger, E., Conrads, K.A., Fontaine, K.A., Rees, C.R., Rossmann, M.G., Isern, S., Samudrala, R. and Michael, S.F. 2010. Structural Optimization and De Novo Design of Dengue Virus Entry Inhibitory Peptides. *PLOS Neglected Tropical Diseases*. 4(6), p.e721.

Cote, R.H. 2021. Photoreceptor phosphodiesterase (PDE6): activation and inactivation mechanisms during visual transduction in rods and cones. *Pflügers Archiv - European Journal of Physiology*. 473(9), pp.1377–1391.

Craik, D.J., Fairlie, D.P., Liras, S. and Price, D. 2013. The Future of Peptide-based Drugs. *Chemical Biology & Drug Design*. 81(1), pp.136–147.

Cristóbal, I., Rincón, R., Manso, R., Madoz-Gúrpide, J., Caramés, C., del Puerto-Nevado, L., Rojo, F. and García-Foncillas, J. 2014. Hyperphosphorylation of PP2A in colorectal cancer and the potential therapeutic value showed by its forskolin-induced dephosphorylation and activation. *Biochimica Et Biophysica Acta*. 1842(9), pp.1823–1829.

Crocetti, L., Floresta, G., Cilibrizzi, A. and Giovannoni, M.P. 2022. An Overview of PDE4 Inhibitors in Clinical Trials: 2010 to Early 2022. *Molecules*. 27(15), p.4964.

Cui, X., Wu, Y., Fan, D., Gao, N., Ming, Y., Wang, P. and An, J. 2018. Peptides P4 and P7 derived from E protein inhibit entry of dengue virus serotype 2 via interacting with ß3 integrin. *Antiviral Research*. 155, pp.20–27.

Cullinane, C., Brett, A., Devane, L., McCullough, P.W., Cooke, F. and Neary, P. 2023. The protective role of phosphodiesterase inhibitors in preventing colorectal cancer and advanced colorectal polyps: a systematic review and meta-analysis. *Colorectal Disease*. 25(10), pp.1949–1959.

Dando, T.M. and Perry, C.M. 2003. Enfuvirtide. *Drugs*. 63(24), pp.2755–2766.

D'Andrea, M.R., Qiu, Y., Haynes-Johnson, D., Bhattacharjee, S., Kraft, P. and Lundeen, S. 2005. Expression of PDE11A in Normal and Malignant Human Tissues. *Journal of Histochemistry & Cytochemistry*. 53(7), pp.895–903.

Danese, S., Neurath, M.F., Kopoń, A., Zakko, S.F., Simmons, T.C., Fogel, R., Siegel, C.A., Panaccione, R., Zhan, X., Usiskin, K. and Chitkara, D. 2020.

Effects of Apremilast, an Oral Inhibitor of Phosphodiesterase 4, in a Randomized Trial of Patients With Active Ulcerative Colitis. *Clinical Gastroenterology and Hepatology*. 18(11), pp.2526-2534.e9.

Danielsen, S.A., Eide, P.W., Nesbakken, A., Guren, T., Leithe, E. and Lothe, R.A. 2015. Portrait of the PI3K/AKT pathway in colorectal cancer. *Biochimica et Biophysica Acta (BBA) - Reviews on Cancer*. 1855(1), pp.104–121.

Davies, H., Bignell, G.R., Cox, C., Stephens, P., Edkins, S., Clegg, S., Teague, J., Woffendin, H., Garnett, M.J., Bottomley, W., Davis, N., Dicks, E., Ewing, R., Floyd, Y., Gray, K., Hall, S., Hawes, R., Hughes, J., Kosmidou, V., Menzies, A., Mould, C., Parker, A., Stevens, C., Watt, S., Hooper, S., Wilson, R., Jayatilake, H., Gusterson, B.A., Cooper, C., Shipley, J., Hargrave, D., Pritchard-Jones, K., Maitland, N., Chenevix-Trench, G., Riggins, G.J., Bigner, D.D., Palmieri, G., Cossu, A., Flanagan, A., Nicholson, A., Ho, J.W.C., Leung, S.Y., Yuen, S.T., Weber, B.L., Seigler, H.F., Darrow, T.L., Paterson, H., Marais, R., Marshall, C.J., Wooster, R., Stratton, M.R. and Futreal, P.A. 2002. Mutations of the BRAF gene in human cancer. *Nature*. 417(6892), pp.949–954.

Deaton, A.M. and Bird, A. 2011. CpG islands and the regulation of transcription. *Genes & Development*. 25(10), p.1010.

DeLano, W.L. 2002. Pymol: An open-source molecular graphics tool. *CCP4 Newsl. Protein Crystallogr*. 40(1), pp.82–92.

Desman, G., Waintraub, C. and Zippin, J.H. 2014. Investigation of cAMP microdomains as a path to novel cancer diagnostics. *Biochimica et Biophysica Acta (BBA) - Molecular Basis of Disease*. 1842(12, Part B), pp.2636–2645.

Dhillon, S. 2023. Adagrasib: First Approval. *Drugs*. 83(3), pp.275–285.

Di Guglielmo, M.D., Perdue, L., Adeyemi, A., van Golen, K.L. and Corao, D.U. 2018. Immunohistochemical Staining for Uroguanylin, a Satiety Hormone, is Decreased in Intestinal Tissue Specimens From Female Adolescents With Obesity. *Pediatric and Developmental Pathology*. 21(3), pp.285–295.

Di, L. 2015. Strategic Approaches to Optimizing Peptide ADME Properties. *The AAPS Journal*. 17(1), pp.134–143.

Diaz, C., Lin, L., Martinez, L.J., Eckels, K.H., Campos, M., Jarman, R.G., Barrera, R.D.L., Lepine, E., Toussaint, J.-F., Febo, I., Innis, B.L., Thomas, S.J. and Schmidt, A.C. 2018. Phase I Randomized Study of a Tetravalent Dengue Purified Inactivated Vaccine in Healthy Adults from Puerto Rico. *The American Journal of Tropical Medicine and Hygiene*. 98(5), p.1435.

DiPilato, L. and Zhang, J. 2009. The role of membrane microdomains in shaping ß2-adrenergic receptor -mediated cAMP dynamics. *Molecular BioSystems*. 5(8), pp.832–837.

Dowdy, S.F., Gallagher, C.J., Vitarella, D. and Brown, J. 2023. A technology evaluation of the atypical use of a CPP-containing peptide in the

formulation and performance of a clinical botulinum toxin product. *Expert Opinion on Drug Delivery*. 20(9), pp.1157–1166.

Du, P., Zhang, X., Huang, C.-C., Jafari, N., Kibbe, W.A., Hou, L. and Lin, S.M. 2010. Comparison of Beta-value and M-value methods for quantifying methylation levels by microarray analysis. *BMC Bioinformatics*. 11(1), p.587.

Dukes, C.E. 1932. The classification of cancer of the rectum. *The Journal of Pathology and Bacteriology*. 35(3), pp.323–332.

Dunne, P.D. and Arends, M.J. 2024. Molecular pathological classification of colorectal cancer—an update. *Virchows Archiv*. 484(2), pp.273–285.

Duval, A. and Hamelin, R. 2002. Mutations at Coding Repeat Sequences in Mismatch Repair-deficient Human Cancers: Toward a New Concept of Target Genes for Instability1. *Cancer Research*. 62(9), pp.2447–2454.

Edgar, R., Domrachev, M. and Lash, A.E. 2002. Gene Expression Omnibus: NCBI gene expression and hybridization array data repository. *Nucleic Acids Research*. 30(1), pp.207–210.

Edwards, J. and Ritchie, A. 2023. INCISE mutational data – Longitudinal polyp study (Nov 2021). Available at: https://researchdata.gla.ac.uk/1307/. Accessed: September 2024.

Edwards, N.J., Oberti, M., Thangudu, R.R., Cai, S., McGarvey, P.B., Jacob, S., Madhavan, S. and Ketchum, K.A. 2015. The CPTAC Data Portal: A Resource for Cancer Proteomics Research. *Journal of Proteome Research*. 14(6), pp.2707–2713.

El-Ashmawy, N.E., Khedr, N.F., El-Bahrawy, H.A. and El-Adawy, S.A. 2018. Roflumilast, type 4 phosphodiesterase inhibitor, attenuates inflammation in rats with ulcerative colitis via down-regulation of iNOS and elevation of cAMP. *International Immunopharmacology*. 56, pp.36–42.

Elshazly, S.M., Elhassanny, A.E.M. and Mahmoud, N.M. 2020. Cilostazol protects against acetic acid-induced colitis in rats: Possible role for cAMP/SIRT1 pathway. *European Journal of Pharmacology*. 881, p.173234.

Emeny, J.M. and Morgan, M.J. 1979. Regulation of the Interferon System: Evidence that Vero Cells have a Genetic Defect in Interferon Production. *Journal of General Virology*. 43(1), pp.247–252.

Epstein, P.M., Basole, C. and Brocke, S. 2021. The Role of PDE8 in T Cell Recruitment and Function in Inflammation. *Frontiers in Cell and Developmental Biology*. 9.

Fajardo, A.M., Piazza, G.A. and Tinsley, H.N. 2014. The Role of Cyclic Nucleotide Signaling Pathways in Cancer: Targets for Prevention and Treatment. *Cancers*. 6(1), pp.436–458.

Farkas, Ö., Lajkó, E., Kalabay, M. and Enyedi, K.N. 2022. How to Scramble? A 'Wise Way' to Achieve a Useful Control Peptide Sequence.

Farouq, M.A.H., Acevedo, R., Ferro, V.A., Mulheran, P.A. and Al Qaraghuli, M.M. 2022. The Role of Antibodies in the Treatment of SARS-CoV-2 Virus Infection, and Evaluating Their Contribution to Antibody-Dependent Enhancement of Infection. *International Journal of Molecular Sciences*. 23(11), p.6078.

Faucz, F.R., Horvath, A., Rothenbuhler, A., Almeida, M.Q., Libé, R., Raffin-Sanson, M.-L., Bertherat, J., Carraro, D.M., Soares, F.A., de Campos Molina, G., Campos, A.H., Alexandre, R.B., Bendhack, M.L., Nesterova, M. and Stratakis, C.A. 2011. Phosphodiesterase 11A (PDE11A) Genetic Variants May Increase Susceptibility to Prostatic Cancer. *The Journal of Clinical Endocrinology & Metabolism*. 96(1), pp.E135–E140.

Feng, Z. and Xu, B. 2016. Inspiration from the mirror: D-amino acid containing peptides in biomedical approaches. *Biomolecular Concepts*. 7(3), pp.179–187.

Fernandez, L., Bustos, R.H., Zapata, C., Garcia, J., Jauregui, E. and Ashraf, G.M. 2018. Immunogenicity in Protein and Peptide Based-Therapeutics: An Overview. *Current Protein and Peptide Science*. 19(10), pp.958–971.

Fernández, X.M. and Birney, E. 2010. Ensembl Genome Browser *In*: M. R. Speicher, A. G. Motulsky and S. E. Antonarakis, eds. *Vogel and Motulsky's Human Genetics* [Online]. Berlin, Heidelberg: Springer, pp.923–939.

Fisher, D.A., Smith, J.F., Pillar, J.S., St. Denis, S.H. and Cheng, J.B. 1998. Isolation and Characterization of PDE8A, a Novel Human cAMP-Specific Phosphodiesterase. *Biochemical and Biophysical Research Communications*. 246(3), pp.570–577.

Foersch, S., Glasner, C., Woerl, A.-C., Eckstein, M., Wagner, D.-C., Schulz, S., Kellers, F., Fernandez, A., Tserea, K., Kloth, M., Hartmann, A., Heintz, A., Weichert, W., Roth, W., Geppert, C., Kather, J.N. and Jesinghaus, M. 2023. Multistain deep learning for prediction of prognosis and therapy response in colorectal cancer. *Nature Medicine*. 29(2), pp.430–439.

Förster, Th. 1948. Zwischenmolekulare Energiewanderung und Fluoreszenz. *Annalen der Physik*. 437(1–2), pp.55–75.

Forte, L.R. 2004. Uroguanylin and guanylin peptides: pharmacology and experimental therapeutics. *Pharmacology & Therapeutics*. 104(2), pp.137–162.

Fosgerau, K. and Hoffmann, T. 2015. Peptide therapeutics: current status and future directions. *Drug Discovery Today*. 20(1), pp.122–128.

Francis, S.H., Busch, J.L., Corbin, J.D. and Sibley, D. 2010. cGMP-dependent protein kinases and cGMP phosphodiesterases in nitric oxide and cGMP action. *Pharmacological Reviews*. 62(3), pp.525–563.

Freedman, D.O. 2023. A new dengue vaccine (TAK-003) now WHO recommended in endemic areas; what about travellers? *Journal of Travel Medicine*. 30(7), p.taad132.

Frei, J.C., Kielian, M. and Lai, J.R. 2015. Comprehensive mapping of functional epitopes on dengue virus glycoprotein E DIII for binding to broadly neutralizing antibodies 4E11 and 4E5A by phage display. *Virology*. 485, pp.371–382.

Gadhwal, A.K., Ankit, B.S., Chahar, C., Tantia, P., Sirohi, P. and Agrawal, R.P. 2016. Effect of Carica papaya Leaf Extract Capsule on Platelet Count in Patients of Dengue Fever with Thrombocytopenia. *The Journal of the Association of Physicians of India*. 64(6), pp.22–26.

Galiatsatos, P. and Foulkes, W.D. 2006. Familial Adenomatous Polyposis. *Official journal of the American College of Gastroenterology | ACG*. 101(2), p.385.

Gamanuma, M., Yuasa, K., Sasaki, T., Sakurai, N., Kotera, J. and Omori, K. 2003. Comparison of enzymatic characterization and gene organization of cyclic nucleotide phosphodiesterase 8 family in humans. *Cellular Signalling*. 15(6), pp.565–574.

Gamet, L., Murat, J.-C., Remaury, A., Remesy, C., Valet, P., Paris, H. and Denis-Pouxviel, C. 1992. Vasoactive intestinal peptide and forskolin regulate proliferation of the HT29 human colon adenocarcinoma cell line. *Journal of Cellular Physiology*. 150(3), pp.501–509.

Gao, G.F., Parker, J.S., Reynolds, S.M., Silva, T.C., Wang, L.-B., Zhou, W., Akbani, R., Bailey, M., Balu, S., Berman, B.P., Brooks, D., Chen, H., Cherniack, A.D., Demchok, J.A., Ding, L., Felau, I., Gaheen, S., Gerhard, D.S., Heiman, D.I., Hernandez, K.M., Hoadley, K.A., Jayasinghe, R., Kemal, A., Knijnenburg, T.A., Laird, P.W., Mensah, M.K.A., Mungall, A.J., Gordon Robertson, A., Shen, H., Tarnuzzer, R., Wang, Z., Wyczalkowski, M., Yang, L., Zenklusen, J.C., Zhang, Z., Liang, H. and Noble, M.S. 2019. Before and After: A Comparison of Legacy and Harmonized TCGA Data at the Genomic Data Commons. *Cell systems*. 9(1), pp.24-34.e10.

Garcia, M., Wehbe, M., Lévêque, N. and Bodet, C. 2017. Skin innate immune response to flaviviral infection. *European Cytokine Network*. 28(2), pp.41–51.

García-Foncillas, J., Sunakawa, Y., Aderka, D., Wainberg, Z., Ronga, P., Witzler, P. and Stintzing, S. 2019. Distinguishing Features of Cetuximab and Panitumumab in Colorectal Cancer and Other Solid Tumors. *Frontiers in Oncology*. 9.

Geller, R., Andino, R. and Frydman, J. 2013. Hsp90 Inhibitors Exhibit Resistance-Free Antiviral Activity against Respiratory Syncytial Virus. *PLOS ONE*. 8(2), p.e56762.

Genther Williams, S.M., Kuznicki, A.M., Andrade, P., Dolinski, B.M., Elbi, C., O'Hagan, R.C. and Toniatti, C. 2015. Treatment with the PARP inhibitor, niraparib, sensitizes colorectal cancer cell lines to irinotecan regardless of MSI/MSS status. *Cancer Cell International*. 15(1), p.14.

Ghaedi, H. 2024. Methylation analysis. Available at: https://github.com/hamidghaedi/Methylation_Analysis. Accessed: September 2024.

Giaretti, W., Venesio, T., Prevosto, C., Lombardo, F., Ceccarelli, J., Molinu, S. and Risio, M. 2004. Chromosomal instability and APC gene mutations in human sporadic colorectal adenomas. *The Journal of Pathology*. 204(2), pp.193–199.

Gibbons, A.V., Lin, J.E., Kim, G.W., Marszalowicz, G.P., Li, P., Stoecker, B.A., Blomain, E.S., Rattan, S., Snook, A.E., Schulz, S. and Waldman, S.A. 2013. Intestinal GUCY2C Prevents TGF-ß Secretion Coordinating Desmoplasia and Hyperproliferation in Colorectal Cancer. *Cancer Research*. 73(22), pp.6654–6666.

Giovannucci, E. 2022. Molecular Biologic and Epidemiologic Insights for Preventability of Colorectal Cancer. *JNCI Journal of the National Cancer Institute*. 114(5), pp.645–650.

Glasner, D.R., Ratnasiri, K., Puerta-Guardo, H., Espinosa, D.A., Beatty, P.R. and Harris, E. 2017. Dengue virus NS1 cytokine-independent vascular leak is dependent on endothelial glycocalyx components. *PLOS Pathogens*. 13(11), p.e1006673.

Glick, B.R. 1995. Metabolic load and heterologous gene expression. *Biotechnology Advances*. 13(2), pp.247–261.

Glyn, T., Williams, S., Whitehead, M., Eglinton, T., West, N. and Purcell, R.V. 2024. Digital spatial profiling identifies molecular changes involved in development of colitis-associated colorectal cancer. *Frontiers in Oncology*. 14.

Gmeiner, W.H. 2024. Recent Advances in Therapeutic Strategies to Improve Colorectal Cancer Treatment. *Cancers*. 16(5), p.1029.

Goldberg, R.M. 2005. Advances in the Treatment of Metastatic Colorectal Cancer. *The Oncologist*. 10(S3), pp.40–48.

González-Lodeiro, L.G., Martín Dunn, A., Martín Prieto, D., Medina-Carrasco, D., García de Castro, L.E., Maldonado Bauzá, D., Chinea Santiago, G. and Huerta Galindo, V. 2024. Dominant epitopes of cross-reactive anti-domain III human antibody response change from early to late convalescence of infection with dengue virus. *Journal of Medical Virology*. 96(2), p.e29443.

Good, S.S., Shannon, A., Lin, K., Moussa, A., Julander, J.G., La Colla, P., Collu, G., Canard, B. and Sommadossi, J.-P. 2021. Evaluation of AT-752, a Double Prodrug of a Guanosine Nucleotide Analog with In Vitro and In Vivo Activity against Dengue and Other Flaviviruses. *Antimicrobial Agents and Chemotherapy*. 65(11), 10.1128/aac.00988-21.

Gopal, G.J. and Kumar, A. 2013. Strategies for the Production of Recombinant Protein in Escherichia coli. *The Protein Journal*. 32(6), pp.419–425.

Govindarajan, D., Meschino, S., Guan, L., Clements, D.E., ter Meulen, J.H., Casimiro, D.R., Coller, B.-A.G. and Bett, A.J. 2015. Preclinical development of a dengue tetravalent recombinant subunit vaccine: Immunogenicity and protective efficacy in nonhuman primates. *Vaccine*. 33(33), pp.4105–4116.

Grady, W.M. and Carethers, J.M. 2008. Genomic and Epigenetic Instability in Colorectal Cancer Pathogenesis. *Gastroenterology*. 135(4), pp.1079–1099.

Grandi, F.C., Modi, H., Kampman, L. and Corces, M.R. 2022. Chromatin accessibility profiling by ATAC-seq. *Nature Protocols*. 17(6), pp.1518–1552.

Greally, M., Kelly, C.M. and Cercek, A. 2018. HER2: An emerging target in colorectal cancer. *Current Problems in Cancer*. 42(6), pp.560–571.

Gribble, F.M. and Reimann, F. 2016. Enteroendocrine Cells: Chemosensors in the Intestinal Epithelium. *Annual Review of Physiology*. 78(Volume 78, 2016), pp.277–299.

Gristan, Y.D., Patel, P. and Moosavi, L. 2024. Folinic Acid *In*: *StatPearls* [Online]. Treasure Island (FL): StatPearls Publishing.

Gromowski, G.D., Roehrig, J.T., Diamond, M.S., Lee, J.C., Pitcher, T.J. and Barrett, A.D.T. 2010. Mutations of an antibody binding energy hot spot on domain III of the dengue 2 envelope glycoprotein exploited for neutralization escape. *Virology*. 407(2), pp.237–246.

de Groot, N.S., Pallarés, I., Avilés, F.X., Vendrell, J. and Ventura, S. 2005. Prediction of 'hot spots' of aggregation in disease-linked polypeptides. *BMC Structural Biology*. 5(1), p.18.

Guidotti, G., Brambilla, L. and Rossi, D. 2017. Cell-Penetrating Peptides: From Basic Research to Clinics. *Trends in Pharmacological Sciences*. 38(4), pp.406–424.

Gurevich, E.V. and Gurevich, V.V. 2015. Beyond traditional pharmacology: new tools and approaches. *British Journal of Pharmacology*. 172(13), pp.3229–3241.

Hackett, F., Collins, C., Strath, M. and Blackman, M. 2014. Cyclic Nucleotide (cAMP and cGMP) Assays and Capture ELISA for Quantitative Analysis of Plasmodium falciparum Blood-stage Egress. *BIO-PROTOCOL*. 4(5).

Halstead, S.B., Mahalingam, S., Marovich, M.A., Ubol, S. and Mosser, D.M. 2010. Intrinsic antibody-dependent enhancement of microbial infection in macrophages: disease regulation by immune complexes. *The Lancet Infectious Diseases*. 10(10), pp.712–722.

Han, P., Fu, Y., Luo, M., He, J., Liu, J., Liao, J., Tian, D. and Yan, W. 2014. BVES Inhibition Triggers Epithelial-Mesenchymal Transition in Human Hepatocellular Carcinoma. *Digestive Diseases and Sciences*. 59(5), pp.992–1000.

Han, X., Mann, E., Gilbert, S., Guan, Y., Steinbrecher, K.A., Montrose, M.H. and Cohen, M.B. 2011. Loss of Guanylyl Cyclase C (GCC) Signaling Leads to Dysfunctional Intestinal Barrier. *PLOS ONE*. 6(1), p.e16139.

Hansen, T.F., Qvortrup, C. and Pfeiffer, P. 2021. Angiogenesis Inhibitors for Colorectal Cancer. A Review of the Clinical Data. *Cancers*. 13(5), p.1031.

Harmel-Laws, E., Mann, E.A., Cohen, M.B. and Steinbrecher, K.A. 2013. Guanylate Cyclase C Deficiency Causes Severe Inflammation in a Murine Model of Spontaneous Colitis. *PLOS ONE*. 8(11), p.e79180.

Hassin, O., Nataraj, N.B., Shreberk-Shaked, M., Aylon, Y., Yaeger, R., Fontemaggi, G., Mukherjee, S., Maddalena, M., Avioz, A., Iancu, O., Mallel, G., Gershoni, A., Grosheva, I., Feldmesser, E., Ben-Dor, S., Golani, O., Hendel, A., Blandino, G., Kelsen, D., Yarden, Y. and Oren, M. 2022. Different hotspot p53 mutants exert distinct phenotypes and predict outcome of colorectal cancer patients. *Nature Communications*. 13(1), p.2800.

Hayes, H.C., P. Luk, L.Y. and Tsai, Y.-H. 2021. Approaches for peptide and protein cyclisation. *Organic & Biomolecular Chemistry*. 19(18), pp.3983–4001.

He, X.C., Zhang, J., Tong, W.-G., Tawfik, O., Ross, J., Scoville, D.H., Tian, Q., Zeng, X., He, X., Wiedemann, L.M., Mishina, Y. and Li, L. 2004. BMP signaling inhibits intestinal stem cell self-renewal through suppression of Wnt–β-catenin signaling. *Nature Genetics*. 36(10), pp.1117–1121.

He, Y., Zhou, J., Gao, H., Liu, C., Zhan, P. and Liu, X. 2024. Broad-spectrum antiviral strategy: Host-targeting antivirals against emerging and re-emerging viruses. *European Journal of Medicinal Chemistry*. 265, p.116069.

Helander, H.F. and Fändriks, L. 2014. Surface area of the digestive tract – revisited. *Scandinavian Journal of Gastroenterology*. 49(6), pp.681–689.

Henninot, A., Collins, J.C. and Nuss, J.M. 2018. The Current State of Peptide Drug Discovery: Back to the Future? *Journal of Medicinal Chemistry*. 61(4), pp.1382–1414.

Hewitt, R.E., Powe, D.G., Carter, G.I. and Turner, D.R. 1993. Desmoplasia and its relevance to colorectal tumour invasion. *International Journal of Cancer*. 53(1), pp.62–69.

Heyer, J., Yang, K., Lipkin, M., Edelmann, W. and Kucherlapati, R. 1999. Mouse models for colorectal cancer. *Oncogene*. 18(38), pp.5325–5333.

Hillson, L.V.S., McCulloch, A.K., Edwards, J., Dunne, P.D., O'Cathail, S.M. and Roxburgh, C.S. 2024. Radiation-induced changes in gene expression in rectal cancer specimens. *Clinical and Translational Oncology*. 26(6), pp.1419–1428.

Ho, M.-R., Tsai, T.-T., Chen, C.-L., Jhan, M.-K., Tsai, C.-C., Lee, Y.-C., Chen, C.-H. and Lin, C.-F. 2017. Blockade of dengue virus infection and viral

cytotoxicity in neuronal cells in vitro and in vivo by targeting endocytic pathways. *Scientific Reports*. 7(1), p.6910.

Hoffman, W., Lakkis, F.G. and Chalasani, G. 2016. B Cells, Antibodies, and More. *Clinical Journal of the American Society of Nephrology*. 11(1), p.137.

Hofmarcher, T. and Lindgren, P. 2020. The cost of cancers of the digestive system in Europe. *IHE Report*. 6.

Holch, J.W., Ricard, I., Stintzing, S., Modest, D.P. and Heinemann, V. 2017. The relevance of primary tumour location in patients with metastatic colorectal cancer: A meta-analysis of first-line clinical trials. *European Journal of Cancer*. 70, pp.87–98.

Hong, T.S., Clark, J.W. and Haigis, K.M. 2012. Cancers of the Colon and Rectum: Identical or Fraternal Twins? *Cancer Discovery*. 2(2), pp.117–121.

Höpfner, M., Maaser, K., Barthel, B., von Lampe, B., Hanski, C., Riecken, E.O., Zeitz, M. and Scherübl, H. 2001. Growth inhibition and apoptosis induced by P2Y2 receptors in human colorectal carcinoma cells: involvement of intracellular calcium and cyclic adenosine monophosphate. *International Journal of Colorectal Disease*. 16(3), pp.154–166.

Hopp, T.P. and Woods, K.R. 1983. A computer program for predicting protein antigenic determinants. *Molecular Immunology*. 20(4), pp.483–489.

Hoter, A., El-Sabban, M.E. and Naim, H.Y. 2018. The HSP90 Family: Structure, Regulation, Function, and Implications in Health and Disease. *International Journal of Molecular Sciences*. 19(9), p.2560.

Hou, Y., Wren, A., Mylarapu, N., Browning, K., Islam, B.N., Wang, R., Vega, K.J. and Browning, D.D. 2022a. Inhibition of Colon Cancer Cell Growth by Phosphodiesterase Inhibitors Is Independent of cGMP Signaling. *Journal of Pharmacology and Experimental Therapeutics*. 381(1), pp.42–53.

Hou, Y., Wren, A., Mylarapu, N., Browning, K., Islam, B.N., Wang, R., Vega, K.J. and Browning, D.D. 2022b. Inhibition of Colon Cancer Cell Growth by Phosphodiesterase Inhibitors Is Independent of cGMP Signaling. *The Journal of Pharmacology and Experimental Therapeutics*. 381(1), pp.42–53.

Howe, M.K., Speer, B.L., Hughes, P.F., Loiselle, D.R., Vasudevan, S. and Haystead, T.A.J. 2016. An inducible heat shock protein 70 small molecule inhibitor demonstrates anti-dengue virus activity, validating Hsp70 as a host antiviral target. *Antiviral Research*. 130, pp.81–92.

Hrdlickova, R., Toloue, M. and Tian, B. 2017. RNA-Seq methods for transcriptome analysis. *WIREs RNA*. 8(1), p.e1364.

Hrobowski, Y.M., Garry, R.F. and Michael, S.F. 2005. Peptide inhibitors of dengue virus and West Nile virus infectivity. *Virology Journal*. 2(1), p.49.

Hsien Lai, S., Zervoudakis, G., Chou, J., Gurney, M.E. and Quesnelle, K.M. 2020. PDE4 subtypes in cancer. *Oncogene*. 39(19), pp.3791–3802.

Htun, H.L., Yeo, T.W., Tam, C.C., Pang, J., Leo, Y.S. and Lye, D.C. 2018. Metformin Use and Severe Dengue in Diabetic Adults. *Scientific Reports*. 8(1), p.3344.

Hu, T., Wu, Z., Wu, S., Chen, S. and Cheng, A. 2021. The key amino acids of E protein involved in early flavivirus infection: viral entry. *Virology Journal*. 18, p.136.

Hu, Y., Jiang, Q., Zhai, X., Liu, L. and Hong, Y. 2023. Screening and validation of the optimal panel of reference genes in colonic epithelium and relative cancer cell lines. *Scientific Reports*. 13(1), p.17777.

Huang, K.-C., Lee, M.-C., Wu, C.-W., Huang, K.-J., Lei, H.-Y. and Cheng, J.-W. 2008. Solution structure and neutralizing antibody binding studies of domain III of the dengue-2 virus envelope protein. *Proteins: Structure, Function, and Bioinformatics*. 70(3), pp.1116–1119.

Huang, W., Sundquist, J., Sundquist, K. and Ji, J. 2019. Use of Phosphodiesterase 5 Inhibitors Is Associated With Lower Risk of Colorectal Cancer in Men With Benign Colorectal Neoplasms. *Gastroenterology*. 157(3), pp.672-681.e4.

Humphries, A. and Wright, N.A. 2008. Colonic crypt organization and tumorigenesis. *Nature Reviews Cancer*. 8(6), pp.415–424.

Hung, J.-J., Hsieh, M.-T., Young, M.-J., Kao, C.-L., King, C.-C. and Chang, W. 2004. An External Loop Region of Domain III of Dengue Virus Type 2 Envelope Protein Is Involved in Serotype-Specific Binding to Mosquito but Not Mammalian Cells. *Journal of Virology*. 78(1), pp.378–388.

Iacopetta, B. 2003. TP53 mutation in colorectal cancer. *Human Mutation*. 21(3), pp.271–276.

Ijsselsteijn, R., Jansen, J.G. and de Wind, N. 2020. DNA mismatch repair-dependent DNA damage responses and cancer. *DNA Repair*. 93, p.102923.

Isa, D.M., Chin, S.P., Chong, W.L., Zain, S.M., Rahman, N.A. and Lee, V.S. 2019. Dynamics and binding interactions of peptide inhibitors of dengue virus entry. *Journal of Biological Physics*. 45(1), pp.63–76.

Islam, B.N., Sharman, S.K. and Browning, D.D. 2018. Clinical utility of plecanatide in the treatment of chronic idiopathic constipation. *International Journal of General Medicine*. 11, pp.323–330.

Islam, B.N., Sharman, S.K., Hou, Y., Bridges, A.E., Singh, N., Kim, S., Kolhe, R., Trillo-Tinoco, J., Rodriguez, P.C., Berger, F.G., Sridhar, S. and Browning, D.D. 2017. Sildenafil Suppresses Inflammation-Driven Colorectal Cancer in Mice. *Cancer Prevention Research*. 10(7), pp.377–388.

Islam, B.N., Sharman, S.K., Hou, Y., Wang, R., Ashby, J., Li, H., Liu, K., Vega, K.J. and Browning, D.D. 2022. Type-2 cGMP-dependent protein kinase suppresses proliferation and carcinogenesis in the colon epithelium. *Carcinogenesis*. 43(6), pp.584–593.

Islam, M.S., Gopalan, V., Lam, A.K. and Shiddiky, M.J.A. 2023. Current advances in detecting genetic and epigenetic biomarkers of colorectal cancer. *Biosensors and Bioelectronics*. 239, p.115611.

Jackson, S.E. 2013. Hsp90: Structure and Function *In*: S. Jackson, ed. *Molecular Chaperones* [Online]. Berlin, Heidelberg: Springer, pp.155–240.

Jain, S., Vimal, N., Angmo, N., Sengupta, M. and Thangaraj, S. 2023. Dengue Vaccination: Towards a New Dawn of Curbing Dengue Infection. *Immunological Investigations*. 52(8), pp.1096–1149.

Jaiswal, A.S. and Narayan, S. 2011. Assembly of the base excision repair complex on abasic DNA and role of adenomatous polyposis coli on its functional activity. *Biochemistry*. 50(11), pp.1901–1909.

Jani, R.K. 2023. Gastrointestinal Tract and Digestion Challenges in Chronic Diseases and Applications of Functional Foods and Nutraceuticals *In*: *Molecular Mechanisms of Action of Functional Foods and Nutraceuticals for Chronic Diseases*. CRC Press.

Jensen, J., Brennesvik, E.O., Lai, Y.-C. and Shepherd, P.R. 2007. GSK-3β regulation in skeletal muscles by adrenaline and insulin: Evidence that PKA and PKB regulate different pools of GSK-3. *Cellular Signalling*. 19(1), pp.204–210.

Ji, X. and Li, Z. 2020. Medicinal chemistry strategies toward host targeting antiviral agents. *Medicinal Research Reviews*. 40(5), pp.1519–1557.

Jiang, J., Liu, H.-L., Tao, L., Lin, X.-Y., Yang, Y.-D., Tan, S.-W. and Wu, B. 2018. Let-7d inhibits colorectal cancer cell proliferation through the CST1/p65 pathway. *International Journal of Oncology*. 53(2), pp.781–790.

Jiang, L., Lan, T., Chen, Y., Sang, J., Li, Y., Wu, M., Tao, Y., Wang, Y., Qian, H. and Gu, L. 2013. PKG II inhibits EGF/EGFR-induced migration of gastric cancer cells. *PloS One*. 8(4), p.e61674.

Jimenez-Solem, E., Rasmussen, M.H., Christensen, M. and Knop, F.K. 2010. Dulaglutide, a long-acting GLP-1 analog fused with an Fc antibody fragment for the potential treatment of type 2 diabetes. *Current Opinion in Molecular Therapeutics*. 12(6), pp.790–797.

Johansson, M.E.V., Ambort, D., Pelaseyed, T., Schütte, A., Gustafsson, J.K., Ermund, A., Subramani, D.B., Holmén-Larsson, J.M., Thomsson, K.A., Bergström, J.H., van der Post, S., Rodriguez-Piñeiro, A.M., Sjövall, H., Bäckström, M. and Hansson, G.C. 2011. Composition and functional role of the mucus layers in the intestine. *Cellular and Molecular Life Sciences*. 68(22), pp.3635–3641.

Johnson, A.J. and Roehrig, J.T. 1999. New Mouse Model for Dengue Virus Vaccine Testing. *Journal of Virology*. 73(1), pp.783–786.

Johnson, J.L. 2012. Evolution and function of diverse Hsp90 homologs and cochaperone proteins. *Biochimica et Biophysica Acta (BBA) - Molecular Cell Research*. 1823(3), pp.607–613.

Jonker, D.J., O'Callaghan, C.J., Karapetis, C.S., Zalcberg, J.R., Tu, D., Au, H.-J., Berry, S.R., Krahn, M., Price, T., Simes, R.J., Tebbutt, N.C., Hazel, G. van, Wierzbicki, R., Langer, C. and Moore, M.J. 2007. Cetuximab for the Treatment of Colorectal Cancer. *New England Journal of Medicine*. 357(20), pp.2040–2048.

Jwad, R., Weissberger, D. and Hunter, L. 2020. Strategies for Fine-Tuning the Conformations of Cyclic Peptides. *Chemical Reviews*. 120(17), pp.9743–9789.

Kaksonen, M. and Roux, A. 2018. Mechanisms of clathrin-mediated endocytosis. *Nature Reviews Molecular Cell Biology*. 19(5), pp.313–326.

Kalayanarooj, S. 2011. Clinical Manifestations and Management of Dengue/DHF/DSS. *Tropical Medicine and Health*. 39(4 Suppl), pp.83–87.

Kallás Esper G., Cintra Monica A.T., Moreira José A., Patiño Elizabeth G., Braga Patricia Emilia, Tenório Juliana C.V., Infante Vanessa, Palacios Ricardo, de Lacerda Marcus Vínicius Guimarães, Batista Pereira Dhelio, da Fonseca Allex Jardim, Gurgel Ricardo Queiroz, Coelho Ivo Castelo-Branco, Fontes Cor Jesus Fernandes, Marques Ernesto T.A., Romero Gustavo Adolfo Sierra, Teixeira Mauro Martins, Siqueira André M., Barral Aldina Maria Prado, Boaventura Viviane Sampaio, Ramos Fabiano, Elias Júnior Erivaldo, Cassio de Moraes José, Covas Dimas T., Kalil Jorge, Precioso Alexander Roberto, Whitehead Stephen S., Esteves-Jaramillo Alejandra, Shekar Tulin, Lee Jung-Jin, Macey Julieta, Kelner Sabrina Gozlan, Coller Beth-Ann G., Boulos Fernanda Castro, and Nogueira Mauricio L. 2024. Live, Attenuated, Tetravalent Butantan–Dengue Vaccine in Children and Adults. *New England Journal of Medicine*. 390(5), pp.397–408.

Kamemura, N., Murakami, S., Komatsu, H., Sawanoi, M., Miyamoto, K., Ishidoh, K., Kishimoto, K., Tsuji, A. and Yuasa, K. 2017. Type II cGMP-dependent protein kinase negatively regulates fibroblast growth factor signaling by phosphorylating Raf-1 at serine 43 in rat chondrosarcoma cells. *Biochemical and Biophysical Research Communications*. 483(1), pp.82–87.

Kang, C. and Syed, Y.Y. 2020. Bulevirtide: First Approval. *Drugs*. 80(15), pp.1601–1605.

Kang, X., Zhang, R., Kwong, T.N., Lui, R.N., Wu, W.K., Sung, J.J., Yu, J. and Wong, S.H. 2021. Serrated neoplasia in the colorectum: gut microbiota and molecular pathways. *Gut Microbes*. 13(1), p.1863135.

Kangawa, Y., Yoshida, T., Maruyama, K., Okamoto, M., Kihara, T., Nakamura, M., Ochiai, M., Hippo, Y., Hayashi, S. and Shibutani, M. 2017. Cilostazol and enzymatically modified isoquercitrin attenuate experimental colitis and colon cancer in mice by inhibiting cell proliferation and inflammation. *Food and Chemical Toxicology*. 100, pp.103–114.

Karamchandani, D.M., Chetty, R., King, T.S., Liu, X., Westerhoff, M., Yang, Z., Yantiss, R.K. and Driman, D.K. 2020. Challenges with colorectal cancer staging: results of an international study. *Modern Pathology*. 33(1), pp.153–163.

Kastrinos, F. and Syngal, S. 2011. Inherited Colorectal Cancer Syndromes. *The Cancer Journal*. 17(6), p.405.

Kasture, P.N., Nagabhushan, K.H. and Kumar, A. 2016. A Multi-centric, Double-blind, Placebo-controlled, Randomized, Prospective Study to Evaluate the Efficacy and Safety of Carica papaya Leaf Extract, as Empirical Therapy for Thrombocytopenia associated with Dengue Fever. *The Journal of the Association of Physicians of India*. 64(6), pp.15–20.

Katz, C., Levy-Beladev, L., Rotem-Bamberger, S., Rito, T., D. Rüdiger, S.G. and Friedler, A. 2011. Studying protein – protein interactions using peptide arrays. *Chemical Society Reviews*. 40(5), pp.2131–2145.

Katzelnick, L.C., Gresh, L., Halloran, M.E., Mercado, J.C., Kuan, G., Gordon, A., Balmaseda, A. and Harris, E. 2017. Antibody-dependent enhancement of severe dengue disease in humans. *Science*. 358(6365), pp.929–932.

Kawashima, D., Kanda, T., Murata, T., Saito, S., Sugimoto, A., Narita, Y. and Tsurumi, T. 2013. Nuclear Transport of Epstein-Barr Virus DNA Polymerase Is Dependent on the BMRF1 Polymerase Processivity Factor and Molecular Chaperone Hsp90. *Journal of Virology*. 87(11), pp.6482–6491.

Keravis, T. and Lugnier, C. 2010. Cyclic Nucleotide Phosphodiesterases (PDE) and Peptide Motifs. *Current Pharmaceutical Design*. 16(9), pp.1114–1125.

Kesteleyn, B., Bonfanti, J.-F., Bardiot, D., De Boeck, B., Goethals, O., Kaptein, S.J.F., Stoops, B., Coesemans, E., Fortin, J., Muller, P., Doublet, F., Carlens, G., Koukni, M., Smets, W., Raboisson, P., Chaltin, P., Simmen, K., Loock, M.V., Neyts, J., Marchand, A. and Jonckers, T.H.M. 2024. Discovery of JNJ-1802, a First-in-Class Pan-Serotype Dengue Virus NS4B Inhibitor. *Journal of Medicinal Chemistry*. 67(5), pp.4063–4082.

Khaliq, A.M., Erdogan, C., Kurt, Z., Turgut, S.S., Grunvald, M.W., Rand, T., Khare, S., Borgia, J.A., Hayden, D.M., Pappas, S.G., Govekar, H.R., Kam, A.E., Reiser, J., Turaga, K., Radovich, M., Zang, Y., Qiu, Y., Liu, Y., Fishel, M.L., Turk, A., Gupta, V., Al-Sabti, R., Subramanian, J., Kuzel, T.M., Sadanandam, A., Waldron, L., Hussain, A., Saleem, M., El-Rayes, B., Salahudeen, A.A. and Masood, A. 2022. Refining colorectal cancer classification and clinical stratification through a single-cell atlas. *Genome Biology*. 23, p.113.

Kim, D.U., Kwak, B. and Kim, S.-W. 2019. Phosphodiesterase 4B is an effective therapeutic target in colorectal cancer. *Biochemical and Biophysical Research Communications*. 508(3), pp.825–831.

Kim, D.U., Nam, J., Cha, M.D. and Kim, S.-W. 2019. Inhibition of phosphodiesterase 4D decreases the malignant properties of DLD-1 colorectal cancer cells by repressing the AKT/mTOR/Myc signaling pathway. *Oncology Letters*. 17(3), pp.3589–3598.

Kim, E.-J. and Juhnn, Y.-S. 2015. Cyclic AMP Signaling Reduces Sirtuin 6 Expression in Non-small Cell Lung Cancer Cells by Promoting Ubiquitin-Proteasomal Degradation via Inhibition of the Raf-MEK-ERK (Raf/Mitogen-activated Extracellular Signal-regulated Kinase/Extracellular Signal-

regulated Kinase) Pathway *. *Journal of Biological Chemistry*. 290(15), pp.9604–9613.

Kim, S.Y. and Kim, T.I. 2018. Serrated neoplasia pathway as an alternative route of colorectal cancer carcinogenesis. *Intestinal Research*. 16(3), pp.358–365.

Kimberlin, D.W. and Whitley, R.J. 1996. Antiviral resistance: mechanisms, clinical significance, and future implications. *Journal of Antimicrobial Chemotherapy*. 37(3), pp.403–421.

Kojima, M., Wakai, K., Tokudome, S., Tamakoshi, K., Toyoshima, H., Watanabe, Y., Hayakawa, N., Suzuki, K., Hashimoto, S., Ito, Y. and Tamakoshi, A. 2004. Bowel movement frequency and risk of colorectal cancer in a large cohort study of Japanese men and women. *British Journal of Cancer*. 90(7), pp.1397–1401.

Koliaraki, V., Pallangyo, C.K., Greten, F.R. and Kollias, G. 2017. Mesenchymal Cells in Colon Cancer. *Gastroenterology*. 152(5), pp.964–979.

Kong, G., Lee, H., Vo, T.-T.T., Juang, U., Kwon, S.H., Park, Jisoo, Park, Jongsun and Kim, S.-H. 2022. Functional characteristics and research trends of PDE11A in human diseases (Review). *Molecular Medicine Reports*. 26(4), pp.1–10.

Kong, X.-D. and Heinis, C. 2021. Towards the Development of Orally Available Peptide Therapeutics. *CHIMIA*. 75(6), p.514.

Kotera, J., Fujishige, K., Imai, Y., Kawai, E., Michibata, H., Akatsuka, H., Yanaka, N. and Omori, K. 1999. Genomic origin and transcriptional regulation of two variants of cGMP-binding cGMP-specific phosphodiesterases. *European Journal of Biochemistry*. 262(3), pp.866–873.

Kothai Ramalingam, Christina S Varghese, Chinchu Elias, Gigi M Mathew, and Arul Balasubramanian 2019. A retrospective study on the effect of Vitamin C in the management of dengue fever in three different states of India. *International Journal of Research in Pharmaceutical Sciences*. 10(4), pp.2670–2673.

Kouzmenko, A.P., Takeyama, K., Kawasaki, Y., Akiyama, T. and Kato, S. 2008. Truncation mutations abolish chromatin-associated activities of adenomatous polyposis coli. *Oncogene*. 27(36), pp.4888–4899.

Kuhn, R.J., Zhang, W., Rossmann, M.G., Pletnev, S.V., Corver, J., Lenches, E., Jones, C.T., Mukhopadhyay, S., Chipman, P.R., Strauss, E.G., Baker, T.S. and Strauss, J.H. 2002. Structure of Dengue Virus: Implications for Flavivirus Organization, Maturation, and Fusion. *Cell*. 108(5), pp.717–725.

Kumar, S. and Sherman, M.Y. 2023. Resistance to TOP-1 Inhibitors: Good Old Drugs Still Can Surprise Us. *International Journal of Molecular Sciences*. 24(8), p.7233.

Kunkel, T.A. and Erie, D.A. 2005. DNA mismatch repair. *Annual Review of Biochemistry*. 74, pp.681–710.

Kurtzhals, P., Østergaard, S., Nishimura, E. and Kjeldsen, T. 2023. Derivatization with fatty acids in peptide and protein drug discovery. *Nature Reviews Drug Discovery*. 22(1), pp.59–80.

Laetsch, T.W. and Hong, D.S. 2021. Tropomyosin Receptor Kinase Inhibitors for the Treatment of TRK Fusion Cancer. *Clinical Cancer Research*. 27(18), pp.4974–4982.

Lakhter, A.J. and Naidu, S.R. 2017. Cyclic AMP-Epac signaling pathway contributes to repression of PUMA transcription in melanoma cells. *Melanoma Research*. 27(5), p.411.

Lambrechts, L., Scott, T.W. and Gubler, D.J. 2010. Consequences of the Expanding Global Distribution of Aedes albopictus for Dengue Virus Transmission. *PLOS Neglected Tropical Diseases*. 4(5), p.e646.

Lamiable, A., Thévenet, P., Rey, J., Vavrusa, M., Derreumaux, P. and Tufféry, P. 2016. PEP-FOLD3: faster de novo structure prediction for linear peptides in solution and in complex. *Nucleic Acids Research*. 44(Web Server issue), pp.W449–W454.

Landy, J., Ronde, E., English, N., Clark, S.K., Hart, A.L., Knight, S.C., Ciclitira, P.J. and Al-Hassi, H.O. 2016. Tight junctions in inflammatory bowel diseases and inflammatory bowel disease associated colorectal cancer. *World Journal of Gastroenterology*. 22(11), pp.3117–3126.

Lau, J.L. and Dunn, M.K. 2018. Therapeutic peptides: Historical perspectives, current development trends, and future directions. *Bioorganic & Medicinal Chemistry*. 26(10), pp.2700–2707.

Le Jeune, I.R., Shepherd, M., Van Heeke, G., Houslay, M.D. and Hall, I.P. 2002. Cyclic AMP-dependent Transcriptional Up-regulation of Phosphodiesterase 4D5 in Human Airway Smooth Muscle Cells: IDENTIFICATION AND CHARACTERIZATION OF A NOVEL PDE4D5PROMOTER*. *Journal of Biological Chemistry*. 277(39), pp.35980–35989.

Lechuga, S., Braga-Neto, M.B., Naydenov, N.G., Rieder, F. and Ivanov, A.I. 2023. Understanding disruption of the gut barrier during inflammation: Should we abandon traditional epithelial cell lines and switch to intestinal organoids? *Frontiers in Immunology*. 14.

Lee, A., Lebedyeva, I., Zhi, W., Senthil, V., Cheema, H., Brands, M.W., Bush, W., Lambert, N.A., Snipes, M. and Browning, D.D. 2023. A Non-Systemic Phosphodiesterase-5 Inhibitor Suppresses Colon Proliferation in Mice. *International Journal of Molecular Sciences*. 24(11), p.9397.

Lee, A.C.-L., Harris, J.L., Khanna, K.K. and Hong, J.-H. 2019. A Comprehensive Review on Current Advances in Peptide Drug Development and Design. *International Journal of Molecular Sciences*. 20(10), p.2383.

Lee, H. and Han, B. 2024a. General solution to inflated type I and II errors in multi-subject single-cell differential gene expression analysis. , 2023.01.09.523212.

Lee, H. and Han, B. 2024b. Pseudobulk with proper offsets has the same statistical properties as generalized linear mixed models in single-cell case-control studies. *Bioinformatics (Oxford, England)*. 40(8), p.btae498.

Lee, H., Park, S., Kong, G., Kwon, S.H., Park, Jisoo, Park, Jongsun and Kim, S.-H. 2022. Phosphodiesterase 11 A (PDE11A), a potential biomarker for glioblastoma. *Toxicological Research*. 38(3), pp.409–415.

Lee, K., Lindsey, A.S., Li, N., Gary, B., Andrews, J., Keeton, A.B. and Piazza, G.A. 2015. ß-catenin nuclear translocation in colorectal cancer cells is suppressed by PDE10A inhibition, cGMP elevation, and activation of PKG. *Oncotarget*. 7(5), pp.5353–5365.

Lee, K.J., Chang, W.-C.L., Chen, X., Valiyaveettil, J., Ramirez-Alcantara, V., Gavin, E., Musiyenko, A., Madeira da Silva, L., Annamdevula, N.S., Leavesley, S.J., Ward, A., Mattox, T., Lindsey, A.S., Andrews, J., Zhu, B., Wood, C., Neese, A., Nguyen, A., Berry, K., Maxuitenko, Y., Moyer, M.P., Nurmemmedov, E., Gorman, G., Coward, L., Zhou, G., Keeton, A.B., Cooper, H.S., Clapper, M.L. and Piazza, G.A. 2021. Suppression of Colon Tumorigenesis in Mutant Apc Mice by a Novel PDE10 Inhibitor that Reduces Oncogenic ß-Catenin. *Cancer Prevention Research*. 14(11), pp.995–1008.

Lee, M.F., Anasir, M.I. and Poh, C.L. 2023. Development of novel antiviral peptides against dengue serotypes 1-4. *Virology*. 580, pp.10–27.

Lee, M.F., Voon, G.Z., Lim, H.X., Chua, M.L. and Poh, C.L. 2022. Innate and adaptive immune evasion by dengue virus. *Frontiers in Cellular and Infection Microbiology*. 12.

Lee, M.F., Wu, Y.S. and Poh, C.L. 2023. Molecular Mechanisms of Antiviral Agents against Dengue Virus. *Viruses*. 15(3), p.705.

Lee, R., Wolda, S., Moon, E., Esselstyn, J., Hertel, C. and Lerner, A. 2002. PDE7A is expressed in human B-lymphocytes and is up-regulated by elevation of intracellular cAMP. *Cellular Signalling*. 14(3), pp.277–284.

Lee, T.I. and Young, R.A. 2013. Transcriptional Regulation and Its Misregulation in Disease. *Cell*. 152(6), pp.1237–1251.

Leeson, P.D. and Empfield, J.R. 2010. Reducing the Risk of Drug Attrition Associated with Physicochemical Properties *In*: J. E. Macor, ed. *Annual Reports in Medicinal Chemistry* [Online]. Academic Press, pp.393–407.

Leggett, B.A. and Worthley, D.L. 2009. Synchronous colorectal cancer: not just bad luck? *Gastroenterology*. 137(5), pp.1559–1562.

Lenharo, M. 2024. Brazil's record dengue surge: why a vaccine campaign is unlikely to stop it. *Nature*. 627(8003), pp.250–251.

Lescar, J., Soh, S., Lee, L.T., Vasudevan, S.G., Kang, C. and Lim, S.P. 2018. The Dengue Virus Replication Complex: From RNA Replication to Protein-Protein Interactions to Evasion of Innate Immunity *In*: R. Hilgenfeld and S. G. Vasudevan, eds. *Dengue and Zika: Control and Antiviral Treatment Strategies* [Online]. Singapore: Springer, pp.115–129.

Leslie, A., Carey, F.A., Pratt, N.R. and Steele, R.J.C. 2002. The colorectal adenoma–carcinoma sequence. *BJS (British Journal of Surgery)*. 89(7), pp.845–860.

Li, J., Guo, B.-C., Sun, L.-R., Wang, J.-W., Fu, X.-H., Zhang, S.-Z., Poston, G. and Ding, K.-F. 2014. TNM staging of colorectal cancer should be reconsidered by T stage weighting. *World Journal of Gastroenterology : WJG*. 20(17), pp.5104–5112.

Li, J., Richter, K. and Buchner, J. 2011. Mixed Hsp90–cochaperone complexes are important for the progression of the reaction cycle. *Nature Structural & Molecular Biology*. 18(1), pp.61–66.

Li, Nan, Chen, X., Zhu, B., Ramírez-Alcántara, V., Canzoneri, J.C., Lee, K., Sigler, S., Gary, B., Li, Y., Zhang, W., Moyer, M.P., Salter, E.A., Wierzbicki, A., Keeton, A.B. and Piazza, G.A. 2015. Suppression of ß-catenin/TCF transcriptional activity and colon tumor cell growth by dual inhibition of PDE5 and 10. *Oncotarget*. 6(29), pp.27403–27415.

Li, N., Lee, K., Xi, Y., Zhu, B., Gary, B.D., Ramírez-Alcántara, V., Gurpinar, E., Canzoneri, J.C., Fajardo, A., Sigler, S., Piazza, J.T., Chen, X., Andrews, J., Thomas, M., Lu, W., Li, Y., Laan, D.J., Moyer, M.P., Russo, S., Eberhardt, B.T., Yet, L., Keeton, A.B., Grizzle, W.E. and Piazza, G.A. 2015. Phosphodiesterase 10A: a novel target for selective inhibition of colon tumor cell growth and ß-catenin-dependent TCF transcriptional activity. *Oncogene*. 34(12), pp.1499–1509.

Li, N., Xi, Y., Tinsley, H.N., Gurpinar, E., Gary, B.D., Zhu, B., Li, Y., Chen, X., Keeton, A.B., Abadi, A.H., Moyer, M.P., Grizzle, W.E., Chang, W., Clapper, M.L. and Piazza, G.A. 2013. Sulindac selectively inhibits colon tumor cell growth by activating the cGMP/PKG pathway to suppress Wnt/ß-catenin signaling. *Molecular cancer therapeutics*. 12(9), pp.1848–1859.

Li, P., Lin, J.E., Chervoneva, I., Schulz, S., Waldman, S.A. and Pitari, G.M. 2007. Homeostatic Control of the Crypt-Villus Axis by the Bacterial Enterotoxin Receptor Guanylyl Cyclase C Restricts the Proliferating Compartment in Intestine. *The American Journal of Pathology*. 171(6), pp.1847–1858.

Li, P., Schulz, S., Bombonati, A., Palazzo, J.P., Hyslop, T.M., Xu, Y., Baran, A.A., Siracusa, L.D., Pitari, G.M. and Waldman, S.A. 2007. Guanylyl Cyclase C Suppresses Intestinal Tumorigenesis by Restricting Proliferation and Maintaining Genomic Integrity. *Gastroenterology*. 133(2), pp.599–607.

Li, P., Wuthrick, E., Rappaport, J.A., Kraft, C., Lin, J.E., Marszalowicz, G., Snook, A.E., Zhan, T., Hyslop, T.M. and Waldman, S.A. 2017. GUCY2C Signaling Opposes the Acute Radiation-Induced GI Syndrome. *Cancer Research*. 77(18), pp.5095–5106.

Li, X., Dong, Z., Liu, Y., Song, W., Pu, J., Jiang, G., Wu, Y., Liu, L. and Huang, X. 2021. A Novel Role for the Regulatory Nod-Like Receptor NLRP12 in Anti-Dengue Virus Response. *Frontiers in Immunology*. 12.

Li, Y., Clark, K.A. and Tan, Z. 2018. Methods for engineering therapeutic peptides. *Chinese Chemical Letters*. 29(7), pp.1074–1078.

Li, Y.-H., Tao, P.-Z., Liu, Y.-Z. and Jiang, J.-D. 2004. Geldanamycin, a Ligand of Heat Shock Protein 90, Inhibits the Replication of Herpes Simplex Virus Type 1 In Vitro. *Antimicrobial Agents and Chemotherapy*. 48(3), pp.867–872.

Li, Z.-N. and Luo, Y. 2023. HSP90 inhibitors and cancer: Prospects for use in targeted therapies (Review). *Oncology Reports*. 49(1), pp.1–13.

Lim, S.P. 2019. Dengue drug discovery: Progress, challenges and outlook. *Antiviral Research*. 163, pp.156–178.

Lin, C.S., Chow, S., Lau, A., Tu, R. and Lue, T.F. 2001. Identification and regulation of human PDE5A gene promoter. *Biochemical and Biophysical Research Communications*. 280(3), pp.684–692.

Lin, J.E., Colon-Gonzalez, F., Blomain, E., Kim, G.W., Aing, A., Stoecker, B., Rock, J., Snook, A.E., Zhan, T., Hyslop, T.M., Tomczak, M., Blumberg, R.S. and Waldman, S.A. 2016. Obesity-Induced Colorectal Cancer Is Driven by Caloric Silencing of the Guanylin–GUCY2C Paracrine Signaling Axis. *Cancer Research*. 76(2), pp.339–346.

Lin, J.E., Snook, A.E., Li, P., Stoecker, B.A., Kim, G.W., Magee, M.S., Garcia, A.V.M., Valentino, M.A., Hyslop, T., Schulz, S. and Waldman, S.A. 2012. GUCY2C opposes systemic genotoxic tumorigenesis by regulating AKT-dependent intestinal barrier integrity. *PloS One*. 7(2), p.e31686.

Lin, K.W. 2019. mSEPT9 Blood Test (Epi proColon) for Colorectal Cancer Screening. *American Family Physician*. 100(1), pp.10–11.

Lindquist, S. and Craig, E.A. 1988. The heat-shock proteins. *Annual Review of Genetics*. 22(Volume 22, 1988), pp.631–677.

Liu, D., Wu, A., Cui, L., Hao, R., Wang, Y., He, J. and Guo, D. 2014. Hepatitis B Virus Polymerase Suppresses NF-κB Signaling by Inhibiting the Activity of IKKs via Interaction with Hsp90ß. *PLOS ONE*. 9(3), p.e91658.

Liu, H., Tang, J.R., Choi, Y.H., Napolitano, M., Hockman, S., Taira, M., Degerman, E. and Manganiello, V.C. 2006. Importance of cAMP-response Element-binding Protein in Regulation of Expression of the Murine Cyclic Nucleotide Phosphodiesterase 3B (Pde3b) Gene in Differentiating 3T3-L1 Preadipocytes *. *Journal of Biological Chemistry*. 281(30), pp.21096–21113.

Liu, J., Zhang, X., Chen, G., Shao, Q., Zou, Y., Li, Z., Su, H., Li, M. and Xu, Y. 2023. Drug repurposing and structure-based discovery of new PDE4 and PDE5 inhibitors. *European Journal of Medicinal Chemistry*. 262, p.115893.

Liu, Q., Herrmann, A. and Huang, Q. 2019. Surface Binding Energy Landscapes Affect Phosphodiesterase Isoform-Specific Inhibitor Selectivity. *Computational and Structural Biotechnology Journal*. 17, pp.101–109.

Lok, S.-M., Costin, J.M., Hrobowski, Y.M., Hoffmann, A.R., Rowe, D.K., Kukkaro, P., Holdaway, H., Chipman, P., Fontaine, K.A., Holbrook, M.R., Garry, R.F., Kostyuchenko, V., Wimley, W.C., Isern, S., Rossmann, M.G. and Michael, S.F. 2012. Release of Dengue Virus Genome Induced by a Peptide Inhibitor. *PLOS ONE*. 7(11), p.e50995.

Lomana, M.G. de, Svensson, F., Volkamer, A., Mathea, M. and Kirchmair, J. 2022. Consideration of predicted small-molecule metabolites in computational toxicology. *Digital Discovery*. 1(2), pp.158–172.

Loo, Y.-M. and Gale, M. 2011. Immune Signaling by RIG-I-like Receptors. *Immunity*. 34(5), pp.680–692.

Lozano Terol, G., Gallego-Jara, J., Sola Martínez, R.A., Cánovas Díaz, M. and de Diego Puente, T. 2019. Engineering protein production by rationally choosing a carbon and nitrogen source using E. coli BL21 acetate metabolism knockout strains. *Microbial Cell Factories*. 18(1), p.151.

Lu, C.-Y., Chang, Y.-C., Hua, C.-H., Chuang, C., Huang, S.-H., Kung, S.-H., Hour, M.-J. and Lin, C.-W. 2017. Tubacin, an HDAC6 Selective Inhibitor, Reduces the Replication of the Japanese Encephalitis Virus via the Decrease of Viral RNA Synthesis. *International Journal of Molecular Sciences*. 18(5), p.954.

Lü, J., Yang, C., Zhang, Y. and Pan, H. 2018. Selection of Reference Genes for the Normalization of RT-qPCR Data in Gene Expression Studies in Insects: A Systematic Review. *Frontiers in Physiology*. 9, p.1560.

Lubbe, W.J., Zuzga, D.S., Zhou, Z., Fu, W., Pelta-Heller, J., Muschel, R.J., Waldman, S.A. and Pitari, G.M. 2009. Guanylyl Cyclase C Prevents Colon Cancer Metastasis by Regulating Tumor Epithelial Cell Matrix Metalloproteinase-9. *Cancer Research*. 69(8), pp.3529–3536.

Lucas, K.A., Pitari, G.M., Kazerounian, S., Ruiz-Stewart, I., Park, J., Schulz, S., Chepenik, K.P. and Waldman, S.A. 2000. Guanylyl Cyclases and Signaling by Cyclic GMP. *Pharmacological Reviews*. 52(3), pp.375–414.

Luckheeram, R.V., Zhou, R., Verma, A.D. and Xia, B. 2012. $CD4^+$T Cells: Differentiation and Functions. *Journal of Immunology Research*. 2012, p.e925135.

Luo, R., Fongwen, N., Kelly-Cirino, C., Harris, E., Wilder-Smith, A. and Peeling, R.W. 2019. Rapid diagnostic tests for determining dengue serostatus: a systematic review and key informant interviews. *Clinical Microbiology and Infection*. 25(6), pp.659–666.

Lutz, S. 2010. Beyond directed evolution—semi-rational protein engineering and design. *Current Opinion in Biotechnology*. 21(6), pp.734–743.

Luzak, B., Siarkiewicz, P. and Boncler, M. 2022. An evaluation of a new high-sensitivity PrestoBlue assay for measuring cell viability and drug cytotoxicity using EA.hy926 endothelial cells. *Toxicology in Vitro*. 83, p.105407.

Ma, C.S., Deenick, E.K., Batten, M. and Tangye, S.G. 2012. The origins, function, and regulation of T follicular helper cells. *Journal of Experimental Medicine*. 209(7), pp.1241–1253.

Ma, D., Wu, P., Egan, R.W., Billah, M.M. and Wang, P. 1999. Phosphodiesterase 4B gene transcription is activated by lipopolysaccharide and inhibited by interleukin-10 in human monocytes. *Molecular Pharmacology*. 55(1), pp.50–57.

MacArthur, R.D. and Novak, R.M. 2008. Maraviroc: The First of a New Class of Antiretroviral Agents. *Clinical Infectious Diseases*. 47(2), pp.236–241.

Mahindra, A., Tejeda, G., Rossi, M., Janha, O., Herbert, I., Morris, C., Morgan, D.C., Beattie, W., Montezano, A.C., Hudson, B., Tobin, A.B., Bhella, D., Touyz, R.M., Jamieson, A.G., Baillie, G.S. and Blair, C.M. 2021. Peptides derived from the SARS-CoV-2 receptor binding motif bind to ACE2 but do not block ACE2-mediated host cell entry or pro-inflammatory cytokine induction. *PLOS ONE*. 16(11), p.e0260283.

Mahmood, B., Damm, M.M.B., Jensen, T.S.R., Backe, M.B., Dahllöf, M.S., Poulsen, S.S., Bindslev, N. and Hansen, M.B. 2016. Phosphodiesterases in non-neoplastic appearing colonic mucosa from patients with colorectal neoplasia. *BMC Cancer*. 16(1), p.938.

Makaremi, S., Asadzadeh, Z., Hemmat, N., Baghbanzadeh, A., Sgambato, A., Ghorbaninezhad, F., Safarpour, H., Argentiero, A., Brunetti, O., Bernardini, R., Silvestris, N. and Baradaran, B. 2021. Immune Checkpoint Inhibitors in Colorectal Cancer: Challenges and Future Prospects. *Biomedicines*. 9(9), p.1075.

Mäkinen, M.J. 2007. Colorectal serrated adenocarcinoma. *Histopathology*. 50(1), pp.131–150.

Maksimovic, J., Phipson, B. and Oshlack, A. 2016. A cross-package Bioconductor workflow for analysing methylation array data. , p.055087.

Malavige, G.N., Wijewickrama, A., Fernando, S., Jeewandara, C., Ginneliya, A., Samarasekara, S., Madushanka, P., Punchihewa, C., Paranavitane, S., Idampitiya, D., Wanigatunga, C., Dissanayake, H., Prathapan, S., Gomes, L., Aman, S.A.B., John, A.S. and Ogg, G.S. 2018. A preliminary study on efficacy of rupatadine for the treatment of acute dengue infection. *Scientific Reports*. 8(1), p.3857.

Mallapaty, S. 2022. Dengue vaccine poised for roll-out but safety concerns linger. *Nature*. 611(7936), pp.434–435.

Mann, E.A., Harmel-Laws, E., Cohen, M.B. and Steinbrecher, K.A. 2013. Guanylate cyclase C limits systemic dissemination of a murine enteric pathogen. *BMC Gastroenterology*. 13(1), p.135.

Manoff, S.B., Sausser, M., Falk Russell, A., Martin, J., Radley, D., Hyatt, D., Roberts, C.C., Lickliter, J., Krishnarajah, J., Bett, A., Dubey, S., Finn, T. and Coller, B.-A. 2019. Immunogenicity and safety of an investigational tetravalent recombinant subunit vaccine for dengue: results of a Phase I randomized clinical trial in flavivirus-naïve adults. *Human Vaccines & Immunotherapeutics*. 15(9), pp.2195–2204.

Mansour, A.I. and Abu-Naser, S.S. 2019. Knowledge Based System for the Diagnosis of Dengue Disease. *International Journal of Academic Health and Medical Research (IJAHMR)*. 3(4), pp.12–19.

Manz, S.M., Losa, M., Fritsch, R. and Scharl, M. 2021. Efficacy and side effects of immune checkpoint inhibitors in the treatment of colorectal cancer. *Therapeutic Advances in Gastroenterology*. 14, p.17562848211002018.

Mármol, I., Sánchez-de-Diego, C., Pradilla Dieste, A., Cerrada, E. and Rodriguez Yoldi, M.J. 2017. Colorectal Carcinoma: A General Overview and Future Perspectives in Colorectal Cancer. *International Journal of Molecular Sciences*. 18(1), p.197.

Maurice, D.H., Ke, H., Ahmad, F., Wang, Y., Chung, J. and Manganiello, V.C. 2014. Advances in targeting cyclic nucleotide phosphodiesterases. *Nature Reviews. Drug Discovery*. 13(4), pp.290–314.

Maurya, N.S., Kushwaha, S., Vetukuri, R.R. and Mani, A. 2023. Unlocking the Potential of the CA2, CA7, and ITM2C Gene Signatures for the Early Detection of Colorectal Cancer: A Comprehensive Analysis of RNA-Seq Data by Utilizing Machine Learning Algorithms. *Genes*. 14(10), p.1836.

Mazumder, R., Hu, Z.-Z., Vinayaka, C.R., Sagripanti, J.-L., Frost, S.D.W., Kosakovsky Pond, S.L. and Wu, C.H. 2007. Computational analysis and identification of amino acid sites in dengue E proteins relevant to development of diagnostics and vaccines. *Virus Genes*. 35(2), pp.175–186.

McBride, A., Chanh, H.Q., Fraser, J.F., Yacoub, S. and Obonyo, N.G. 2020. Microvascular dysfunction in septic and dengue shock: Pathophysiology and implications for clinical management. *Global Cardiology Science & Practice*. 2020(2), p.e202029.

McEwan, D.G., Brunton, V.G., Baillie, G.S., Leslie, N.R., Houslay, M.D. and Frame, M.C. 2007. Chemoresistant KM12C Colon Cancer Cells Are Addicted to Low Cyclic AMP Levels in a Phosphodiesterase 4–Regulated Compartment via Effects on Phosphoinositide 3-Kinase. *Cancer Research*. 67(11), pp.5248–5257.

McQuade, R., Stojanovska, V., C. Bornstein, J. and Nurgali, K. 2017. Colorectal Cancer Chemotherapy: The Evolution of Treatment and New Approaches. *Current Medicinal Chemistry*. 24(15), pp.1537–1557.

Md-Sani, S.S., Md-Noor, J., Han, W.-H., Gan, S.-P., Rani, N.-S., Tan, H.-L., Rathakrishnan, K., A-Shariffuddin, M.A. and Abd-Rahman, M. 2018. Prediction of mortality in severe dengue cases. *BMC Infectious Diseases*. 18(1), p.232.

Mehta, A. and Patel, B.M. 2019. Therapeutic opportunities in colon cancer: Focus on phosphodiesterase inhibitors. *Life Sciences*. 230, pp.150–161.

Mei, X.-L., Yang, Y., Zhang, Y.-J., Li, Y., Zhao, J.-M., Qiu, J.-G., Zhang, W.-J., Jiang, Q.-W., Xue, Y.-Q., Zheng, D.-W., Chen, Y., Qin, W.-M., Wei, M.-N. and Shi, Z. 2015. Sildenafil inhibits the growth of human colorectal cancer in vitro and in vivo. *American Journal of Cancer Research*. 5(11), pp.3311–3324.

Mendoza, R.U., Valenzuela, S. and Dayrit, M. 2020. A Crisis of Confidence: The Case of Dengvaxia in the Philippines.

Miauton, A., Audran, R., Besson, J., Hajjami, H.M.-E., Karlen, M., Warpelin-Decrausaz, L., Sene, L., Schaufelberger, S., Faivre, V., Faouzi, M., Hartley, M.-A., Spertini, F. and Genton, B. 2024. Safety and immunogenicity of a synthetic nanoparticle-based, T cell priming peptide vaccine against dengue in healthy adults in Switzerland: a double-blind, randomized, vehicle-controlled, phase 1 study. *eBioMedicine*. 99.

Miklos, W., Heffeter, P., Pirker, C., Hager, S., Kowol, C.R., van Schoonhoven, S., Stojanovic, M., Keppler, B.K. and Berger, W. 2016. Loss of phosphodiesterase 4D mediates acquired triapine resistance via Epac-Rap1-Integrin signaling. *Oncotarget*. 7(51), pp.84556–84574.

Miyazaki, K. and Arnold, F.H. 1999. Exploring Nonnatural Evolutionary Pathways by Saturation Mutagenesis: Rapid Improvement of Protein Function. *Journal of Molecular Evolution*. 49(6), pp.716–720.

Modis, Y., Ogata, S., Clements, D. and Harrison, S.C. 2003. A ligand-binding pocket in the dengue virus envelope glycoprotein. *Proceedings of the National Academy of Sciences*. 100(12), pp.6986–6991.

Modis, Y., Ogata, S., Clements, D. and Harrison, S.C. 2004. Structure of the dengue virus envelope protein after membrane fusion. *Nature*. 427(6972), pp.313–319.

Modis, Y., Ogata, S., Clements, D. and Harrison, S.C. 2005. Variable Surface Epitopes in the Crystal Structure of Dengue Virus Type 3 Envelope Glycoprotein. *Journal of Virology*. 79(2), pp.1223–1231.

Mohammadi, P., Hesari, M., Chalabi, M., Salari, F. and Khademi, F. 2022. An overview of immune checkpoint therapy in autoimmune diseases. *International Immunopharmacology*. 107, p.108647.

Mojarad, E.N., Kuppen, P.J., Aghdaei, H.A. and Zali, M.R. 2013. The CpG island methylator phenotype (CIMP) in colorectal cancer. *Gastroenterology and Hepatology From Bed to Bench*. 6(3), pp.120–128.

Montoro, D.T., Haber, A.L., Rood, J.E., Regev, A. and Rajagopal, J. 2020. A Synthesis Concerning Conservation and Divergence of Cell Types across Epithelia. *Cold Spring Harbor Perspectives in Biology*. 12(11), p.a035733.

Moon, S.Y., Kim, K.D., Yoo, J., Lee, J.-H. and Hwangbo, C. 2021. Phytochemicals Targeting JAK–STAT Pathways in Inflammatory Bowel Disease: Insights from Animal Models. *Molecules*. 26(9), p.2824.

Mori, S. and Barth, H.G. 1999. *Size Exclusion Chromatography*. Springer Science & Business Media.

Moroder, L. 2005. Isosteric replacement of sulfur with other chalcogens in peptides and proteins. *Journal of Peptide Science*. 11(4), pp.187–214.

Morrison, J. and García-Sastre, A. 2014. STAT2 signaling and dengue virus infection. *JAK-STAT*. 3(1), p.e27715.

Morrison, K.L. and Weiss, G.A. 2001. Combinatorial alanine-scanning. *Current Opinion in Chemical Biology*. 5(3), pp.302–307.

Movsesian, M. 2016. Novel approaches to targeting PDE3 in cardiovascular disease. *Pharmacology & Therapeutics*. 163, pp.74–81.

Mueller-Langer, F. 2013. Neglected infectious diseases: Are push and pull incentive mechanisms suitable for promoting drug development research? *Health Economics, Policy and Law*. 8(2), pp.185–208.

Mukherjee, Soumita, Roy, S., Mukherjee, Shruti, Harikishore, A., Bhunia, A. and Mandal, A.K. 2024. 14-3-3 interaction with phosphodiesterase 8A sustains PKA signaling and downregulates the MAPK pathway. *Journal of Biological Chemistry*. 300(3).

Müller, M.F., Ibrahim, A.E.K. and Arends, M.J. 2016. Molecular pathological classification of colorectal cancer. *Virchows Archiv*. 469(2), pp.125–134.

Murakami, T., Kurosawa, T., Fukushima, H., Shibuya, T., Yao, T. and Nagahara, A. 2022. Sessile serrated lesions: Clinicopathological characteristics, endoscopic diagnosis, and management. *Digestive Endoscopy*. 34(6), pp.1096–1109.

Murata, K., Kameyama, M., Fukui, F., Ohigashi, H., Hiratsuka, M., Sasaki, Y., Kabuto, T., Mukai, M., Mammoto, T., Akedo, H., Ishikawa, O. and Imaoka, S. 1999. Phosphodiesterase type III inhibitor, cilostazol, inhibits colon cancer cell motility. *Clinical & Experimental Metastasis*. 17(6), pp.525–530.

Murata, K., Sudo, T., Kameyama, M., Fukuoka, H., Mukai, M., Doki, Y., Sasaki, Y., Ishikawa, O., Kimura, Y. and Imaoka, S. 2000. Cyclic AMP specific phosphodiesterase activity and colon cancer cell motility. *Clinical & Experimental Metastasis*. 18(7), pp.599–604.

Murata, T., Shimizu, K., Hiramoto, K. and Tagawa, T. 2009. Phosphodiesterase 3 (PDE3): Structure, Localization and Function. *Cardiovascular & Hematological Agents in Medicinal Chemistry (Formerly*. 7(3), pp.206–211.

Murugesan, A. and Manoharan, M. 2020. Chapter 16 - Dengue Virus *In*: M. M. Ennaji, ed. *Emerging and Reemerging Viral Pathogens* [Online]. Academic Press, pp.281–359.

Musheshe, N., Oun, A., Sabogal-Guáqueta, A.M., Trombetta-Lima, M., Mitchel, S.C., Adzemovic, A., Speek, O., Morra, F., van der Veen, C.H.J.T., Lezoualc'h, F., Cheng, X., Schmidt, M. and Dolga, A.M. 2022. Pharmacological Inhibition of Epac1 Averts Ferroptosis Cell Death by Preserving Mitochondrial Integrity. *Antioxidants*. 11(2), p.314.

Muttenthaler, M., King, G.F., Adams, D.J. and Alewood, P.F. 2021. Trends in peptide drug discovery. *Nature Reviews Drug Discovery*. 20(4), pp.309–325.

Nanaware, N., Banerjee, A., Mullick Bagchi, S., Bagchi, P. and Mukherjee, A. 2021. Dengue Virus Infection: A Tale of Viral Exploitations and Host Responses. *Viruses*. 13(10), p.1967.

Nasirudeen, A.M.A., Wong, H.H., Thien, P., Xu, S., Lam, K.-P. and Liu, D.X. 2011. RIG-I, MDA5 and TLR3 Synergistically Play an Important Role in Restriction of Dengue Virus Infection. *PLOS Neglected Tropical Diseases*. 5(1), p.e926.

National Cancer Institute 2024. Bioinformatics Pipeline: mRNA Analysis - GDC Docs. Available at: https://docs.gdc.cancer.gov/Data/Bioinformatics_Pipelines/Expression_mRNA_Pipeline/. Accessed: October 2024.

Neckers, L., Blagg, B., Haystead, T., Trepel, J.B., Whitesell, L. and Picard, D. 2018. Methods to validate Hsp90 inhibitor specificity, to identify off-target effects, and to rethink approaches for further clinical development. *Cell Stress and Chaperones*. 23(4), pp.467–482.

Nesvizhskii, A.I. 2014. Proteogenomics: concepts, applications and computational strategies. *Nature Methods*. 11(11), pp.1114–1125.

Ngono, A.E. and Shresta, S. 2018. Immune Response to Dengue and Zika. *Annual Review of Immunology*. 36(Volume 36, 2018), pp.279–308.

Nguyen, N.M., Chanh, H.Q., Tam, D.T.H., Vuong, N.L., Chau, N.T.X., Chau, N.V.V., Phong, N.T., Trieu, H.T., Luong Thi Hue, T., Cao Thi, T., Dinh The, T., Duyen, H.T.L., Van, N.T.T., Nguyen Than Ha, Q., Rivino, L., Gallagher, P., Jones, N.K., Geskus, R.B., Kestelyn, E. and Yacoub, S. 2021. Metformin as adjunctive therapy for dengue in overweight and obese patients: a protocol for an open-label clinical trial (MeDO). *Wellcome Open Research*. 5, p.160.

Nicholls, C.M.R., Sevvana, M. and Kuhn, R.J. 2020. Chapter Two - Structure-guided paradigm shifts in flavivirus assembly and maturation mechanisms *In*: M. Kielian, T. C. Mettenleiter and M. J. Roossinck, eds. *Advances in Virus Research* [Online]. Virus Assembly and Exit Pathways. Academic Press, pp.33–83.

Nielsen, M., Morreau, H., Vasen, H.F.A. and Hes, F.J. 2011. MUTYH-associated polyposis (MAP). *Critical Reviews in Oncology/Hematology*. 79(1), pp.1–16.

Nikolovska, K., Seidler, U.E. and Stock, C. 2022. The Role of Plasma Membrane Sodium/Hydrogen Exchangers in Gastrointestinal Functions: Proliferation and Differentiation, Fluid/Electrolyte Transport and Barrier Integrity. *Frontiers in Physiology*. 13.

Niles, R.M., Ludwig, K.W. and Makarski, J.S. 1979. Differential Growth Inhibition in Two Human Carcinoma Cell Lines by Cyclic Adenosine 5′-Monophosphate Analogs2. *JNCI: Journal of the National Cancer Institute*. 63(4), pp.909–911.

Nishi, K., Luo, H., Ishikura, S., Doi, K., Iwaihara, Y., Wills, L., Baillie, G.S., Sakata, T., Shirasawa, S. and Tsunoda, T. 2017. Apremilast Induces Apoptosis of Human Colorectal Cancer Cells with Mutant KRAS. *Anticancer Research*. 37(7), pp.3833–3839.

Nkongolo, S., Ni, Y., Lempp, F.A., Kaufman, C., Lindner, T., Esser-Nobis, K., Lohmann, V., Mier, W., Mehrle, S. and Urban, S. 2014. Cyclosporin A inhibits hepatitis B and hepatitis D virus entry by cyclophilin-independent interference with the NTCP receptor. *Journal of Hepatology*. 60(4), pp.723–731.

Nome, T., Thomassen, G.O., Bruun, J., Ahlquist, T., Bakken, A.C., Hoff, A.M., Rognum, T., Nesbakken, A., Lorenz, S., Sun, J., Barros-Silva, J.D., Lind, G.E., Myklebost, O., Teixeira, M.R., Meza-Zepeda, L.A., Lothe, R.A. and Skotheim, R.I. 2013. Common Fusion Transcripts Identified in Colorectal Cancer Cell Lines by High-Throughput RNA Sequencing. *Translational Oncology*. 6(5), pp.546–553.

Nongthombam, P.D. and Haobam, R. 2024. Targeting phosphodiesterase 4 as a potential therapy for Parkinson's disease: a review. *Molecular Biology Reports*. 51(1), p.510.

Nummela, P., Zafar, S., Veikkolainen, E., Ukkola, I., Cinella, V., Ayo, A., Asghar, M.Y., Välimäki, N., Törnquist, K., Karhu, A., Laakkonen, P., Aaltonen, L.A. and Ristimäki, A. 2024. mutation inhibits growth and induces phosphodiesterase 4D expression in colorectal cancer cell lines. *International Journal of Cancer*. 154(11), pp.1987–1998.

Nurgali, K., Jagoe, R.T. and Abalo, R. 2018. Editorial: Adverse Effects of Cancer Chemotherapy: Anything New to Improve Tolerance and Reduce Sequelae? *Frontiers in Pharmacology*. 9.

Obi, J.O., Gutiérrez-Barbosa, H., Chua, J.V. and Deredge, D.J. 2021. Current Trends and Limitations in Dengue Antiviral Research. *Tropical Medicine and Infectious Disease*. 6(4), p.180.

O'Hurley, G., Sjöstedt, E., Rahman, A., Li, B., Kampf, C., Pontén, F., Gallagher, W.M. and Lindskog, C. 2014. Garbage in, garbage out: A critical evaluation of strategies used for validation of immunohistochemical biomarkers. *Molecular Oncology*. 8(4), pp.783–798.

Oishi, K., Saito, M., Mapua, C.A. and Natividad, F.F. 2007. Dengue illness: clinical features and pathogenesis. *Journal of Infection and Chemotherapy*. 13(3), pp.125–133.

Omori, K. and Kotera, J. 2007. Overview of PDEs and Their Regulation. *Circulation Research*. 100(3), pp.309–327.

Pačínková, A. and Popovici, V. 2019. Cross-platform Data Analysis Reveals a Generic Gene Expression Signature for Microsatellite Instability in Colorectal Cancer. *BioMed Research International*. 2019(1), p.6763596.

Paes, D., Xie, K., Wheeler, D.G., Zook, D., Prickaerts, J. and Peters, M. 2021. Inhibition of PDE2 and PDE4 synergistically improves memory consolidation processes. *Neuropharmacology*. 184, p.108414.

Palanichamy Kala, M., St John, A.L. and Rathore, A.P.S. 2023. Dengue: Update on Clinically Relevant Therapeutic Strategies and Vaccines. *Current Treatment Options in Infectious Diseases*. 15(2), pp.27–52.

Panya, A., Bangphoomi, K., Choowongkomon, K. and Yenchitsomanus, P. 2014. Peptide Inhibitors Against Dengue Virus Infection. *Chemical Biology & Drug Design*. 84(2), pp.148–157.

Panya, A., Sawasdee, N., Junking, M., Srisawat, C., Choowongkomon, K. and Yenchitsomanus, P. 2015. A Peptide Inhibitor Derived from the Conserved Ectodomain Region of DENV Membrane (M) Protein with Activity Against Dengue Virus Infection. *Chemical Biology & Drug Design*. 86(5), pp.1093–1104.

Panya, A., Sawasdee, N., Songprakhon, P., Tragoolpua, Y., Rotarayanont, S., Choowongkomon, K. and Yenchitsomanus, P. 2020. A Synthetic Bioactive Peptide Derived from the Asian Medicinal Plant Acacia catechu Binds to Dengue Virus and Inhibits Cell Entry. *Viruses*. 12(11), p.1267.

Papaneophytou, C.P. and Kontopidis, G. 2014. Statistical approaches to maximize recombinant protein expression in *Escherichia coli*: A general review. *Protein Expression and Purification*. 94, pp.22–32.

Parang, B., Kaz, A.M., Barrett, C.W., Short, S.P., Ning, W., Keating, C.E., Mittal, M.K., Naik, R.D., Washington, M.K., Revetta, F.L., Smith, J.J., Chen, X., Wilson, K.T., Brand, T., Bader, D.M., Tansey, W.P., Chen, R., Brentnall, T.A., Grady, W.M. and Williams, C.S. 2017. BVES regulates c-Myc stability via PP2A and suppresses colitis-induced tumorigenesis. *Gut*. 66(5), pp.852–862.

Pardoll, D.M. 2012. The blockade of immune checkpoints in cancer immunotherapy. *Nature Reviews Cancer*. 12(4), pp.252–264.

Park, J. and Edwards, J. 2021. Colorectal cancer GRI TMA cohort. Available at: https://researchdata.gla.ac.uk/1227/. Accessed: September 2024.

Patel, A., Patel, M., Yang, X. and Mitra, A.K. 2014. Recent Advances in Protein and Peptide Drug Delivery: A Special Emphasis on Polymeric Nanoparticles. *Protein and peptide letters*. 21(11), pp.1102–1120.

Patel, K. and Dauphine, L. 2020. Of Mosquitoes and Models: Tracking Disease by Satellite. Available at: https://earthobservatory.nasa.gov/features/disease-vector. Accessed: April 2024.

Patel, S.S., Rauscher, M., Kudela, M. and Pang, H. 2023. Clinical Safety Experience of TAK-003 for Dengue Fever: A New Tetravalent Live Attenuated Vaccine Candidate. *Clinical Infectious Diseases*. 76(3), pp.e1350–e1359.

Pearson, C.A.B., Abbas, K.M., Clifford, S., Flasche, S. and Hladish, T.J. 2019. Serostatus testing and dengue vaccine cost–benefit thresholds. *Journal of the Royal Society Interface*. 16(157), p.20190234.

Peng, T., Gong, J., Jin, Y., Zhou, Y., Tong, R., Wei, X., Bai, L. and Shi, J. 2018. Inhibitors of phosphodiesterase as cancer therapeutics. *European Journal of Medicinal Chemistry*. 150, pp.742–756.

Pérez-Carbonell, L., Alenda, C., Payá, A., Castillejo, A., Barberá, V.M., Guillén, C., Rojas, E., Acame, N., Gutiérrez-Aviñó, F.J., Castells, A., Llor, X., Andreu, M., Soto, J.-L. and Jover, R. 2010. Methylation Analysis of MLH1 Improves the Selection of Patients for Genetic Testing in Lynch Syndrome. *The Journal of Molecular Diagnostics : JMD*. 12(4), p.498.

Perry, S.T., Buck, M.D. and Shresta, S. 2011. Better late than never: antivirals for dengue. *Expert Review of Anti-infective Therapy*. 9(7), pp.755–757.

Peters, T.J., Buckley, M.J., Statham, A.L., Pidsley, R., Samaras, K., V Lord, R., Clark, S.J. and Molloy, P.L. 2015. De novo identification of differentially methylated regions in the human genome. *Epigenetics & Chromatin*. 8(1), p.6.

Phillips, S. f., Pemberton, J. h., Shorter, R. g. and Talbot, I.C. 1993. The Large Intestine: Physiology, Pathophysiology and Disease. *Histopathology*. 23(4), pp.391–391.

Phue, J.-N., Lee, S.J., Trinh, L. and Shiloach, J. 2008. Modified Escherichia coli B (BL21), a superior producer of plasmid DNA compared with Escherichia coli K (DH5α). *Biotechnology and Bioengineering*. 101(4), pp.831–836.

Piccini, L.E., Castilla, V. and Damonte, E.B. 2015. Dengue-3 Virus Entry into Vero Cells: Role of Clathrin-Mediated Endocytosis in the Outcome of Infection. *PLOS ONE*. 10(10), p.e0140824.

Pino, M.S. and Chung, D.C. 2010. The Chromosomal Instability Pathway in Colon Cancer. *Gastroenterology*. 138(6), pp.2059–2072.

Pintado Silva, J. and Fernandez-Sesma, A. 2023. Challenges on the development of a dengue vaccine: a comprehensive review of the state of the art. *Journal of General Virology*. 104(3), p.001831.

Pinto, E.M., Faucz, F.R., Paza, L.Z., Wu, G., Fernandes, E.S., Bertherat, J., Stratakis, C.A., Lalli, E., Ribeiro, R.C., Rodriguez-Galindo, C., Figueiredo, B.C. and Zambetti, G.P. 2020. Germline Variants in Phosphodiesterase

Genes and Genetic Predisposition to Pediatric Adrenocortical Tumors. *Cancers*. 12(2), p.506.

Pirhaghi, M., Mamashli, F., Moosavi-Movahedi, F., Arghavani, P., Amiri, A., Davaeil, B., Mohammad-Zaheri, M., Mousavi-Jarrahi, Z., Sharma, D., Langel, Ü., Otzen, D.E. and Saboury, A.A. 2024. Cell-Penetrating Peptides: Promising Therapeutics and Drug-Delivery Systems for Neurodegenerative Diseases. *Molecular Pharmaceutics*. 21(5), pp.2097–2117.

Piroozkhah, Moein, Aghajani, A., Jalali, P., Shahmoradi, A., Piroozkhah, Mobin, Tadlili, Y. and Salehi, Z. 2023. Guanylate cyclase-C Signaling Axis as a theragnostic target in colorectal cancer: a systematic review of literature. *Frontiers in Oncology*. 13.

Pisal, D.S., Kosloski, M.P. and Balu-Iyer, S.V. 2010. Delivery of Therapeutic Proteins. *Journal of Pharmaceutical Sciences*. 99(6), pp.2557–2575.

Pitari, G.M., Li, P., Lin, J.E., Zuzga, D., Gibbons, A.V., Snook, A.E., Schulz, S. and Waldman, S.A. 2007. The Paracrine Hormone Hypothesis of Colorectal Cancer. *Clinical Pharmacology & Therapeutics*. 82(4), pp.441–447.

Pleiman, J.K., Irving, A.A., Wang, Z., Toraason, E., Clipson, L., Dove, W.F., Deming, D.A. and Newton, M.A. 2018. The conserved protective cyclic AMP-phosphodiesterase function PDE4B is expressed in the adenoma and adjacent normal colonic epithelium of mammals and silenced in colorectal cancer. *PLOS Genetics*. 14(9), p.e1007611.

Pockley, A.G. 2003. Heat shock proteins as regulators of the immune response. *The Lancet*. 362(9382), pp.469–476.

Pollaro, L. and Heinis, C. 2010. Strategies to prolong the plasma residence time of peptidedrugs. *MedChemComm*. 1(5), pp.319–324.

Poole, R.M. and Nowlan, M.L. 2014. Albiglutide: first global approval. *Drugs*. 74(8), pp.929–938.

Popat, S. and Houlston, R.S. 2005. A systematic review and meta-analysis of the relationship between chromosome 18q genotype, DCC status and colorectal cancer prognosis. *European Journal of Cancer*. 41(14), pp.2060–2070.

Porath, J. 1988. IMAC—Immobilized metal ion affinity based chromatography. *TrAC Trends in Analytical Chemistry*. 7(7), pp.254–259.

Porter, K.R., Ewing, D., Chen, L., Wu, S.-J., Hayes, C.G., Ferrari, M., Teneza-Mora, N. and Raviprakash, K. 2012. Immunogenicity and protective efficacy of a vaxfectin-adjuvanted tetravalent dengue DNA vaccine. *Vaccine*. 30(2), pp.336–341.

Posit team 2024. RStudio: Integrated Development Environment for R. *Posit Software, PBC, Boston, MA*.

Prodromou, C. 2016. Mechanisms of Hsp90 regulation. *Biochemical Journal*. 473(16), pp.2439–2452.

Qiu, N., Hou, H., Guo, T., Lv, Y., zhou, Y., Zhang, Fang-fang, Zhang, Feng, Wang, X., Chen, W., Gao, Y., Chen, M., Zhang, X., Zhang, H. and Wang, H. 2024. Phosphodiesterase 8 (PDE8): Distribution and Cellular Expression and Association with Alzheimer's Disease. *Neurochemical Research*. 49(8), pp.1993–2004.

Quach, M.E., Chen, W. and Li, R. 2018. Mechanisms of platelet clearance and translation to improve platelet storage. *Blood*. 131(14), pp.1512–1521.

Quinlan, A.R. and Hall, I.M. 2010. BEDTools: a flexible suite of utilities for comparing genomic features. *Bioinformatics*. 26(6), pp.841–842.

R Core Team 2023. R: A Language and Environment for Statistical Computing. *R Foundation for Statistical Computing, Vienna, Austria*.

Ramesh, S., Johnson, P., Fadlalla, K., Moore, A., Huang, C.-H., Berry, K., Maxuitenko, Y.Y., Chen, X., Keeton, A.B., Zhou, G. and Piazza, G. 2023. Novel sulindac derivatives for colorectal cancer chemoprevention that target cGMP phosphodiesterases to suppress Wnt/β-catenin transcriptional activity. *Cancer Insight*. 3(1), pp.42–54.

Rappaport, J.A., Entezari, A.A., Caspi, A., Caksa, S., Jhaveri, A.V., Stanek, T.J., Ertel, A., Kupper, J., Fortina, P.M., McMahon, S.B., Jaynes, J.B., Snook, A.E. and Waldman, S.A. 2022. A β-Catenin-TCF-Sensitive Locus Control Region Mediates GUCY2C Ligand Loss in Colorectal Cancer. *Cellular and Molecular Gastroenterology and Hepatology*. 13(4), pp.1276–1296.

Rappaport, J.A. and Waldman, S.A. 2020. An update on guanylyl cyclase C in the diagnosis, chemoprevention, and treatment of colorectal cancer. *Expert review of clinical pharmacology*. 13(10), pp.1125–1137.

Rappaport, J.A. and Waldman, S.A. 2018. The Guanylate Cyclase C—cGMP Signaling Axis Opposes Intestinal Epithelial Injury and Neoplasia. *Frontiers in Oncology*. 8.

Rathore, A.P.S., Haystead, T., Das, P.K., Merits, A., Ng, M.-L. and Vasudevan, S.G. 2014. Chikungunya virus nsP3 & nsP4 interacts with HSP-90 to promote virus replication: HSP-90 inhibitors reduce CHIKV infection and inflammation *in vivo*. *Antiviral Research*. 103, pp.7–16.

Reale, M.A., Hu, G., Zafar, A.I., Getzenberg, R.H., Levine, S.M. and Fearon, E.R. 1994. Expression and alternative splicing of the deleted in colorectal cancer (DCC) gene in normal and malignant tissues. *Cancer Research*. 54(16), pp.4493–4501.

Rerksuppaphol, S. and Rerksuppaphol, L. 2018. A Randomized Controlled Trial of Zinc Supplementation as Adjuvant Therapy for Dengue Viral Infection in Thai Children. *International Journal of Preventive Medicine*. 9(1), p.88.

Reyes-del Valle, J., Chávez-Salinas, S., Medina, F. and del Angel, R.M. 2005. Heat Shock Protein 90 and Heat Shock Protein 70 Are Components of

Dengue Virus Receptor Complex in Human Cells. *Journal of Virology*. 79(8), pp.4557–4567.

Rezaul, K., Murphy, M., Lundgren, D.H., Wilson, L. and Han, D.K. 2010. Combined mass spectrometry- and immunohistochemistry-based approach to determine protein expression in archival melanoma – proof of principle. *Pigment Cell & Melanoma Research*. 23(6), pp.849–852.

Riddell, I.A. 2018. Cisplatin and Oxaliplatin: Our Current Understanding of Their Actions. *Metal Ions in Life Sciences*. 18, /books/9783110470734/9783110470734-007/9783110470734-007.xml.

Ritchie, M.E., Phipson, B., Wu, D., Hu, Y., Law, C.W., Shi, W. and Smyth, G.K. 2015. limma powers differential expression analyses for RNA-sequencing and microarray studies. *Nucleic Acids Research*. 43(7), p.e47.

Rivino, L. 2018. Understanding the Human T Cell Response to Dengue Virus *In*: R. Hilgenfeld and S. G. Vasudevan, eds. *Dengue and Zika: Control and Antiviral Treatment Strategies* [Online]. Singapore: Springer, pp.241–250.

Roberts, R.A., Kavanagh, S.L., Mellor, H.R., Pollard, C.E., Robinson, S. and Platz, S.J. 2014. Reducing attrition in drug development: smart loading preclinical safety assessment. *Drug Discovery Today*. 19(3), pp.341–347.

Roby, J.A., Esser-Nobis, K., Dewey-Verstelle, E.C., Fairgrieve, M.R., Schwerk, J., Lu, A.Y., Soveg, F.W., Hemann, E.A., Hatfield, L.D., Keller, B.C., Shapiro, A., Forero, A., Stencel-Baerenwald, J.E., Savan, R. and Gale, M. 2020. Flavivirus Nonstructural Protein NS5 Dysregulates HSP90 to Broadly Inhibit JAK/STAT Signaling. *Cells*. 9(4), p.899.

Rodríguez, A., Rodríguez, M., Córdoba, J.J. and Andrade, M.J. 2015. Design of Primers and Probes for Quantitative Real-Time PCR Methods *In*: C. Basu, ed. *PCR Primer Design* [Online]. New York, NY: Springer, pp.31–56.

Roehrig, J.T., Bolin, R.A. and Kelly, R.G. 1998. Monoclonal Antibody Mapping of the Envelope Glycoprotein of the Dengue 2 Virus, Jamaica. *Virology*. 246(2), pp.317–328.

Rosty, C., Hewett, D.G., Brown, I.S., Leggett, B.A. and Whitehall, V.L.J. 2013. Serrated polyps of the large intestine: current understanding of diagnosis, pathogenesis, and clinical management. *Journal of Gastroenterology*. 48(3), pp.287–302.

Rothan, H.A., Mohamed, Z., Paydar, M., Rahman, N.A. and Yusof, R. 2014. Inhibitory effect of doxycycline against dengue virus replication in vitro. *Archives of Virology*. 159(4), pp.711–718.

Roy, S.K. and Bhattacharjee, S. 2021. Dengue virus: epidemiology, biology, and disease aetiology. *Canadian Journal of Microbiology*. 67(10), pp.687–702.

Saba, M.V., Barkla, D.H. and Tutton, P.J.M. 1990. Influence of adenosine cyclic nucleotide analogs on growth of human colon tumor cell lines. *Life Sciences*. 47(4), pp.307–311.

Sabbah, D.A., Hajjo, R. and Sweidan, K. 2020. Review on Epidermal Growth Factor Receptor (EGFR) Structure, Signaling Pathways, Interactions, and Recent Updates of EGFR Inhibitors. *Current Topics in Medicinal Chemistry*. 20(10), pp.815–834.

Sadahiro, S., Ohmura, T., Saito, T. and Suzuki, S. 1991. Relationship between length and surface area of each segment of the large intestine and the incidence of colorectal cancer. *Cancer*. 68(1), pp.84–87.

Sadek, M.S., Cachorro, E., El-Armouche, A. and Kämmerer, S. 2020. Therapeutic Implications for PDE2 and cGMP/cAMP Mediated Crosstalk in Cardiovascular Diseases. *International Journal of Molecular Sciences*. 21(20), p.7462.

Saeedan, A., Rastogi, S. and Ansari, M. 2020. Roflumilast counteracts DMH-induced preneoplastic colon damage in albino Wistar rats. *Human & Experimental Toxicology*. 39(11), pp.1545–1555.

Salje, H., Alera, M.T., Chua, M.N., Hunsawong, T., Ellison, D., Srikiatkhachorn, A., Jarman, R.G., Gromowski, G.D., Rodriguez-Barraquer, I., Cauchemez, S., Cummings, D.A.T., Macareo, L., Yoon, I.-K., Fernandez, S. and Rothman, A.L. 2021. Evaluation of the extended efficacy of the Dengvaxia vaccine against symptomatic and subclinical dengue infection. *Nature Medicine*. 27(8), pp.1395–1400.

Salovaara, R., Roth, S., Loukola, A., Launonen, V., Sistonen, P., Avizienyte, E., Kristo, P., Järvinen, H., Souchelnytskyi, S., Sarlomo-Rikala, M. and Aaltonen, L.A. 2002. Frequent loss of SMAD4/DPC4 protein in colorectal cancers. *Gut*. 51(1), pp.56–59.

Sample, V., DiPilato, L.M., Yang, J.H., Ni, Q., Saucerman, J.J. and Zhang, J. 2012. Regulation of nuclear PKA revealed by spatiotemporal manipulation of cyclic AMP. *Nature Chemical Biology*. 8(4), pp.375–382.

Sanchez, J., Carter, T.R., Cohen, M.S. and Blagg, B.S.J. 2020. Old and New Approaches to Target the Hsp90 Chaperone. *Current Cancer Drug Targets*. 20(4), pp.253–270.

Sanders, B., Koldijk, M. and Schuitemaker, H. 2015. Inactivated Viral Vaccines *In*: B. K. Nunnally, V. E. Turula and R. D. Sitrin, eds. *Vaccine Analysis: Strategies, Principles, and Control* [Online]. Berlin, Heidelberg: Springer, pp.45–80.

Sankaradoss, A., Jagtap, S., Nazir, J., Moula, S.E., Modak, A., Fialho, J., Iyer, M., Shastri, J.S., Dias, M., Gadepalli, R., Aggarwal, A., Vedpathak, M., Agrawal, S., Pandit, A., Nisheetha, A., Kumar, A., Bordoloi, M., Shafi, M., Shelar, B., Balachandra, S.S., Damodar, T., Masika, M.M., Mwaura, P., Anzala, O., Muthumani, K., Sowdhamini, R., Medigeshi, G.R., Roy, R., Pattabiraman, C., Krishna, S. and Sreekumar, E. 2022. Immune profile and responses of a novel dengue DNA vaccine encoding an EDIII-NS1 consensus design based on Indo-African sequences. *Molecular Therapy*. 30(5), pp.2058–2077.

Santana, L.M.R., Baquero, O.S., Maeda, A.Y., Nogueira, J.S. and Chiaravalloti Neto, F. 2022. Spatio-temporal dynamics of dengue-related deaths and associated factors. *Revista do Instituto de Medicina Tropical de São Paulo*. 64, p.e30.

Sanz-Pamplona, R., Cordero, D., Berenguer, A., Lejbkowicz, F., Rennert, H., Salazar, R., Biondo, S., Sanjuan, X., Pujana, M.A., Rozek, L., Giordano, T.J., Ben-Izhak, O., Cohen, H.I., Trougouboff, P., Bejhar, J., Sova, Y., Rennert, G., Gruber, S.B. and Moreno, V. 2011. Gene Expression Differences between Colon and Rectum Tumors. *Clinical Cancer Research*. 17(23), pp.7303–7312.

Sapio, L., Salzillo, A., Ragone, A., Illiano, M., Spina, A. and Naviglio, S. 2020. Targeting CREB in Cancer Therapy: A Key Candidate or One of Many? An Update. *Cancers*. 12(11), p.3166.

Sarker, A., Dhama, N. and Gupta, R.D. 2023. Dengue virus neutralizing antibody: a review of targets, cross-reactivity, and antibody-dependent enhancement. *Frontiers in Immunology*. 14.

Sasaki, T., Kotera, J. and Omori, K. 2004. Transcriptional activation of phosphodiesterase 7B1 by dopamine D1 receptor stimulation through the cyclic AMP/cyclic AMP-dependent protein kinase/cyclic AMP-response element binding protein pathway in primary striatal neurons. *Journal of Neurochemistry*. 89(2), pp.474–483.

Sassone-Corsi, P. 2012. The Cyclic AMP Pathway. *Cold Spring Harbor Perspectives in Biology*. 4(12), p.a011148.

Satija, R., Farrell, J.A., Gennert, D., Schier, A.F. and Regev, A. 2015. Spatial reconstruction of single-cell gene expression data. *Nature Biotechnology*. 33(5), pp.495–502.

Sawicki, T., Ruszkowska, M., Danielewicz, A., Niedźwiedzka, E., Arłukowicz, T. and Przybyłowicz, K.E. 2021. A Review of Colorectal Cancer in Terms of Epidemiology, Risk Factors, Development, Symptoms and Diagnosis. *Cancers*. 13(9), p.2025.

Schatoff, E.M., Leach, B.I. and Dow, L.E. 2017. WNT Signaling and Colorectal Cancer. *Current Colorectal Cancer Reports*. 13(2), pp.101–110.

Schein, C.H. and Noteborn, M.H.M. 1988. Formation of Soluble Recombinant Proteins in Escherichia Coli is Favored by Lower Growth Temperature. *Bio/Technology*. 6(3), pp.291–294.

Scheufler, C., Brinker, A., Bourenkov, G., Pegoraro, S., Moroder, L., Bartunik, H., Hartl, F.U. and Moarefi, I. 2000. Structure of TPR Domain–Peptide Complexes: Critical Elements in the Assembly of the Hsp70–Hsp90 Multichaperone Machine. *Cell*. 101(2), pp.199–210.

Schmid, M.A., Diamond, M.S. and Harris, E. 2014. Dendritic Cells in Dengue Virus Infection: Targets of Virus Replication and Mediators of Immunity. *Frontiers in Immunology*. 5.

Schmidt, A.G., Yang, P.L. and Harrison, S.C. 2010. Peptide Inhibitors of Dengue-Virus Entry Target a Late-Stage Fusion Intermediate. *PLOS Pathogens*. 6(4), p.e1000851.

Schmidt, W.-P., Suzuki, M., Thiem, V.D., White, R.G., Tsuzuki, A., Yoshida, L.-M., Yanai, H., Haque, U., Tho, L.H., Anh, D.D. and Ariyoshi, K. 2011. Population Density, Water Supply, and the Risk of Dengue Fever in Vietnam: Cohort Study and Spatial Analysis. *PLOS Medicine*. 8(8), p.e1001082.

Schmittgen, T.D. and Livak, K.J. 2008. Analyzing real-time PCR data by the comparative CT method. *Nature Protocols*. 3(6), pp.1101–1108.

Schudt, C., Hatzelmann, A., Beume, R. and Tenor, H. 2011. Phosphodiesterase Inhibitors: History of Pharmacology *In*: S. H. Francis, M. Conti and M. D. Houslay, eds. *Phosphodiesterases as Drug Targets* [Online]. Berlin, Heidelberg: Springer, pp.1–46.

Screaton, G., Mongkolsapaya, J., Yacoub, S. and Roberts, C. 2015. New insights into the immunopathology and control of dengue virus infection. *Nature Reviews Immunology*. 15(12), pp.745–759.

See, K.C. 2022. Vaccination for the Prevention of Infection among Immunocompromised Patients: A Concise Review of Recent Systematic Reviews. *Vaccines*. 10(5), p.800.

Selvarajan, V., Tram, N.D.T., Xu, J., Ngen, S.T.Y., Koh, J.-J., Teo, J.W.P., Yuen, T.-Y. and Ee, P.L.R. 2023. Stapled ß-Hairpin Antimicrobial Peptides with Improved Stability and Activity against Drug-Resistant Gram-Negative Bacteria. *Journal of Medicinal Chemistry*. 66(13), pp.8498–8509.

Shailubhai, K., Yu, H.H., Karunanandaa, K., Wang, J.Y., Eber, S.L., Wang, Y., Joo, N.S., Kim, H.D., Miedema, B.W., Abbas, S.Z., Boddupalli, S.S., Currie, M.G. and Forte, L.R. 2000. Uroguanylin Treatment Suppresses Polyp Formation in the ApcMin/+ Mouse and Induces Apoptosis in Human Colon Adenocarcinoma Cells via Cyclic GMP. *Cancer Research*. 60(18), pp.5151–5157.

Sharman, S.K., Islam, B.N., Hou, Y., Singh, N., Berger, F.G., Sridhar, S., Yoo, W. and Browning, D.D. 2018. Cyclic-GMP–Elevating Agents Suppress Polyposis in ApcMin Mice by Targeting the Preneoplastic Epithelium. *Cancer Prevention Research*. 11(2), pp.81–92.

Shukla, R., Ramasamy, V., Shanmugam, R.K., Ahuja, R. and Khanna, N. 2020. Antibody-Dependent Enhancement: A Challenge for Developing a Safe Dengue Vaccine. *Frontiers in Cellular and Infection Microbiology*. 10.

Sicca, F., Neppelenbroek, S. and Huckriede, A. 2018. Effector mechanisms of influenza-specific antibodies: neutralization and beyond. *Expert Review of Vaccines*. 17(9), pp.785–795.

Sidaway, P. 2019. Microenvironment plasticity confers cetuximab resistance. *Nature Reviews Clinical Oncology*. 16(9), pp.527–527.

Sievers, F. and Higgins, D.G. 2018. Clustal Omega for making accurate alignments of many protein sequences. *Protein Science*. 27(1), pp.135–145.

Sinicrope, F.A. 2018. Lynch Syndrome-Associated Colorectal Cancer. *The New England Journal of Medicine*. 379(8), pp.764–773.

Siri, S., Zhao, Y., Maier, F., Pierce, D.M. and Feng, B. 2020. The Macro- and Micro-Mechanics of the Colon and Rectum I: Experimental Evidence. *Bioengineering*. 7(4), p.130.

Smith, S.A., de Alwis, A.R., Kose, N., Harris, E., Ibarra, K.D., Kahle, K.M., Pfaff, J.M., Xiang, X., Doranz, B.J., de Silva, A.M., Austin, S.K., Sukupolvi-Petty, S., Diamond, M.S. and Crowe, J.E. 2013. The Potent and Broadly Neutralizing Human Dengue Virus-Specific Monoclonal Antibody 1C19 Reveals a Unique Cross-Reactive Epitope on the bc Loop of Domain II of the Envelope Protein. *mBio*. 4(6), 10.1128/mbio.00873-13.

Sobhani, I., Tap, J., Roudot-Thoraval, F., Roperch, J.P., Letulle, S., Langella, P., Corthier, G., Nhieu, J.T.V. and Furet, J.P. 2011. Microbial Dysbiosis in Colorectal Cancer (CRC) Patients. *PLOS ONE*. 6(1), p.e16393.

Söderberg, O., Leuchowius, K.-J., Gullberg, M., Jarvius, M., Weibrecht, I., Larsson, L.-G. and Landegren, U. 2008. Characterizing proteins and their interactions in cells and tissues using the *in situ* proximity ligation assay. *Methods*. 45(3), pp.227–232.

Soderling, S.H., Bayuga, S.J. and Beavo, J.A. 1998. Identification and Characterization of a Novel Family of Cyclic Nucleotide Phosphodiesterases *. *Journal of Biological Chemistry*. 273(25), pp.15553–15558.

Soderling, S.H. and Beavo, J.A. 2000. Regulation of cAMP and cGMP signaling: new phosphodiesterases and new functions. *Current Opinion in Cell Biology*. 12(2), pp.174–179.

Soo, K.-M., Khalid, B., Ching, S.-M. and Chee, H.-Y. 2016. Meta-Analysis of Dengue Severity during Infection by Different Dengue Virus Serotypes in Primary and Secondary Infections. *PLOS ONE*. 11(5), p.e0154760.

Souza, L.R., Colonna, J.G., Comodaro, J.M. and Naveca, F.G. 2022. Using amino acids co-occurrence matrices and explainability model to investigate patterns in dengue virus proteins. *BMC Bioinformatics*. 23(1), p.80.

Spano, J.-P., Lagorce, C., Atlan, D., Milano, G., Domont, J., Benamouzig, R., Attar, A., Benichou, J., Martin, A., Morere, J.-F., Raphael, M., Penault-Llorca, F., Breau, J.-L., Fagard, R., Khayat, D. and Wind, P. 2005. Impact of EGFR expression on colorectal cancer patient prognosis and survival. *Annals of Oncology*. 16(1), pp.102–108.

Spiegelberg, H.L. 2009. Biological Role of Different Antibody Classes. *International Archives of Allergy and Applied Immunology*. 90(Suppl. 1), pp.22–27.

Spinelli, A. 2022. Colorectal Cancer: Minimally Invasive Surgery *In*: S. R. Steele, T. L. Hull, N. Hyman, J. A. Maykel, T. E. Read and C. B. Whitlow, eds. *The ASCRS Textbook of Colon and Rectal Surgery* [Online]. Cham: Springer International Publishing, pp.619–642.

Srikanth, B., Reddy, L., Biradar, S., Shamanna, M., Mariguddi, D.D. and Krishnakumar, M. 2019. An open-label, randomized prospective study to evaluate the efficacy and safety of Carica papaya leaf extract for thrombocytopenia associated with dengue fever in pediatric subjects. *Pediatric Health, Medicine and Therapeutics*. 10(null), pp.5–11.

Srikiatkhachorn, A., Mathew, A. and Rothman, A.L. 2017. Immune-mediated cytokine storm and its role in severe dengue. *Seminars in Immunopathology*. 39(5), pp.563–574.

Srisutthisamphan, K., Jirakanwisal, K., Ramphan, S., Tongluan, N., Kuadkitkan, A. and Smith, D.R. 2018. Hsp90 interacts with multiple dengue virus 2 proteins. *Scientific Reports*. 8(1), p.4308.

St John, A.L., Rathore, A.P., Raghavan, B., Ng, M.-L. and Abraham, S.N. 2013. Contributions of mast cells and vasoactive products, leukotrienes and chymase, to dengue virus-induced vascular leakage R. Medzhitov, ed. *eLife*. 2, p.e00481.

St. John, A.L. and Rathore, A.P.S. 2019. Adaptive immune responses to primary and secondary dengue virus infections. *Nature Reviews Immunology*. 19(4), pp.218–230.

Standring, S. 2019. The Anatomy of the Large Intestine *In*: M. Parker and W. Hohenberger, eds. *Lower Gastrointestinal Tract Surgery: Vol.1, Laparoscopic procedures* [Online]. Cham: Springer International Publishing, pp.27–89.

Stark, G.R., Kerr, I.M., Williams, B.R.G., Silverman, R.H. and Schreiber, R.D. 1998. HOW CELLS RESPOND TO INTERFERONS.

Steinbrecher, K.A., Wowk, S.A., Rudolph, J.A., Witte, D.P. and Cohen, M.B. 2002a. Targeted Inactivation of the Mouse Guanylin Gene Results in Altered Dynamics of Colonic Epithelial Proliferation. *The American Journal of Pathology*. 161(6), pp.2169–2178.

Steinbrecher, K.A., Wowk, S.A., Rudolph, J.A., Witte, D.P. and Cohen, M.B. 2002b. Targeted Inactivation of the Mouse Guanylin Gene Results in Altered Dynamics of Colonic Epithelial Proliferation. *The American Journal of Pathology*. 161(6), pp.2169–2178.

Sucharov, C.C., Nakano, S.J., Slavov, D., Schwisow, J.A., Rodriguez, E., Nunley, K., Medway, A., Stafford, N., Nelson, P., McKinsey, T.A., Movsesian, M., Minobe, W., Carroll, I.A., Taylor, M.R.G. and Bristow, M.R. 2019. A PDE3A Promoter Polymorphism Regulates cAMP-Induced Transcriptional Activity in Failing Human Myocardium. *Journal of the American College of Cardiology*. 73(10), pp.1173–1184.

Sukupolvi-Petty, S., Austin, S.K., Purtha, W.E., Oliphant, T., Nybakken, G.E., Schlesinger, J.J., Roehrig, J.T., Gromowski, G.D., Barrett, A.D., Fremont, D.H. and Diamond, M.S. 2007. Type- and Subcomplex-Specific Neutralizing Antibodies against Domain III of Dengue Virus Type 2 Envelope Protein Recognize Adjacent Epitopes. *Journal of Virology*. 81(23), pp.12816–12826.

Sun, B., Sundström, K.B., Chew, J.J., Bist, P., Gan, E.S., Tan, H.C., Goh, K.C., Chawla, T., Tang, C.K. and Ooi, E.E. 2017. Dengue virus activates cGAS through the release of mitochondrial DNA. *Scientific Reports*. 7(1), p.3594.

Sun, D. and Nassal, M. 2006. Stable HepG2- and Huh7-based human hepatoma cell lines for efficient regulated expression of infectious hepatitis B virus. *Journal of Hepatology*. 45(5), pp.636–645.

Sung, H., Ferlay, J., Siegel, R.L., Laversanne, M., Soerjomataram, I., Jemal, A. and Bray, F. 2021. Global Cancer Statistics 2020: GLOBOCAN Estimates of Incidence and Mortality Worldwide for 36 Cancers in 185 Countries. *CA: A Cancer Journal for Clinicians*. 71(3), pp.209–249.

Susmi, T.F., Rahman, A., Khan, Md.M.R., Yasmin, F., Islam, Md.S., Nasif, O., Alharbi, S.A., Batiha, G.E.-S. and Hossain, M.U. 2021. Prognostic and clinicopathological insights of phosphodiesterase 9A gene as novel biomarker in human colorectal cancer. *BMC Cancer*. 21(1), p.577.

Sutton, S.S., Magagnoli, J., Cummings, T.H. and Hardin, J.W. 2020. The Association Between Phosphodiesterase-5 Inhibitors and Colorectal Cancer in a National Cohort of Patients. *Clinical and Translational Gastroenterology*. 11(6), p.e00173.

Suzuki, H., Watkins, D.N., Jair, K.-W., Schuebel, K.E., Markowitz, S.D., Dong Chen, W., Pretlow, T.P., Yang, B., Akiyama, Y., van Engeland, M., Toyota, M., Tokino, T., Hinoda, Y., Imai, K., Herman, J.G. and Baylin, S.B. 2004. Epigenetic inactivation of SFRP genes allows constitutive WNT signaling in colorectal cancer. *Nature Genetics*. 36(4), pp.417–422.

Swift, M.L. 1997. GraphPad Prism, Data Analysis, and Scientific Graphing. *Journal of Chemical Information and Computer Sciences*. 37(2), pp.411–412.

Swinnen, J.V., Joseph, D.R. and Conti, M. 1989. The mRNA encoding a high-affinity cAMP phosphodiesterase is regulated by hormones and cAMP. *Proceedings of the National Academy of Sciences of the United States of America*. 86(21), pp.8197–8201.

Swinnen, J.V., Tsikalas, K.E. and Conti, M. 1991. Properties and hormonal regulation of two structurally related cAMP phosphodiesterases from the rat Sertoli cell. *The Journal of Biological Chemistry*. 266(27), pp.18370–18377.

Szabó, G.T., Mahiny, A.J. and Vlatkovic, I. 2022. COVID-19 mRNA vaccines: Platforms and current developments. *Molecular Therapy: The Journal of the American Society of Gene Therapy*. 30(5), pp.1850–1868.

Tabernero, J., Velez, L., Trevino, T.L., Grothey, A., Yaeger, R., Van Cutsem, E., Wasan, H., Desai, J., Ciardiello, F., Yoshino, T., Gollerkeri, A., Maharry, K., Christy-Bittel, J. and Kopetz, S. 2021. Management of adverse events from the treatment of encorafenib plus cetuximab for patients with *BRAF* V600E-mutant metastatic colorectal cancer: insights from the BEACON CRC study. *ESMO Open*. 6(6), p.100328.

Taguwa, S., Maringer, K., Li, X., Bernal-Rubio, D., Rauch, J.N., Gestwicki, J.E., Andino, R., Fernandez-Sesma, A. and Frydman, J. 2015. Defining Hsp70 Subnetworks in Dengue Virus Replication Reveals Key Vulnerability in Flavivirus Infection. *Cell*. 163(5), pp.1108–1123.

Taha, E.A., Ono, K. and Eguchi, T. 2019. Roles of Extracellular HSPs as Biomarkers in Immune Surveillance and Immune Evasion. *International Journal of Molecular Sciences*. 20(18), p.4588.

Tamas, K., Walenkamp, A.M.E., de Vries, E.G.E., van Vugt, M.A.T.M., Beets-Tan, R.G., van Etten, B., de Groot, D.J.A. and Hospers, G.A.P. 2015. Rectal and colon cancer: Not just a different anatomic site. *Cancer Treatment Reviews*. 41(8), pp.671–679.

Tassone, G., Mazzorana, M. and Pozzi, C. 2022. Structural Basis of Parasitic HSP90 ATPase Inhibition by Small Molecules. *Pharmaceuticals*. 15(11), p.1341.

Thomas, S.J. and Yoon, I.-K. 2019. A review of Dengvaxia®: development to deployment. *Human Vaccines & Immunotherapeutics*. 15(10), pp.2295–2314.

Thompson, W.J., Piazza, G.A., Li, H., Liu, L., Fetter, J., Zhu, B., Sperl, G., Ahnen, D. and Pamukcu, R. 2000. Exisulind Induction of Apoptosis Involves Guanosine 3′,5′-Cyclic Monophosphate Phosphodiesterase Inhibition, Protein Kinase G Activation, and Attenuated β-Catenin. *Cancer Research*. 60(13), pp.3338–3342.

Thomson, H.J., Busuttil, A., Eastwood, M.A., Smith, A.N. and Elton, R.A. 1986. The submucosa of the human colon. *Journal of Ultrastructure and Molecular Structure Research*. 96(1), pp.22–30.

Thul, P.J. and Lindskog, C. 2018. The human protein atlas: A spatial map of the human proteome. *Protein Science : A Publication of the Protein Society*. 27(1), pp.233–244.

Tibbo, A.J., Mika, D., Dobi, S., Ling, J., McFall, A., Tejeda, G.S., Blair, C., MacLeod, R., MacQuaide, N., Gök, C., Fuller, W., Smith, B.O., Smith, G.L., Vandecasteele, G., Brand, T. and Baillie, G.S. 2022. Phosphodiesterase type 4 anchoring regulates cAMP signaling to Popeye domain-containing proteins. *Journal of Molecular and Cellular Cardiology*. 165, pp.86–102.

Tinsley, H.N., Gary, B.D., Thaiparambil, J., Li, N., Lu, W., Li, Y., Maxuitenko, Y.Y., Keeton, A.B. and Piazza, G.A. 2010. Colon Tumor Cell Growth-Inhibitory Activity of Sulindac Sulfide and Other Nonsteroidal Anti-

Inflammatory Drugs Is Associated with Phosphodiesterase 5 Inhibition. *Cancer Prevention Research*. 3(10), pp.1303–1313.

Tkačová, J. and Angelovičová, M. 2012. Heat Shock Proteins (HSPs): a Review. *SCIENTIFIC PAPERS ANIMAL SCIENCE AND BIOTECHNOLOGIES*. 45(1), pp.349–349.

Torlakovic, E.E., Gomez, J.D., Driman, D.K., Parfitt, J.R., Wang, C., Benerjee, T. and Snover, D.C. 2008. Sessile Serrated Adenoma (SSA) vs. Traditional Serrated Adenoma (TSA). *The American Journal of Surgical Pathology*. 32(1), p.21.

Torras-Llort, M. and Azorín, F. 2003. Functional characterization of the human phosphodiesterase 7A1 promoter. *Biochemical Journal*. 373(Pt 3), pp.835–843.

Trieu, E.P., Gross, J.K. and Targoff, I.N. 2009. Immunoprecipitation-western blot for proteins of low abundance. *Methods in Molecular Biology (Clifton, N.J.)*. 536, pp.259–275.

Tsai, L.-C.L. and Beavo, J.A. 2012. Regulation of Adrenal Steroidogenesis by the High-affinity Phosphodiesterase 8 Family. *Hormone and metabolic research = Hormon- und Stoffwechselforschung = Hormones et metabolisme*. 44(10), pp.790–794.

Tsai, W.-Y., Lai, C.-Y., Wu, Y.-C., Lin, H.-E., Edwards, C., Jumnainsong, A., Kliks, S., Halstead, S., Mongkolsapaya, J., Screaton, G.R. and Wang, W.-K. 2013. High-Avidity and Potently Neutralizing Cross-Reactive Human Monoclonal Antibodies Derived from Secondary Dengue Virus Infection. *Journal of Virology*. 87(23), pp.12562–12575.

Tsheten, T., Clements, A.C.A., Gray, D.J., Adhikary, R.K., Furuya-Kanamori, L. and Wangdi, K. 2021. Clinical predictors of severe dengue: a systematic review and meta-analysis. *Infectious Diseases of Poverty*. 10(1), p.123.

Tsukahara, T., Matsuda, Y. and Haniu, H. 2013. Cyclic Phosphatidic Acid Stimulates cAMP Production and Inhibits Growth in Human Colon Cancer Cells. *PLOS ONE*. 8(11), p.e81139.

Tsunoda, T., Ota, T., Fujimoto, T., Doi, K., Tanaka, Y., Yoshida, Y., Ogawa, M., Matsuzaki, H., Hamabashiri, M., Tyson, D.R., Kuroki, M., Miyamoto, S. and Shirasawa, S. 2012. Inhibition of Phosphodiesterase-4 (PDE4) activity triggers luminal apoptosis and AKT dephosphorylation in a 3-D colonic-crypt model. *Molecular Cancer*. 11(1), p.46.

Tully, D. and Griffiths, C.L. 2021. Dengvaxia: the world's first vaccine for prevention of secondary dengue. *Therapeutic Advances in Vaccines and Immunotherapy*. 9, p.25151355211015839.

Ubol, S., Phuklia, W., Kalayanarooj, S. and Modhiran, N. 2010. Mechanisms of Immune Evasion Induced by a Complex of Dengue Virus and Preexisting Enhancing Antibodies. *The Journal of Infectious Diseases*. 201(6), pp.923–935.

Uhlen, M., Oksvold, P., Fagerberg, L., Lundberg, E., Jonasson, K., Forsberg, M., Zwahlen, M., Kampf, C., Wester, K., Hober, S., Wernerus, H., Björling, L. and Ponten, F. 2010. Towards a knowledge-based Human Protein Atlas. *Nature Biotechnology*. 28(12), pp.1248–1250.

Unal, E.B., Gursoy, A. and Erman, B. 2009. Conformational energies and entropies of peptides, and the peptide–protein binding problem. *Physical Biology*. 6(3), p.036014.

Uno, N. and Ross, T.M. 2018. Dengue virus and the host innate immune response. *Emerging Microbes & Infections*.

Vaish, A., Verma, S., Agarwal, A., Gupta, L. and Gutch, M. 2012. Effect of vitamin E on thrombocytopenia in dengue fever. *Annals of Tropical Medicine and Public Health*. 5(4), p.282.

Vales, S., Kryukova, J., Chandra, S., Smagurauskaite, G., Payne, M., Clark, C.J., Hafner, K., Mburu, P., Denisov, S., Davies, G., Outeiral, C., Deane, C.M., Morris, G.M. and Bhattacharya, S. 2023. Discovery and pharmacophoric characterization of chemokine network inhibitors using phage-display, saturation mutagenesis and computational modelling. *Nature Communications*. 14(1), p.5763.

Vázquez, S., Guzmán, M.G., Guillen, G., Chinea, G., Pérez, A.B., Pupo, M., Rodriguez, R., Reyes, O., Garay, H.E., Delgado, I., García, G. and Alvarez, M. 2002. Immune response to synthetic peptides of dengue prM protein. *Vaccine*. 20(13), pp.1823–1830.

Verma, S., Goand, U.K., Husain, A., Katekar, R.A., Garg, R. and Gayen, J.R. 2021. Challenges of peptide and protein drug delivery by oral route: Current strategies to improve the bioavailability. *Drug Development Research*. 82(7), pp.927–944.

Vermeulen, L., De Sousa E Melo, F., van der Heijden, M., Cameron, K., de Jong, J.H., Borovski, T., Tuynman, J.B., Todaro, M., Merz, C., Rodermond, H., Sprick, M.R., Kemper, K., Richel, D.J., Stassi, G. and Medema, J.P. 2010. Wnt activity defines colon cancer stem cells and is regulated by the microenvironment. *Nature Cell Biology*. 12(5), pp.468–476.

Vicini, E. and Conti, M. 1997. Characterization of an Intronic Promoter of a Cyclic Adenosine 3′,5′-Monophosphate (cAMP)-Specific Phosphodiesterase Gene that Confers Hormone and cAMP Inducibility. *Molecular Endocrinology*. 11(7), pp.839–850.

Victor, K., Jacob, J. and Cafiso, D.S. 1999. Interactions Controlling the Membrane Binding of Basic Protein Domains: Phenylalanine and the Attachment of the Myristoylated Alanine-Rich C-Kinase Substrate Protein to Interfaces. *Biochemistry*. 38(39), pp.12527–12536.

Vodenkova, S., Buchler, T., Cervena, K., Veskrnova, V., Vodicka, P. and Vymetalkova, V. 2020. 5-fluorouracil and other fluoropyrimidines in colorectal cancer: Past, present and future. *Pharmacology & Therapeutics*. 206, p.107447.

Walker, D.L., Bhagwate, A.V., Baheti, S., Smalley, R.L., Hilker, C.A., Sun, Z. and Cunningham, J.M. 2015. DNA Methylation Profiling: Comparison of Genome-Wide Sequencing Methods and the Infinium Human Methylation 450 Bead Chip. *Epigenomics*. 7(8), pp.1287–1302.

Wallace, D., Canouet, V., Garbes, P. and Wartel, T.A. 2013. Challenges in the clinical development of a dengue vaccine. *Current Opinion in Virology*. 3(3), pp.352–356.

Wang, C. and Luo, D. 2021. The metabolic adaptation mechanism of metastatic organotropism. *Experimental Hematology & Oncology*. 10(1), p.30.

Wang, D., Deng, C., Bugaj-Gaweda, B., Kwan, M., Gunwaldsen, C., Leonard, C., Xin, X., Hu, Y., Unterbeck, A. and De Vivo, M. 2003. Cloning and characterization of novel PDE4D isoforms PDE4D6 and PDE4D7. *Cellular Signalling*. 15(9), pp.883–891.

Wang, H., Li, Z., Ou, Q., Wu, X., Nagasaka, M., Shao, Y., Ou, S.I. and Yang, Y. 2022. NTRK fusion positive colorectal cancer is a unique subset of CRC with high TMB and microsatellite instability. *Cancer Medicine*. 11(13), pp.2541–2549.

Wang, J.P., Liu, P., Latz, E., Golenbock, D.T., Finberg, R.W. and Libraty, D.H. 2006. Flavivirus Activation of Plasmacytoid Dendritic Cells Delineates Key Elements of TLR7 Signaling beyond Endosomal Recognition1. *The Journal of Immunology*. 177(10), pp.7114–7121.

Wang, P., Wu, P., Egan, R.W. and Billah, M.M. 2001. Human phosphodiesterase 8A splice variants: cloning, gene organization, and tissue distribution. *Gene*. 280(1), pp.183–194.

Wang, Q.-Y. and Shi, P.-Y. 2015. Flavivirus Entry Inhibitors. *ACS Infectious Diseases*. 1(9), pp.428–434.

Wang, R., Islam, B.N., Bridges, A., Sharman, S.K., Hu, M., Hou, Y., Somanath, P.R., Venable, L., Singh, N., Kim, S., Sridhar, S., Hofmann, F. and Browning, D.D. 2017. cGMP Signaling Increases Antioxidant Gene Expression by Activating Forkhead Box O3A in the Colon Epithelium. *The American Journal of Pathology*. 187(2), pp.377–389.

Wang, R., Kwon, I.-K., Thangaraju, M., Singh, N., Liu, K., Jay, P., Hofmann, F., Ganapathy, V. and Browning, D.D. 2012. Type 2 cGMP-dependent protein kinase regulates proliferation and differentiation in the colonic mucosa. *American Journal of Physiology-Gastrointestinal and Liver Physiology*. 303(2), pp.G209–G219.

Wang, R., Li, J., Zhou, X., Mao, Y., Wang, Wendong, Gao, S., Wang, Wei, Gao, Y., Chen, K., Yu, S., Wu, X., Wen, L., Ge, H., Fu, W. and Tang, F. 2022. Single-cell genomic and transcriptomic landscapes of primary and metastatic colorectal cancer tumors. *Genome Medicine*. 14(1), p.93.

Wang, S., Zhang, Z., Qian, W., Ji, D., Wang, Q., Ji, B., Zhang, Y., Zhang, C., Sun, Ye, Zhu, C. and Sun, Yueming 2018. Angiogenesis and vasculogenic mimicry are inhibited by 8-Br-cAMP through activation of the cAMP/PKA

pathway in colorectal cancer. *OncoTargets and Therapy*. 11, pp.3765–3774.

Wang, X., Ni, D., Liu, Y. and Lu, S. 2021. Rational Design of Peptide-Based Inhibitors Disrupting Protein-Protein Interactions. *Frontiers in Chemistry*. 9.

Wang, Y., Chen, Y., Li, Y., Lan, T. and Qian, H. 2014. Type II cGMP-dependent protein kinase inhibits RhoA activation in gastric cancer cells. *Molecular Medicine Reports*. 9(4), pp.1444–1452.

Wang, Y., Jin, F., Wang, R., Li, F., Wu, Y., Kitazato, K. and Wang, Yifei 2017. HSP90: a promising broad-spectrum antiviral drug target. *Archives of Virology*. 162(11), pp.3269–3282.

Watanaveeradej, V., Simasathien, S., Mammen, M.P., Nisalak, A., Tournay, E., Kerdpanich, P., Samakoses, R., Putnak, R.J., Gibbons, R.V., Yoon, I.-K., Jarman, R.G., Barrera, R.D.L., Moris, P., Eckels, K.H., Thomas, S.J. and Innis, B.L. 2016. Long-Term Safety and Immunogenicity of a Tetravalent Live-Attenuated Dengue Vaccine and Evaluation of a Booster Dose Administered to Healthy Thai Children. *The American Journal of Tropical Medicine and Hygiene*. 94(6), pp.1348–1358.

Waterhouse, A.M., Procter, J.B., Martin, D.M.A., Clamp, M. and Barton, G.J. 2009. Jalview Version 2—a multiple sequence alignment editor and analysis workbench. *Bioinformatics*. 25(9), pp.1189–1191.

Wehbe, N., Slika, H., Mesmar, J., Nasser, S.A., Pintus, G., Baydoun, S., Badran, A., Kobeissy, F., Eid, A.H. and Baydoun, E. 2020. The Role of Epac in Cancer Progression. *International Journal of Molecular Sciences*. 21(18), p.6489.

Wei, H., Zhang, Y., Jia, Y., Chen, X., Niu, T., Chatterjee, A., He, P. and Hou, G. 2024. Heat shock protein 90: biological functions, diseases, and therapeutic targets. *MedComm*. 5(2), p.e470.

Wei, Z., Fang, Y., Gosztyla, M.L., Li, A.J., Huang, W., LeClair, C.A., Simeonov, A., Tao, D. and Xia, M. 2021. A direct peptide reactivity assay using a high-throughput mass spectrometry screening platform for detection of skin sensitizers. *Toxicology Letters*. 338, pp.67–77.

Weinberg, D.S., Lin, J.E., Foster, N.R., Della'Zanna, G., Umar, A., Seisler, D., Kraft, W.K., Kastenberg, D.M., Katz, L.C., Limburg, P.J. and Waldman, S.A. 2017. Bioactivity of Oral Linaclotide in Human Colorectum for Cancer Chemoprevention. *Cancer Prevention Research*. 10(6), pp.345–354.

Weinstein, J.N., Collisson, E.A., Mills, G.B., Shaw, K.M., Ozenberger, B.A., Ellrott, K., Shmulevich, I., Sander, C. and Stuart, J.M. 2013. The Cancer Genome Atlas Pan-Cancer Analysis Project. *Nature genetics*. 45(10), pp.1113–1120.

Weiser, M.R. 2018. AJCC 8th Edition: Colorectal Cancer. *Annals of Surgical Oncology*. 25(6), pp.1454–1455.

Whitehead, S.S. 2016. Development of TV003/TV005, a single dose, highly immunogenic live attenuated dengue vaccine; what makes this vaccine different from the Sanofi-Pasteur CYD™ vaccine? *Expert Review of Vaccines*. 15(4), pp.509–517.

Whitt, J.D., Li, N., Tinsley, H.N., Chen, X., Zhang, W., Li, Y., Gary, B.D., Keeton, A.B., Xi, Y., Abadi, A.H., Grizzle, W.E. and Piazza, G.A. 2012. A Novel Sulindac Derivative that Potently Suppresses Colon Tumor Cell Growth by Inhibiting cGMP Phosphodiesterase and β-Catenin Transcriptional Activity. *Cancer Prevention Research*. 5(6), pp.822–833.

Wild, C.T., Shugars, D.C., Greenwell, T.K., McDanal, C.B. and Matthews, T.J. 1994. Peptides corresponding to a predictive alpha-helical domain of human immunodeficiency virus type 1 gp41 are potent inhibitors of virus infection. *Proceedings of the National Academy of Sciences*. 91(21), pp.9770–9774.

Wilken, L. and Rimmelzwaan, G.F. 2020. Adaptive Immunity to Dengue Virus: Slippery Slope or Solid Ground for Rational Vaccine Design? *Pathogens*. 9(6), p.470.

Williams, C.S., Zhang, B., Smith, J.J., Jayagopal, A., Barrett, C.W., Pino, C., Russ, P., Presley, S.H., Peng, D., Rosenblatt, D.O., Haselton, F.R., Yang, J.-L., Washington, M.K., Chen, X., Eschrich, S., Yeatman, T.J., El-Rifai, W., Beauchamp, R.D. and Chang, M.S. 2011. BVES regulates EMT in human corneal and colon cancer cells and is silenced via promoter methylation in human colorectal carcinoma. *The Journal of Clinical Investigation*. 121(10), pp.4056–4069.

Williams, G.H. and Stoeber, K. 2012. The cell cycle and cancer. *The Journal of Pathology*. 226(2), pp.352–364.

Wilson, C., Lin, J.E., Li, P., Snook, A.E., Gong, J., Sato, T., Liu, C., Girondo, M.A., Rui, H., Hyslop, T. and Waldman, S.A. 2014. The Paracrine Hormone for the GUCY2C Tumor Suppressor, Guanylin, Is Universally Lost in Colorectal Cancer. *Cancer Epidemiology, Biomarkers & Prevention*. 23(11), pp.2328–2337.

Wollner, C.J., Richner, M., Hassert, M.A., Pinto, A.K., Brien, J.D. and Richner, J.M. 2021. A Dengue Virus Serotype 1 mRNA-LNP Vaccine Elicits Protective Immune Responses. *Journal of Virology*. 95(12), 10.1128/jvi.02482-20.

World Health Organization 2024. Dengue and severe dengue. Available at: https://www.who.int/news-room/fact-sheets/detail/dengue-and-severe-dengue. Accessed: May 2024.

World Health Organization 2009. *Dengue: Guidelines for Diagnosis, Treatment, Prevention and Control*. World Health Organization.

World Health Organization 2019. Ten health issues WHO will tackle this year. Available at: https://www.who.int/news-room/spotlight/ten-threats-to-global-health-in-2019. Accessed: April 2024.

Wright, T.A., Gemmell, A.O., Tejeda, G.S., Blair, C.M. and Baillie, G.S. 2023. Cancer: Phosphodiesterase type 4C (PDE4C), the forgotten subfamily as a therapeutic target. *The International Journal of Biochemistry & Cell Biology*. 162, p.106453.

Wu, J., Sun, L., Chen, X., Du, F., Shi, H., Chen, C. and Chen, Z.J. 2013. Cyclic GMP-AMP Is an Endogenous Second Messenger in Innate Immune Signaling by Cytosolic DNA. *Science*. 339(6121), pp.826–830.

Wu, Y., Chen, Y., Qu, R., Lan, T. and Sang, J. 2012. Type II cGMP-dependent protein kinase inhibits EGF-triggered signal transduction of the MAPK/ERK-mediated pathway in gastric cancer cells. *Oncology Reports*. 27(2), pp.553–558.

Wu, Y.-L., Jiang, T., Huang, W., Wu, X.-Y., Zhang, P.-J. and Tian, Y.-P. 2022. Genome-wide methylation profiling of early colorectal cancer using an Illumina Infinium Methylation EPIC BeadChip. *World Journal of Gastrointestinal Oncology*. 14(4), p.935.

Xi, Y. and Xu, P. 2021. Global colorectal cancer burden in 2020 and projections to 2040. *Translational Oncology*. 14(10), p.101174.

Xia, Y. and Liang, T.J. 2019. Development of Direct-acting Antiviral and Host-targeting Agents for Treatment of Hepatitis B Virus Infection. *Gastroenterology*. 156(2), pp.311–324.

Xie, Y.-H., Chen, Y.-X. and Fang, J.-Y. 2020. Comprehensive review of targeted therapy for colorectal cancer. *Signal Transduction and Targeted Therapy*. 5(1), pp.1–30.

Xu, H., Zhang, Z., Li, P., Lu, X., Chen, B. and Lan, T. 2020. Expression of PKG2 in ovarian cancer and its effect on epidermal growth factor receptor. *Journal of B.U.ON.: official journal of the Balkan Union of Oncology*. 25(2), pp.729–735.

Xu, X., Yu, Y., Liu, M., Liang, L. and Liu, T. 2022. Efficacy and safety of regorafenib and fruquintinib as third-line treatment for colorectal cancer: a narrative review. *Translational Cancer Research*. 11(1), pp.276–287.

Yaeger, R., Weiss, J., Pelster, M.S., Spira, A.I., Barve, M., Ou, S.-H.I., Leal, T.A., Bekaii-Saab, T.S., Paweletz, C.P., Heavey, G.A., Christensen, J.G., Velastegui, K., Kheoh, T., Der-Torossian, H. and Klempner, S.J. 2023. Adagrasib with or without Cetuximab in Colorectal Cancer with Mutated KRAS G12C. *New England Journal of Medicine*. 388(1), pp.44–54.

Yalaz, C., Bridges, E., Alham, N.K., Zois, C.E., Chen, J., Bensaad, K., Miar, A., Pires, E., Muschel, R.J., McCullagh, J.S.O. and Harris, A.L. 2024. Cone photoreceptor phosphodiesterase PDE6H inhibition regulates cancer cell growth and metabolism, replicating the dark retina response. *Cancer & Metabolism*. 12(1), p.5.

Yalla, K., Elliott, C., Day, J.P., Findlay, J., Barratt, S., Hughes, Z.A., Wilson, L., Whiteley, E., Popiolek, M., Li, Y., Dunlop, J., Killick, R., Adams, D.R., Brandon, N.J., Houslay, M.D., Hao, B. and Baillie, G.S. 2018. FBXW7

regulates DISC1 stability via the ubiquitin-proteosome system. *Molecular Psychiatry*. 23(5), pp.1278–1286.

Yamamoto, S., Nakanishi, K. and Matsuno, R. 1988. *Ion-Exchange Chromatography of Proteins*. CRC Press.

Yap, S.S.L., Nguyen-Khuong, T., Rudd, P.M. and Alonso, S. 2017. Dengue Virus Glycosylation: What Do We Know? *Frontiers in Microbiology*. 8.

Yauch, L.E. and Shresta, S. 2008. Mouse models of dengue virus infection and disease. *Antiviral Research*. 80(2), pp.87–93.

Ye, J., Zeng, B., Zhong, M., Li, H., Xu, L., Shu, J., Wang, Y., Yang, F., Zhong, C., Ye, X., He, X. and Ouyang, D. 2021. Scutellarin inhibits caspase-11 activation and pyroptosis in macrophages *via* regulating PKA signaling. *Acta Pharmaceutica Sinica B*. 11(1), pp.112–126.

Yi, H., Wang, K., Jin, J., Jin, H., Yang, L., Zou, Y., Du, B. and Liu, X. 2018. Elevated Adenylyl Cyclase 9 Expression Is a Potential Prognostic Biomarker for Patients with Colon Cancer. *Medical Science Monitor*. 24, pp.19–25.

Yoshizawa, J., Yoshida, K., Fujikawa, T., Tanabe, A. and Sakurai, K. 1995. [Inhibitory effects of Forskolin on hepatic metastasis from human colon cancer in nude mice]. *Nihon Geka Gakkai Zasshi*. 96(1), pp.26–30.

Young, C.L., Britton, Z.T. and Robinson, A.S. 2012. Recombinant protein expression and purification: a comprehensive review of affinity tags and microbial applications. *Biotechnology Journal*. 7(5), pp.620–634.

Yu, L.C.-H. 2018. Microbiota dysbiosis and barrier dysfunction in inflammatory bowel disease and colorectal cancers: exploring a common ground hypothesis. *Journal of Biomedical Science*. 25(1), p.79.

Zaccolo, M. 2011. Spatial control of cAMP signalling in health and disease. *Current Opinion in Pharmacology*. 11(6), pp.649–655.

Zagórska, A. 2020. Phosphodiesterase 10 (PDE10) inhibitors: an updated patent review (2014-present). *Expert Opinion on Therapeutic Patents*. 30(2), pp.147–157.

Zambon, A.C., Wilderman, A., Ho, A. and Insel, P.A. 2011. Increased Expression of the Pro-apoptotic Protein BIM, a Mechanism for cAMP/Protein Kinase A (PKA)-induced Apoptosis of Immature T Cells. *Journal of Biological Chemistry*. 286(38), pp.33260–33267.

Zapadka, K.L., Becher, F.J., Gomes dos Santos, A.L. and Jackson, S.E. 2017. Factors affecting the physical stability (aggregation) of peptide therapeutics. *Interface Focus*. 7(6), p.20170030.

Zellweger, R.M. and Shresta, S. 2014. Mouse Models to Study Dengue Virus Immunology and Pathogenesis. *Frontiers in Immunology*. 5.

Zhai, Z., Yu, X., Yang, B., Zhang, Y., Zhang, L., Li, X. and Sun, H. 2017. Colorectal cancer heterogeneity and targeted therapy: Clinical

implications, challenges and solutions for treatment resistance. *Seminars in Cell & Developmental Biology*. 64, pp.107–115.

Zhang, H., Kong, Q., Wang, J., Jiang, Y. and Hua, H. 2020. Complex roles of cAMP–PKA–CREB signaling in cancer. *Experimental Hematology & Oncology*. 9(1), p.32.

Zhang, H., Liu, Y., Liu, J., Chen, J., Wang, J., Hua, H. and Jiang, Y. 2024. cAMP-PKA/EPAC signaling and cancer: the interplay in tumor microenvironment. *Journal of Hematology & Oncology*. 17(1), p.5.

Zhang, L. and Shay, J.W. 2017. Multiple Roles of APC and its Therapeutic Implications in Colorectal Cancer. *JNCI: Journal of the National Cancer Institute*. 109(8), p.djw332.

Zhang, M., Sun, J., Li, M. and Jin, X. 2020. Modified mRNA-LNP Vaccines Confer Protection against Experimental DENV-2 Infection in Mice. *Molecular Therapy Methods & Clinical Development*. 18, pp.702–712.

Zhang, T., Luu, M.D.A., Dolga, A.M., Eisel, U.L.M. and Schmidt, M. 2023. The old second messenger cAMP teams up with novel cell death mechanisms: potential translational therapeutical benefit for Alzheimer's disease and Parkinson's disease. *Frontiers in Physiology*. 14.

Zhang, T.-M., Huang, T. and Wang, R.-F. 2018. Cross talk of chromosome instability, CpG island methylator phenotype and mismatch repair in colorectal cancer. *Oncology Letters*. 16(2), pp.1736–1746.

Zhang, W., Chipman, P.R., Corver, J., Johnson, P.R., Zhang, Y., Mukhopadhyay, S., Baker, T.S., Strauss, J.H., Rossmann, M.G. and Kuhn, R.J. 2003. Visualization of membrane protein domains by cryo-electron microscopy of dengue virus. *Nature Structural & Molecular Biology*. 10(11), pp.907–912.

Zhang, X. and Yu, W. 2022. Heat shock proteins and viral infection. *Frontiers in Immunology*. 13, p.947789.

Zhang, Y., Zhang, W., Ogata, S., Clements, D., Strauss, J.H., Baker, T.S., Kuhn, R.J. and Rossmann, M.G. 2004. Conformational Changes of the Flavivirus E Glycoprotein. *Structure*. 12(9), pp.1607–1618.

Zhao, Lili, Liu, J., He, C., Yan, R., Zhou, K., Cui, Q., Meng, X., Li, X., Zhang, Y., Nie, Y., Zhang, Y., Hu, R., Liu, Y., Zhao, Lian, Chen, M., Xiao, W., Tian, J., Zhao, Y., Cao, L., Zhou, L., Lin, A., Ruan, C. and Dai, K. 2017. Protein kinase A determines platelet life span and survival by regulating apoptosis. *The Journal of Clinical Investigation*. 127(12), pp.4338–4351.

Zhao, Y., Wang, Y., Zhao, J., Zhang, Z., Jin, M., Zhou, F., Jin, C., Zhang, J., Xing, J., Wang, N., He, X. and Ren, T. 2021a. PDE2 Inhibits PKA-Mediated Phosphorylation of TFAM to Promote Mitochondrial Ca2+-Induced Colorectal Cancer Growth. *Frontiers in Oncology*. 11, p.663778.

Zhao, Y., Wang, Y., Zhao, J., Zhang, Z., Jin, M., Zhou, F., Jin, C., Zhang, J., Xing, J., Wang, N., He, X. and Ren, T. 2021b. PDE2 Inhibits PKA-Mediated

Phosphorylation of TFAM to Promote Mitochondrial Ca2+-Induced Colorectal Cancer Growth. *Frontiers in Oncology*. 11.

Zheng, L. and Zhou, Z.-Z. 2023. An overview of phosphodiesterase 9 inhibitors: Insights from skeletal structure, pharmacophores, and therapeutic potential. *European Journal of Medicinal Chemistry*. 259, p.115682.

Zhou, W., Triche, T.J., Jr, Laird, P.W. and Shen, H. 2018. SeSAMe: reducing artifactual detection of DNA methylation by Infinium BeadChips in genomic deletions. *Nucleic Acids Research*. 46(20), p.e123.

Zhu, X., Zelmer, A. and Wellmann, S. 2017. Visualization of Protein-protein Interaction in Nuclear and Cytoplasmic Fractions by Co-immunoprecipitation and In Situ Proximity Ligation Assay. *Journal of Visualized Experiments : JoVE*. (119), p.55218.

Zolla, L. 2008. Proteomics studies reveal important information on small molecule therapeutics: a case study on plasma proteins. *Drug Discovery Today*. 13(23), pp.1042–1051.

Zompi, S. and Harris, E. 2012. Animal Models of Dengue Virus Infection. *Viruses*. 4(1), pp.62–82.

Zuzga, D.S., Pelta-Heller, J., Li, P., Bombonati, A., Waldman, S.A. and Pitari, G.M. 2012. Phosphorylation of vasodilator-stimulated phosphoprotein Ser239 suppresses filopodia and invadopodia in colon cancer. *International Journal of Cancer*. 130(11), pp.2539–2548.

Zyla, J., Papiez, A., Zhao, J., Qu, R., Li, X., Kluger, Y., Polanska, J., Hatzis, C., Pusztai, L. and Marczyk, M. 2023. Evaluation of zero counts to better understand the discrepancies between bulk and single-cell RNA-Seq platforms. *Computational and Structural Biotechnology Journal*. 21, pp.4663–4674.